

KLIWAS Schriftenreihe KLIWAS-27/2014

Comparison of three regional coupled ocean
atmosphere models for the North Sea under
today's and future climate conditions

Koblenz, im Juli 2014



BUNDESAMT FÜR
SEESCHIFFFAHRT
UND
HYDROGRAPHIE



Max-Planck-Institut
für Meteorologie



SMHI





Der Bericht darf nur ungekürzt vervielfältigt werden. Die Vervielfältigung und eine Veröffentlichung bedürfen der schriftlichen Genehmigung der BfG.

KLIWAS Schriftenreihe KLIWAS-27/2014

Comparison of three regional coupled ocean atmosphere models for the North Sea under today's and future climate conditions

Authors:

Katharina Bülow¹, Christian Dieterich², Alberto Elizalde³, Matthias Gröger², Hartmut Heinrich¹, Sabine Hüttl-Kabus¹, Birgit Klein¹, Bernhard Mayer⁴, H.E. Markus Meier², Uwe Mikolajewicz³, Nikesh Narayan¹, Thomas Pohlmann⁴, Gudrun Rosenhagen⁵, Semjon Schimanke², Dmitry Sein⁶, Jian Su⁴

(1) Federal Maritime and Hydrographic Agency (BSH), Hamburg, Germany, (2) Swedish Meteorological and Hydrological Institute (SMHI), Norköpping, Sweden, (3) Max Planck Institute for Meteorology, Hamburg, Germany, (4) Institute of Oceanography, University Hamburg, Hamburg, Germany, (5) German Meteorological Service (DWD), Marine Meteorological Monitoring Centre, Hamburg, Germany, (6) Alfred Wegener Institute (AWI), Bremerhaven, Germany

DOI:

10.5675/Kliwas_27/2014

Page

Chapter

Contents

09		LIST OF TABLES
09		LIST OF FIGURES
25	1	ABSTRACT
26	2	INTRODUCTION
28	3	DESCRIPTION OF MODELS AND DATASETS
28	3.1	REMO
29	3.2	MPI-OM
31	3.3	HAMSOM
31	3.4	REMO-HAMSOM
32	3.5	RCA4-NEMO-NORDIC
34	3.6	CLIMATOLOGIES
36	4	COMPARISON OF THE THREE COUPLED ATMOSPHERE OCEAN MODELS TO THE CLIMATOLOGIES
37	4.1	ANNUAL CYCLE OF THE MEAN SEA SURFACE AND BOTTOM TEMPERATURE
38	4.2	ANNUAL CYCLE OF THE MEAN SEA SURFACE AND BOTTOM SALINITY
39	4.3	SEASONAL AND ANNUAL MEANS OF TEMPERATURE AND SALINITY AT THE SEA SURFACE AND THE BOTTOM
42	4.4	VERTICAL DISTRIBUTION OF TEMPERATURE AND SALINITY ALONG TRANSECTS
42	4.4.1	TEMPERATURE AND SALINITY TRANSECTS ALONG 56 °N
43	4.4.2	TEMPERATURE AND SALINITY TRANSECTS ALONG 58 °N
45	5	ANALYSIS OF THE SCENARIO RUNS
45	5.1	REMO-MPIOM
45	5.1.1	TEMPERATURE
48	5.1.2	SALINITY
53	5.1.3	SEA SURFACE HEIGHT

Page

Chapter

Contents

54	5.2	REMO-HAMSOM
54	5.2.1	TEMPERATURE
57	5.2.2	SALINITY
60	5.2.3	SEA SURFACE HEIGHT
61	5.3	RCA4-NEMO-NORDIC
61	5.3.1	TEMPERATURE
63	5.3.2	SALINITY
65	5.3.3	SEA SURFACE HEIGHT
66	5.4	COMPARISON OF THE THREE MODELS
66	5.4.1	TEMPERATURE
71	5.4.2	SALINITY
77	5.4.3	SEA SURFACE HEIGHT
80	6	SUMMARY AND KEY ACHIEVEMENTS
84	7	DISCUSSION AND OUTLOOK
86	8	LIST OF ABBREVIATIONS AND ACRONYMS
88	9	REFERENCES
93	10	APPENDIX 1: FIGURES FROM THE VALIDATION ANALYSIS IN CHAPTER 4
151	11	APPENDIX 2: FIGURES FROM THE SRES A1B SIMULATIONS IN CHAPTER 5

Page

Table

List of Tables

28	1	COUPLED OCEAN ATMOSPHERE MODELS
78	5.4.1	ADDITIONAL COMPONENTS OF SEA LEVEL RISE NOT INCLUDED IN THE SIMULATIONS. SOURCE IPCC REPORT 2013

Page

Figure

List of Figures

30	3.2.1	THE GRID OF MPI-OM AND COUPLING AREAS WITH THE ATMOSPHERIC MODEL DOMAIN
30	3.2.2	SCHEME FOR THE COUPLING OF THE MODEL COMPONENTS
31	3.4.1	MODEL CONFIGURATION OF REMO-HAMSOM (COUPLED HINDCAST)
32	3.4.2	COUPLED DOMAINS OF REMO AND HAMSOM
33	3.5.1	THE COUPLED MODEL RCA4-NEMO-NORDIC SET-UP AND MODEL DOMAIN
36	4.1	NORTH SEA DOMAIN USED TO CALCULATE AVERAGE PROPERTIES AND LOCATION OF TRANSECTS
47	5.1.1	COMPARISON OF TEMPERATURE CHANGES IN MPIOM/REMO RUN 215 IN THE FAR FUTURE IN THE ATMOSPHERE AND IN THE OCEAN
50	5.1.2	FAR FUTURE CHANGES OF PRECIPITATION, EVAPORATION RATE AND THE NET SURFACE FRESH WATER FLUX BASED ON THE REFERENCE PERIOD 1961-1990
51	5.1.3	SUM OF RUNOFF FROM RIVERS DRAINING INTO THE NORTH SEA AND INTO THE BALTIC IN KM³/YEAR
52	5.1.4	MULTI-DECAL VARIABILITY OF SEA SURFACE SALINITY IN THE 20TH CENTURY
52	5.1.5	COMPARISON OF SEA SURFACE SALINITY TIME SERIES FROM THE NORTH SEA AND BALTIC

Page

Figure

List of Figures

56	5.2.1	COMPARISON OF TEMPERATURE CHANGES IN HAMSOM/REMO RUN 202 IN THE FAR FUTURE IN THE ATMOSPHERE AND IN THE OCEAN
59	5.2.2	FAR FUTURE CHANGES OF PRECIPITATION, EVAPORATION RATE AND THE NET SURFACE FRESH WATER FLUX BASED ON THE REFERENCE PERIOD 1970-1999
62	5.3.1	COMPARISON OF TEMPERATURE CHANGES IN NEMO-NORDIC/RCA4 RUN 470 IN THE FAR FUTURE IN THE ATMOSPHERE AND IN THE OCEAN
64	5.3.2	FAR FUTURE CHANGES OF PRECIPITATION, EVAPORATION RATE AND THE NET SURFACE FRESH WATER FLUX BASED ON THE REFERENCE PERIOD 1970-1999
75	5.4.1	SMOOTHED TIME SERIES (21 YEAR RUNNING MEAN APPLIED) OF AVERAGE SEA SURFACE SALINITY FROM THE THREE MODEL SIMULATIONS. AN OFFSET OF +0.4 HAS BEEN ADDED TO THE NEMO-NORDIC DATA TO ADJUST THE TOO LOW SALINITIES. ADDITIONALLY SALINITY TIME SERIES CHARACTERIZING THE ATLANTIC INFLOW HAVE BEEN INCLUDED. THESE HAVE BEEN SELECTED FROM SINGLE GRID POINT DATA FROM THE MPIOM RUN 215 AT THE SHELF EDGE
79	5.4.2	PROJECTED CHANGES OF ANNUAL MEAN SEA LEVELS AT THE TIDE GAUGE STATION IN CUXHAVEN FROM THE CLIMATE SIMULATION OF MPIOM, HAMSOM AND NEMO-NORDIC. THE OBSERVATIONAL TIME SERIES IS INCLUDED TO DENOTE THE EVOLUTION DURING THE 20TH CENTURY. IN ORDER TO MAKE THE TIME SERIES COMPARABLE, THE LAND MOVEMENT AT CUXHAVEN HAS BEEN CORRECTED AND THE MODELLED TIME SERIES HAVE BEEN ADJUSTED FOR THE GIA COMPONENT TAKEN FROM PELTIER'S (2004) ICE-5G MODEL

Appendix

Appendix 1:

- Figure 4.1.1A: The mean annual cycle of sea surface temperatures [°C] for MPIOM run 253, HAMSOM 201, NEMO-Nordic run 477, BSH observations and KNSC over the time period 1986-1999. The means are representing averages over the North Sea area. 93**
- Figure 4.1.2A: Difference of the mean annual cycle of sea surface temperatures between KNSC for the time period 1986-1999 and modelled data [°C]: MPIOM run 253, HAMSOM 201, NEMO-Nordic run 477, BSH observations. The means are representing averages over the North Sea area. 94**
- Figure 4.1.3A: The mean annual cycle of sea surface temperatures [°C] for NEMO-Nordic run 477, KNSC, BSH observations, BHC, NCEP and ERA40 over the time period 1971 till 2000. The means are representing averages over the North Sea area. 95**
- Figure 4.1.4A: Difference of the mean annual cycle of the sea surface temperatures between KNSC for the time period 1971-2000 and modelled data in [°C]: NEMO-Nordic run 477, BSH observations, BHC, NCEP, ERA40. The means are representing averages over the North Sea area. 96**
- Figure 4.1.5A: The mean annual cycle of bottom temperatures [°C]: MPIOM run 253 1986-1999, HAMSOM run 201 1986-1999, NEMO-Nordic run 477 1986-1999, NEMO-Nordic run 477 1971-2000, BHC 1971-2000. The means are representing averages over the North Sea area 97**
- Figure 4.1.6A: Difference of the mean annual cycle of the bottom temperatures between BHC 1971-2000 and modelled data [°C]: MPIOM run 253 1986-1999, HAMSOM run 201 1986-1999, NEMO run 477 1986-1999, NEMO-Nordic run 477 1971-2000. The means are representing averages over the North Sea area. 98**
- Figure 4.2.1A: The mean annual cycle of sea surface salinity [psu] for MPIOM run 253, HAMSOM 201, NEMO-Nordic run 477 and KNSC over the time period 1986-1999. The means are representing averages over the North Sea area. 99**
- Figure 4.2.2A: Difference of the mean annual cycle of sea surface salinity [psu] between KNSC for the time period 1986-1999 and modelled data: MPIOM run 253, HAMSOM 201, and NEMO-Nordic run 477. The means are representing averages over the North Sea area. 100**
- Figure 4.2.3A: The mean annual cycle of sea surface salinity [psu] for NEMO-Nordic run 477, KNSC, BHC over the time period 1971 till 2000. The means are representing averages over the North Sea area. 101**
- Figure 4.2.4A: Difference of the mean annual cycle of the sea surface salinity [psu] between KNSC for the time period 1971-2000 and modelled data: NEMO-Nordic run 477 and BHC. The means are representing averages over the North Sea area. 102**
- Figure 4.2.5A: The mean annual cycle of bottom salinity [psu] for MPIOM run 253 1986-1999, HAMSOM 1986-1999, NEMO-Nordic run 477 1986-1999, NEMO-Nordic run 477 1971-2000, and BHC. The means are representing averages over the North Sea area. 103**
- Figure 4.2.6A: Difference of the mean annual cycle of the sea surface salinity [psu] between BHC for the time period 1971-2000 and modelled data: MPIOM run 253 1986-1999, HAMSOM 1986-**

1999, NEMO-Nordic run 477 1986-1999, NEMO-Nordic run 477 1971-2000. The means are representing averages over the North Sea area.	104
Figure 4.3.1A: Seasonal and annual means of sea surface temperature [°C] from BHC and KNSC for the period 1971-2000 and their differences (lower row).	105
Figure 4.3.2A: Seasonal and annual means of sea surface salinity [psu] from BHC and KNSC for the period 1971-2000 and their differences (lower row).	106
Figure 4.3.3A: Seasonal and annual means of sea surface temperature [°C] averaged over the period 1986-1999: MPIOM (run 253), HAMSOM (run 201) and NEMO-Nordic (run 477).	107
Figure 4.3.4A: Differences of modelled seasonal and annual means of sea surface temperature [°C] averaged over the period 1986-1999 to the KNSC: MPIOM (run 253), HAMSOM (run 201) and NEMO-Nordic (run 477).	108
Figure 4.3.5A: Differences of modelled seasonal and annual means of sea surface temperature [°C] averaged over the period 1986-1999 to the BHC (1971-2000): MPIOM (run 253), HAMSOM (run 201) and NEMO-Nordic (run 477).	109
Figure 4.3.6A: Seasonal and annual means of sea surface salinity [psu] averaged over the period 1986-1999. The mean sea surface salinity results from MPIOM (run 253), from HAMSOM (run 201) and from NEMO-Nordic (run 477).	110
Figure 4.3.7A: Differences of modelled seasonal and annual means of sea surface salinity [psu] averaged over the period 1986-1999 to the KNSC: MPIOM (run 253), HAMSOM (run 201) and NEMO-Nordic (run 477).	111
Figure 4.3.8A: Differences of modelled seasonal and annual means of sea surface salinity [psu] (1986-1999) to the BHC (1971-2000): MPIOM (run 253), HAMSOM (run 201) and from NEMO-Nordic (run 477).	112
Figure 4.3.9A: Seasonal and annual means of sea surface temperature [°C] averaged over the period 1986-1999. Mean sea surface temperature results from MPIOM (run 253), from the KNSC and difference between model results and KNSC.	113
Figure 4.3.10A: Seasonal and annual means of sea surface temperature [°C]. Mean sea surface temperature results from MPIOM (run 253) averaged over the period 1986-1999, mean surface temperature from the BHC averaged over the period 1971-2000 and the difference between model results and climatology.	114
Figure 4.3.11A: Seasonal and annual means of sea surface temperature [°C] averaged over the period 1986-1999: HAMSOM (run 201), KNSC and difference between the model results and climatology.	115
Figure 4.3.12A: Seasonal and annual means of sea surface temperature [°C]. Mean sea surface temperature results from HAMSOM (run 201) averaged over the period 1986-1999, mean surface temperature from the BHC averaged over the period 1971-2000 and difference between the model results and climatology.	116
Figure 4.3.13A: Seasonal and annual means of sea surface temperature [°C] averaged over the period 1986-1999: NEMO-Nordic (run 477), KNSC, and difference between the model results and climatology.	117
Figure 4.3.14A: Seasonal and annual means of sea surface temperature [°C] averaged over the period 1971-2000: NEMO-Nordic (run 477), BHC, and difference between the model results and climatology.	118

Figure 4.3.15A: Seasonal and annual means of sea surface salinity [psu] averaged over the period 1986-1999: MPIOM (run 253), KNSC, and difference between the model results and climatology.	119
Figure 4.3.16A: Seasonal and annual means of sea surface salinity [psu]: MPIOM (run 253) averaged over the period 1986-1999, BHC averaged over the period 1971-2000, and difference between the model results and climatology.	120
Figure 4.3.17A: Seasonal and annual means of sea surface salinity [psu] averaged over the period 1986-1999: HAMSOM (run 201), KNSC, and difference between the model results and climatology.	121
Figure 4.3.18A: Seasonal and annual means of sea surface salinity [psu]: HAMSOM (run 201) averaged over the period 1986-1999, BHC averaged over the period 1971-2000 and difference between the model results and climatology.	122
Figure 4.3.19A: Seasonal and annual means of sea surface salinity [psu] averaged over the period 1986-1999: NEMO-Nordic (run 477), KNSC, and difference between the model results and climatology.	123
Figure 4.3.20A: Seasonal and annual means of sea surface salinity [psu] averaged over the period 1971-2000: NEMO-Nordic (run 477), BHC, difference between the model results and climatology.	124
Figure 4.3.21A: Seasonal and annual means of bottom temperature [°C] averaged over the period 1986-1999: MPIOM (run 253), HAMSOM (run 201), and NEMO-Nordic (run 477) over the time period 1970-1999.	125
Figure 4.3.22A: Differences of modelled seasonal and annual means of bottom temperature [°C] averaged over the period 1986-1999 to the BHC (1971-2000): MPIOM (run 253), HAMSOM (run 201), and NEMO-Nordic (run 477) over the time period 1970-1999.	126
Figure 4.3.23A: Seasonal and annual means of bottom salinity [psu] averaged over the period 1986-1999: MPIOM (run 253), HAMSOM (run 201), and NEMO-Nordic (run 477) over the time period 1970-1999.	127
Figure 4.3.24A: Differences of modelled seasonal and annual means of bottom salinity [psu] averaged over the period 1986-1999 to the BHC (1971-2000): MPIOM (run 253), HAMSOM (run 201), and NEMO-Nordic (run 477) over the time period 1970-1999.	128
Figure 4.3.25A: Seasonal and annual means of bottom temperature [°C]: MPIOM (run 253) averaged over the period 1986-1999, BHC averaged over the period 1971-2000, and difference between the model results and climatology.	129
Figure 4.3.26A: Seasonal and annual means of bottom temperature [°C]: HAMSOM (run 201) averaged over the period 1986-1999, BHC averaged over the period 1971-2000, and difference between the model results and climatology.	130
Figure 4.3.27A: Seasonal and annual means of bottom temperature [°C] averaged over the period 1971-2000: NEMO-Nordic (run 477), BHC, and difference between the model results and climatology.	131
Figure 4.3.28A: Seasonal and annual means of bottom salinity [psu]: MPIOM (run 253) averaged over the period 1986-1999, BHC averaged over the period 1971-2000, and difference between the model results and the climatology.	132

Figure 4.3.29A: Seasonal and annual means of bottom salinity [psu]: HAMSOM (run 201) averaged over the period 1986-1999, BHC averaged over the period 1971-2000, and difference between the model results and the climatology. 133

Figure 4.3.30A: Seasonal and annual means of bottom salinity [psu] averaged over the period 1971-2000: NEMO-Nordic (run 477), BHC, and difference between the model results and the climatology. 134

Figure 4.4.1A: The mean February temperature [°C] from the KNSC for the time period 1986-1999 is presented for transect along 56 °N left and along 58 °N (right). Bottom: The mean February salinity [psu] from the KNSC for the time period 1986-1999 is presented for transect along 56 °N (left) and along 58 °N (right). Figure 4.4.3 will present transect along 58 °N to a depth of 400 m. 135

Figure 4.4.2A: The mean August temperature [°C] from the KNSC for the time period 1986-1999 is presented for transect along 56 °N left and along 58 °N (right). Bottom: The mean August salinity [psu] from the KNSC for the time period 1986-1999 is presented for transect along 56 °N (left) and along 58 °N (right). 136

Figure 4.4.3A: The mean February temperature [°C] from the KNSC for the time period 1986-1999 is presented for transect along 56 °N left and along 58 °N depth to 400 m (right). Bottom: The mean February salinity [psu] from the KNSC for the time period 1986-1999 is presented for transect along 56 °N (left) and along 58 °N depth to 400 m (right). 137

Figure 4.4.4A: The mean August temperature [°C] from the KNSC for the time period 1986-1999 is presented for transect along 56 °N left and along 58 °N depth to 400 m (right). Bottom: The mean August salinity [psu] from the KNSC for the time period 1986-1999 is presented for transect along 56 °N (left) and along 58 °N depth to 400 m (right). 138

Figure 4.4.5A: The mean February temperature [°C] for the time period 1986-1999 is presented for transect along 56 °N. Mean simulated temperature by MPIOM, HAMSOM and NEMO-Nordic is presented on the left hand side and on the right hand side the difference between each model result and the temperature from the KNSC. 139

Figure 4.4.6A: The mean February salinity [psu] for the time period 1986-1999 is presented for transect along 56 °N. Mean simulated salinity by MPIOM, HAMSOM and NEMO-Nordic is presented on the left hand side and on the right hand side the difference between each model result and the temperature from the KNSC. 140

Figure 4.4.7A: The mean August temperature [°C] for the time period 1986-1999 is presented for transect along 56 °N. Mean simulated temperature by MPIOM, HAMSOM and NEMO-Nordic is presented on the left hand side and on the right hand side the difference between each model result and the temperature from the KNSC. 141

Figure 4.4.8A: The mean August salinity [psu] for the time period 1986-1999 is presented for transect along 56 °N. Mean simulated salinity by MPIOM, HAMSOM and NEMO-Nordic is presented on the left hand side and on the right hand side the difference between each model result and the temperature from the KNSC. 142

Figure 4.4.9A: The mean February temperature [°C] for the time period 1986-1999 is presented for transect along 58 °N. Mean simulated temperature by MPIOM, HAMSOM and NEMO-Nordic is presented on the left hand side and on the right hand side the difference between each model result and the temperature from the KNSC. Figure 4.4.13 will present transect along 58 °N to a depth of 400 m. 143

Figure 4.4.10A: The mean February salinity [psu] for the time period 1986-1999 is presented for transect along 58 °N. Mean simulated salinity by MPIOM, HAMSOM and NEMO-Nordic is presented on the left hand side and on the right hand side the difference between each model result and the temperature from the KNSC. 144

Figure 4.4.11A: The mean August temperature [°C] for the time period 1986-1999 is presented for transect along 58 °N. Mean simulated temperature by MPIOM, HAMSOM and NEMO-Nordic is presented on the left hand side and on the right hand side the difference between each model result and the temperature from the KNSC. 145

Figure 4.4.12A: The mean August salinity [psu] for the time period 1986-1999 is presented for transect along 58 °N. Mean simulated salinity by MPIOM, HAMSOM and NEMO-Nordic is presented on the left hand side and on the right hand side the difference between each model result and the temperature from the KNSC. 146

Figure 4.4.13A: The mean February temperature [°C] for the time period 1986-1999 is presented for transect along 58 °N. Mean simulated temperature by MPIOM, HAMSOM and NEMO-Nordic is presented on the left hand side and on the right hand side the difference between each model result and the temperature from the KNSC. 147

Figure 4.4.14A: The mean February salinity [psu] for the time period 1986-1999 is presented for transect along 58 °N. Mean simulated salinity by MPIOM, HAMSOM and NEMO-Nordic is presented on the left hand side and on the right hand side the difference between each model result and the temperature from the KNSC. 148

Figure 4.4.15A: The mean August temperature [°C] for the time period 1986-1999 is presented for transect along 58 °N. Mean simulated temperature by MPIOM, HAMSOM and NEMO-Nordic is presented on the left hand side and on the right hand side the difference between each model result and the temperature from the KNSC. 149

Figure 4.4.16A: The mean August salinity [psu] for the time period 1986-1999 is presented for transect along 58 °N. Mean simulated salinity by MPIOM, HAMSOM and NEMO-Nordic is presented on the left hand side and on the right hand side the difference between each model result and the temperature from the KNSC. 150

Appendix 2:

Figure 5.1.1A: Seasonal and annual means of sea surface temperature [°C] for MPIOM run 215 (A1B scenario run). The upper row shows averages for the period 1970-1999, the middle row for 2021-2050 and the lower row for 2070-2099. 152

Figure 5.1.2A: Comparison of seasonal and annual means of sea surface temperature [°C] for MPIOM run 215 for the base period 1970-1999 with climatological means from the BHC. The upper row shows average model distributions, the middle row observed climatological means and the lower row the differences between the two data sets. 153

Figure 5.1.3A: Comparison of seasonal and annual means of sea surface temperature [°C] for MPIOM run 215 for the base period 1970-1999 with climatological means from the KNSC. The upper row shows average model distributions, the middle row observed climatological means and the lower row the differences between the two data sets. 154

Figure 5.1.4A: Seasonal and annual means of bottom temperature [°C] for MPIOM run 215 (A1B scenario run). The upper row shows averages for the period 1970-1999, the middle row for 2021-2050 and the lower row for 2070-2099. 155

Figure 5.1.5A: Comparison of seasonal and annual means of bottom temperature [°C] for MPIOM run 215 for the base period 1970-1999 with BHC means. The upper row shows average

model distributions, the middle row observed climatological means and the lower row the differences between the two data sets.	156
Figure 5.1.6A: Comparison of seasonal and annual means of bottom temperature [°C] for MPI-OM run 215 for the base period 1970-1999 with KNSC means. The upper row shows average model distributions, the middle row observed climatological means and the lower row the differences between the two data sets.	157
Figure 5.1.7A: Changes in seasonal and annual sea surface temperature [°C] for MPIOM run 215 (A1B scenario run). Upper panel from (1970-1999) to (2021-2050) and lower panel from (1970-1999) to (2070-2099).	158
Figure 5.1.8A: Changes in seasonal and annual bottom temperature [°C] for MPIOM run 215 (A1B scenario run). Upper panel from (1970-1999) to (2021-2050) and lower panel from (1970-1999) to (2070-2099).	159
Figure 5.1.9A: Time series of seasonal and annual means of sea surface temperature [°C] for MPIOM run 215 (A1B scenario run) from 1920-2099. The temperatures represent averages over the North Sea area given in Figure 4.1.	160
Figure 5.1.10A: The mean annual cycle of sea surface temperatures [°C] for MPIOM run 215 (A1B scenario run) for 1970-1999, 2021-2050 and 2070-2099. The means are representing averages over the North Sea area given in Figure 4.1. The error bars are indicating time variability.	161
Figure 5.1.11A: Time series of seasonal and annual means of bottom temperature [°C] for MPI-OM run 215 (A1B scenario run) from 1920-2099. The temperatures represent averages over the North Sea area given in Figure 4.1.	162
Figure 5.1.12A: The mean annual cycle of bottom temperatures [°C] for MPIOM run 215 (A1B scenario run) 1970-1999, 2021-2050 and 2070-2099. The means are representing averages over the North Sea area given in Figure 4.1. The error bars are indicating time variability.	163
Figure 5.1.13A: Seasonal and annual means of sea surface salinity [psu] for MPIOM run 215 (A1B scenario run). The upper row shows averages for the period 1970-1999, the middle row for 2021-2050 and the lower row for 2070-2099.	164
Figure 5.1.14A: Comparison of seasonal and annual means of sea surface salinity [psu] for MPI-OM run 215 for the base period 1970-1999 with BHC means. The upper row shows average model distributions, the middle row observed climatological means and the lower row the differences between the two data sets.	165
Figure 5.1.15A: Comparison of seasonal and annual means of sea surface salinity [psu] for MPI-OM run 215 for the base period 1970-1999 with KNSC means. The upper row shows average model distributions, the middle row observed climatological means and the lower row the differences between the two data sets.	166
Figure 5.1.16A: Seasonal and annual means of bottom salinity [psu] for MPIOM run 215 (A1B scenario run). The upper row shows averages for the period 1970-1999, the middle row for 2021-2050 and the lower row for 2070-2099.	167
Figure 5.1.17A: Comparison of seasonal and annual means of bottom salinity [psu] for MPIOM run 215 for the base period 1970-1999 with climatological BHC means. The upper row shows averages model distributions, the middle row observed climatological means and the lower row the differences between the two data sets.	168

- Figure 5.1.18A:** Comparison of seasonal and annual means of bottom salinity [psu] for MPIOM run 215 for the base period 1970-1999 with KNSC means. The upper row shows average model distributions, the middle row observed climatological means and the lower row the differences between the two data sets. 169
- Figure 5.1.19A:** Changes in seasonal and annual sea surface salinity [psu] for MPIOM run 215 (A1B scenario run). Upper panel from (1970-1999) to (2021-2050) and lower panel from (1970-1999) to (2070-2099). 170
- Figure 5.1.20A:** Changes in seasonal and annual bottom salinity [psu] for MPIOM run 215 (A1B scenario). Upper panel from (1970-1999) to (2021-2050) and lower panel from (1970-1999) to (2070-2099). The contour interval is 0.5 °C. 171
- Figure 5.1.21A:** Time series of seasonal and annual means of sea surface salinity [psu] for MPIOM run 215 (A1B scenario run) from 1920-2099. The salinities represent averages over the North Sea area given in Figure 4.1. 172
- Figure 5.1.22A:** The mean annual cycle of sea surface salinity [psu] for MPIOM run 215 (A1B scenario run) for 1970-1999 (blue), 2021-2050 (green) and 2070-2099 (red). The means are representing averages over the North Sea area given in Figure 4.1. The error bars are indicating time variability. 173
- Figure 5.1.23A:** Time series of seasonal and annual means of bottom salinity [psu] for MPIOM run 215 (A1B scenario run) from 1920-2099. The salinities represent averages over the North Sea area given in Figure 4.1. 174
- Figure 5.1.24A:** The mean annual cycle of bottom salinity [psu] for MPIOM run 215 (A1B scenario run) for 1970-1999 (blue), 2021-2050 (green) and 2070-2099 (red). The means are representing averages over the North Sea area given in Figure 4.1. The error bars are indicating time variability. 175
- Figure 5.1.25A:** Seasonal and annual means of sea surface height [m] for MPIOM run 215 (A1B scenario run). The upper row shows averages for the period 1970-1999, the middle row for 2021-2050 and the lower row for 2070-2099. 176
- Figure 5.1.26A:** Changes in seasonal and annual sea surface height [m] for MPIOM run 215 (A1B scenario run). Upper panel from (1970-1999) to (2021-2050) and in lower panel from (1970-1999) to (2070-2099). 177
- Figure 5.1.27A:** Time series of seasonal and annual means of sea surface height [m] for MPIOM run 215 (A1B scenario run) from 1920-2099. The sea surface heights represent averages over the North Sea area given in Figure 4.1. 178
- Figure 5.1.28A:** The mean annual cycle of sea surface height [m] for MPIOM run 215 (A1B scenario run) 1970-1999 (blue), 2021-2050 (green) and 2070-2099 (red). The means are representing averages over the North Sea area given in Figure 4.1. The error bars are indicating time variability. 179
- Figure 5.2.1A:** Seasonal and annual means of sea surface temperature [°C] for HAMSOM run 202 (A1B scenario run). The upper row shows averages for the period 1970-1999, the middle row for 2021-2050 and the lower row for 2070-2099. 180
- Figure 5.2.2A:** Comparison of seasonal and annual means of sea surface temperature [°C] for HAMSOM run 202 for the base period 1970-1999 with BHC means. The upper row shows average model distributions, the middle row observed climatological means and the lower row the differences between the two data sets. 181

Figure 5.2.3A: Comparison of seasonal and annual means of sea surface temperature [°C] for HAMSOM run 202 for the base period 1970-1999 with KNCS means. The upper row shows average model distributions, the middle row observed climatological means and the lower row the differences between the two data sets. 182

Figure 5.2.4A: Seasonal and annual means of bottom temperature [°C] for HAMSOM run 202 (A1B scenario run). The upper row shows averages for the period 1970-1999, the middle row for 2021-2050 and the lower row for 2070-2099. 183

Figure 5.2.5A: Comparison of seasonal and annual means of bottom temperature [°C] for HAMSOM run 202 for the base period 1970-1999 with BHC means. The upper row shows average model distributions, the middle row observed climatological means and the lower row the differences between the two data sets. 184

Figure 5.2.6A: Comparison of seasonal and annual means of bottom temperature [°C] for HAMSOM run 202 for the base period 1970-1999 with KNCS means. The upper row shows average model distributions, the middle row observed climatological means and the lower row the differences between the two data sets. 185

Figure 5.2.7A: Changes in seasonal and annual sea surface temperature [°C] for HAMSOM run 202 (A1B scenario run). Upper panel from (1970-1999) to (2021-2050) and lower panel from (1970-1999) to (2070-2099). 186

Figure 5.2.8A: Changes in seasonal and annual bottom temperature [°C] for HAMSOM run 202 (A1B scenario run). Upper panel from (1970-1999) to (2021-2050) and lower panel from (1970-1999) to (2070-2099). The contour interval is 0.5 °C. 187

Figure 5.2.9A: Time series of seasonal and annual means of sea surface temperature [°C] for HAMSOM run 202 (A1B scenario run) from 1950-2099. The temperatures represent averages over the North Sea area given in Figure 4.1. 188

Figure 5.2.10A: The mean annual cycle of sea surface temperatures [°C] for HAMSOM run 202 (A1B scenario run) for 1970-1999 (blue), 2021-2050 (green) and 2070-2099 (red). The means are representing averages over the North Sea area given in Figure 4.1. The error bars are indicating time variability. 189

Figure 5.2.11A: Time series of seasonal and annual means of bottom temperature [°C] for HAMSOM run 202 (A1B scenario run) from 1950-2099. The temperatures represent averages over the North Sea area given in Figure 4.1. 190

Figure 5.2.12A: The mean annual cycle of bottom temperatures [°C] for HAMSOM run 202 (A1B scenario run) for 1970-1999 (blue), 2021-2050 (green) and 2070-2099 (red). The means are representing averages over the North Sea area given in Figure 4.1. The error bars are indicating time variability. 191

Figure 5.2.13A: Seasonal and annual means of sea surface salinity [psu] for HAMSOM run 202 (A1B scenario run). The upper row shows averages for the period 1970-1999, the middle row for 2021-2050 and the lower row for 2070-2099. 192

Figure 5.2.14A: Comparison of seasonal and annual means of sea surface salinity [psu] for HAMSOM run 202 for the base period 1970-1999 with BHC means. The upper row shows average model distributions, the middle row observed climatological means and the lower row the differences between the two data sets. 193

Figure 5.2.15A: Comparison of seasonal and annual means of sea surface salinity [psu] for HAMSOM run 202 for the base period 1970-1999 with KNCS means. The upper row shows av-

erage model distributions, the middle row observed climatological means and the lower row the differences between the two data sets. 194

Figure 5.2.16A: Seasonal and annual means of bottom salinity [psu] for HAMSOM run 202 (A1B scenario run). The upper row shows averages for the period 1970-1999, the middle row for 2021-2050 and the lower row for 2070-2099. 195

Figure 5.2.17A: Comparison of seasonal and annual means of bottom salinity [psu] for HAMSOM run 202 for the base period 1970-1999 with BHC means. The upper row shows average model distributions, the middle row observed climatological means and the lower row the differences between the two data sets. 196

Figure 5.2.18A: Comparison of seasonal and annual means of bottom salinity [psu] for HAMSOM run 202 for the base period 1970-1999 with KNSC means. The upper row shows average model distributions, the middle row observed climatological means and the lower row the differences between the two data sets. 197

Figure 5.2.19A: Changes in seasonal and annual sea surface salinity [psu] for HAMSOM run 202 (A1B scenario run). Upper panel from (1970-1999) to (2021-2050) and lower panel from (1970-1999) to (2070-2099). 198

Figure 5.2.20A: Changes in seasonal and annual bottom salinity [psu] for HAMSOM run 202 (A1B scenario run). Upper panel from (1970-1999) to (2021-2050) and lower panel from (1970-1999) to (2070-2099). The contour interval is 0.5 °C. 199

Figure 5.2.21A: Time series of seasonal and annual means of sea surface salinity [psu] for HAMSOM run 202 (A1B scenario run) from 1950-2099. The salinities represent averages over the North Sea area given in Figure 4.1. 200

Figure 5.2.22A: The mean annual cycle of sea surface salinity [psu] for HAMSOM run 202 (A1B scenario run) for 1970-1999, 2021-2050 and 2070-2099. The means are representing averages over the North Sea area given in Figure 4.1. The error bars are indicating time variability. 201

Figure 5.2.23A: Time series of seasonal and annual means of bottom salinity [psu] for HAMSOM run 202 (A1B scenario run) from 1950-2099. The salinities represent averages over the North Sea area given in Figure 4.1. 202

Figure 5.2.24A: The mean annual cycle of bottom salinity [psu] for HAMSOM run 202 (A1B scenario run) for 1970-1999, 2021-2050 and 2070-2099. The means are representing averages over the North Sea area given in Figure 4.1. The error bars are indicating time variability. 203

Figure 5.2.25A: Seasonal and annual means of sea surface height [m] for HAMSOM run 202 (A1B scenario run). The upper row shows averages for the period 1970-1999, the middle row for 2021-2050 and the lower row for 2070-2099. 204

Figure 5.2.26A: Changes in seasonal and annual sea surface height [m] for HAMSOM run 202 (A1B scenario run). Upper panel from (1970-1999) to (2021-2050) and lower panel from (1970-1999) to (2070-2099). 205

Figure 5.2.27A: Time series of seasonal and annual means of sea surface height [m] for HAMSOM run 202 (A1B scenario run) from 1950-2099. The sea surface heights represent averages over the North Sea area given in Figure 4.1. 206

Figure 5.2.28A: The mean annual cycle of sea surface height [m] for HAMSOM run 202 (A1B scenario run) 1970-1999 (blue), 2021-2050 (green) and 2070-2099 (red). The means are represent-

	ing averages over the North Sea area given in Figure 4.1. The error bars are indicating time variability.	207
	Figure 5.3.1A: Seasonal and annual means of sea surface temperature [°C] for NEMO-Nordic run 470 (A1B scenario run). The upper row shows averages for the period 1970-1999, the middle row for 2021-2050 and the lower row for 2070-2099.	208
	Figure 5.3.2A: Comparison of seasonal and annual means of sea surface temperature [°C] for NEMO-Nordic run 470 for the base period 1970-1999 with BHC means. The upper row shows average model distributions, the middle row observed climatological means and the lower row the differences between the two data sets.	209
	Figure 5.3.3A: Comparison of seasonal and annual means of sea surface temperature [°C] for NEMO-Nordic run 470 for the base period 1970-1999 with KNSC means. The upper row shows average model distributions, the middle row observed climatological means and the lower row the differences between the two data sets.	210
	Figure 5.3.4A: Seasonal and annual means of bottom temperature [°C] for NEMO-Nordic run 470 (A1B scenario run). The upper row shows averages for the period 1970-1999, the middle row for 2021-2050 and the lower row for 2070-2099.	211
	Figure 5.3.5A: Comparison of seasonal and annual means of bottom temperature [°C] for NEMO-Nordic run 470 for the base period 1970-1999 with BHC means. The upper row shows average model distributions, the middle row observed climatological means and the lower row the differences between the two data sets.	212
	Figure 5.3.6A: Comparison of seasonal and annual means of bottom temperature [°C] for NEMO-Nordic run 470 for the base period 1970-1999 with KNSC means. The upper row shows average model distributions, the middle row observed climatological means and the lower row the differences between the two data sets.	213
	Figure 5.3.7A: Changes in seasonal and annual sea surface temperature [°C] for NEMO-Nordic run 470 (A1B scenario run). Upper panel from (1970-1999) to (2021-2050) and lower panel from (1970-1999) to (2070-2099).	214
	Figure 5.3.8A: Changes in seasonal and annual bottom temperature [°C] for NEMO-Nordic run 470 (A1B scenario run). Upper panel from (1970-1999) to (2021-2050) and lower panel from (1970-1999) to (2070-2099). The contour interval is 0.5 °C.	215
	Figure 5.3.9A: Time series of seasonal and annual means of sea surface temperature [°C] for NEMO-Nordic run 470 (A1B scenario run) from 1970-2099. The temperatures represent averages over the North Sea area given in Figure 4.1.	216
	Figure 5.3.10A: The mean annual cycle of sea surface temperatures [°C] for NEMO-Nordic run 470 (A1B scenario run) for 1970-1999 (blue), 2021-2050 (green) and 2070-2099 (red). The means are representing averages over the North Sea area given in Figure 4.1.	217
	Figure 5.3.11A: Time series of seasonal and annual means of bottom temperature [°C] for NEMO-Nordic run 470 (A1B scenario run) from 1970-2099. The temperatures represent averages over the North Sea area given in Figure 4.1.	218
	Figure 5.3.12A: The mean annual cycle of bottom temperatures [°C] for NEMO-Nordic run 470 (A1B scenario run) for 1970-1999, 2021-2050 and 2070-2099. The means are representing averages over the North Sea area given in Figure 4.1.	219

Figure 5.3.13A: Seasonal and annual means of sea surface salinity [psu] for NEMO-Nordic run 470 (A1B scenario run). The upper row shows averages for the period 1970-1999, the middle row for 2021-2050 and the lower row for 2070-2099. 220

Figure 5.3.14A: Comparison of seasonal and annual means of sea surface salinity [psu] for NEMO-Nordic run 470 for the base period 1970-1999 with BHC means. The upper row shows average model distributions, the middle row observed climatological means and the lower row the differences between the two data sets. 221

Figure 5.3.15A: Comparison of seasonal and annual means of sea surface salinity [psu] for NEMO-Nordic run 470 for the base period 1970-1999 with KNSC means. The upper row shows average model distributions, the middle row observed climatological means and the lower row the differences between the two data sets. 222

Figure 5.3.16A: Seasonal and annual means of bottom salinity [psu] for NEMO-Nordic run 470 (A1B scenario run). The upper row shows averages for the period 1970-1999, the middle row for 2021-2050 and the lower row for 2070-2099. 223

Figure 5.3.17A: Comparison of seasonal and annual means of bottom salinity [psu] for NEMO-Nordic run 470 for the base period 1970-1999 with BHC means. The upper row shows average model distributions, the middle row observed climatological means and the lower row the differences between the two data sets. 224

Figure 5.3.18A: Comparison of seasonal and annual means of bottom salinity [psu] for NEMO-Nordic run 470 for the base period 1970-1999 with KNSC means. The upper row shows average model distributions, the middle row observed climatological means and the lower row the differences between the two data sets. 225

Figure 5.3.19A: Changes in seasonal and annual sea surface salinity [psu] for NEMO-Nordic run 470 (A1B scenario run). Upper panel from (1970-1999) to (2021-2050) and lower panel from (1970-1999) to (2070-2099). 226

Figure 5.3.20A: Changes in seasonal and annual bottom salinity [psu] for NEMO-Nordic run 470 (A1B scenario run). Upper panel from (1970-1999) to (2021-2050) and lower panel from (1970-1999) to (2070-2099). 227

Figure 5.3.21A: Time series of seasonal and annual means of sea surface salinity [psu] for NEMO-Nordic run 470 (A1B scenario run) from 1970-2099. The salinities represent averages over the North Sea area given in Figure 4.1. 228

Figure 5.3.22A: The mean annual cycle of sea surface salinity [psu] for NEMO-Nordic run 470 (A1B scenario run) for 1970-1999, 2021-2050 and 2070-2099. The means are representing averages over the North Sea area given in Figure 4.1. 229

Figure 5.3.23A: Time series of seasonal and annual means of bottom salinity [psu] for NEMO-Nordic run 470 (A1B scenario run) from 1970-2099. The salinities represent averages over the North Sea area given in Figure 4.1. 230

Figure 5.3.24A: The mean annual cycle of bottom salinity [psu] for NEMO-Nordic run 470 (A1B scenario run) for 1970-1999, 2021-2050 and 2070-2099. The means are representing averages over the North Sea area given in Figure 4.1. 231

Figure 5.3.25A: Seasonal and annual means of sea surface height [m] for NEMO-Nordic run 470 (A1B scenario run). The upper row shows averages for the period 1970-1999, the middle row for 2021-2050 and the lower row for 2070-2099. 232

Figure 5.3.26A: Changes in seasonal and annual sea surface height [m] for NEMO-Nordic run 470 (A1B scenario run). Upper panel from (1970-1999) to (2021-2050) and lower panel from (1970-1999) to (2070-2099).	233
Figure 5.3.27A: Time series of seasonal and annual means of sea surface height [m] for NEMO-Nordic run 470 (A1B scenario run) from 1970-2099. The sea surface heights represent averages over the North Sea area given in Figure 4.1.	234
Figure 5.3.28A: The mean annual cycle of sea surface height [m] for NEMO-Nordic run 470 (A1B scenario run) for 1970-1999, 2021-2050 and 2070-2099. The means are representing averages over the North Sea area given in Figure 4.1.	235
Figure 5.4.1A: Seasonal and annual means of sea surface temperature [°C] for the period 1970-1999. Upper row MPIOM run 215, middle row HAMSOM run 202 and lower row NEMO-Nordic run 470 (all A1B scenario).	236
Figure 5.4.2A: Seasonal and annual means of sea surface temperature [°C] for the period 2021-2050. Upper row MPIOM run 215, middle row HAMSOM run 202 and lower row NEMO-Nordic run 470 (all A1B scenario).	237
Figure 5.4.3A: Seasonal and annual means of sea surface temperature [°C] for the period 2070-2050. Upper row MPIOM run 215, middle row HAMSOM run 202 and lower row NEMO-Nordic run 470 (all A1B scenario).	238
Figure 5.4.4A: Seasonal and annual means of bottom temperature [°C] for the period 1970-1999. Upper row MPIOM run 215, middle row HAMSOM run 202 and lower row NEMO-Nordic run 470 (all A1B scenario).	239
Figure 5.4.5A: Seasonal and annual means of bottom temperature [°C] for the period 2021-2050. Upper row MPIOM run 215, middle row HAMSOM run 202 and lower row NEMO-Nordic run 470 (all A1B scenario).	240
Figure 5.4.6A: Seasonal and annual means of bottom temperature [°C] for the period 2070-2050. Upper row MPIOM run 215, middle row HAMSOM run 202 and lower row NEMO-Nordic run 470 (all A1B scenario).	241
Figure 5.4.7A: Changes in seasonal and annual means of sea surface temperature [°C] from (1970-1999) to (2021-2050). Upper row MPIOM run 215, middle row HAMSOM run 202 and lower row NEMO-Nordic run 470 (all A1B scenario).	242
Figure 5.4.8A: Changes in seasonal and annual means of sea surface temperature [°C] from (1970-1999) to (2070-2099). Upper row MPIOM run 215, middle row HAMSOM run 202 and lower row NEMO-Nordic run 470 (all A1B scenario).	243
Figure 5.4.9A: Changes in seasonal and annual means of bottom temperature [°C] from (1970-1999) to (2021-2050). Upper row MPIOM run 215, middle row HAMSOM run 202 and lower row NEMO-Nordic run 470 (all A1B scenario).	244
Figure 5.4.10A: Changes in seasonal and annual means of bottom temperature [°C] from (1970-1999) to (2070-2099). Upper row MPIOM run 215, middle row HAMSOM run 202 and lower row NEMO-Nordic run 470 (all A1B scenario).	245
Figure 5.4.11A: Time series of seasonal and annual means of sea surface temperature [°C] for MPIOM run 215, HAMSOM run 202 and NEMO-Nordic run 470. The temperatures represent averages over the North Sea area given in Figure 4.1.	246
Figure 5.4.12A: left: mean annual cycle of sea surface temperatures [°C] for 1970-1990 for MPIOM run 215, HAMSOM run 202 and NEMO-Nordic run 470. Right: differences in mean annual	

cycle to the averaging period 1970-1999, 2021-2050 as dotted line and 2070-2099 as dashed line. The means are representing averages over the North Sea area given in Figure 4.1.	247
Figure 5.4.13A: Time series of seasonal and annual means of bottom temperature [°C] for MPIOM run 215, HAMSOM run 202 and NEMO-Nordic run 470. The temperatures represent averages over the North Sea area given in Figure 4.1.	248
Figure 5.4.14A: left: mean annual cycle of bottom temperatures [°C] for 1970-1990 for MPIOM run 215, HAMSOM run 202 and NEMO-Nordic run 470. Right: differences in mean annual cycle to the averaging period 1970-1999, 2021-2050 as dotted line and 2070-2099 as dashed line. The means are representing averages over the North Sea area given in Figure 4.1.	249
Figure 5.4.15A: Seasonal and annual means of sea surface salinity [psu] for the period 1970-1999. Upper row MPIOM run 215, middle row HAMSOM run 202 and lower row NEMO-Nordic run 470 (all A1B scenario).	250
Figure 5.4.16A: Seasonal and annual means of sea surface salinity [psu] for the period 2021-2050. Upper row MPIOM run 215, middle row HAMSOM run 202 and lower row NEMO-Nordic run 470 (all A1B scenario).	251
Figure 5.4.17A: Seasonal and annual means of sea surface salinity [psu] for the period 2070-2050. Upper row MPIOM run 215, middle row HAMSOM run 202 and lower row NEMO-Nordic run 470 (all A1B scenario).	252
Figure 5.4.18A: Seasonal and annual means of bottom salinity [psu] for the period 1970-1999. Upper row MPIOM run 215, middle row HAMSOM run 202 and lower row NEMO-Nordic run 470 (all A1B scenario).	253
Figure 5.4.19A: Seasonal and annual means of bottom salinity [psu] for the period 2021-2050. Upper row MPIOM run 215, middle row HAMSOM run 202 and lower row NEMO-Nordic run 470 (A1B scenario).	254
Figure 5.4.20A: Seasonal and annual means of bottom salinity [psu] for the period 2070-2090. Upper row MPIOM run 215, middle row HAMSOM run 202 and lower row NEMO-Nordic run 470 (all A1B scenario).	255
Figure 5.4.21A: Changes in seasonal and annual means of sea surface salinity [psu] from (1970-1999) to (2021-2050). Upper row MPIOM run 215, middle row HAMSOM run 202 and lower row NEMO-Nordic run 470 (all A1B scenario).	256
Figure 5.4.22A: Changes in seasonal and annual means of sea surface salinity [psu] from (1970-1999) to (2070-2099). Upper row MPIOM run 215, middle row HAMSOM run 202 and lower row NEMO-Nordic run 470 (all A1B scenario).	257
Figure 5.4.23A: Changes in seasonal and annual means of bottom salinity [psu] from (1970-1999) to (2021-2050). Upper row MPIOM run 215, middle row HAMSOM run 202 and lower row NEMO-Nordic run 470 (all A1B scenario).	258
Figure 5.4.24A: Changes in seasonal and annual means of bottom salinity [psu] from (1970-1999) to (2070-2099). Upper row MPIOM run 215, middle row HAMSOM run 202 and lower row NEMO-Nordic run 470 (all A1B scenario).	259
Figure 5.4.25A: Time series of seasonal and annual means of sea surface salinity [psu] for MPIOM run 215, HAMSOM run 202 and NEMO-Nordic run 470. The salinities represent averages over the North Sea area given in Figure 4.1.	260
Figure 5.4.26A: left: mean annual cycle of sea surface salinity [psu] for 1970-1990 for MPIOM run 215, HAMSOM run 202 and NEMO-Nordic run 470. Right: differences in mean annual	

cycle to the averaging period 1970-1999, 2021-2050 as dotted line and 2070-2099 as dashed line. The means are representing averages over the North Sea area given in Figure 4.1. 261

Figure 5.4.27A: Time series of seasonal and annual means of bottom salinity [psu] for MPIOM run 215, HAMSOM run 202 and NEMO-Nordic run 470. The salinities represent averages over the North Sea area given in Figure 4.1. 262

Figure 5.4.28A: left: mean annual cycle of bottom salinity [psu] for 1970-1990 for MPIOM run 215, HAMSOM run 202 and NEMO-Nordic run 470. Right: differences in mean annual cycle to the averaging period 1970-1999, 2021-2050 as dotted line and 2070-2099 as dashed line. The means are representing averages over the North Sea area given in Figure 4.1. 263

Figure 5.4.29A: Seasonal and annual means of sea surface height [m] for the period 1970-1999. Upper row MPIOM run 215, middle row HAMSOM run 202 and lower row NEMO-Nordic run 470 (all A1B scenario). 264

Figure 5.4.30A: Seasonal and annual means of sea surface height [m] for the period 2021-2050. Upper row MPIOM run 215, middle row HAMSOM run 202 and lower row NEMO-Nordic run 470 (all A1B scenario). 265

Figure 5.4.31A: Seasonal and annual means of sea surface height [m] for the period 2070-2099. Upper row MPIOM run 215, middle row HAMSOM run 202 and lower row NEMO-Nordic run 470 (all A1B scenario). 266

Figure 5.4.32A: Changes in seasonal and annual means of sea surface height [m] from (1970-1999) to (2021-2050). Upper row MPIOM run 215, middle row HAMSOM run 202 and lower row NEMO-Nordic run 470 (all A1B scenario). 267

Figure 5.4.33A: Changes in seasonal and annual means of sea surface height [m] from (1970-1999) to (2070-2099). Upper row MPIOM run 215, middle row HAMSOM run 202 and lower row NEMO-Nordic run 470 (all A1B scenario). 268

Figure 5.4.34A: Time series of seasonal and annual means of sea surface height [m] for MPIOM run 215, HAMSOM run 202 and NEMO-Nordic run 470. The sea surface heights represent averages over the North Sea area given in Figure 4.1. 269

Figure 5.4.35A: left: mean annual cycle of sea surface height [m] for 1970-1990 for MPIOM run 215, HAMSOM run 202 and NEMO-Nordic run 470. Right: differences in mean annual cycle to the averaging period 1970-1999, 2021-2050 as dotted line and 2070-2099 as dashed line. The means are representing averages over the North Sea area given in Figure 4.1. 270

1 Abstract

Coupled Ocean
Atmosphere
Models

BSH
DWD
IfM Hamburg
MPI Hamburg
SMHI
AWI

The Federal Ministry of Transport, Building and Urban Development (BMVBS) had launched the research program KLIWAS in 2009 to obtain an expert view on the potential impacts of climate change for the German inland waterways and coastal waters. For the North Sea area it was important to obtain estimates on the potential changes of physical parameters such as temperature, salinity and sea level which could be used as boundary conditions in the impact models of the adjacent estuaries.

For this purpose three fully coupled ocean atmosphere models were constructed for the North Sea region, that have performed simulations for today's climate and for the SRES Scenario A1B. All three coupled models are able to successfully simulate the main hydrological and circulation features in the North Sea with comparable patterns. Yearly and seasonal means of the sea surface and bottom temperature and salinity have been compared to observations to validate the models hindcast runs. Although the validation was a success, this exercise has highlighted some discrepancies in the individual models. But the scenario simulations have shown that these are not strongly influenced by the climate change signal and spatial patterns remain the same throughout the simulations. The climate change signal is described for the near future (2021-2050) and the far future (2070-2099), by comparing the seasonal and annual mean sea surface and bottom temperatures as well as salinity and sea surface height to the control period (1970-1999). Robust trends have been detected in all three models for the parameters temperature and sea surface height which predicts increasing values for the end of the 21st century. Trends in salinity were influenced by assumptions on terrestrial discharge and the formulation of boundary conditions. Since the signal to noise ratio in this parameter is low due to large internal variability no robust signal could be determined although all models predicted decreasing salinities.

2 Introduction

The latest IPCC assessment report (IPCC 5TH ASSESSMENT REPORT, 2013), like the preceding 4th report, has given clear evidence on the human influence on the climate system. The evidence is based on observations of increasing greenhouse gas concentrations in the atmosphere, positive radiative forcing, observed warming in the ocean, and increased understanding of the climate system. While much progress has been achieved for the climate system as a whole, many questions remain when assessing the extent to which not just global mean but also spatial patterns of change will develop across the globe. Natural internal variability constitutes a major influence on the climate at the regional scale and particularly in the near-term. This represents a major difficulty in the detection and attribution of climate change signals at the regional scale. But in the context of vulnerability, resilience of coastal societies and sustainable development, regional and local changes are the most relevant. Regional sea level change for example, one of the key indicators of anthropogenic global warming, has far-reaching consequences for coastal societies.

Local climate information can in principle be obtained directly from global models. Their horizontal resolution is often too coarse to resolve features that are important on the regional scale. Therefore, dynamical downscaling is applied and the regional coupled atmosphere-ocean models complement globally coupled models (AOGCMs) by generating region-specific climate information.

In the present study we present climate projections for the North Sea from a set of three different models: a global model with variable resolution (so-called ‘stretched grid’) with higher resolution over the North European Shelf and two regional climate models (RCMs) which are applied over a limited-area domain and receive their boundary conditions the global climate model output.

For the first time three different climate simulations for the North Sea have been performed using fully coupled atmosphere ocean high resolution models, which imply a free exchange of momentum, heat freshwater fluxes between the models at the air-sea interface.

Two different tasks are carried out in this report. First we assess the quality and the uncertainty of the models in calculating present-day climate conditions based on simulations driven with reanalysis data (NCEP or ERA40). These are compared to observations in order to define the model uncertainty range for present-day climate conditions. Secondly, we analyse the climate projections of the three models to determine the range and robustness of the climate signal for selected variables. It is important to keep in mind, that these results for the scenario runs are only three possible future

developments for one single emission scenario. The report will start in chapter 3 with a short description of the model components and the datasets used for the validation, which is described in chapter 4. The results of the climate change simulations for the SRES scenario A1B are presented in chapter 5. The majority of figures for chapters 4 and 5 are presented in Annex 1 and Annex 2. This report ends with a summary, key achievements and an outlook.

Coupled Ocean
Atmosphere
Models

BSH
DWD
IfM Hamburg
MPI Hamburg
SMHI
AWI

This work has been carried out in the KLIWAS Project 1.03 and 2.01.

3 Description of models and datasets

The results of three different coupled atmosphere ocean modelling experiments are analysed. The coupled models are the global ocean model MPI-OM coupled to the regional climate model REMO and the regional North Sea model HAMSOM coupled to REMO as well as the results of the regional ocean model NEMO-Nordic coupled to the regional climate model RCA4. Key information about each model systems and its components will be given in the following chapter and are also summarized in Table 1.

Institute Atmosphere model Ocean model	Resolution	Hydrological Model	Boundary forcing:	
			Today's climate	A1B Scenario
MPI-Met Hamburg RCM: REMO MPI-OM	REMO: horizontal: 37 km MPI-OM: horizontal: 5-13 km vertical: 27 levels	HD Model is coupled to REMO and MPI-OM	REMO: NCEP MPI-OM: n.a.	REMO: ECHAM5_r3 MPI-OM: n.a.
IfM Hamburg RCM: REMO HAMSOM	REMO: horizontal: 37 km HAMSOM: horizontal: 3 km vertical: 30 levels	Runoff is prescribed from observations	REMO: NCEP HAMSOM: MPI-OM	REMO: ECHAM5_r3 HAMSOM: MPI-OM
SMHI, Norrköping RCM: RCA4 NEMO-Nordic	RCA4: Horizontal: 20 km NEMO-Nordic: horizontal 3,7 km vertical: 56 levels	Runoff is prescribed from the E-HYPE ERA-interim run	RCA4: ERA40 NEMO-Nordic: monthly climatology	RCA4: ECHAM5_r3 NEMO-Nordic: MPI-OM

Table 1: Coupled ocean atmosphere models

3.1 REMO

The regional climate model REMO (JACOB AND PODZUN, 1997, JACOB, 2001) is a three-dimensional, hydrostatic atmospheric circulation model which solves the discretized primitive equations of atmospheric motion. It is based on the 'Europa-Modell'

of the German Weather service (MAJEWSKI ET AL., 1995) and the physical parameterizations are taken from the global climate model ECHAM-4 (ROECKNER ET AL., 1996). REMO is a hydrostatic model and can be used for a horizontal resolution up to 10 km. For horizontal discretization REMO uses a spherical Arakawa-C grid in which all variables, except the wind components, are defined in the centre of the respective grid box. The grid box centres are defined on a rotated latitude-longitude coordinate system. In the vertical, variations of the prognostic variables (except surface pressure) are represented by a hybrid vertical coordinate system and 31 vertical levels are used for this experiment. As a ‘Limited Area Model’, REMO needs lateral boundary forcing data like temperature, wind, surface pressure and moisture and surface boundary conditions such as the temporally variable sea surface temperature and sea ice extent. The temporal evolution of the surface boundary conditions over sea are taken from the MPI-OM run. The lateral boundary conditions can be prepared using reanalysis data (here NCEP, KALNAY ET AL., 1996) for validation simulations or from global climate models (here ECHAM) for climate simulation scenarios.

3.2 MPI-OM

The Max-Planck-Institute Ocean Model (MPI-OM, formerly C-HOPE, MAIER-REIMER, 1997; MARSLAND ET AL., 2003) is a primitive equation model (z-level, with Boussinesq and incompressibility assumptions) formulated on an orthogonal curvilinear Arakawa C-grid. The model includes a dynamic-thermodynamic sea ice model with viscous-plastic rheology (HIBLER, 1979). It has a free surface and uses a mass flux boundary condition for salinity. A simple bottom boundary layer scheme is included as well as the standard set of sub-grid scale parameterizations (e.g. isopycnal diffusion, Richardson number dependent vertical diffusivities, a simple mixed layer scheme including the effect of wind mixing at the surface, and eddy induced tracer transport according to GENT ET AL. (1995). A full tidal potential was included in the simulations.

The blue line in the Fig. 3.2.1 depicts the domain finally chosen to perform the regionally coupled simulations of REMO-MPI-OM. The atmospheric grid size is 181x181 grid boxes with 27 vertical levels with a horizontal resolution of 0.33×0.33 degrees. The ocean domain is global with a bipolar projection. The grid is represented by the grey lines in the Fig. 3.2.1. The poles are located in Central Europe and North America. The domain resolution is variable from approximately 300 km at the geographical South Pole up to 5 – 13 km in the North Sea.

The model time step for the atmosphere model is 150 seconds and 600 seconds for the ocean model. The model coupling has been run using the concurrent mode. The coupling time step is 2 hours.

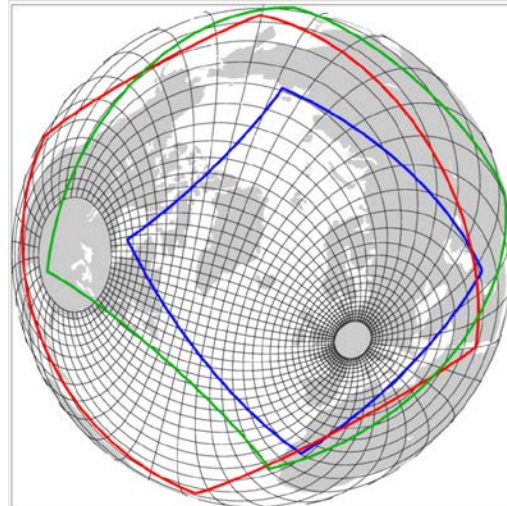


Figure 3.2.1: The grid of MPI-OM and coupling areas with the atmospheric model domain. The blue line indicates the coupling area of REMO-MPI-OM in the present setup.

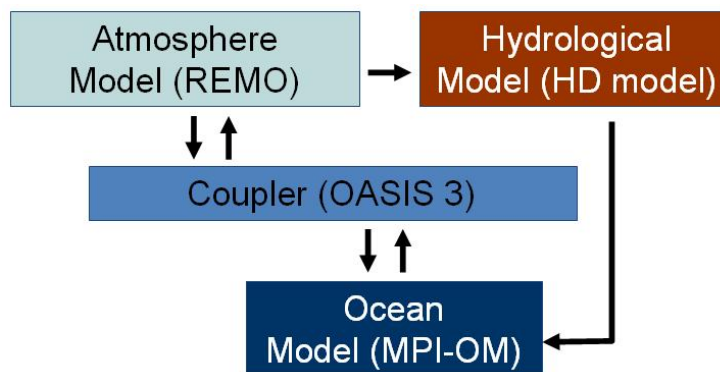


Figure 3.2.2: Scheme for the coupling of the model components.

The coupling between the REMO atmosphere model and the MPI-OM ocean model (Fig. 3.2.2) was carried out using the OASIS coupler developed by CERFACS (VALCKE, 2012). OASIS is used for the exchange of variables and for synchronization of the coupling times only. A conservative bilinear interpolation routine is integrated in the MPI-OM model to interpolate fields between REMO and MPI-OM model grids. The hydrological model HD model (HAGEMANN AND DÜMENIL, 1998, HAGEMANN AND DÜMENIL, 1999, HAGEMANN AND JACOB, 2007) makes its own interpolation for REMO fields. REMO calculates heat, freshwater and momentum fluxes for each grid box and receives in turn SST, sea ice thickness and compactness from the ocean model. The atmosphere-ocean coupling frequency is set to 2 hours and the calculation of the river routing is performed every 24 hours (ELIZALDE ET AL.; 2010, SEIN ET AL. 2012). A similar configuration without the river routing has been used for

Indonesian rainfall (ALDRIAN ET AL., 2005) and Arctic sea ice studies (MIKOLAJEWICZ, 2005).

Coupled Ocean
Atmosphere
Models

BSH
DWD
IfM Hamburg
MPI Hamburg
SMHI
AWI

3.3 HAMSOM

HAMSOM is a high-resolution 3-D baroclinic, free surface, primitive equation equation model. The use of relatively long time steps is possible in HAMSOM, since terms limiting the time-step are treated implicitly (BACKHAUS, 1985). This advantage enables HAMSOM to perform long-term simulations, and is thus suitable for climate studies. HAMSOM has been intensively validated in the North Sea (POHLMANN, 1996, 2006). The horizontal resolution of HAMSOM is ~3 km; it has 30 vertical levels and includes tidal constituents. In the coupled experiment only the M2 tides are included, because they are the major component. The open boundaries (northern boundary, English Channel, Baltic Outflow) are provided by the data of MPI-OM (chapter 3.2). Boundary conditions have to be applied only under outflow conditions, details are described by CHEN ET AL. (2013).

3.4 REMO-HAMSOM

The regional coupling system includes the regional ocean model HAMSOM, the regional climate model REMO and the coupler OASIS3 (Fig. 3.4.1). The coupled system REMO-HAMSOM (SCHRUM, 2001; SCHRUM ET AL., 2003) is modified to a high resolution regional atmosphere-ocean model via heat flux coupling. In this coupled model system the atmospheric part REMO is identical to the atmospheric part in the coupled model REMO-MPI-OM, therefore details about REMO can be found in Chapter 3.1.

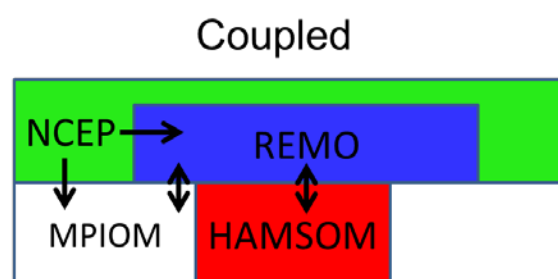


Figure 3.4.1: Model configuration of REMO-HAMSOM (coupled hindcast)

The global ocean model MPI-OM provides the boundary conditions for the regional ocean model HAMSOM. HAMSOM is initialised with the data from world ocean atlas (BOYER ET AL, 2005). The atmospheric model REMO uses NCEP reanalysis data as boundary forcing but the SST outside the North Sea is provided by the global ocean model MPI-OM (Fig. 3.4.2) (chapter 3.2).

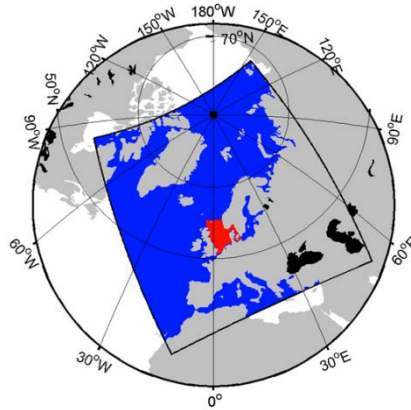


Figure 3.4.2: Coupled domains of REMO and HAMSOM. The blue colour refers to the domain of REMO, while the red colour refers to the domain of HAMSOM.

In the scenario run the lateral boundaries for REMO are provided by the IPCC SRES A1B scenario run ECHAM5_r3. The coupler is OASIS3 (VALCKE, 2012) and the coupling time step is 3 hours. At each coupling time step, REMO provides heat fluxes, turbulent fluxes (wind stress) and water fluxes to HAMSOM. HAMSOM in return exchanges SST to REMO.

3.5 RCA4-NEMO-Nordic

RCA4-NEMO-Nordic is a regional, coupled climate model at the SMHI (DIETERICH ET AL., 2013). It consists of the atmosphere model RCA4 in a model domain covering the East Atlantic and Europe (KUPIAINEN ET AL., 2013) and the NEMO setup for the North Sea and Baltic Sea (HORDOIR ET AL., 2013). RCA4-NEMO-Nordic is a fully coupled atmosphere-ice-ocean model (Fig. 3.5.1), where the different components are coupled every 3 hours using the OASIS3 coupler (VALCKE, 2012). The coupler exchanges the surface temperatures of open water and sea ice together with the ice fraction and ice albedo to the atmosphere model. From the atmosphere the ocean-ice model receives the momentum fluxes and pressure at the surface, the shortwave and non-solar heat fluxes and the freshwater fluxes due to the evaporation - precipitation. The river discharge is prescribed based on the E-HYPE ERA-interim run (LINDSTRÖM ET AL., 2010). During the period 1961 to 1979 a monthly climatology is applied based on the 30-year period 1979 to 2008. During the period 1979 to 2000 daily output of the E-HYPE ERA-interim run is applied. For the period 2001 to 2099 the monthly climatology with a 10% runoff increase in the Bothnian Sea and Bothnian Bay is prescribed.

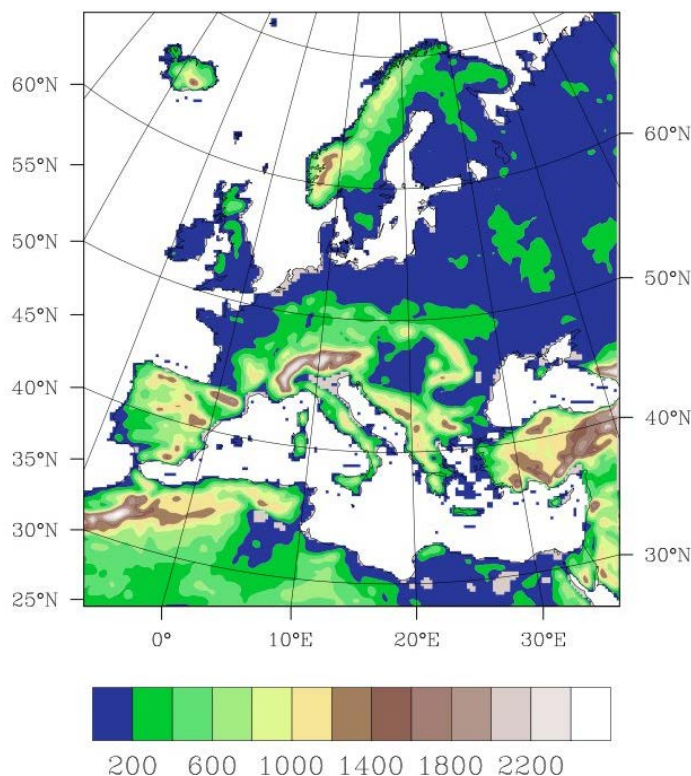
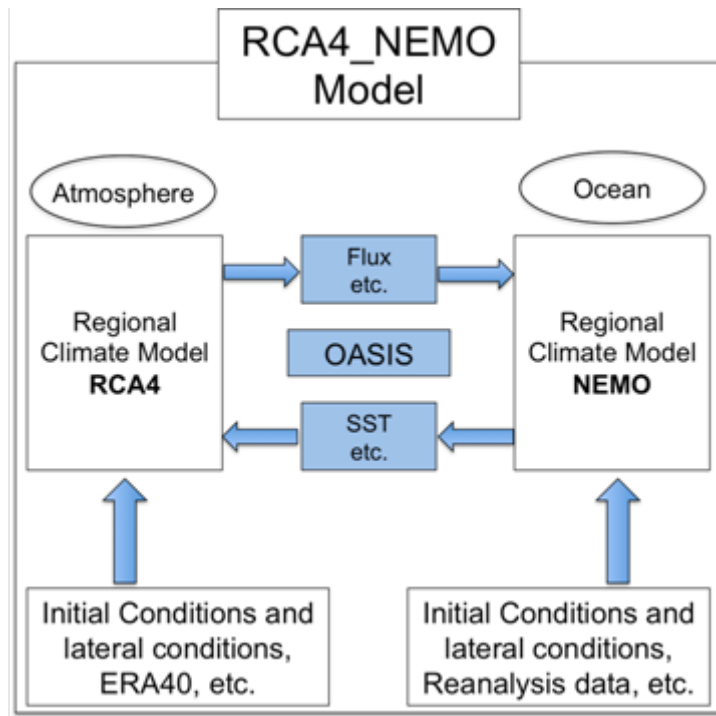


Figure 3.5.1: Top: The coupled model RCA4-NEMO-Nordic (DIETERICH ET AL., 2013). Bottom: Model domain.

To simulate today's climate, RCA4 uses ERA40 reanalysis as boundary forcing (UPPALA ET AL., 2005) and NEMO-Nordic uses monthly means of temperature and salinity from the World Ocean Atlas (LEVITUS AND BOYER, 1994). The 11 tidal constituents are taken from the data of the Oregon State University global tidal model (EG-

BERT AND EROFEEVA, 2002). For the initialisation of NEMO-Nordic, temperature and salinity are based on the Janssen climatology (JANSSEN ET AL., 1999). The barotropic transport across the open boundaries is prescribed using climatological monthly mean sea surface heights extracted from the REMO_MPIOM run for the 50-year historical period. The scenario run starts in 1961. The atmosphere is started from rest, the ice from ice free conditions and the ocean from an interpolated state of the RCO-reanalysis by LIU ET AL. (2013). RCA4 itself uses boundary conditions from ECHAM5_r3.

3.6 Climatologies

The coupled hindcast simulations of the coupled models are compared to two different regional climatologies for the North Sea area.

One of these data sets is the climatology from BERX AND HUGHES (2009), hereafter abbreviated as BHC. It consists of a 30-year (1971-2000) estimate of mean conditions and the annual cycle for surface and near-bed temperature and salinity of the NW European shelf seas, with a resolution of $1/6^\circ$ longitude and $1/10^\circ$ latitude.

Secondly, the KLIWAS North Sea Climatology, hereafter abbreviated as KNSC, for hydrographic and atmospheric parameters is used for comparison. This is the first version (1.0) of a hydrographic climatology for the region 47°N to 65°N , 15°W to 15°E (BERSCH ET AL., 2013). It contains monthly and yearly mean temperature and salinity data at 179 depth levels on a 0.25° latitude and 0.5° longitude grid for the period 1890 to 2011.

Both climatologies provide information at adequate resolution to resolve oceanographic features at the Northwest European shelf. The BHC offers more than twice the resolution than the KNSC, but only at two selected levels. One of the major improvements of the BHC compared to other existing climatologies such as JANSSEN ET AL. (1999) is the focus on the more recent climatological time period 1971-2000. The KNSC on the other hand is a flexible tool that allows the user to build climatologies for a selected time period based on the available monthly means for each of the grid cells. In our analysis here we have built climatologies for the periods 1970-1999 and 1986-1999.

The observational data from which the gridded climatologies are created are unevenly distributed in time and space. THE BHC follows the methodology described by JANSSEN ET AL. (1999) to grid the data. A smoothing was necessary to reduce the noise caused by the uneven spatial and temporal distribution of input data and a smoothing radius of 85 km was selected. In the case of the KNSC a mean annual and monthly cycle was removed from the data for each grid cell prior to averaging. Because the grid cells in this analysis are much larger than those used in the BHC the

averages were built on larger samples and only a weak smoothing was applied to reduce the noise (STAMMER ET AL., 2014).

Because of the different methodologies used in the construction of the climatological data sets and their different spatial resolution we chose to use both data sets for the comparisons to the model simulations to give additional support to the analysis. The climatologies have been compared to each other and to observations to determine their uncertainty.

Coupled Ocean
Atmosphere
Models

BSH
DWD
IfM Hamburg
MPI Hamburg
SMHI
AWI

4 Comparison of the three coupled atmosphere ocean models to the climatologies

The three coupled simulations are validated for today's climate of the North Sea. The hydrodynamic conditions of the North Sea simulated by the global ocean model MPIOM coupled to the regional climate model REMO (in the following text abbreviated as MPIOM), the regional shelf model HAMSOM coupled to REMO (abbreviated as HAMSOM) and the regional ocean model NEMO-Nordic coupled to the regional climate model RCA4 (abbreviated as NEMO-Nordic) are compared to the KNSC from the Integrated Climate Data Centre (ICDC) and the BHC. All three model simulations are available for the overlapping time period 1986 till 1999. The KNSC offers temperature and salinity for different depth and on a monthly temporal resolution. Therefore it is most suited as a consistent reference for the validation. The KNSC will also be compared to other observations and the BHC to gain an impression of its uncertainty. Details about the climatologies and the models are presented in Chapter 3. Time series of average quantities will be presented based on the averaging area displayed in Fig. 4.1.

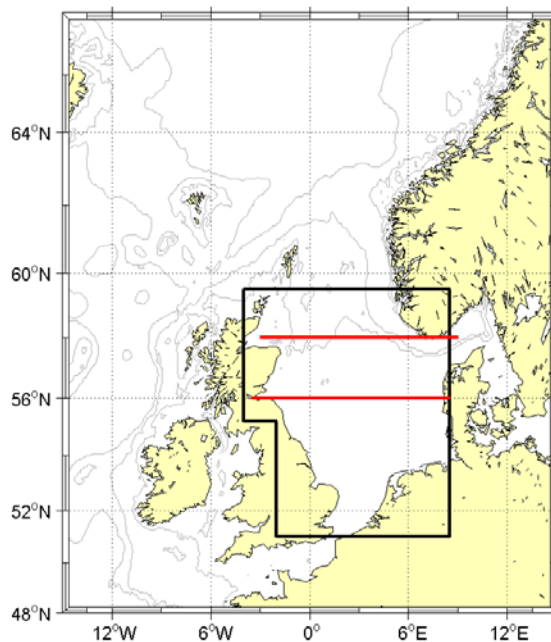


Figure 4.1: North Sea domain used to calculate average properties and location of transects.

4.1 Annual cycle of the mean sea surface and bottom temperature

The mean annual cycle of the sea surface temperature averaged over of the North Sea (Fig. 4.1) simulated by the three coupled models compares reasonably well to the KNSC for the time period 1986-1999 (Fig. 4.1.1A¹). Additionally, the mean sea surface temperatures from another SST data set collected by BSH (LOEWE ET AL., 2013) is included in the comparison. The annual cycle of the sea surface temperature is an important property governing biological processes in the North Sea. Amplitude and timing of the annual cycle are set by the atmospheric forcing and the vertical exchange of water masses, e.g. the mixed layer development.

The annual cycle from the KNSC is subtracted from the annual cycle of the model results and the observed SST to emphasize the deviations in the annual cycle (Fig. 4.1.2A). MPIOM mainly underestimates the mean sea surface temperature except for the months October till December. In summer (May till August) the underestimation of the sea surface temperature is most pronounced at about -1 °C. HAMSOM underestimates the mean sea surface temperature during the whole year with values ranging between -0.5 °C to maximum values of -1.2 °C in August. NEMO-Nordic on the other hand overestimates the sea surface temperature from April till December by +0.2 °C to +0.6 °C in July and shows underestimation only from January to March with -0.4 °C to -0.2 °C. The observed sea surface temperature from the BSH deviates by ±0.2 °C from the KNSC.

The sea surface temperature in the North Sea is strongly influenced by the temperature of the atmospheric model coupled to the ocean model. The atmospheric models of the coupled systems use different reanalysis data as boundary forcing. REMO uses NCEP reanalysis data as boundary forcing and RCA4 uses ERA40 reanalysis data. Therefore, the annual cycle of SST from NCEP and ERA40 is included in the comparison (Fig. 4.1.3A). To complete the analysis of uncertainties in the reference data the BHC is included in the comparison. This required an averaging period of 1971-2000 for all data sets because the Berx and Hughes data are only available as climatological means.

The difference between the reanalysis data NCEP, ERA40, BSH observations and the BHC to the KNSC (Fig. 4.1.4A) is very small ±0.2 °C and cannot explain the differences between the modelled annual cycles. Some differences are noted however, the BHC is much warmer in December than the other observational data sets, the BSH observations are warmer in summer than the rest of the data sets and ERA40 is the only data set which is warmer than the KNSC from January till March (Fig. 4.1.4A).

The difference between the modelled annual cycle of SST from NEMO-Nordic and the KNSC is twice as high as the maximum deviation between the observational data sets (Fig. 4.1.4A). The differences of the annual cycle of MPIOM and HAMSOM to

¹ All figure numbers ending with an „A“ are shown in the corresponding Appendix!

the KNSC are even higher than the maximum deviation of the NEMO-Nordic (Fig. 4.1.2A).

The mean annual cycle of the bottom temperatures averaged over the North Sea area (Fig. 4.1.5A) show a smaller amplitude than the sea surface temperatures. The minimum of the BHC is in March (6 °C) and its maximum is in September (11 °C). The sea surface temperature and the bottom temperature average over the whole North Sea area are very similar during the winter season from November till April.

The annual cycle of the bottom temperature from the BHC is subtracted from the model results (Fig. 4.1.6A). The differences between the models to the climatology are similar in all three models. In April and May all model results show colder bottom temperatures than the climatology. MPIOM and HAMSOM show higher differences than NEMO-Nordic and underestimate the bottom temperatures by more than 0.5 °C respectively 1.0 °C in April. In late summer, July till October all models show 0.5 °C warmer bottom temperature than the BHC.

The difference between the annual cycle of the NEMO-Nordic results for two time periods 1986-1999 and 1971-2000 is less than 0.1 °C. The bottom temperatures are similar for the two time periods 1971-2000 and 1986-1999, therefore the BHC can also be compared to MPIOM and HAMSOM for which only data for the later period are available.

4.2 Annual cycle of the mean sea surface and bottom salinity

The mean annual cycle of the sea surface salinity averaged over of the North Sea simulated by the three coupled models is compared to the KNSC for the time period 1986-1999 (Fig. 4.2.1A). The observed mean North Sea salinity shows a weak annual cycle with amplitude in the order of 0.2 psu with its maximum in winter and a minimum in summer, but also with noticeable month to month variations. MPIOM overestimates salinities throughout most of the year while HAMSOM is quite close to the climatology except for the summer months when overestimations occur. NEMO-Nordic on the other hand underestimates the sea surface salinity throughout the whole year and shows exaggerated annual amplitude. The maximum underestimation in NEMO-Nordic is from May to September around -0.3 to -0.4 psu (Fig. 4.2.2A).

The mean annual cycle of the sea surface salinity averaged over the North Sea from the BHC is compared to the KNSC for the time period 1971-2000 (Fig. 4.2.3A) to assess the uncertainty in the observational data. The sea surface salinity of the BHC is about 0.1 till 0.2 psu higher than the sea surface salinity of the KNSC and shows a slight shift in the annual cycle (Fig. 4.2.4A).

The mean annual cycle of the bottom salinity averaged over the North Sea from the BHC is compared to the results of the three models (Fig. 4.2.5A). The mean North Sea bottom salinity shows a small annual cycle with amplitude in the order of 0.1 psu

with its maximum in winter and a minimum in summer. The difference between the annual cycle of the bottom salinity of the model results and the annual cycle of the BHC is between 0.05 and -0.25 psu (Fig. 4.2.6A).

4.3 Seasonal and annual means of temperature and salinity at the sea surface and the bottom

The horizontal distribution of sea surface temperature and salinity from the three coupled models will be compared to the KNSC and BHC. The annual mean difference and the differences for winter (December till February), spring (March till May), summer (June till August) and autumn (September till November) will be displayed.

Each of the two climatologies has its own advantages. The KNSC is available for the same years as the model results from 1986-1999, but it is not available homogeneous for the whole North Sea, while the climatology of Berx and Hughes is available for the whole North Sea for the surface and for the bottom layer but only as an average over the time period 1971-2000.

The mean sea surface temperature in the BHC for the period 1971-2000 is characterized by a gradient from the northwest (North Atlantic) to the southeast (German and Dutch coast), with decreasing values from 8 °C in the northwest to 5 °C in the southeast in the winter and increasing values in the summer from 11 °C in the northwest to 16 °C in the southeast (Fig. 4.3.1A). The advection of heat with the inflow of Atlantic Water through the English Channel is clearly visible in all seasons except summer. The differences between the sea surface temperatures of the two climatologies are small (less than ± 0.5 °C). The largest differences between the two data sets are noted along the Norwegian coast in summer where the BHC is by at least 1 °C colder than the KNSC.

The sea surface salinity fields are dominated by the strong contrast between the low salinity waters along the eastern coast and high salinity waters in the north and south (Fig. 4.3.2A). Along the Dutch, German and Danish coasts fresh water discharge from the rivers reduce the salinity. The Skagerrak is influenced by the fresh Baltic Sea outflow which continues northward along the Norwegian Coast in the Norwegian Coastal Current. Seasonal changes in sea surface salinity are comparatively small, especially in the western part of the North Sea. Along the east coast of the North Sea the fresh water discharge from the rivers reaches a maximum extent in summer and in the North the area affected by the Baltic Sea outflow also increases. The salinity differences between the two climatologies are less than ± 0.5 psu for large parts of the North Sea. Areas which are influenced by fresh water discharge from the rivers in the south or by the Baltic Sea outflow at the mouth of the Skagerrak differ substantially between the climatologies (± 1 psu or more).

The horizontal distributions of the sea surface temperature from the three coupled models (Fig. 4.3.3) are compared to the two climatologies (Fig. 4.3.4A and 4.3.5A).

The differences between the model results and the climatologies show distinct horizontal pattern and differ between the coastal regions and the central North Sea.

In winter the annual cycle averaged over the whole North Sea area showed an underestimation of the sea surface temperature (Fig. 4.1.2A) in all models, but all models show 1°C higher sea surface temperatures along the Norwegian coast than the BHC (Fig. 4.3.5A, be aware that no KNSC data is available for this region). MPIOM and NEMO-Nordic show more than 0.5 °C higher sea surface temperatures in the English Channel and adjacent region than both climatologies (Fig. 4.3.4A, and 4.3.5A). HAMSOM has its boundary in the Channel at 51 °N. MPIOM overestimates the sea surface temperature in the German Bight by 1 °C in winter (compared to the BHC). Very close to the Dutch, German and Danish coast HAMSOM is 1 °C colder in winter and 2°C warmer in summer. In spring MPIOM and HAMSOM underestimate the sea surface temperature in the southern German Bight by more than 1 °C compared to the KNSC and by more than 2 °C compared to the BHC. In summer MPIOM and HAMSOM show 1-2 °C less warming of the SST in the central North Sea. NEMO-Nordic is 1°C warmer than the climatologies in most areas except of the Scottish coastal waters. In autumn MPIOM and NEMO-Nordic show at least 1 °C higher sea surface temperatures in the English Channel and along the eastern coast.

The horizontal difference for the sea surface salinity between the model results and the climatologies are presented in Fig. 4.3.7A and 4.3.8A. The highest positive differences between the model results and the climatologies occur in summer along the Norwegian Coast. In the MPIOM simulation the plume of the Baltic outflow in the North Sea is simulated as a narrow boundary current close to the Norwegian coast (Fig. 4.3.6A). The width of the jet is too narrow compared to the observations (Fig. 4.3.7A and 4.3.8A) and because of the strong restriction of the fresh Baltic waters to the coast too little Baltic water is simulated further offshore creating high salinity deviations on either side of the jet. The results from the HAMSOM model also show high salinity differences compared to the climatologies on the seaward side of the Norwegian Coastal Current. But the very low salinity water of the Baltic outflow is not progressing much around the southern tip of Norway (Fig. 4.3.6A). Waters found in the Norwegian Coastal Current north of that point are more saline than in observations even close to land (Fig. 4.3.7A and 4.3.8A). The outflow of the low salinity waters from the Baltic is well established and continues along the eastern boundary current in the Norwegian Coastal Current in the NEMO-Nordic simulation (Fig. 4.3.6A), but the extent of fresh water from the Baltic close to the coast is exaggerated, especially in summer, in extent and amplitude. This creates the large signal of fresh salinity differences in the Skagerrak and west of it with differences >2 psu compared to the observations (Fig. 4.3.7A and 4.3.8A). These particular regional differences between the model results and the climatologies are observed through the whole year just a less pronounced than in summer.

For all seasons HAMSOM and NEMO-Nordic are at least 1 psu fresher than the climatologies in most parts along the Dutch, German and Danish Coast, which are influenced by fresh water discharge (Fig. 4.3.7A, 4.3.8A). The results from MPIOM show the opposite. The MPIOM results are 1 psu saltier than the climatologies in the regions along the east coast. Each model is separately compared to the climatologies in Fig. 4.3.9A to 4.3.20A.

The mean bottom temperatures of MPIOM and HAMSOM for the time period 1986-1999 and for NEMO-Nordic 1971-2000 is shown in Fig.4.3.21A and are compared to the bottom temperatures of Berx and Hughes 1971-2000 (Fig. 4.3.22A). The differences between the model results and the climatology are between ± 1 °C in winter (Fig. 4.3.22A). The Atlantic water coming from the south is warmer in the model results of MPIOM and NEMO-Nordic compared to the climatology. The bottom temperature of HAMSOM is 0.5 °C to 1 °C colder in the southern North Sea. The bottom temperatures along the Norwegian coast are warmer in all model results in winter compared to the climatology. Through the warming at the surface stratification is established in late spring. The bottom temperatures in the deeper regions 50-100 m between 54 °N - 57 °N are not affected and show a remaining patch of much colder temperatures (Fig. 4.3.21A). Also all models show the warm Atlantic water in the Fair Island Current and the Scottish coastal waters (Fig.4.3.21A). In summer the bottom temperatures differ between the model results and the climatology between ± 2 °C (Fig. 4.3.22A). The results of HAMSOM are much warmer than the climatology along the Dutch, German and Danish coast. This area is well mixed even in summer and the surface temperatures of HAMSOM are warmer in summer, too (Fig. 4.3.5A). The results of NEMO-Nordic are warmer than the climatology in the shallow regions of the North Sea south of the Dogger Bank.

The North Sea mean bottom salinity of MPIOM and HAMSOM for the time period 1986-1999 and for NEMO-Nordic 1971-200 is shown in Fig. 4.3.23A and is compared to the bottom salinity of Berx and Hughes 1971-2000 (Fig. 4.3.24A). The differences between the results of each model and the climatology do not vary much between the seasons (Fig. 4.3.24A). The salinity of MPIOM is much higher than the salinity of the BHC along the German coast, which is most pronounced in winter. The Atlantic water entering the North Sea from the South and from the North is 0.25 psu saltier than the climatology. In the central North Sea the salinity of MPIOM is 0.25 psu less than the salinity of the climatology. The results of HAMSOM and NEMO-Nordic show similar results compared to the climatology. The salinity is 0.25 psu higher in the model results compared to the climatology along the East coast. But the salinity in the central, north and east North Sea is 0.25 till 1 psu higher in the climatology than in NEMO-Nordic and HAMSOM, with increasing differences towards the coast. There is only one exception in the area around 8 °E and 54 °N, where the salinity is less in the climatology, than in the model results.

The comparison of bottom temperature and salinity for each model and the BHC can be found in Fig. 4.3.25A-4.3.30A.

4.4 Vertical distribution of temperature and salinity along transects

The simulated vertical distribution of temperature and salinity of the coupled models MPIOM, HAMSOM and NEMO-Nordic are compared to the KNSC (1986-1999) for the months of February and August. Transects along 56 °N and 58 °N are chosen as examples. We examine situations in the annual cycle when the water column is well mixed in winter and the development of seasonal stratification during summer. For this we have chosen the months of February and August to represent these situations since the observational data coverage along the sections is best for these two months.

In the observations the temperature in the North Sea is well mixed in winter on both sections (Fig. 4.4.1A, upper panel) and stratification develops in summer (Fig. 4.4.2A, upper panel). In summer warm surface waters are separated from cold bottom waters by the thermocline, a strong vertical temperature gradient. In the central and northern North Sea the thermocline is well pronounced from April/May to September, where as in the north-western region and in the shallow southern North Sea strong tidal currents and bottom friction prevent thermal stratification (OSPAR COMMISSION, 2000). The mean depth of the thermocline ranges from about 20 to 40 m in the KNSC. The salinity distribution in the North Sea is characterized by the fresh water discharge of the rivers along the southern continental coast and the Baltic Sea outflow as well as by the inflow of saline Atlantic waters from the North and from the English Channel (Fig. 4.4.1A and 4.4.2A lower panel). Figure 4.4.3A and 4.4.4A also show the vertical temperature and salinity distribution along 58 °N but to a depth of 400 m.

4.4.1 Temperature and salinity transects along 56 °N

In February all model results show a similar structure of the vertical temperature distribution along 56 °N (Fig. 4.4.5A). The water body is mixed and all models show the coldest water along the east coast with temperatures of 3 °C for HAMSOM and NEMO-Nordic and 4 °C for MPIOM. In the central North Sea the temperature is 6 °C for all models. All models differ from the KNSC between 0.5 °C and -1 °C. The front between the large warm pool in the central North Sea and the cold coastal waters between 3 °E - 4 °E in the KNSC shows a high variability of 2 °C (Fig. 4.4.1A upper left). This variability seems too high and is caused by the poor availability of observations. At this location there are large positive and negative differences to the climatology to the models which could be related to a slight shift in the location of the front in the models and the much coarser resolution of the climatology.

The salinity gradient of 2 psu from the coasts to the central North Sea is well represented by all models (Fig. 4.4.6A). The results from MPIOM are around 0.2 psu fresher than the results from the KNSC except for a small region along the coast. NEMO-Nordic and HAMSOM are fresher than the KNSC in the eastern part of the North Sea and saltier in the western half. The differences between the surface salinities of the models and the climatologies (Fig. 4.3.7A, 4.3.8A, 4.3.24A) therefore apply to the whole water column.

In August all model results show a region of warm and well mixed temperatures in the shallow area at the east coast of the North Sea (Fig. 4.4.7A). Stratification starts at 7 °E towards the west in HAMSOM and NEMO-Nordic and in the MPIOM results at 6 °E (this difference is caused by the vertical resolution of the MPIOM model). The decrease of surface temperature from 16 °C in the east to 13 °C in the west is depicted by all models. All models are around 1 °C warmer than the KNSC directly at the eastern coast. The KNSC shows a similar W-E gradient but its warm surface layer reaches a depth of at least 20 m from the east coast to 1 °E (Fig. 4.4.2A). MPIOM and HAMSOM underestimate the mixed layer temperature by up to 1.5 °C for most of the section. The thermocline in the central North Sea (1 °W – 4 °E) between 20 - 50 m depth is depicted by all models. HAMSOM shows less temperature decrease between surface water and deep water. The deep water in HAMSOM is about 1 °C warmer than the KNSC and 0.5 – 1 °C colder in MPIOM and NEMO-Nordic (Fig. 4.4.7A).

The vertical salinity distribution in August along 56 °N is characterized by a strong gradient from the east coast to the west coast (Fig. 4.4.8A). The differences of the salinity distribution are not as distinguished between February and August as for the temperature. In August NEMO-Nordic distributes the freshwater from the east coast 4° further to the west in the upper 20 m than MPIOM, HAMSOM and the KNSC. The MPIOM results are around 0.2 psu fresher than the results from the KNSC. NEMO-Nordic and HAMSOM are fresher than the KNSC in the eastern part of the North Sea and saltier in the western half.

4.4.2 Temperature and salinity transects along 58 °N

The transect along 58 °N is covers the inflow from the Atlantic, the deep Norwegian trench and the connection to the Baltic Sea (Fig. 4.1). In February all models show the warm (7°C) and saline (~35 psu) inflow branches between 2 °W and 4 °E from the North Atlantic (Fig. 4.4.9A and Fig. 4.4.10A). The cold (~3 °C) and fresh (31 psu) water influenced by the outflow from the Baltic Sea is confined over the deep trench (east of 6 °E) for MPIOM and HAMSOM, but reaches further west in NEMO-Nordic. Compared to the climatology NEMO-Nordic is therefore 1.5 °C colder and up to 1 psu fresher between 2 °E -5° E. The salinity in the KNSC is higher than in the models and this is most pronounced in the Baltic outflow. The difference decreases from -2.5 psu at the east to +0.5 psu in the west.

All models show a stratified water column in August of varying depth and extent (Fig. 4.4.11A). All model results show colder temperatures than the KNSC in the region influenced by the Baltic outflow. The KNSC temperature east of 6 °E is warmer than 16 °C above 20 m (Fig. 4.4.2A). This is not represented by any of the models. In the MPIOM results east of 4 °E the warmer waters from the surface are mixed into deeper layers than in the climatology. The 34 psu isohaline has a different position in the climatology and in the model results (Fig. 4.4.12A). In all model results it reaches greater depth at 7 °E and reaches the surface at around 5 °E in HAM-SOM and MPIOM, which is further east than in the climatology and the NEMO-Nordic results.

5 Analysis of the scenario runs

In this chapter we first present the results from each model individually and analyse the climate change signals for the SRES A1B scenario in the respective runs. The analysis focuses on the parameters temperature, salinity and sea surface height. The horizontal distribution of each parameter and its changes are presented as 30 year means for the time slices 1970-1999, 2021-2050 and 2070-2099 defined by the KLIWAS project as climatic periods representing the present day, near and far future climate. Time series of North Sea averages for each property are presented to visualize the temporal variability which is significant in most of the time series and simulations. For the control period (1970-1999) comparisons to both observational climatologies (BHC and KNSC) are shown since the scenario run can differ from the hindcast simulation described in chapter 4. The last section in this chapter will show comparisons between the three models and will discuss the robustness of the climate change signals.

5.1 REMO-MPIOM

5.1.1 Temperature

In order to distinguish between different runs performed with the Max-Planck ocean model we will use MPIOM in the following to refer to the regionally coupled run with the atmospheric model REMO as described in chapter 3, compared to the globally coupled runs with ECHAM5. These will be referenced as MPIOM_G.

The sea surface temperature (SST) fields of the SRES A1B run from MPIOM (Fig. 5.1.1A) demonstrate the gradual increase of temperatures through the course of the simulation, whereas the spatial pattern remain basically unchanged. The control period (1970-1990) in the scenario run shows the same structures than the hindcast simulation, but the mean seasonal and annual fields are even slightly cooler (~ 0.5 °C) than in the hindcast (compare Figs. 4.3.9A, 4.3.10A, 5.1.2A, and 5.1.3A). But one has to keep in mind that the averaging period for the hindcast only comprises the second half of 30 years which already showed some warming at least in the observational record. Additionally, it has already been noted that the atmospheric boundary conditions from the ECHAM5-run3 simulations missed a warming signal at the end of 20th century. The cool bias in the scenario run for the period 1970-1999 (Fig. 5.1.2A and 5.1.3A) is persistent through all seasons and reaches maxima between 1.5 °C - 2.0 °C in the southern North Sea between 54 °N - 57 °N. This cool bias leads to the local minimum between latitudes 54 and 57 °N in winter and spring. Because of the persistence of the strong local biases in this band the SST gradient towards the German Bight is confined to a narrow area in summer. As already noted in Chapter 4 the in-

flow of Atlantic water from the north and through the Atlantic is well matched with observations.

The bottom temperature fields (Fig. 5.1.4A) show the strong temperature increase towards the shallow southern North Sea in summer and the influence of local topographic features such as the Dogger Bank. The temperature increase is gradual throughout the course of the century similar to the surface. As for the surface fields it is evident that the fields from the scenario run are showing the same structures but lower temperatures than the hindcast simulations (Fig. 4.3.25A). The temperatures at the shelf break in the scenario run do not differ much from the hindcast experiments and simulated oceanic conditions in the deep ocean outside the North Sea are therefore also approximately 1 °C too warm (Fig. 5.1.5A, 5.1.6A) compared to observations. It is the central North Sea where the free climate runs experiences stronger cold temperature biases than in other regions. The patch of cold water between 54 °N - 57 °N is a remnant of the ventilated waters from the winter period which was formed by heat exchange with the atmosphere. Re-stratification in spring and summer shelters this water too early from the surface heating and a cool bottom patch remains. South of this pool in the well mixed waters of the southern North Sea the temperatures of the bottom layer are too high.

The temporal evolution of sea surface temperature is given as difference plots between the climatic periods in Fig. 5.1.7A. The climatic periods have been defined for the entire KLIWAS project to represent changes in the near and far future. The calculated differences depend on the choice of the averaging period of 30 years because of the pronounced decadal variability in the time records and the values shown here do not imply linear trends. The upper panels in Fig. 5.1.7A give the time evolution until the near future as the difference between the time periods 2021-2050 and 1970-1999 and for the far future in the lower panels as the difference between 2070-2099 and 1970-1999. The temperature increase until the near future is generally below 1.0 °C except for the outflow from the Baltic Sea where higher increases are visible for all seasons. In the far future the temperature increase is in the range between 2 and 2.5 °C with a slightly stronger warming in winter than in summer. An interesting feature is the tongue of lower temperature increase associated with the inflow of Atlantic Water through the English Channel and from the north. Highest increases are simulated in the central and eastern North Sea.

The temporal evolution of bottom water temperature is given as difference plots between the climatic periods in Fig. 5.1.8A. For the near future it is more homogenous than the corresponding surface fields (Fig. 5.1.7A) because the Baltic outflow is not influencing the horizontal distributions. The amount of temperature increase is similar to the surface and amounts to less than 1.0 °C in the near future for most of the North Sea. In the far future the differential heating of the Atlantic Waters becomes

much more important and lower temperature increases are notable in the northern North Sea and in the English Channel area.

Coupled Ocean
Atmosphere
Models

BSH
DWD
IfM Hamburg
MPI Hamburg
SMHI
AWI

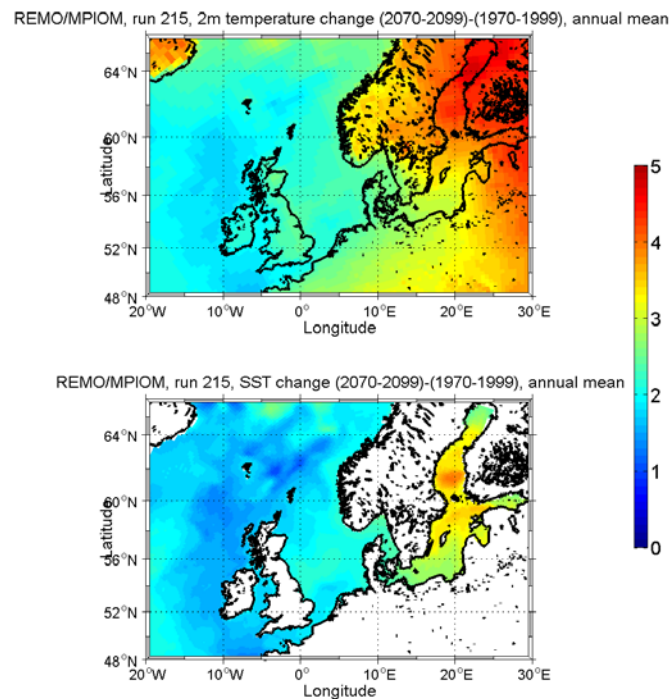


Figure 5.1.1: Comparison of temperature changes in MPIOM/REMO run 215 in the far future (2070-2099 to 1970-1999) in the atmosphere (upper panel) and in the ocean (lower panel).

The North Sea is influenced by both the maritime climate of the North Atlantic and the continental climate in the east. Due to the alternating dominance of the two regimes the transition zone is characterized by high variability (BACKHAUS, 1989). As far as the climate change signal is concerned the atmospheric and oceanic changes mimic each other (Fig. 5.1.1). But the air temperature shows a stronger increase of temperatures over the continent in the east compared to areas under maritime influence. In the MPIOM/REMO simulation the maritime influences dominate the North Sea proper, even at the eastern coast.

The time series of average North Sea surface temperatures (Fig. 5.1.9A, Fig. 4.1 for averaging area) shows the earlier mentioned flat evolution at the end of the 20th century and delayed start of the temperature increase in the 21st century. There is strong inter-annual variability superimposed on the long-term trend which reflects natural modes of variability. There are several modes of variability, which are particularly important in the North Sea area (see GROSSMANN AND KLOTZBECK, 2009), namely the North Atlantic Oscillation (NAO), the Atlantic Multi-Decadal Oscillation (AMO) and the Atlantic Meridional Mode (AMM). While one would expect the NAO variability to be dominating in winter and spring the inter-annual variability appears to be particularly strong also in the summer records. The highest year to year differences are

found in summer and fall and amount to $0.86\text{ }^{\circ}\text{C}$ (averaged over entire time series). Variability in the spring record seems to decrease towards the end of the simulation period.

The stronger warming in winter relative to the summer is also recognized in the annual cycle of the spatially averaged sea surface temperature (Fig. 5.1.10A). The annual cycle in the consecutive averaging periods does not differ significantly within the error bars representing the temporal variability of the 30 year means, but the far future annual cycle is distinct from today's. The range and magnitude of the annual cycle in the free climate run are similar to the hindcast simulation (Fig. 4.1.1A) and are therefore a bit too cool compared to observations especially during April-August.

The time series of average North Sea bottom temperatures (Fig. 5.1.11A) has similar timing than the corresponding surface time series (Fig. 5.1.9A) but reduced year to year variability in summer and fall ($0.55, 0.53\text{ }^{\circ}\text{C}$ compared to $0.85, 0.86\text{ }^{\circ}\text{C}$ at the surface). This is due to the insulating effect of stratification in the deeper parts of the North Sea.

The amplitude of the annual cycle of the bottom temperatures (Fig. 5.1.12A) is much smaller than the corresponding surface cycle and the maximum temperatures are delayed from August at the surface (Fig. 5.1.10A) to September at the bottom. While temperatures at the surface and the bottom are similar in winter and spring because of the strong vertical mixing, they differ as much as $4\text{ }^{\circ}\text{C}$ at the end of summer. Compared to the corresponding hindcast simulations (Fig. 4.1.5A and 4.1.6A) scenario run is about $0.5\text{ }^{\circ}\text{C}$ cooler in winter and spring and more than $1.0\text{ }^{\circ}\text{C}$ in summer. The large increase of the bias to observations in the scenario run in summer compared to the hindcast is due to the cold patch in the central North Sea where remnants of the winter water are capped too early by a mixed layer to receive more heating from the surface.

5.1.2 Salinity

The sea surface salinity fields inside the North Sea proper (Fig. 5.1.13A) are mostly dominated by the strong contrast between the low salinity waters along the eastern coasts and high salinity waters in the north and south. The spatial patterns are not changing during the course of the simulation but salinities are decreasing slightly towards the end of the 21st century.

Compared to the corresponding hindcast simulations (Figs. 4.3.15A, 4.3.16A, 5.1.14A, and 5.1.15A) the surface salinities in the free climate run are notably higher in the Atlantic waters outside the North Sea associated with different large scale salinity patterns in the sub-polar North Atlantic. Both, the hindcast and the climate simulations reveal a too narrow Norwegian Coastal Current (NCC) compared to observations and thus, too low salinities in the narrow jet as discussed in chapter 4. In com-

parison to observations (Figs. 5.1.14A, 5.1.15A) this is evident from the high salinity deviations at both sides of the jet.

Observations would suggest that the simulated sea surface salinities (SSS) are too high in the German Bight (i.e. along the West and North Frisian coastal zone) in the hindcast (Figs. 4.3.15A, 4.3.16A) as well as in the free climate run (Figs. 5.1.14A, 5.1.15A) and that the fresh water plumes from the rivers Elbe and Weser therefore do not extend far enough offshore. But, the 16 m surface layer of the model is inadequate in the shallow areas close to the estuaries to describe the river plume correctly. In the area of the river plume of the Rhine (around 4 °E) too low salinities are simulated compared to observations from the BHC (Fig. 5.1.14A), but only to a lesser extent when using the KNSC (Fig.5.1.15A).

The bottom salinity fields (Fig. 5.1.16A) are similar to the surface fields except for the deep Norwegian Trench where high salinity waters are flowing in at depth compared to low salinity outflow of Baltic Waters at the surface. The highest salinities seem to be associated with the inflow of Atlantic Water in the Trench and a second branch is indicated over the Shetland-Orkney plateau. Although the high salinities over the Norwegian Trench are depicted slightly different in the two observational data sets (Fig. 5.1.17A, Fig. 5.1.18A) both climatologies agree that the simulated salinities are slightly too high. The inflow through the Fair Isle Channel between the Orkneys and Shetlands and the retroflexion of the saline waters at the 100 m isobaths (known as Dooley Current) are realistically modelled (HOWARTH, 2001; HOLT AND PROCTOR, 2008). The spatial patterns are mostly conserved though the climate periods and a light freshening is shown towards the end of the century which is strongest in the southern parts of the North Sea (Fig. 5.1.16A). Compared to the hindcast (Fig. 4.3.28A) the salinities are generally higher, which reduces the fresh salinity bias of the hindcast especially in the northern parts of the North Sea.

The salinity budget of the North Sea is strongly influenced by the inflow from the Atlantic. Salinity changes in the North Sea will therefore to a large degree depend on the North Atlantic salinity evolution and changes in the wind driven inflow. SSS decreases only slightly until the near future, but a strong decrease is projected for the far future (Fig. 5.1.19A). The amplitude of the freshening depends on our choice of the averaging periods and is not statistically significant for the near future, given the high multi-decadal variability in the salinity record (Fig. 5.1.21A). The strongest decreases in the far future are associated with the Baltic Sea outflow (Fig. 5.1.19A) where salinity decreases by more than 2 psu. This decrease is limited to the narrow band of the Norwegian Coastal Current and does not seem to spread substantially out of the current. A second band of stronger salinity decrease is simulated in the southern North Sea. The salinity decrease there is between 0.25-0.5 psu. Both the freshening of the Baltic Sea outflow and along the Continental coast can be attributed to increasing

precipitation rates and river runoff, associated with the enhanced hydrological cycle and moister climate of the A1B scenario.

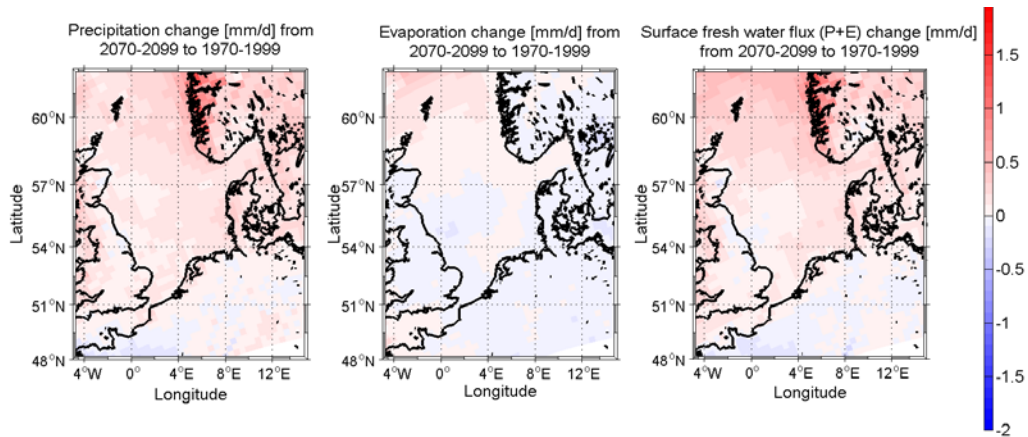


Figure 5.1.2: Far future changes of precipitation (left), evaporation rate (middle) and the net surface fresh water flux (right) based on the reference period 1961-1990.

The changes of surface fluxes of fresh water in the far future are shown in Fig. 5.1.2. One of the major conclusions from the EU ENSEMBLES project was that northern Europe is expected to receive larger amounts of rain while southern Europe is expected to get less rain (VAN DEN LINDEN ET AL., 2009). But the variability among the ENSEMBLES RCMs was considerable and the boundary between the two regimes highly variable (DEQUE ET AL., 2011). REMO in the setup used here follows that general pattern and predicts increased rainfall over the entire North Sea area with strongest rainfall changes over the Norwegian coastal mountain range. The net surface fresh water flux is mostly dominated by precipitation, since changes in evaporation are comparatively smaller. The changes in the net fresh water flux are thus showing a clear W to E decrease with two areas of higher positive anomalies in the greater German Bight area and off Norway.

Runoff has been calculated in the MPIOM simulations from the integrated hydrological model. Fig. 5.1.3 shows the sum of runoff from all rivers draining into the North Sea and respectively into the Baltic. The mean 20th century runoff for the North Sea amounts to 375 ± 41 km³/year, which is about 25% higher than the climatological value of 300 km³/year (DAMM, 1997). Values for the Baltic are 565 ± 67 km³/year and are also higher (27%) than the climatological value of 444 km³/year quoted in the literature (BERGSTRÖM AND CARLSSON, 1994). But experience from the ENSEMBLES project (VAN DEN LINDEN ET AL., 2009) has shown that at high resolution (25km compared to 50 km) almost all of the RCMs, including REMO, tended to simulate more precipitation (RAUSCHER ET AL., 2009) that resulted in an increased wet bias over some regions.

Whilst the North Sea time series of runoff (Fig. 5.1.3) is dominated by strong inter-annual fluctuations no obvious trend is found. The Baltic runoff in contrast is strongly increasing after 2000 with increasing inter-annual amplitude. Freshening of the Baltic Sea outflow thus seems to receive a contribution from terrestrial discharge, while this does not seem to be the case for the rivers discharging into the North Sea. The increased freshening in the southern North Sea must therefore be attributed to the enhanced precipitation over sea or changes in the advective transports.

The seasonal cycle of precipitation is linked to the temperature contrast between sea and land, while inter-annual variations correlate with the strength of the westerly circulation. ALTEMA AND LENDERINK (2014) have reported on the influence of the North Sea on coastal precipitation in future climate and focused their analysis on the coasts of the Netherlands. In their simulations they found a small increase of coastal precipitation for all seasons except spring.

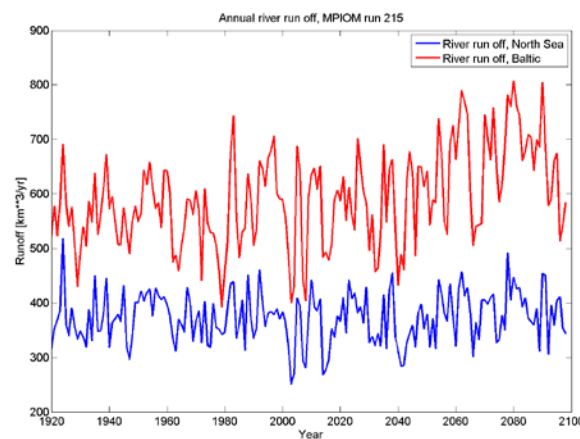


Figure 5.1.3: Sum of runoff from rivers draining into the North Sea (blue) and into the Baltic (red) in km^3/year .

Bottom salinity differences (Fig. 5.1.20A) are also small for the near future. In the far future the only area of stronger salinity decrease is the shallow southern North Sea, where bottom conditions are similar to the surface. Salinities in the deep Norwegian Trench do not change much in contrast to the surface.

The time series of average North Sea SSS (Fig. 5.1.21A) shows pronounced multi-decadal variability and a superimposed salinity decrease after 2020. The period of the multi-decadal variability is in the order of 40 years with peak to peak amplitudes of 0.15 psu during the 20th century (Fig. 5.1.4). The inter-annual variability is also strong and effects all seasons (Fig. 5.1.21A). It has mean amplitudes of 0.10 psu for the annual values and reaches highest values (0.14 psu) in summer. The range of variability in the surface salinity is similar to the hindcast simulations.

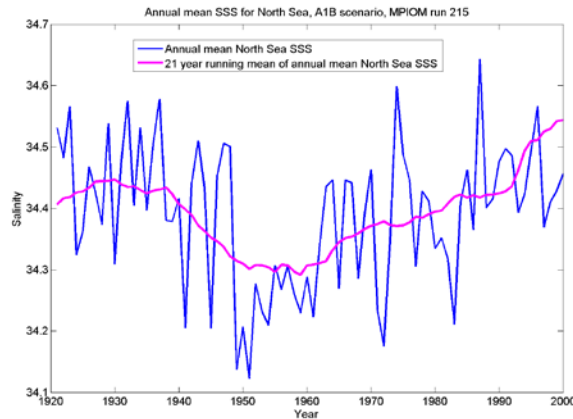


Figure 5.1.4: Multi-decadal variability of sea surface salinity in the 20th century. The multi-decadal variability has been highlighted by a 21 year moving average applied to the yearly mean data from MPIOM run 215.

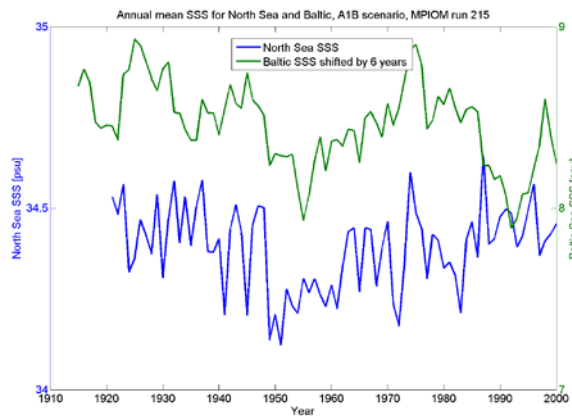


Figure 5.1.5: Comparison of sea surface salinity time series from the North Sea (blue) and Baltic (green). The record from the Baltic is leading by 6 years and has been shifted accordingly in the figure.

The time series of the averaged sea surface salinity in the North Sea and Baltic vary in parallel, but the signal in the Baltic leads by 6 years (Fig. 5.1.5). The causes for the multi-decadal variability in the Baltic have been investigated in modelling studies (MEIER AND KAUKER, 2003; GUSTAFSSON AND ANDERSON, 2001) and in observational studies (WINSOR ET AL., 2001; ZORITA AND LAINE, 2000). Among the factors that have been proposed are decadal variations of accumulated volume of fresh water from the rivers and net precipitation and large scale pressure differences over the North Sea and Scandinavia. In agreement with our findings here the studies reported multi-decadal variations on time scales of 35 years (MEIER AND KAUKER, 2003). GUSTAFSSON AND ANDERSON (2001) have focused in their study on the physical mechanisms controlling the exchange of water between the North Sea and Baltic and found that north-south pressure gradients across the North Sea and sea level in the Kattegat were highly correlated. One has to keep in mind that the horizontal and vertical resolution of the MPIOM is not sufficient to resolve the exchange through the

straits properly. Nonetheless it is encouraging to see that the time scales of variability are similar. Further investigations are needed to explore the physical mechanisms connecting the SSS variability in North Sea and Baltic.

The annual cycle of sea surface salinity (Fig. 5.1.22A) shows a minimum during May to July which is related to increased river runoff. Compared to the hindcast simulation (Fig. 4.2.1A) the minimum is shifted one month earlier (June) while the observations would suggest that the minimum is reached even later (August). The temporal evolution shows increasing rates of salinity decrease (Fig. 5.1.23A). While the salinities during the first two KLIWAS climate averaging periods are nearly indistinguishable given the amount of temporal variability, the last period becomes distinct. Due to the high level of multi-decadal variability this conclusion is also affected by the choice of the averaging period.

The time series of average North Sea bottom salinities (Fig. 5.1.23A) shows similar levels of inter-annual variability than the surface records. But the amplitude of the multi-decadal variability is much reduced compared to the surface.

The amplitude of the annual cycle of salinity at the bottom (Fig. 5.1.24A) is not very pronounced during the 1970-1999 climate period. In this it is similar to the hindcast simulation (Fig. 4.2.5A) although the higher salinity values in the scenario run agree better with the observed cycle. The annual range increases slightly in the last period (2070-2099) while the entire annual cycle shifts to lower salinities.

5.1.3 Sea surface height

The sea surface height fields of MPIOM displayed a small offset of 0.6 m to the records from tide gauge. In order to make the model more compatible with observations 0.6 m was added as a constant to the simulated SSH data.

The sea level fields of the SRES A1B scenario run from MPIOM (Fig. 5.1.25A) demonstrate a gradual increase of water levels throughout the course of the century, while the spatial patterns remain basically the same. Sea level changes that originate from the melting of ice shields and glaciers or from glacial isostatic adjustment (GIA) have not been included in these figures. The spatial patterns in the climate simulation do not differ significantly from the hindcast simulation (not shown for the hindcast). The seasonal cycle of SSH (see also Fig. 5.1.28A) is visible in the seasonal means of Fig. 5.1.25A in all three time periods. The minimum in spring is caused by the low temperatures while the increase in summer and fall is due to rising temperatures and increasing winds.

During the near future the mean rise in sea level is below 0.08 m and it increases to more than 0.24 m in the far future (Fig. 5.1.26A). In the far future the largest increase in sea level is noted in spring, related to the stronger warming in the cold than in the warm seasons. The spatial patterns are mostly homogenous in the far future except for slightly increased levels in the eastern North Sea. The stronger increase of sea level at

the eastern coasts could also be related to the surge component of sea level due to wind. Analysis of the mean wind fields has shown a small but consistent increase in westerly winds in the far future compared to 1970-1999 which would result in a higher wind surge.

The time series of average sea level in the North Sea (Fig. 5.1.27A) shows a significant increase of sea level in all seasons only after 2020. Before that period it is mostly dominated by inter-annual variability which is related partly to NAO induced variability. Variability is strong in all seasons but is weakest in summer.

The annual cycle of sea surface height (Fig. 5.1.28A) has a minimum during March and April and shows the above mentioned strong increase of sea level during the later decades of the 21st century for the period 2070-2099. Compared to the hindcast simulations (not shown for the hindcast) the minimum in sea level occurs nearly 2 month earlier. The reason for the change in the annual cycle is subject of future work.

5.2 REMO-HAMSOM

5.2.1 Temperature

The SST fields from the scenario run of HAMSOM (Fig. 5.2.1A) show a gradual increase through the course of the century while the spatial patterns remain basically unchanged. Compared to the hindcast simulation (Fig. 4.3.11A, 4.3.12A and Fig. 5.2.2A, 5.2.3A) the seasonal and annual fields in the scenario run start at similar levels or even slightly cooler. But one has to keep in mind that the averaging period for the hindcast only comprises the second half of 30 years. Comparison of the scenario run with the observational data (Fig. 5.2.2A and 5.2.3A) would suggest that there is a temperature deviation in the order of 1 °C and up to 2 °C along the coast of Jutland. There is a marked seasonality in the temperature biases with cold biases in winter and spring and warm biases in summer resulting in an enhanced seasonal cycle. The temperature biases in the coastal area in HAMSOM have been studied by SU ET AL. (2014). The comparisons between coupled and uncoupled hindcast simulation showed that the dynamic coupling has improved the prediction of climate change impacts in the North Sea and led to reduced deviations from observations in the coastal areas. Root mean square deviations between the coupled and uncoupled hindcast were as high as 5 °C in the German Bight. Another area with larger temperature biases compared to observations (Figs. 5.2.2A, 5.2.3A) is found along the English coast in the area off Newcastle. It is most pronounced in summer and extends towards the southern tip of Norway in autumn. The atmospheric forcing fields in this area need to be investigated in more detail in order to discern the mechanisms that create the cool temperatures. The English Channel model boundary, where boundary conditions from the MPIOM run are specified, is very close to the eastern exit of the Channel in this model set-up. This might be one of the reasons why the advection of warm Atlantic water is less pronounced in the model (Fig. 5.2.1A) than in the obser-

vations (Figs. 5.2.2A and 5.2.3A). The modelled Atlantic tongue is most visible in the autumn fields and nearly absent in winter and spring.

The bottom temperature fields (Fig. 5.2.4A) show a strong temperature gradient towards the shallow southern North Sea in summer and the influence of local features such as the Dogger Bank. There is a very strong temperature contrast between winter (DJF) and summer (JJA) along Jutland which is stronger than in the observations. These patterns are similar to the hindcast simulation (Figs. 4.3.26A, 5.2.5A, and 5.2.6A). Around the Danish mainland the temperatures are too low by about 2 °C in winter and too high by a similar amount in summer based on the BHC.

The spatial patterns of bottom temperature biases (Fig. 5.2.5A, 5.2.6A) differ from the surface fields (Fig. 5.2.2A, 5.2.3A). This is most obvious in summer and fall when a seasonal mixed layer insulates the bottom layer from the atmosphere's influence. The cold pool off Newcastle and in the band towards the southern tip of Norway is showing warm biases in these seasons at the bottom. If this not an advective signal it would point to processes such as re-stratification and vertical mixing by which heat can be transferred downward.

At the surface the temperature change in the near future (2021-2050) is already relatively large and exceeds 1.0 °C almost everywhere (Fig. 5.2.7A). It is strongest in the spring season with warming > 2.0 °C in the eastern part of the North Sea. The temperature change in the far future (2070-2099) is larger than 2.5 °C for most of the North Sea. It has a pronounced maximum in spring when it exceeds 3 °C in the eastern parts of the North Sea. The inflowing Atlantic waters at the English Channel and the north western model boundary show lower temperature increases due to the more maritime influence. This is clearly seen in the annual means for both the near and far future.

The temporal temperature change in the bottom fields (Fig. 5.2.8A) is of similar range than at the surface and has also similar spatial patterns. Stronger spatial gradients are seen in summer and fall in the north western corner of the model area where Atlantic water is entering the North Sea.

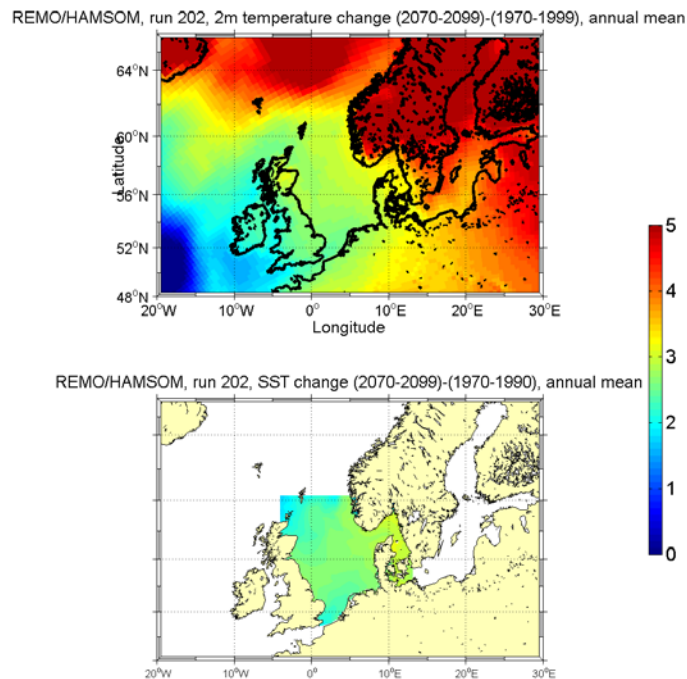


Figure 5.2.1: Comparison of temperature changes in HAMSOM/REMO run 202 in the far future in the atmosphere (upper panel) and in the ocean (lower panel).

The atmospheric 2 m temperature change in the far future (Fig. 5.2.1) shows a very pronounced warming over Norway, Sweden and Finland but also over the Nordic Seas. The strong amplitude of warming of the atmosphere over Sweden and Norway gradually smoothens out over the Skagerrak and Kattegat while the North Sea proper is still dominated by maritime influence from the North Atlantic. The SST mimics the air temperature changes and the increasing sea surface temperature changes in the eastern North Sea are resulting from the stronger heating over land.

Both the HAMSOM and the MPIOM simulation use the same REMO setup to downscale the atmospheric forcing, but show distinctly different air temperature response over land and in the north (compare Fig. 5.2.1 and 5.1.1). The only difference between the two simulations is that ice concentrations in the HAMSOM run were taken from the MPIOM-G run instead of the KLIWAS run described in chapter 5.1.

The time series of average North Sea surface temperatures (Fig. 5.2.9A) shows a nearly linear trend throughout the simulation superimposed with strong inter-annual variability in all seasons. The internal variability seems to decrease in the 21st century in winter and spring while it remains at similar levels for summer and fall.

The shape of the annual cycle of SST (Fig. 5.2.10A) remains unchanged through the simulation and increases by similar amounts between the averaging periods as was already indicated by the nearly linear trend in Fig. 5.2.9A. The seasonal cycle in the scenario run has a similar range than the hindcast simulation (Fig. 4.1.1A, 4.1.2A) for which the comparison with observations indicated a cold bias in the order of 0.5-1.0

°C. The increase of SST is similar in all seasons except for spring when a stronger increase is indicated.

The time series of bottom temperatures (Fig. 5.2.11A) are similar to the surface records (Fig. 5.2.9A) but the warming appears more prominent after 2000. The inter-annual variability is strong in all seasons but for the winter and spring seasons it decreases after 2025, similar to the surface records.

The annual cycle of bottom temperatures (Fig. 5.2.12A) increases by nearly similar amounts from averaging period to averaging period. The maximum of the annual cycle is reached in September which is about a month later than at the surface (Fig. 5.2.10A).

5.2.2 Salinity

The sea surface salinity (SSS, Fig. 5.2.13A) is mostly dominated by the strong contrast between the low salinity waters along the eastern coasts and the high salinity waters in the North and South. The spatial patterns remain basically unchanged through the entire simulation. The period 1970-1999 in the scenario run shows slightly more saline Atlantic waters at the northern boundary than the corresponding period in the hindcast simulation (Figs. 4.3.17A, 4.3.18A, 5.2.14A, and 5.2.15A). But, otherwise it has the same spatial distribution. The boundary conditions supplied by MPIOM in the scenario run had simulated more saline waters at the northern shelf edge compared to the hindcast run.

The very low salinities waters of the Baltic Sea outflow are not progressing much around the southern tip of Norway (Fig. 5.2.13A). Waters found in the Norwegian Coastal Current north of that point are more saline than in the observations (Fig. 5.2.14A, 5.2.15A). The comparison with observations suggests that the model systematically overestimates the salinities of the Baltic Sea outflow outside the Kattegat. The same result was obtained from the hindcast simulation (Figs. 4.3.17A, 4.3.18A).

In the HAMSOM simulation the low salinity waters in the German Bight and along the Frisian coasts show a seasonal cycle (Fig. 5.2.13A). They reach their largest offshore extent during summer and their smallest in winter. The comparison with observations (Figs. 5.2.14A, 5.2.15A) suggests that the offshore extent of the fresh water plume from the Elbe and the Weser rivers is too large especially in spring and fall. Closer to the mouth of these estuaries on the other hand the modelled salinities seem to be too low. The hydrological cycle for these simulations was taken from a monthly mean climatology (DAMM, 1997) and was simulated as a perpetual annual cycle throughout the entire simulation. The large extension of the fresh water plume into the German Bight and northward along the Danish coast might be due to a more pronounced occurrence of easterly winds compared to other models that would spread the low salinity waters offshore and change circulation patterns. Moreover, the HAMSOM simulation shows low salinities in a band along the Belgian and Dutch

coasts that are too low compared to observations (Figs. 5.2.14A, 5.2.15A) and are present in all seasons.

The bottom salinity fields (Fig. 5.2.16A) show the inflow of high saline Atlantic Water in the deep Norwegian Trench while low salinity waters occupy the bottom of the shallow southern North Sea. Only minor changes are noticeable in the salinity fields during the course of the simulation. The horizontal patterns are similar to the hindcast simulations Fig. 4.3.29A, Fig. 5.2.17A, 5.2.18A). The maximum salinities at the northern boundary occur in the east over the Norwegian Trench, as prescribed from the MPIOM simulation (Fig. 5.1.16A). In the observations additional inflow of high salinity waters in the Dooley current follows the 100 m isobaths in a south easterly direction before it retroflects over the Norwegian trench (Fig. 5.2.17A, 5.2.18A. This south easterly turn of high salinity waters at the southern tip of Norway is less pronounced in the model especially in winter and spring when transport into the North Sea is highest (HJOLLO ET AL., 2009; WINTHER AND JOHANESSEN, 2006). Along the east coast of Great Britain the tongue of salinities higher than those in the observations could be due to a too strong influx of water coming from the Atlantic at this location (Fig. 5.2.17A, 5.2.18A).

Changes in salinity are small in the near future (2021-2050) and vary from a small salinity increase in the northern North Sea to decreasing salinities along the southern and eastern coasts (Fig. 5.2.19A). The Kattegat shows strong local features during the near future as well as the far future that need to be investigated further. A continuation of the salinity change signals from the Baltic along the Norwegian coast is not visible in the near future. The salinity decrease in the Baltic Sea outflow is more obvious in the far future (2070-2099) and the advection of the signal out of the Kattegat and Skagerrak is then visible in all seasons, but a stronger continuation along the Norwegian coast is only seen in spring. The rest of the North Sea also experiences a small decrease in salinity in the far future, but at reduced amplitude compared to the freshening of the Baltic. It has to be kept in mind that the river runoff into the North Sea is prescribed as perpetual year during the simulation and increasing fresh water fluxes are only entering the North Sea as precipitation or evaporation changes or advective changes (Baltic Sea Outflow, Atlantic inflow).

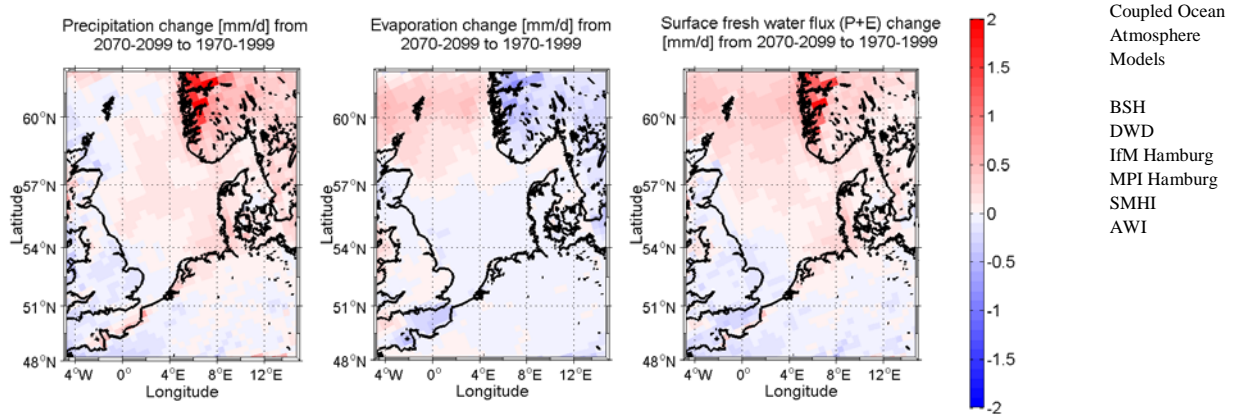


Figure 5.2.2: Far future changes of precipitation (left), evaporation rate (middle) and the net surface fresh water flux (right) based on the reference period 1970-1999.

The changes of the net fresh water fluxes through the surface for the far future that result from rainfall and evaporation are shown in Fig. 5.2.2. The net fields are dominated by changes in rainfall, but are reduced by decreasing evaporation rates. As a result decreasing net fluxes are calculated over the south western North Sea including the Channel area and increasing fluxes in the north with intensification towards the coasts of Denmark and Norway.

The corresponding surface salinity changes (Fig. 5.2.19A) in the far future to some extent follow the surface forcing from the atmosphere but advective signals from the Baltic Outflow and probably also in the Channel inflow must play a role. MATHIS (2013) has noted in his simulation a significant reduction of the inflow through the English Channel and the associated salt inflow. This might explain the salinity decrease in the English Channel area and along the coast.

Spatial bottom salinity changes (Fig. 5.2.20A) are small for the near and far future. In the far future the only area of higher salinity decrease is found in the southern Kattegat. In the near future changes in the bottom salinity range between a small increase in the deeper parts of the North Sea and a small decrease along the southern and eastern coasts as already discussed for the surface fields (Fig. 5.2.19A).

The temporal behaviour of the surface salinity shows a pronounced inter-annual variability (Fig. 5.2.21A) and, superimposed a long-term salinity evolution with increasing salinities during the 20th century followed by a small decrease thereafter.

The temporal changes in the annual cycle of the sea surface salinity SSS (Fig. 5.2.22A) are small and the near future cycle is almost indistinguishable from the reference period 1970-1999 considering the amount of temporal variability. Only slightly larger changes are predicted for the far future but error bars still overlap. The annual cycle shows a minimum in summer in all averaging periods but, like in the hindcast, the amplitude of the annual cycle is reduced compared to observations (Fig. 4.2.1A). The decrease in salinity for the near future is mostly confined to the first half

of the year. The time series of the bottom salinity (Fig. 5.2.23A) shows a more pronounced multi-decadal signal than the corresponding surface salinity time series (Fig. 5.2.21A). The amplitude of the inter-annual variability as well as the long-term variability is much larger than at the surface.

The annual cycle of bottom salinity is not very pronounced (Fig. 5.2.24A) and shows a shallow minimum for the period May-August in all three averaging periods. This is in agreement with observations (Fig. 4.2.25A). The annual cycle in the hindcast simulation was similarly flat, but salinities of the hindcast simulation were much lower and thus differed more from observations.

5.2.3 Sea surface height

The HAMSOM output for the sea surface height (SSH) had originally added the component from ice sheet/glacier melting based on the AR4 assessment of the IPCC (see MATHIS (2013) for details about the added components). Since the other models do not include such contributions we have subtracted the ice/sheet/glacier melt contribution to make the model results comparable.

The sea level fields of the scenario run from HAMSOM (Fig. 5.2.25A) demonstrate the gradual increase of water levels through the course of the century, while the spatial patterns remain basically the same. The patterns in the scenario run do not differ significantly from the hindcast simulation (not shown for the hindcast). The sea level fields show a small seasonal cycle with lowest levels in spring due to low temperatures and higher sea levels in the other seasons as a reaction to warming of the water column and stronger winds.

The SSH rise is small in the near future (Fig. 5.2.26A) when it amounts to 0.08 m. It increases strongly to more than 0.26 m in the far future. At the eastern side of the North Sea a slightly higher sea level rise is noted, partly associated with changes in the Baltic Sea outflow (Fig. 5.2.19A) and the stronger warming of the water column in the east (Fig. 5.2.7A).

The time series of SSH (Fig. 5.2.27A) is nearly flat during the 20th century, followed by a strong and linear increase after 2025. The inter-annual variability is strong during all seasons and remains at similar levels throughout the simulation.

The annual cycle for sea surface height for the three different time slices is shown in Fig. 5.2.28A. It shows the above mentioned minimum of sea level in spring (March/April) and shows the small increase in sea level toward the near future and the stronger increase toward the far future.

5.3 RCA4-NEMO-Nordic

5.3.1 Temperature

The SST fields of the scenario run from NEMO-Nordic (Fig. 5.3.1A) demonstrate the gradual increase of temperatures through the course of the century, while the spatial patterns remain basically unchanged. In the scenario run the control period (1970-1990) shows the same structures than the hindcast simulation, but the mean seasonal and annual fields are noticeably colder (~ 1.0 °C) than in the hindcast (compare Figs. 4.3.13A, 4.3.14A and Figs. 5.3.2A, 5.3.3A). Remember, the averaging period for the hindcast only comprises the second half of 30 years which already showed some warming at least in the observational record.

In the scenario run the inflow of warmer Atlantic water through the English Channel is well established in all seasons (Fig. 5.3.1A). It agrees well with observations in the control period and is most noticeable in fall. NEMO-Nordic simulates very low summer temperatures off the coast of Great Britain north of 54 °N which are 1.5-2.5 °C colder than the observations (Figs. 5.3.2A, 5.3.3A). Winter time cooling appears to be too pronounced along the coast of Jutland resulting in large negative biases compared to the climatologies which persist during spring and summer.

The bottom temperature fields (Fig. 5.3.4A) show the strong temperature increase towards the shallow southern North Sea in summer and the influence of local topographic features such as the Dogger Bank. The temperature increase is gradual throughout the course of the 21st century and spatial patterns remain unchanged.

The difference to observations for the period 1970-1999 (Fig. 5.3.5A, 5.3.6A) differs from the hindcast run in the southern North Sea (Fig. 4.3.27A). While the hindcast had shown strong overestimation of the bottom temperatures especially in summer and fall, this has been reversed to an underestimation of bottom temperature at the southern coasts in the free climate run. From the positive temperature biases between the English coast off Newcastle and the Skagerrak in the hindcast (Fig. 4.3.27A) only a small band remains.

SST changes are small in the near future and nearly homogeneous (Fig. 5.3.7A). These increases amount to more than 0.5 °C for most parts of the North Sea but are less than 0.5 °C in the southern North Sea. In the far future, the temperatures increase around 2 °C.

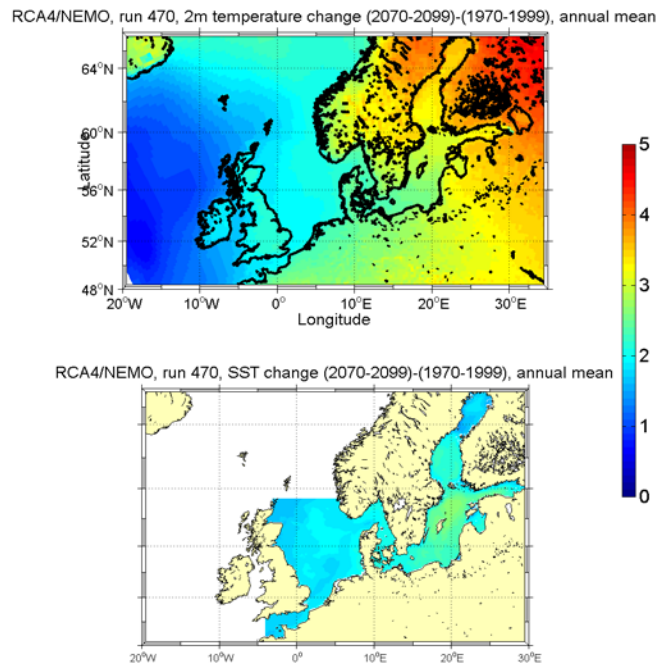


Figure 5.3.1.: Comparison of temperature changes in NEMO-Nordic/RCA4 run 470 in the far future in the atmosphere (upper panel) and in the ocean (lower panel).

Both, the Atlantic Ocean in the west and the continent in the east have an influence on the climate of the North Sea area. In the simulation of the 2 m air temperature evolution of the far future a marked transition appears between the relatively small air temperature increase west of England and stronger temperature increase over the continent in the east (Fig. 5.3.1). Over the North Sea the air temperature changes show only a slight W/E gradient. The SST changes mimic the temperature changes in the atmosphere and show not much spatial pattern in the North Sea and larger warming rates in the central Baltic Sea.

Changes in bottom temperature (Fig. 5.3.8A) are of similar magnitude than those at the sea surface (Fig. 5.3.7A). The spatial patterns are also very similar.

The time series of average SST (Fig. 5.3.9A) is showing a nearly flat time series until 2020 followed by a steady increase thereafter. The superimposed inter-annual variability is strongest in spring and summer amounting to 0.77 °C respectively 0.71 °C, averaged over the entire time series. However, the amplitude of the inter-annual variability is much weaker in the far future and only amounts to 0.52 °C and 0.54 °C. Of all seasons winter variability is the weakest and amounts only to 0.56 °C for the entire time series and decreases in the far future to 0.46 °C.

The annual cycle of SST (Fig. 5.3.10A) in the scenario run shows much colder temperatures in the reference period 1970-1999 than the corresponding hindcast run (Fig. 4.1.1A), especially in summer. While in the hindcast simulation the surface temperatures were overestimated in summer relative to observations, they are underestimated in the scenario run.

The time series of the bottom temperatures (Fig. 5.3.11A) are similar to the surface records (Fig. 5.3.9A) and only show a weak warming after 2020. The inter-annual variability is similar to the surface SST variability in winter and spring (0.44 °C, 0.51 °C) when the water column is well mixed, but much weaker in summer and fall (0.61 °C, 0.38 °C) when stratification has developed and capped the bottom layer. Variability tapers off at the end of the 21st century as already noted for the surface.

The annual cycle of bottom temperature (Fig. 5.3.12A) is thus much smaller than at the surface (Fig. 5.3.10A). The maximum temperatures are delayed by one month compared to the surface. Compared to the hindcast simulation (Fig. 4.2.5A) the temperatures are much reduced especially in summer.

5.3.2 Salinity

The SSS fields (Fig. 5.3.13A) are mostly dominated by the strong contrast between the low salinity waters along the eastern coasts of the North Sea and the high salinity waters in the northern North Sea and the English Channel. These patterns persist during the simulation. However, towards the end of the 21st century, salinities noticeably decrease. The outflow of the low salinity waters from the Baltic is pronounced, but the surface salinities are generally too low, similar to the hindcast simulation (Figs. 4.3.19A, 4.3.20A), and especially the Baltic Sea outflow is exaggerated in extent and magnitude (Figs. 5.3.14A, 5.3.15A).

The salinity biases between model results and observations at 58 °N (Fig. 4.4.13A) give the impression that the outflow is too strongly confined to the upper layers and thus influenced by the Ekman circulation as discussed in chapter 4. It therefore has a too strong zonal component when it has left the Skagerrak.

The inflow of high salinity Atlantic waters from the North occurs over the Orkney Shetland Plateau and progresses mostly southward (Fig. 5.3.14A, 5.3.15A). The strong presence of the Baltic outflow seems to hinder a transport of high salinity Atlantic Waters towards the Skagerrak. The inflow of Atlantic Waters through the English Channel is well noticeable in all seasons. It is pushed offshore after the entrance into the North Sea by coastal waters of low salinity. The magnitude of the coastal low salinity waters is exaggerated along the Dutch and Belgian coast in comparison with observations similar as in the hindcast simulations (Figs. 4.3.20A, 5.3.14A, and 5.3.15A).

The bottom salinity fields (Fig. 5.3.16A) are similar to the surface fields (Fig. 5.3.14A) in the southern North Sea but differ much in the North where the Baltic Sea outflow occupies such a large area at the surface. At depth (Fig. 5.3.16A) it can be seen that the inflow of Atlantic waters occurs in the Norwegian Trench indicated by the high salinities. A second branch of inflow is indicated over the Shetland-Orkney Plateau and follows the 100 m isobaths in the Dooley current. The comparison with observational data (Figs. 5.3.17A, 5.3.18A) shows large areas with negative salinity

bias originating from the Skagerrak. These are probably resulting from vertical mixing with the large Baltic Sea outflow plume at the surface. Salinities in the waters of Atlantic origin (Norwegian Trench, English Channel and at the north western part of the shelf) are slightly overestimated in accordance with the too salty boundary conditions supplied from MPIOM.

In the control period (1970-1999) the salinities in the scenario run (Fig. 5.3.16A) are on average only slightly higher than in the hindcast (Fig. 4.3.30A), except for the Atlantic inflows. The spatial patterns persist throughout the simulation. A light freshening is indicated at the end of the 21st century.

Salinities decrease in in the near and far future compared to the control period of 1970-1999 (Fig. 5.3.19A). The decrease in the near future is mostly small and the signal of the stronger freshening in the Baltic does not reach beyond the Kattegat. In the far future the freshening in the Baltic has increased and the signal now progresses north along the Norwegian coast within the Norwegian Coastal Current. Another zone of stronger salinity decrease is now also found in the southern North Sea. One has to keep in mind that the hydrological cycle in this simulation is prescribed from an ERA-interim run using a perpetual monthly climatology with the modification for 10% increased runoff in the Bothnian Sea and Bothnian Bay.

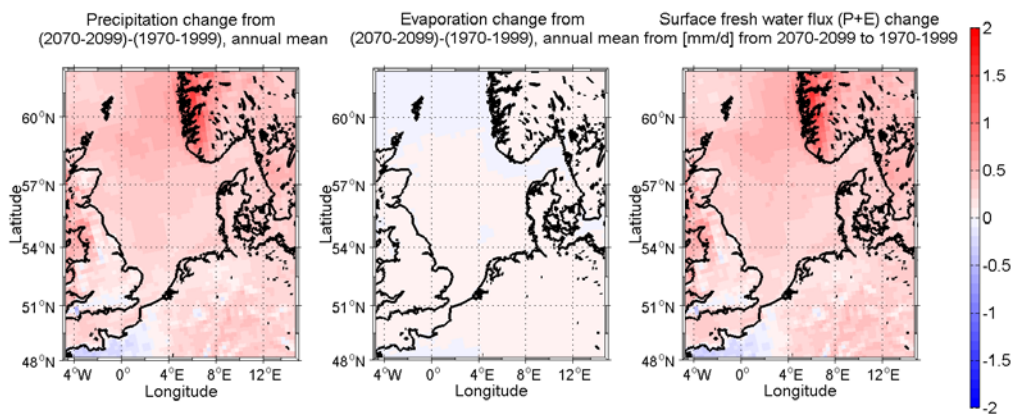


Figure 5.3.2: Far future changes of precipitation (left), evaporation rate (middle) and the net surface fresh water flux (right) based on the reference period 1970-1999.

The changes of surface fluxes of fresh water in the far future are shown in Fig. 5.3.2. They fall in line with the findings from the ENSEMBLES project that projected enhanced rainfall over northern Europe (VAN DEN LINDEN ET AL., 2009). RCA4 in the setup used here follows that general pattern and predicts increased rainfall over the entire North Sea area with strongest annual rainfall changes over the Norwegian coastal mountain range and a N/S gradient in rainfall. The net surface fresh water flux is mostly dominated by precipitation, since changes in evaporation are comparatively small. The changes in the net fresh water flux are thus showing a N/S gradient with two areas of highest positive anomalies off Norway.

Part of the salinity decrease in the far future (Fig. 5.3.19A) is corresponding to the general increase in net freshwater flux into the North Sea, but the indicating enhanced freshening in the south must also have advective sources others than river discharges, maybe from the Baltic Sea outflow.

Changes in bottom salinities are small for the near future and very homogenous (Fig. 5.3.20A). In the far future the only area of a larger salinity decrease is found along to the coast in the southern North Sea, as was also noted for the surface distributions (Fig. 5.3.18A).

While the time series of SSS (Fig. 5.3.21A) shows only long-period variability during the 20th century but no clear trend, the average salinity in the 21st century is showing a continuous decline. The inter-annual variability is strongest in summer (0.15 psu averaged over the entire time series) and remains strong in all seasons throughout the simulation.

In the annual cycle of SSS in the scenario run (Fig. 5.3.22A) a pronounced minimum occurs in summer in all three averaging periods. The period 1970-1990 in the scenario run is slightly more saline than the corresponding hindcast run (Fig. 4.2.1A). The amplitude of the seasonal cycle of both, the scenario run and the hindcast is overestimated compared to observations. The shape of the annual cycle remains unchanged in the three averaging periods and the largest salinity change between averaging periods occurs in the far future (Fig. 5.3.22A).

The time series of bottom salinity (Fig. 5.3.23A) has a smaller inter-annual variability than the surface time series (Fig. 5.3.21A). Maximum variability still occurs in summer but amounts only to 0.09 psu. It also has to be noted that the amplitude of the multi-decadal variability is reduced compared to the surface (Fig. 5.3.21A).

The annual cycle of bottom salinity is very small in all three periods (Fig. 5.3.24A) and shows an indistinct minimum in August. The annual cycle in scenario run for the period 1970-1999 is similar to the hindcast simulation (Fig. 4.2.5A).

5.3.3 Sea surface height

The SSH fields of NEMO-Nordic display a small offset of 0.6 m to the records from tide gauge. In order to make the model more compatible with observations 0.6 m was added as a constant to the simulated SSH data.

The SSH fields of the scenario run from NEMO-Nordic (Fig. 5.3.25A) demonstrate the gradual increase of water levels through the course of the century, while the spatial patterns remain basically the same. In the climate simulation this pattern does not differ significantly from that of the hindcast (not shown for the hindcast). The seasonally averaged fields show a small seasonal cycle with lowest sea levels in spring (due to seasonally low temperatures) and higher sea levels in the other seasons as a reaction to the seasonal warming of the water column and to stronger winds.

The SSH changes are small in the near future where they amount to 0.1 m and increase strongly to more than 0.26 m in the far future (Fig. 5.3.26A). A slightly higher sea level increase is noted at the eastern side of the North Sea, partly associated with changes in the Baltic outflow.

The time series of sea surface height (Fig. 5.3.27A) is nearly flat during the 20th century, followed by a strong and linear increase after 2020. The inter-annual variability is moderate during all seasons (ranging between 0.03-0.04 m averaged over the entire time series) and remains at similar levels throughout the simulation.

The annual cycle of sea surface height (Fig. 5.3.28A) has a minimum in April and a maximum in September similar to the hindcast simulation (not shown for the hindcast). The shape of the annual cycle remains the same in all three averaging periods. A small increase is noted in the near future followed by a significant increase in the far future.

5.4 Comparison of the three models

All three models are able to successfully simulate the main hydrological and the circulation features in the North Sea with comparable patterns. The comparison with observations has highlighted some inconsistencies in the individual models, but the SRES A1B scenario simulations have shown that these are not strongly influenced by the climate change signal and remain constant throughout the simulations. The comparison of the models against each other is thus focusing on the inherent differences between the models and aims at establishing the robustness of the projected climate change signals. Where possible, existing estimates of climate change signals from the literature will be used to put our results in a larger perspective and add information on the robustness.

5.4.1 Temperature

Figure 5.4.1A shows the seasonal and annual distribution of sea surface temperature from the SRES A1B scenario for all three models for the control period 1970-1999. The large scale pattern are similar since sea surface temperature is mostly driven by the atmospheric fluxes, however the advective fluxes from the boundaries also influence the horizontal distributions. The global model MPIOM for example projects a noticeable amount of advection of heat through the English Channel clearly visible in the cold seasons and in the annual mean. The regional model HAMSOM has its boundary very close to the entrance of the English Channel and the advective signal fades away more quickly than in the global model MPIOM. NEMO-Nordic on the other hand includes most of the English Channel in the simulations and gives a representation of the English Channel tongue similar to that of MPIOM.

The northern boundary of the North Sea in NEMO-Nordic is further south than in HAMSOM and it seems that this influences the circulation over the deep Norwegian

Trench, especially the recirculation of the inflowing Atlantic water over the Trench (Fig. 5.4.1A). Compared to MPIOM and HAMSOM the recirculation tongue that reaches from the north into the Skagerrak is the least pronounced. This can best be seen in summer when the inflowing Atlantic waters display a distinct temperature gradient to the warmer waters residing in the Skagerrak. Another region of larger discrepancies is found along the northern coast of Great Britain. The two regional models (HAMSOM and NEMO-Nordic) show a patch of colder waters in summer between Aberdeen and Newcastle while MPIOM is generally warmer and has cold spots that are of more local extent. Future work should include the comparison of local winds and oceanic circulation to determine the causes.

HAMSOM is the only model which simulating a significant warming for coastal areas in summer which is most pronounced in the south along the coast of Jutland (Fig. 5.4.1A). Although the vertical resolution in HAMSOM is much higher than in MPIOM, it is comparable to NEMO-Nordic which does not show similar features. The climate change signal in the atmospheric forcing fields (see chapter 5.2.1) is most pronounced in the HAMSOM/REMO simulation and forces the signal in the ocean. However, the comparison with observations indicates that the coastal warming is too strong in HAMSOM, but the horizontal resolution of 18x11km, respectively 55x28 km in the observational data sets naturally provides smoother versions of the fields. Single station data could therefore provide a more appropriate reference.

The seasonal evolution of the sea surface temperature fields (Figs. 5.4.2A, 5.4.3A) is similar in the three models and thus the fields remain at similar levels to each other, at least at the level of the superimposed climate change signal. This is true for all seasons. The features noted above are also visible in the two future periods.

In the reference period 1970-1999 (Fig. 5.4.4A) the seasonal and annual distribution of the bottom temperature in the scenario runs for all three models show similar features in the cold periods (winter and spring) when the water column is vertically mixed. But they start to diverge in summer and fall when a mixed layer on top of the water column shelters the bottom waters from the atmospheric forcing. A patch of waters in the central North Sea north of 55 °N is much cooler in the MPIOM and NEMO-Nordic simulation than in HAMSOM in the latter seasons. This patch is a remnant of the cooled waters from the winter mixing period. The differences to the observations therefore either point to discrepancies in the timing and intensity/vertical extent of restratification, to the vertical redistribution of heat or to differences in circulation. The frontal gradient between the warmer shallow southern North Sea and the deeper parts to the north in summer is well depicted in all simulations, but the gradients towards the coast are much sharper in the HAMSOM data. The other two averaging periods (Fig. 5.4.5A, 5.4.6A) show similar characteristics.

The differences in the temporal evolution of the sea surface temperature fields is best recognized in Fig. 5.4.7A and Fig. 5.4.8A, since the temporal changes are so much

smaller than the spatial gradients. In the near future (Fig. 5.4.7A) the indicated temperature increase ranges between 1 - 2.0 °C. The largest increase is simulated by HAMSOM, the smallest by NEMO-Nordic. There is not much agreement between the three models as long as small scale features are concerned. One has to keep in mind that all models are showing considerable multi-decadal variability which could influence the representation of the climate change signal, shown here as differences between 30-year means. As the temperature increases towards the far future (Fig. 5.4.8A), the differences to the control period 1970-1999 increase to 2.0-3.0 °C, depending on location and model. The order of the models remains the same as for the near future. Again there is not much agreement in the smaller scale features between the models.

The UK report on marine and coastal projections (LOWE ET AL., 2009) states warming rates of 1.5-4.0 °C for the far future depending on the location. The downscaled climate simulations in this case were made with the POLCOMS model (12 km resolution, see HOLT AND JAMES, 2001 for details about the shelf model) which was forced with atmospheric scenario forcing from the Met Office regional climate model (RCM) which in turn received its forcing from a mid-member of an perturbed physics ensemble from the global coupled model (HADCM3). The range of predicted warming is slightly higher than in our scenarios and the spatial pattern in the POLCOMS simulations point to a much stronger response of the coastal ocean. MATHIS (2013) has carried out an uncoupled climate simulation with HAMSOM. In this simulation HAMSOM was forced with results from the global ocean model MPIOM-G at the lateral boundaries to the open ocean based on the IPCC scenario run. The meteorological forcing at the air-sea interface was taken from the regional atmosphere model REMO, which provides a dynamical downscaling from this IPCC run. A bias correction method relative to ERA40 reanalysis data (UPPALA ET AL., 2005) and WOA-2001 climatology (National Oceanographic Data Center) is applied to the forcing variables, respectively. His analysis showed an increase of the annual mean air temperature over the North Sea area by about 2.1 °C, with a distinctly stronger warming trend in winter than in summer, which is reflected in an increase of annual mean SST by about +1.8 °C. The SRES A1B scenario for the time slice 2072–2097 performed with the Bergen Climate Model (BCM) has been downscaled for the marine climate in the North Sea (ÅDLANDSVIK, 2008) using the Regional Ocean Model System (ROMS). The results are compared to the 20C3M run for the time slice 1972–1997. The downscaling is done by forcing a shelf sea circulation model with atmospheric forcing and open-ocean lateral boundary conditions from the global climate model (BCM). The atmospheric forcing consists of daily averaged fields from BCM using a flux formulation based on BENTSEN AND DRANGE (2000). The results show a warming of the North Sea, with a volume average of 1.4 °C, and a mean SST change of 1.7 °C. The warming is strongest in May–June. Geographically the strongest warming in the North Sea

is found towards Skagerrak–Kattegat in the surface waters and in the central North Sea at 50 m depth.

The uncertainty range in projected SST changes has mainly been attributed to the global climate model providing the forcing. In ensemble studies utilizing different forcing GCMs as for example in the MEECE project large differences in the warming amplitude in the order of 1 °C were detected (WAKELIN ET AL., 2012, HOLT ET AL., 2010). ALHEIT ET AL. (2012) also found a strong influence of the GCM in a multi-model ensemble utilizing ROMS with warming in the North Sea between 0.3-1.1 °C in the annual mean for the near future. Uncertainties due to the regional model physics are smaller and in the order of 1/10 degrees (WAKELIN ET AL., 2012).

Seasonal dependent warming is predicted in some of the studies as well as increased warming in the coastal zone (LOWE ET AL., 2009; WAKELIN ET AL., 2012), but regional and seasonal patterns of projected changes are not consistent between the models because the properties and parameterisation of the regional models influence the regional and seasonal patterns. Potential factors affecting the regional patterns are the depth of the mixed layer, flux parameterisation and local feedbacks. Our results here have shown that the amplitude of the continental warming varies substantially between the three models, although their driving GCM is the same.

The detailed analysis of the potential feedback mechanisms in our models has to remain for future work. In our case this seems to be related to differences in the warming rates over land. SUTTON ET AL., (2007) has noted large differences in the land-sea warming ratio in the CMIP3 model ensemble with ratios ranging between 1.36-1.84. It is important to understand what factors are contributing to the warming contrast between land and sea warming because of the direct impacts on regional warming patterns and the interaction of the land-sea contrast on the atmospheric circulation on regional and local scales. The ENSEMBLES report (VAN DEN LINDEN, 2009) indicates local feedbacks between warming, relative humidity and cloud cover as possible factors contributing to different magnitudes in land surface warming. The temperature change in the bottom layer (Figs. 5.4.9A and 5.4.10A) is also showing clear effects of differences in land-sea heating with maximum temperature increase in the central and eastern North Sea in the simulations by MPIOM and HAMSOM. This is pronounced in the near future in HAMSOM and stands out strongly in the far future in the MPIOM simulations. It is an indication of the more pronounced influence from the inflowing Atlantic waters through the English Channel and from the North. In the NEMO-Nordic simulations, the spatial patterns are less distinct and warming at the bottom is generally a bit weaker.

The comparison of temporal evolution in time series of the sea surface temperature is shown in Fig. 5.4.11A. The time series of annual means show a smaller temperature increases in the NEMO-Nordic run than in MPIOM and HAMSOM, as already discussed on the basis of Fig. 5.4.7A and 5.4.8A. The small temperature changes in the

NEMO-Nordic simulation seem to be mostly due to smaller trends in spring and summer, where the temperature increase is deviating from the other models after 2020. The continental air temperature increase in the annual mean is the weakest in the NEMO-Nordic simulation and the seasonal evolution has to be analysed in addition with the atmospheric circulation to determine the factors contributing to the weak warming. There is not much agreement amongst the models on shorter timescales as one would expect in the scenario runs because of the internal variability in the atmospheric forcing fields. The amount of inter-annual variability is similar in all three models ranging between 0.5, 0.45, 0.42 °C in MPIOM, HAMSOM and NEMO-Nordic for the entire simulation and all three models indicate a decrease of inter-annual variability in the far future (2070-2099). Please note, that seasonally MPIOM displays nearly 50% more inter-annual variability in fall than HAMSOM and NEMO-Nordic (0.86, 0.57, 0.58 °C).

The annual cycle of the sea surface temperatures for the reference period 1970-1999 is very similar for all models (Fig. 5.4.12A) but shows deviations in the maximum temperature of the summer. The characteristic of the annual cycle remains similar in the near and far future with a nearly constant offset for MPIOM and NEMO-Nordic. Only HAMSOM shows a slight change in the annual cycle of sea surface temperature, with higher warming rates in late winter and spring and lower rates in summer.

The comparison of the temporal evolution of the bottom temperatures is shown in Fig. 5.4.13A. Bottom temperatures for the 20th century are very similar in all models. The bottom warming is slower in the MPIOM and NEMO-Nordic than in the HAMSOM runs. The temperature difference between HAMSOM and MPIOM and NEMO-Nordic therefore increases in time. This is probably due to the cold patch in the MPIOM and NEMO-Nordic simulation in the central North Sea and the larger amounts of heat transferred downward by HAMSOM. The differences are clearly linked to the periods when the ocean is warm (summer and fall) and the strength and timing of the development of a surface mixed layer is important for the amount of vertical mixing. The synchronization of the MPIOM and HAMSOM time series is very obvious for the annual mean time series but also for the other seasons.

The annual cycle of bottom temperature (Fig. 5.4.14A) shows significantly larger amplitude in the HAMSOM simulation than in the MPIOM or NEMO-Nordic simulations. The maximum temperature difference in the annual cycle of the models between the models occurs during the summer maximum. The corresponding hindcast runs (Fig. 4.1.5A, 4.1.6A) suggest that HAMSOM overestimates the amplitude of annual cycle. HAMSOM simulates the most pronounced seasonal variations in the warming rates with larger warming in spring and smaller warming in late summer as already noted for the sea surface temperature in Fig. 5.4.12A.

5.4.2 Salinity

Figure 5.4.15A shows the seasonal and annual distribution of the sea surface salinity from the scenario run for all three models for the reference period 1970-1999. The extent of the fresh water tongues from the river plumes in the southern North Sea and the Baltic Sea outflow is represented differently by the models. All models show a coastal zone of very low salinities along entire continental coast while the climatologies show pronounced river plumes only in the vicinity of Elbe and Rhine. The seaward extension of the river plumes is also different between the models. MPIOM salinities are too high in the German Bight compared to observations and the fresh water plume from the rivers Elbe and Weser reaches not far enough offshore. One has to keep in mind that the vertical resolution in MPIOM is not adequate to describe the river plume correctly. In the area of the river Rhine plume (about 4 °E) all three models simulate too low salinities compared to observations by. HAMSOM simulates a too large extent of the fresh water plume from Elbe and Weser in all seasons, especially in spring and fall. The other two time periods (Fig. 5.4.16A and 5.4.17A) are giving similar results.

As noted before, the representation of the Baltic outflow and its continuation north as the Norwegian Coastal Current is different between the models (Fig. 5.4.14A). In the MPIOM simulation the Norwegian Coastal Current is too narrow. This is shown as collocated patches of high and low salinity anomalies across the axes of the current when compared to observations. HAMSOM simulates at the southern tip of Norway a fresh tongue that is much reduced in extend and thus too high salinities along the northern parts of the current. It seems that too much of the low salinity waters from the Baltic is retained in the Kattegat. This can best be seen when comparing the summer fields to observations. NEMO-Nordic simulates a very wide Norwegian Coastal Current with a more pronounced zonal flow of the fresh water plume along 57 °N. The modelled outflow from the Baltic in NEMO-Nordic spreads mostly in the surface layer as can be seen from the vertical sections at 58 °N (Fig. 4.4.15AA) and, it is not reaching deep enough.

All models probably lack horizontal resolution to properly represent the mesoscale activities connected to the NCC. FOSSUM (2006) has shown in simulation of the Norwegian Coastal Current that one of its main characteristics is its high temporal and spatial variability. One of the areas where the mesoscale variability is most pronounced is the area off the southern tip of Norway where the NCC turns northward. FOSSUM (2006) found a correspondence between the seasonal dependency of the baroclinic instability and outbreak events of low-salinity water from the Skagerrak. Neither the grid size of the MPIOM in the Norwegian Trench (15x15km) nor the much higher resolution of HAMSOM and NEMO-Nordic (3-4 km) are sufficiently small enough to properly resolve the mesoscale activity (JOHANNESSEN ET AL., 1989). The role of the Baltic Sea outflow in the climate simulations deserves further investigations and also the dynamics in the area of the Norwegian Coastal Current.

WINTHER AND JOHANESSEN (2006) have therefore compensated for resolution in their model study with HYCOM by implementing a numerical scheme to improve the dynamical representation of the eddy physics.

The bottom salinity (Fig. 5.4.18A) shows different pathways of the inflowing Atlantic waters from the north. In the HAMSOM model these waters follow the topography in the Norwegian Trench less strongly than in MPIOM although it receives its boundary conditions from MPIOM. Instead HAMSOM shows a larger advection of high saline water along the British coast. NEMO-Nordic on the other hand shows a more pronounced inflow via the Shetland and Orkney plateau. The temporal changes in all models (Fig. 5.4.19A, 5.4.20A) are much smaller than the spatial gradients and are therefore almost unnoticeable in the horizontal maps for the different time slices.

It should be recalled that salinity time series showed strong multi decadal variability in all three models (see chapter 5.1-5.3) and that the signal to noise ratio for the climatic change signal is low. The 30-year means for the climatic periods critically depend on the averaging periods and can differ between the models since the temporal evolution is not isochronic. The spatial patterns and amplitudes of the salinity change discussed next in Fig. 5.4.21A and 5.4.22A for the surface salinity and in Fig. 5.4.23A and 5.4.24A for the bottom salinity should therefore also be interpreted with care.

Figure 5.4.21A shows the temporal changes in SSS in the near future as difference between the averaging period 2021-2050 and the reference period 1970-1999. The salinity changes are much smaller than 0.25 psu and differ considerably between the models. The signal to noise ratio is low for the near future when the climate signal is still weak compared to the inherent time variability. While MPIOM and NEMO-Nordic predict a small salinity decrease in the North Sea proper, HAMSOM indicates a small salinity increase of similar size for most of the deeper parts of the North Sea. The salinity evolution of the Baltic Sea Outflow is also very different between the models. In the NEMO-Nordic simulation the salinity decrease is already very pronounced in the Kattegat while it is much smaller in the MPIOM run and positive in the HAMSOM simulation.

For the far future there is more agreement about the sign of the surface salinity changes (Fig. 5.4.22A) although the magnitude still varies between the models. However, all models show that the salinity decreases in the entire North Sea. The smallest changes were found in the HAMSOM simulation and differences in the spatial patterns occur between the models. While both MPIOM and NEMO-Nordic show enhanced salinity decrease in the southern North Sea this is missing in HAMSOM. In the HAMSOM simulation river run off has been kept at the mean climatological cycle, but the MPIOM simulation with an integrated hydrodynamic model had indicated that long-term changes of run off were of minor importance. The amplitude of fresh water flux changes from the atmosphere (P-E) seems to play an important role in

changing the salt budget, as well as changes in advective transports of salt from the Atlantic and the Baltic.

The strong salinity decrease in the Baltic Sea is clearly seen in all simulations in the far future, but the pathway of the outflow in the North Sea is different in all three models (Fig. 5.4.22A). The HAMSOM simulation had prescribed the transport of the low salinity waters from the Baltic Sea as a mean climatological cycle. The chosen boundary conditions contribute to the small averaged salinity change in the North Sea deduced from the HAMSOM simulation. In the NEMO-Nordic simulation the salinity change signal is spread over a much larger area in the North Sea.

Other existing model comparisons (WAKELIN ET AL., 2012, FRIOCOURT ET AL., 2013) have attributed limited predictive capacity for the salt and fresh water changes. But comparison of model results is often complicated by unknown assumptions and approaches for terrestrial water fluxes, Atlantic boundary conditions and relaxation scheme. Based on the comparison of our small ensemble of only three models, the salinity change signal does not appear to be robust and depend on the specific model setup.

Model resolution as well as decadal variability seems to influence the sea surface salinity in the simulations. The projected changes in the North Sea to a large extent seem to depend on the evolution of salinity in the North Atlantic. GRÖGER ET AL. (2013) have diagnosed much higher salinity decay in the North Sea (~ 0.7 psu) consistent with the intensified hydrological cycle and the substantial freshening of the North Atlantic. A comparison of a low resolution uncoupled MPIOM run (GRÖGER ET AL., 2013) with the high resolution coupled MPIOM run analysed here has revealed that the sub-polar gyre extended to far eastwards and southward in the low resolution setup while the frontal position of the subarctic front is much better represented in the regionally coupled setup. Although both MPIOM simulations in low and high resolution have shown a freshening of the sub-polar gyre and a salinification of the subtropical gyre, a substantial reduction in the sub-polar salinity decrease is seen in the high resolution run. Similar results to GRÖGER ET AL. (2013) have been obtained by an uncoupled run of the HAMSOM model with boundary conditions derived from the global low resolution MPIOM_G/ECHAM5 setup (MATHIS, 2013), where a drop of the North Sea salinity by about -0.6 psu by 2100 was diagnosed. FRIOCOURT ET AL. (2012) attributed projections of the freshening in the near future to decreasing winter inflow. In addition, the projected salinity change strongly depends on the choice of the GCM (HOLT ET AL., 2012; WAKELIN ET AL., 2012). Their results showed GCM related variability in the order of 1 psu. According to their analysis the choice of the regional model and assumptions made on runoff contribute as second order effects, compared to the GCM. The regional projections from the UK Marine Report (LOWE ET AL., 2009) give a salinity decrease of ~ 0.2 psu for the North Sea

which is nearly homogeneous. There is no indication of changes in the Baltic Sea outflow in this run.

The differences in the temporal evolution of the bottom salinity fields can best be seen in Fig. 5.4.23A and Fig. 5.4.24A, since the temporal changes are again much smaller than the spatial gradients. Overall the changes in the near future in the bottom salinity fields (Fig. 5.4.23A) are small and similar to the surface fields (Fig. 5.4.21A). One has to be careful when interpreting the differences in spatial patterns between the models because of the large multi-decadal variability in this property with potentially different temporal evolutions. This holds especially true for the near future, and HAMSOM shows distinctly different patterns than MPIOM and NEMO-Nordic.

Although both shelf models, HAMSOM and NEMO-Nordic, receive their boundary conditions from MPIOM, this is only applied under inflow conditions and probably most prevailing in the deep Norwegian Trench. In this area both MPIOM and HAMSOM show weak signs of increasing salinities in the near future (Fig. 5.4.23A). NEMO-Nordic has a very southerly model boundary and indicates a very weak bottom salinity change in the near future. Even so the HAMSOM field indicates a small salinity increase over an extended area in the North these are probably not significant because of the high temporal variability.

In the far future (Fig. 5.4.24A) the climate change signal is increasing and bottom salinities decrease more strongly in all three models. Again, HAMSOM is showing different patterns while MPIOM and NEMO-Nordic are showing more similar spatial patterns.

The time series of the sea surface salinity (Fig. 5.4.25A) give very clear indications of the differences between the models. The lower salinities of the NEMO-Nordic simulation stand out among the three models, although the change signal is comparable to the MPIOM run. The levels of inter-annual variability are at similar levels for NEMO-Nordic and MPIOM but much reduced in the HAMSOM run (0.09, 0.10 and 0.06 psu for the annual means and averaged over the entire time series). Some of the larger events stand out in all three time series; however the temporal evolution seems to be independent of each other.

The low frequency variability of the North Sea SSS time series for all three models is shown in Fig. 5.4.1. Two auxiliary time series from grid points at the shelf edge that are constructed from the MPIOM scenario run have been added to represent the salinity evolution in the inflowing Atlantic water. The time series at the shelf edge at -0.8°W stands for the inflow over the Orkney-Shetland shelf while the time series at 2.2°E represents the deeper inflow at the Norwegian Trench. All models simulate a similarly strong increase until 2020. The amplitude of Atlantic salinity variability matches the multi-decadal variability of the North Sea time series for most of the 20th century, but the time series deviate after 2020.

MPIOM and NEMO-Nordic show mostly synchronous behaviour in the 21st century with only minor difference in the amplitude (Fig. 5.4.1). HAMSOM on the other hand has a more reduced amplitude than the other models. The close correspondence to the time variability in the inflowing Atlantic Ocean surface salinity seems to indicate that in HAMSOM the variability on salinity is mostly driven by changes in the Atlantic Ocean. The much larger freshening in the MPIOM and NEMO-Nordic runs is related to Baltic freshening. In HAMSOM the representation of the Baltic Outflow in the near and far future is obviously problematic. The closed model boundary in the Kattegat area results in incorrect SSH gradients over the course of the time.

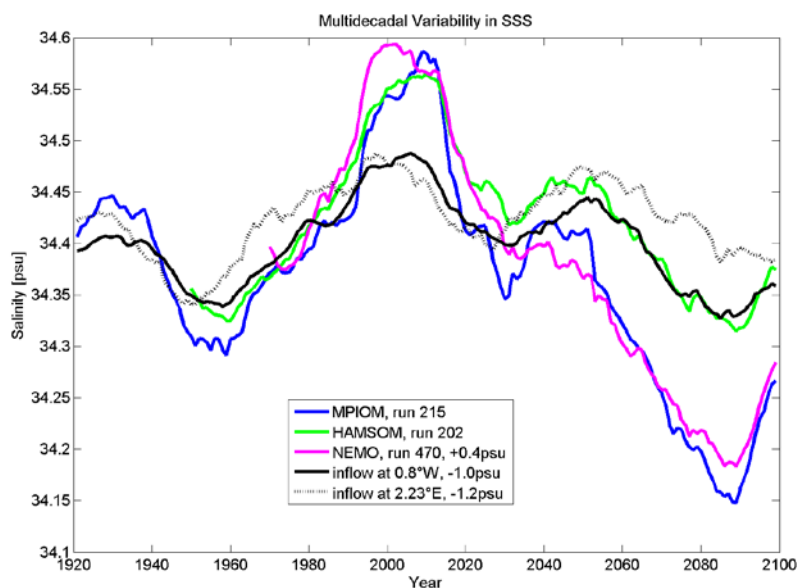


Figure 5.4.1: Smoothed time series (21year running mean applied) of average sea surface salinity from the three model simulations. An offset of +0.4 psu has been added to the NEMO-Nordic data to adjust the too low salinities. Additionally salinity time series characterizing the Atlantic inflow have included. These have been selected from single grid point data from the MPIOM run 215 at the shelf edge.

The annual cycle of salinity is also different for the three models (Fig. 5.4.26A). The annual range is much larger in NEMO-Nordic than in MPIOM and HAMSOM. As noted above in the discussion of the individual model runs, for MPIOM and HAMSOM the annual cycle is in better agreement with observations for than for NEMO-Nordic as far as range and timing of the annual cycle are concerned. None of the models indicates larger changes in the shape of the annual cycle of sea surface salinity.

The time series of bottom salinity in (Fig. 5.4.27A) give indications of the differences between the models on inter-annual and multi-decadal time scales. The amplitude of the inter-annual variability is strongest in MPIOM, and, slightly weaker in HAMSOM and NEMO-Nordic (0.08, 0.07 and 0.07 psu for the annual mean, when averaged over the entire period). But for the multi-decadal variability MPIOM shows the largest

Coupled Ocean
Atmosphere
Models

amplitude while HAMSOM is nearly flat. The annual mean time series vary out of phase between the three models.

BSH
DWD
IfM Hamburg
MPI Hamburg
SMHI
AWI

The annual cycle of the bottom salinity is very similar between HAMSOM and MPIOM, while NEMO-Nordic shows a delayed salinity minimum (Fig. 5.4.28A). But the future evolution of bottom salinity is also more similar between MPIOM and NEMO-Nordic as has already been discussed based on the spatial patterns (Fig. 5.4.23A, 5.4.24A).

5.4.3 Sea Surface height

The sea surface height fields in the reference period (1970-1999) are overall similar in all models (Fig. 5.4.29A). All of them indicate the expected increase of sea level towards the German Bight and the gradient towards the Baltic Sea with a strong upward jump in the Kattegat. The gradient towards the Baltic is strongest in MPIOM and weakest in HAMSOM. One should keep in mind that HAMSOM is bounded to the North Sea and does not include the Baltic Sea. The sea level gradients over the Norwegian trench are different between the models and thus the circulation must be different. The continuation of the low sea levels from the Atlantic into the Norwegian Trench is strongest in the MPIOM simulation and much weaker in NEMO-Nordic. These spatial features extend into the near and far future (Fig. 5.4.30A, 5.4.31A).

The temporal changes in the sea level fields for the near and far future are depicted in Fig. 5.4.32A and 5.4.33A. In these projected sea level changes only the steric fraction is included but no losses of continental ice and changes in the glacial isostatic adjustments (GIA). The three models show very good agreement in indicating for the near future a sea level rise between 0.06-0.10 m depending on location and model. This increases in the far future to 0.24-0.32 m, again dependent on model and location. (When adding the values published in the latest IPCC report for ice loss and terrestrial water storage for the far future (Tab. 5.4.1) the total sea level rise amounts to 0.55-0.63 m). The changes in the SSH in HAMSOM and NEMO-Nordic originate from the global MPIOM and are supplied as boundary condition to the two regional models. The steric changes in the North Sea are very small.

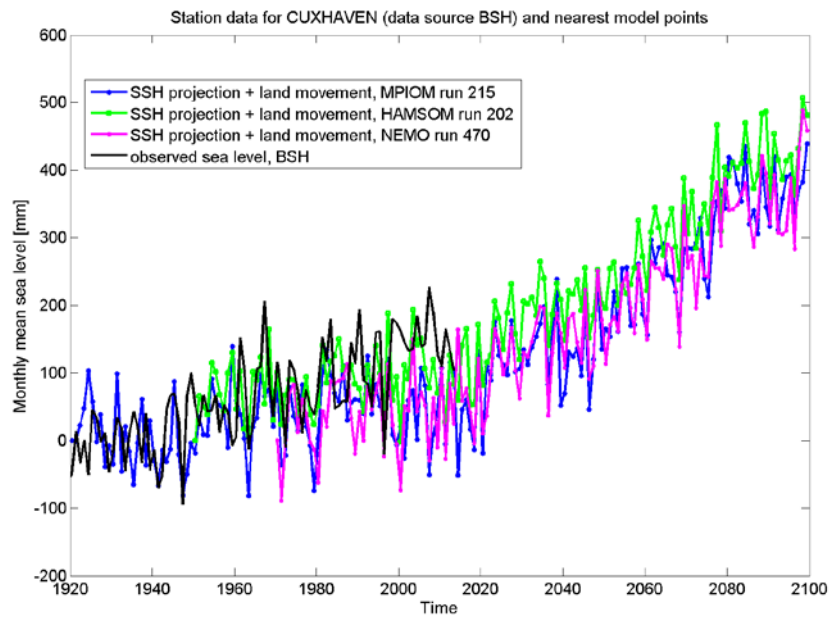
There is not much agreement amongst the model with regard to the small scale features. But HAMSOM consistently gives the higher sea level rise rates which are related to the larger warming rates. In UK marine report (LOWE ET AL., 2009) an ensemble of 11 models projects sea level rise between 0.09 and 0.48 m until 2100 for the North Sea area based on the thermal expansion. Adding ice melt and vertical land movement components to these regional expansion rates gives medium estimates of sea level rise for the English coast until 2100 between 0.21–0.68 m for London and 0.07–0.54 m for Edinburgh (5th to 95th percentile for the medium emissions scenario). The UKCP09 considered even stronger sea level increases up to 2 m in extreme scenarios for planning purposes, although increases up to 1m were considered more likely even under higher scenarios. The climate scenarios for sea level rise for the Netherlands (VAN DEN HURK ET AL., 2006) are presented for the target years 2050 and 2100 relative to 1990. The estimate of the thermal expansion is also based on the analysis of GCM runs that have been performed for the 4th IPCC Assessment Report. For the year 2050, values of global temperature rise of +1 °C and +2 °C are used, following the definition of climate change scenarios adopted for the report. The target values for 2100 are +2 °C and +4 °C respectively. They are a mixture of different SRES scenarios as different GCMs reach different global temperature rise under a

given scenario. However, given the temperature development in our models it is most appropriate to compare the sea level rise with the low scenario estimate. It agrees well with the estimates given here and the mean values are 0.09 m for 2050 and 0.24 m for 2100.

SLR 2081–2100 relative to 1986–2005 in m	A1B: Mean value, lower and upper bound [m]	RCP8.5 : Mean value, lower and upper bound [m]
Glaciers	0.14, 0.08, 0.21	0.16, 0.09, 0.23
Greenland SMB	0.05, 0.02, 0.12	0.07, 0.03, 0.16
Antarctica SMB	-0.03, -0.06, -0.01	-0.04, -0.07, -0.01
Greenland ice-sheets rapid dynamics	0.04, 0.01, 0.06	0.05, 0.02, 0.07
Antarctica ice-sheets rapid dynamics	0.07, -0.01, 0.16	0.07, -0.01, 0.16
Land water storage	0.04, -0.01, 0.09	0.04, -0.01, 0.09
Sum of components:	0.31	0.35

Tab. 5.4.1: Additional components of sea level rise not included in the simulations. Source IPCC report 2013 (IPCC, 2013),

The IPCC report (IPCC, 2013) for the first time gives regional information about sea level rise in form of selected time series. The time series at Ijmunden/NL presented in the IPCC report is located in the North Sea and can be used for comparison. The amount of sea level rise in the southern North Sea is mainly set by the large scale pattern in the North Atlantic. The steric changes in the North Sea itself are much too small to compete with the Atlantic. LANDERER ET AL. (2007) have described this effect as common for all shelf seas. Here we have constructed a virtual tide gauge record at Cuxhaven (Fig. 5.4.2). The sea level rise values shown for Ijmunden in the IPCC report are close to the global mean showing a range of sea level rise based on the CMIP5 models between 0.22 and 0.8 m and an ensemble mean of 0.45 m for all models and RCPs. Our three models show a sea level rise in the order of 0.40 m at Cuxhaven and differ only by less than 0.05 m. It should be noted that the curves in Fig. 5.4.2 are in a reference frame relative to land and about 0.05 m of the projected sea level rise is related to the subsidence of the land at the Cuxhaven tide gauge.



Coupled Ocean
Atmosphere
Models

BSH
DWD
IfM Hamburg
MPI Hamburg
SMHI
AWI

Figure 5.4.2: Projected changes of annual mean sea levels at the tide gauge station in Cuxhaven from the climate simulation of MPIOM, HAMSOM and NEMO-Nordic. The observational time series is included to denote the evolution during the 20th century. In order to make the time series comparable, the land movement at Cuxhaven has been corrected and the modelled time series have been adjusted for the GIA component taken from PELTIER'S (2004) ICE-5G model.

The time series of sea surface height in Fig. 5.4.34A shows the more pronounced increase of the sea level in the HAMSOM simulation compared to the other two models which are basically indistinguishable. The larger increase in sea surface height in the annual mean time series of HAMSOM is evident in all seasons but it seems larger in spring and in summer. The temporal variation in all models about the same which is not unexpected since the signal comes to a large part from the global steric height change which is prescribed in the two regional models from the MPIOM boundary conditions.

In the annual cycles of the three models (Fig. 5.4.35A) there is more similar between MPIOM and HAMSOM than with NEMO-Nordic. While MPIOM and HAMSOM have their minimum of sea level in March it is delayed in NEMO-Nordic. None of the model indicates larger changes in the shape of the annual cycle in the near future, but for the far future a slightly larger increase in late winter/early spring can be seen in all three models.

6 Summary and key achievements

Hindcasts:

For the first time a set of three fully coupled ocean atmosphere simulations (REMO-MPIOM, REMO-HAMSOM and RCA4-NEMO-Nordic) for the North Sea are available. While coupled coarse resolution global models of the climate system have been in use for decades, only very few studies have been published so far on fully coupled, high-resolution, ocean-atmosphere-ice-land models which resolve small regional scales and which permit local feedbacks in shelf seas such as the North Sea. It has already been shown in the past (SCHRUM ET AL., 2003) that coupling reduces the drift of parameters which arise from the accumulation of small imbalances in the heat fluxes that occur in the uncoupled system.

In this KLIWAS study simulations have been performed for today's climate and for the SRES Scenario A1B. All three coupled models are able to successfully simulate the present day main hydrological and circulation features in the North Sea. Nevertheless, a comparison of the model outputs with observations has highlighted some imperfections in the individual models, but the scenario simulations have shown that these are not strongly influenced by the climate change signal and remain the same throughout the simulations.

The comparison of the North Sea sea surface temperature annual cycle for the reference period (1971-1999) with observations and re-analyses (e.g. KNSC and BHC, the BSH observations, NCEP and ERA40) shows deviations of ± 0.2 °C between each other. A comparison of the coupled hindcast runs with the KNSC for the period 1986-1999 shows that the sea surface temperature averaged over the North Sea in HAMSOM and MPIOM is underestimated by about 1 °C in summer and overestimated by around 0.5 °C by NEMO-Nordic. In winter all models and the BSH sea surface temperature are colder than the KNSC.

The differences of the sea surface temperature between the three coupled models and the climatologies show large-scale horizontal patterns. In winter MPIOM and NEMO-Nordic show more than 0.5 °C warmer sea surface temperatures in the English Channel and adjacent regions than both, the KNSC and BHC. At the east coast the results from MPIOM are warmer in autumn and winter and here the HAMSOM results are by 2 °C warmer in summer.

The North Sea mean sea surface salinity of the BHC (1971-1999) and of MPIOM and HAMSOM (1986-1999) is about 0.1 till 0.2 psu higher than the sea surface salinity of the KNSC for most of the year. NEMO-Nordic underestimates the sea surface salinity

during the whole year with highest deviations from May to September around -0.3 till -0.4 psu.

Locally the sea surface salinity differs up to 2 psu between the climatologies and the respective model results. The simulated salinities differ distinctly in the northeastern part of the North Sea, which is influenced by the Baltic outflow and North Atlantic inflow. In the regions influenced by fresh water discharge from the rivers along the Dutch, German and Danish Coast HAMSOM and NEMO-Nordic are 1 psu fresher than the climatologies in all seasons. MPIOM is 1 psu saltier than the climatologies.

The differences between the modelled mean North Sea bottom temperature and the BHC show a similar behavior like the surface waters. In April and May all model results show temperatures 0.2 to 0.5 °C colder than the climatology. In late summer, July till October all models show 0.5 °C warmer bottom temperatures. The horizontal differences between the model results and the climatology are between ± 1 °C in winter and much higher in summer and autumn. The Atlantic water coming from the south and from the North is in winter warmer in the model results than in the climatology.

The mean North Sea bottom salinity shows a small annual cycle with amplitude in the order of 0.1 psu with its maximum in winter and a minimum in summer. The difference between the annual cycle of the bottom salinity of the model results and the annual cycle of the BHC vary between 0.05 and -0.25 psu. The differences of the bottom salinity show high horizontal variability, which show difference between ± 2 psu along the east coast.

Scenario runs:

In the KLIWAS scenario runs the temperature change signal emerges as a robust result in our ensemble. A strong long-term trend is visible in all models, even if inter-annual variability is substantial. The sea surface temperature fields of the SRES A1B scenario run from MPIOM, HAMSOM and NEMO-Nordic demonstrate a gradual increase of temperatures through the course of the simulation, whereas the spatial pattern remain basically unchanged. The temperature increase until the near future (2021-2050) is generally below 1.0 °C except for the outflow from the Baltic Sea where higher increases are visible for all seasons in MPIOM and HAMSOM. The models give comparable change signals of SST in the far future (2070-2099) between 2-3 °C but differ by 0.5 °C although the driving GCM is the same. But rates of land warming are simulated differently in the three models and seem to affect the range of the warming over sea and also the spatial patterns. In contrast to previous simulations published in the literature none of our models shows signatures of enhanced warming in the southern North Sea. The shape of the annual cycle is mostly preserved throughout the simulations, the model with the strong land warming (HAMSOM) is the only one that indicate more substantial changes in the annual cycle and shows stronger warming in late winter/spring.

The sea surface salinity fields inside the North Sea proper are dominated by the strong contrast between the low salinity waters along the eastern coasts and high salinity waters in the north and south. The spatial patterns are mostly conserved through the climate periods. The salinity change signal differs significantly between the models and it has to be considered that there is pronounced and long-periodic variability in this property which leads to a small signal to noise ratio. All models indicate a freshening of the North Sea in the far future but at different amplitudes between -0.05 and -0.25 psu. The implementation of terrestrial discharge has been different in the models, and only the MPIOM run included a hydrological model. River discharge was kept constant in the HAMSOM run, while NEMO-Nordic has runoff from an ERA-interim run where the runoff in the Bothnian Sea and the Bothnian Bay is increased by 10% at the end of the 21st century. But based on the MPIOM changes in river discharge were of minor importance for the North Sea, while strongly increasing river runoff was found for the river basins discharging into the Baltic Sea. The Baltic Sea outflow is simulated differently in all models and resolution seemed to be a problem representing the Norwegian Coastal Current (NCC) properly.

Because of the small size and shallow topography of the North Sea the climate change signal in the North Sea is mostly determined by external forces and cannot be modified strongly in the shelf sea. This requires a close examination of the climate signal in the external boundary conditions (atmospheric, oceanic and terrestrial). However, due to the coarse GCM resolution and unresolved small scales, these boundary conditions often suffer from considerable biases at regional scales. In the KLIWAS studies, the far field oceanic changes in hydrological properties and circulation are transferred from the GCM in form of boundary conditions for the North Sea. The stretched grid set-up of the global model in our ensemble (MPIOM) is offering much higher resolution (15-20 km) than standard IPCC GCM output and thus offers more realism in the boundary conditions which in turn are used by HAMSOM and NEMO-Nordic. To overcome shortcomings in the lateral boundary data previous studies have often used bias corrections, which helped to drive the hindcast climate closer to the observed climate, but had the disadvantage that the set of forcing parameters was no longer consistent. Additionally, it could not be ensured that the predictive capability of the model remains intact because of the assumptions of unchanged variability. Therefore, we have chosen not to use bias corrections in our ensemble.

The smaller salinity change in the order of 0.25 psu in our high-resolution setup of the MPIOM compared to a much larger change of 0.7 psu in the low-resolution setup by GRÖGER ET AL. (2013) has been attributed to differences in the large scale salinity evolution in the North Atlantic. Biases in the large scale circulation introduced at the lateral boundaries have been discussed in chapter 5 based on comparisons with observations and the hindcast runs.

The steric changes in the North Sea are moderate in all three models and close to the global mean. They amount to 25-28 cm in the far future and adding the contributions from global melt that are taken from the latest IPCC report increases sea level rise to the order of 60 cm. The sea level rise in the North Sea is basically set by the sea level rise at the northern shelf edge as it is determined by the larger sea level rise in the deep Atlantic. It is therefore not surprising that the sea level rise is the same in all models since the boundary conditions are taken from the MPIOM run.

Coupled Ocean
Atmosphere
Models

BSH
DWD
IfM Hamburg
MPI Hamburg
SMHI
AWI

7 Discussion and outlook

In the IPCC assessments a multi-model approach has proven successful in order to estimate uncertainties in projections of future climate conditions. This procedure has been adopted for many regional studies as well. Previous studies have identified the driving GCM being responsible for the variability in the climate change signals for example in temperature.

The KLIWAS ensemble was driven with only one GCM. In order to address the GCM uncertainty properly it is necessary to create a larger ensemble that includes other CGMs.

The A1B scenario was mandatory for the KLIWAS project and due to time constraints no other scenario could be performed with all models but part of the uncertainty is also arising from scenario choice. It is advisable in the future to include runs into the ensemble that are based on other scenarios and also scenarios that have higher climate change signals and could get closer to threshold in the climate system and feedback loops. The downscaling of the Representative Concentration Pathways (RCP) scenarios created for the IPCC AR4 has already been started and analysis of the new simulations remains future work.

From the literature review it has also become obvious that the choice of the regional model and the model biases are crucial for the regional pattern of climate change signal and the seasonality of the projected change. These patterns are of even greater importance for the subsequent impact models. Further investigations are needed that examine the influence of the domain size and the location and specification of boundary conditions for the regional model results as well as analysis of local feedbacks which are important for setting the land/sea warming ratio.

The temperature change appears as a robust signal, but the model spread is not much smaller than the amplitude of the projected change and seems to depend on the choice of the regional model.

Projected salinity changes on the other hand don't seem to be robust. An extension of the regional model across the shelf break into the Atlantic and into the Baltic Sea seems crucial to improve the model projections as well as careful consideration of the boundary conditions. Picking the boundary conditions from global GCMs is most often not based on specific consideration such as being representative of the ensemble mean changes, but more often incidental. Artificial drift and large scale spatial biases can be inherited from the driving GCM and affect RCM results. Therefore a more consistent experimental design of GCMs is needed to address the impact for the climate change signal in the North Sea.

In this report the focus was on the climatological mean, but most of the parameters also show strong variability from year to year and pronounced spatial patterns. This pronounced natural climate variability forms an additional challenge. Future work is required to study the representation of these models of natural variability in the models in the terms of spatial patterns and amplitudes. Internal variability in the RCM is not necessarily the same as in the observed climate and can impact the analysis of the climate change signal.

Coupled Ocean
Atmosphere
Models

BSH
DWD
IfM Hamburg
MPI Hamburg
SMHI
AWI

So far changes in the circulation have not been included in our assessment, but clearly play an important role. Finer coastal scales ($< 3\text{km}$) and higher frequency processes also remain for future work. Our studies presented here have focused on changes in the mean properties. Extremes have not been analysed. This would require higher temporal resolution in the model output or implementation of diagnostic parameters during the simulation.

8 List of Abbreviations and Acronyms

AMM	Atlantic Meridional mode, natural mode of climate variability
AMO	Atlantic Multidecadal Oscillation, natural mode of climate variability
AOGCM	Atmosphere Ocean General Circulation model
BCM	Bergen Climate Model
BHC	Berx and Hughes Climatology
BSH	Bundesamt für Seeschifffahrt und Hydrographie
CERFACS	Centre Européen de Recherche et de Formation Avancée en Calcul Scientifique
DWD	Deutscher Wetter Dienst
ECHAM	atmospheric general circulation model developed at Max Planck Institute of Meteorology (MPI) (C-HOPE, ECHAM4 and ECHAM5)
E-HPYE	Pan-European hydrological model
ERA40	Extended Reanalysis Envisaged
ERA_interim	Extended Reanalysis Envisaged
HAMSOM	Hamburg Shelf Ocean Model
HD-model	Hydrological Model
ICDC	Integrated Climate Data Center
IPCC	Intergovernmental Panel on Climate Change
IFM	Institut für Meereskunde
KNSC	KLIWAS North Sea Climatology
MEECE	Marine Ecosystem evolution in a changing Environment, FP7 project
MPI	Max Planck Institute
MPI-OM	Max-Planck Institute Ocean Model
NAO	North Atlantic Oscillation, natural mode of climate variability
NCC	Norwegian Coastal Current
NCEP	National Centers for Environmental Prediction
NEMO	Nucleus for European Modelling of the Ocean
NEMO-NORDIC	North Sea-Baltic Sea setup of NEMO
OASIS	Ocean Atmosphere Sea Ice Soil
POLCOMS	Proudman Oceanographic Laboratory Coastal Ocean Modelling System
RCA4	Rosby Center Regional Climate Model (Version 4)
RCM	Regional Climate Model
RCO-reanalysis	Rosby Center Ocean Model Reanalysis

REMO	Regional Model	Coupled Ocean Atmosphere Models
ROMS	Regional Ocean Modelling Sytem (University of Bergen)	
SLR	Sea Level Rise	BSH
SMHI	Swedish Meteorological and Hydrological Institute	DWD
SRES A1B	Emission scenario defined by the Special Report on Emissions Scenario	IfM Hamburg
SSH	Sea surface height	MPI Hamburg
SSS	Sea surface salinity	SMHI
SST	Sea Surface Temperature	AWI
WOA-2001	World Ocean Atlas (2001)	

9 References

- Ådlandsvik, B. (2008): Marine downscaling of a future climate scenario for the North Sea. *Tellus A*, 60(3):451–458, doi:10.1111/j.1600-0870.2008.00311.x.
- Aldrian, E., Sein, D., Jacob, D., Gates, L., and Podzun, R. (2005): Modelling Indonesian rainfall with a coupled regional model. *Climate Dynamics*, 25(1):1–17.
- Alheit, J., Ådlandsvik, B., Boersma, M., Daewel, U., Diekmann, R., Flöter, J., Hufnagl, M., Johannessen, T., Kong, S-M, Mathis, M., Möllmann, C., Peck, M., Pohlmann, T., Temming, A., Shchekinova, E., Skogen, M., Sundby, S., Wagner, C. (2012): ERANET MarinERA: Verbundprojekt 189592 ECO-DRIVE. Förderkennzeichen: 03F603, Schlußbericht. Bundesministerium für Bildung und Forschung, 53170 Bonn.
- Altema, J.J. and Lenderink, G. (2014): The influence of the North Sea on coastal precipitation in the Netherlands in the present-day and future climate, *Climate Dynamics* 42, 505-519, doi:10.1007/s00382-013-166.5-4.
- Backhaus, J. O., (1985): A three-dimensional model for the simulation of shelf sea dynamics. *Deutsche Hydrographische Zeitschrift*, 38, 165-187.
- Backhaus, J. O. (1989): The North Sea and the climate. *Dana*, 8, pp 69-82.
- Bentsen, M. and Drange, H. (2000): Parameterizing surface fluxes in ocean models using the NCEP/NCAR reanalysis data. In: *RegClim General Technical Report Volume 4* (eds T. Iversen and B. Høisaker), Norwegian Meteorological Institute, 149–158.
- Bergström, S. and Carlsson, S. (1994): River runoff to the Baltic Sea: 1950-1990, *Ambio*, 23, 280-287.
- Bersch, M., Gouretski, V. and Sadikni, R. (2013): The hydrographic climatology of the North Sea and surrounding regions, Centre for Earth System Research and Sustainability (CEN), University of Hamburg, doi: 10.1594/WDCC/KNSC_hyd_v1.0.
- Berx, B. and Hughes, B. (2009): Climatology of surface and near-bed temperature and salinity on the north-west European continental shelf for 1971–2000. *Continental Shelf Research*, Volume 29, Issue 19, 2286-2292, ISSN 0278-4343, <http://dx.doi.org/10.1016/j.csr.2009.09.006>.
- Boyer, T., Levitus, S., Garcia, H., Locarnini, R.A., Stephens, C., Antonov, J. (2005): Objective analyses of annual, seasonal and monthly Temperature and salinity for the world ocean on a 0.25° grid. *International Journal of Climatology* 25 (7), 931-945.
- Chen, X., Liu, C., O'Driscoll, K., Mayer, B., Su, J. and Pohlmann, T. (2013): On the nudging terms at open boundaries in regional ocean models. *Ocean Modelling*, 66, 14-25.
- Damm, P. E. (1997): Die saisonale Salzgehalts- und Frischwasserverteilung in der Nordsee und ihre Bilanzierung. *Berichte aus dem ZMK, Reihe B, Ozeanographie* 28, 259 pp, Hamburg, Inst. für Meereskunde.
- Déqué, M., Somot, S., Sanchez-Gomez, E., Goodess, C. M., Jacob, D., Lenderink, G. and Christensen, O.B. (2011): The spread amongst ENSEMBLES regional scenarios: regional climate models, driving general circulation models and interannual variability, *Clim Dyn*, DOI 10.1007/s00382-011-1053-x.

Dieterich, C., Schimanke, S., Wang, S., Väli, G., Liu, Y., Hordoir, R., Axell, L., Höglund, A. and Meier, H.E.M. (2013): Evaluation of the SMHI coupled atmosphere-ice-ocean model RCA4_NEMO SMHI-Report, RO 47, ISSN 0283-1112.

Egbert, G.D and Erofeeva, S.Y. (2002): Efficient inverse modelling of barotropic ocean tides. *Journal of Atmospheric and Oceanic Technology*, 19 (2), 183-204.

Elizalde, A., Sein, D., Mikolajewick, U. and Jacob, D. (2010): Technical Report: Atmosphere-ocean-hydrology coupled regional climate model. Max Planck Institute for Meteorology. Available at www.remo-rcm.de/fileadmin/user_upload/remo/UBA/pdf/TechnicalReport.pdf or by email alberto.elizalde@zmaw.de

Friocourt, Y.F., Skogen, M., Stolte, W. and Albrechtsen, J. (2012): Marine downscaling of a future climate scenario in the North Sea and possible effects on dinoflagellate harmful algal blooms, *Food Additives & Contaminants: Part A*, 29:10,1630-1646, DOI: 10.1080/19440049.2012.714079

Fossum, I. (2006): Analysis of instability and mesoscale motion off southern Norway. *J. Geophys. Res.*, Vol. 111, C08006, doi:10.1029/2005JC003228, 17pp.

Gent, P. R., Willebrand, J. McDougall, T. and McWilliams, J.C. (1995), Parameterizing eddy-induced tracer transports in ocean circulation models, *J. Phys. Oceanogr.*, 25 463–474.

Gröger, M., Maier-Reimer, E, Mikolajewicz, U., Moll, A., Sein, D (2013): NW European shelf under climate warming: implications for open ocean – shelf exchange, primary production, and carbon absorption. *Biogeosciences*, 10, 3767-3792.

Grossmann, I., Klotzbach, P.J. (2009): A review of North Atlantic modes of natural variability and their driving mechanisms. *J. Geophys. Res.-Atmos.* 114.

Gustafsson, B. G., and Andersson, H.C. (2001): Modeling the exchange of the Baltic Sea from the meridional atmospheric pressure difference across the North Sea, *J. Geophys. Res.*, 106, 19731–19744.

Hagemann, S. and Dümenil, L. (1998): A parametrization of the lateral waterflow for the global scale. *Climate Dynamics*, 14:17–31.

Hagemann, S. and Dümenil, L. (1999): Application of a global discharge model to atmospheric model simulations in the baltex region. *Nordic Hydrology*, 30, 209–230.

Hagemann, S. and Jacob, D. (2007): Gradient in the climate change signal of european discharge predicted by a multi-model ensemble. *Climatic Change*, 81, 309–327.

Hibler, W. D. (1979): A dynamic thermodynamic sea ice model *J. Phys. Oceanogr.*, 1979, 9, 815-846.

Hjøllo, S. S., Skogen, M. D. and Svendsen, E. (2009): Exploring currents and heat within the North Sea using a numerical model. *Journal of Marine Systems*, 78, 180–192, doi:10.1016/j.jmarsys.2009.06.001.

Holt, J. T. and James, I. D. (2001): An s-coordinate density evolving model of the northwest European continental shelf. 1. Model description and density structure. *J. Geophys. Res.*, Vol. 106 (C7), 14015-14034.

Holt, J., and Proctor, R. (2008): The seasonal circulation and volume transport on the northwest European continental shelf: A fine-resolution model study. *J. Geophys. Res.*, Vol. 113, C06021, doi:10.1029/2006JC004034, 20pp.

Holt, J., Wakelin, S., Lowe, J., Tinker, J. (2010): The potential impacts of climate change on the hydrography of the northwest European Continental shelf. *Progress in Oceanography* 86, 361-379.

Holt, J., Butenschon, M., Wakelin, S.L., Artioli, Y. and Allen, J.I. (2012): Oceanic controls on the primary production of the northwest European continental shelf: model experiments under recent past conditions and a potential future scenario. *Biogeosciences* 9, 97-117.

Hordoir, R., An, B.W., Haapala, J., Dieterich, C., Schimanke, S., Höglund, A. and Meier, H.E.M. (2013): BaltiX: A 3D Ocean Modelling Configuration for Baltic & North Sea Exchange Analysis. SMHI-Report, Oceanography 115, ISSN 0283-7714.

Howarth, M. J. (2001): North Sea Circulation, 1st edition of Encyclopedia of Ocean Sciences, Vol. 1, pp 1912–1921, Elsevier Ltd.

IPCC, 2013: Climate Change 2013: The Physical Science Basis. Contribution of Working Group I to the Fifth Assessment Report of the Intergovernmental Panel on Climate Change [Stocker, T.F., D. Qin, G.-K. Plattner, M. Tignor, S.K. Allen, J. Boschung, A. Nauels, Y. Xia, V. Bex and P.M. Midgley (eds.)]. Cambridge University Press, Cambridge, United Kingdom and New York, NY, USA, 1535 pp.

Jacob, D. (2001): A note to the simulation of the annual and interannual variability of the water budget over the Baltic Sea drainage basin. *Meteorology and Atmospheric Physics*, 77, 61–73.

Jacob, D. and Podzun, R. (1997): Sensitivity studies with the regional climate model REMO. *Meteorology and Atmospheric Physics*, 63:119–129.

Janssen, F., Schrum, C. and Backhaus, J.O. (1999): A climatological dataset for Temperature and Salinity in the North Sea and the Baltic Sea. *Deutsche Hydrographische Zeitung*, Supplement 9.

Johannessen, J. A., E. Svendsen, S. Sandven, Johannessen, O.M. and Lygre, K. (1989): Three-dimensional structure of mesoscale eddies in the Norwegian Coastal Current. *J. Phys. Oceanogr.*, 19, 3 – 19.

Kalnay et al. (1996): The NCEP/NCAR 40-year reanalysis project. *Bull. Amer. Meteor. Soc.*, 77, 437-470.

Kupiainen, M., Jansson, C., Samuelsson, P., Jones, C., Willén, U., Hansson, U., Ullerstig, A., Wang, S. and Döscher, R. (2013): Rossby Centre regional atmospheric model, RCA4. Rossby Center New Letter , <http://www.smhi.se/en/Research/Research-departments/climate-research-rossby-centre2-552/1.16562>.

Landerer, F.W., Jungclaus, J. H, and Marotzke, J. (2007): Regional Dynamic and Steric Sea Level Change in Response to the IPCC-A1B Scenario, *J. Phys. Oceanogr.*, Vol. 37, 296-312, doi: 10.1175/JPO3013.1.

Levitus, S. and Boyer, T.P. (1994): World Ocean Atlas 1994, Vol. 4: temperature, NOAA Atlas NESDIS 4, 117pp.

Lindström, G., Pers, C.P., Rosberg, R., Strömqvist, J., Arheimer, B. (2010): Development and test of the HYPE (Hydrological Predictions for the Environment) model – A water quality model for different spatial scales. *Hydrology Research* 41.3-4:295-319.

Liu, Y., Meier, H. E. M. and Axell, L. (2013), Reanalyzing temperature and salinity on decadal time scales using the ensemble optimal interpolation data assimilation method and a 3-D ocean circulation model of the Baltic Sea, *J. Geophys. Res. Oceans*, 118, 5536–5554, doi: [10.1002/jgrc.20384](https://doi.org/10.1002/jgrc.20384)

Loewe, P., Klein, H., Frohse, A., Schulz, A. and Schmelzer, N. (2013): Meeresphysik, Temperatur, p. 142-155, in: Loewe, P., H. Klein and S. Weigelt-Krenz (eds.), System Nordsee, 2006 & 2007: Zustand und Entwicklungen], Berichte des BSH, Nr. 49, Bundesamt für Seeschifffahrt und Hydrographie, Hamburg und Rostock, 2013.

Lowe, J. A., Howard, T. P., Pardaens, A., Tinker, J., Holt, J., Wakelin, S., Milne, G., Leake, J., Wolf, J., Horsburgh, K., Reeder, T., Jenkins, G., Ridley, J., Dye, S., Bradley, S. (2009): UK Climate Projections science report: Marine and coastal projections. Met Office Hadley Centre, Exeter, UK, 99pp.

- Maier-Reimer, E. (1997): Design of a closed boundary regional model of the Arctic Ocean, paper presented at Workshop on Polar Processes in Global Climate, Bull. Amer. Meteor. Soc., 13–15 Nov. 1996.
- Majewski, D., Doms, G., Edelmann, W., Gertz, M., Hanisch, T., Heise, E., Link, A., Prohl, P., Schaettler, U. and Ritter, B. (1995): Documentation of the EM/DM System, Deutscher Wetterdienst. Technical Report, Offenbach.
- Marsland, S. J., Haak, H., Jungclaus, J. H., Latif, M., and Röske, F. (2003): The Max Planck Institute global ocean/sea ice model with orthogonal curvilinear coordinates. *Ocean Modelling*, 5(2), 91–127.
- Mathis, M., (2013): Projected Forecast of Hydrodynamic Conditions in the North Sea for the 21st Century. PhD Thesis, University of Hamburg, 182 pp.
- Meier, H. E. M., and Kauker, F (2003): Modeling decadal variability of the Baltic Sea: 2. Role of freshwater inflow and large-scale atmospheric circulation for salinity, *J. Geophys. Res.*, 108(C11), 3368, doi:10.1029/2003JC001799.
- Mikolajewicz, U. (2005): Simulating arctic sea ice variability with a coupled regional atmosphere-ocean-sea ice model. *Meteorologische Zeitschrift*, 14, No.6, 793–800.
- OSPAR Commission (2000): Quality Status Report 2000, Region II – Greater North Sea. OSPAR Commission, London. 136 + xiii pp.
- Peltier, W.R. (2004): Global glacial isostasy and the surface if the ice-age earth: The ICE-5G (VM2) Model and GRACE, *Ann. Rev. Earth Planet. Sci.*, Vol. 32, 111–49, doi: 10.1146/annurev.earth.32.082503.144359.
- Pohlmann, T. (1996): Predicting the thermocline in a circulation model of the North Sea .1. Model description, calibration and verification. *Continental Shelf Research*, 16 (2), 131-146.
- Pohlmann, T. (2006): A meso-scale model of the central and southern North Sea: Consequences of an improved resolution. *Continental Shelf Research*, Vol. 16, No. 2, 131-146.
- Rauscher S.A., Coppola E., Piani C. and Giorgi, F. (2009): Resolution effects on regional climate model simulations of seasonal precipitation over Europe. *Climate Dynamics*, Vol. 32, 2-3, 273-285, doi:10.1007/s00382-009-0607-7.
- Roeckner, E., Arpe, K., Bengtsson, L., Christoph, M., Claussen, M., Dümenil, L., Esch, M., Giorgetta, M., Schlese, U. and Schulzweida, U. (1996): Report no.218 the atmospheric general circulation model echam4: Model description and simulation of present day climate., Technical report, Max Planck Institute for Meteorology.
- Schrum, C. (2001): Regionalization of climate change for the North Sea and Baltic Sea. *Climate Research*, 18 (1-2), 31-37.
- Schrum, C., Huebner, U., Jacob, D., Podzun, R. (2003): A coupled atmosphere/ice/ocean model for the North Sea and the Baltic Sea. *Climate Dynamics*, 21 (2), 131-151.
- Sein, D.V., M. Gröger, Maier-Reimer, E. and Mikolajewicz, U. (2012): Modeling anthropogenic Climate Change of the northwest European Shelves and the northeast Atlantic. *Geophysical Research Abstracts Vol. 14*, EGU2012-8828.
- Stammer, D., Bersch, M., Sadikni, R., Jahnke-Bornemann, A. Gouretski, V., Hinrichs, I., Heinrich, H., Klein, B., Klein, H., Schade, N., Rosenhagen, G., Tinz, B., Lefebvre, Ch. (2014): Die KLIWAS Nordseeklimatologie für ozeanographische und meteorologische In-Situ Daten, KLIWAS Schriftenreihe Band 59/2014, doi:10.5675/Kliwas_59/2014_Nordseeklimatologie.

Su, J., Yang, H., Pohlmann, Th., Ganske, A., Klein, B., Klein, H. and N. Narayan (2014): A regional coupled atmosphere-ocean model system REMO/HAMSOM for the North Sea. *Kliwas Schriftenreihe*, Band 60/2014, doi: 10.5675/Kliwas_60/2014_REMO_HAMSOM.

Sutton R.T., Dong B.-W. and Gregory J.M. (2007): Land/sea warming ratio in response to climate change: IPCC AR4 model results and comparison with observations. *Geophysical Research Letters*. 34, L02701, doi:10.1029/2006 GL028164.

Uppala, S.M., Kallberg, P.W., Simmons, A.J., Andrae, U., Da Costa Bechtold, V., Fiorino, M., Gibson, J.K., Haseler, J., Hernandez, A., Kelly, G.A., Li, X., Onogi, K., Saarinen, S., Allan, R.P., Andersson, E., Arpe, K., Balmaseda, M.A., Beljaars, A.C.M., Van De Berg, L., Bidlot, J., Bormann, N., Caires, S., Chevallier, F., Dethof, A., Dragosavac, M., Fisher, M., Fuentes, M., Hagemann, S., Holm, E., Hoskins, B.J., Isaksen, L., Janssen, P.A.E.M., Jenne, R., McNally, A.P., Mahfouf, J.F., Morcrette, J.J., Rayner, N.A., Saunders, R.W., Simon, P., Sterl, A., Trenberth, K.E., Untch, A., Vasiljevic, D., Viterbo, P., and Woollen, J. (2005): The ERA-40 re-analysis. *Quarterly Journal of the Royal Meteorological Society*, 131, 2961-3012.

Valcke, S. (2012): The OASIS3 coupler: a European climate modelling community software;. *Geoscientific Model Development Discussions*, Vol. 5, 2012, 2139-2178, doi:10.5194/gmd-5-2139-2012.

van den Hurk, B., Klein Tank, A., Lenderink, G., van Ulden, A., van Oldenborgh, G. J., Katsman, C., van den Brink, G., Keller, F., Bessembinder, J., Burgers, G., Komen, G., Hazeleger, W. and Drijfhout, S. (2006): KNMI Climate Change Scenarios 2006 for the Netherlands. KNMI Scientific Report WR 2006-01, 82 pp.

van der Linden P. and Mitchell, J.F.B. (eds.) (2009): ENSEMBLES: Climate Change and its Impacts: Summary of research and results from the ENSEMBLES project. Met Office Hadley Centre, FitzRoy Road, Exeter EX1 3PB, UK. 160pp.

Wakelin, S., Daewel, U., Schrum, C., Holt, J., Butenschön, M., Artioli, Y., Beecham, J., Lynam, C. and Mackinson, S. (2012): MEECE deliverable D3.4: Synthesis report for Climate Simulations Part 3: NE Atlantic / North Sea.

Winsor, P., Rodhe, J. and Omstedt, A. (2001): Baltic Sea ocean climate: An analysis of 100 yr of hydrographic data with focus on the freshwater budget, *Clim. Res.*, 18, 5 – 15.

Winther, N. G., and Johannessen, J. A. (2006): North Sea circulation: Atlantic inflow and its destination. *J. Geophys. Res.*, 111, C12018, doi:10.1029/2005J.C003310, 12pp.

Woodworth, P.L. and R. Player (2003): The Permanent Service for Mean Sea Level: an update to the 21st century. *Journal of Coastal Research*, 19, 287-295.

Zorita, E., and Laine, A. (2000): Dependence of salinity and oxygen concentrations in the Baltic Sea on large-scale atmospheric circulation, *Clim. Res.*, 14, 25– 41.

10 Appendix 1: Figures from the validation analysis in chapter 4

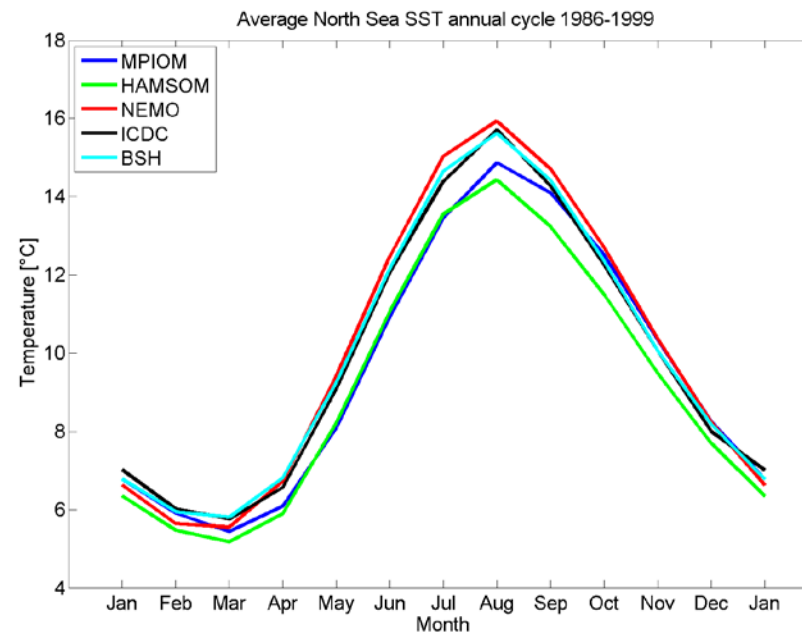


Figure 4.1.1A: The mean annual cycle of sea surface temperatures [°C] for MPIOM run 253 (blue), HAMSOM 201 (green), NEMO-Nordic run 477 (red), BSH observations (cyan) and the KNSC (ICDC, black) over the time period 1986-1999. The means are representing averages over the North Sea area.

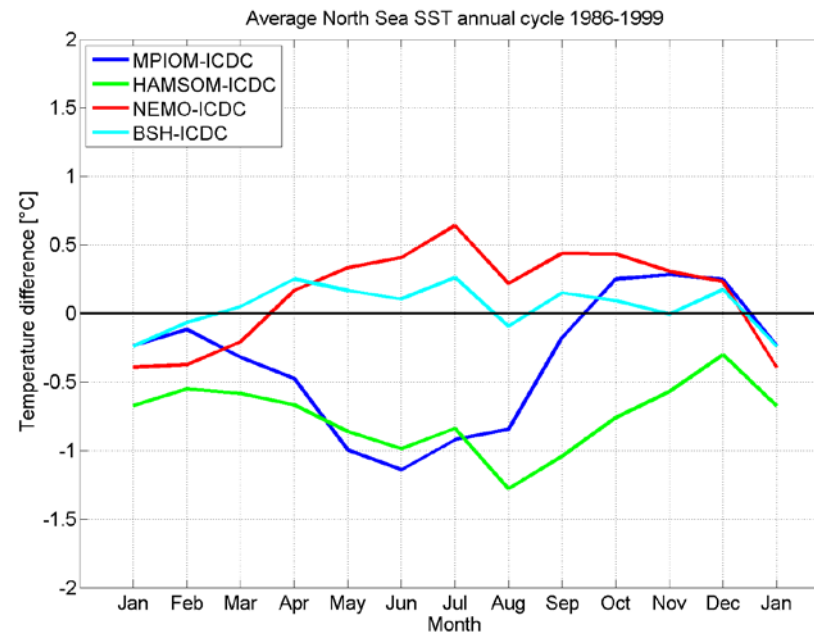


Figure 4.1.2A: Difference of the mean annual cycle of sea surface temperatures between KNSC for the time period 1986-1999 and modelled data [°C]: MPIOM run 253 (blue), HAMSOM 201 (green), NEMO-Nordic run 477 (red), BSH observations (cyan). The means are representing averages over the North Sea area.

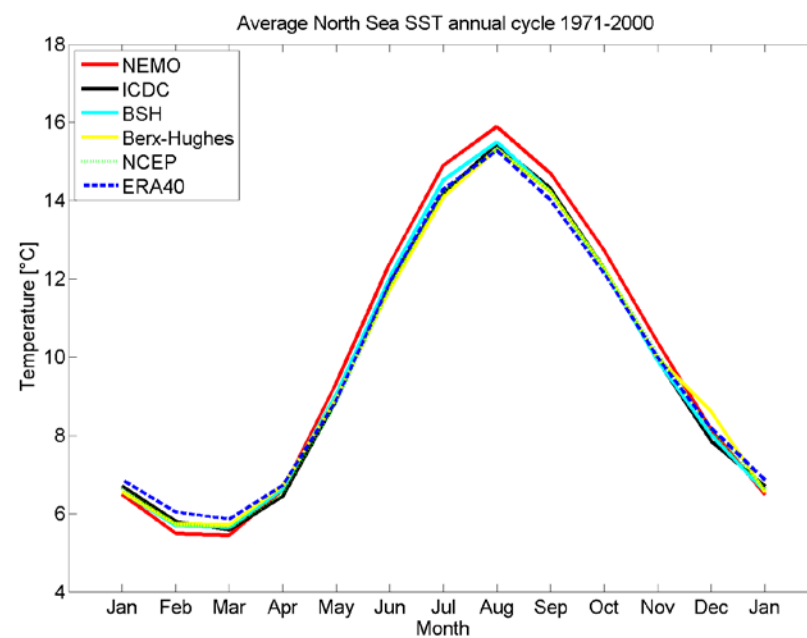


Figure 4.1.3A: The mean annual cycle of sea surface temperatures [°C] for NEMO-Nordic run 477 (red), KNSC (ICDC, black), BSH observations (cyan), BHC (yellow), NCEP (green) and ERA40 (blue) over the time period 1971 till 2000. The means are representing averages over the North Sea area.

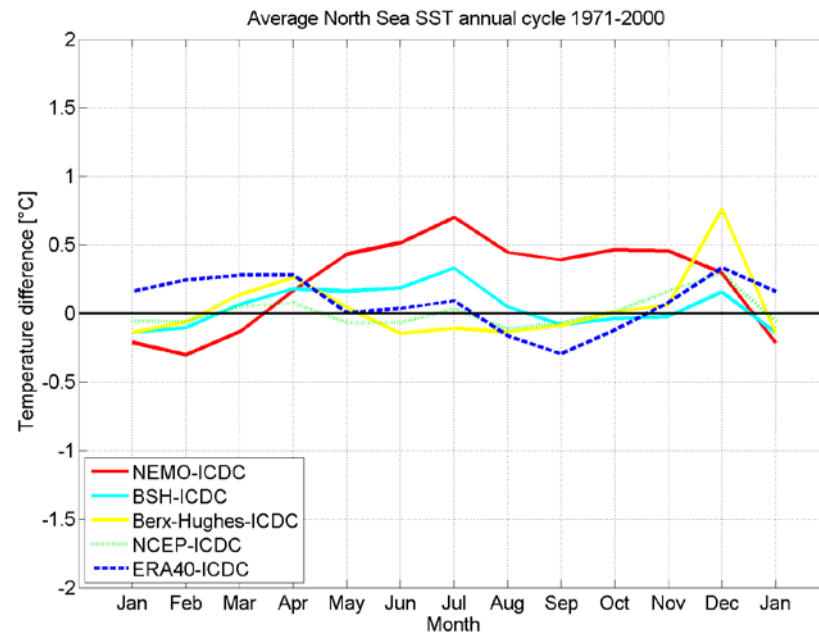


Figure 4.1.4A: Difference of the mean annual cycle of the sea surface temperatures between KNSC for the time period 1971-2000 and modelled data [°C]: NEMO-Nordic run 477 (red), BSH observations (cyan), BHC (yellow), NCEP (green), ERA40 (blue). The means are representing averages over the North Sea area.

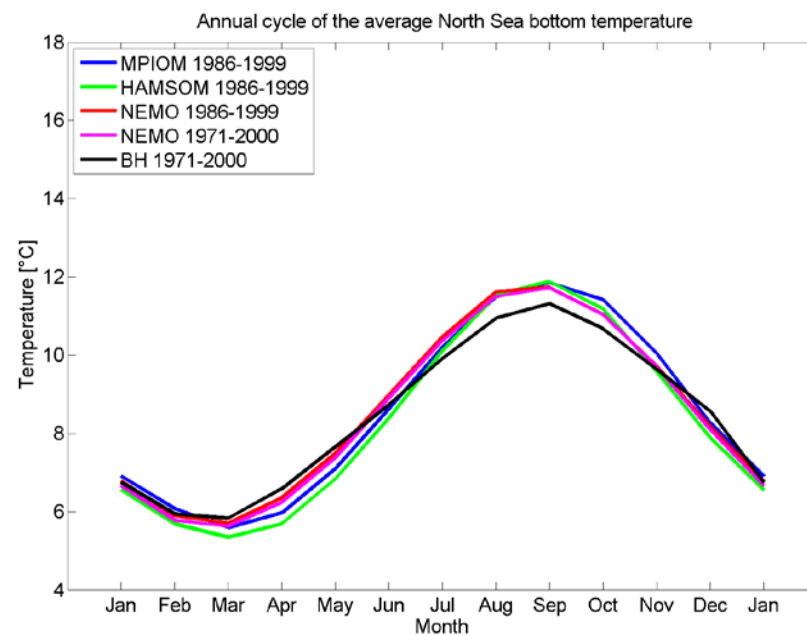


Figure 4.1.5A: The mean annual cycle of bottom temperatures [°C]: MPIOM run 253 1986-1999 (blue), HAMSOM run 201 1986-1999 (green), NEMO-Nordic run 477 1986-1999 (red), NEMO-Nordic run 477 1971-2000 (magenta), BHC 1971-2000 (black). The means are representing averages over the North Sea area.

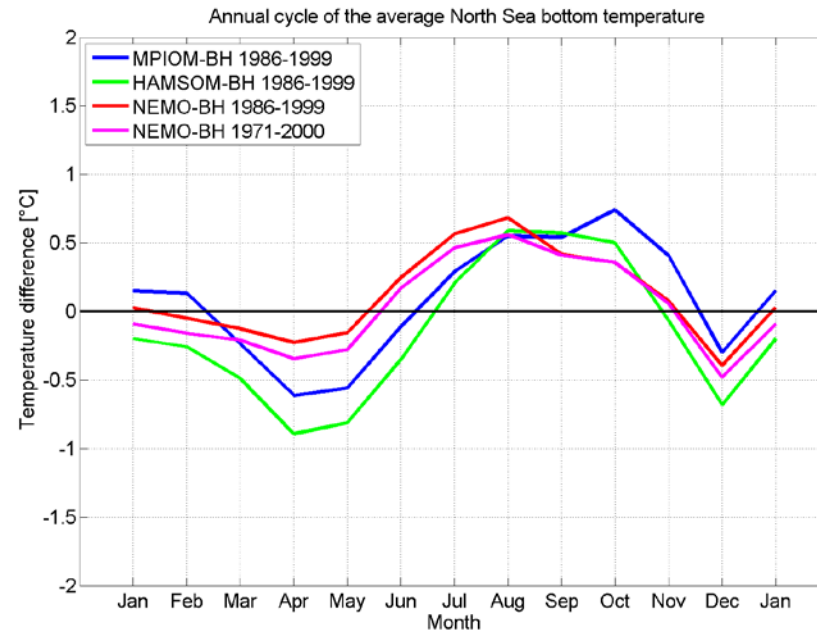


Figure 4.1.6A: Difference of the mean annual cycle of the bottom temperatures between BHC 1971-2000 and modelled data [°C]: MPIOM run 253 1986-1999 (blue), HAMSOM run 201 1986-1999 (green), NEMO-Nordic run 477 1986-1999 (red), NEMO-Nordic run 477 1971-2000 (magenta). The means are representing averages over the North Sea area.

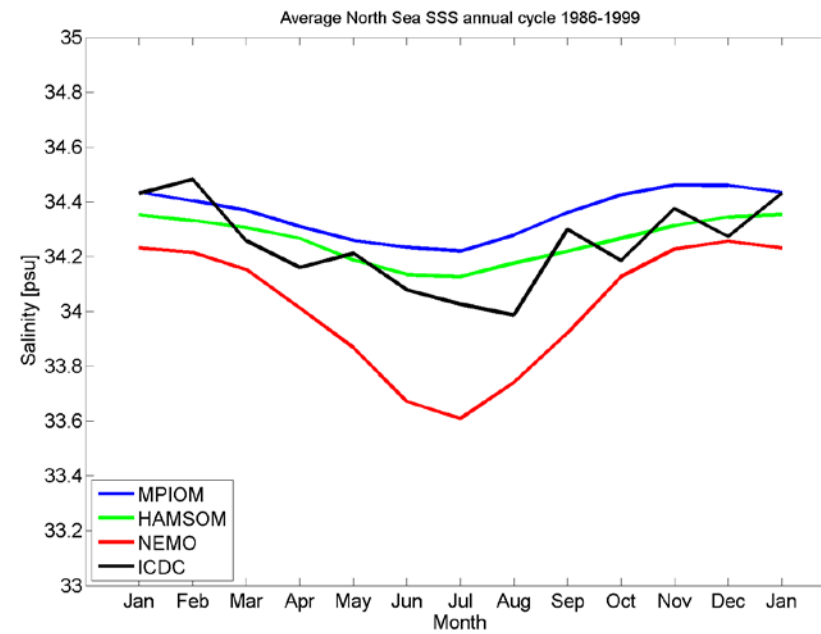


Figure 4.2.1A: The mean annual cycle of sea surface salinity [psu] for MPIOM run 253 (blue), HAMSOM 201 (green), NEMO-Nordic run 477 (red) and KNSC (black) over the time period 1986-1999. The means are representing averages over the North Sea area.

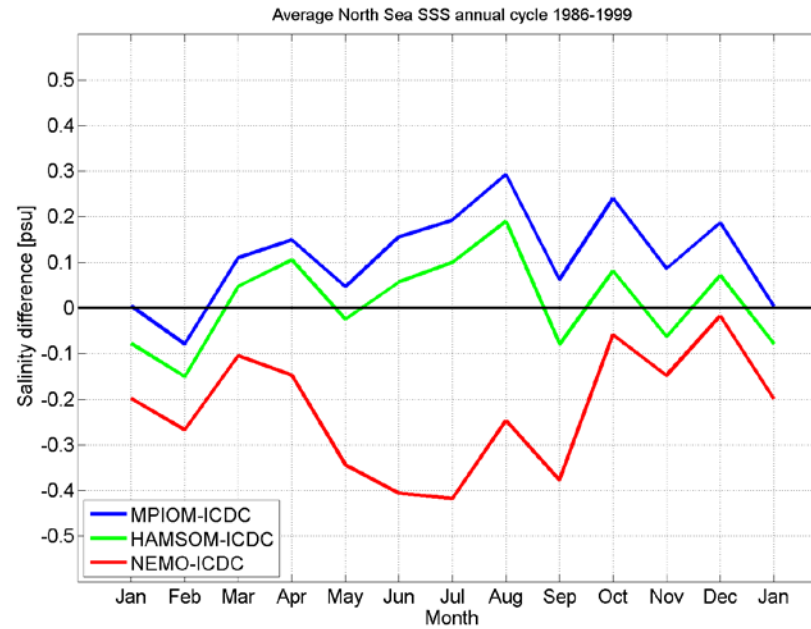


Figure 4.2.2A: Difference of the mean annual cycle of sea surface salinity [psu] between KNSC for the time period 1986-1999 and modelled data: MPIOM run 253 (blue), HAMSOM 201 (green), and NEMO-Nordic run 477 (red). The means are representing averages over the North Sea area.

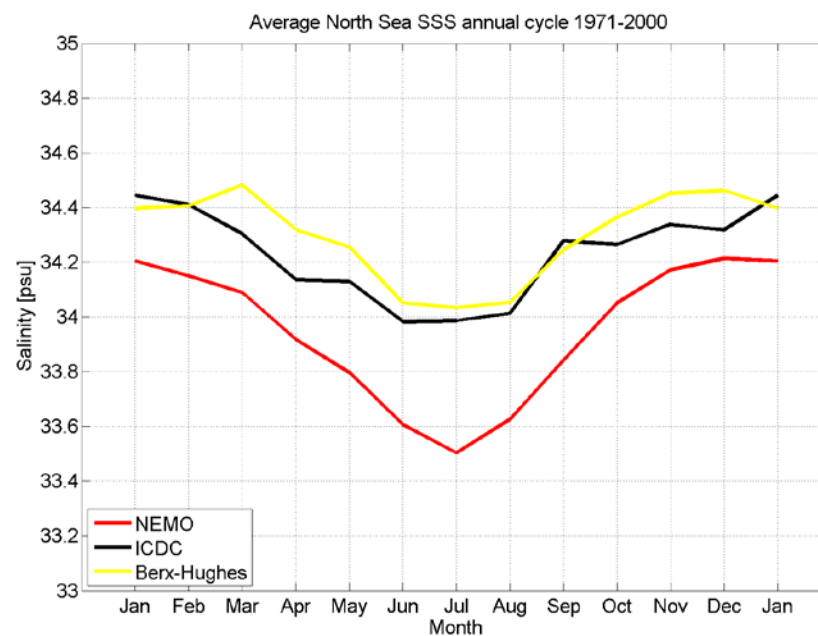


Figure 4.2.3A: The mean annual cycle of sea surface salinity [psu] for NEMO-Nordic run 477 (red), KNSC (black), BHC (yellow) over the time period 1971 till 2000. The means are representing averages over the North Sea area.

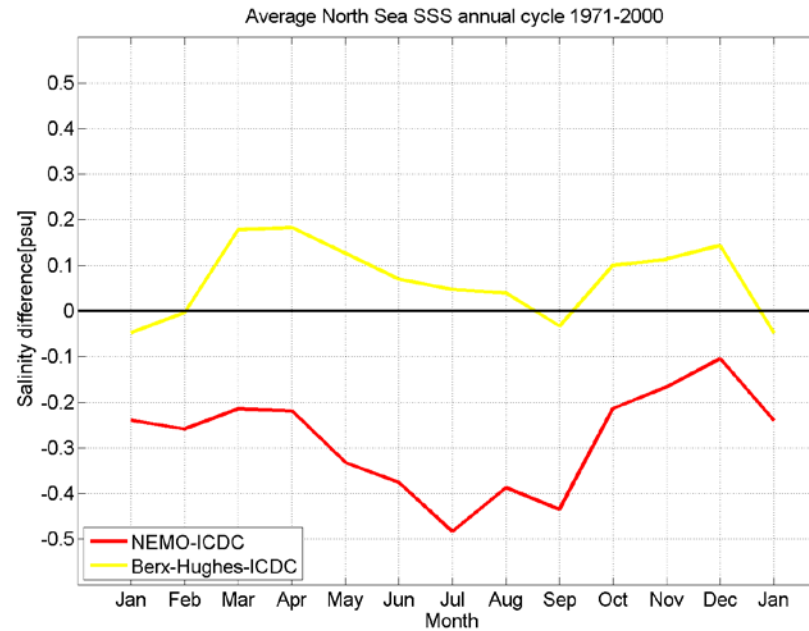


Figure 4.2.4A: Difference of the mean annual cycle of the sea surface salinity [psu] between KNSC for the time period 1971-2000 and modelled data: NEMO-Nordic run 477 (red), BHC (yellow). The means are representing averages over the North Sea area.

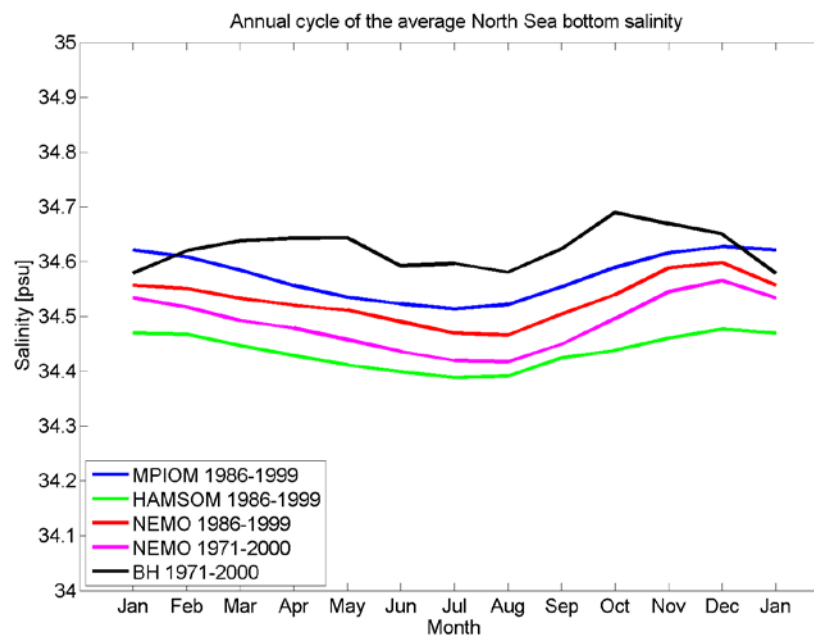


Figure 4.2.5A: The mean annual cycle of bottom salinity [psu] for MPIOM run 253 1986-1999 (blue), HAMSOM 1986-1999 (green), NEMO-Nordic run 477 1986-1999 (red), NEMO-Nordic run 477 1971-2000 (magenta), BHC (black). The means are representing averages over the North Sea area.

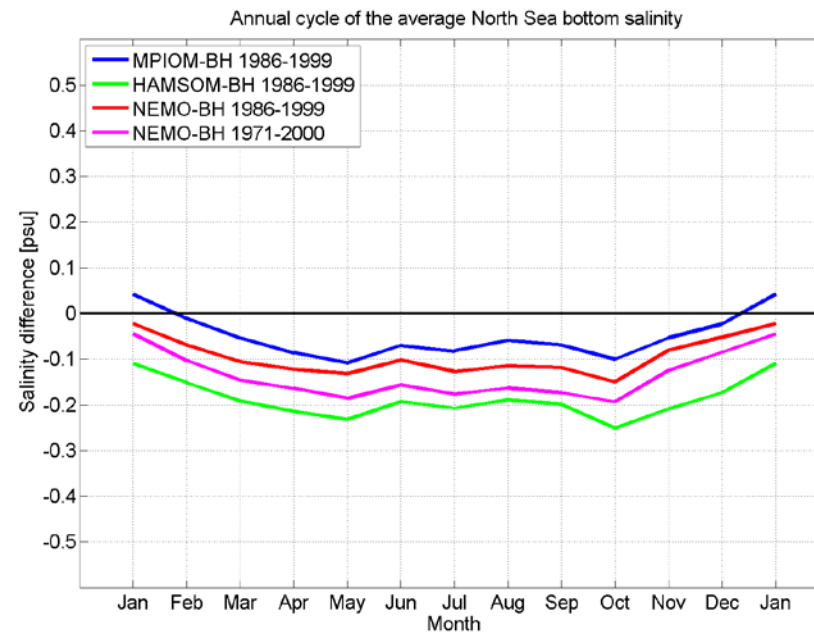


Figure 4.2.6A: Difference of the mean annual cycle of the sea surface salinity [psu] between BHC for the time period 1971-2000 and modelled data: MPIOM run 253 1986-1999 (blue), HAMSOM 1986-1999 (green), NEMO-Nordic run 477 1986-1999 (red), NEMO-Nordic run 477 1971-2000 (magenta). The means are representing averages over the North Sea area.

Seasonal and annual mean sea surface and bottom Temperature and Salinity

Coupled Ocean
Atmosphere
Models

BSH
DWD
IfM Hamburg
MPI Hamburg
SMHI
AWI

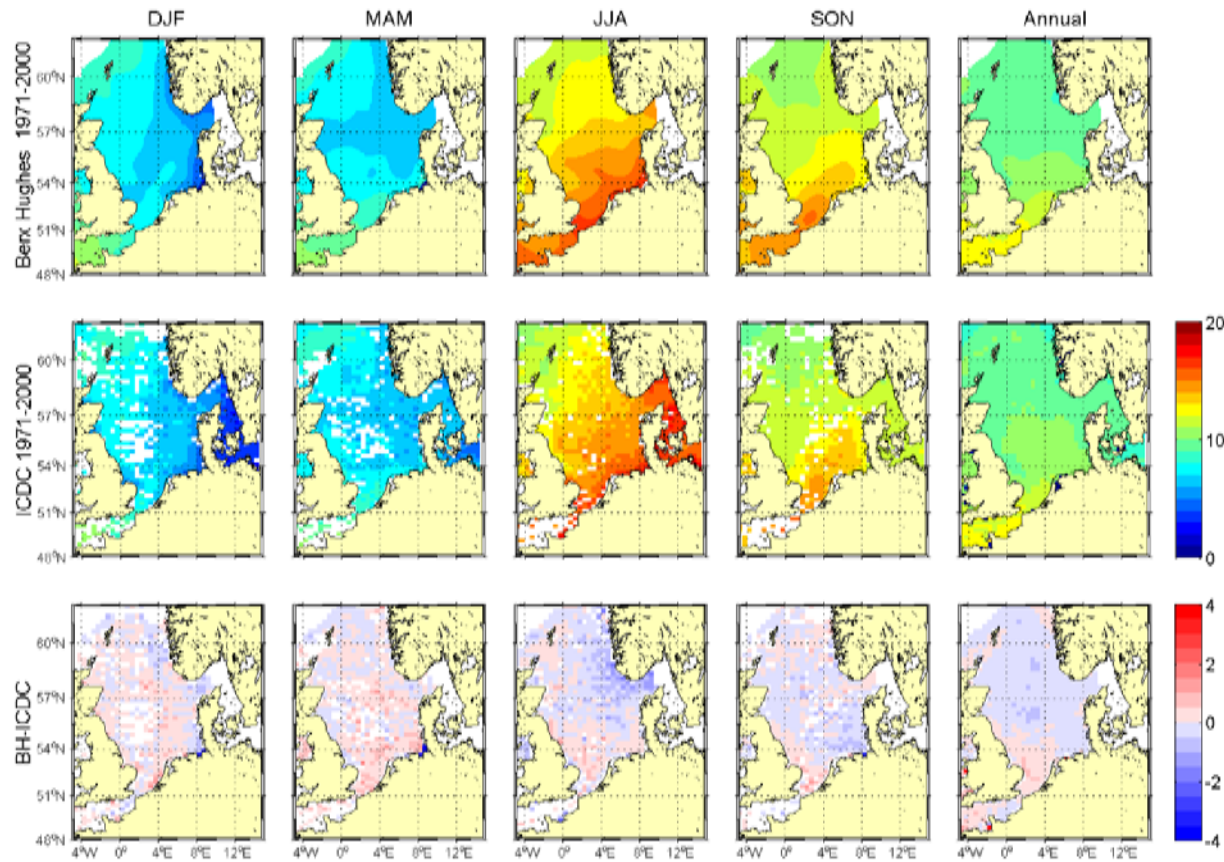


Figure 4.3.1A: Seasonal and annual means of sea surface temperature [°C] from BHC (upper row) and KNSC (ICDC, middle row) for the period 1971-2000 and their differences (lower row).

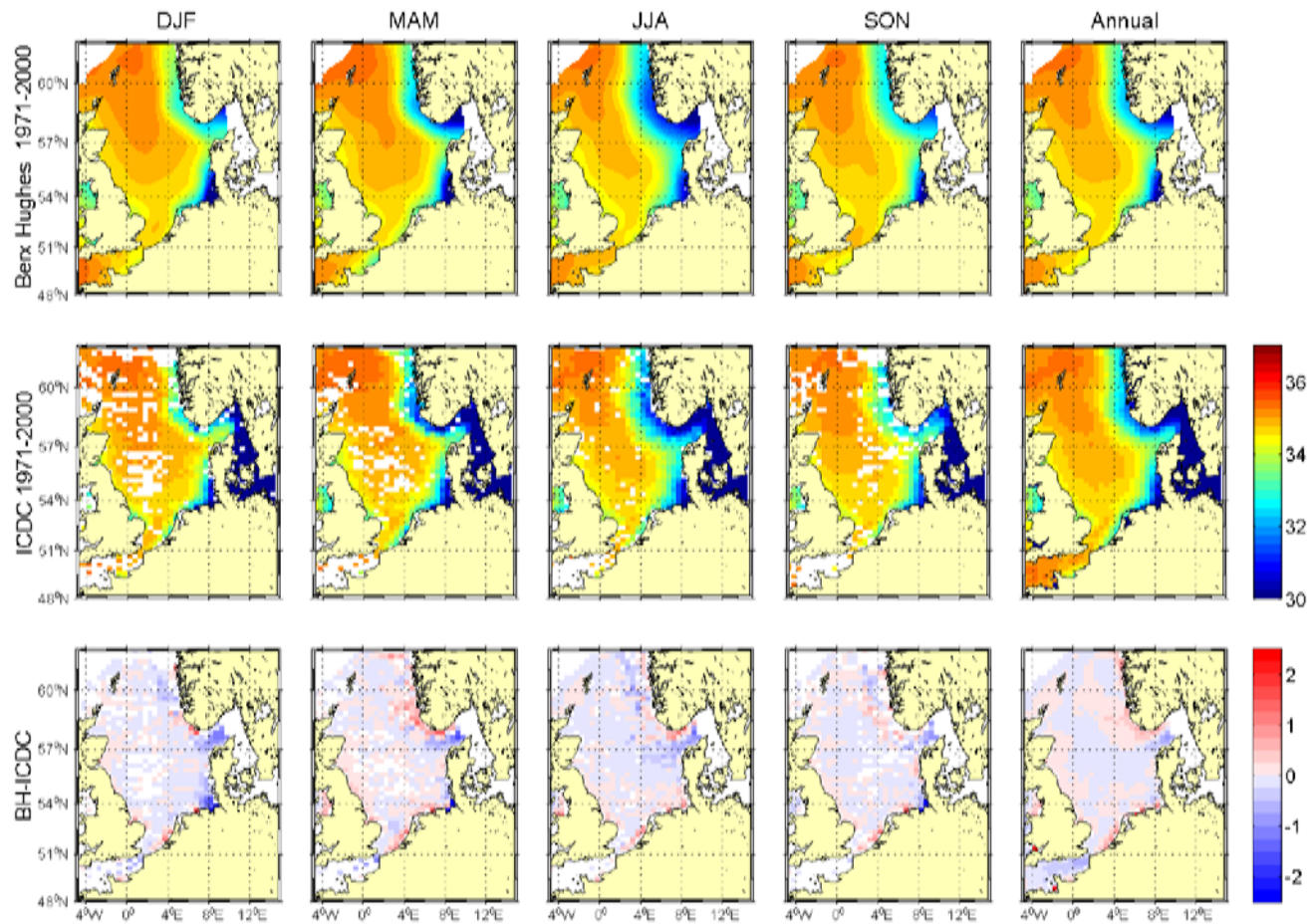


Figure 4.3.2A: Seasonal and annual means of sea surface salinity [psu] from BHC (upper row) and KNSC (ICDC, middle row) for the period 1971-2000 and their differences (lower row).

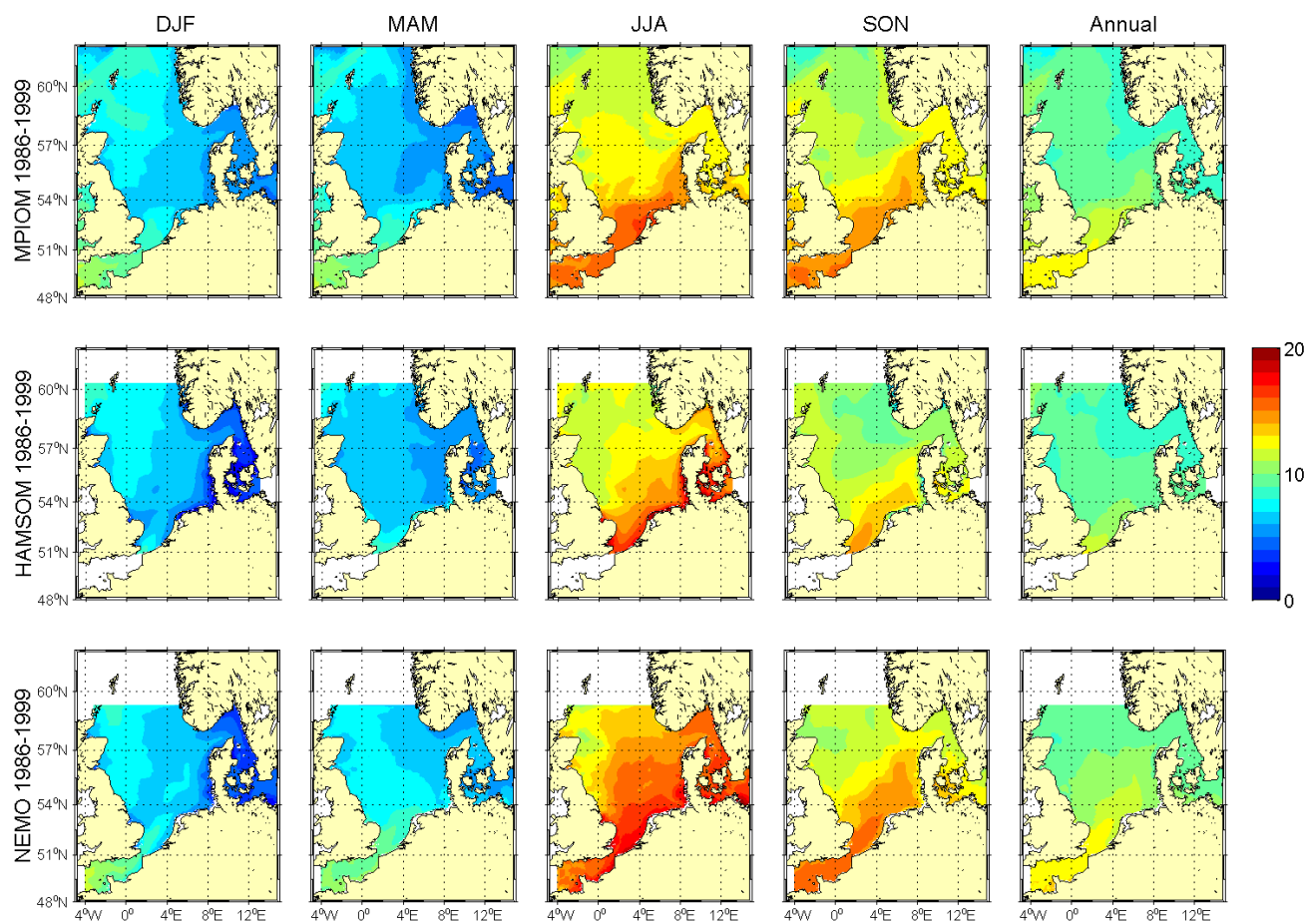


Figure 4.3.3A: Seasonal and annual means of sea surface temperature [°C] averaged over the period 1986-1999. The mean SST results from MPIOM (run 253) are presented in the upper row, in the middle row from HAMSOM (run 201) and in the lower row from NEMO-Nordic (run 477).

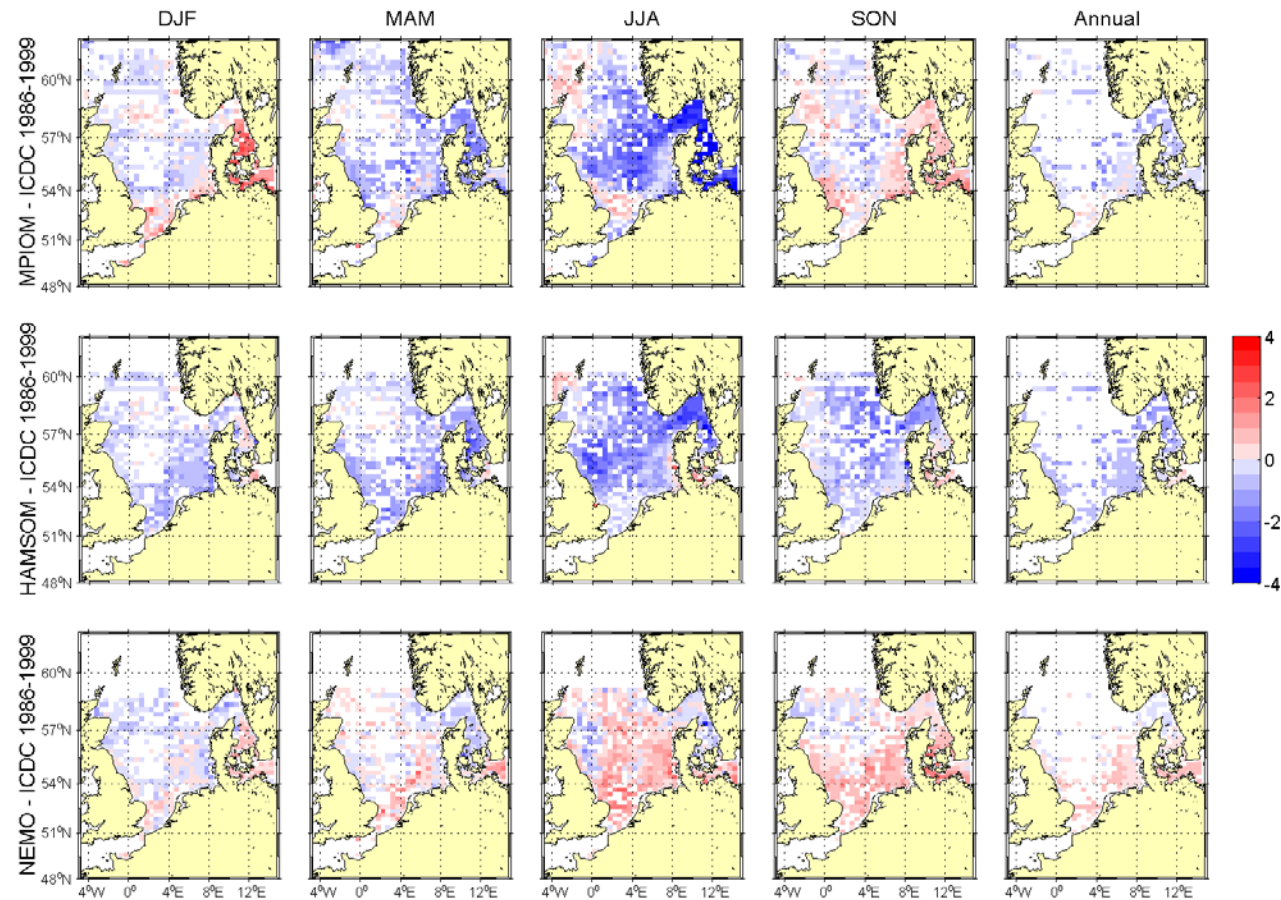


Figure 4.3.4A: Differences of modelled seasonal and annual means of sea surface temperature [°C] averaged over the period 1986-1999 to the KNSC: MPIOM (run 253, upper row), HAMSOM (run 201, middle row) and NEMO-Nordic (run 477, lower row).

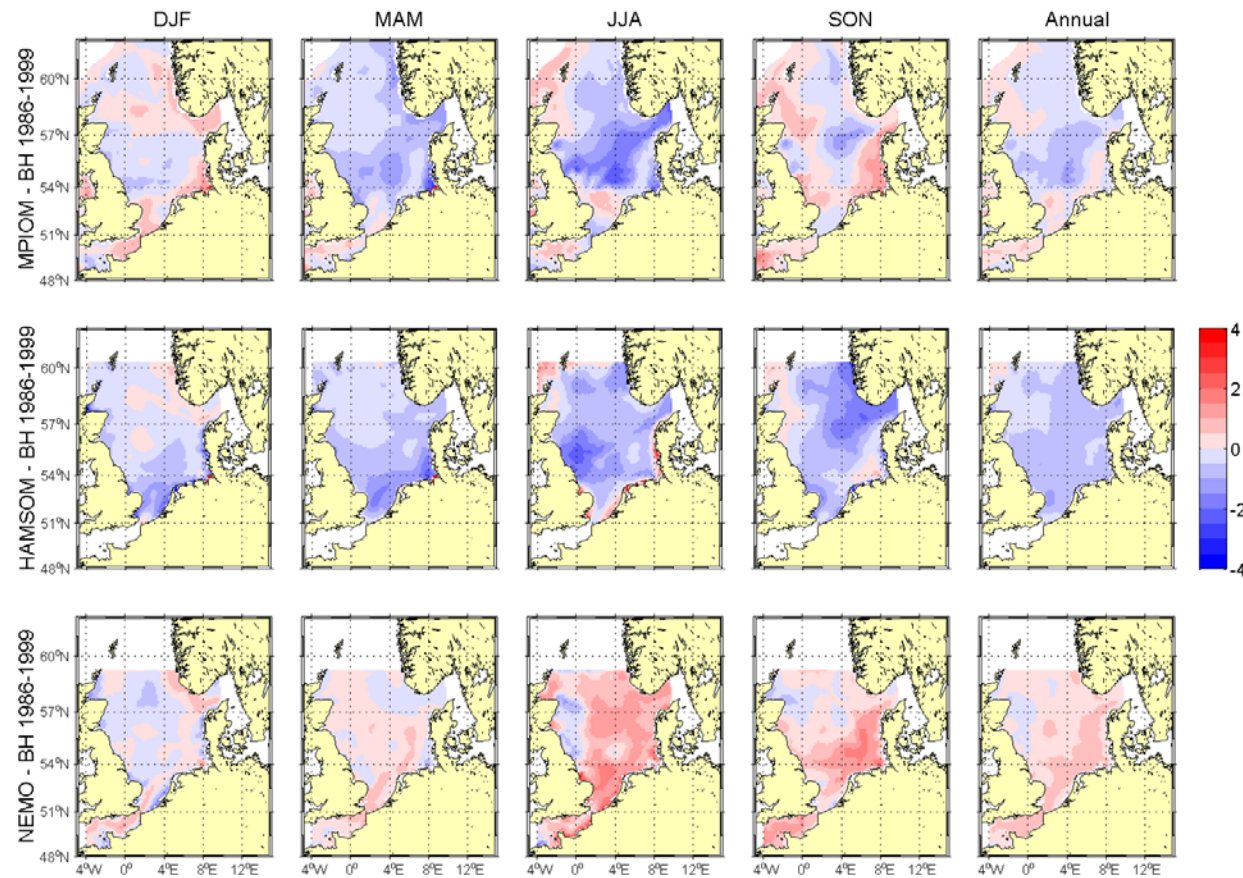


Figure 4.3.5A: Differences of modelled seasonal and annual means of sea surface temperature [°C] averaged over the period 1986-1999 to the BHC (1971-2000): MPIOM (run 253, upper row), HAMSOM (run 201, middle row) and from NEMO-Nordic (run 477, lower row).

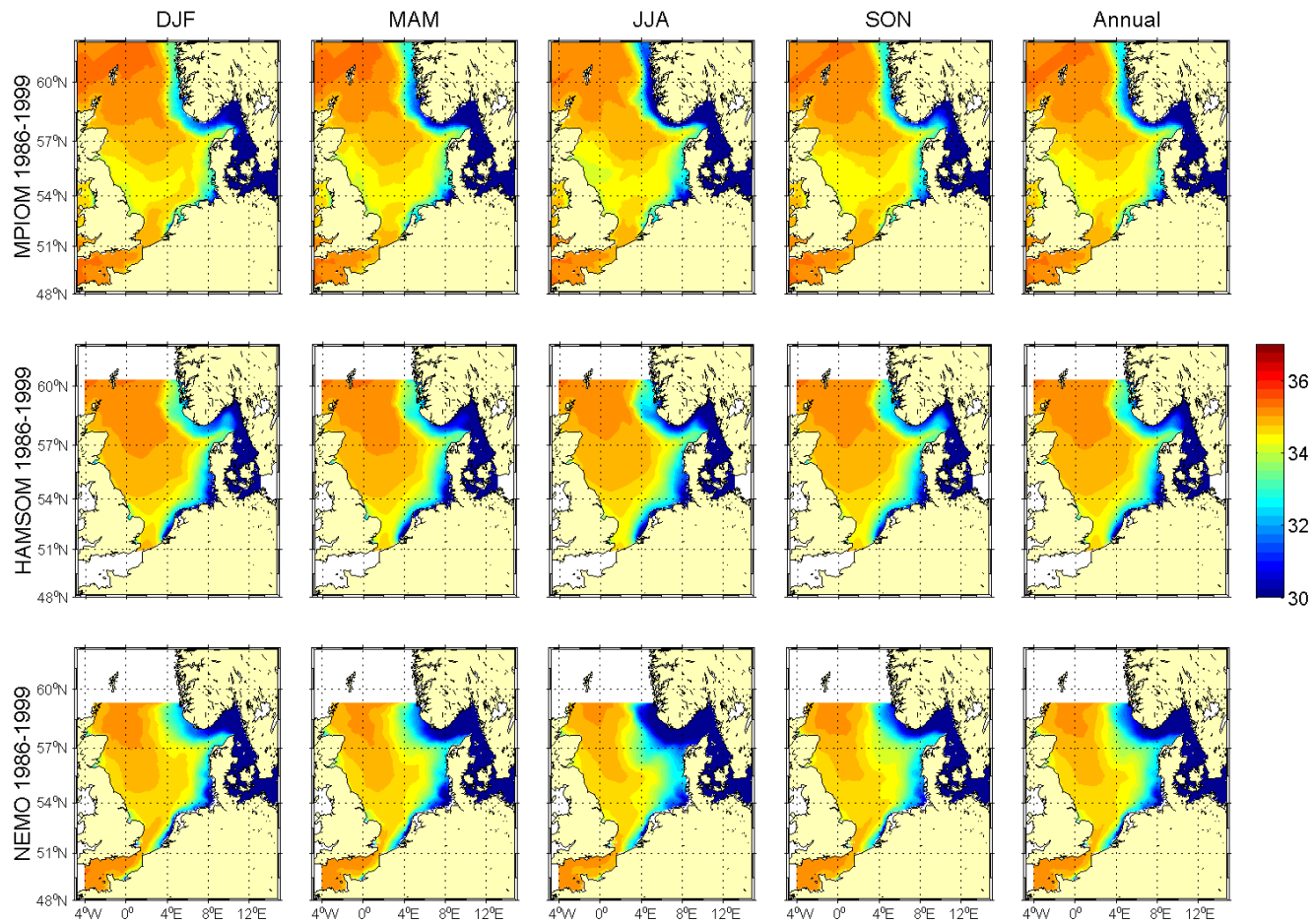


Figure 4.3.6A: Seasonal and annual means of sea surface salinity [psu] averaged over the period 1986-1999. The mean sea surface salinity results from MPI-OM (run 253) are presented in the upper row, in the middle row from HAMSOM (run 201) and in the lower row from NEMO-Nordic (run 477).

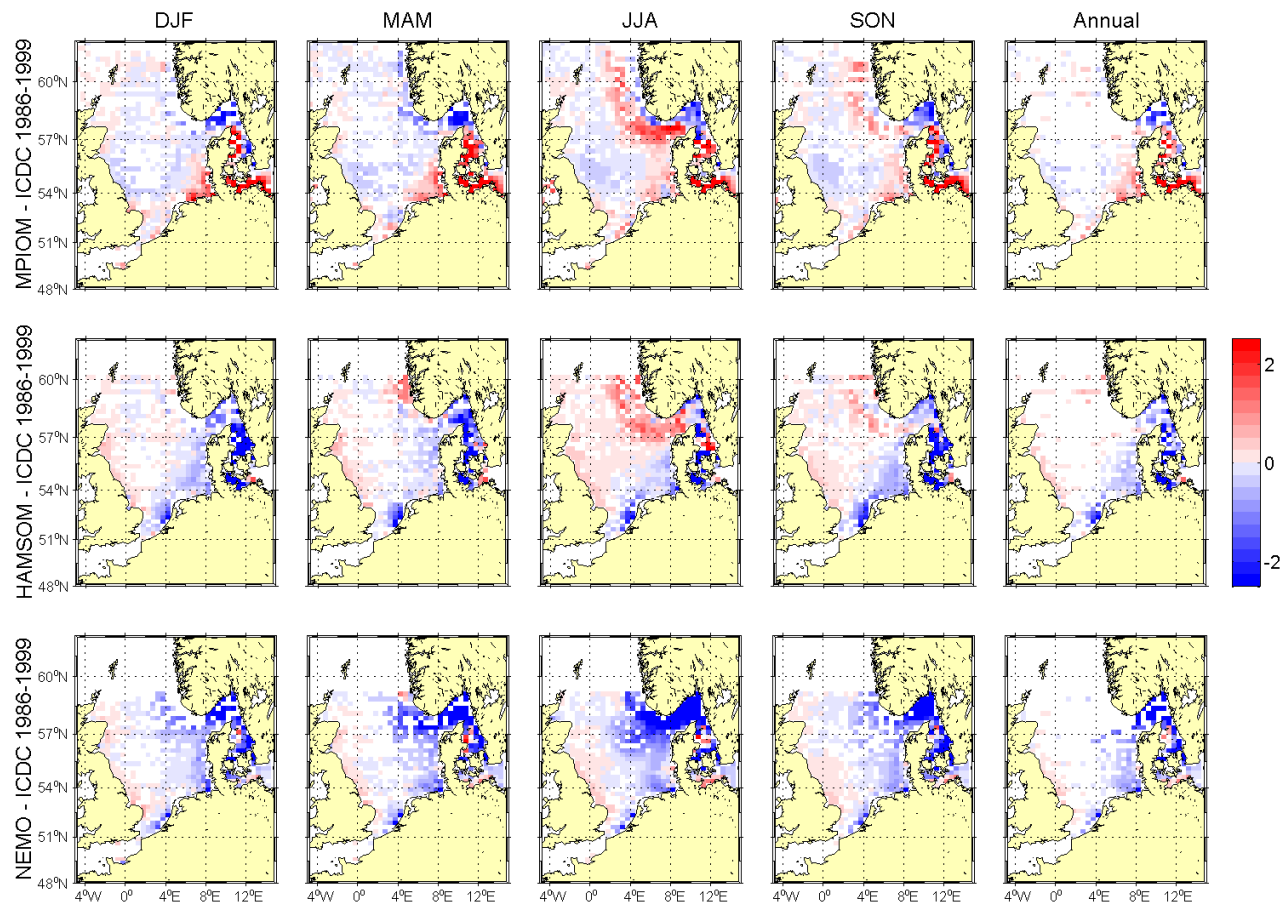


Figure 4.3.7A: Differences of modelled seasonal and annual means of sea surface salinity [psu] averaged over the period 1986-1999 to the KNSC: MPIOM (run 253, upper row), HAMSOM (run 201, middle row) from NEMO-Nordic (run 477, lower row).

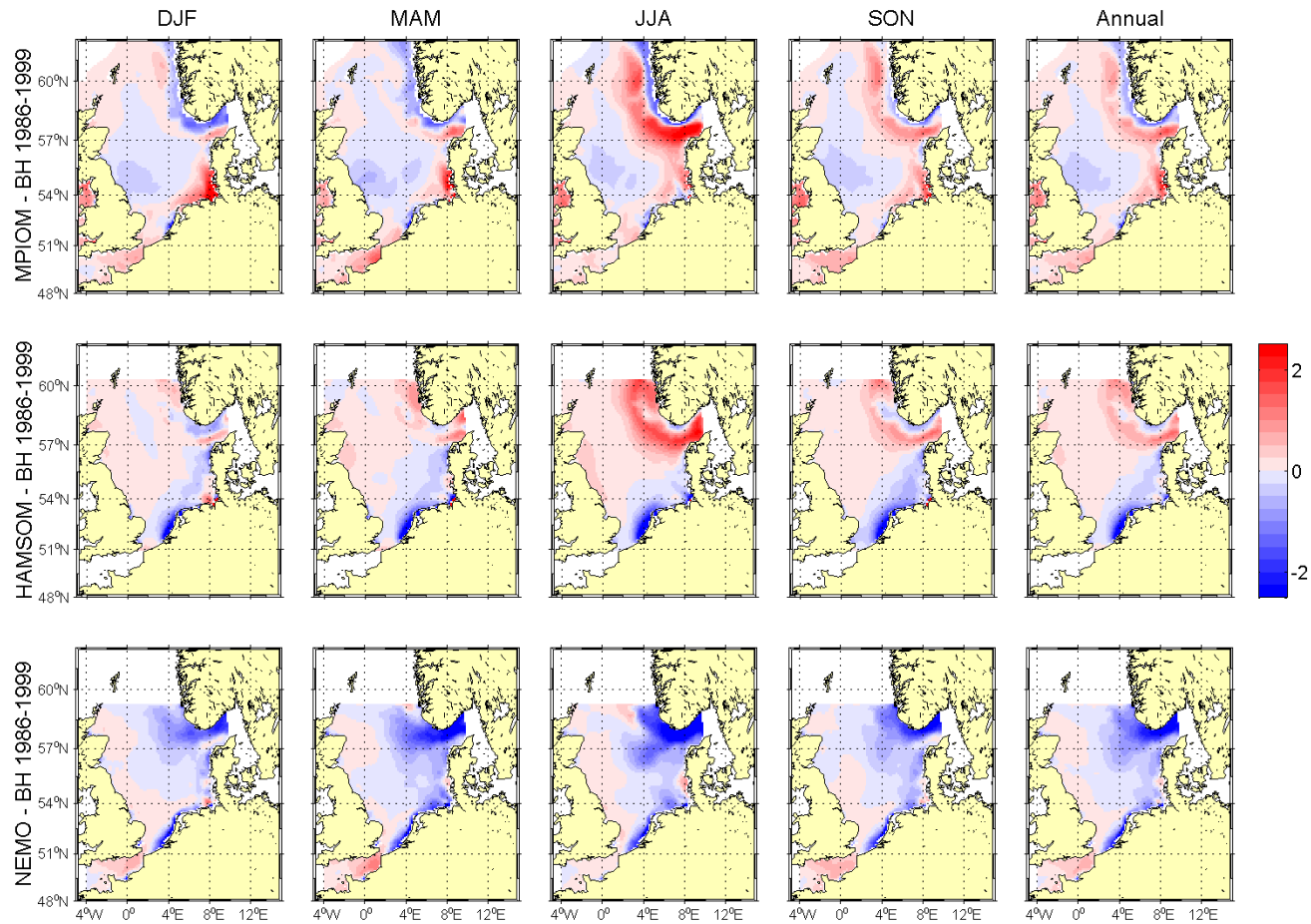


Figure 4.3.8A: Differences of modelled seasonal and annual means of sea surface salinity [psu] (1986-1999) to the BHC (1971-2000): MPIOM (run 253, upper row), HAMSOM (run 201, middle row) and from NEMO-Nordic (run 477, lower row).

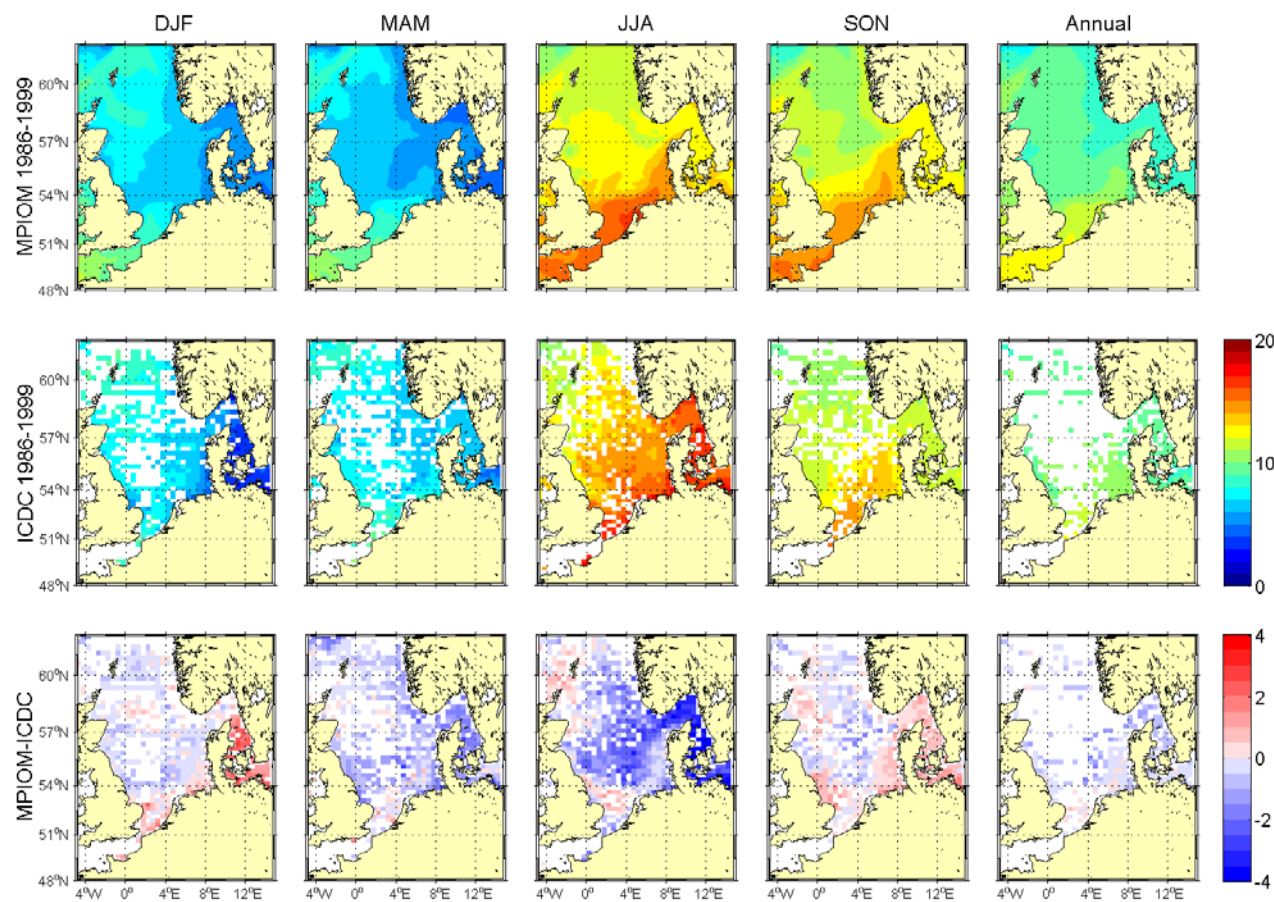


Figure 4.3.9A: Seasonal and annual means of sea surface temperature [°C] averaged over the period 1986-1999: The means of sea surface temperature result from MPIOM (run 253) are presented in the upper row, in the middle KNSC (ICDC) and in the lower row the difference between the model results and the KNSC.

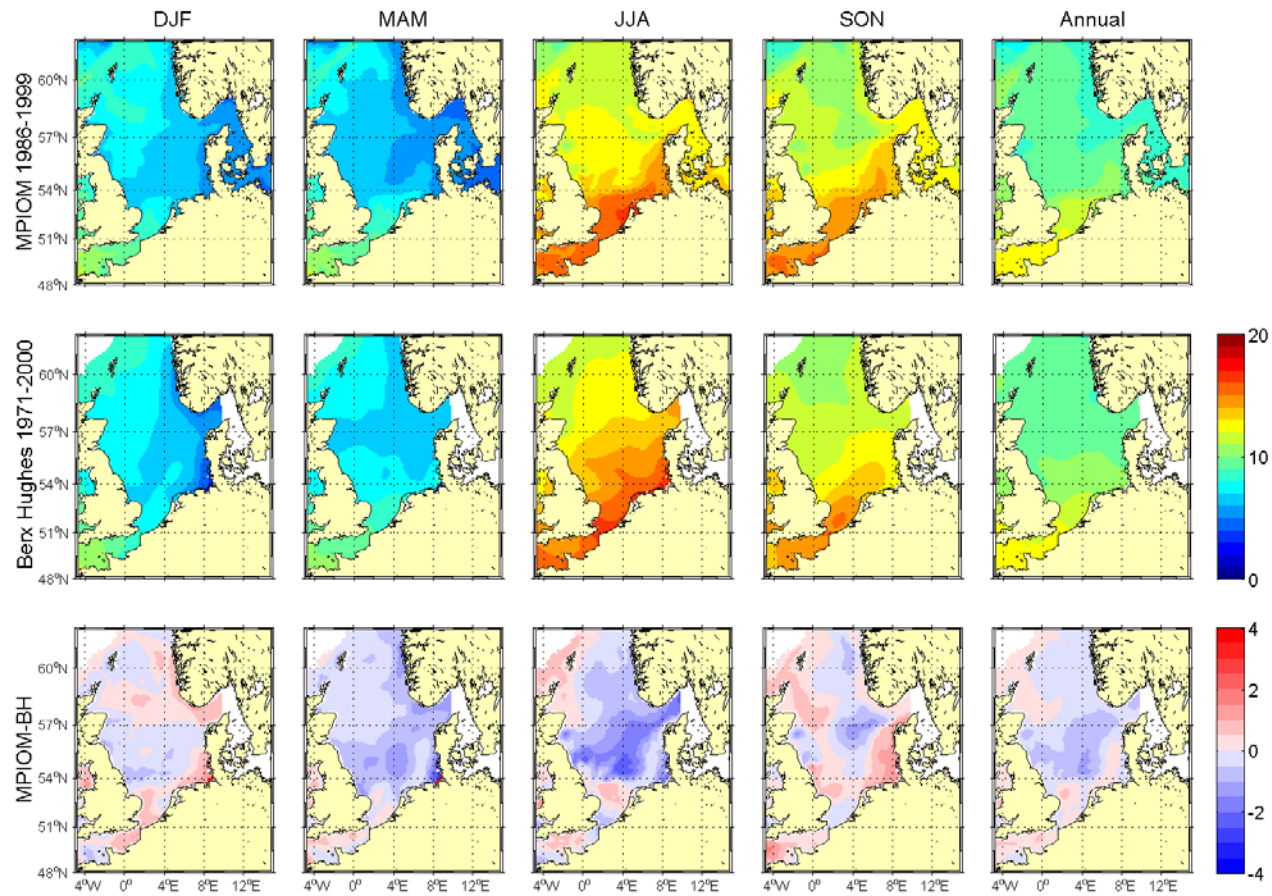


Figure 4.3.10A: Seasonal and annual means of sea surface temperature [°C]: The means of sea surface temperature result from MPIOM (run 253) averaged over the period 1986-1999 are presented in the upper row, in the middle from the BHC averaged over the period 1971-2000 and in the lower row the difference between model results and the climatology.

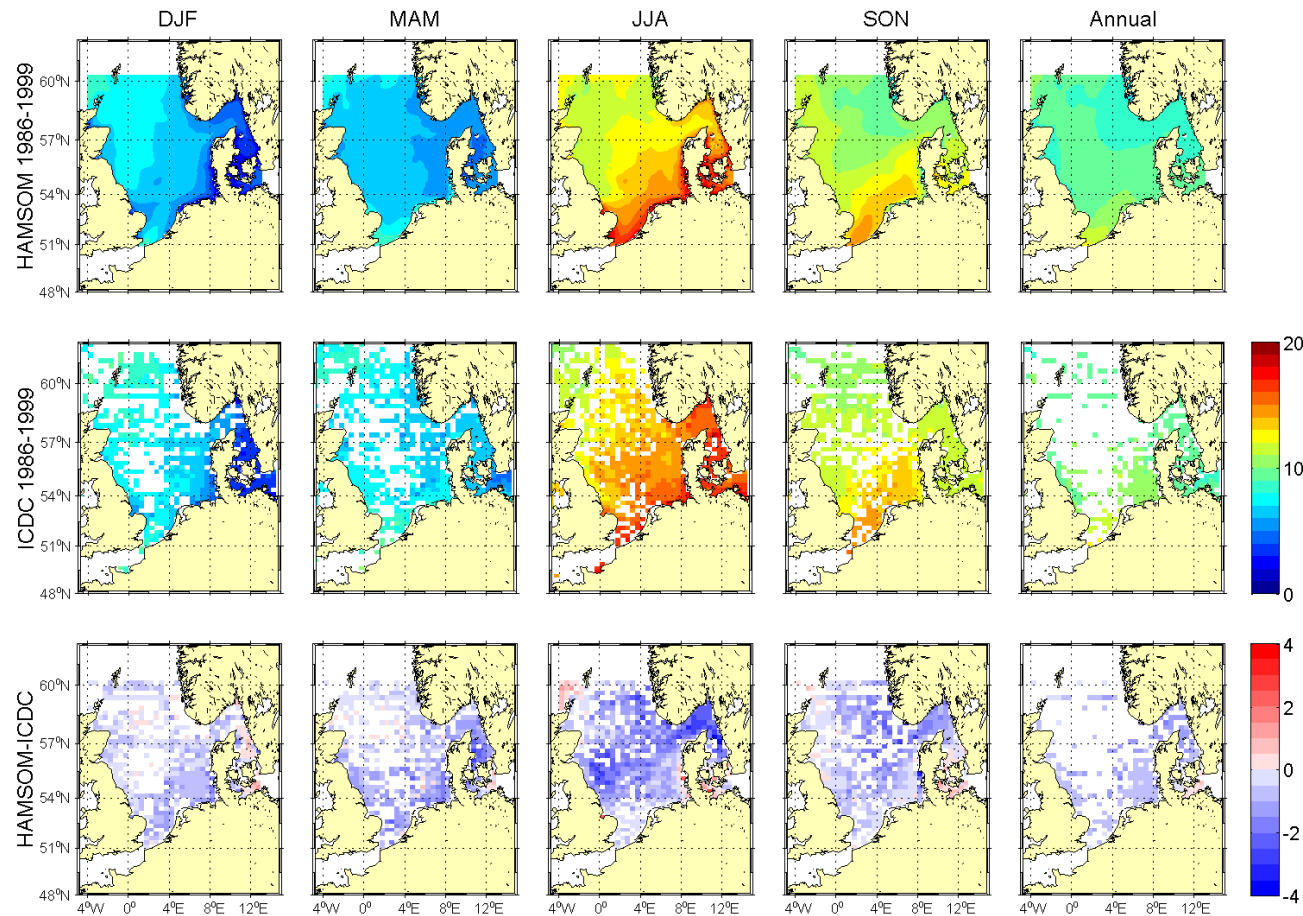


Figure 4.3.11A: Seasonal and annual means of sea surface temperature [°C] averaged over the period 1986-1999: The mean sea surface temperatures from HAMSOm (run 201) are presented in the upper row, in the middle the mean sea surface temperatures from the KNSC and in the lower row the difference between the model results and the climatology.

Coupled Ocean
Atmosphere
Models

BSH
DWD
IfM Hamburg
MPI Hamburg
SMHI
AWI

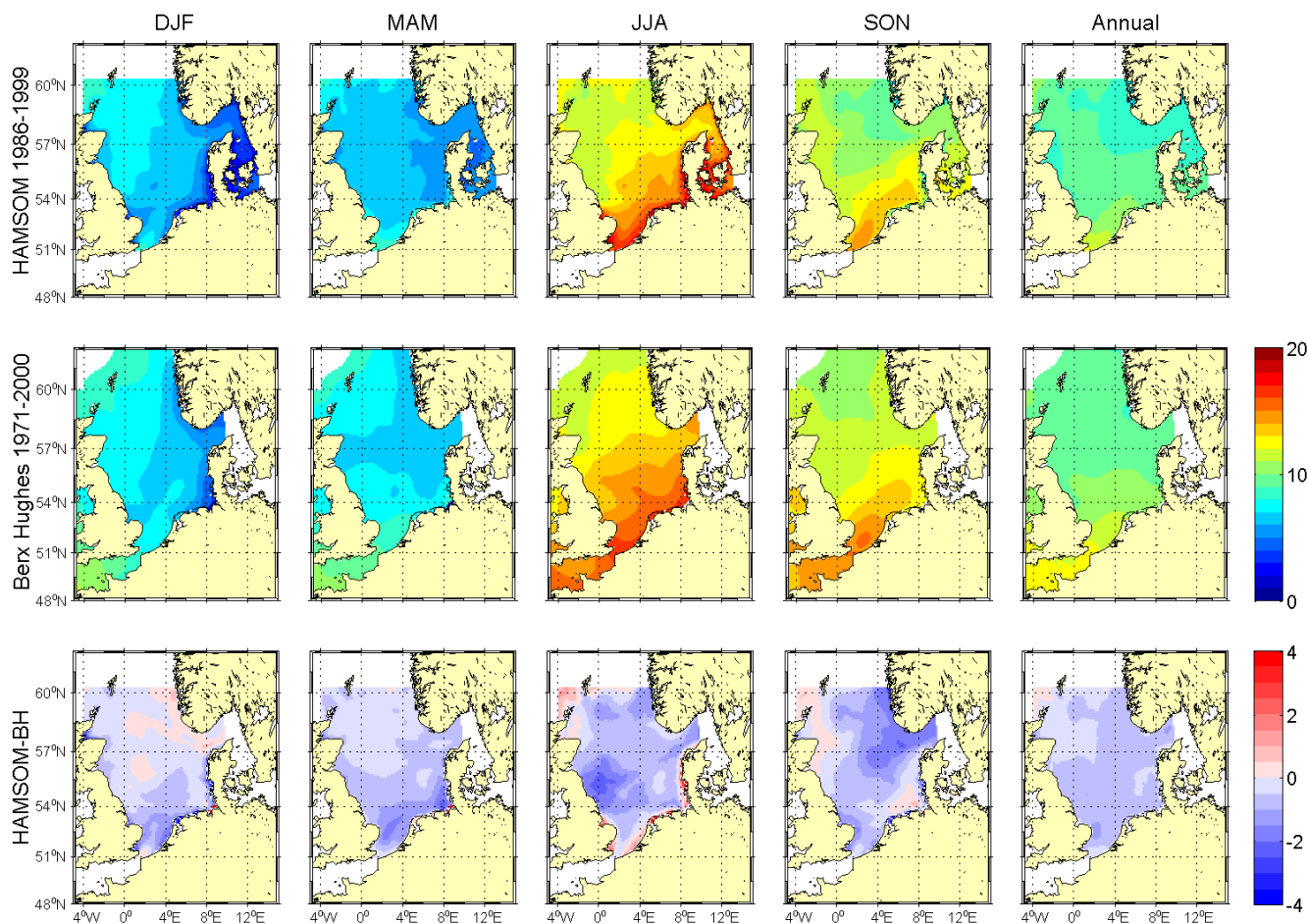


Figure 4.3.12A: Seasonal and annual means of sea surface temperature [°C]: The mean sea surface temperatures from HAMSOM (run 201) averaged over the period 1986-1999 are presented in the upper row, in the middle the mean surface temperatures from the BHC averaged over the period 1971-2000 and in the lower row the difference between the model results and the climatology.

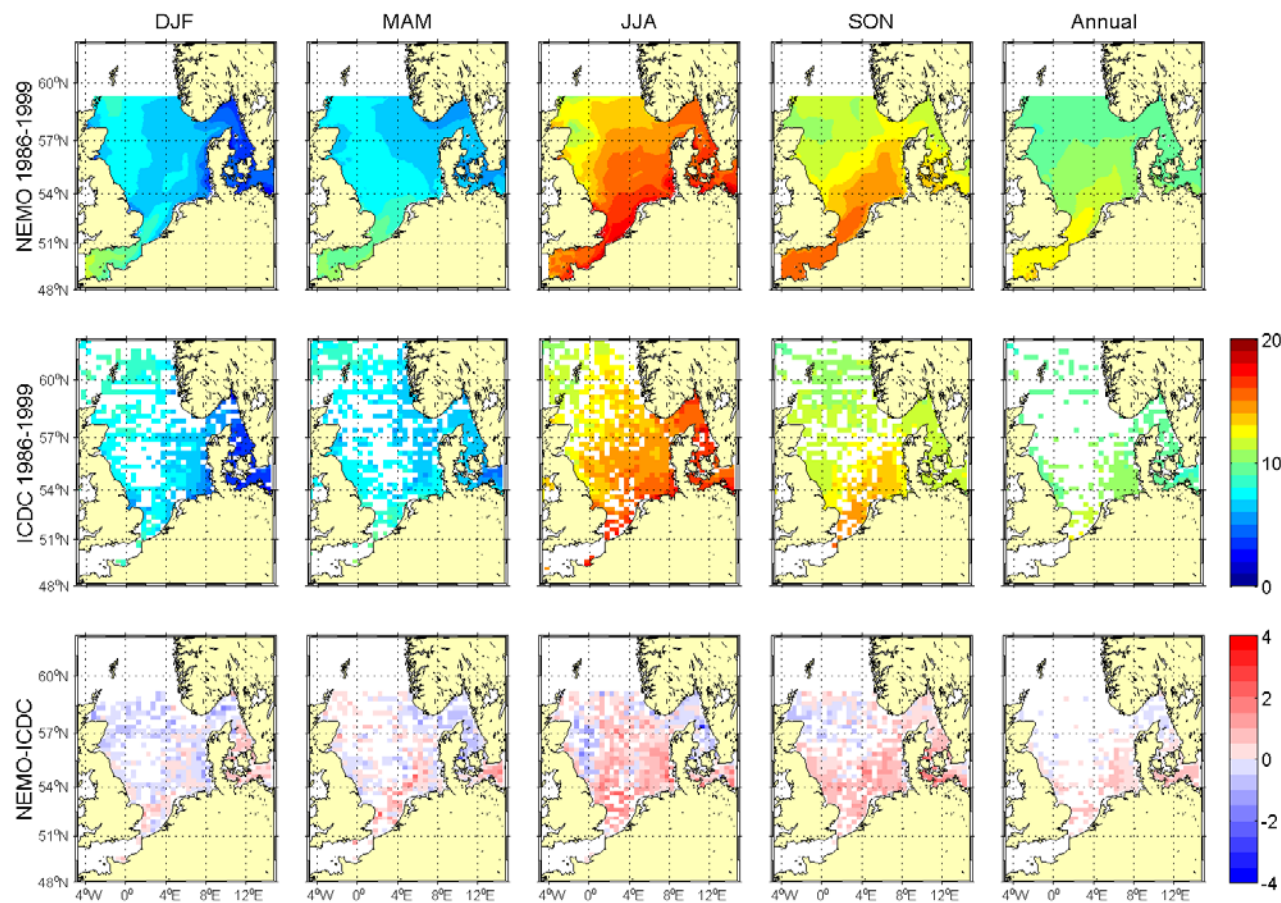


Figure 4.3.13A: Seasonal and annual means of sea surface temperature [°C] averaged over the period 1986-1999: The mean sea surface results from NEMO-Nordic (run 477) are presented in the upper row, in the middle the mean surface temperatures from the KNSC and in the lower row the difference between the model results and the climatology.

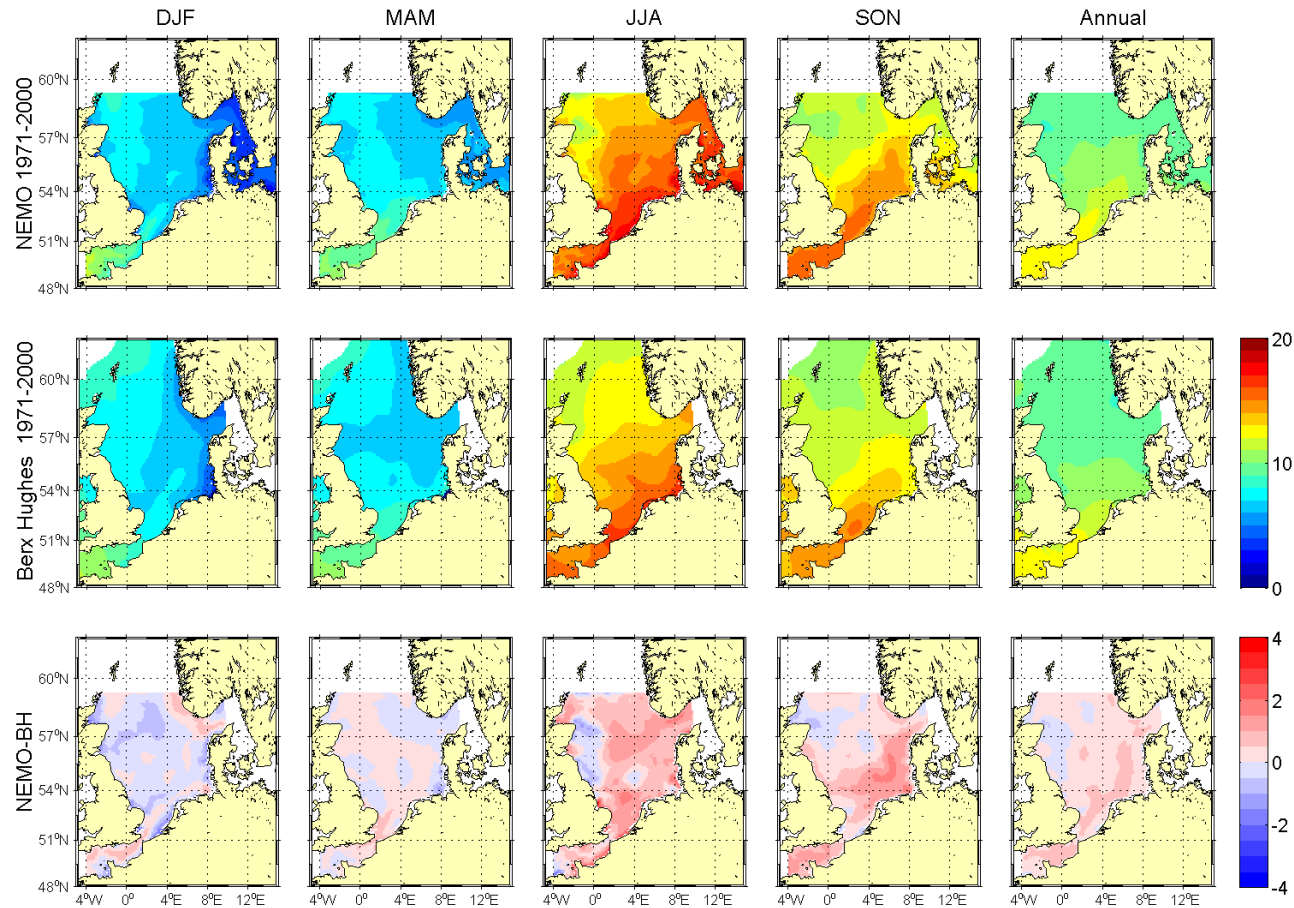


Figure 4.3.14A: Seasonal and annual means of sea surface temperature [°C] averaged over the period 1971-2000: The mean sea surface temperature results from NEMO-Nordic (run 477) are presented in the upper row, in the middle the mean surface temperature from the BHC and in the lower row the difference between the model results and the climatology.

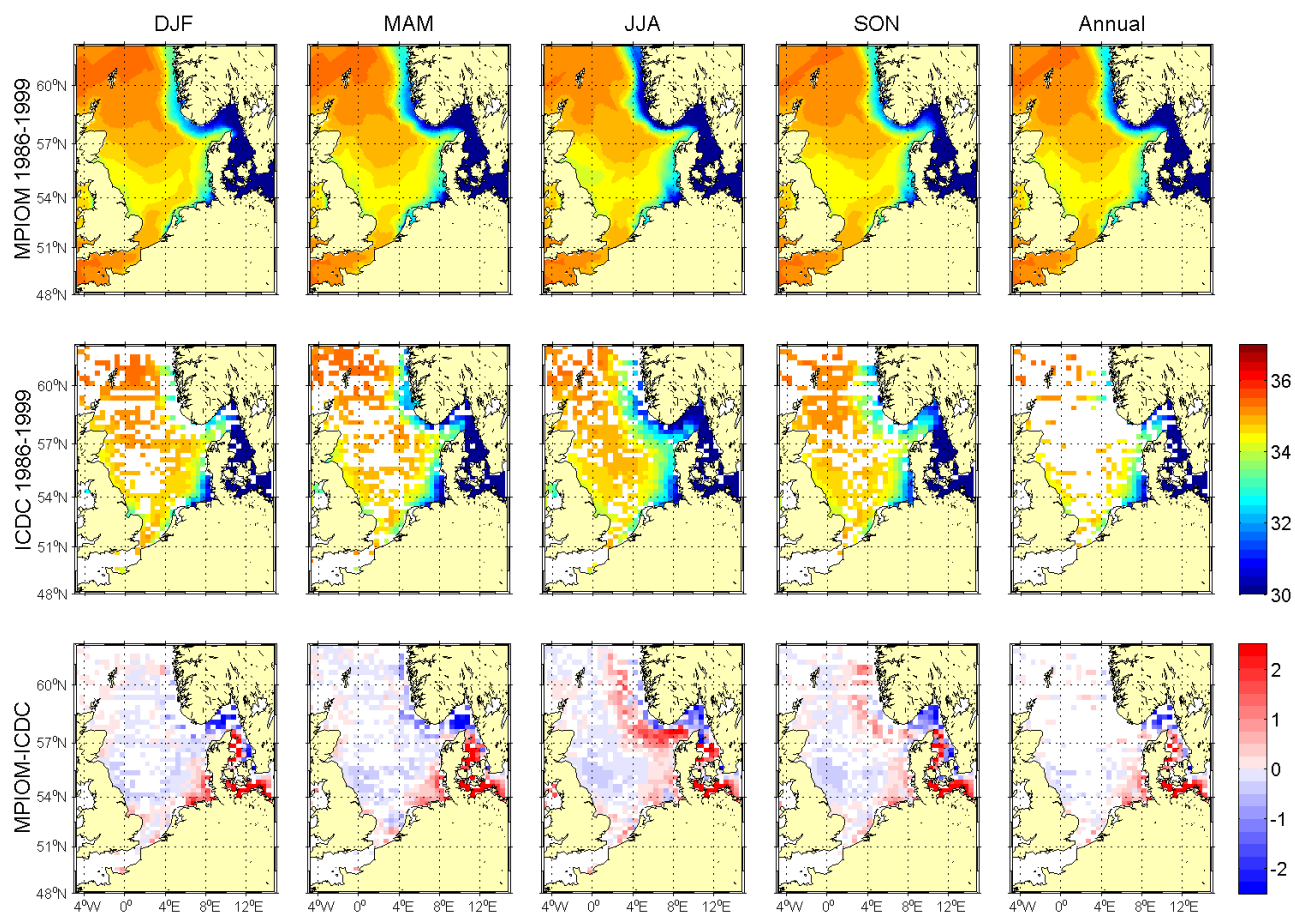


Figure 4.3.15A: Seasonal and annual means of sea surface salinity [psu] averaged over the period 1986-1999: The mean surface salinity results from MPIOM (run 253) are presented in the upper row, in the middle the mean surface salinity from the KNSC and in the lower row the difference between the model results and the climatology.

Coupled Ocean
Atmosphere
Models

BSH
DWD
IfM Hamburg
MPI Hamburg
SMHI
AWI

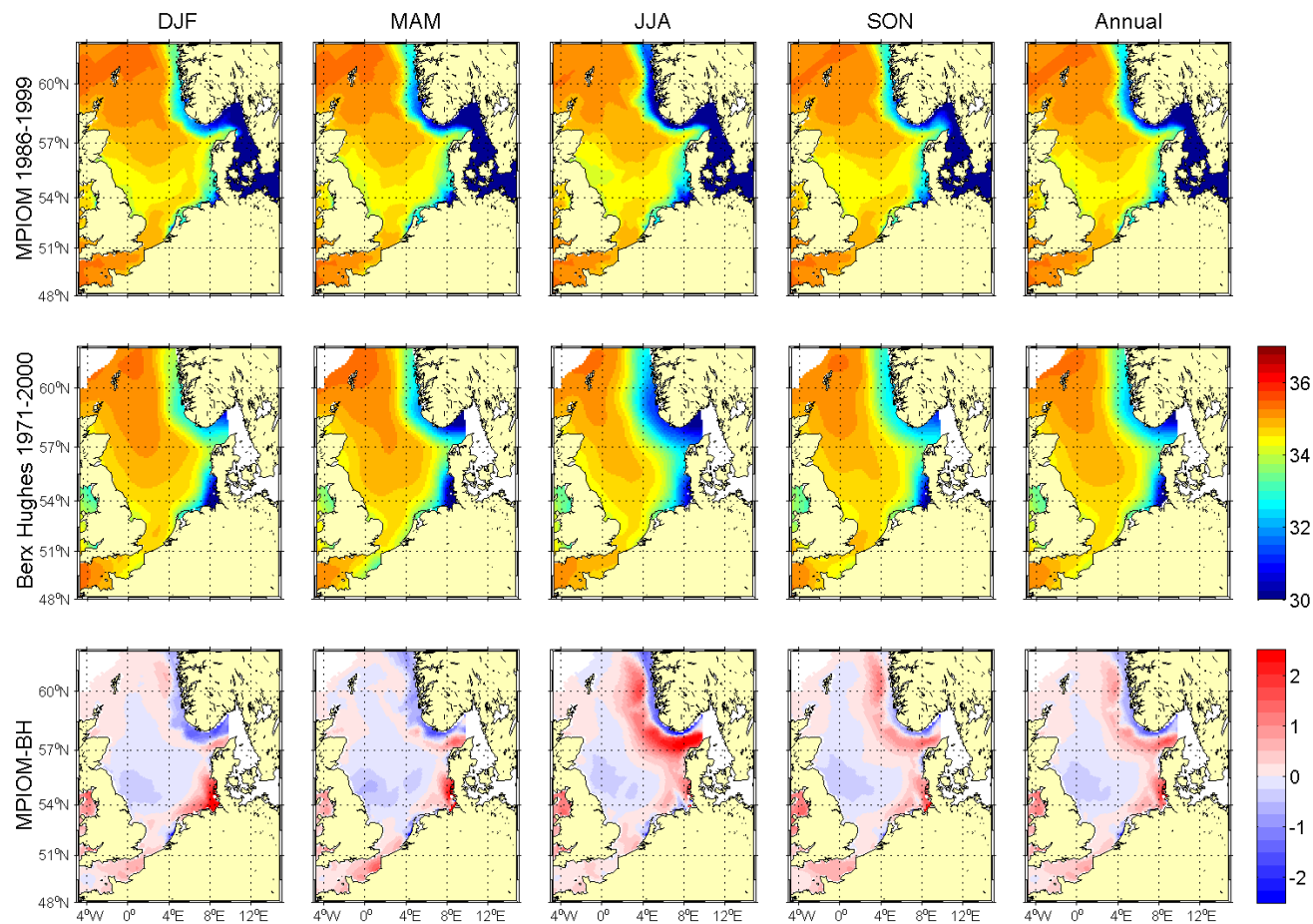


Figure 4.3.16A: Seasonal and annual means of sea surface salinity [psu]: The mean sea surface salinity results from MPIOM (run 253) averaged over the period 1986-1999 are presented in the upper row, in the middle the mean surface salinity from the BHC averaged over the period 1971-2000 and in the lower row the difference between the model results and the climatology.

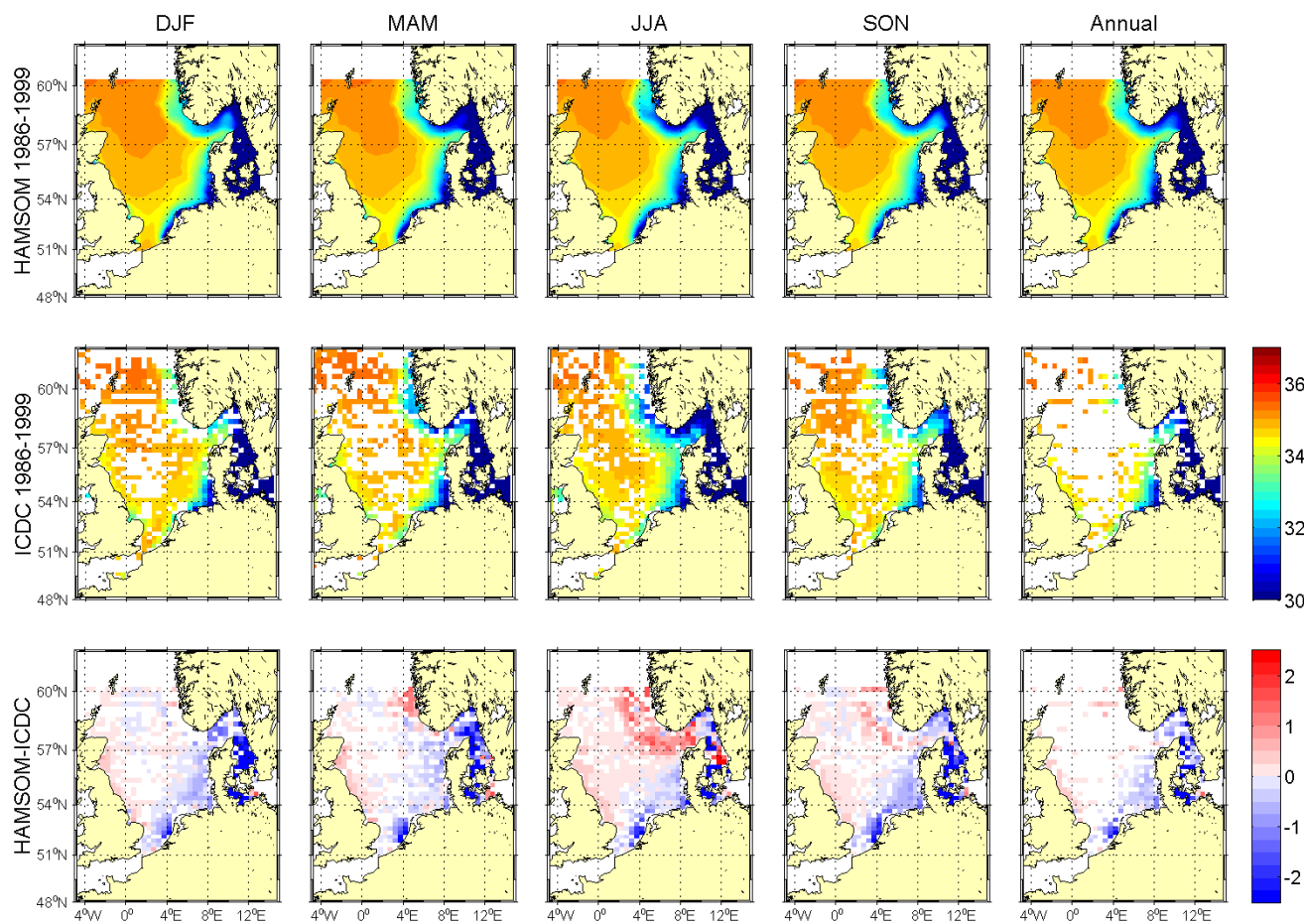


Figure 4.3.17A: Seasonal and annual means of sea surface salinity [psu] averaged over the period 1986-1999: The mean surface salinity results from HAM-SOM (run 201) are presented in the upper row, in the middle the mean surface salinity from the KNSC and in the lower row the difference between the model results and the climatology.

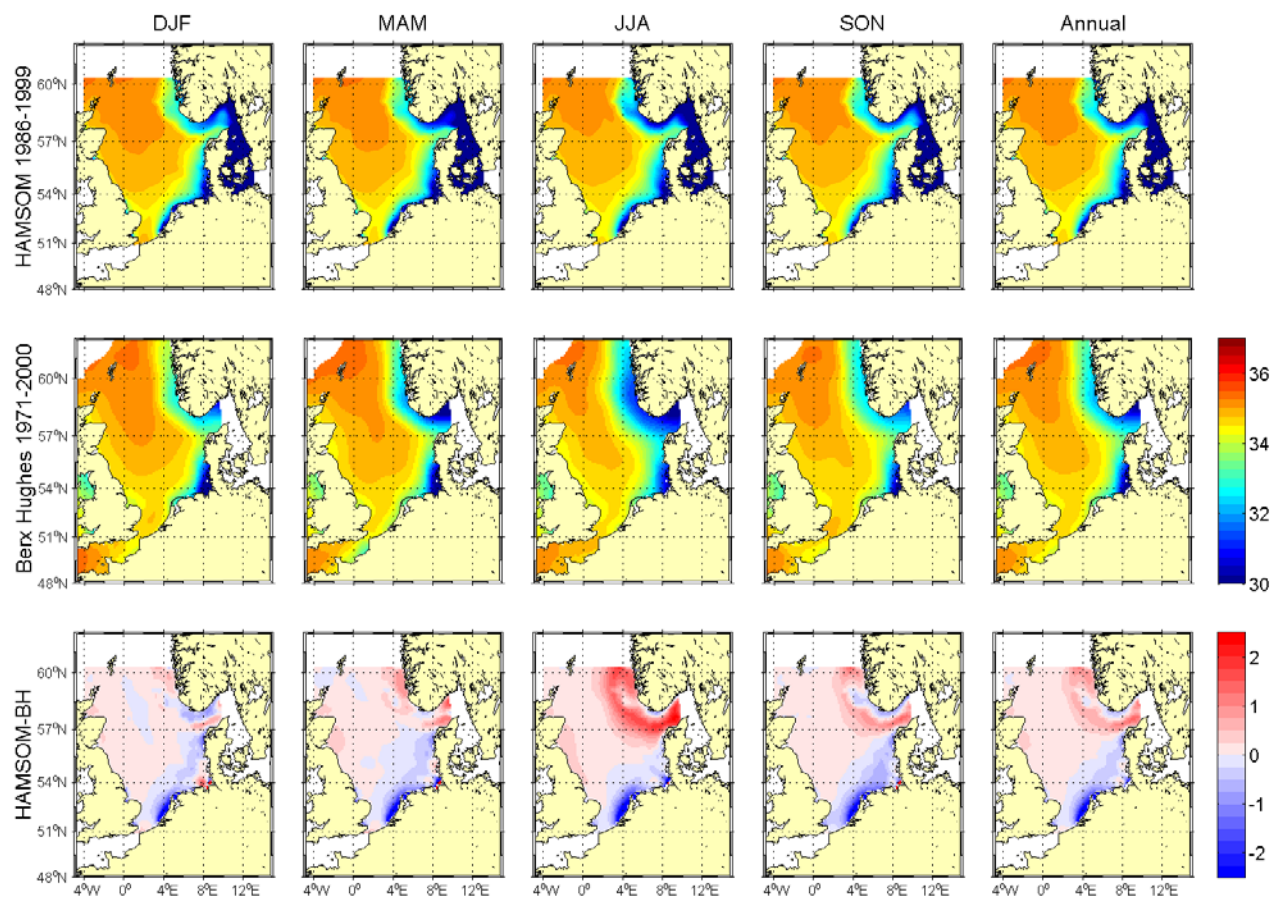


Figure 4.3.18A: Seasonal and annual means of sea surface salinity [psu]: The mean sea surface salinity from HAMSOM (run 201) averaged over the period 1986-1999 are presented in the upper row, in the middle the mean surface salinity from the BHC averaged over the period 1971-2000 and in the lower row the difference between the model results and the climatology.

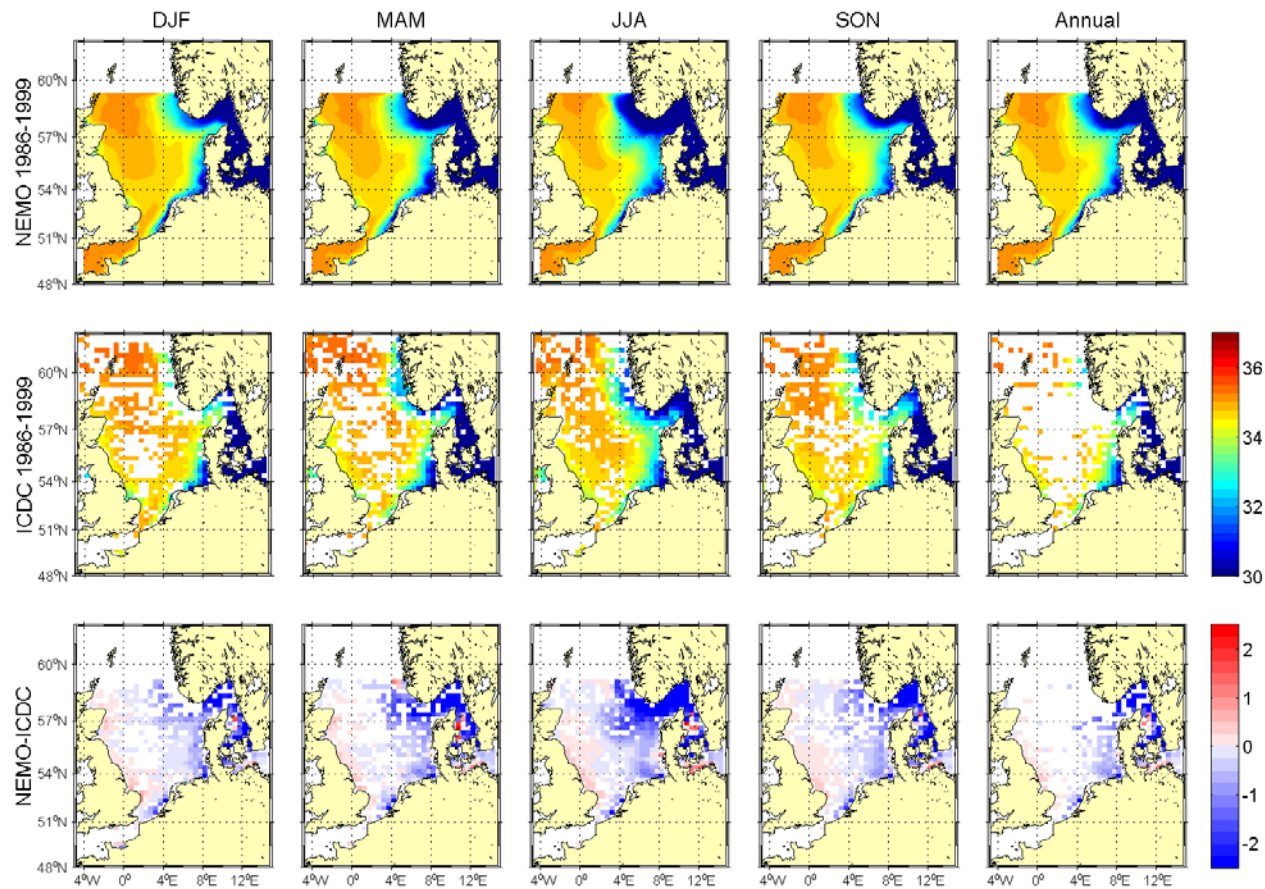


Figure 4.3.19A: Seasonal and annual means of sea surface salinity [psu] averaged over the period 1986-1999: The mean surface salinity from NEMO-Nordic (run 477) are presented in the upper row, in the middle the mean surface salinity from the KNSC and in the lower row the difference between the model results and the climatology.

Coupled Ocean
Atmosphere
Models

BSH
DWD
IfM Hamburg
MPI Hamburg
SMHI
AWI

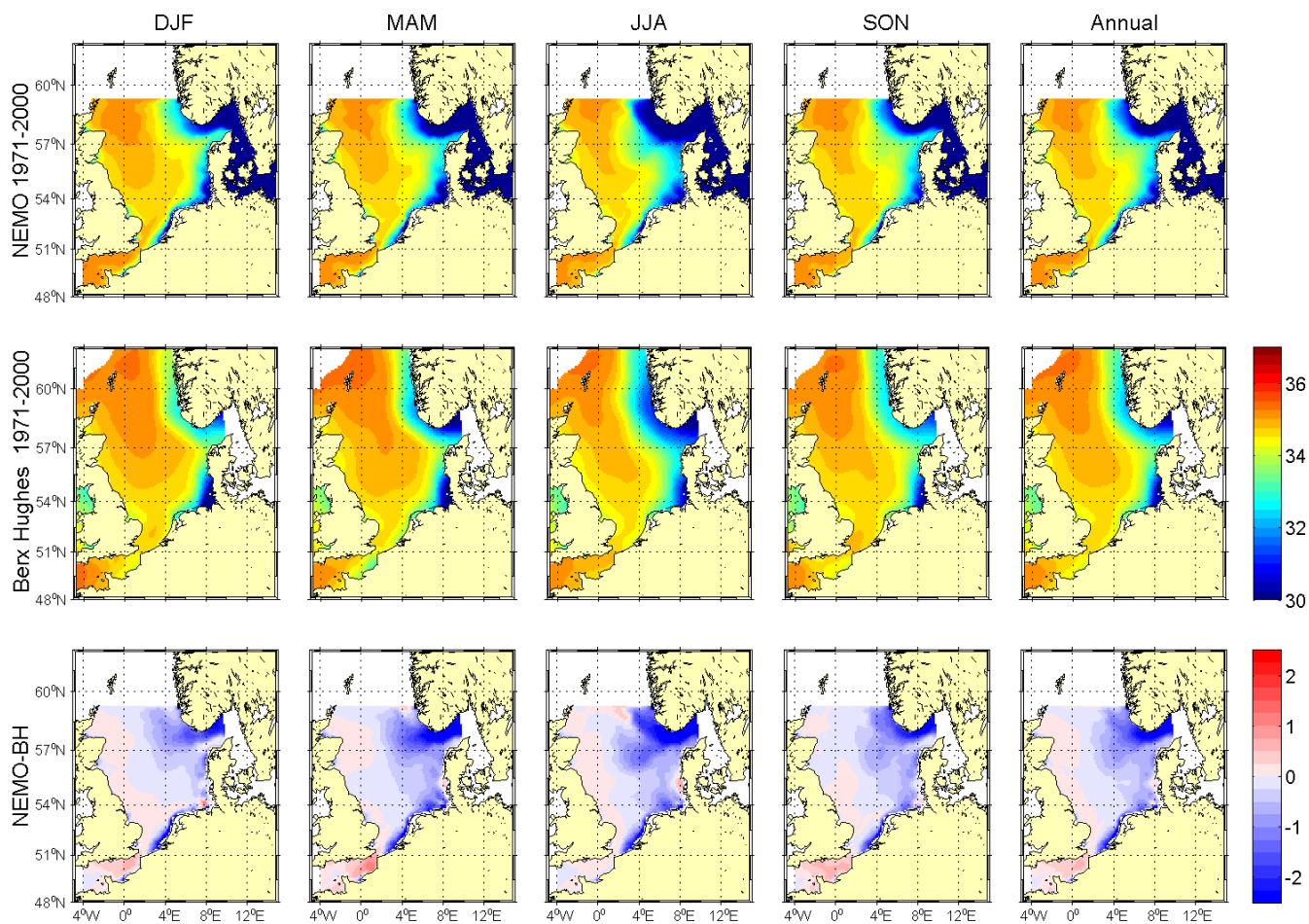


Figure 4.3.20A: Seasonal and annual means of sea surface salinity [psu] averaged over the period 1971-2000: The mean surface salinity from NEMO-Nordic (run 477) are presented in the upper row, in the middle the mean surface salinity from the BHC and in the lower row the difference between the model results and the climatology.

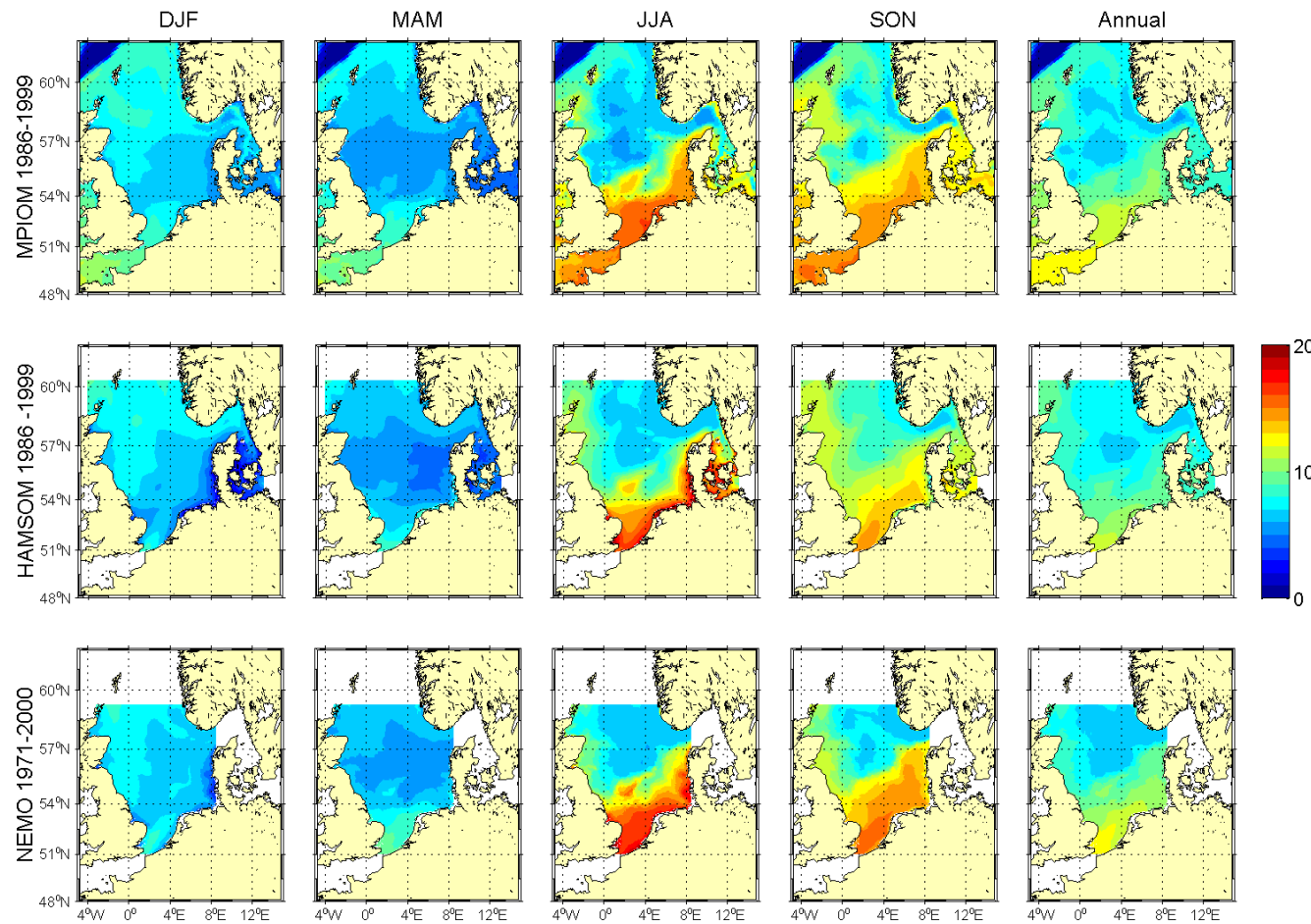


Figure 4.3.21A: Seasonal and annual means of bottom temperature [°C] averaged over the period 1986-1999: The mean bottom temperature results from MPIOM (run 253) are presented in the upper row, in the middle row from HAMSOM (run 201) and in the lower row from the NEMO-Nordic (run 477) over the time period 1970-1999.

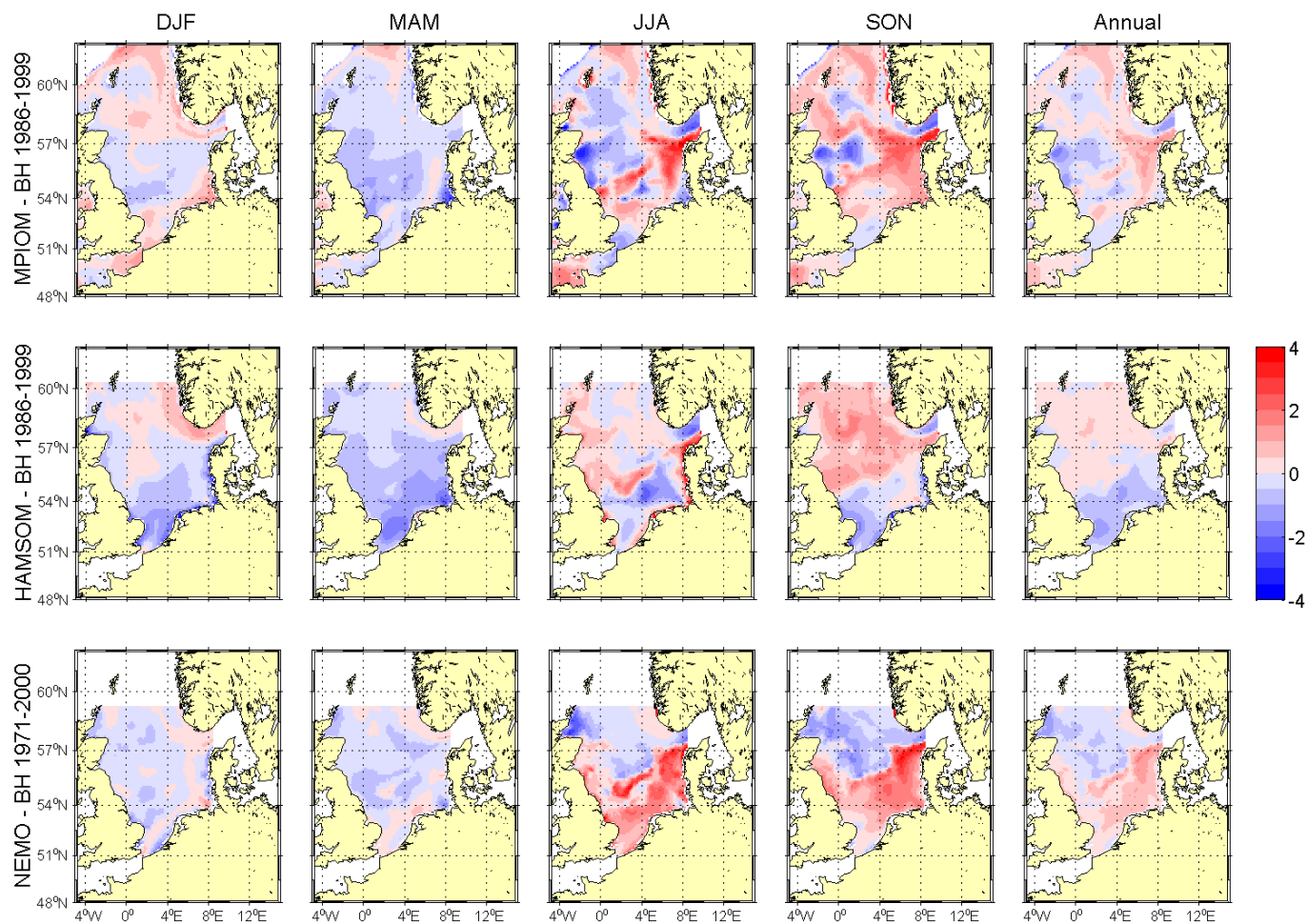


Figure 4.3.22A: Differences of modelled seasonal and annual means of bottom temperature [°C] averaged over the period 1986-1999 to the BHC (1971-2000): MPIOM (run 253) in the upper row, HAMSOM (run 201) in the middle row and in the lower row NEMO-Nordic (run 477) over the time period 1970-1999.

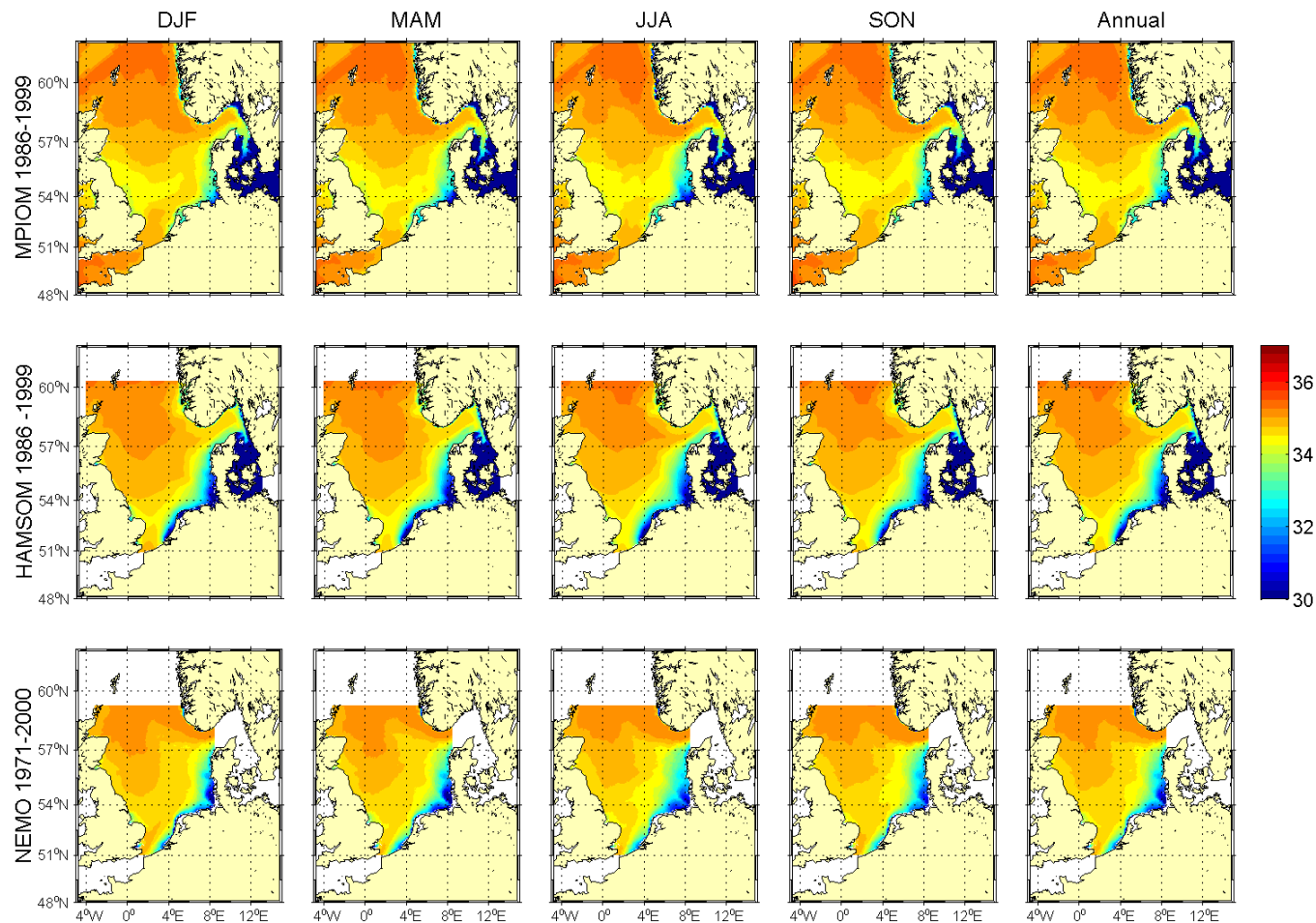


Figure 4.3.23A: Seasonal and annual means of bottom salinity [psu] averaged over the period 1986-1999: The mean bottom salinity results from MPIOM (run 253) are presented in the upper row, in the middle row from HAMSOM (run 201) and in the lower row from NEMO-Nordic (run 477) over the time period 1970-1999.

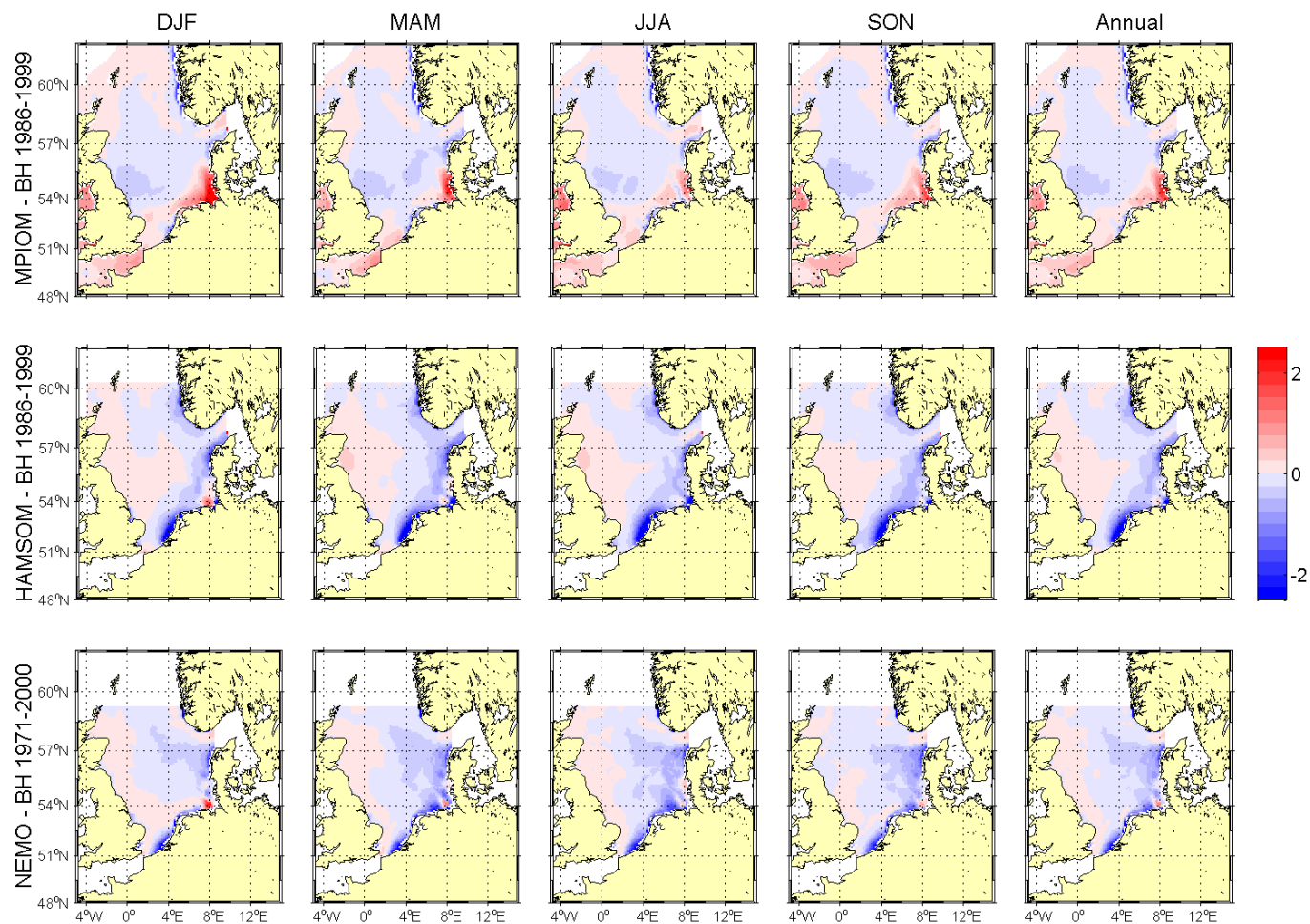


Figure 4.3.24A: Differences of modelled seasonal and annual means of bottom salinity [psu] averaged over the period 1986-1999 to the BHC (1971-2000): MPIOM (run 253) in the upper row, HAMSOM (run 201) in the middle row and NEMO-Nordic (run 477) in the lower row over the time period 1970-1999.

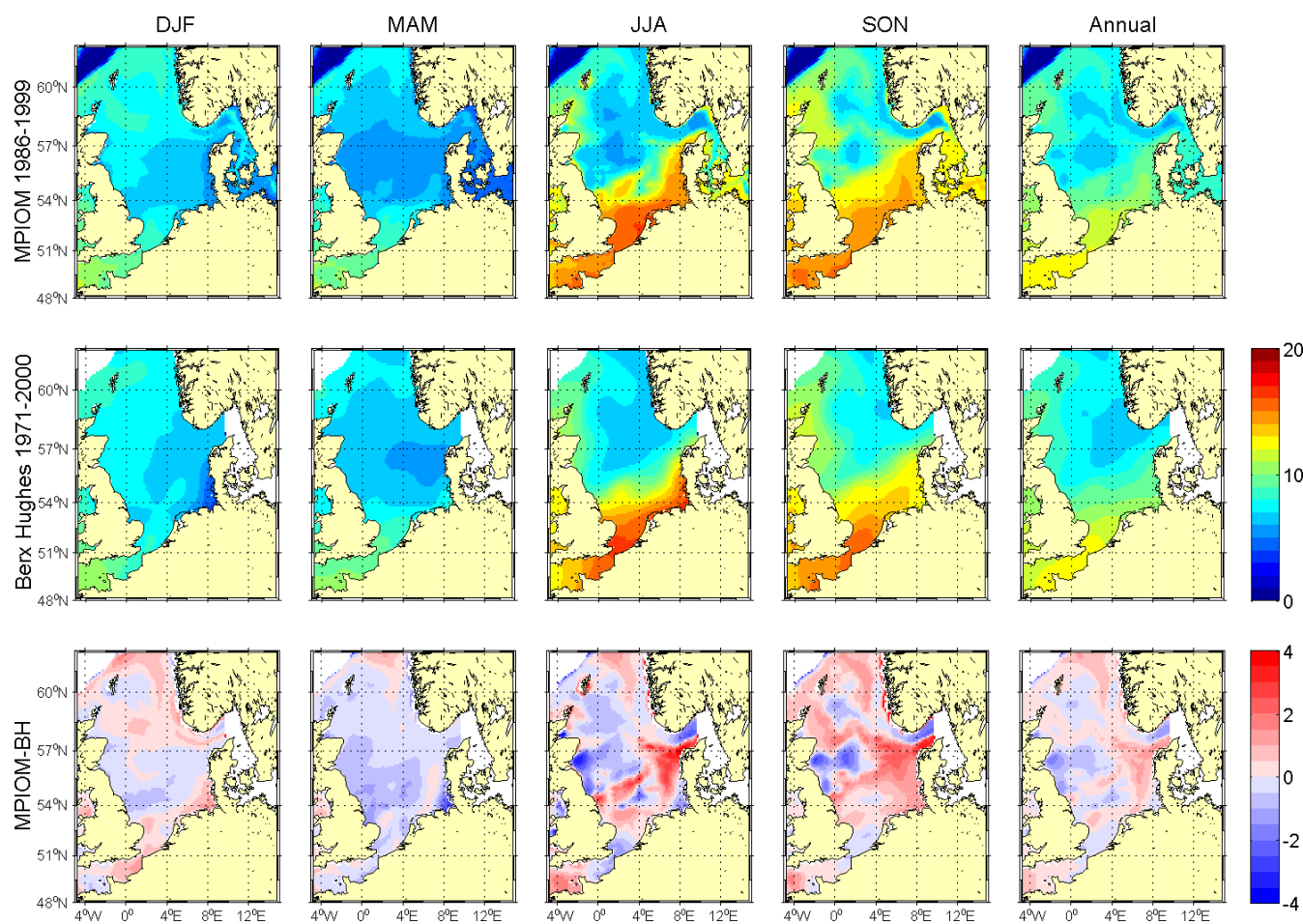


Figure 4.3.25A: Seasonal and annual means of bottom temperature [°C]: The mean bottom temperature results from MPIOM (run 253) averaged over the period 1986-1999 are presented in the upper row, in the middle the mean bottom temperature from the BHC averaged over the period 1971-2000 and in the lower row difference between the model results and the climatology.

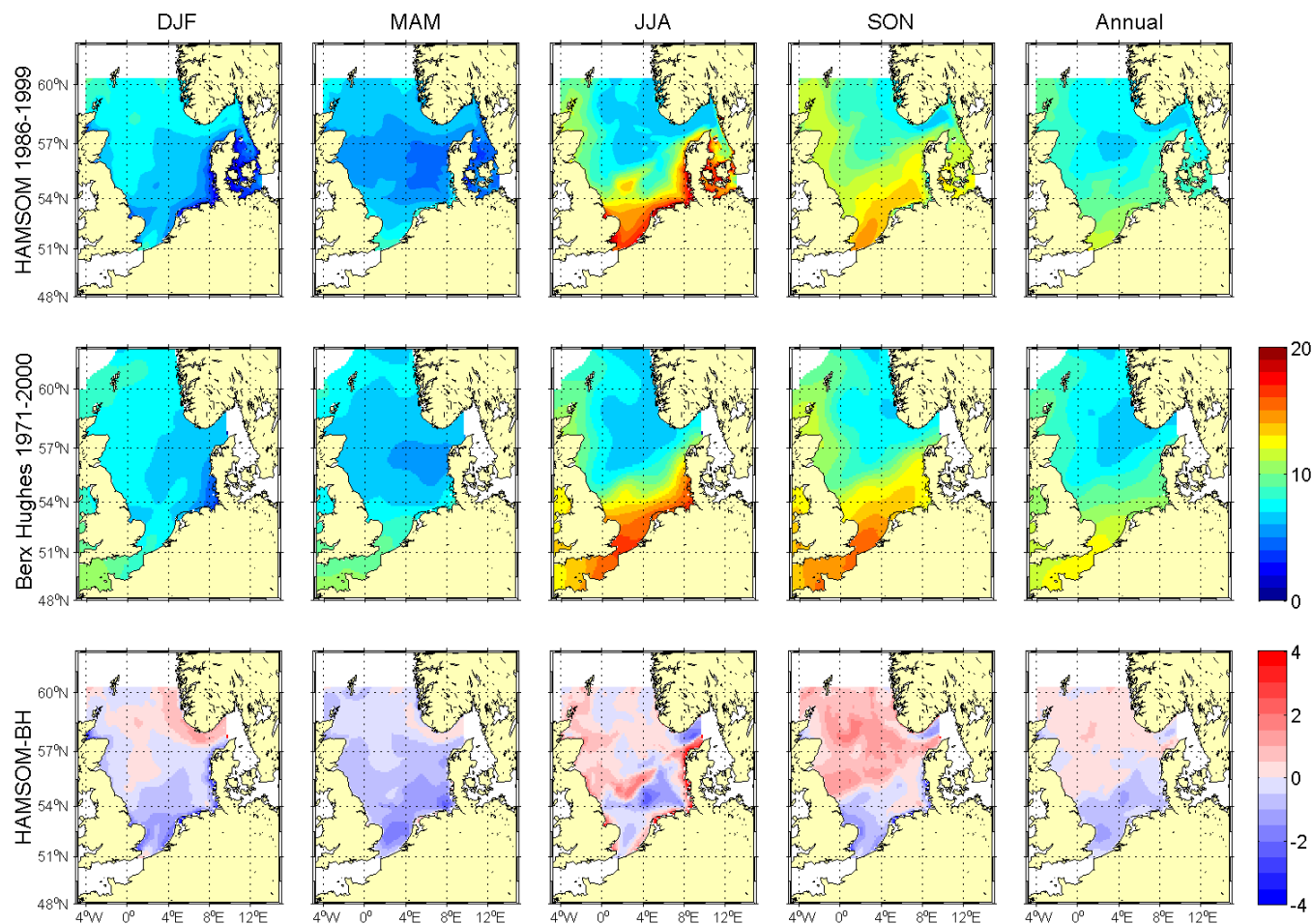


Figure 4.3.26A: Seasonal and annual means of bottom temperature [°C]: The mean bottom temperatures from HAMSOM (run 201) averaged over the period 1986-1999 are presented in the upper row, in the middle row the mean bottom temperature from the BHC averaged over the period 1971-2000 and in the lower row the difference between the model results and the climatology.

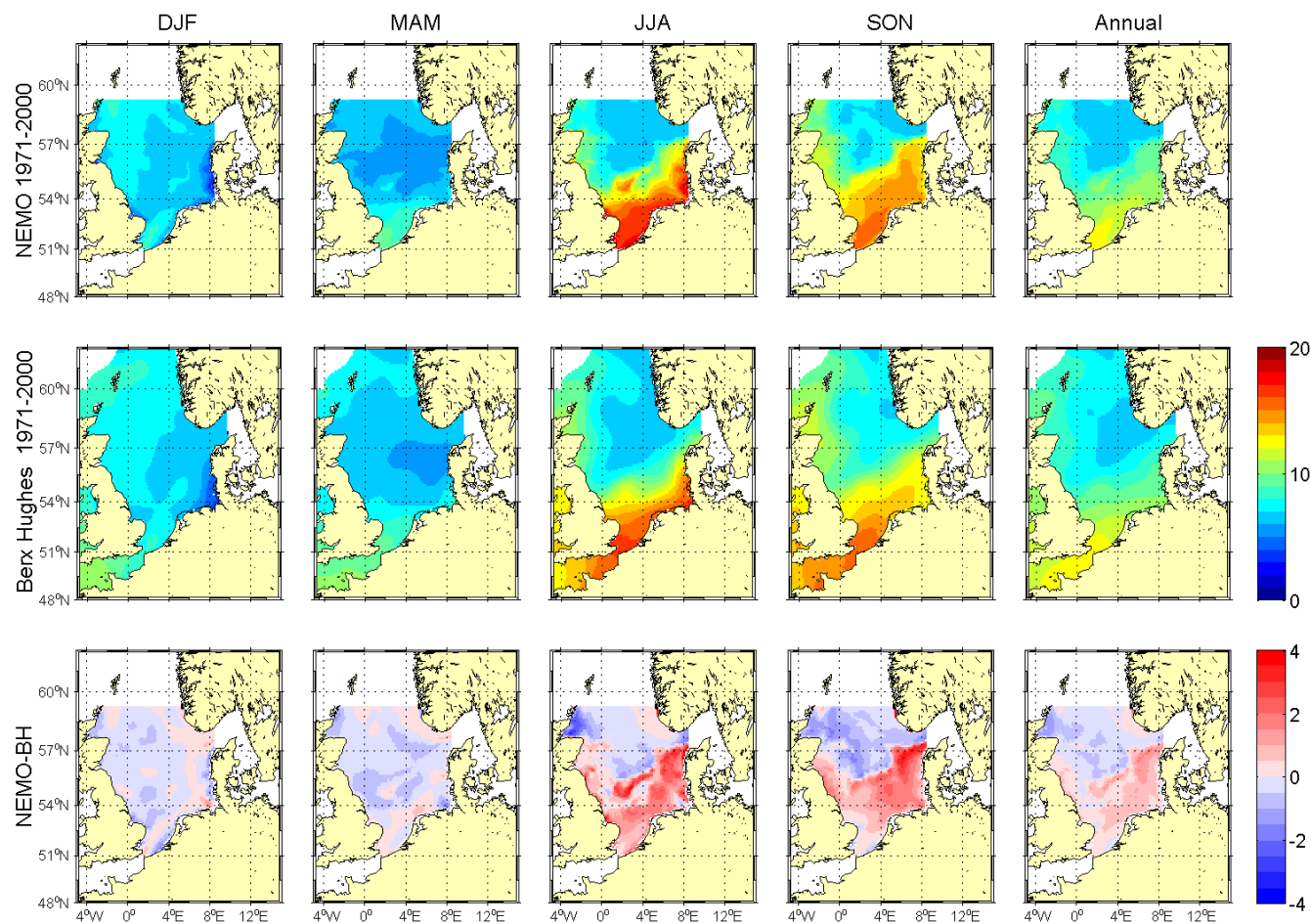


Figure 4.3.27A: Seasonal and annual means of bottom temperature [°C] averaged over the period 1971-2000: The mean bottom temperature results from NEMO-Nordic (run 477) are presented in the upper row, in the middle the bottom temperature from the BHC and in the lower row the difference between the model results and the climatology.

Coupled Ocean
Atmosphere
Models

BSH
DWD
IfM Hamburg
MPI Hamburg
SMHI
AWI

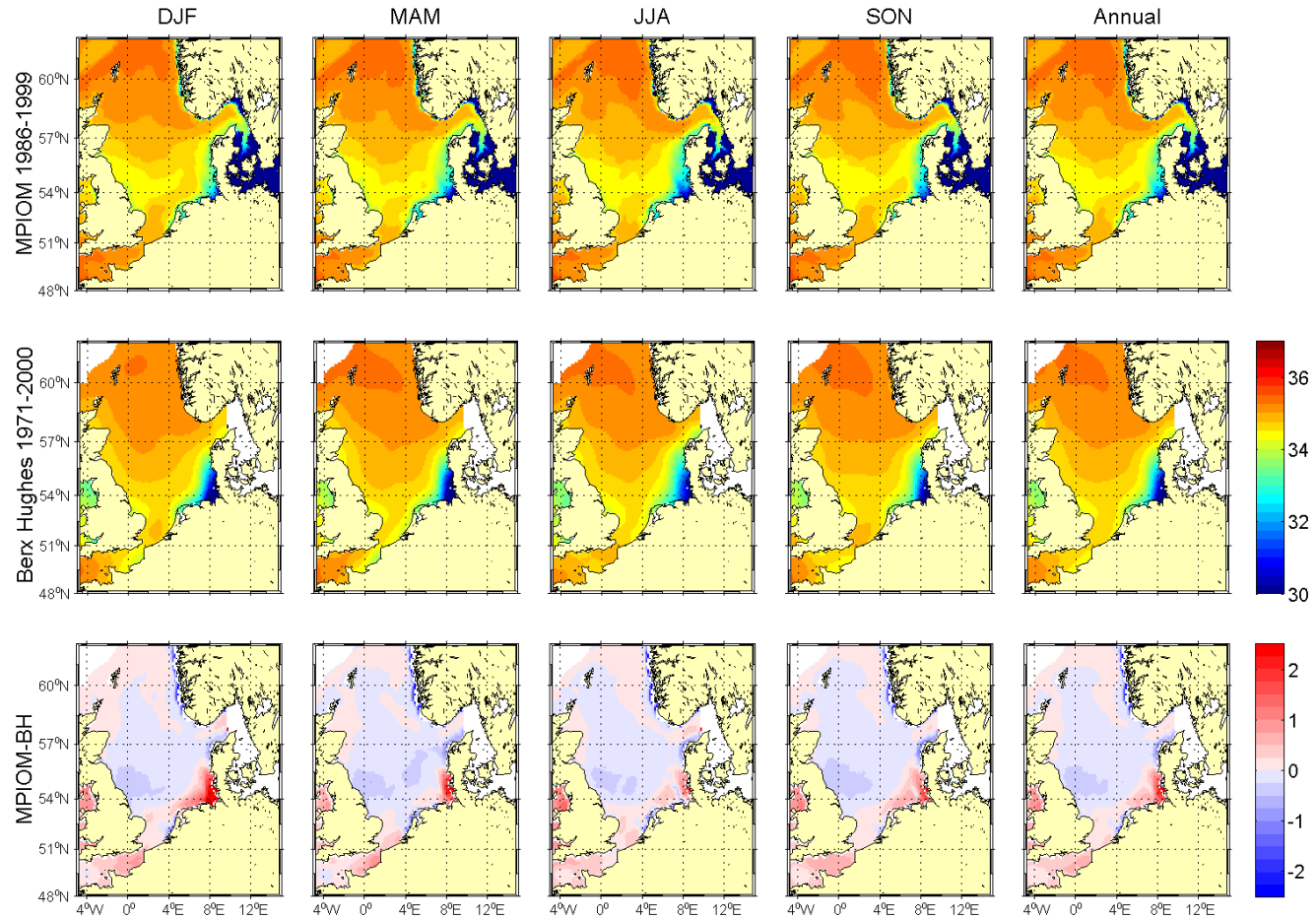


Figure 4.3.28A: Seasonal and annual means of bottom salinity [psu]: The mean bottom salinity from MPIOM (run 253) averaged over the period 1986-1999 are presented in the upper row, in the middle the mean bottom salinity from the BHC averaged over the period 1971-2000 and in the lower row the difference between the model results and the climatology.

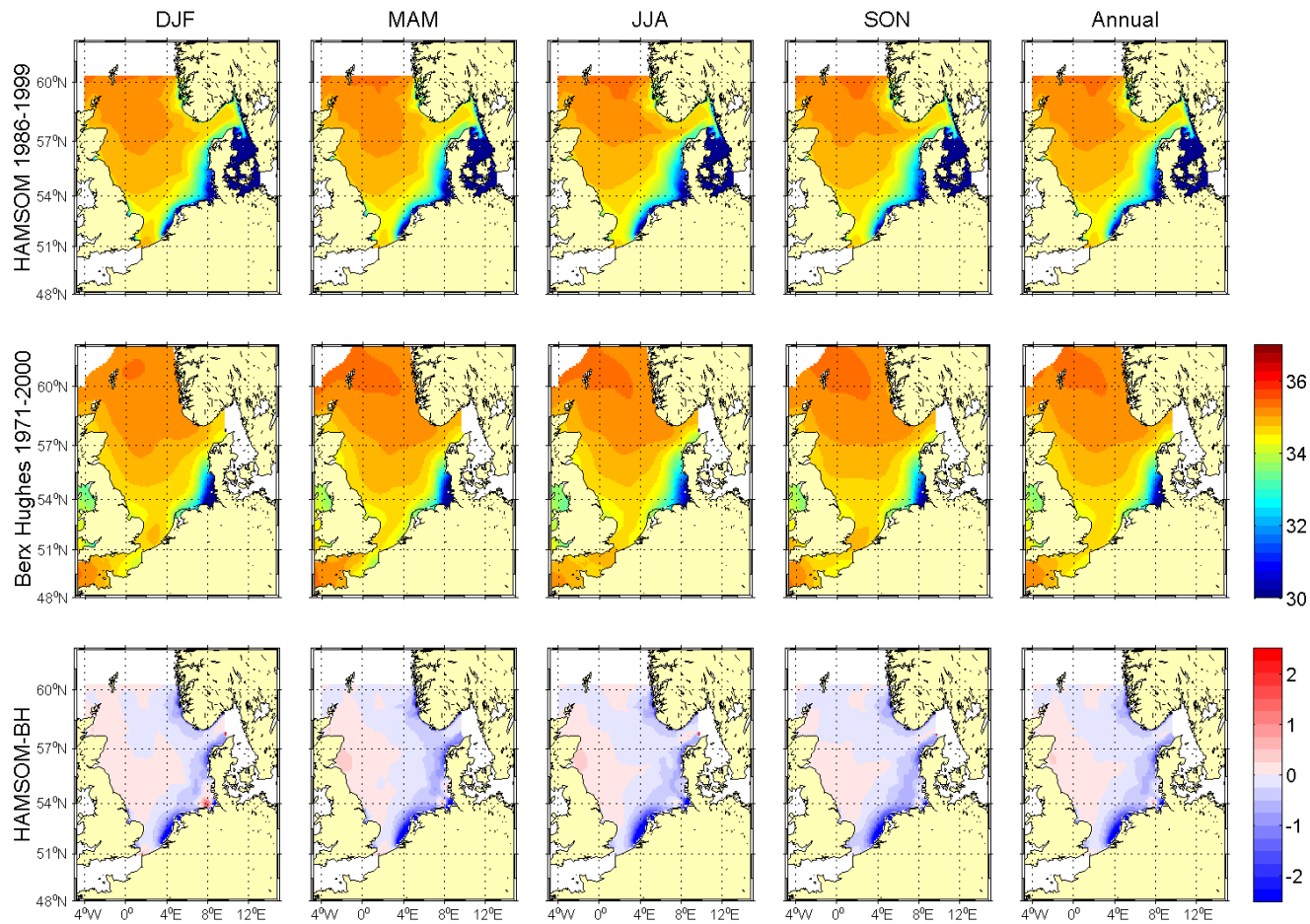


Figure 4.3.29A: Seasonal and annual means of bottom salinity [psu]: The mean bottom salinity results from HAMSOm (run 201) averaged over the period 1986-1999 are presented in the upper row, in the middle row the mean bottom salinity from the BHC averaged over the period 1971-2000 and in the lower row the difference between the model results and the climatology.

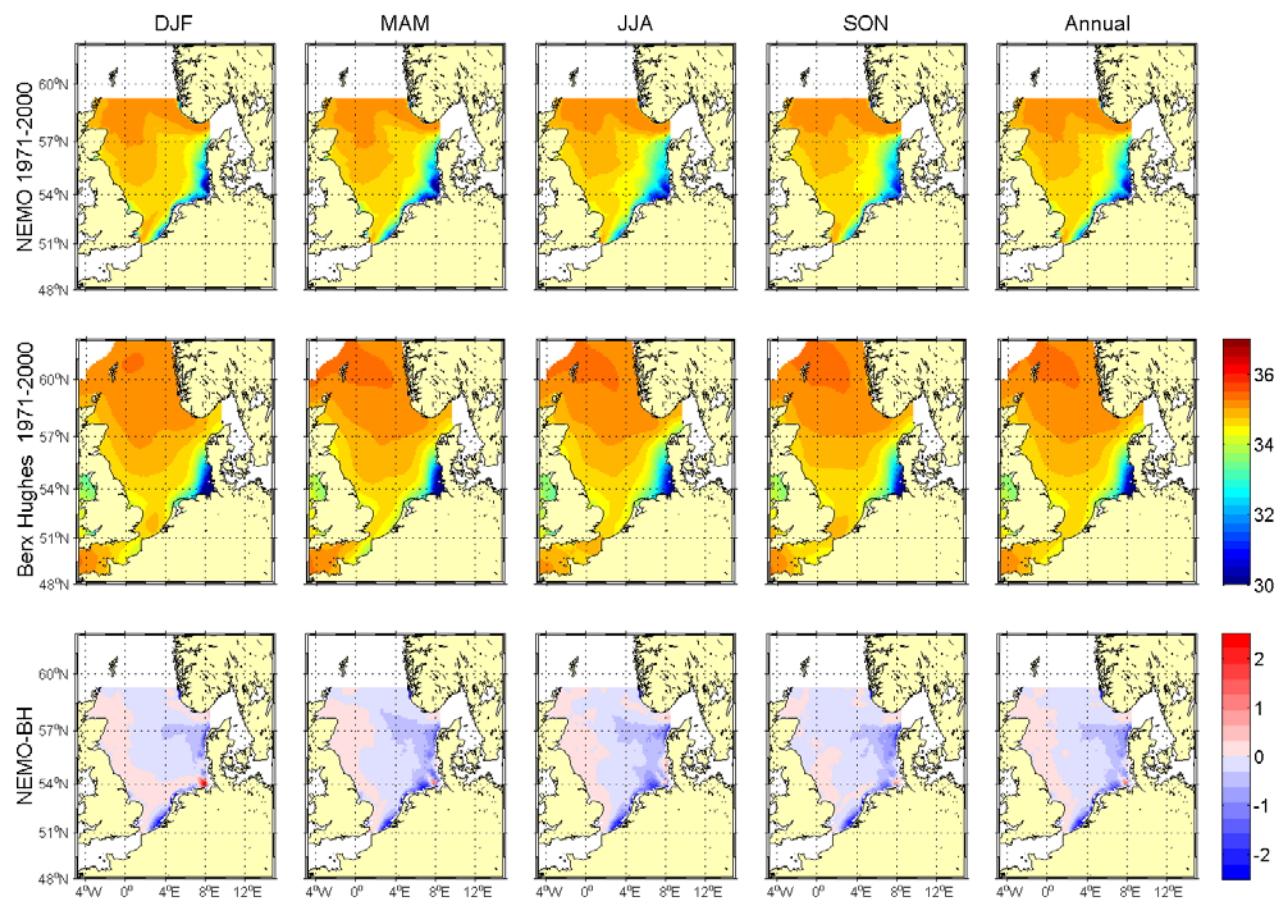


Figure 4.3.30A: Seasonal and annual means of bottom salinity [psu] averaged over the period 1971-2000: The mean bottom salinity results from NEMO-Nordic (run 477) are presented in the upper row, in the middle row the mean bottom salinity from the BHC and in the lower row the difference between the model results and the climatology.

Vertical distribution of temperature and salinity along 56°N and 58°N

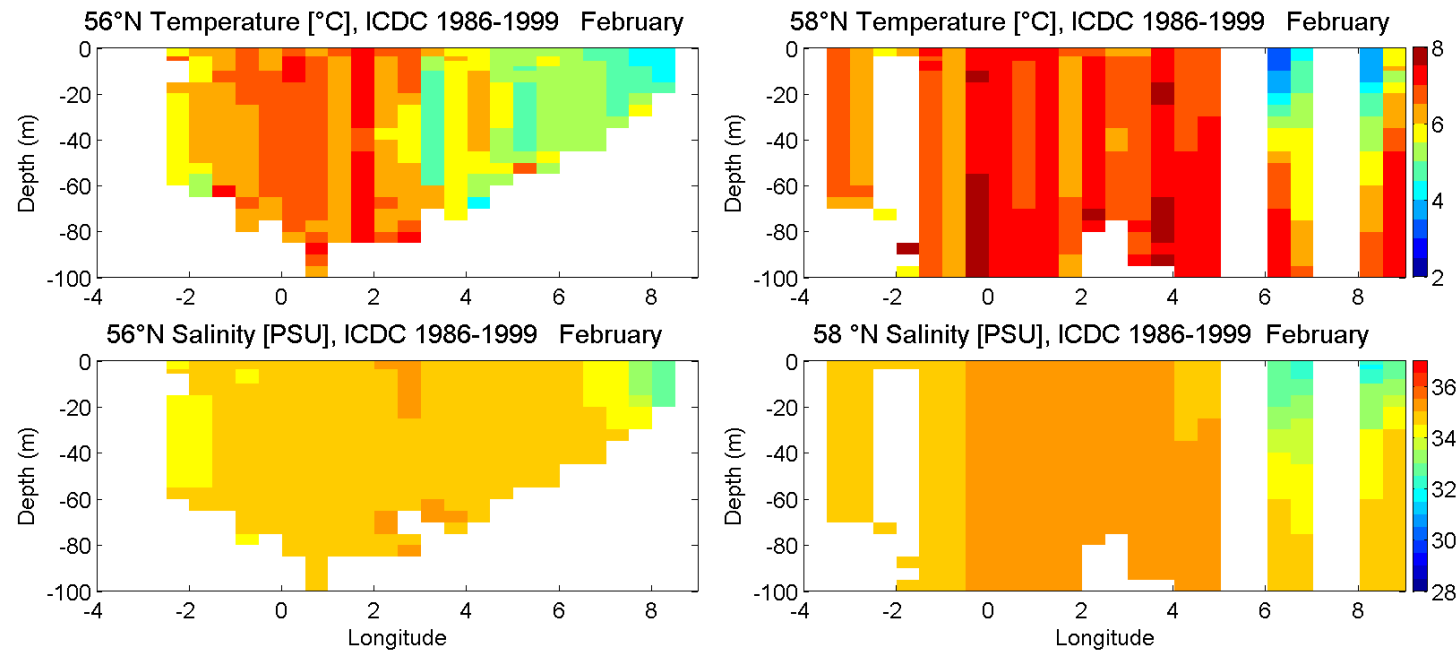


Figure 4.4.1A: The mean February temperature [°C] from the KNCS climatology for the time period 1986-1999 is presented for transect along 56°N left and along 58°N (right). Bottom: The mean February salinity [psu] from the KNCS climatology for the time period 1986-1999 is presented for transect along 56°N (left) and along 58°N (right). Figure 4.4.3 will present transect along 58°N to a depth of -400 m.

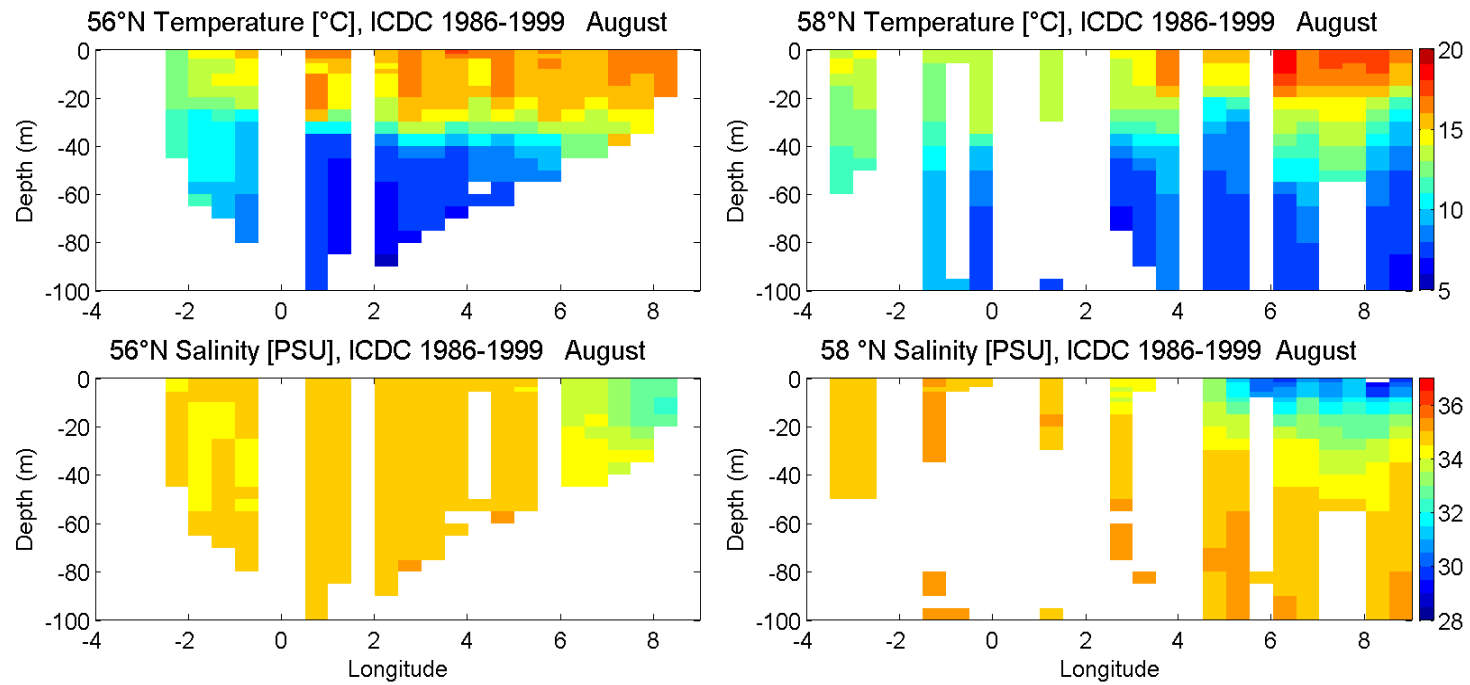


Figure 4.4.2A: The mean August temperature [°C] from the KNSC climatology for the time period 1986-1999 is presented for transect along 56°N left and along 58°N (right). Bottom: The mean August salinity [psu] from the KNSC climatology for the time period 1986-1999 is presented for transect along 56°N (left) and along 58°N (right). Figure 4.4.4 will present transect along 58°N to a depth of -400 m.

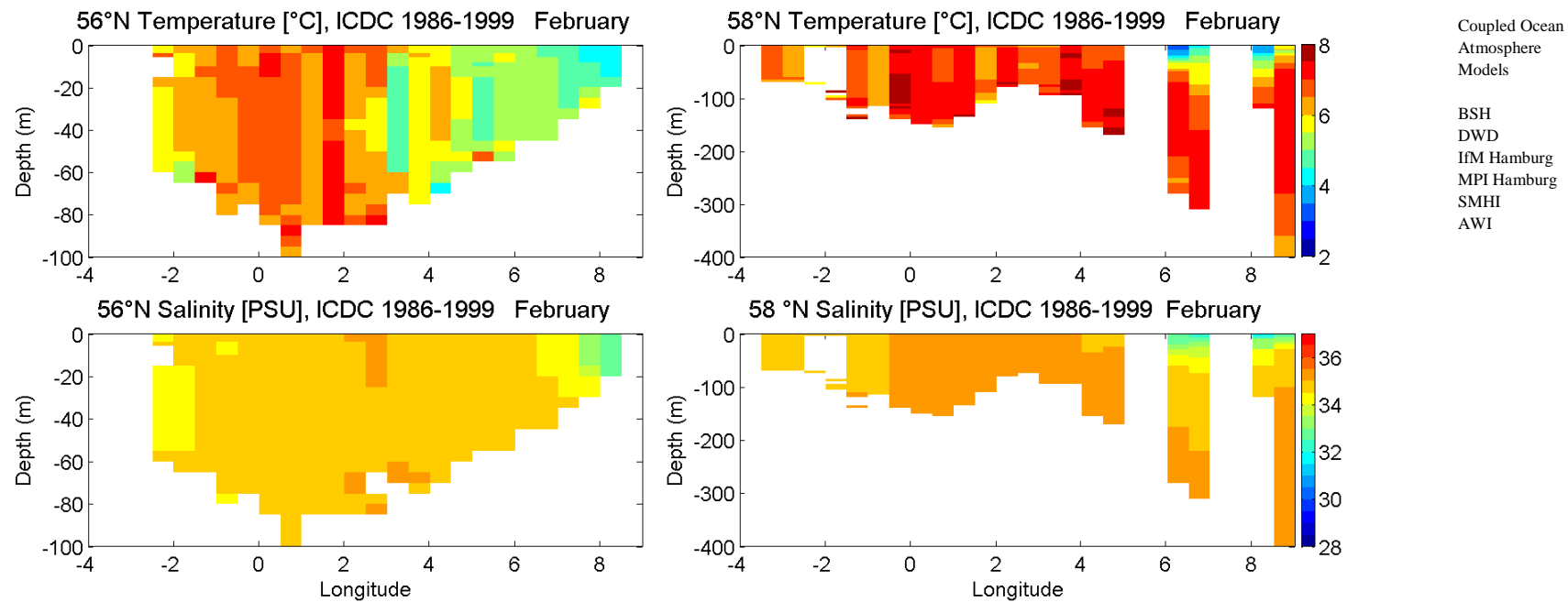


Figure 4.4.3A: The mean February temperature [°C] from the KNSC climatology for the time period 1986-1999 is presented for transect along 56°N left and along 58°N depth to 400 m (right). Bottom: The mean February salinity [psu] from the KNSC climatology for the time period 1986-1999 is presented for transect along 56°N (left) and along 58°N depth to 400 m (right).

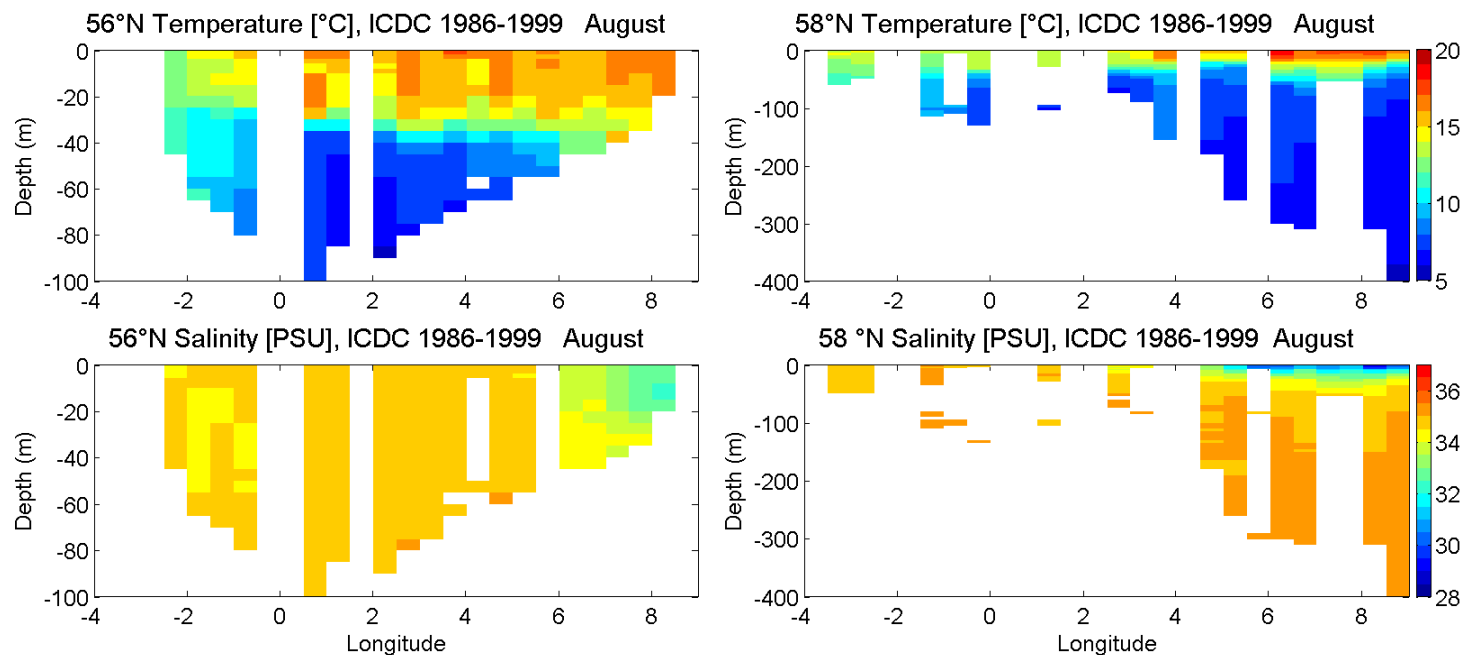


Figure 4.4.4A: The mean August temperature [°C] from the KNSC climatology for the time period 1986-1999 is presented for transect along 56°N left and along 58°N depth to 400 m (right). Bottom: The mean August salinity [psu] from the KNSC climatology for the time period 1986-1999 is presented for transect along 56°N (left) and along 58°N depth to 400 m (right).

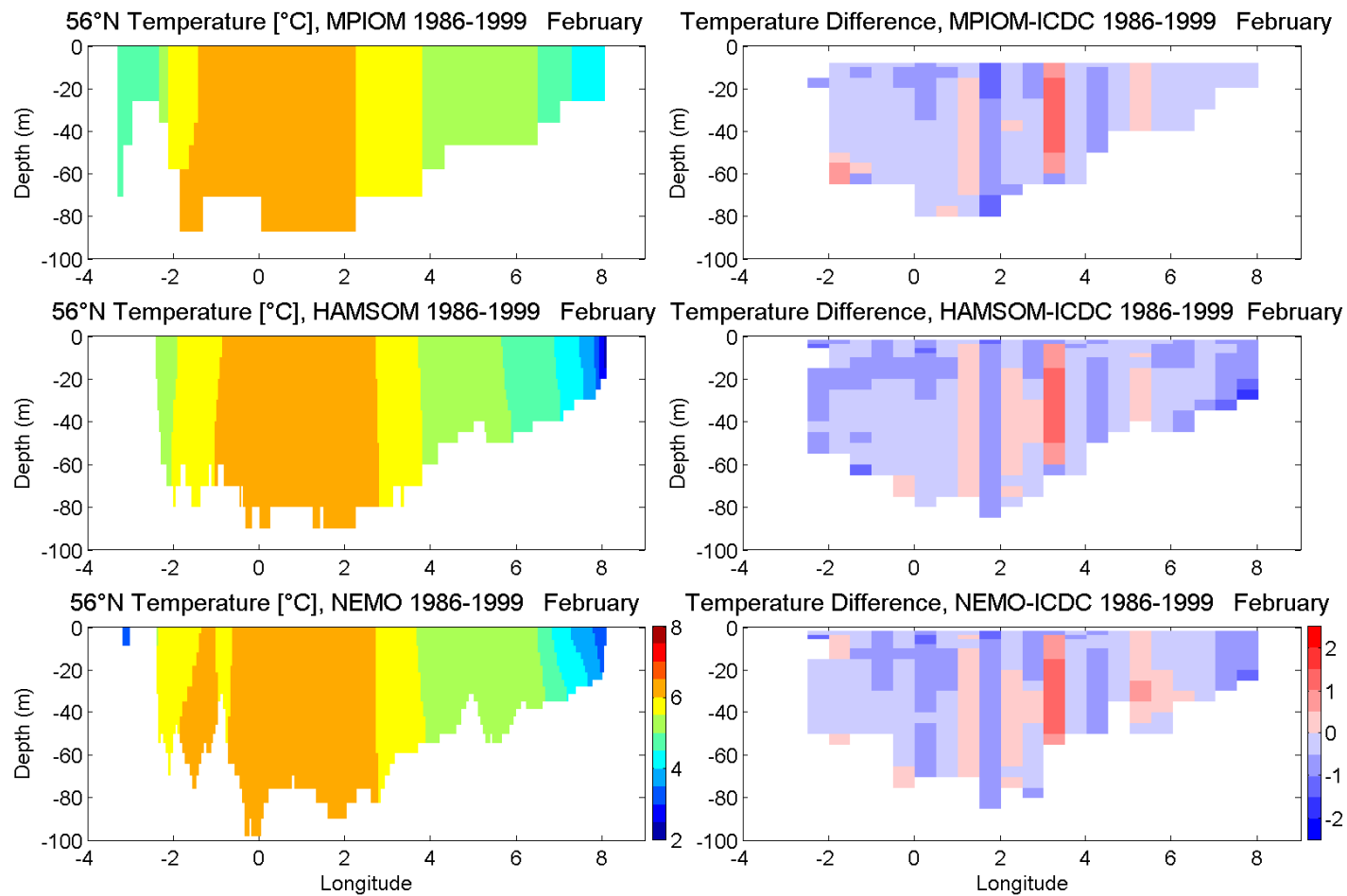


Figure 4.4.5A: The mean February temperature [°C] for the time period 1986-1999 is presented for transect along 56°N. Mean simulated temperature by MPIOM, HAMSOM and NEMO-Nordic (from top to bottom) is presented on the left hand side and on the right hand side the difference between each model result and the temperature from the KNCS climatology.

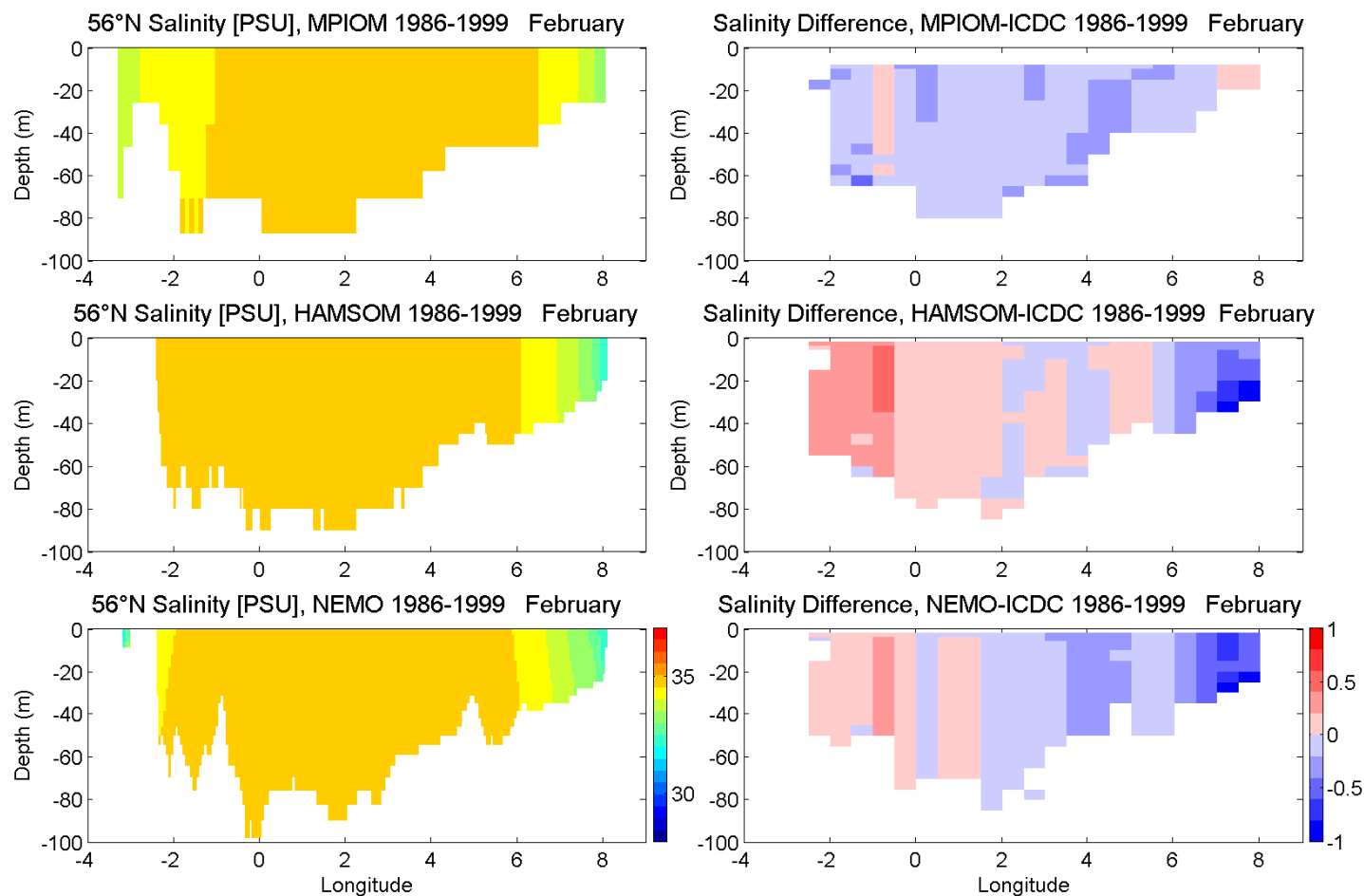


Figure 4.4.6A: The mean February salinity [psu] for the time period 1986-1999 is presented for transect along 56°N. Mean simulated salinity by MPIOM, HAMSOM and NEMO-Nordic (from top to bottom) is presented on the left hand side and on the right hand side the difference between each model result and the temperature from the KNCS climatology.

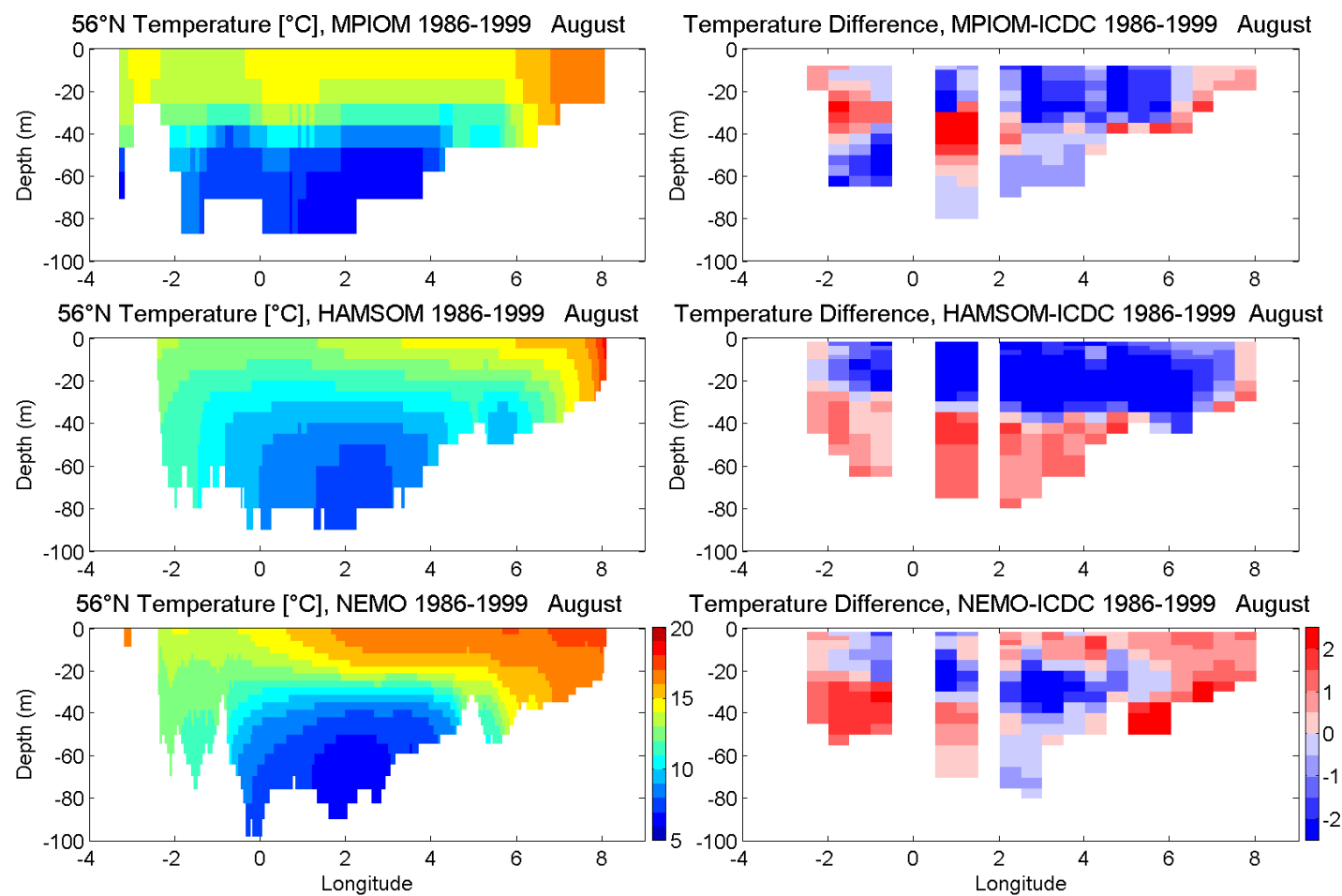


Figure 4.4.7A: The mean August temperature [°C] for the time period 1986-1999 is presented for transect along 56°N. Mean simulated temperature by MPIOM, HAMSOM and NEMO-Nordic (from top to bottom) is presented on the left hand side and on the right hand side the difference between each model result and the temperature from the KNSC climatology.

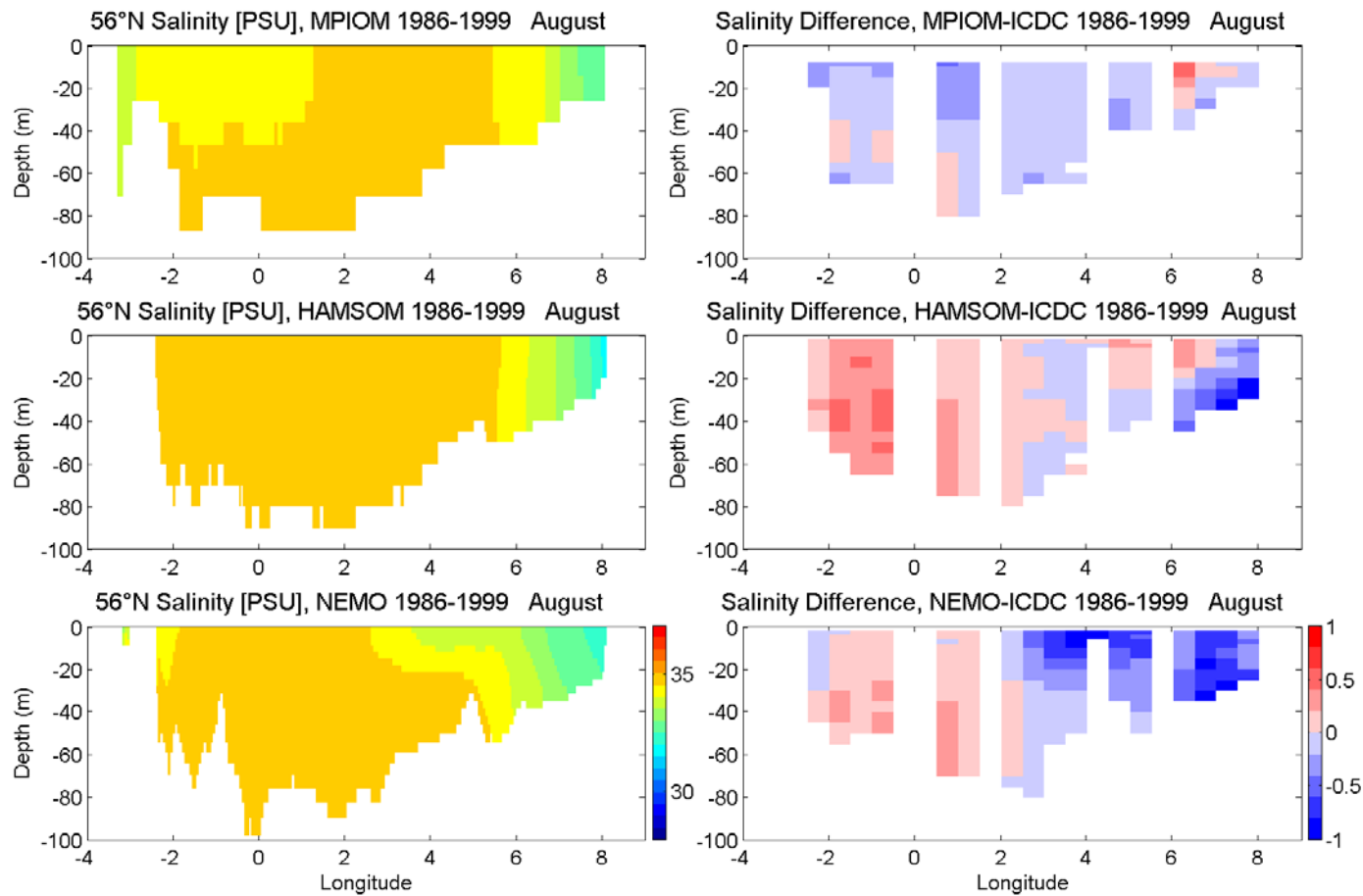


Figure 4.4.8A: The mean August salinity [psu] for the time period 1986-1999 is presented for transect along 56°N. Mean simulated salinity by MPIOM, HAMSOM and NEMO-Nordic (from top to bottom) is presented on the left hand side and on the right hand side the difference between each model result and the temperature from the KNCS climatology.

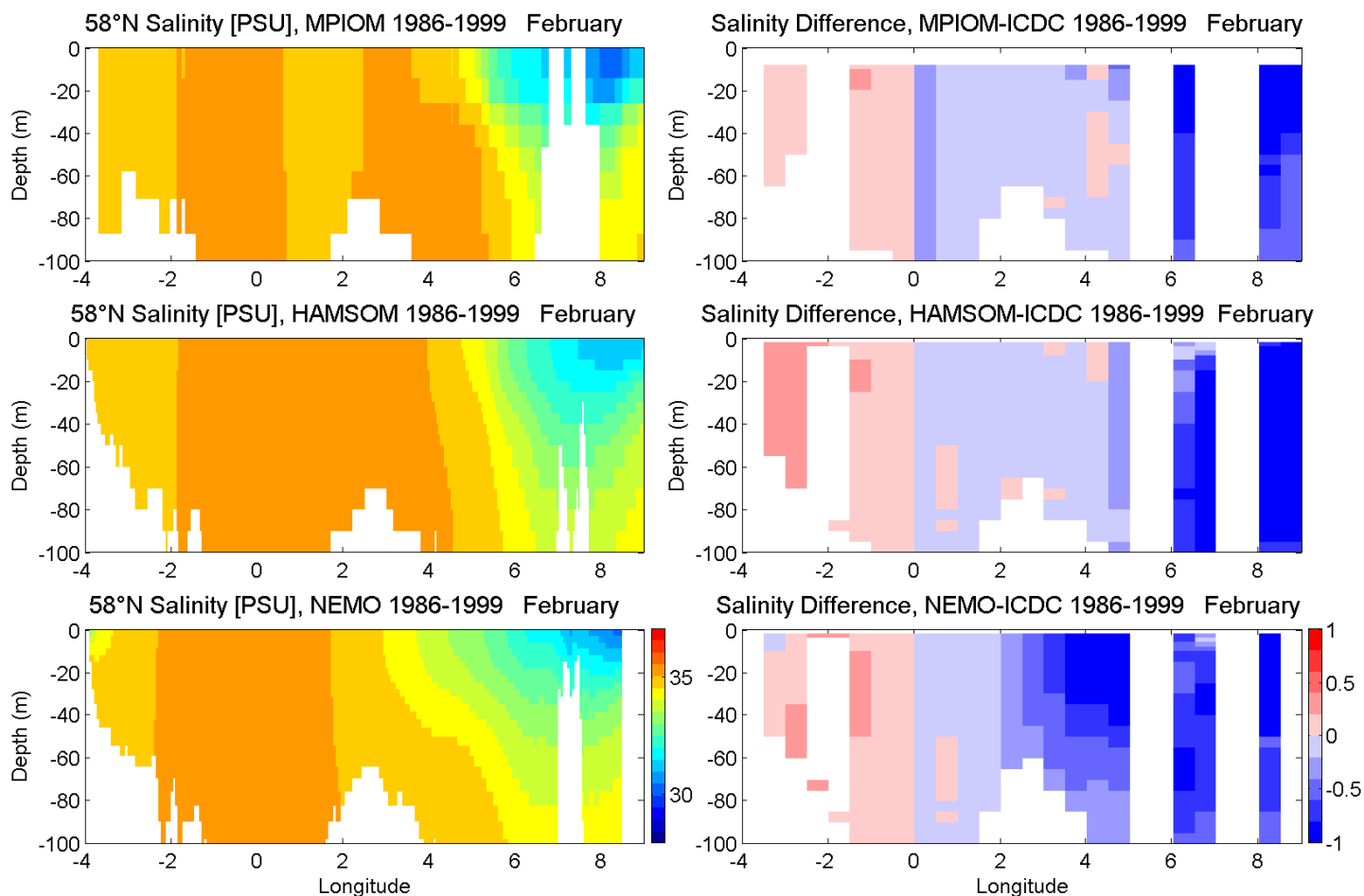


Figure 4.4.10A: The mean February salinity [psu] for the time period 1986-1999 is presented for transect along 58°N. Mean simulated salinity by MPIOM, HAMSOM and NEMO-Nordic (from top to bottom) is presented on the left hand side and on the right hand side the difference between each model result and the temperature from the KNCS climatology. Figure 4.4.14 will present transect along 58°N to a depth of -400 m.

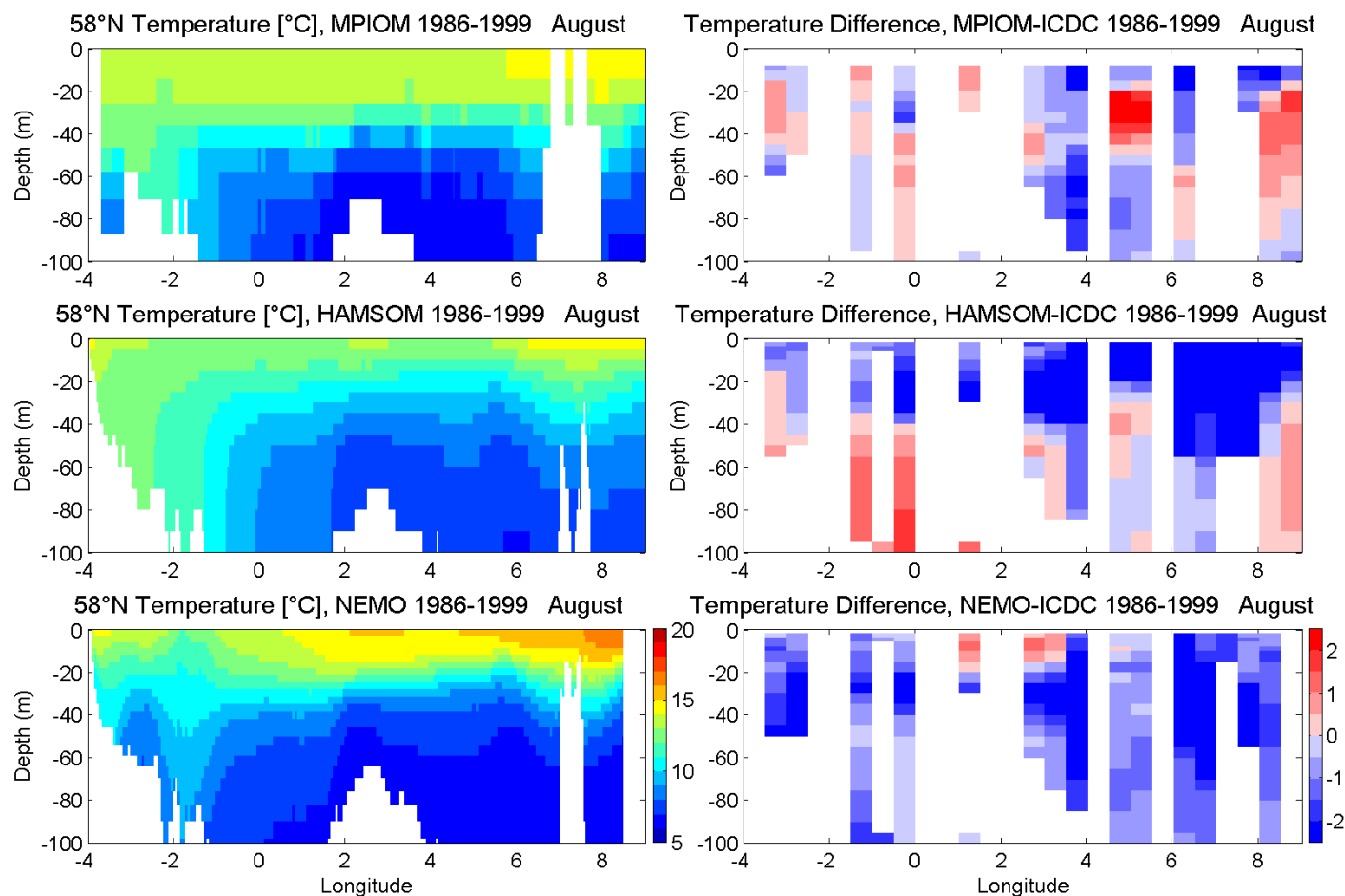


Figure 4.4.11A: The mean August temperature [°C] for the time period 1986-1999 is presented for transect along 58°N. Mean simulated temperature by MPI-OM, HAMSOM and NEMO-Nordic (from top to bottom) is presented on the left hand side and on the right hand side the difference between each model result and the temperature from the KNSC climatology. Figure 4.4.15 will present transect along 58°N to a depth of -400 m.

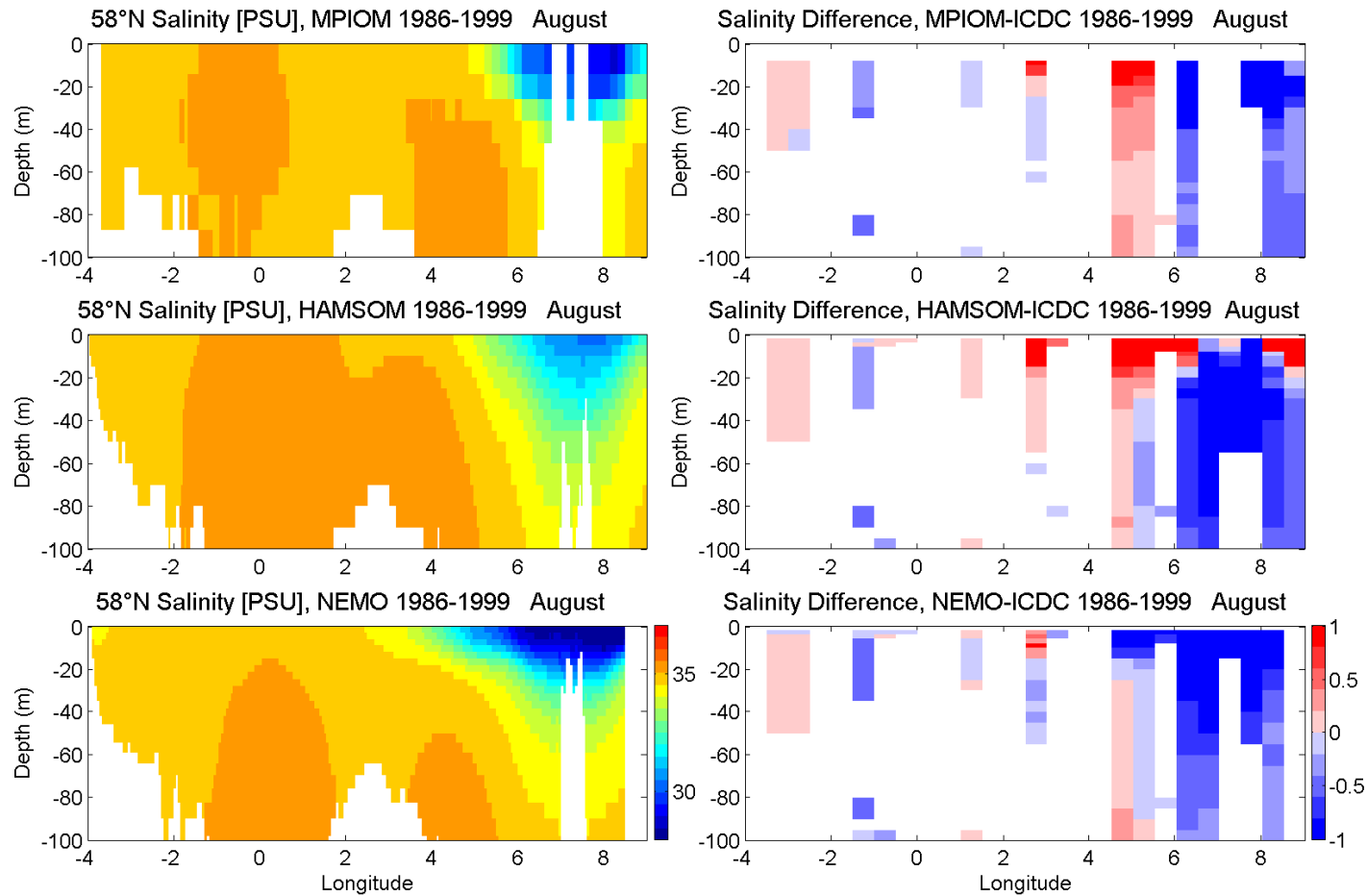


Figure 4.4.12A: The mean August salinity [psu] for the time period 1986-1999 is presented for transect along 58°N. Mean simulated salinity by MPIOM, HAMSOM and NEMO-Nordic (from top to bottom) is presented on the left hand side and on the right hand side the difference between each model result and the temperature from the KNCS climatology. Figure 4.4.16 will present transect along 58°N to a depth of -400 m.

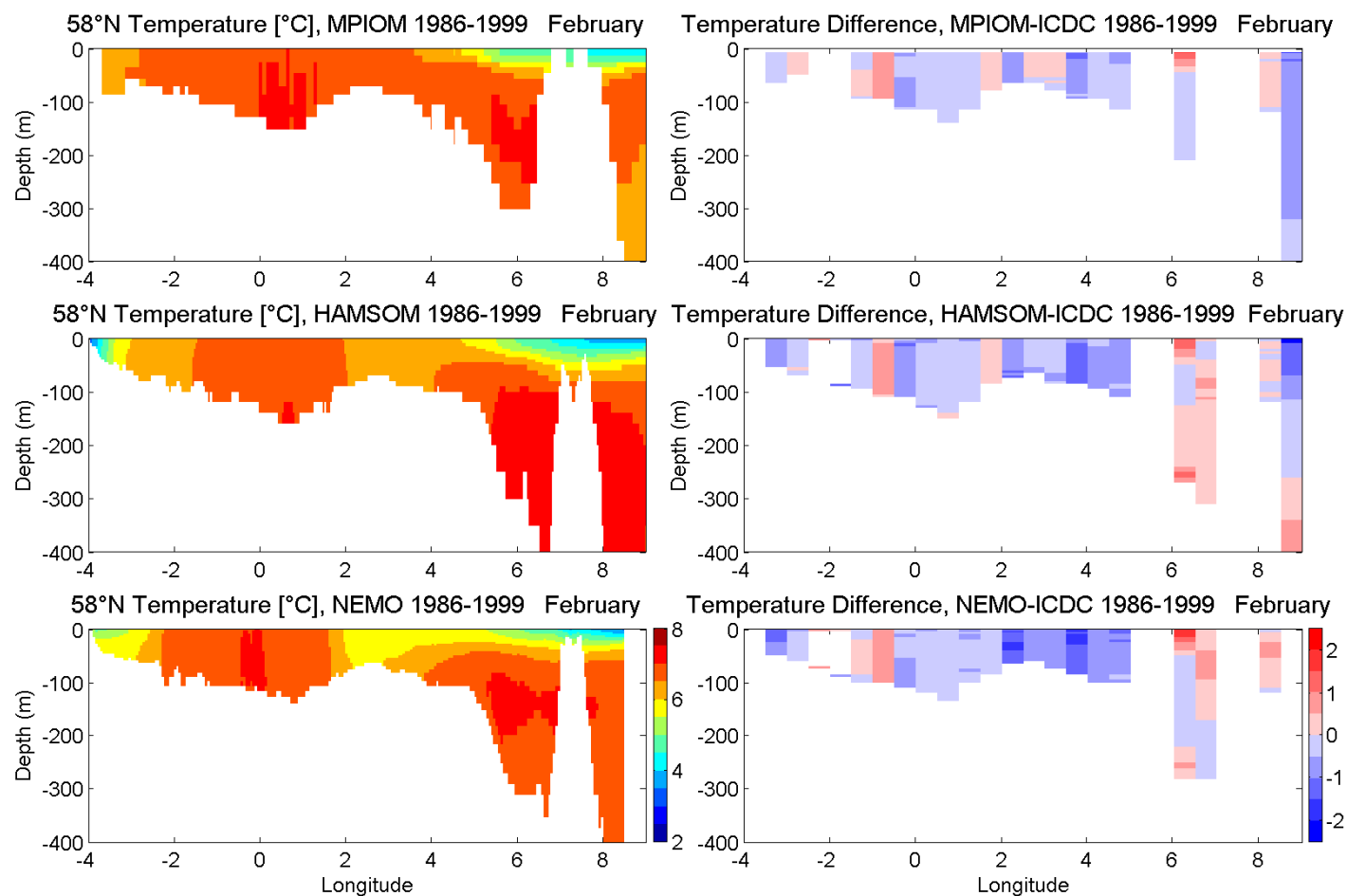


Figure 4.4.13A: The mean February temperature [°C] for the time period 1986-1999 is presented for transect along 58°N. Mean simulated temperature by MPIOM, HAMSOM and NEMO-Nordic (from top to bottom) is presented on the left hand side and on the right hand side the difference between each model result and the temperature from the KNSC climatology.

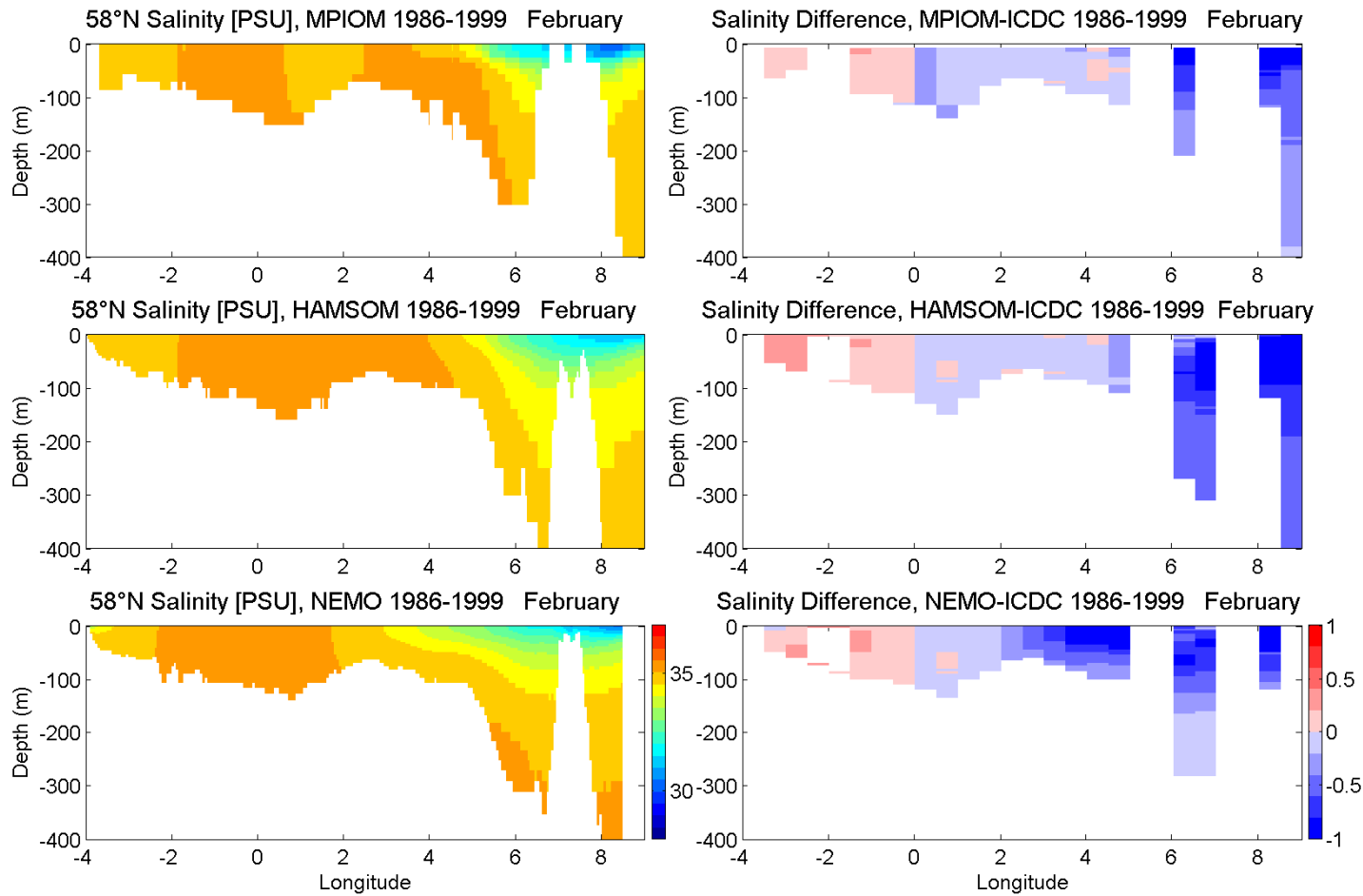


Figure 4.4.14A: The mean February salinity [psu] for the time period 1986-1999 is presented for transect along 58°N. Mean simulated salinity by MPIOM, HAMSOM and NEMO-Nordic (from top to bottom) is presented on the left hand side and on the right hand side the difference between each model result and the temperature from the KNCS climatology.

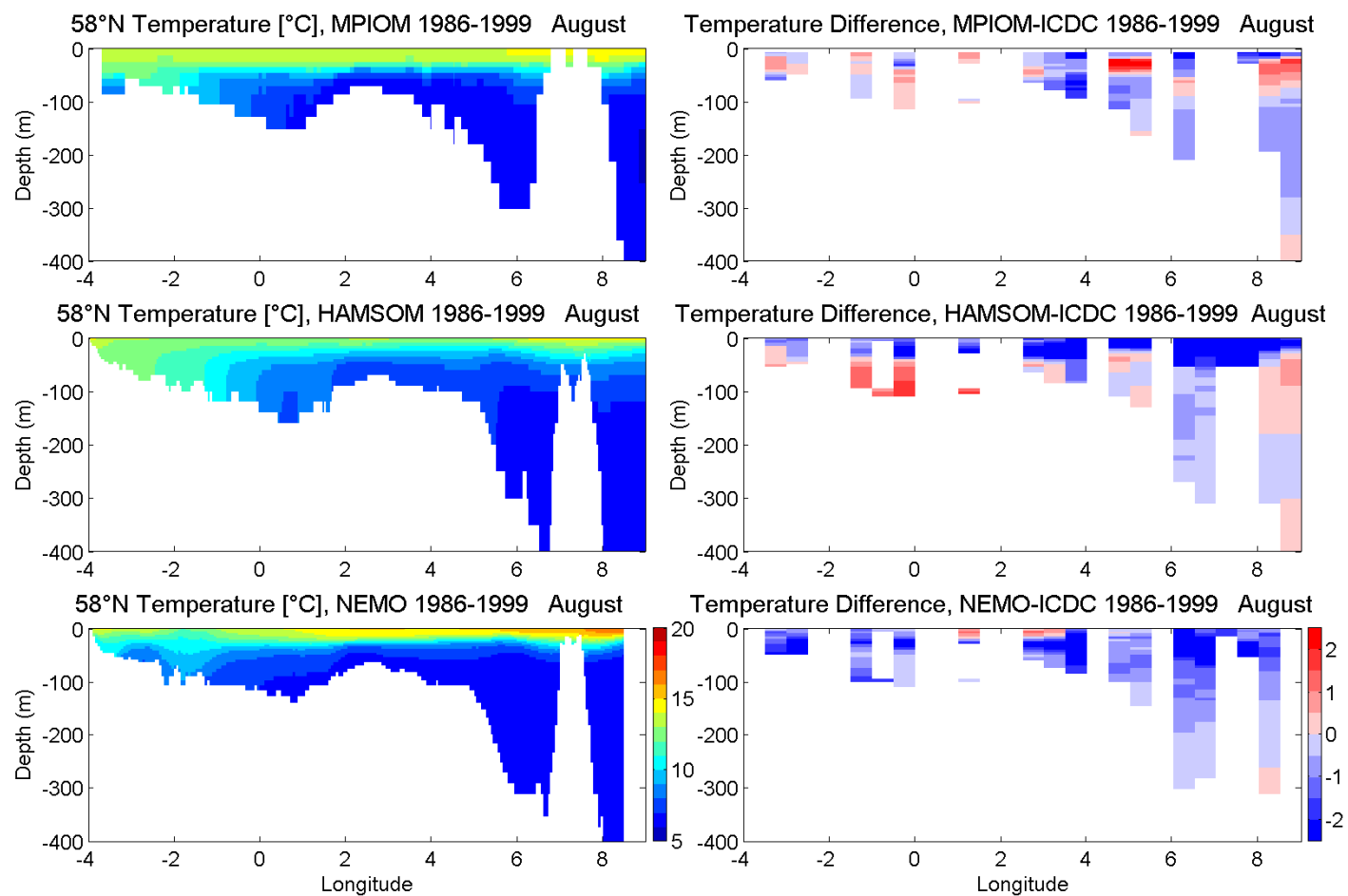


Figure 4.4.15A: The mean August temperature [°C] for the time period 1986-1999 is presented for transect along 58°N. Mean simulated temperature by MPI-OM, HAMSOM and NEMO-Nordic (from top to bottom) is presented on the left hand side and on the right hand side the difference between each model result and the temperature from the KNSC climatology.

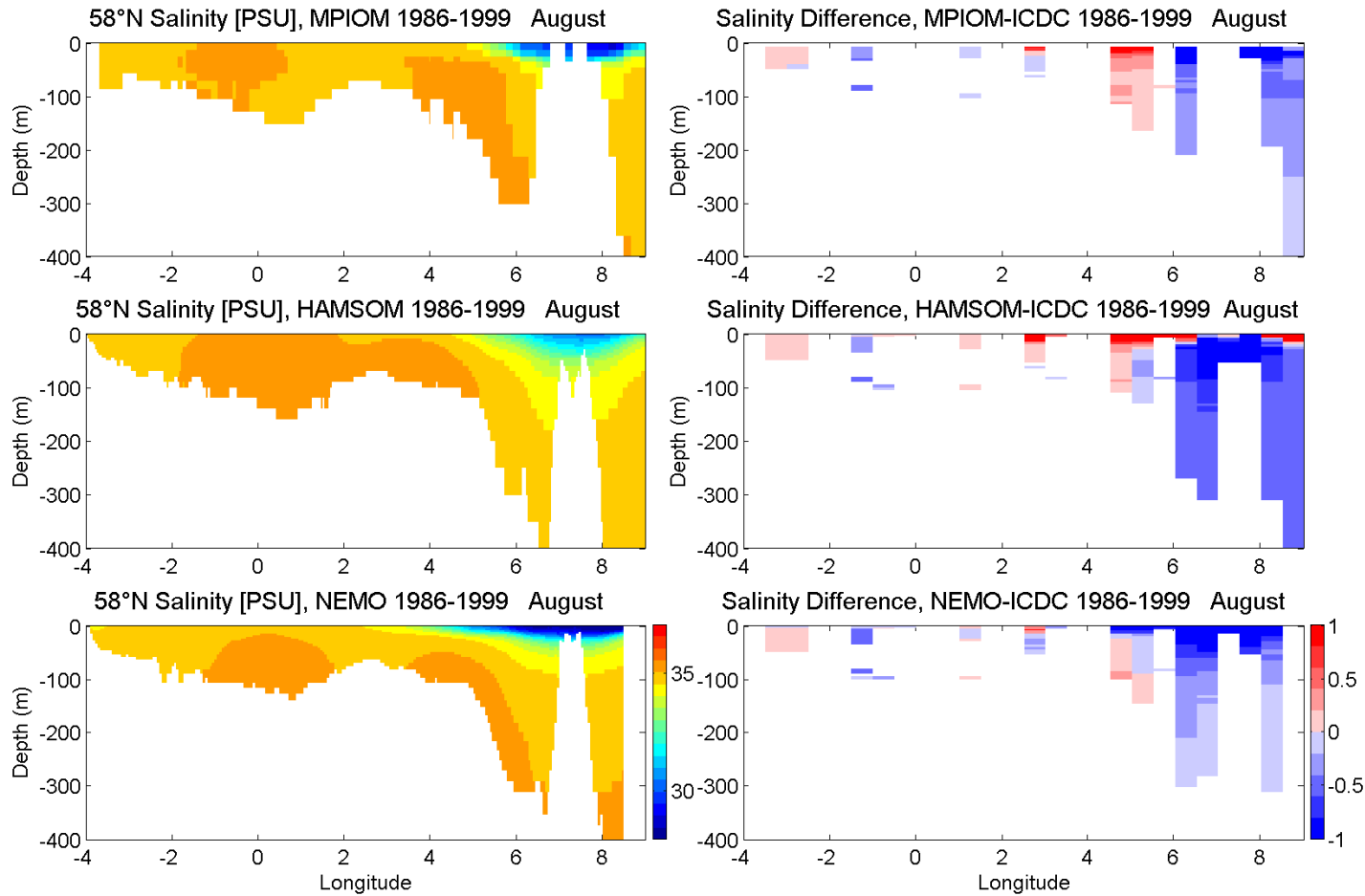


Figure 4.4.16A: The mean August salinity [psu] for the time period 1986-1999 is presented for transect along 58°N. Mean simulated salinity by MPIOM, HAMSOM and NEMO-Nordic (from top to bottom) is presented on the left hand side and on the right hand side the difference between each model result and the temperature from the KNSC climatology.

11 Appendix 2: Figures from the SRES A1B simulations in chapter 5

Coupled Ocean
Atmosphere
Models

BSH
DWD
IfM Hamburg
MPI Hamburg
SMHI
AWI

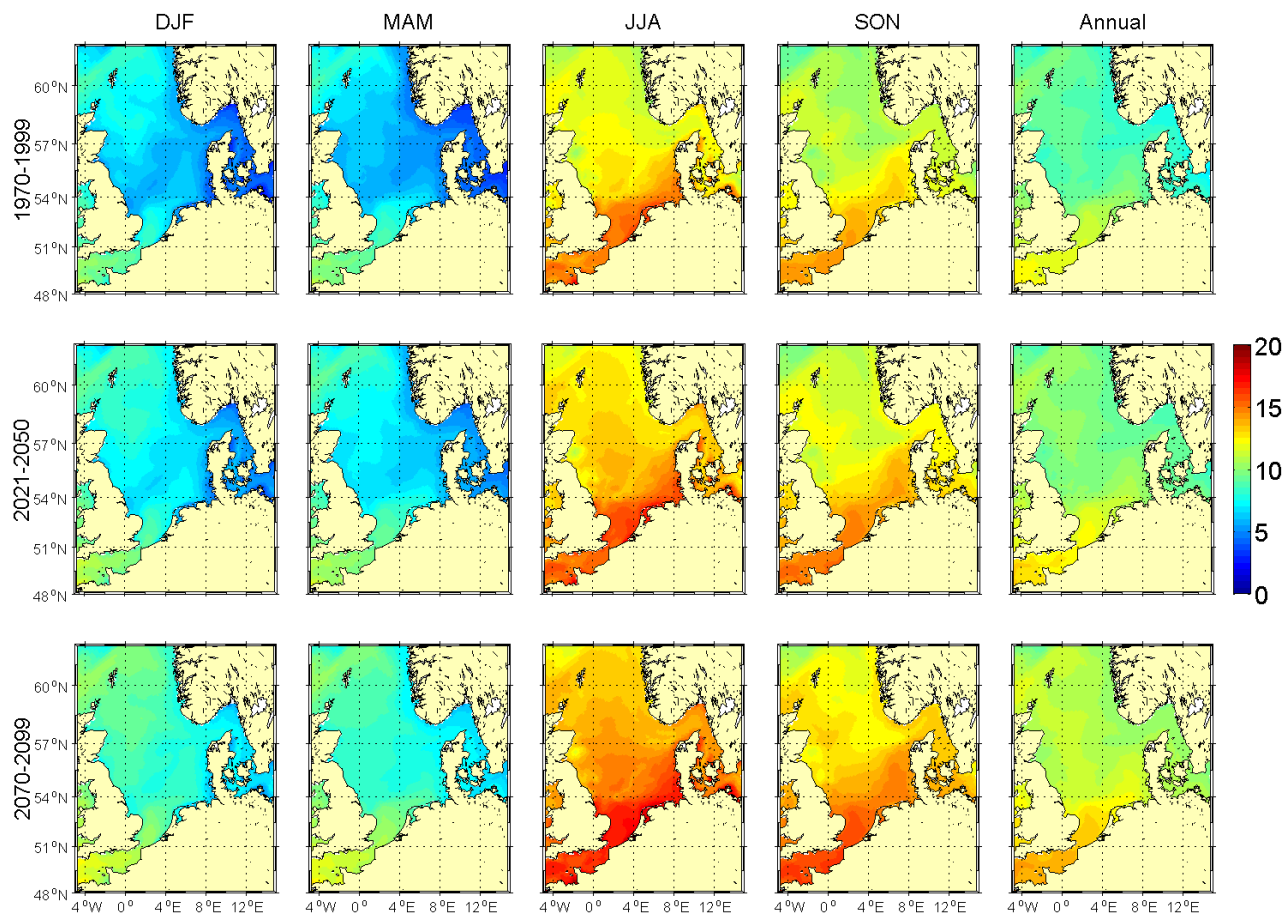


Figure 5.1.1A: Seasonal and annual means of sea surface temperature [°C] for MPIOM run 215 (A1B scenario run). The upper row shows averages for the period 1970-1999, the middle row for 2021-2050 and the lower row for 2070-2099.

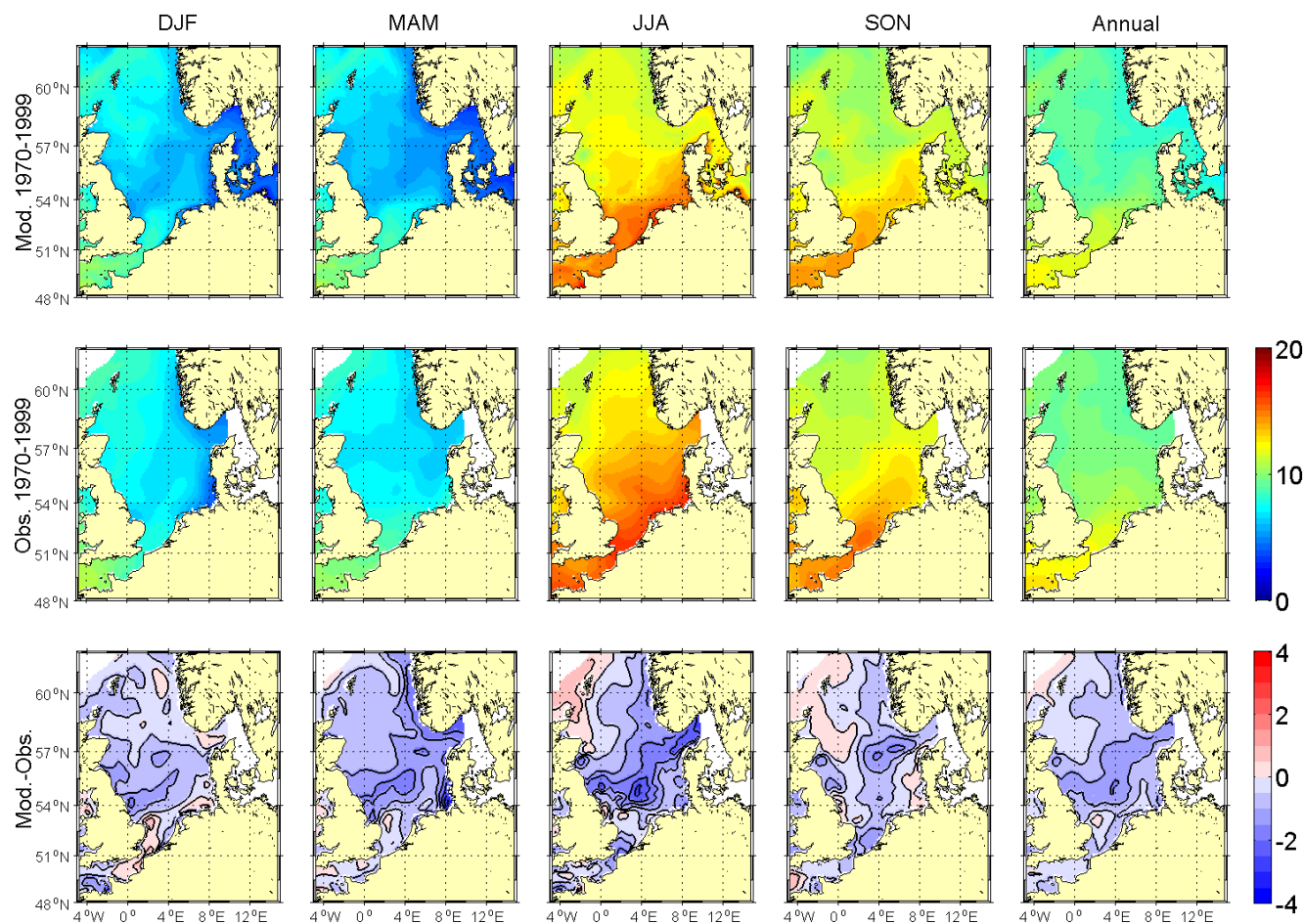


Figure 5.1.2A: Comparison of seasonal and annual means of sea surface temperature [°C] for MPIOM run 215 for the base period 1970-1999 with climatological means from the BHC. The upper row shows average model distributions, the middle row observed climatological means and the lower row difference between the model results and the climatology.

Coupled Ocean
Atmosphere
Models

BSH
DWD
IfM Hamburg
MPI Hamburg
SMHI
AWI

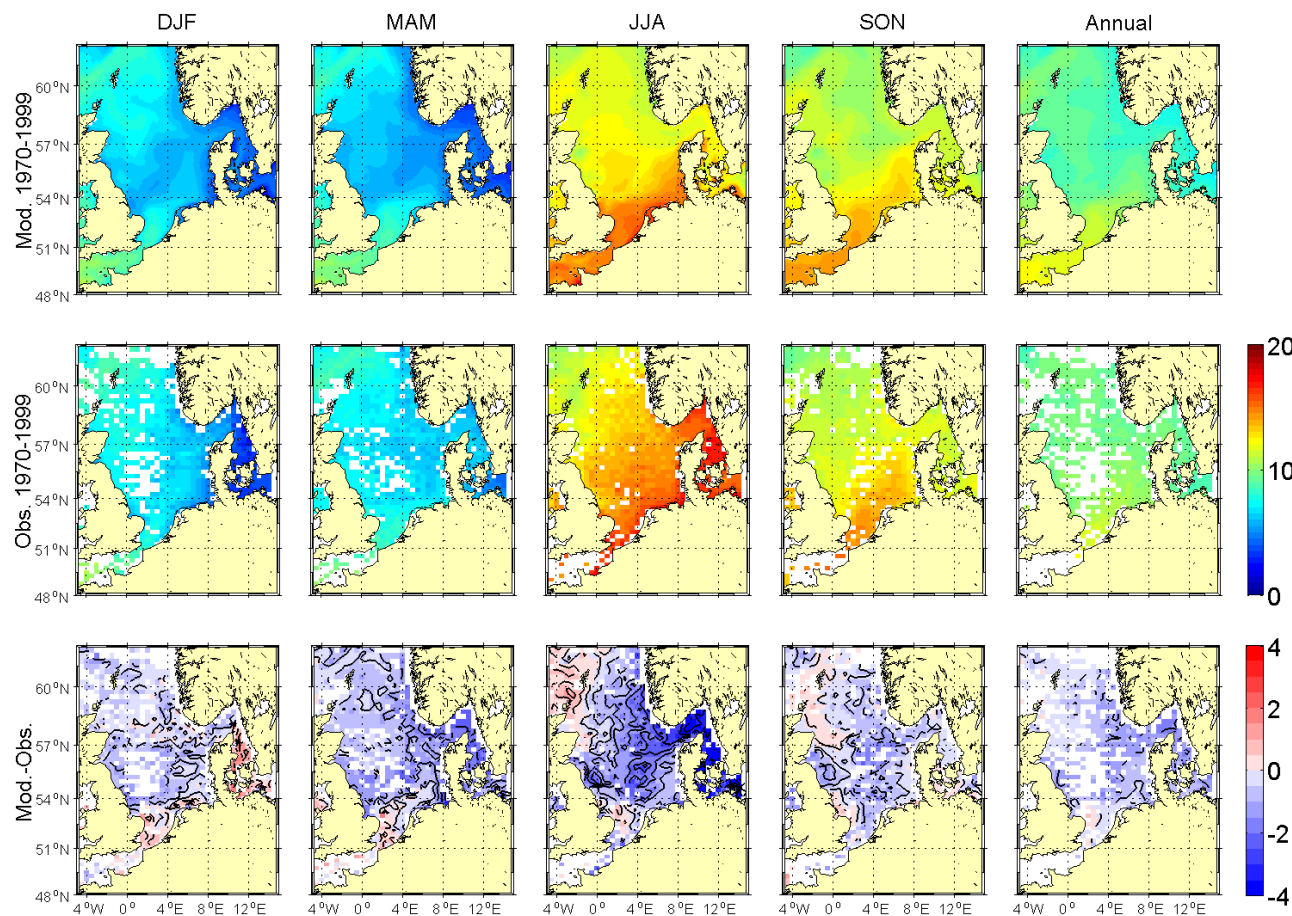


Figure 5.1.3A: Comparison of seasonal and annual means of sea surface temperature [°C] for MPIOM run 215 for the base period 1970-1999 with climatological means from the KNSC. The upper row shows average model distributions, the middle row observed climatological means and the lower row difference between the model results and the climatology.

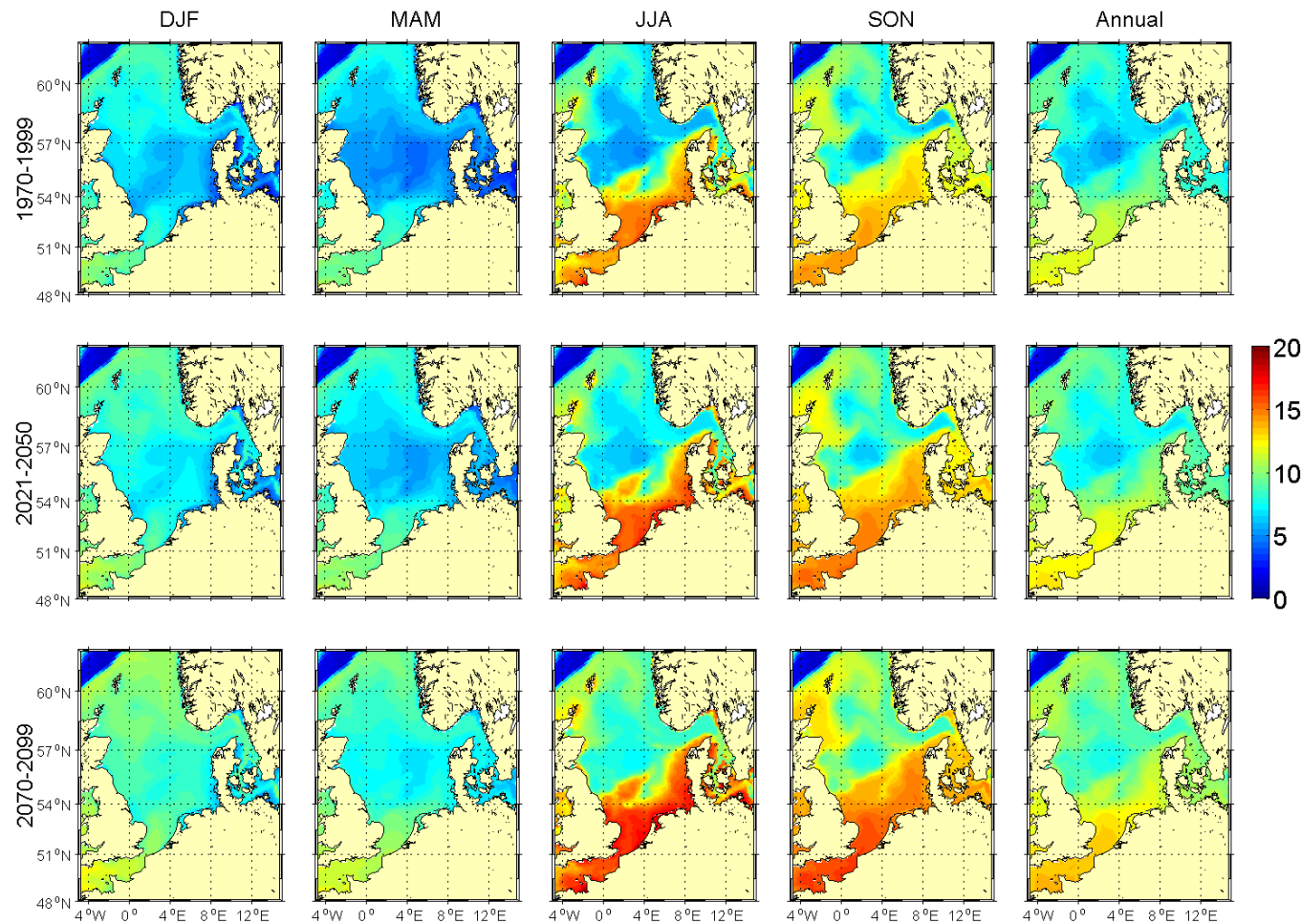


Figure 5.1.4A: Seasonal and annual means of bottom temperature [°C] for MPIOM run 215 (A1B scenario run). The upper row shows averages for the period 1970-1999, the middle row for 2021-2050 and the lower row for 2070-2099.

Coupled Ocean
Atmosphere
Models

BSH
DWD
IfM Hamburg
MPI Hamburg
SMHI
AWI

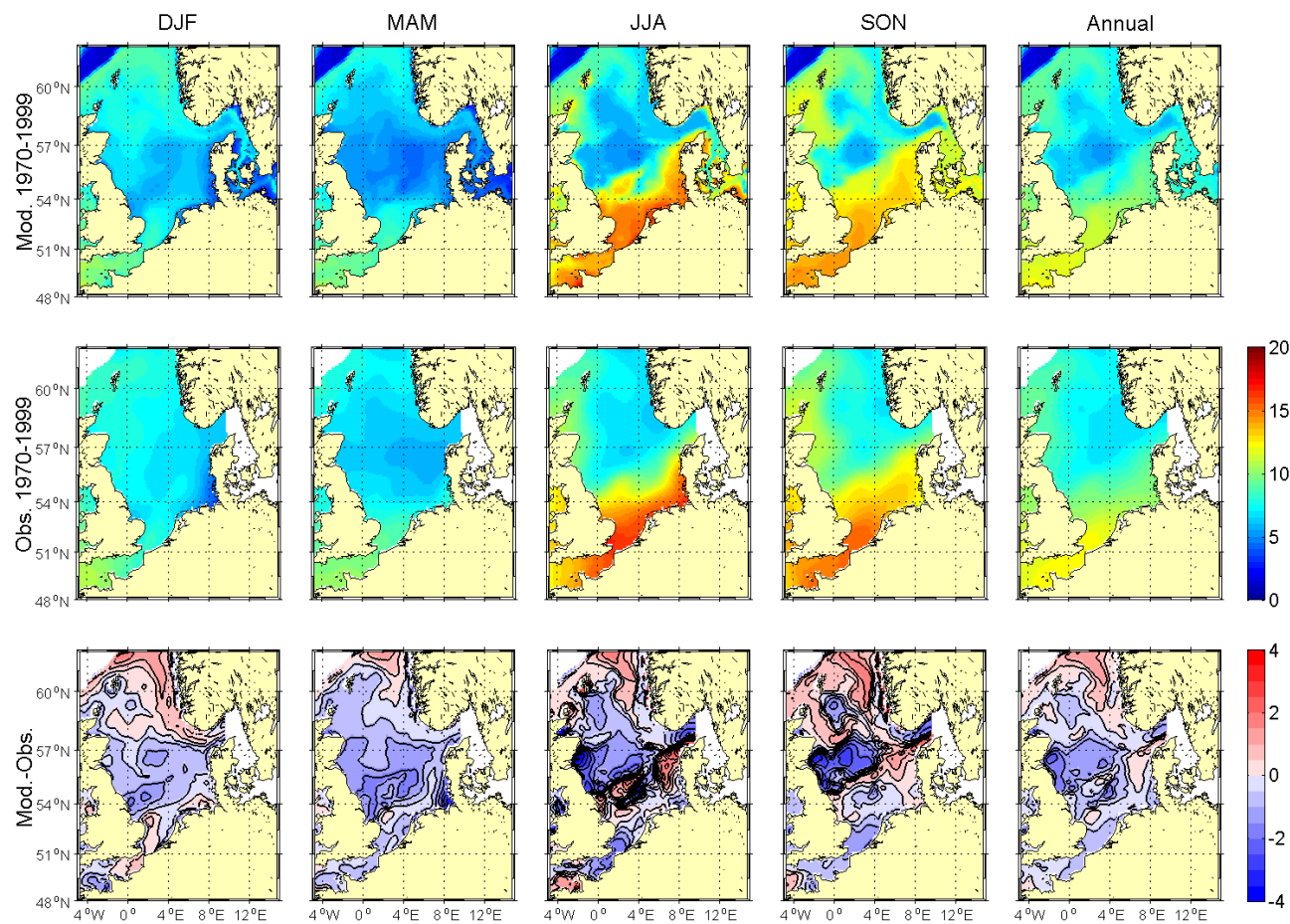


Figure 5.1.5A: Comparison of seasonal and annual means of bottom temperature [°C] for MPIOM run 215 for the base period 1970-1999 with BHC means. The upper row shows average model distributions, the middle row observed climatological means and the lower row the difference between the model results and the climatology.

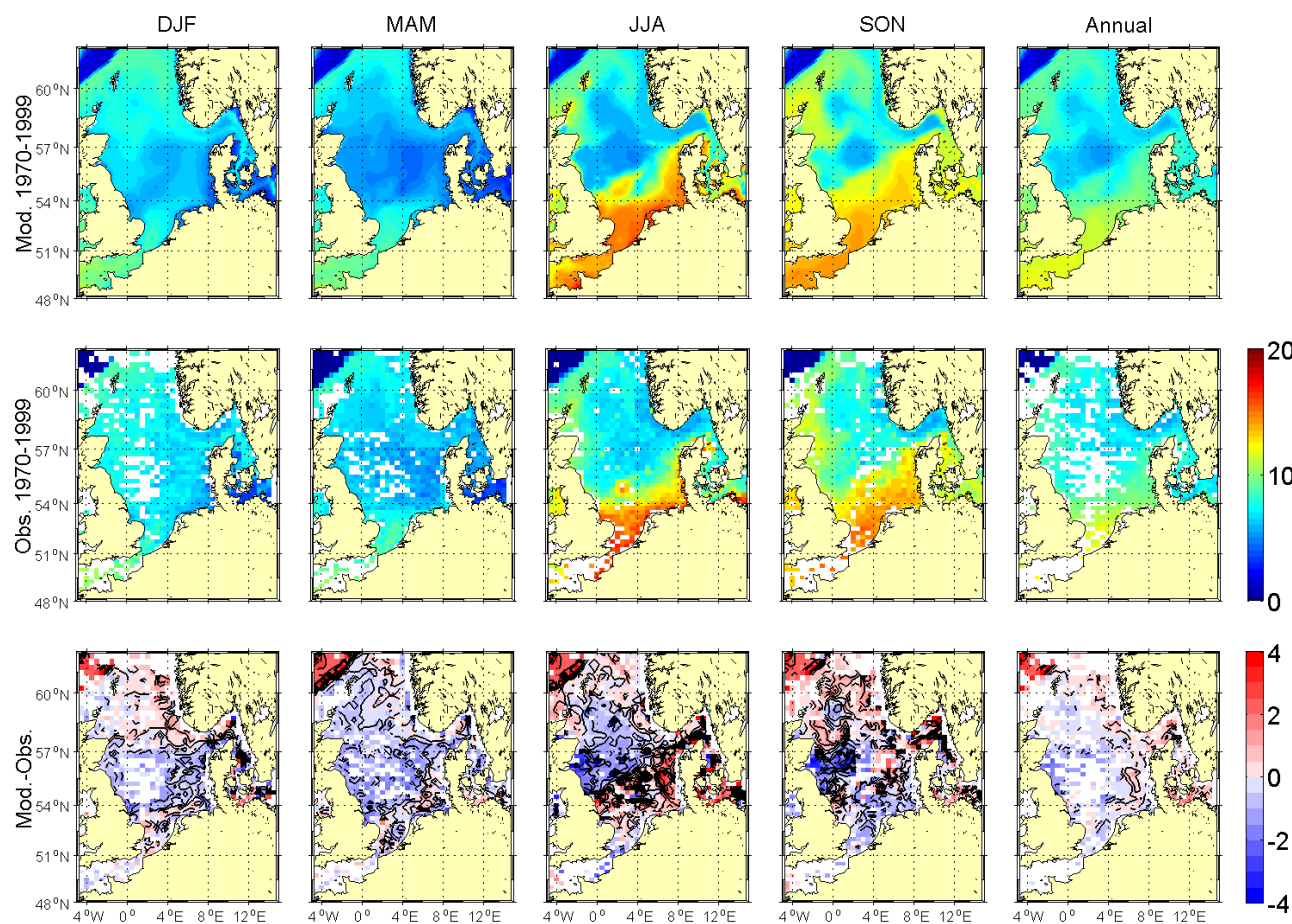


Figure 5.1.6A: Comparison of seasonal and annual means of bottom temperature [°C] for MPIOM run 215 for the base period 1970-1999 with KNSC means. The upper row shows average model distributions, the middle row observed climatological means and the lower row the difference between the model results and the climatology.

Coupled Ocean
Atmosphere
Models

BSH
DWD
IfM Hamburg
MPI Hamburg
SMHI
AWI

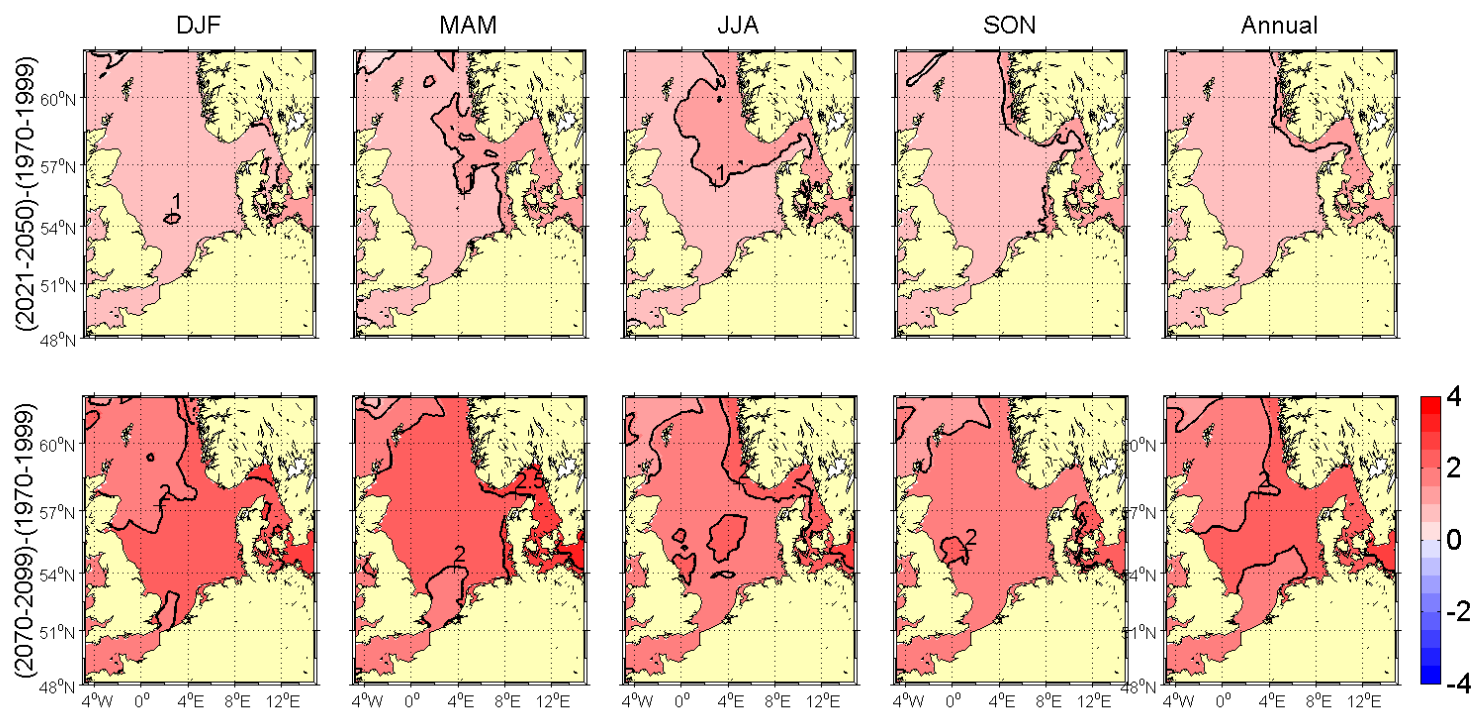


Figure 5.1.7A: Changes in seasonal and annual sea surface temperature [°C] for MPIOM run 215 (A1B scenario run). Upper panel from (1970-1999) to (2021-2050) and lower panel from (1970-1999) to (2070-2099). The contour interval is 0.5 °C. Selected isolines have been labelled for better orientation.

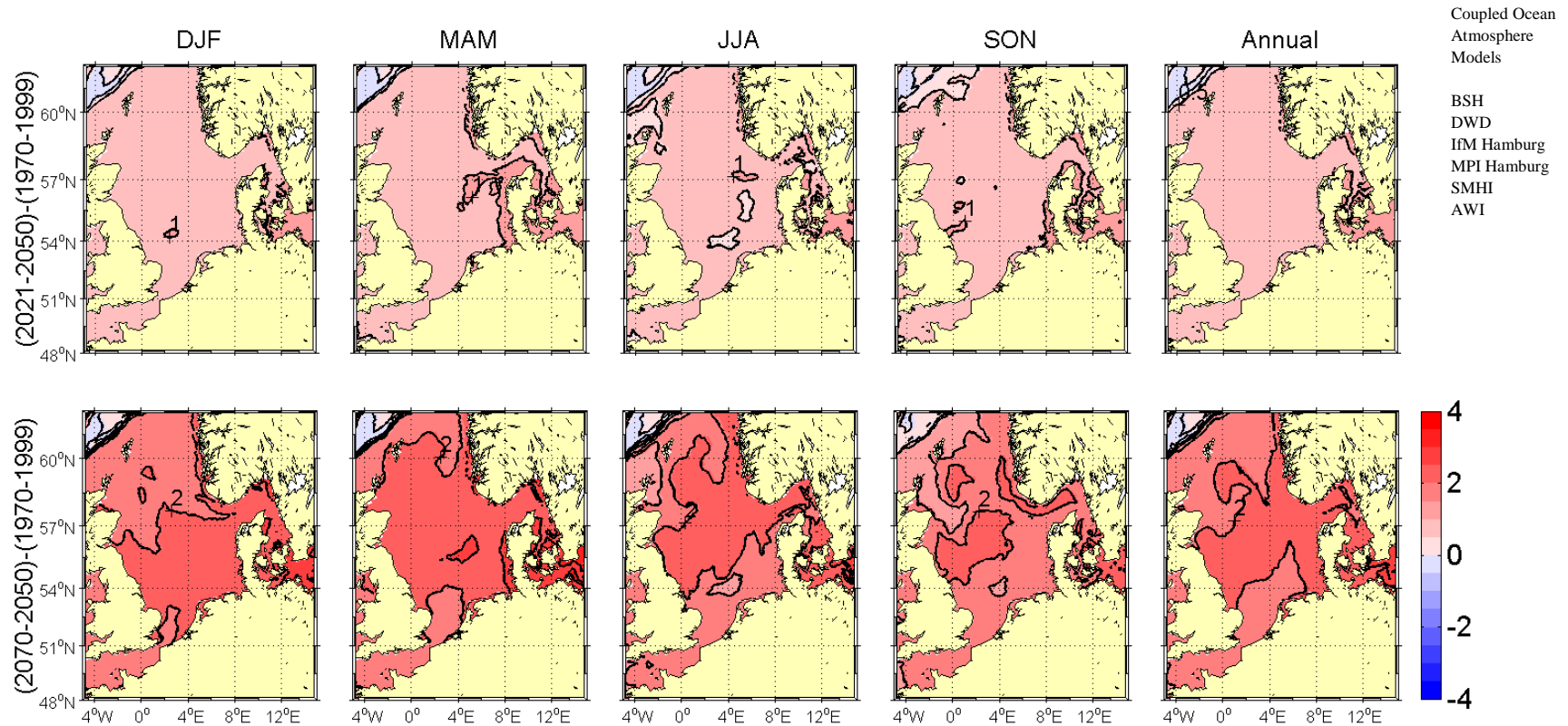


Figure 5.1.8A: Changes in seasonal and annual bottom temperature [°C] for MPIOM run 215 (A1B scenario run). Upper panel from (1970-1999) to (2021-2050) and lower panel from (1970-1999) to (2070-2099). The contour interval is 0.5 °C. Selected isolines have been labelled for better orientation.

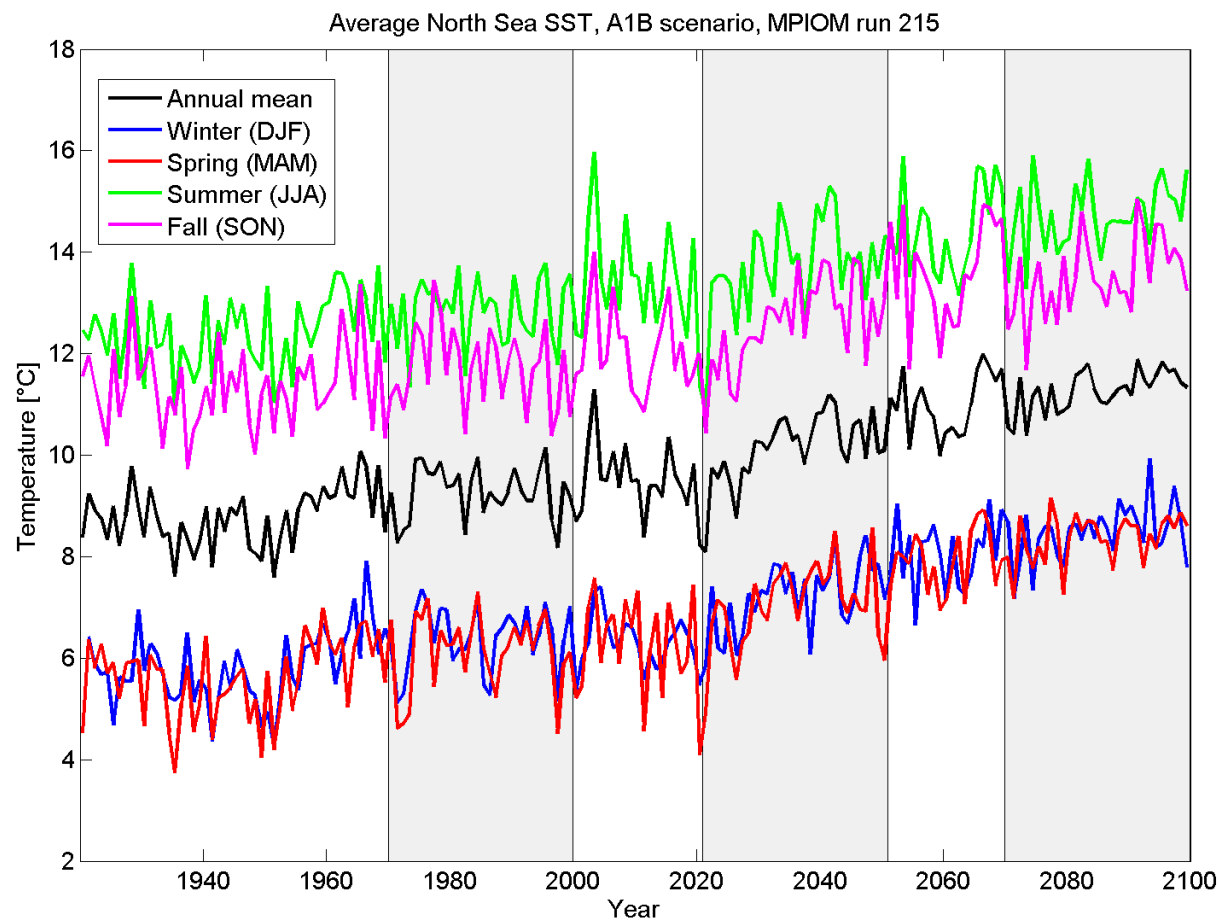


Figure 5.1.9A: Time series of seasonal and annual means of sea surface temperature [°C] for MPIOM run 215 (A1B scenario run) from 1920-2099. The temperatures represent averages over the North Sea area given in Figure 4.1.

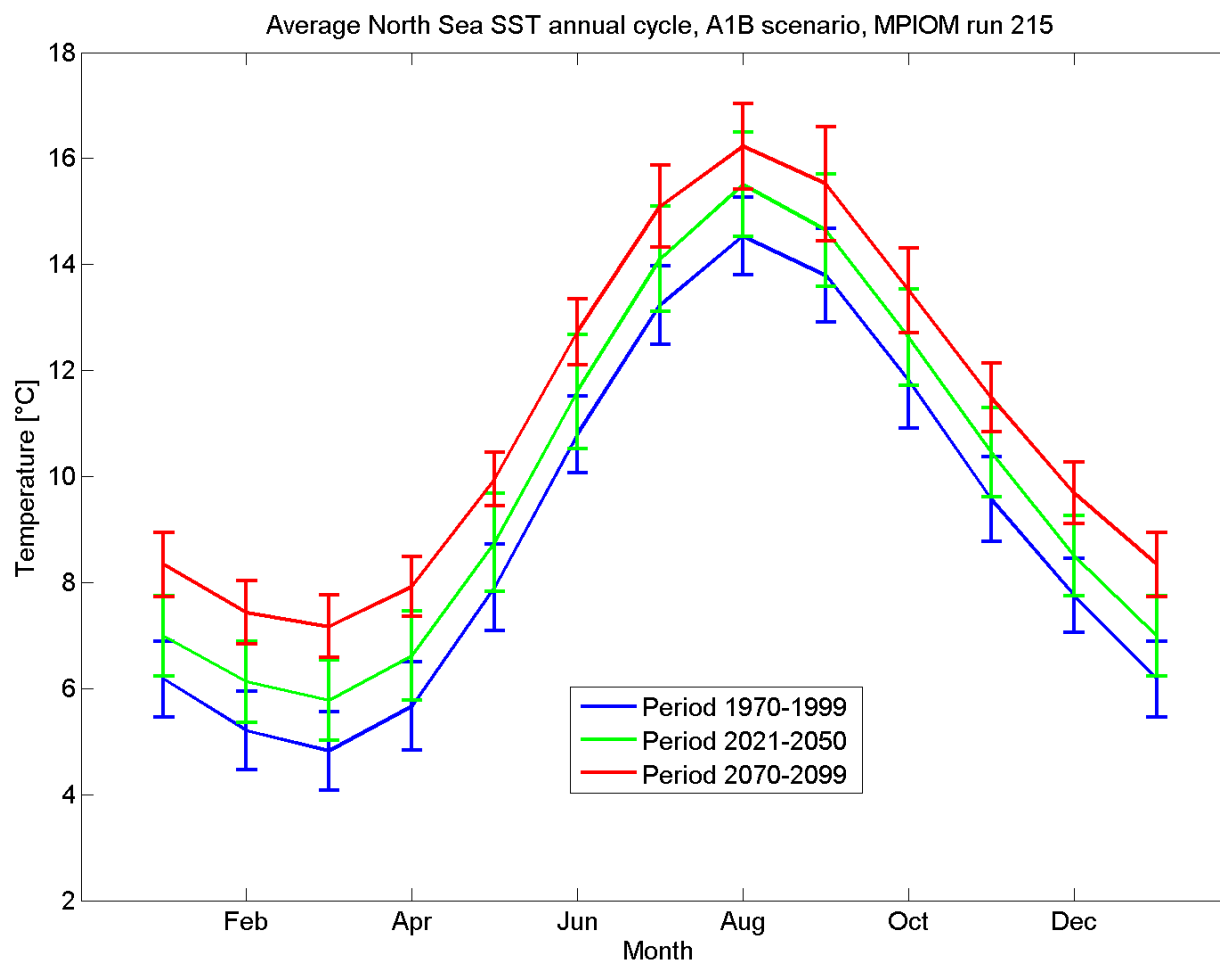


Figure 5.1.10A: The mean annual cycle of sea surface temperatures [°C] for MPIOM run 215 (A1B scenario run) for 1970-1999 (blue), 2021-2050 (green) and 2070-2099 (red). The means are representing averages over the North Sea area given in Figure 4.1. The error bars are indicating time variability.

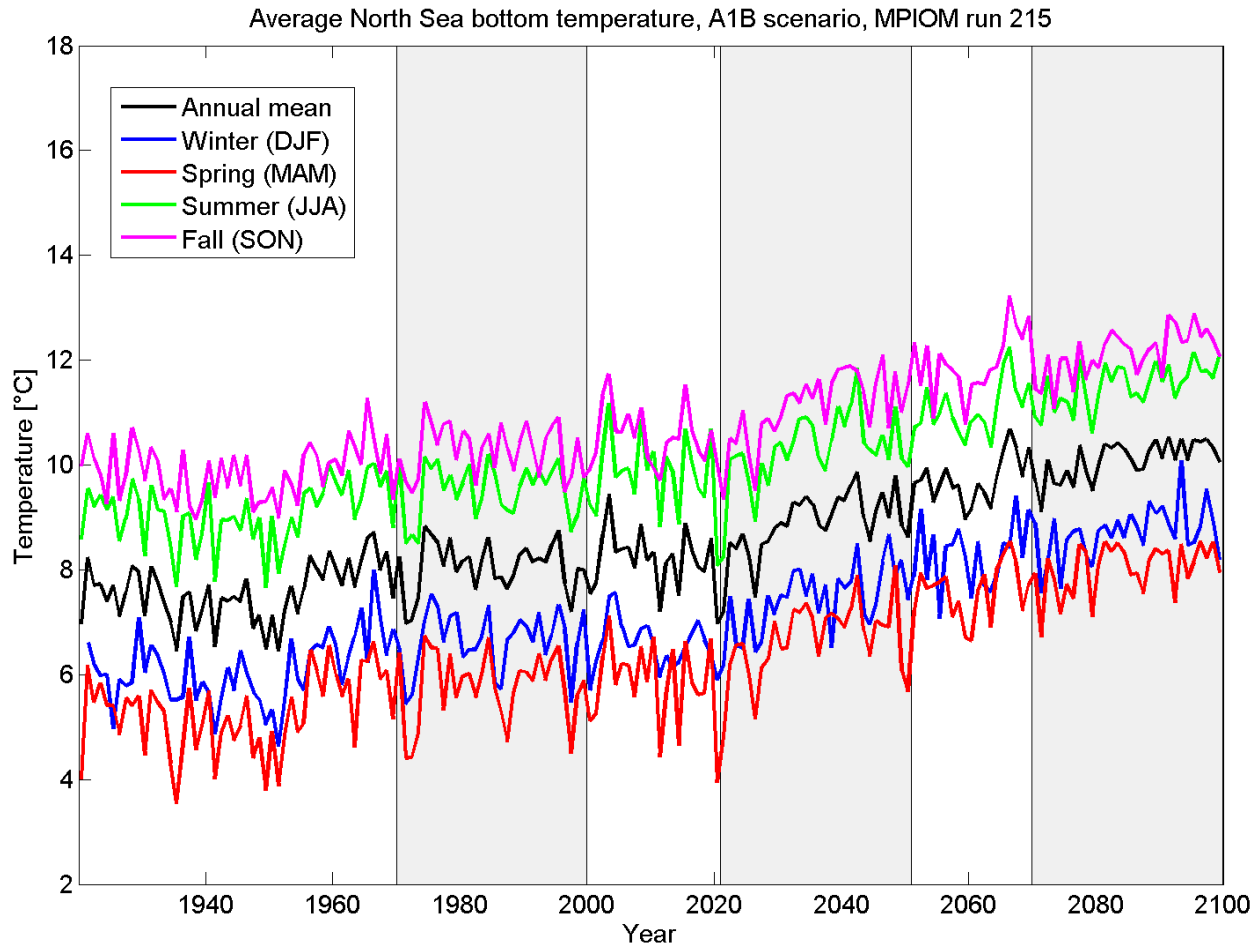


Figure 5.1.11A: Time series of seasonal and annual means of bottom temperature [°C] for MPIOM run 215 (A1B scenario run) from 1920-2099. The temperatures represent averages over the North Sea area given in Figure 4.1.

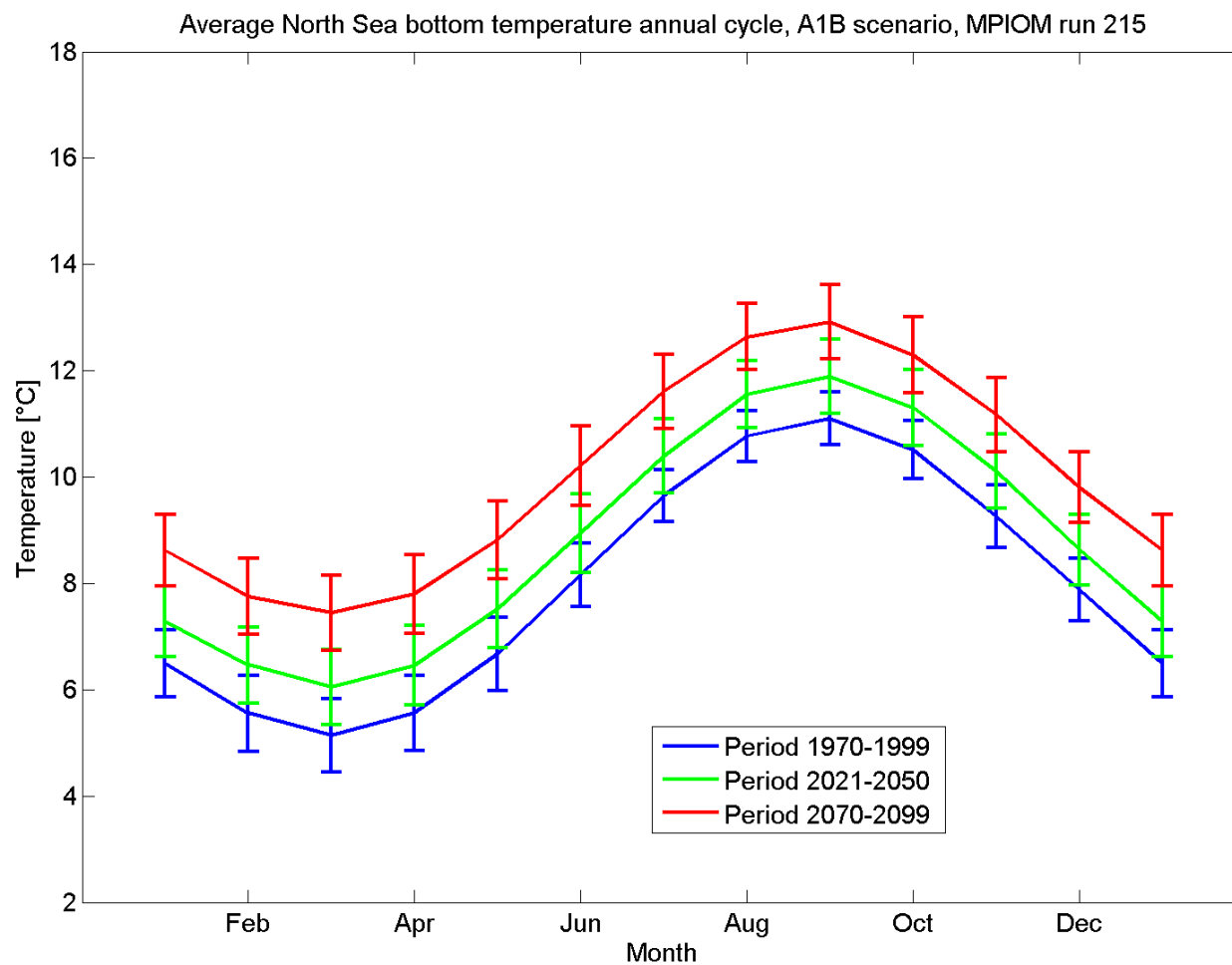


Figure 5.1.12A: The mean annual cycle of bottom temperatures [°C] for MPIOM run 215 (A1B scenario) 1970-1999 (blue), 2021-2050 (green) and 2070-2099 (red). The means are representing averages over the North Sea area given in Figure 4.1. The error bars are indicating time variability.

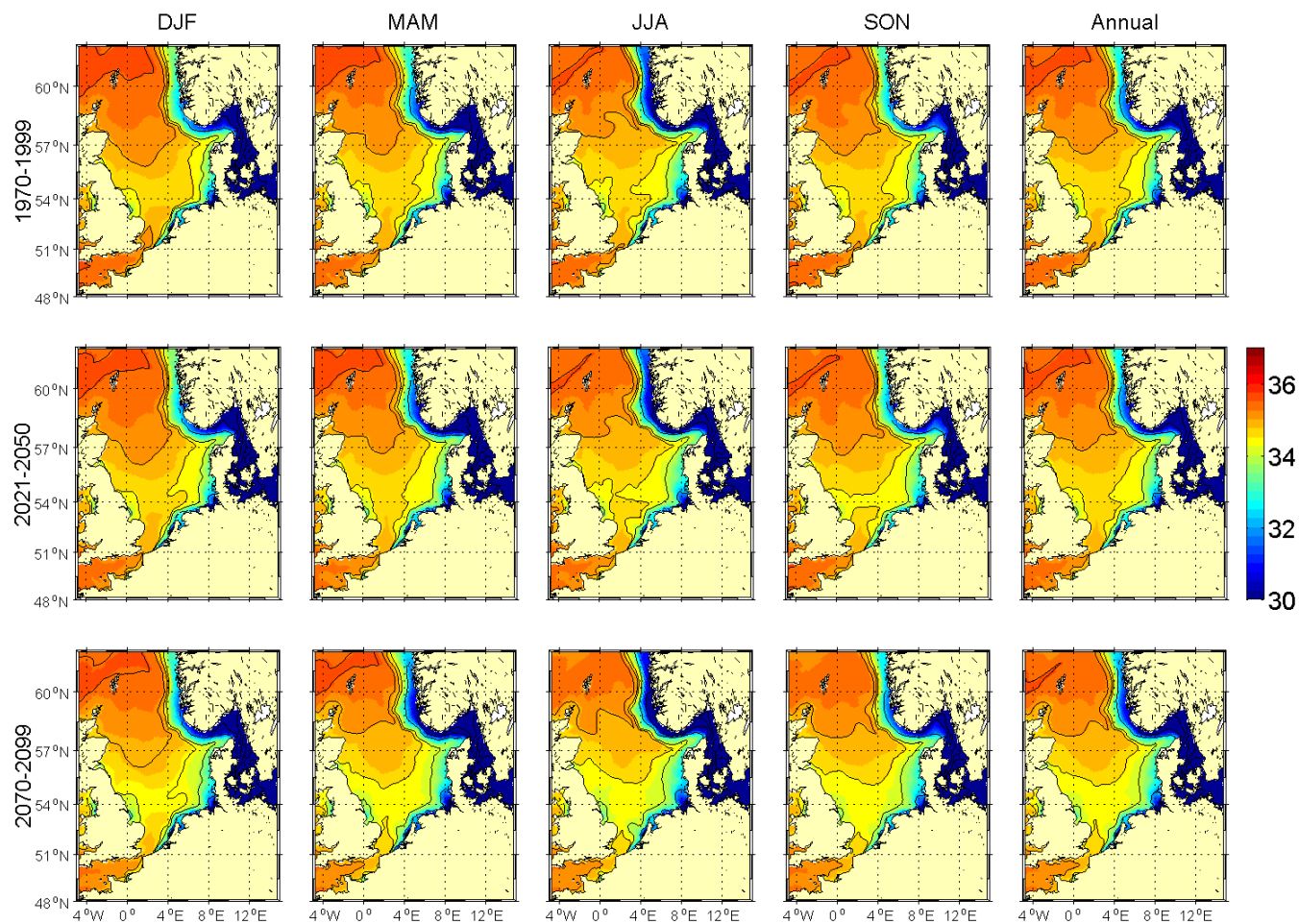


Figure 5.1.13A: Seasonal and annual means of sea surface salinity [psu] for MPIOM run 215 (A1B scenario run). The upper row shows averages for the period 1970-1999, the middle row for 2021-2050 and the lower row for 2070-2099.

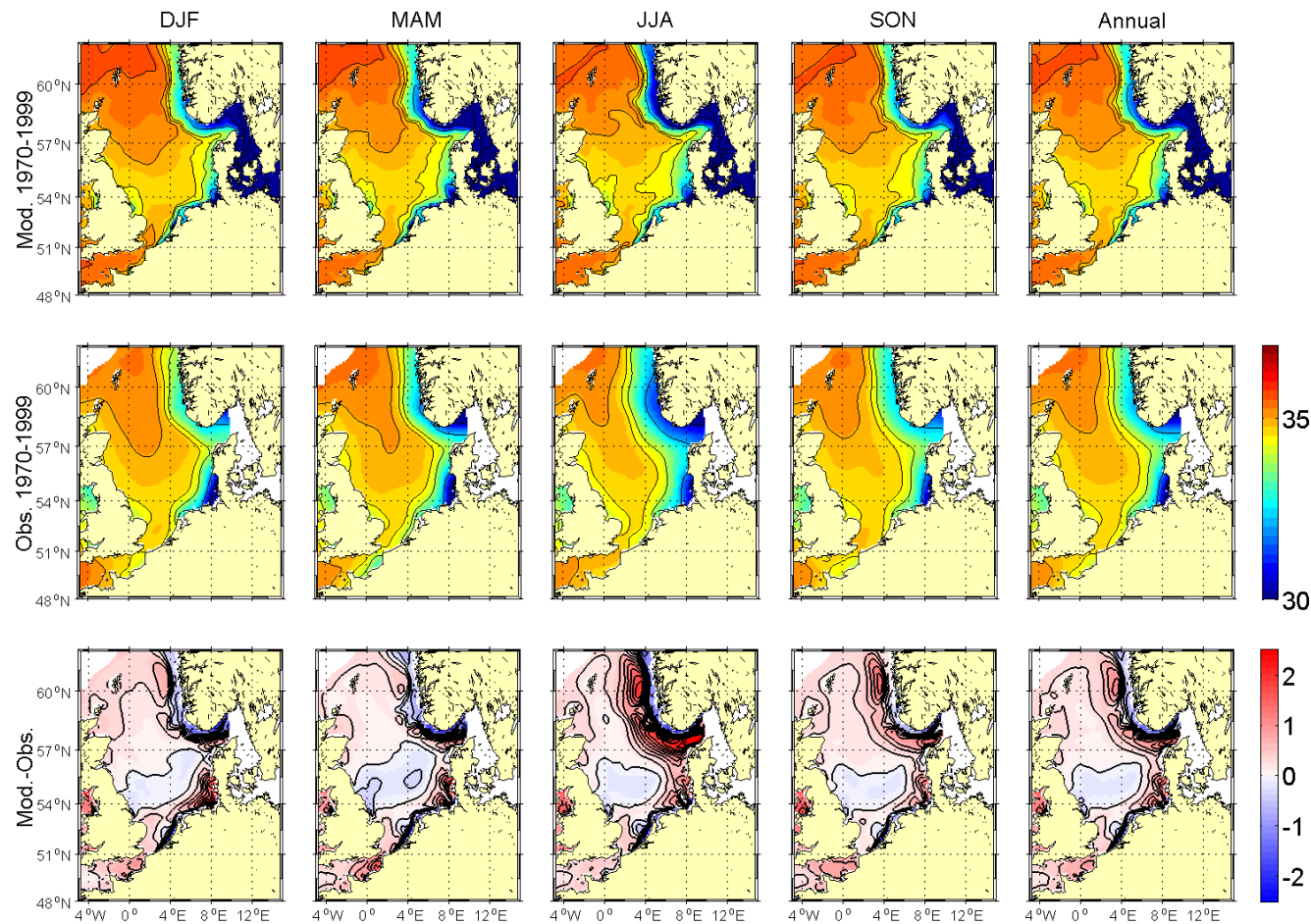


Figure 5.1.14A: Comparison of seasonal and annual means of sea surface salinity [psu] for MPIOM run 215 for the base period 1970-1999 with climatological means from the BHC. The upper row shows average model distributions, the middle row observed climatological means and the lower row the difference between the model results and the climatology.

Coupled Ocean
Atmosphere
Models

BSH
DWD
IfM Hamburg
MPI Hamburg
SMHI
AWI

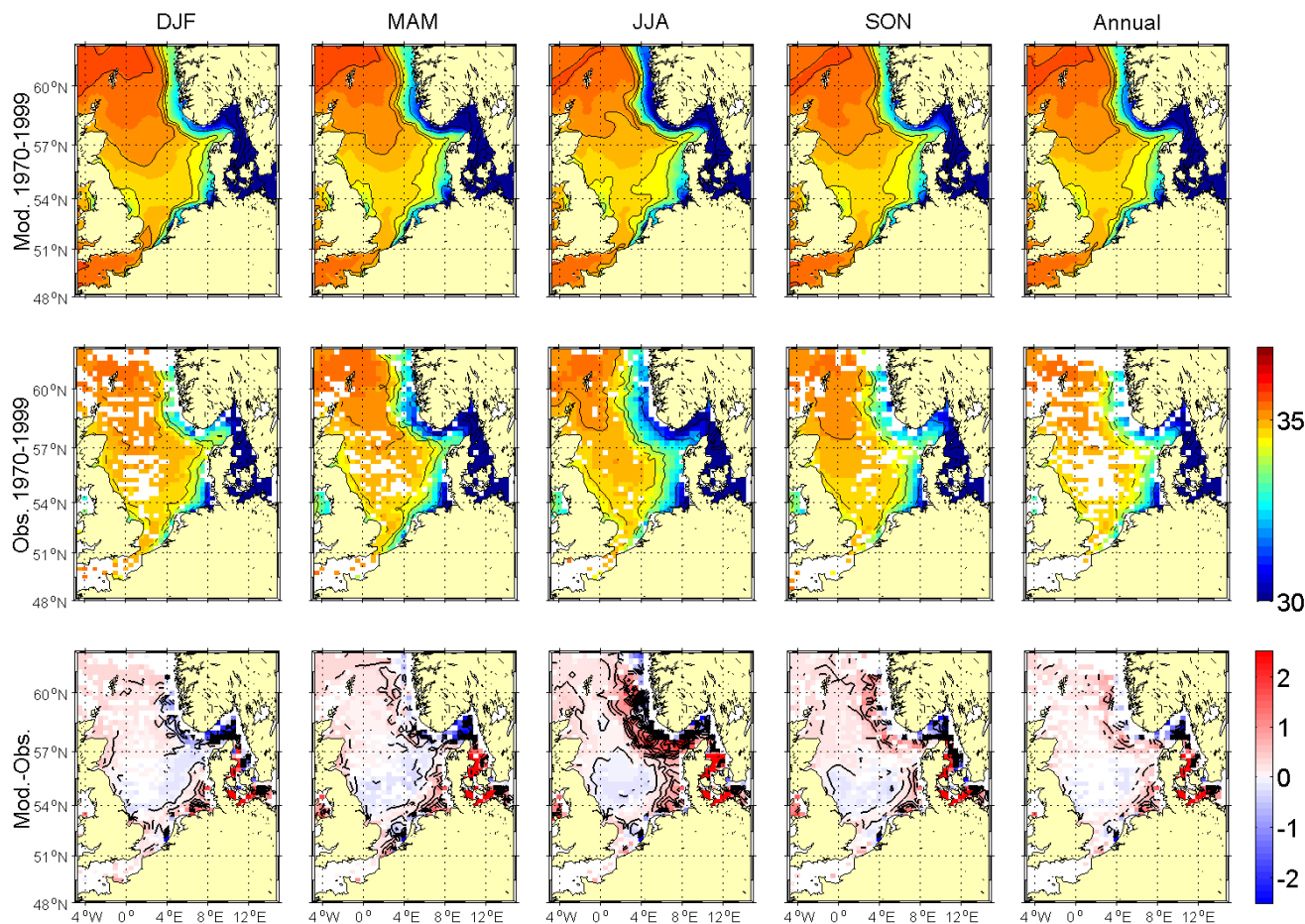


Figure 5.1.15A: Comparison of seasonal and annual means of sea surface salinity [psu] for MPIOM run 215 for the base period 1970-1999 with KNSC means. The upper row shows average model distributions, the middle row observed climatological means and the lower row the difference between the model results and the climatology.

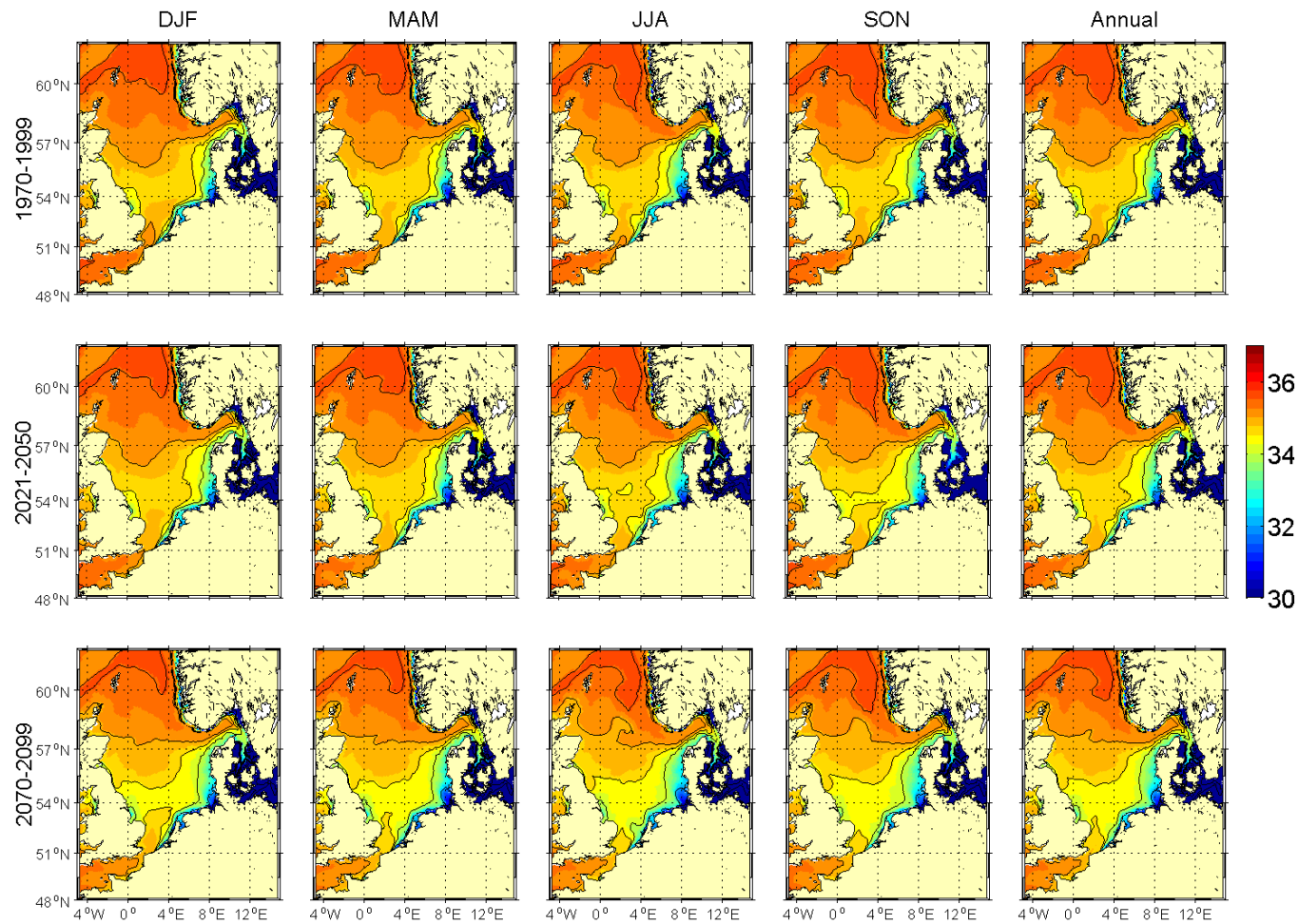


Figure 5.1.16A: Seasonal and annual means of bottom salinity [psu] for MPIOM run 215 (A1B scenario run). The upper row shows averages for the period 1970-1999, the middle row for 2021-2050 and the lower row for 2070-2099.

Coupled Ocean
Atmosphere
Models

BSH
DWD
IfM Hamburg
MPI Hamburg
SMHI
AWI

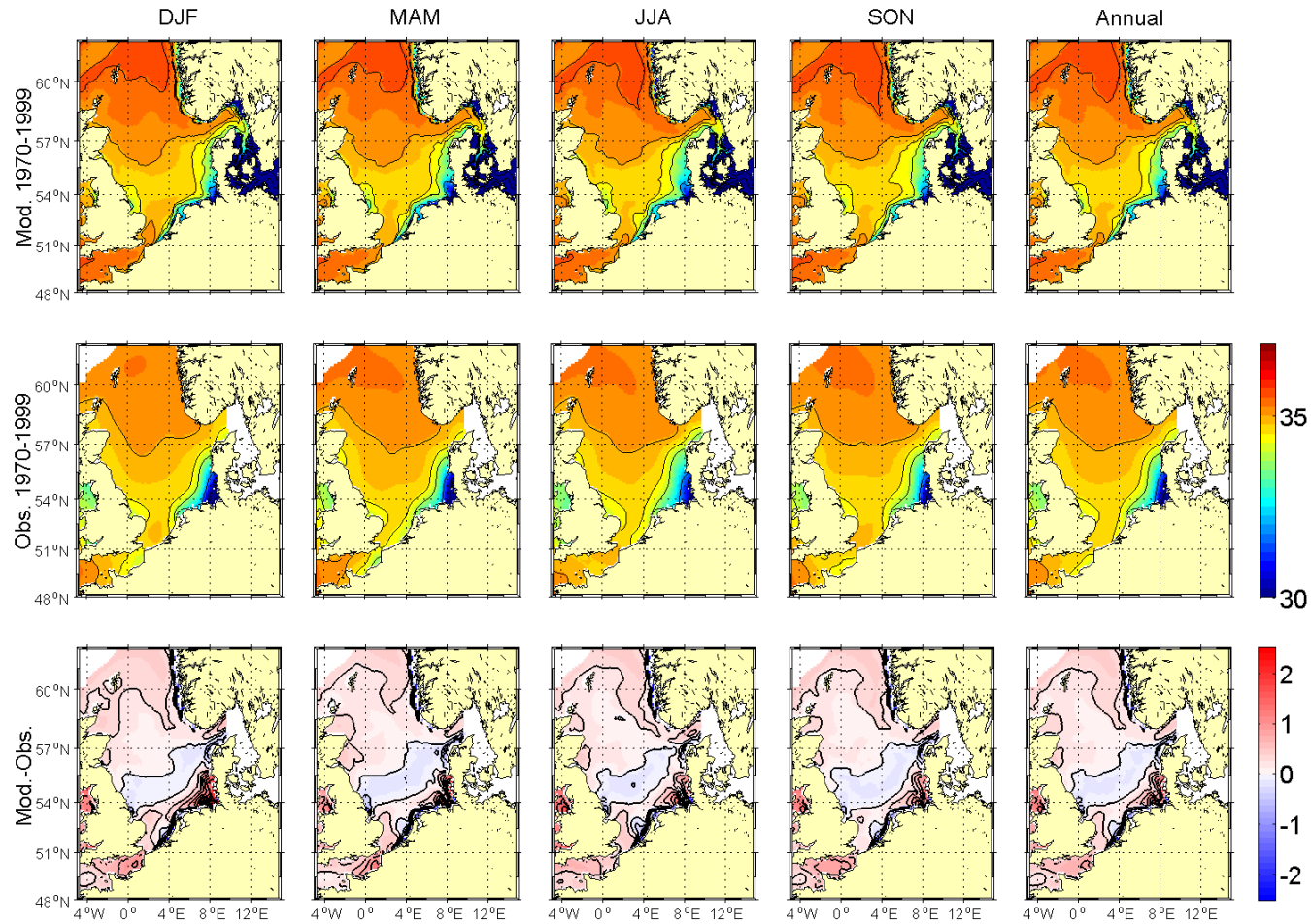
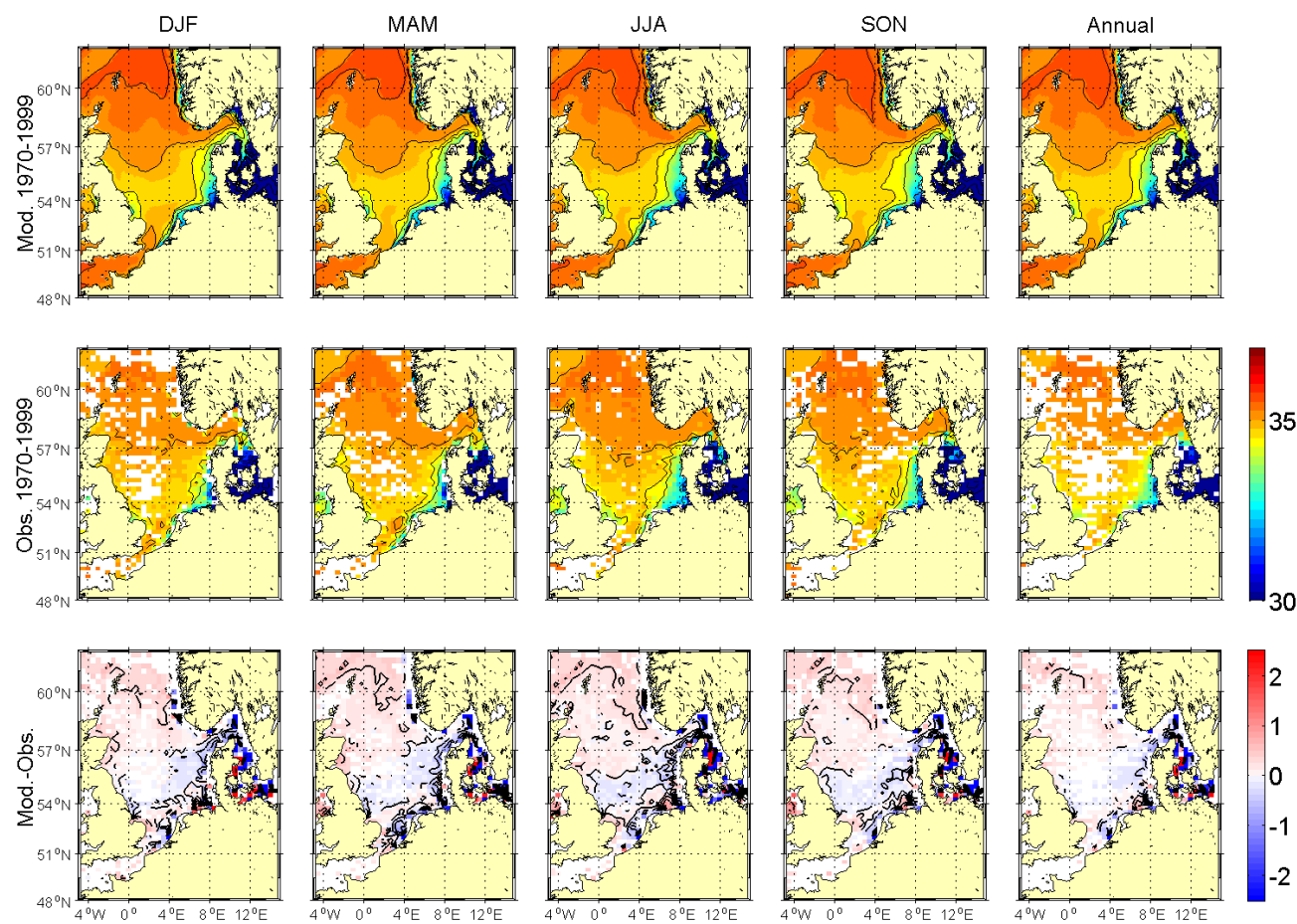


Figure 5.1.17A: Comparison of seasonal and annual means of bottom salinity [psu] for MPIOM run 215 for the base period 1970-1999 with BHC means. The upper period shows average model distributions, the middle row observational means and the lower row the difference between the model results and the climatology.



Coupled Ocean
Atmosphere
Models

BSH
DWD
IfM Hamburg
MPI Hamburg
SMHI
AWI

Figure 5.1.18A: Comparison of seasonal and annual means of bottom salinity [psu] for MPIOM run 215 for the base period 1970-1999 with KNSC means. The upper row shows average model distributions, the middle row observed climatological means and the lower row the difference between the model results and the climatology.

Coupled Ocean
Atmosphere
Models

BSH
DWD
IfM Hamburg
MPI Hamburg
SMHI
AWI

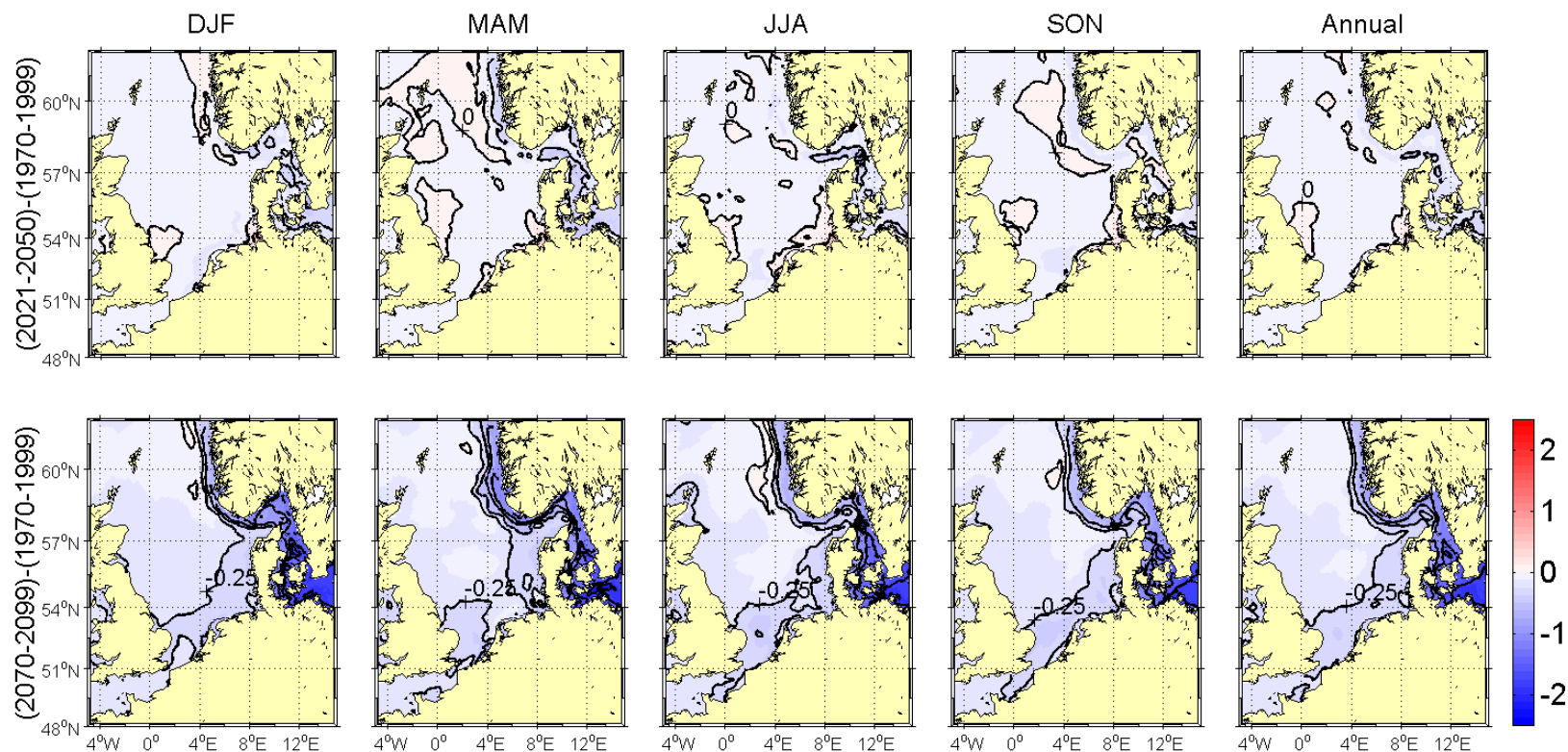


Figure 5.1.19A: Changes in seasonal and annual sea surface salinity [psu] for MPIOM run 215 (A1B scenario run). Upper panel from (1970-1999) to (2021-2050) and lower panel from (1970-1999) to (2070-2099). The contour interval is 0.25 psu. Selected isolines have been labelled for better orientation.

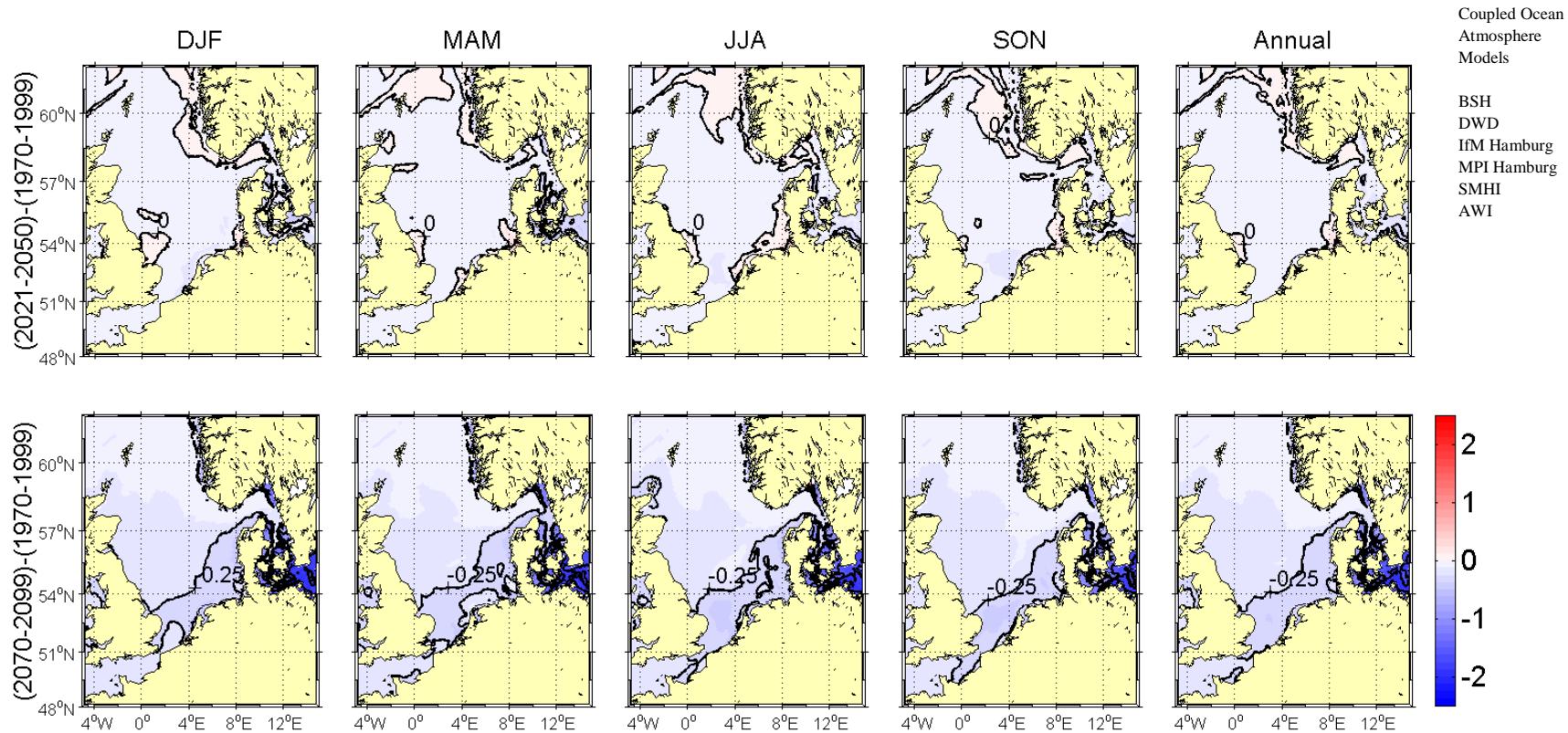


Figure 5.1.20A: Changes in seasonal and annual bottom salinity [psu] for MPIOM run 215 (A1B scenario run). Upper panel from (1970-1999) to (2021-2050) and lower panel from (1970-1999) to (2070-2099). The contour interval is 0.5 °C. Selected isolines have been labelled for better orientation.

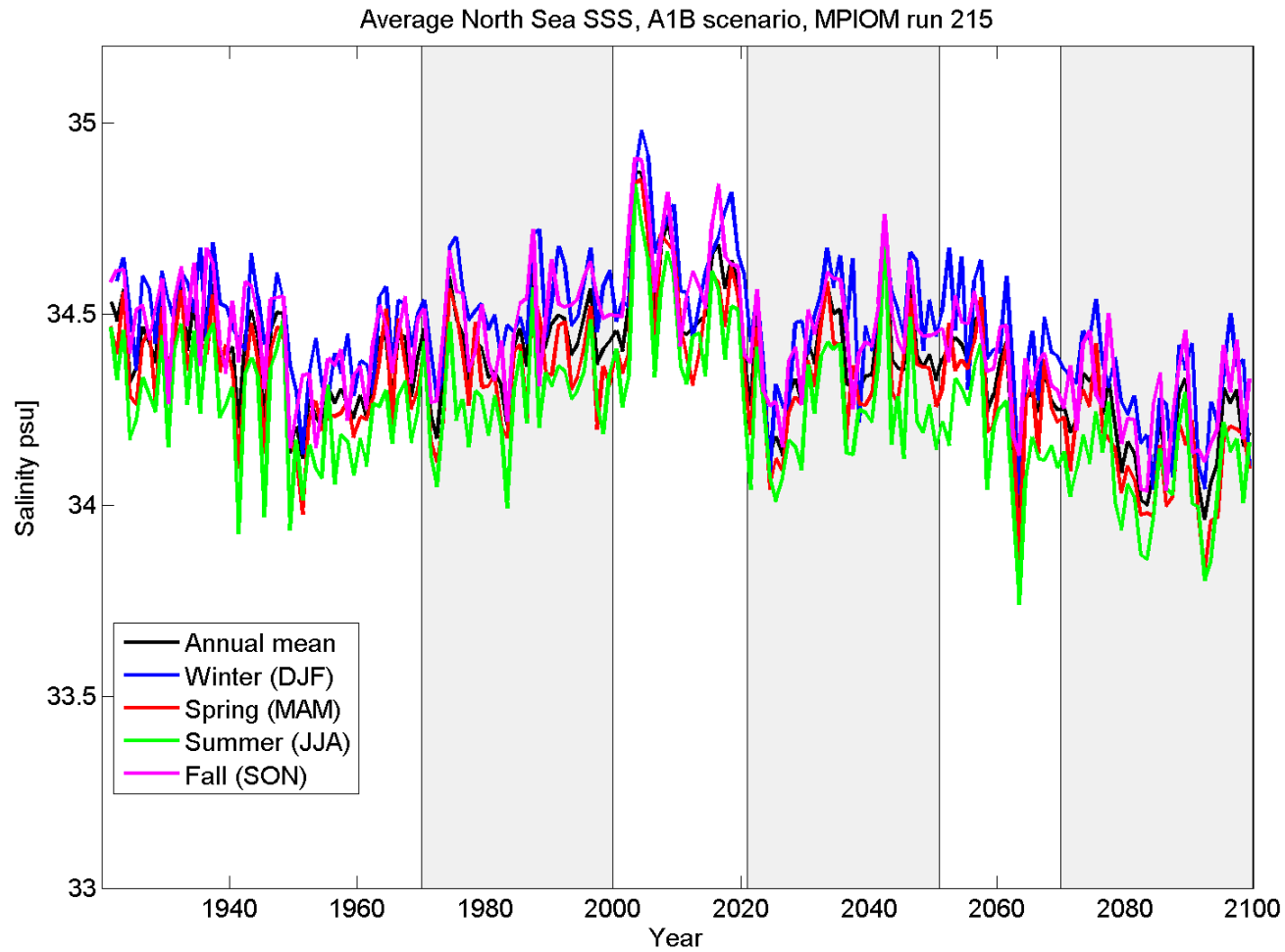


Figure 5.1.21A: Time series of seasonal and annual means of sea surface salinity [psu] for MPIOM run 215 (A1B scenario run) from 1920-2099. The salinities represent averages over the North Sea area given in Figure 4.1.

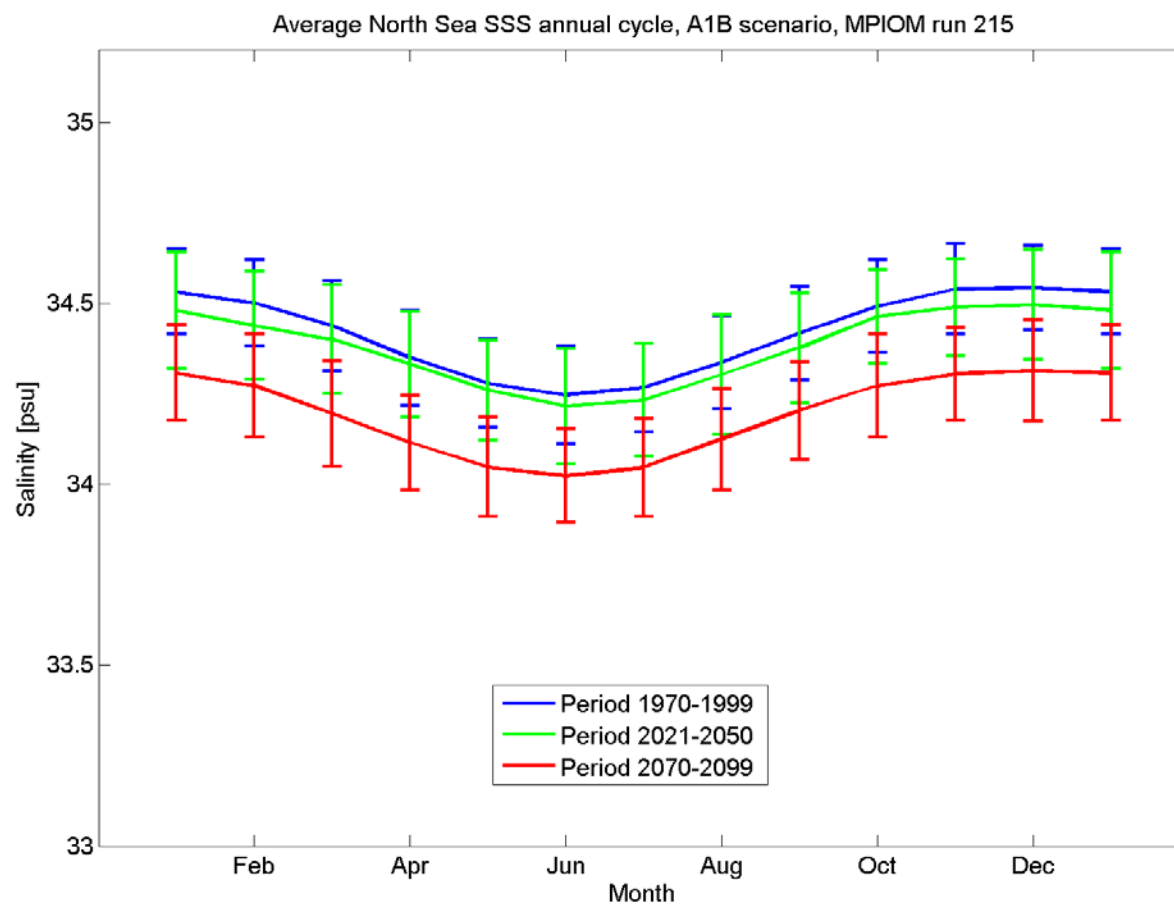


Figure 5.1.22A: The mean annual cycle of sea surface salinity [psu] for MPIOM run 215 (A1B scenario run) for 1970-1999 (blue), 2021-2050 (green) and 2070-2099 (red). The means are representing averages over the North Sea area given in Figure 4.1. The error bars are indicating time variability.

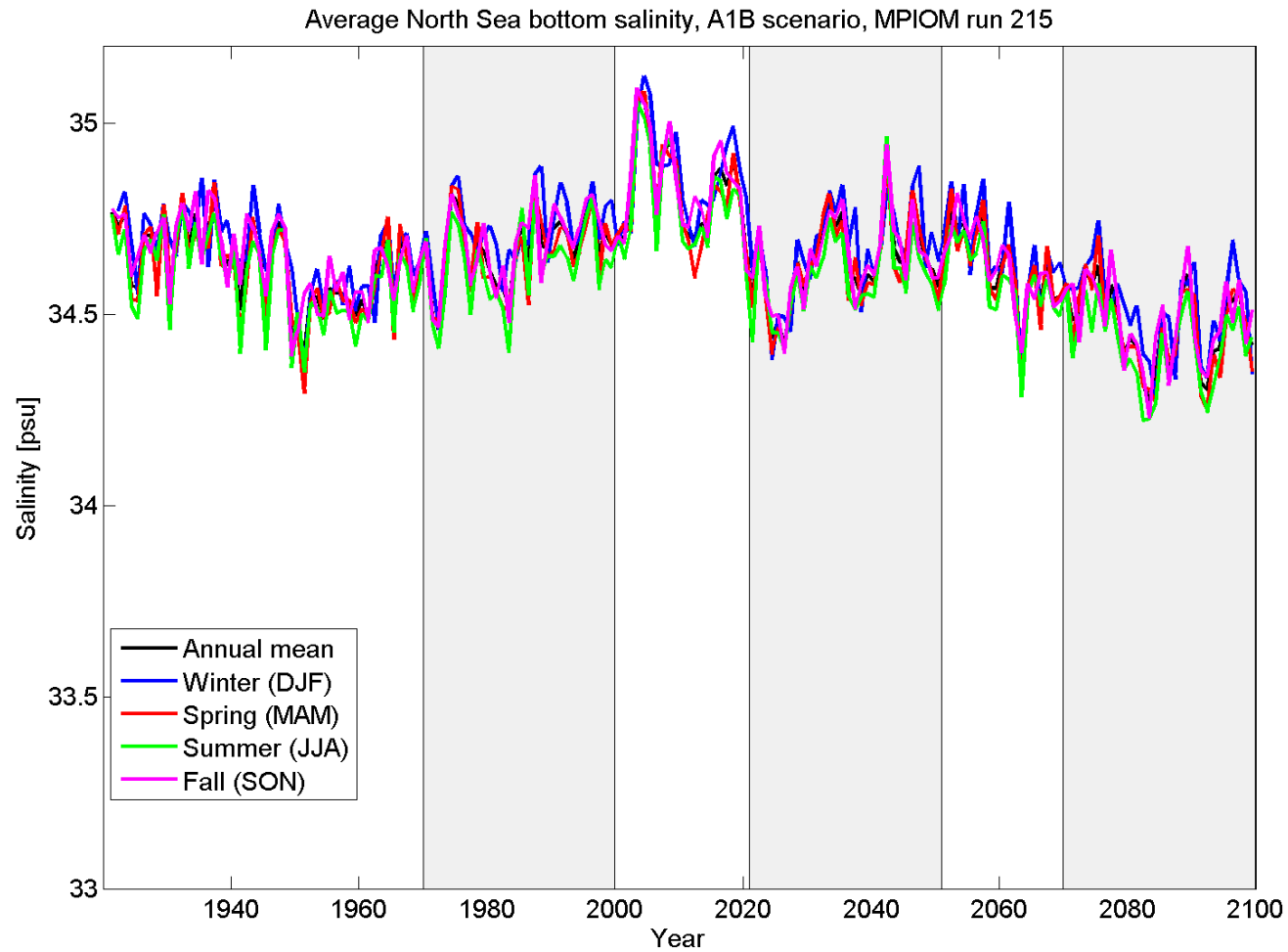


Figure 5.1.23A: Time series of seasonal and annual means of bottom salinity [psu] for MPIOM run 215 (A1B scenario run) from 1920-2099. The salinities represent averages over the North Sea area given in Figure 4.1.

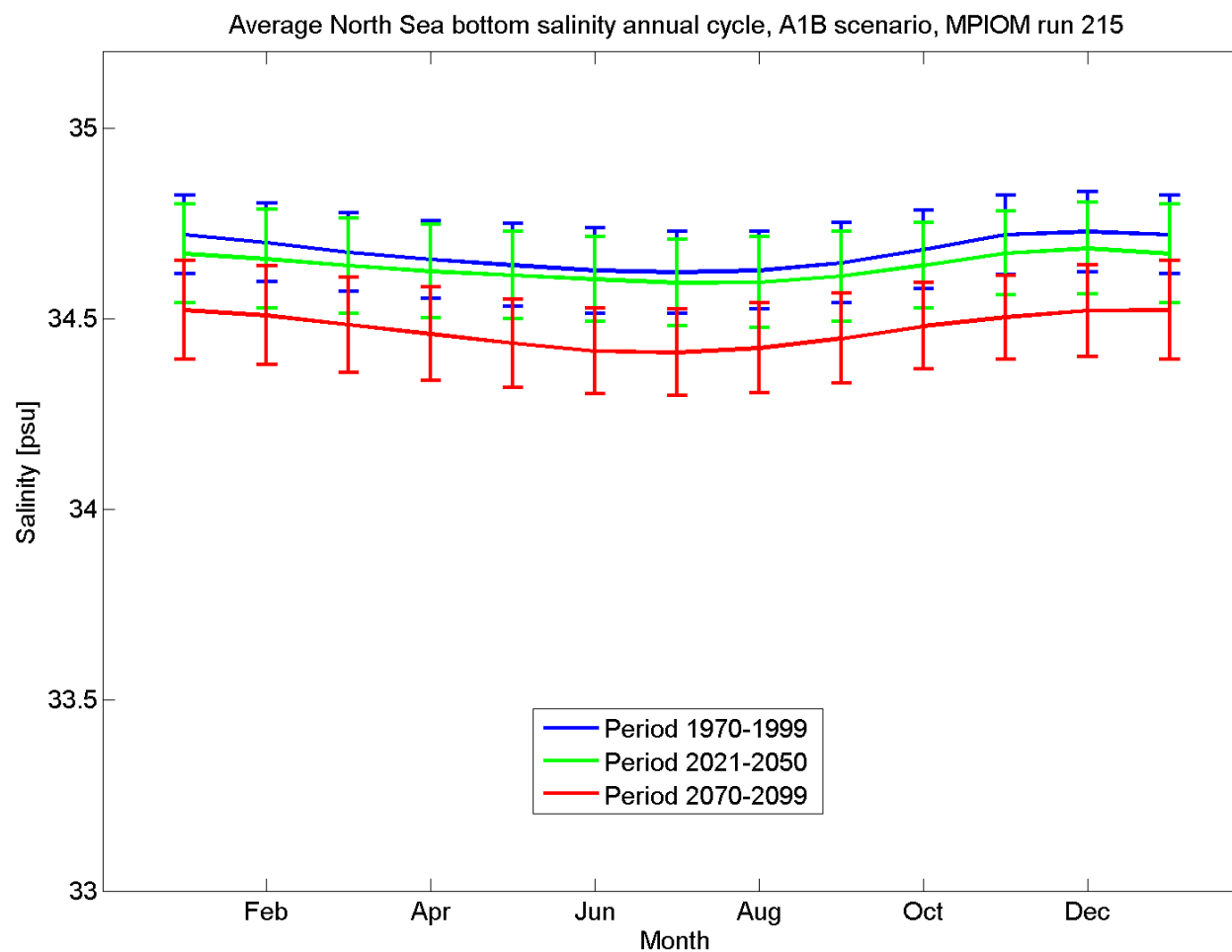


Figure 5.1.24A: The mean annual cycle of bottom salinity [psu] for MPIOM run 215 (A1B scenario run) for 1970-1999 (blue), 2021-2050 (green) and 2070-2099 (red). The means are representing averages over the North Sea area given in Figure 4.1. The error bars are indicating time variability.

Coupled Ocean
Atmosphere
Models

BSH
DWD
IfM Hamburg
MPI Hamburg
SMHI
AWI

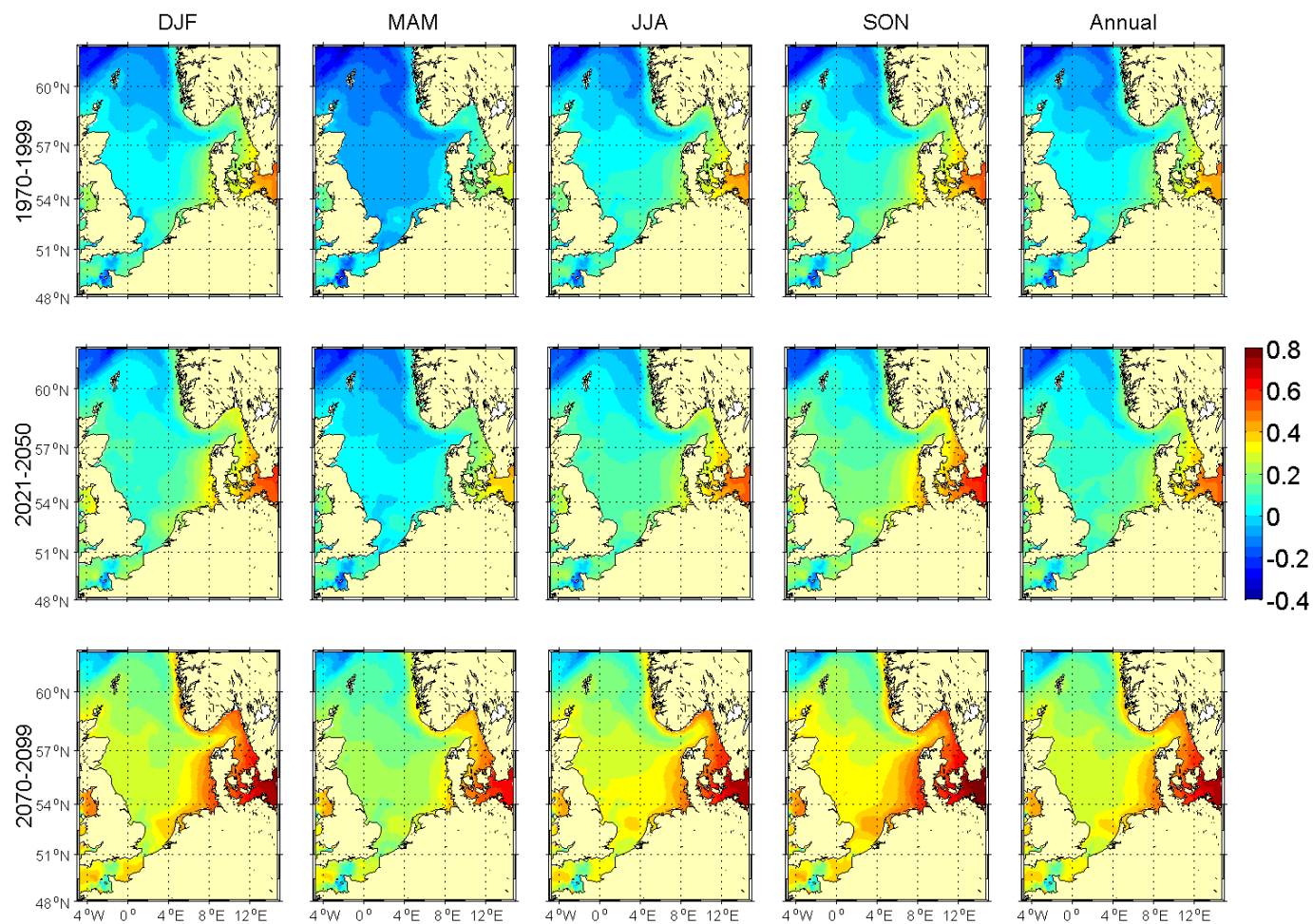


Figure 5.1.25A: Seasonal and annual means of sea surface height [m] for MPIOM run 215 (A1B scenario run). The upper row shows averages for the period 1970-1999, the middle row for 2021-2050 and the lower row for 2070-2099.

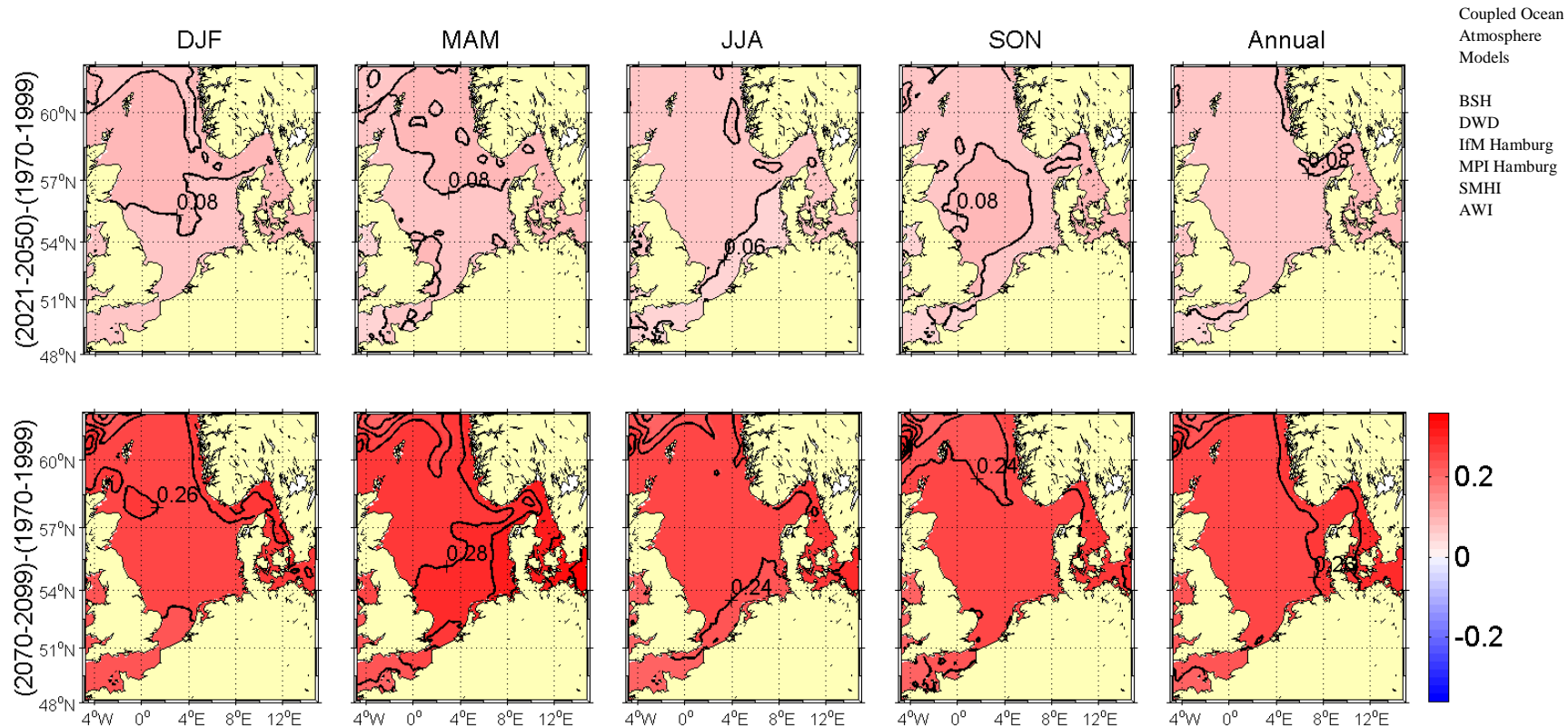


Figure 5.1.26A: Changes in seasonal and annual sea surface height [m] for MPIOM run 215 (A1B scenario run). Upper panel from (1970-1999) to (2021-2050) and in lower panel from (1970-1999) to (2070-2099). The contour interval is 0.02 m. Selected isolines have been labelled for better orientation.

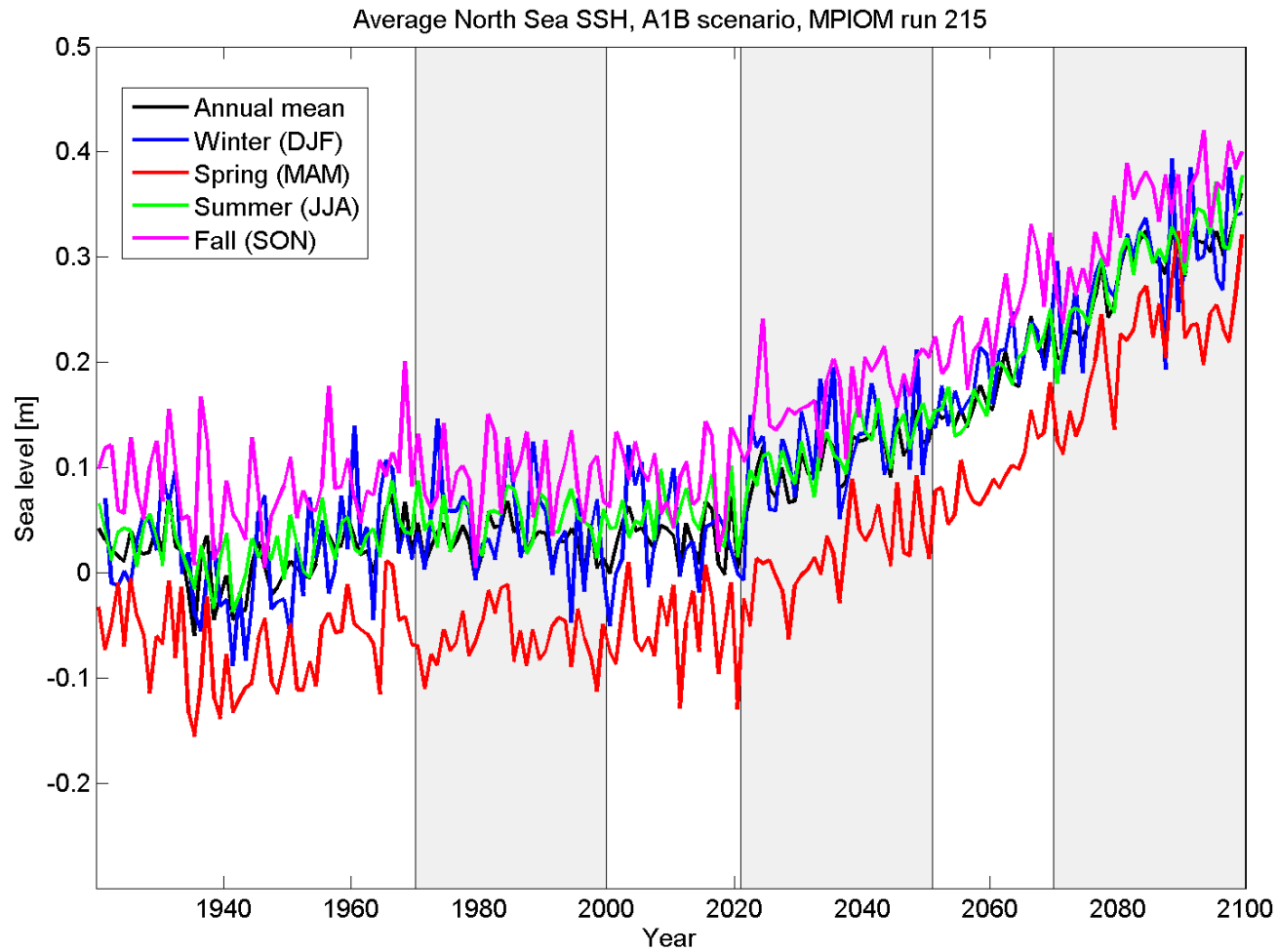


Figure 5.1.27A: Time series of seasonal and annual means of sea surface height [m] for MPIOM run 215 (A1B scenario run) from 1920-2099. The sea surface heights represent averages over the North Sea area given in Figure 4.1.

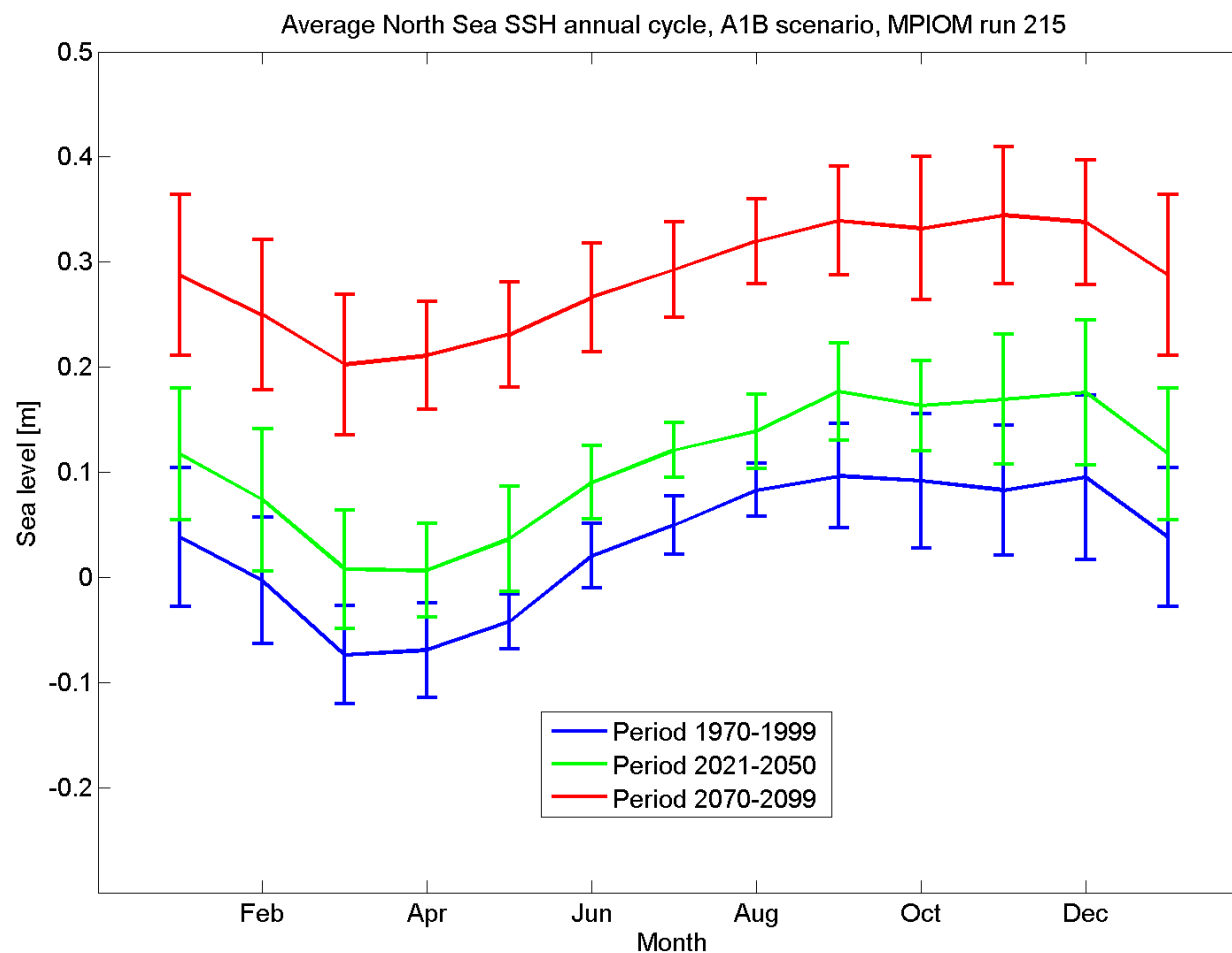


Figure 5.1.28A: The mean annual cycle of sea surface height [m] for MPIOM run 215 (A1B scenario run) 1970-1999 (blue), 2021-2050 (green) and 2070-2099 (red). The means are representing averages over the North Sea area given in Figure 4.1. The error bars are indicating time variability.

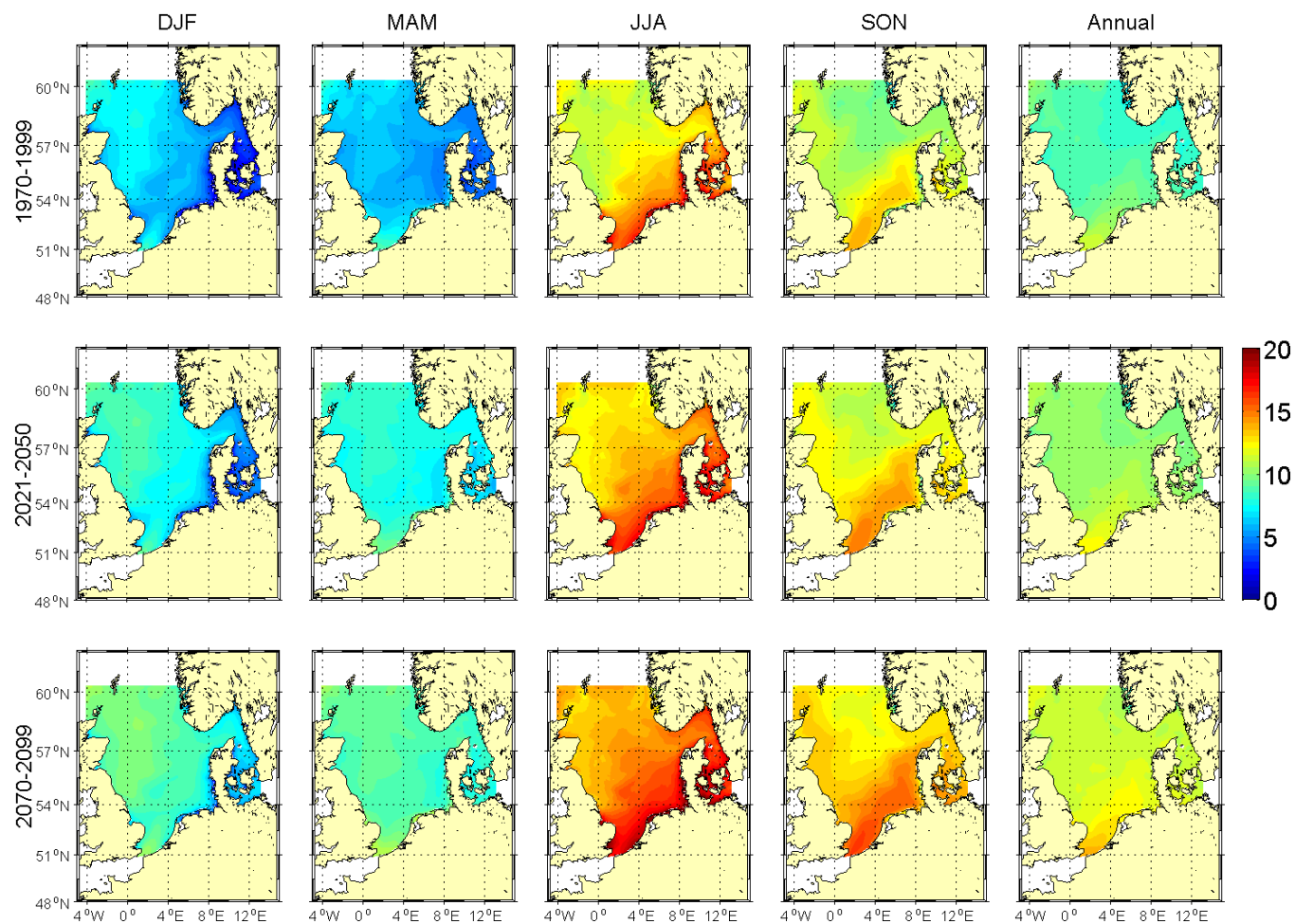


Figure 5.2.1A: Seasonal and annual means of sea surface temperature [°C] for HAMSOM run 202 (A1B scenario run). The upper row shows averages for the period 1970-1999, the middle row for 2021-2050 and the lower row for 2070-2099.

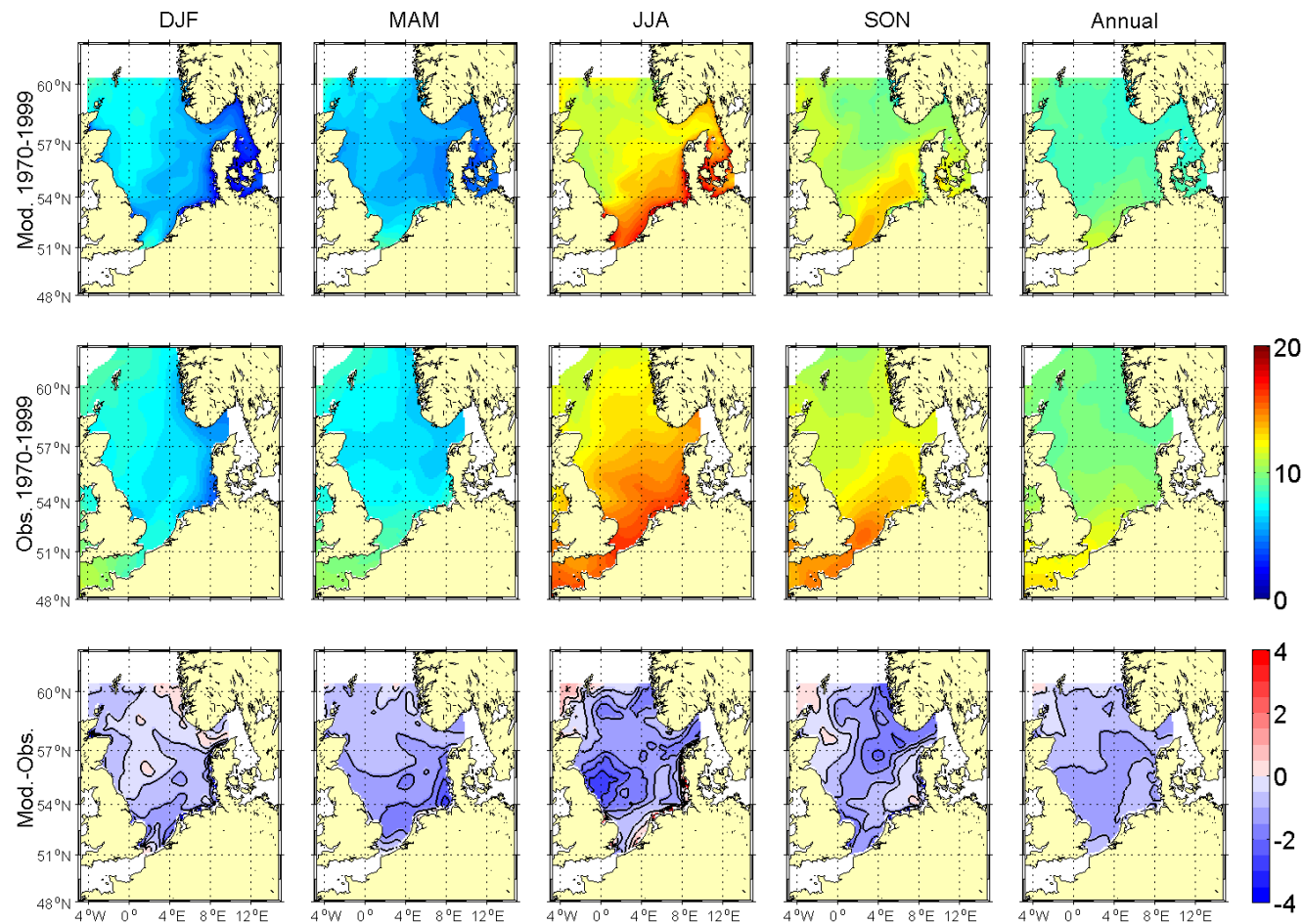


Figure 5.2.2A: Comparison of seasonal and annual means of sea surface temperature [°C] for HAMSOM run 202 for the base period 1970-1999 with BHC means. The upper row shows average model distributions, the middle row observed climatological means and the lower row the difference between the model results and the climatology.

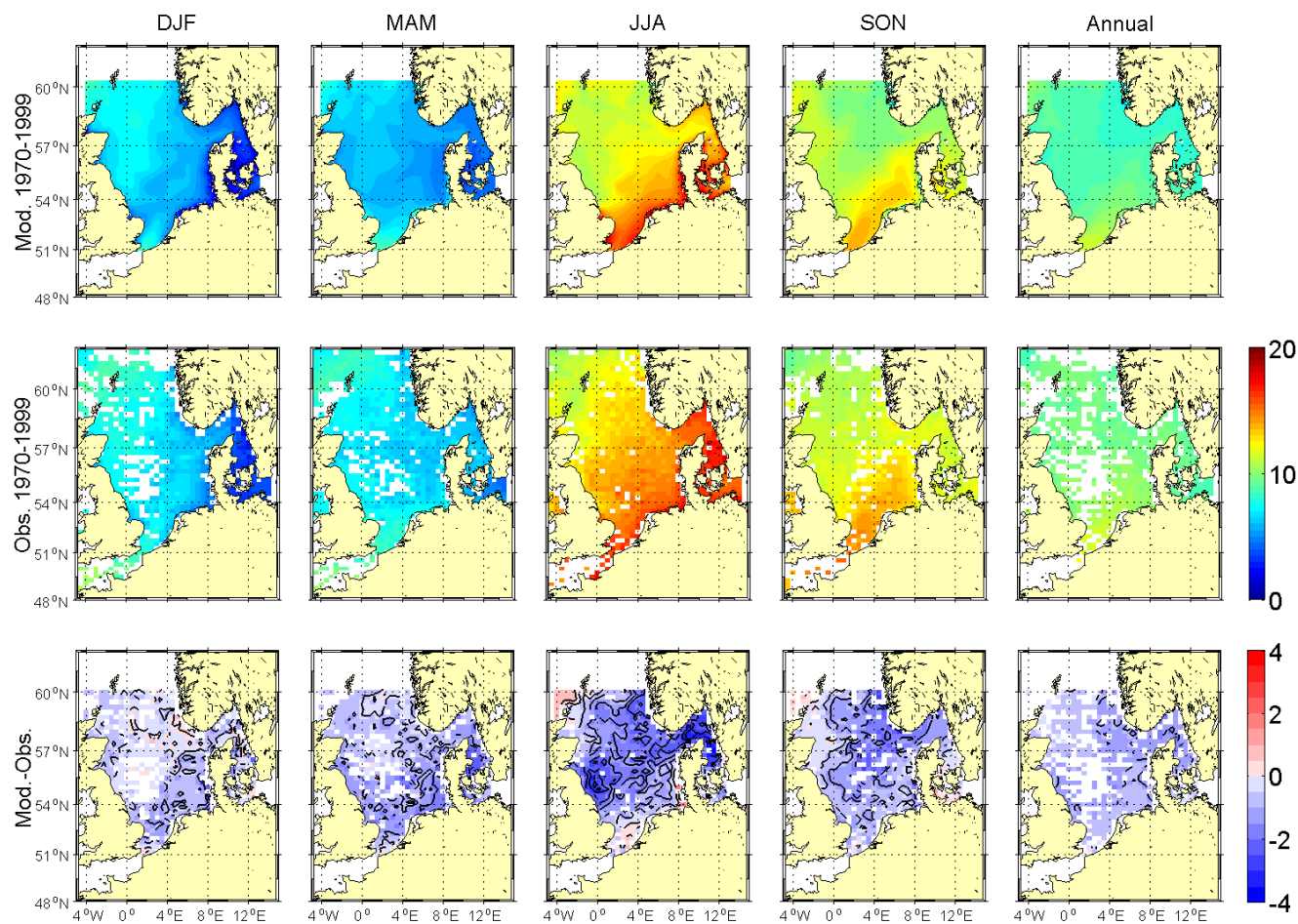


Figure 5.2.3A: Comparison of seasonal and annual means of sea surface temperature [°C] for HAMSOM run 202 for the base period 1970-1999 with KNSC means. The upper row shows average model distributions, the middle row observed climatological means and the lower row the difference between the model results and the climatology.

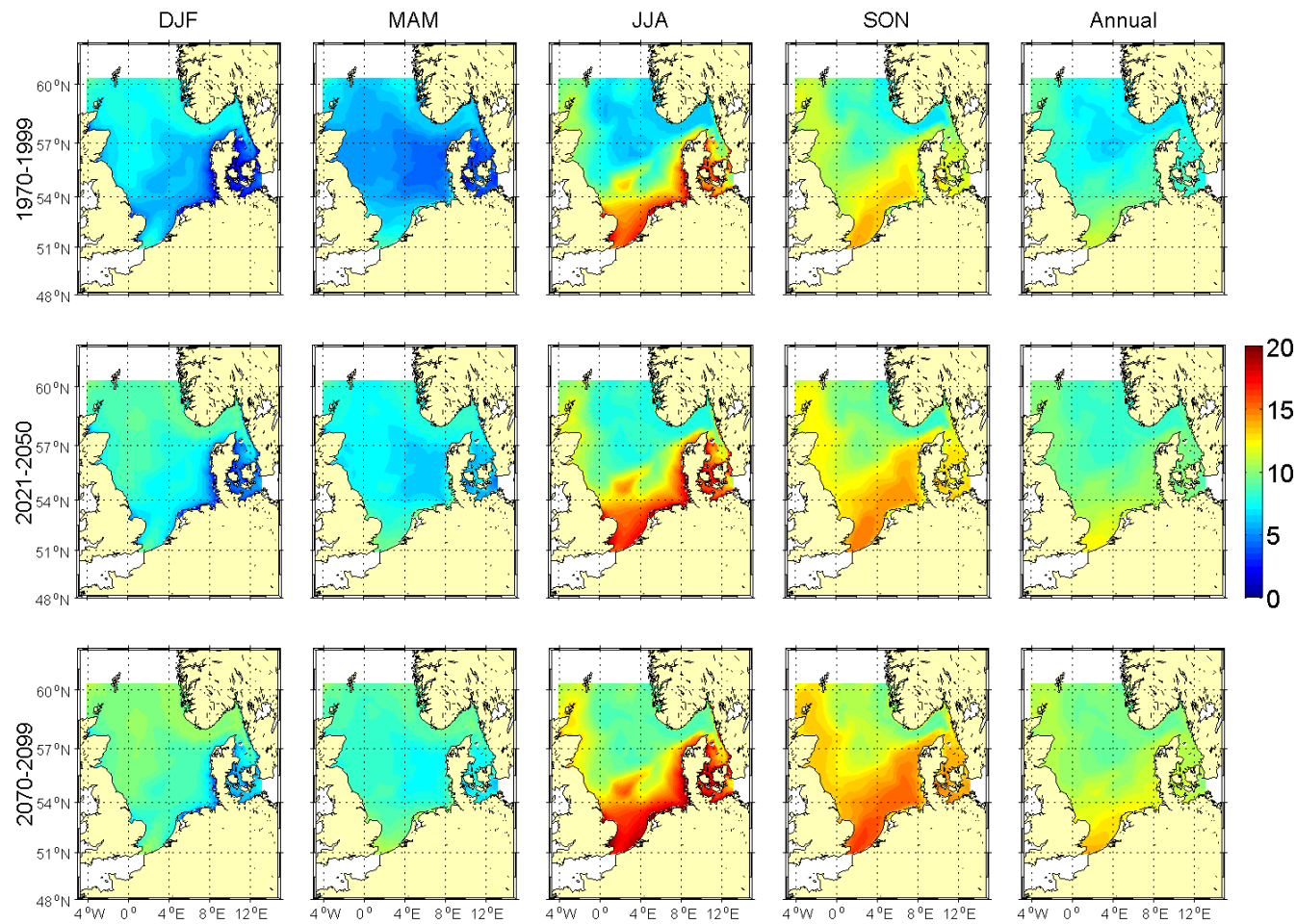


Figure 5.2.4A: Seasonal and annual means of bottom temperature [°C] for HAMSOM run 202 (A1B scenario run). The upper row shows averages for the period 1970-1999, the middle row for 2021-2050 and the lower row for 2070-2099.

Coupled Ocean
Atmosphere
Models

BSH
DWD
IfM Hamburg
MPI Hamburg
SMHI
AWI

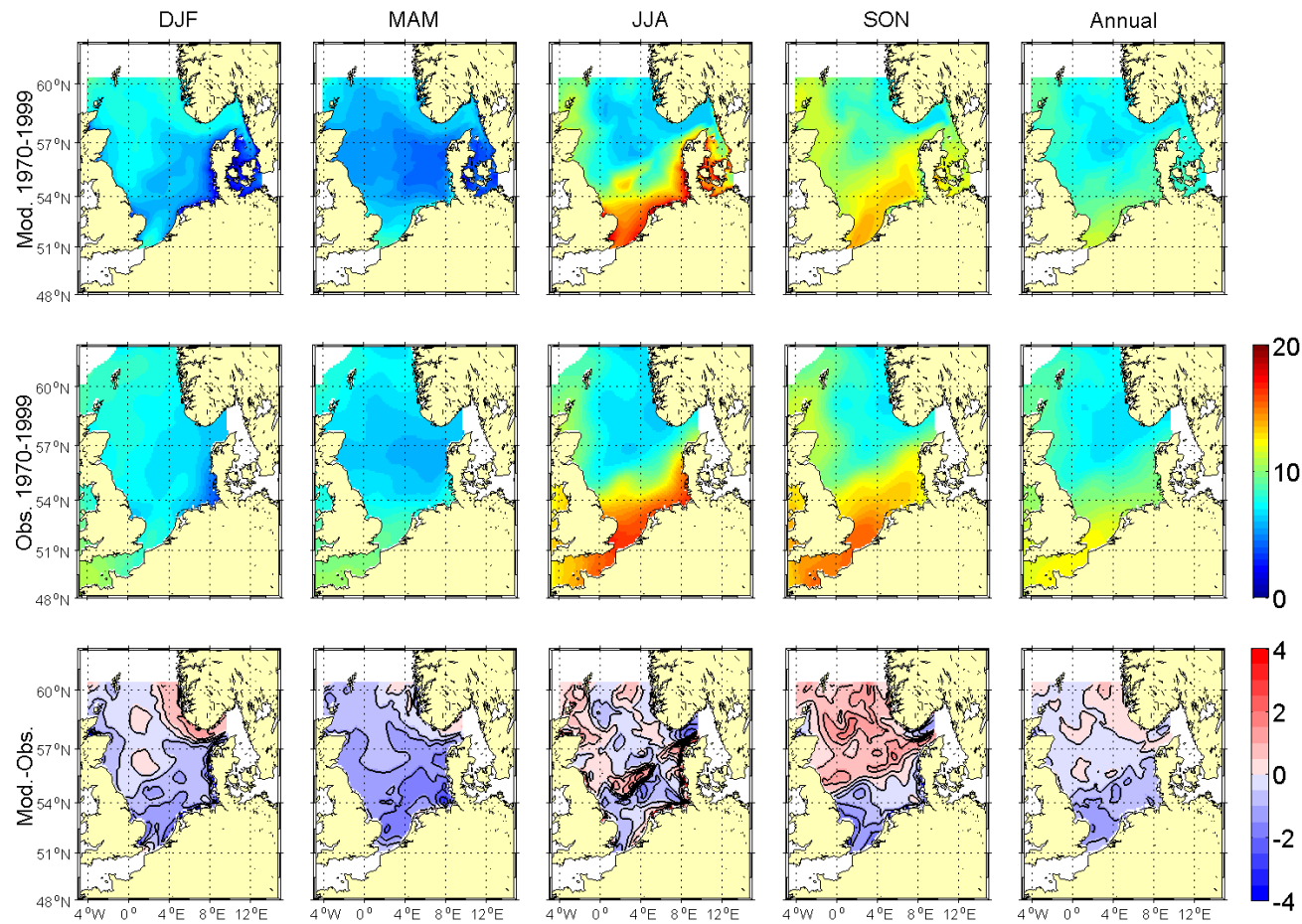
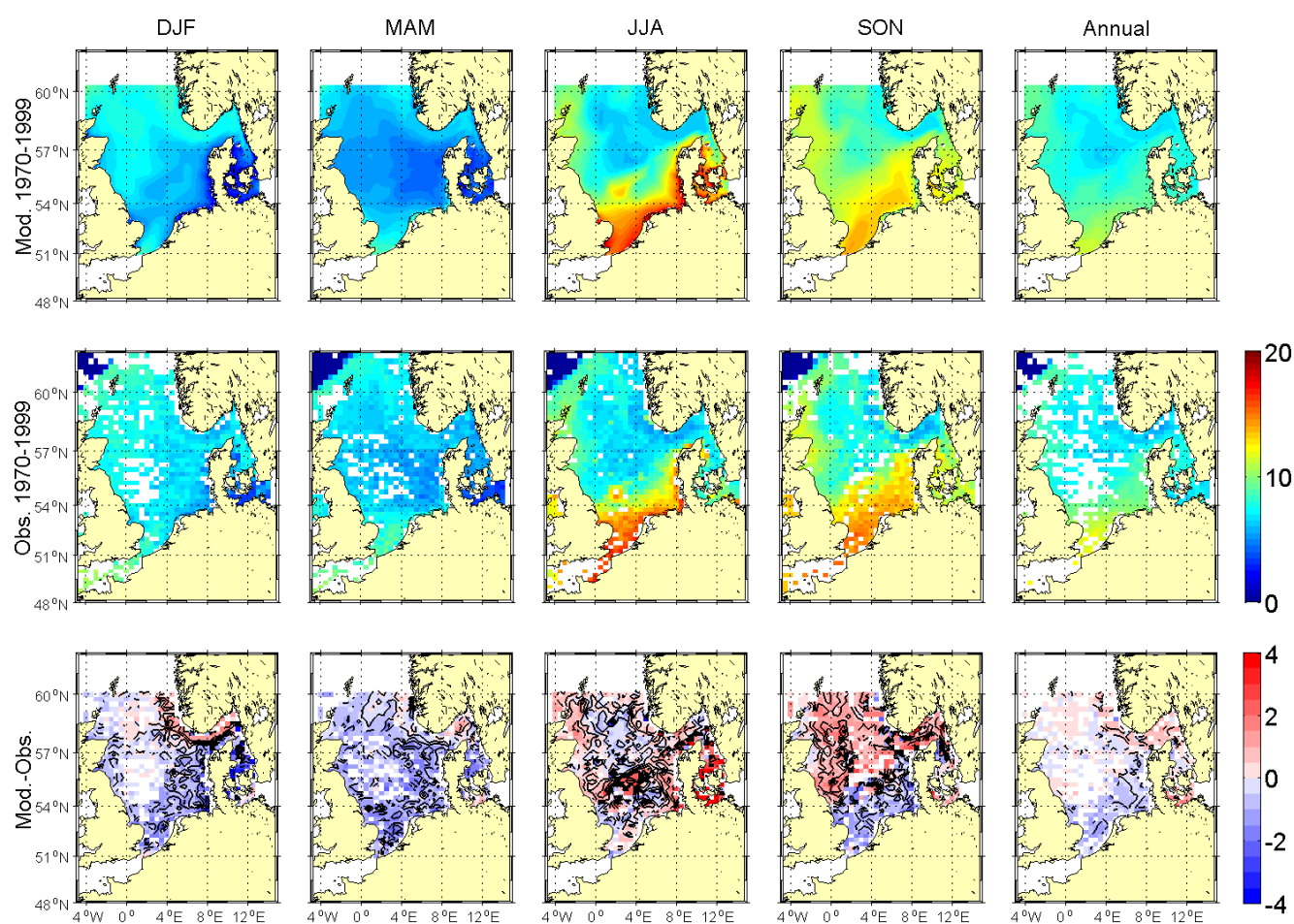


Figure 5.2.5A: Comparison of seasonal and annual means of bottom temperature [°C] for HAMSOM run 202 for the base period 1970-1999 with BHC means. The upper row shows average model distributions, the middle row observed climatological means and the lower row the difference between the model results and the climatology.



Coupled Ocean
Atmosphere
Models

BSH
DWD
IfM Hamburg
MPI Hamburg
SMHI
AWI

Figure 5.2.6A: Comparison of seasonal and annual means of bottom temperature [°C] for HAMSOM run 202 for the base period 1970-1999 with KN5C means. The upper row shows average model distributions, the middle row observed climatological means and the lower row the difference between the model results and the climatology.

Coupled Ocean
Atmosphere
Models

BSH
DWD
IfM Hamburg
MPI Hamburg
SMHI
AWI

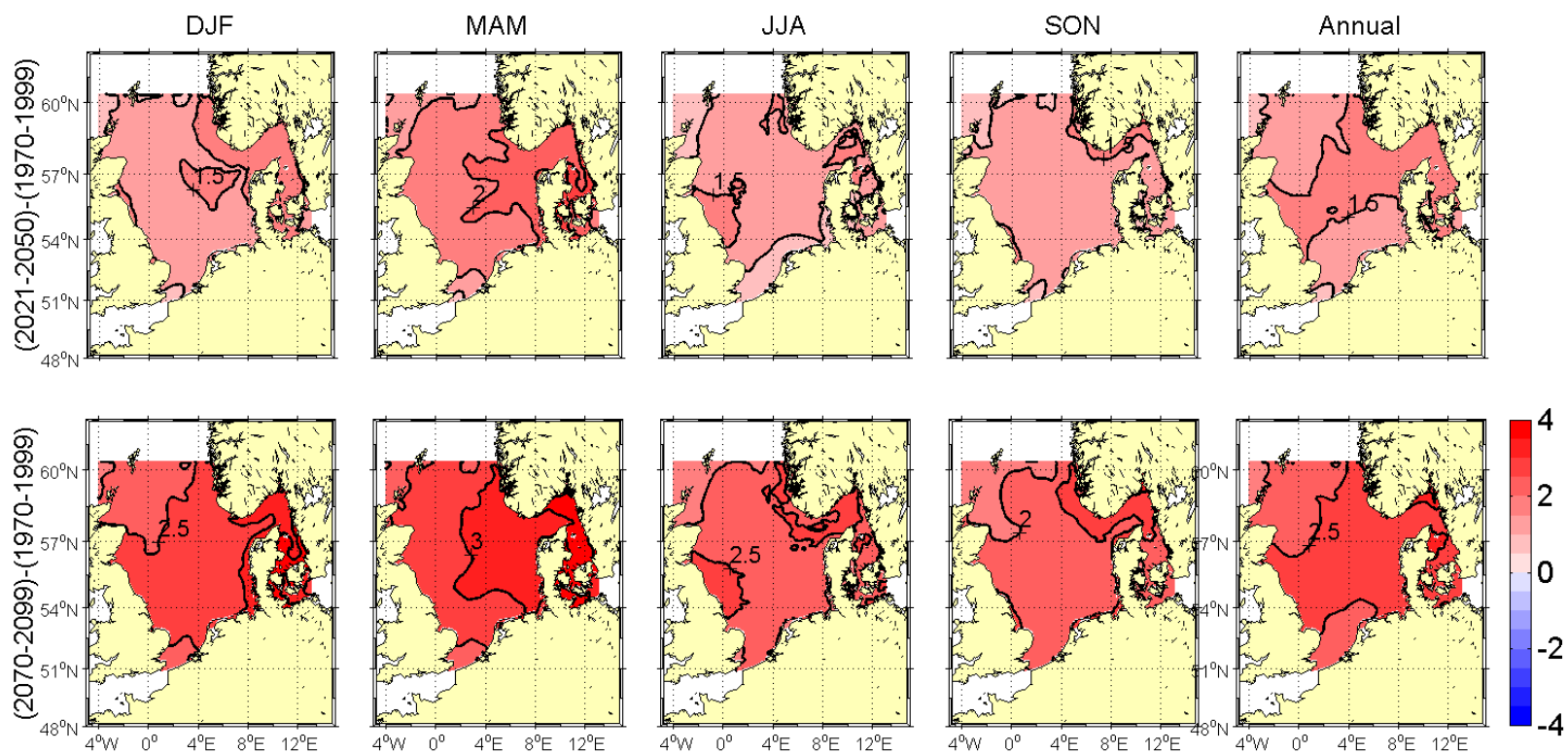


Figure 5.2.7A: Changes in seasonal and annual sea surface temperature [°C] for HAMSOM run 202 (A1B scenario run). Upper panel from (1970-1999) to (2021-2050) and lower panel from (1970-1999) to (2070-2099). The contour interval is 0.5 °C. Selected isolines have been labelled for better orientation.

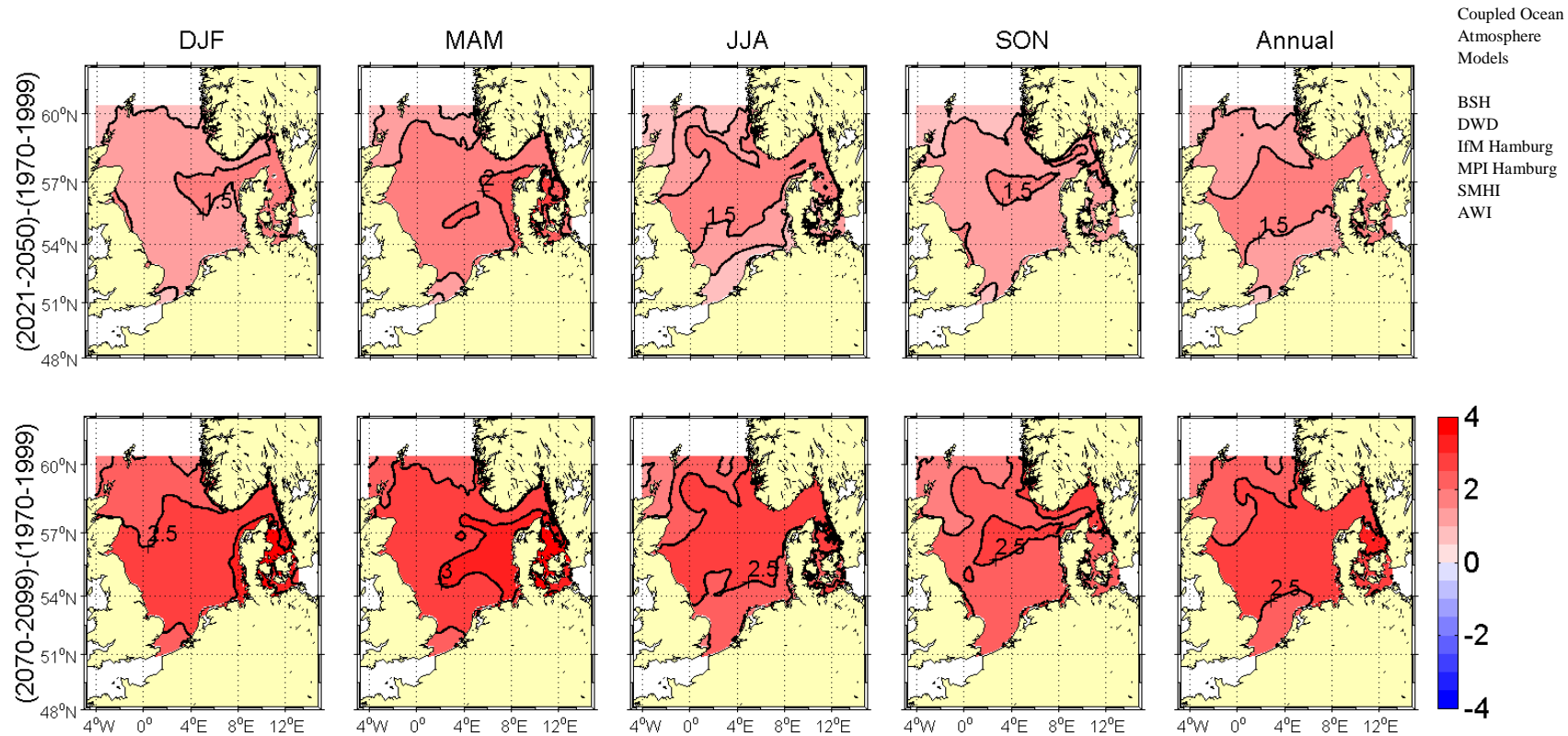


Figure 5.2.8A: Changes in seasonal and annual bottom temperature [°C] for HAMSOM run 202 (A1B scenario run). Upper panel from (1970-1999) to (2021-2050) and lower panel from (1970-1999) to (2070-2099). The contour interval is 0.5 °C. Selected isolines have been labelled for better orientation.

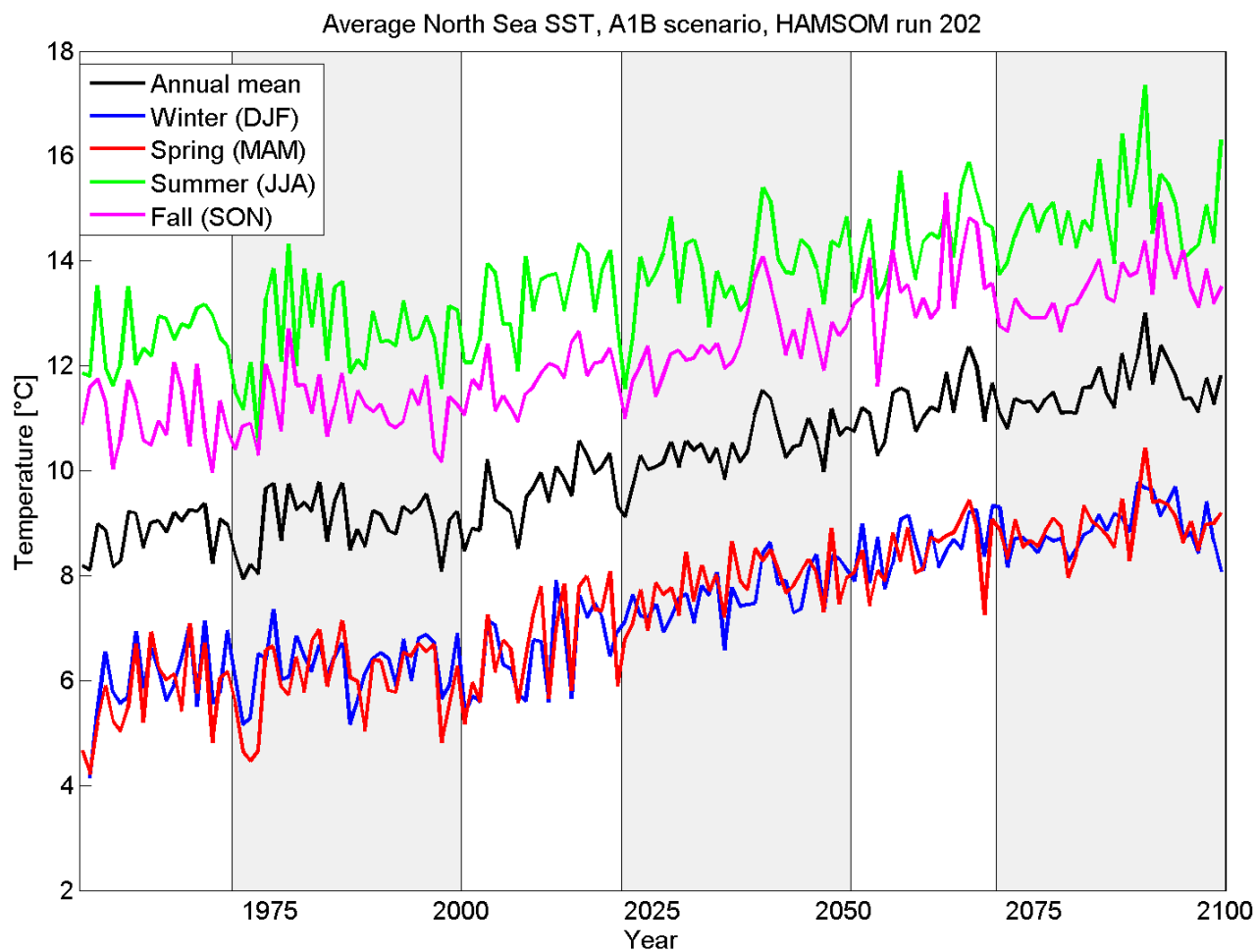


Figure 5.2.9A: Time series of seasonal and annual means of sea surface temperature [°C] for HAMSOM run 202 (A1B scenario run) from 1950-2099. The temperatures represent averages over the North Sea area given in Figure 4.1.

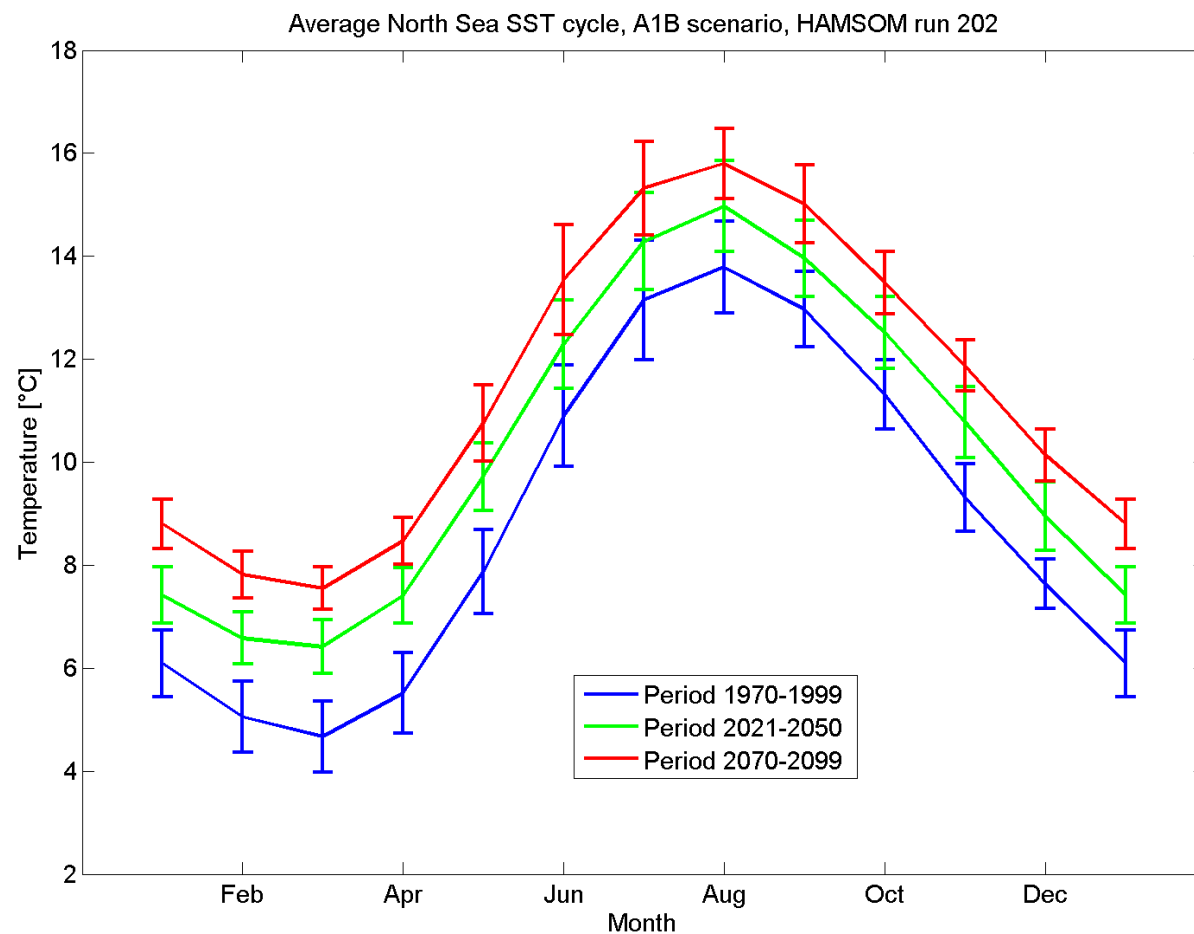


Figure 5.2.10A: The mean annual cycle of sea surface temperatures [°C] for HAMSOM run 202 (A1B scenario run) for 1970-1999 (blue), 2021-2050 (green) and 2070-2099 (red). The means are representing averages over the North Sea area given in Figure 4.1. The error bars are indicating time variability.

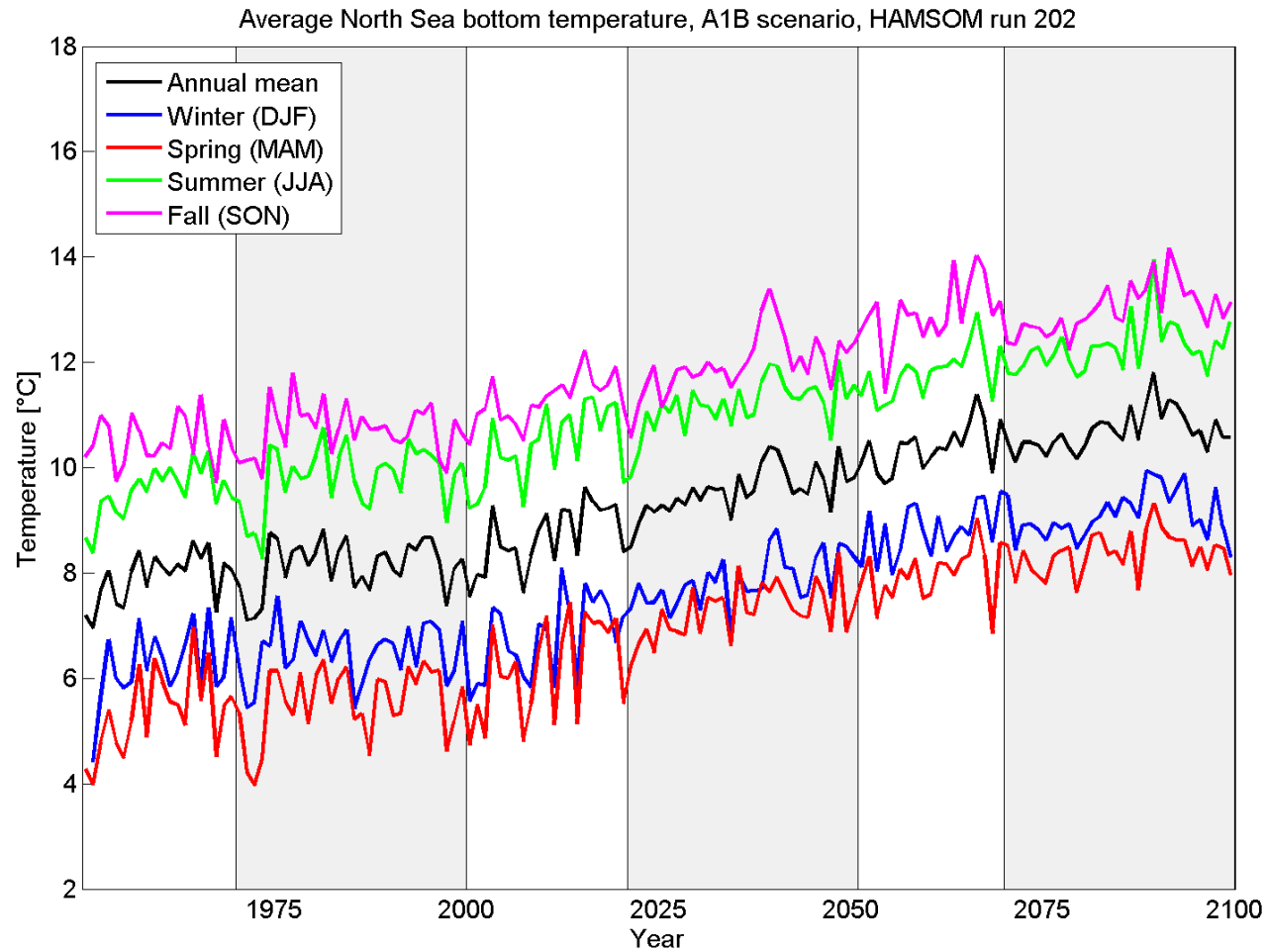


Figure 5.2.11A: Time series of seasonal and annual means of bottom temperature [°C] for HAMSOM run 202 (A1B scenario run) from 1950-2099. The temperatures represent averages over the North Sea area given in Figure 4.1.

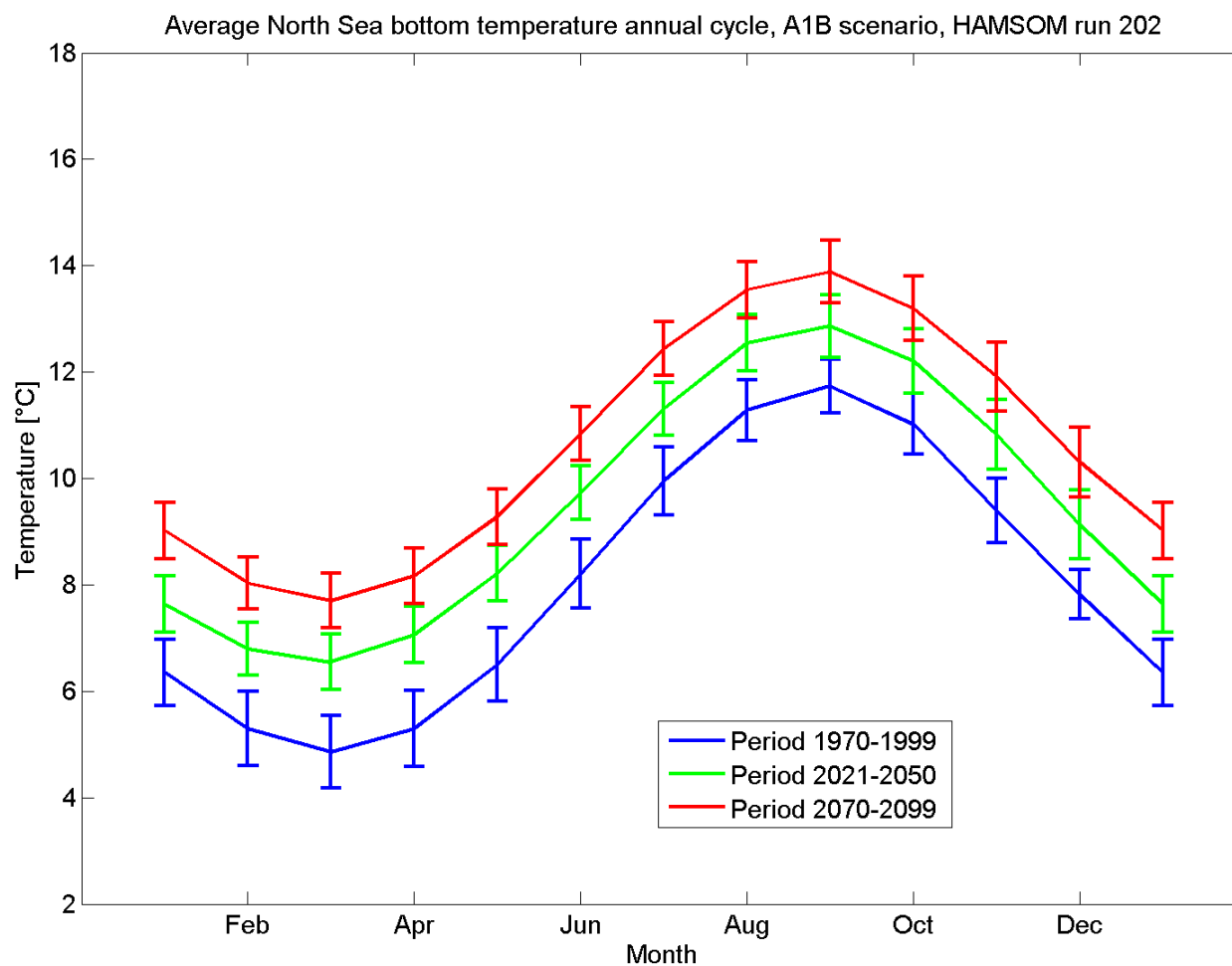


Figure 5.2.12A: The mean annual cycle of bottom temperatures [°C] for HAMSOM run 202 (A1B scenario run) for 1970-1999 (blue), 2021-2050 (green) and 2070-2099 (red). The means are representing averages over the North Sea area given in Figure 4.1. The error bars are indicating time variability.

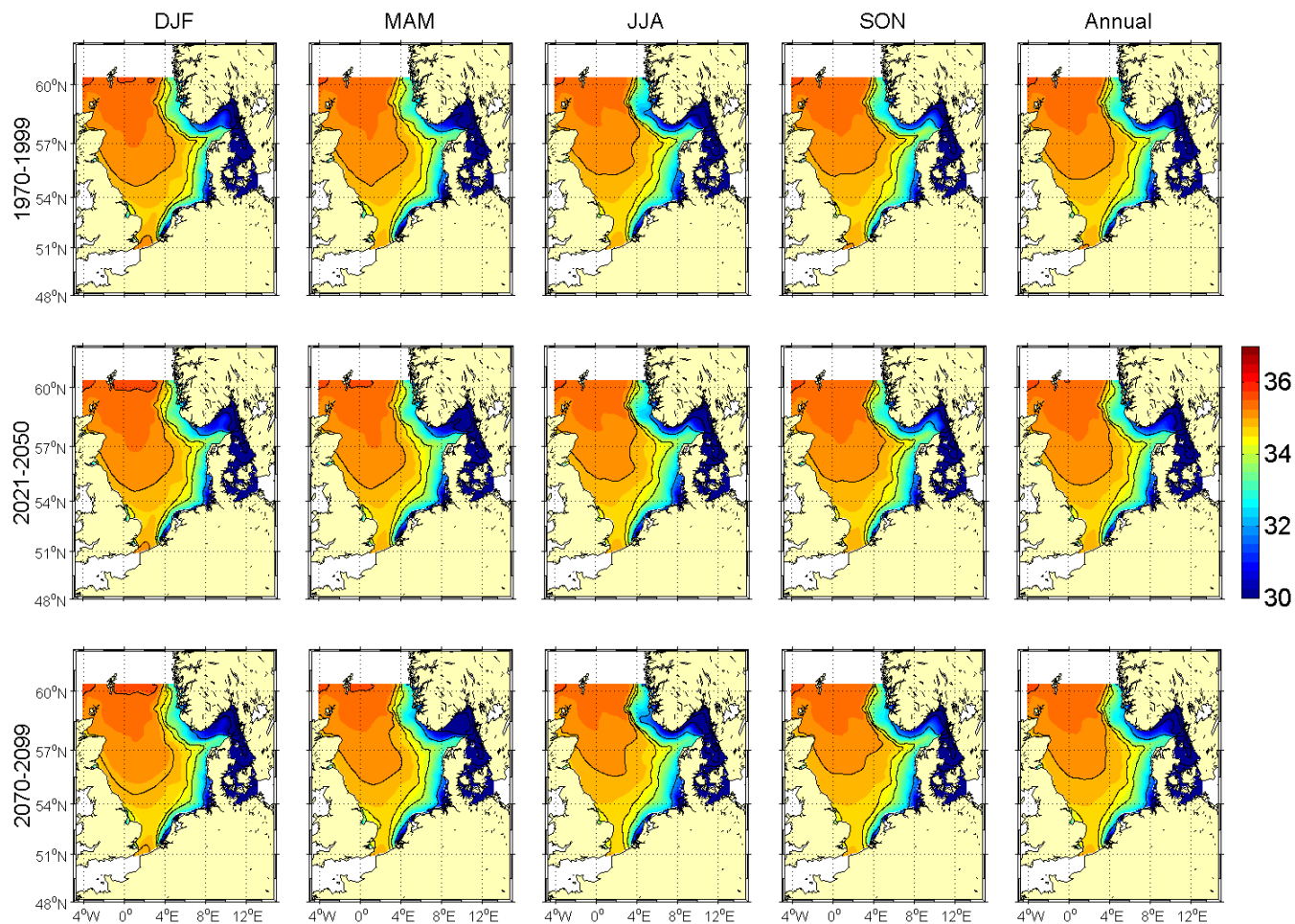


Figure 5.2.13A: Seasonal and annual means of sea surface salinity [psu] for HAMSOM run 202 (A1B scenario run). The upper row shows averages for the period 1970-1999, the middle row for 2021-2050 and the lower row for 2070-2099.

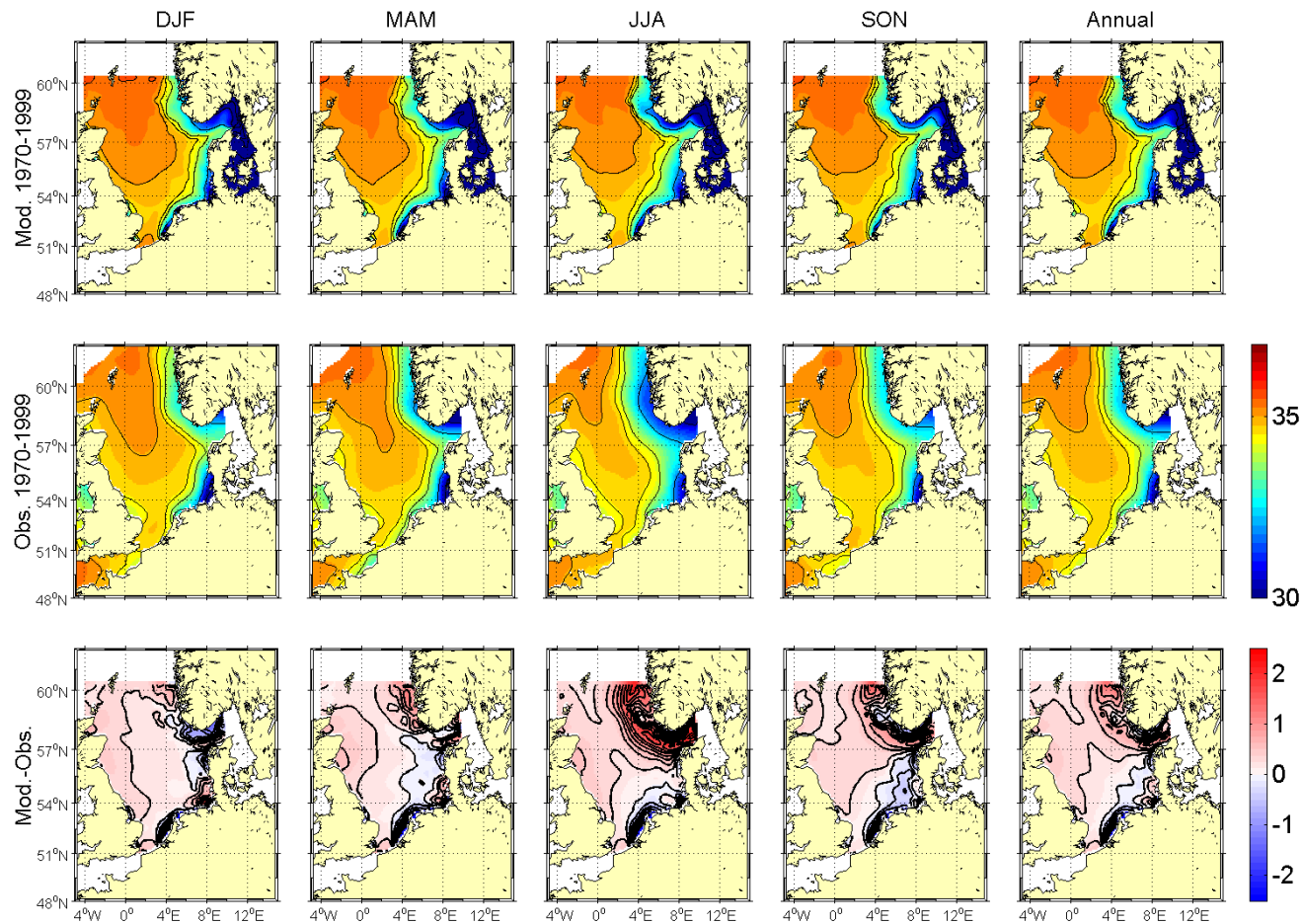


Figure 5.2.14A: Comparison of seasonal and annual means of sea surface salinity [psu] for HAMSOM run 202 for the base period 1970-1999 with BHC means. The upper row shows average model distributions, the middle row observed climatological means and the lower row the difference between the model results and the climatology.

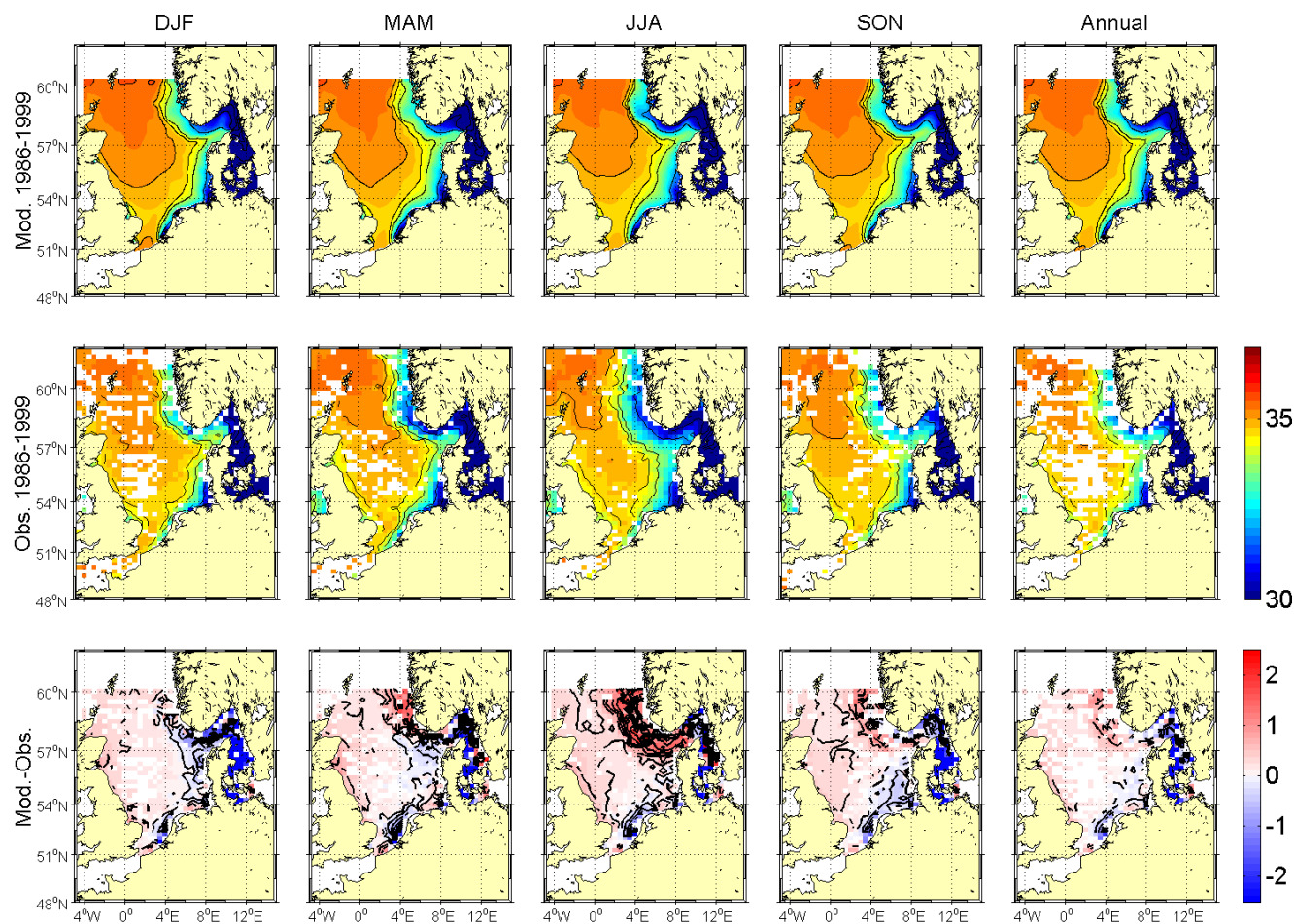


Figure 5.2.15A: Comparison of seasonal and annual means of sea surface salinity [psu] for HAMSOM run 202 for the base period 1970-1999 with KNSC means. The upper row shows average model distributions, the middle row observed climatological means and the lower row the difference between the model results and the climatology.

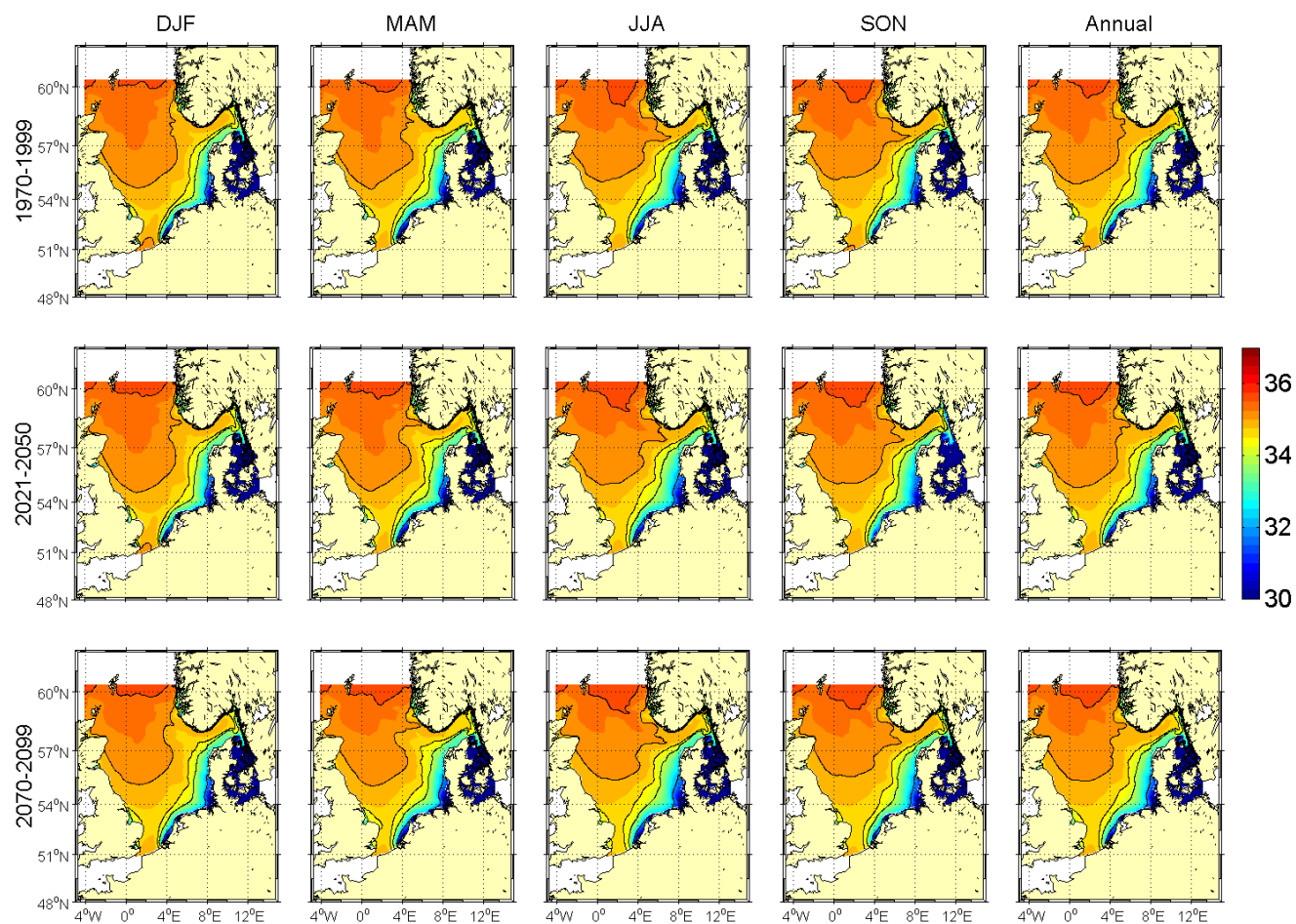


Figure 5.2.16A: Seasonal and annual means of bottom salinity [psu] for HAMSOM run 202 (A1B scenario run). The upper row shows averages for the period 1970-1999, the middle row for 2021-2050 and the lower row for 2070-2099.

Coupled Ocean
Atmosphere
Models

BSH
DWD
IfM Hamburg
MPI Hamburg
SMHI
AWI

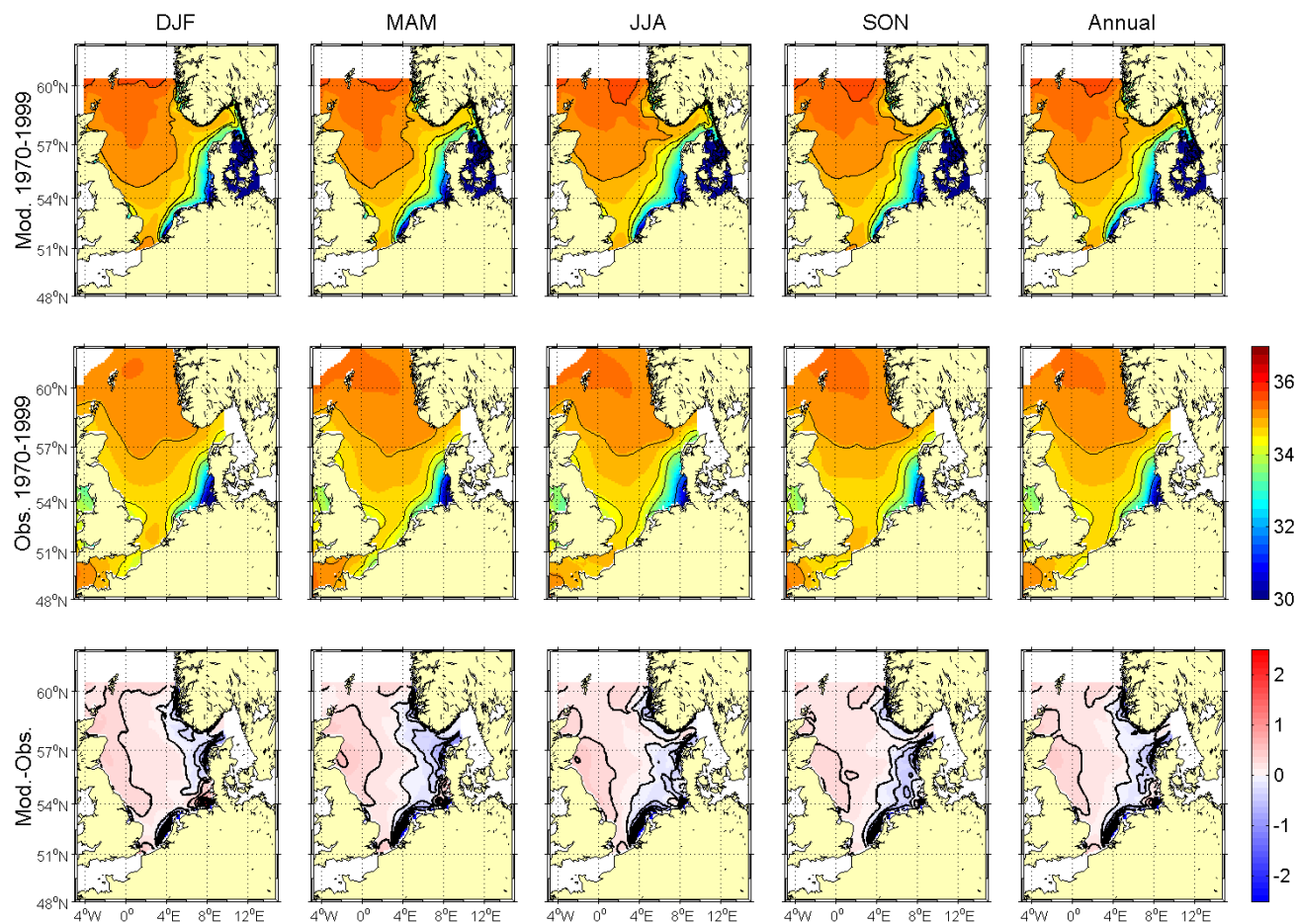
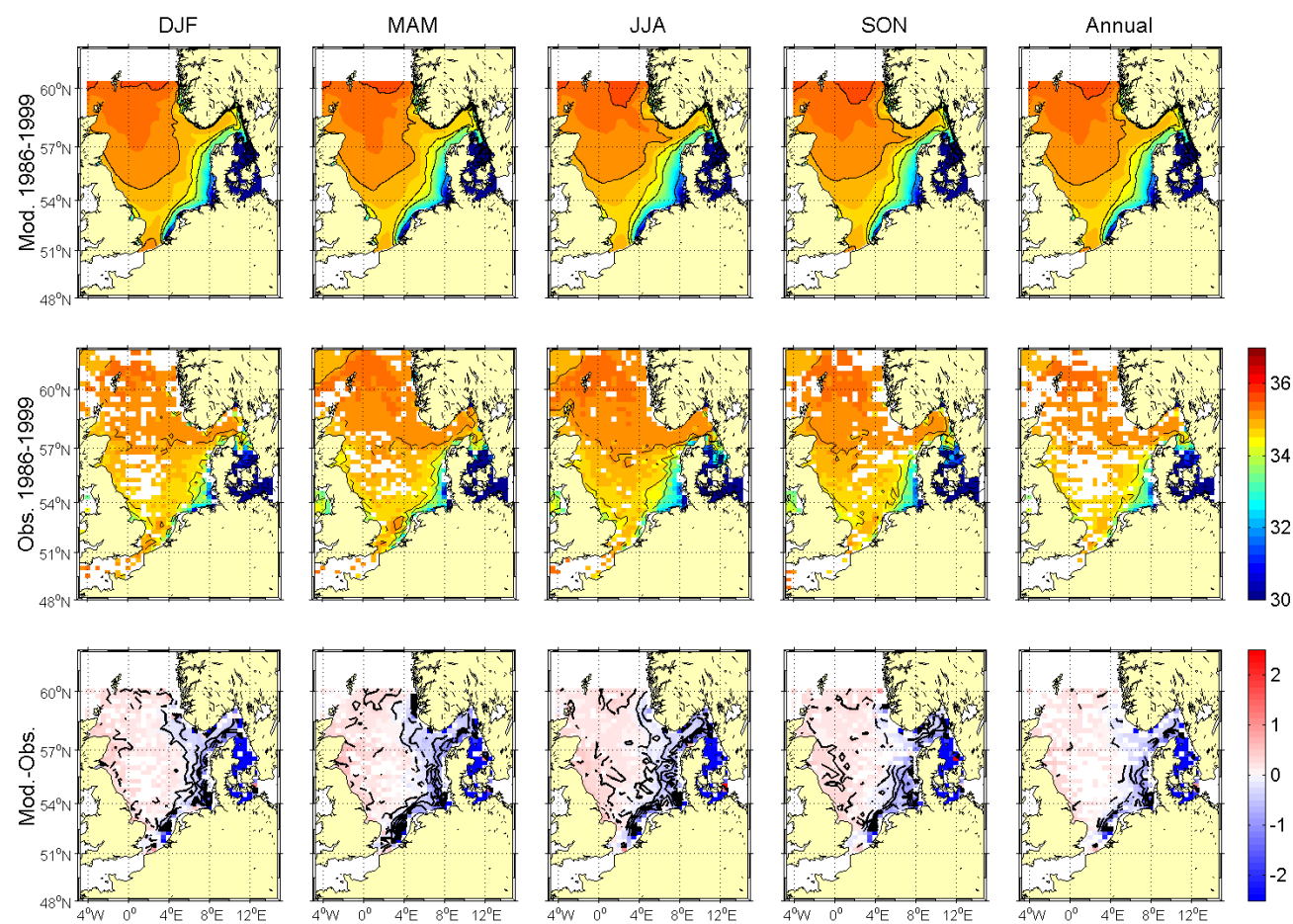


Figure 5.2.17A: Comparison of seasonal and annual means of bottom salinity [psu] for HAMSOM run 202 for the base period 1970-1999 with BHC means. The upper row shows average model distributions, the middle row observed climatological means and the lower row the difference between the model results and the climatology.



Coupled Ocean
Atmosphere
Models

BSH
DWD
IfM Hamburg
MPI Hamburg
SMHI
AWI

Figure 5.2.18A: Comparison of seasonal and annual means of bottom salinity [psu] for HAMSOM run 202 for the base period 1970-1999 with KNSC means. The upper row shows average model distributions, the middle row observed climatological means and the lower row the difference between the model results and the climatology.

Coupled Ocean
Atmosphere
Models

BSH
DWD
IfM Hamburg
MPI Hamburg
SMHI
AWI

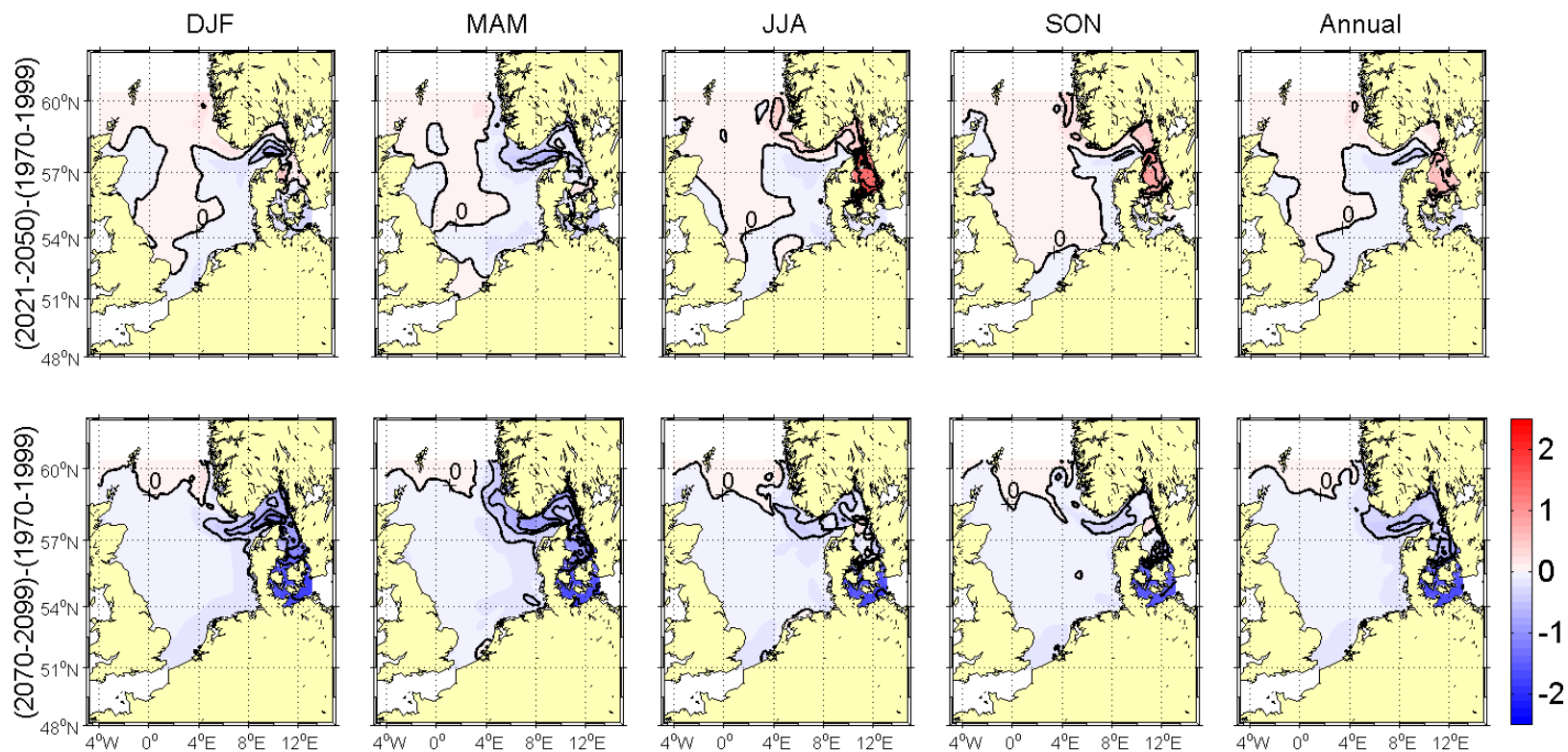


Figure 5.2.19A: Changes in seasonal and annual sea surface salinity [psu] for HAMSOM run 202 (A1B scenario run). Upper panel from (1970-1999) to (2021-2050) and lower panel from (1970-1999) to (2070-2099). The contour interval is 0.25 psu. Selected isolines have been labelled for better orientation.

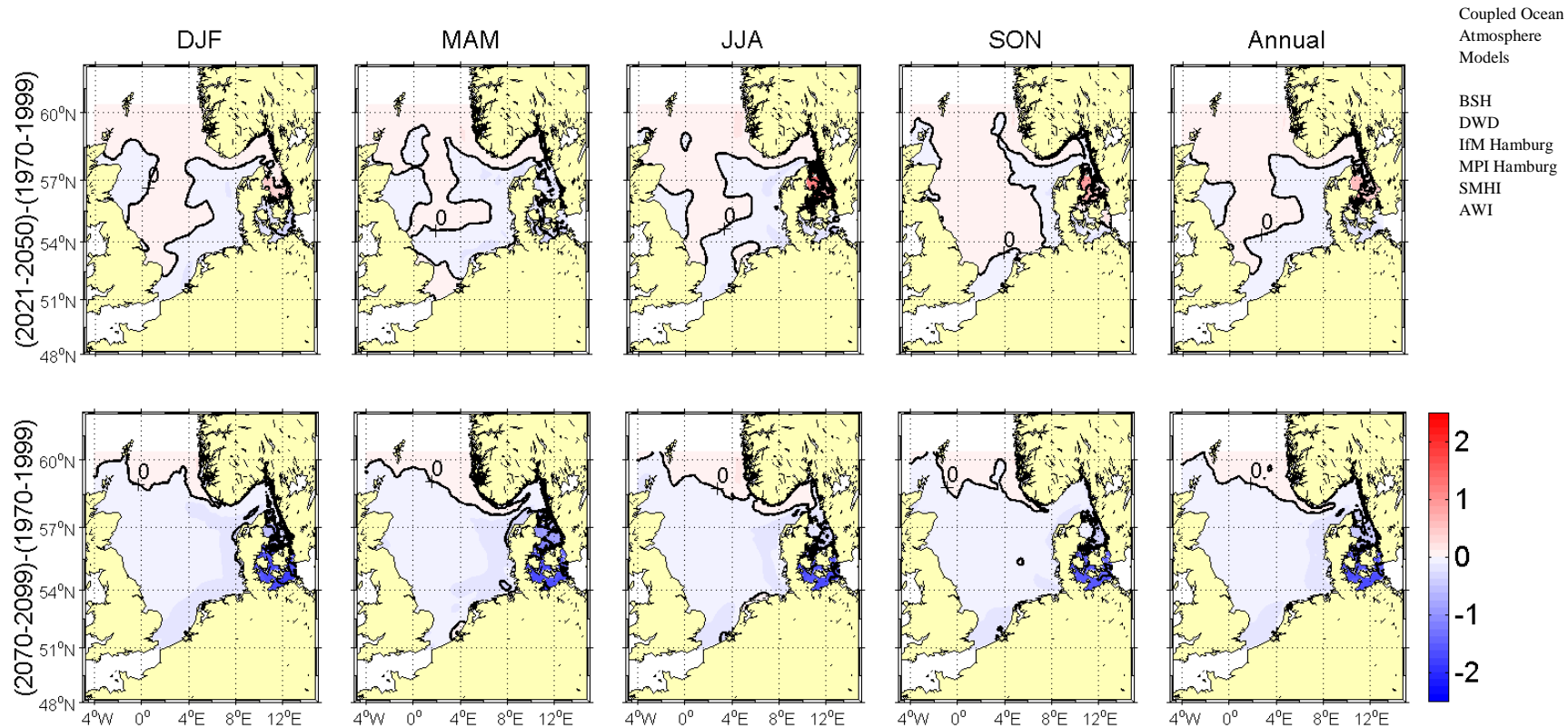


Figure 5.2.20A: Changes in seasonal and annual bottom salinity [psu] for HAMSOM run 202 (A1B scenario run). Upper panel from (1970-1999) to (2021-2050) and lower panel from (1970-1999) to (2070-2099). The contour interval is 0.5 °C. Selected isolines have been labelled for better orientation.

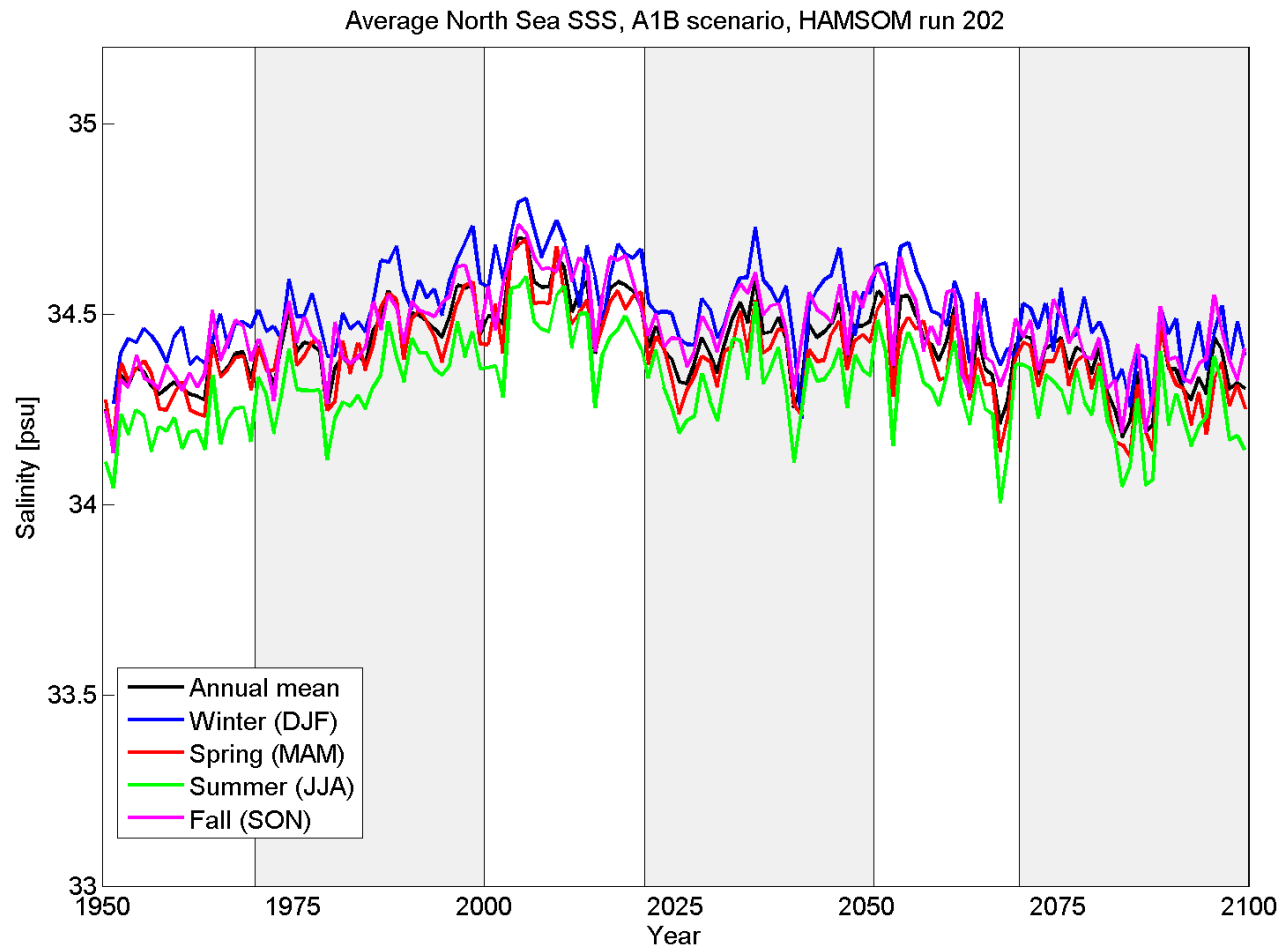


Figure 5.2.21A: Time series of seasonal and annual means of sea surface salinity [psu] for HAMSOM run 202 (A1B scenario run) from 1950-2099. The salinities represent averages over the North Sea area given in Figure 4.1.

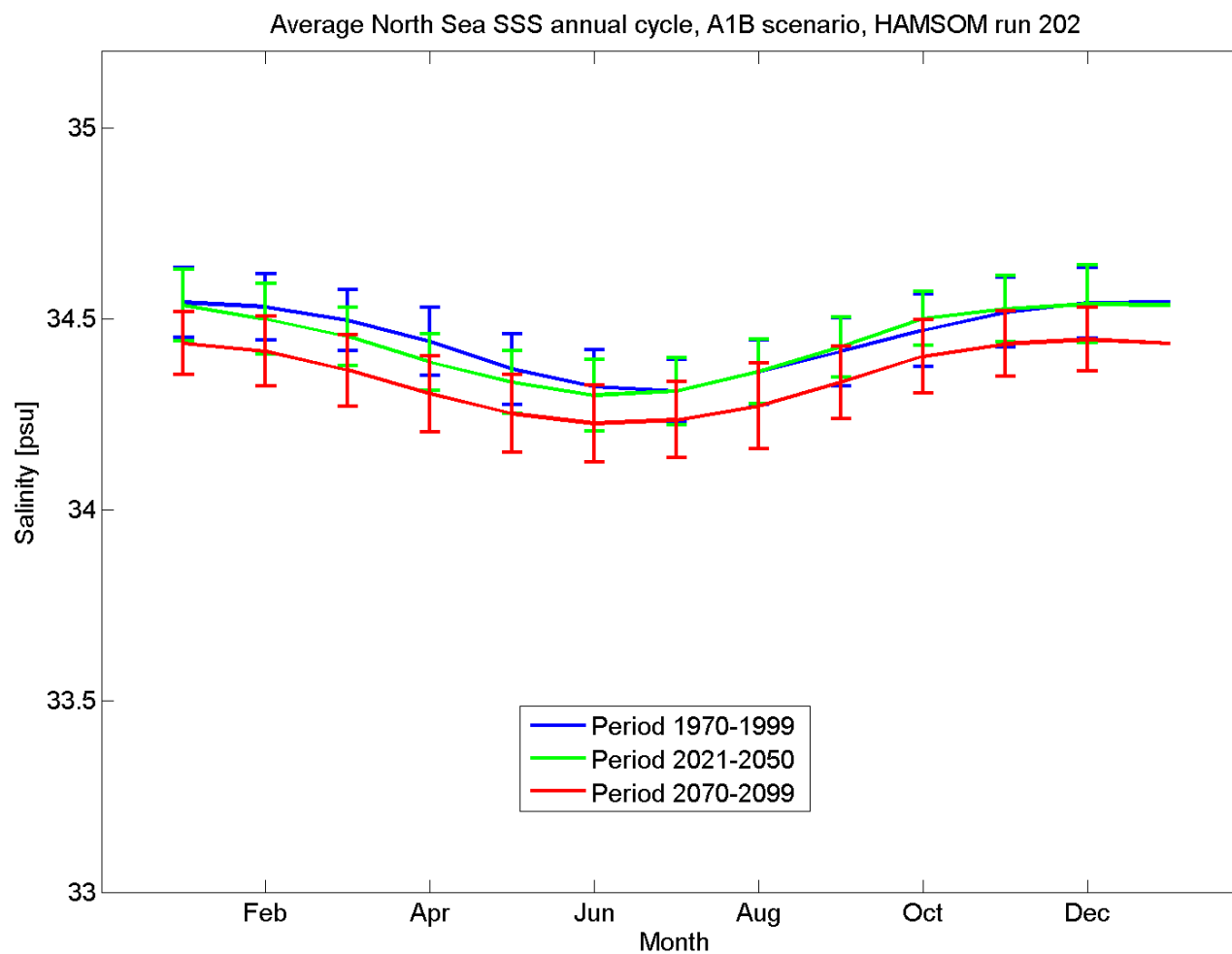


Figure 5.2.22A: The mean annual cycle of sea surface salinity [psu] for HAMSOM run 202 (A1B scenario run) for 1970-1999 (blue), 2021-2050 (green) and 2070-2099 (red). The means are representing averages over the North Sea area given in Figure 4.1. The error bars are indicating time variability.

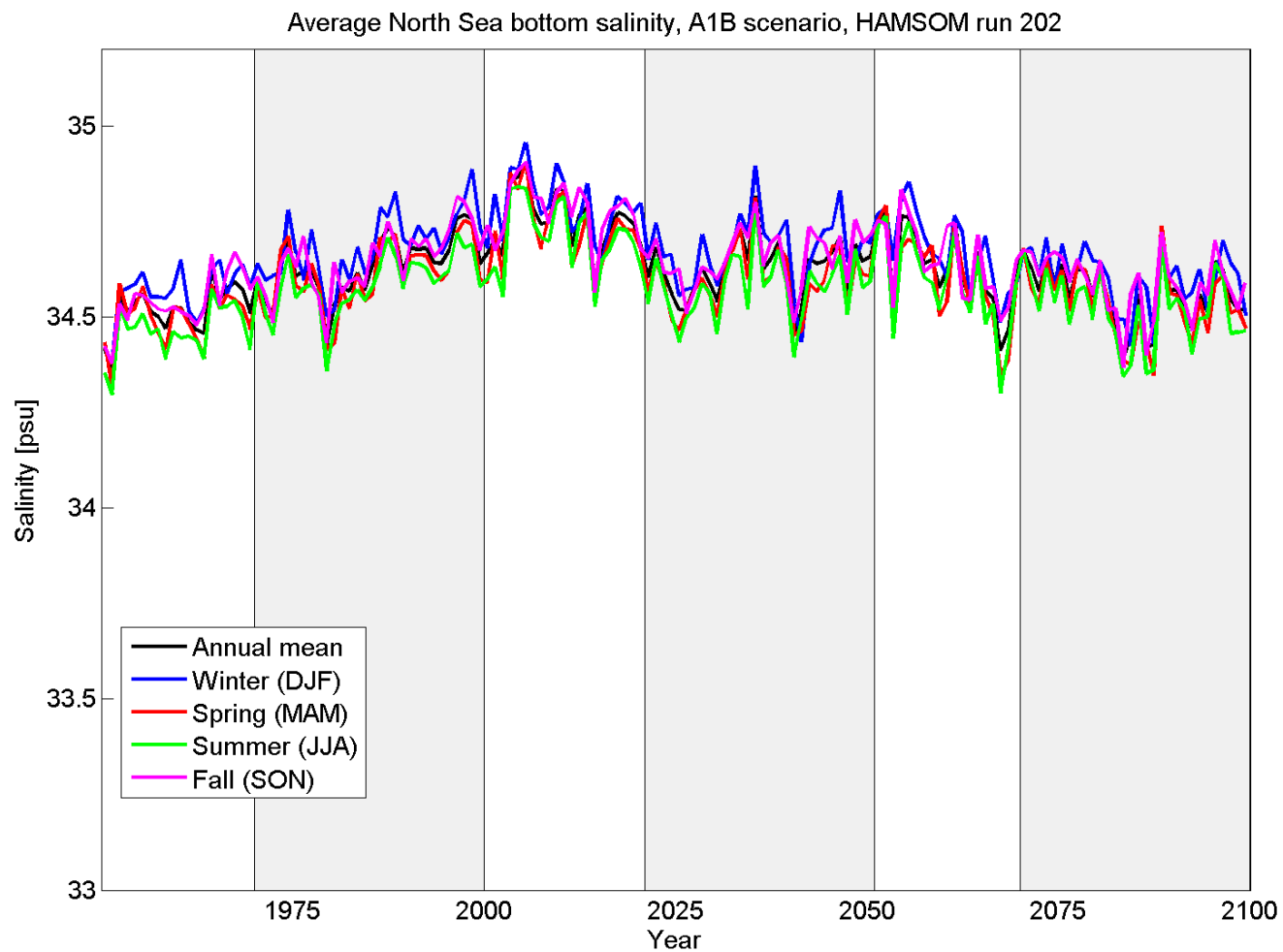


Figure 5.2.23A: Time series of seasonal and annual means of bottom salinity [psu] for HAMSOM run 202 (A1B scenario run) from 1950-2099. The salinities represent averages over the North Sea area given in Figure 4.1.

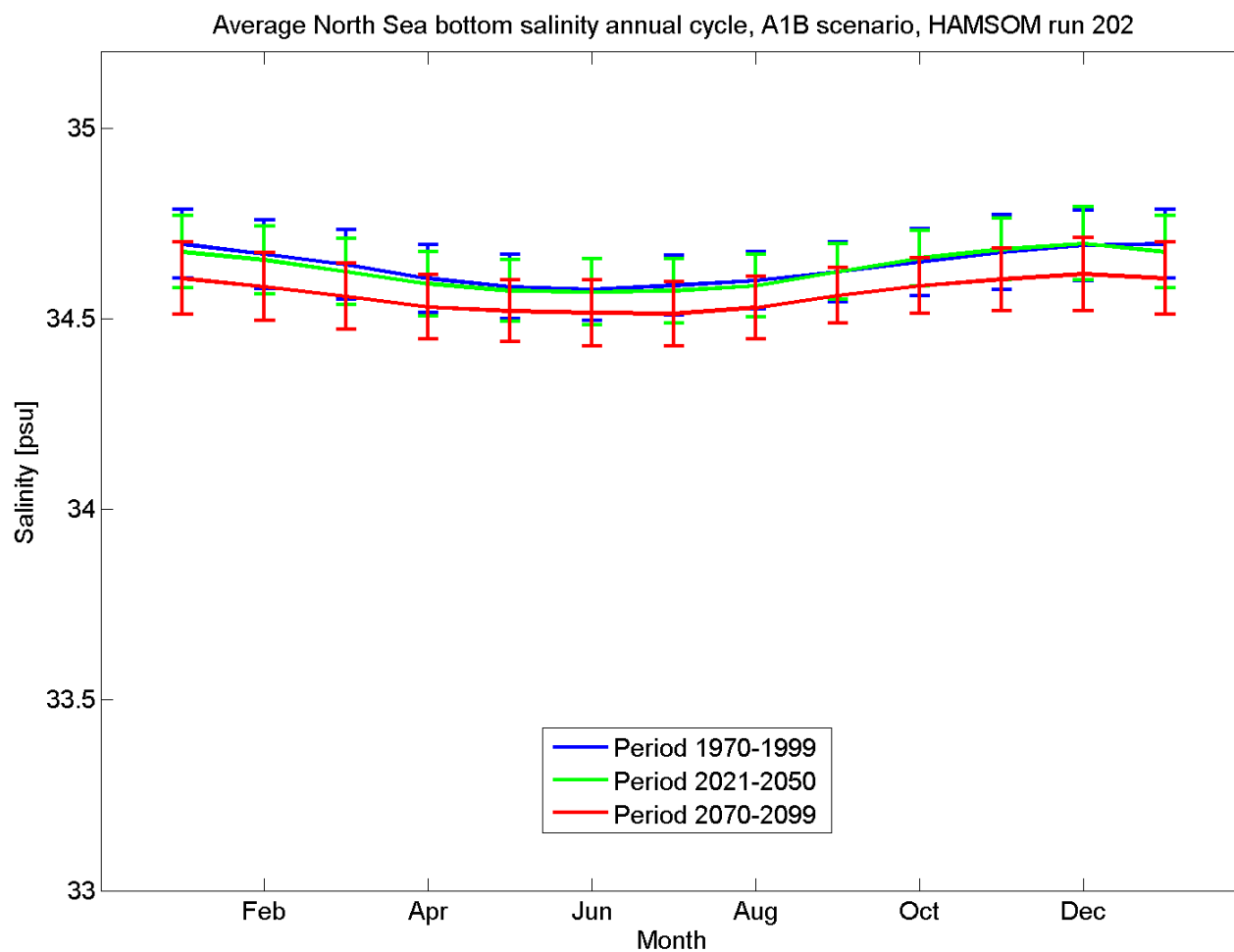


Figure 5.2.24A: The mean annual cycle of bottom salinity [psu] for HAMSOM run 202 (A1B scenario run) for 1970-1999 (blue), 2021-2050 (green) and 2070-2099 (red). The means are representing averages over the North Sea area given in Figure 4.1. The error bars are indicating time variability.

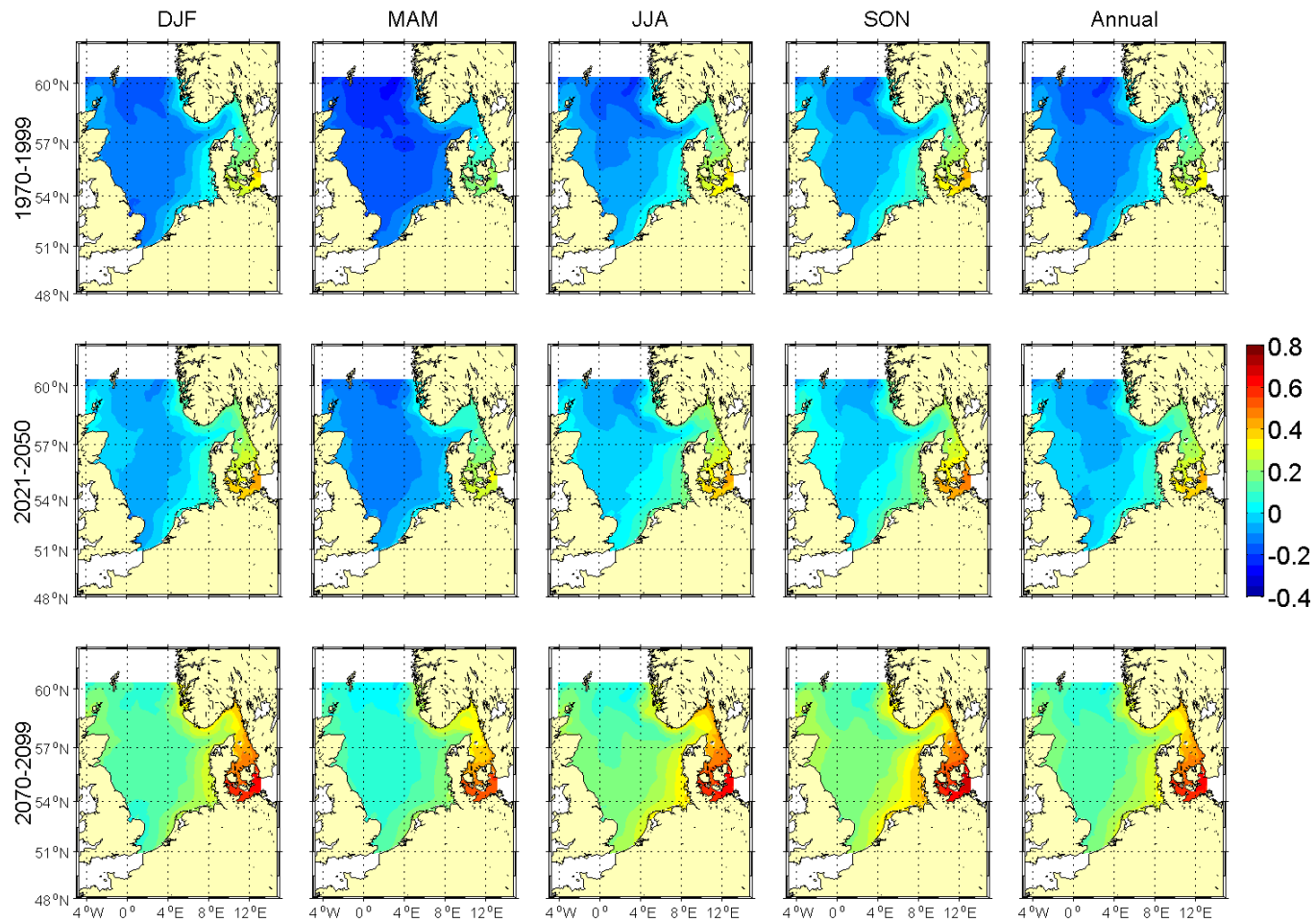


Figure 5.2.25A: Seasonal and annual means of sea surface height [m] for HAMSOM run 202 (A1B scenario run). The upper row shows averages for the period 1970-1999, the middle row for 2021-2050 and the lower row for 2070-2099.

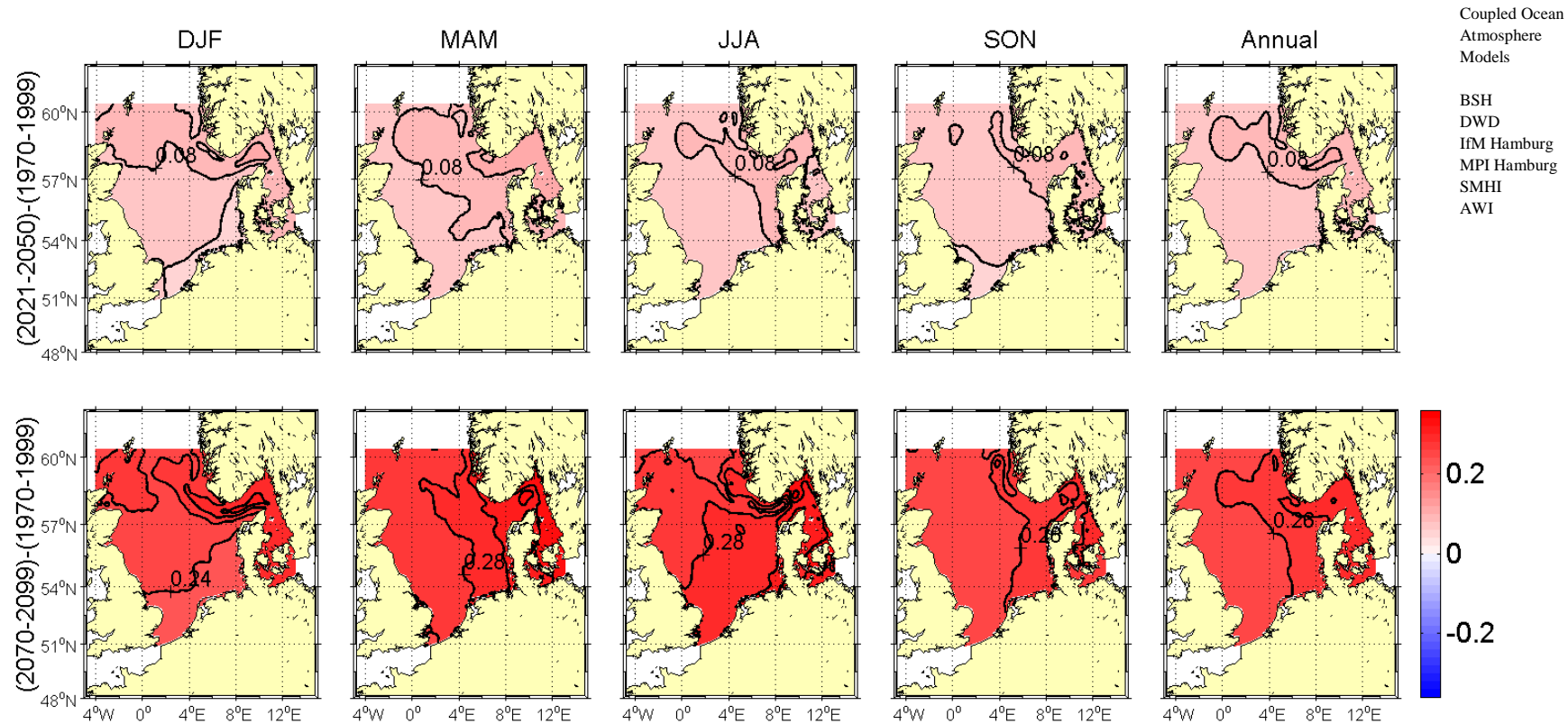


Figure 5.2.26A: Changes in seasonal and annual sea surface height [m] for HAMSOM run 202 (A1B scenario run). Upper panel from (1970-1999) to (2021-2050) and lower panel from (1970-1999) to (2070-2099). The contour interval is 0.02 m. Selected isolines have been labelled for better orientation.

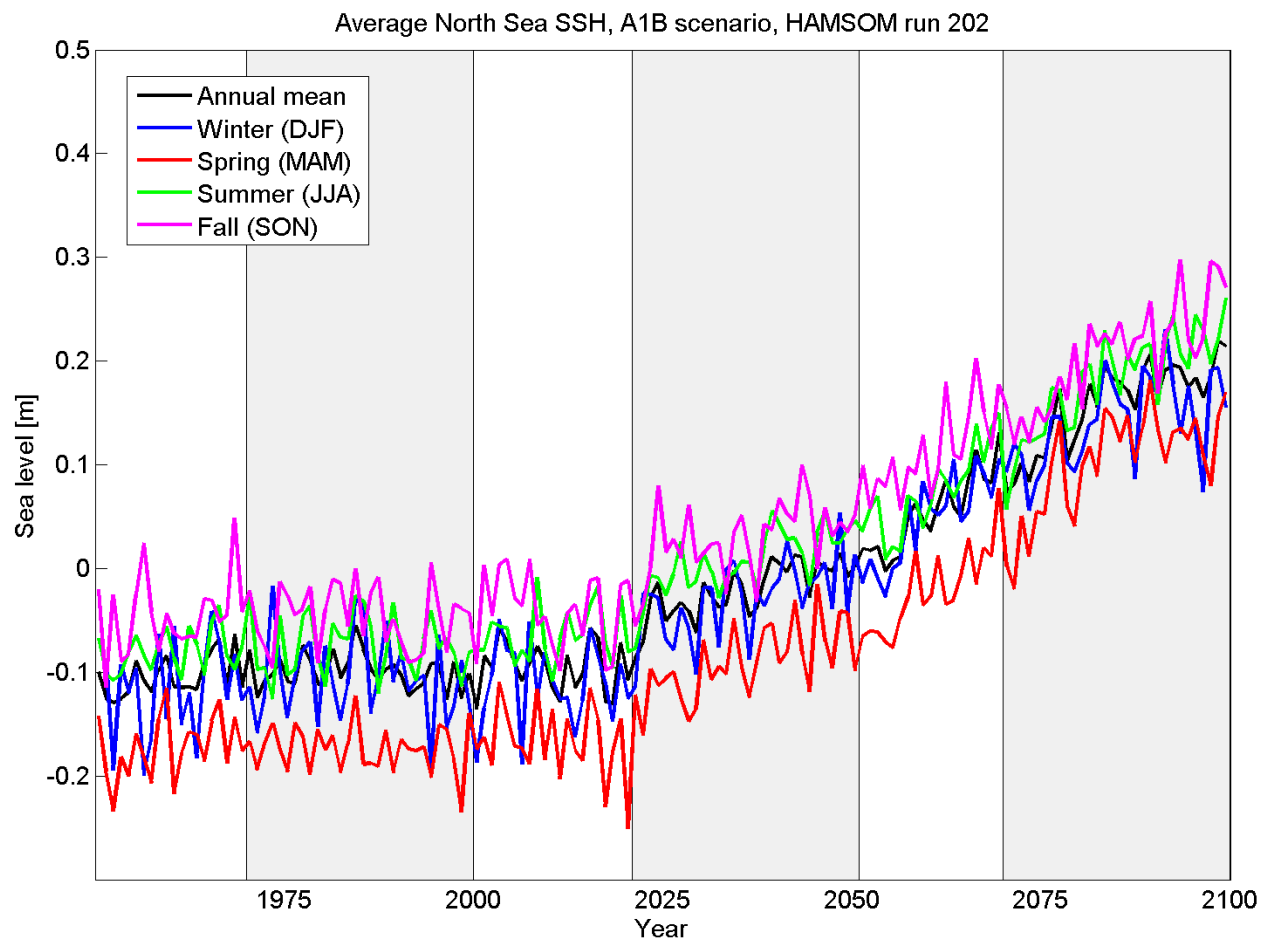


Figure 5.2.27A: Time series of seasonal and annual means of sea surface height [m] for HAMSOM run 202 (A1B scenario run) from 1950-2099. The sea surface heights represent averages over the North Sea area given in Figure 4.1.

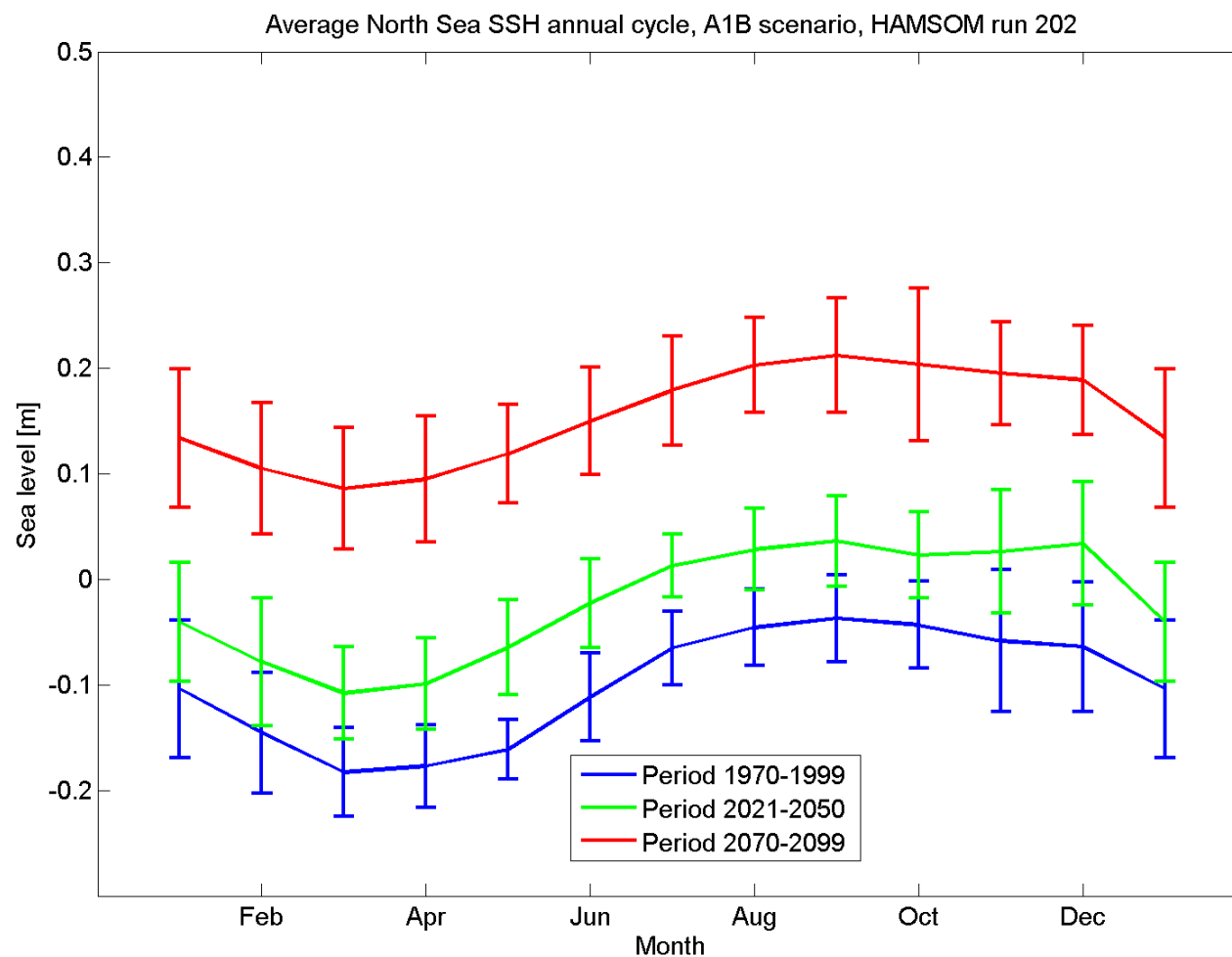


Figure 5.2.28A: The mean annual cycle of sea surface height [m] for HAMSOM run 202 (A1B scenario run) 1970-1999 (blue), 2021-2050 (green) and 2070-2099 (red). The means are representing averages over the North Sea area given in Figure 4.1. The error bars are indicating time variability.

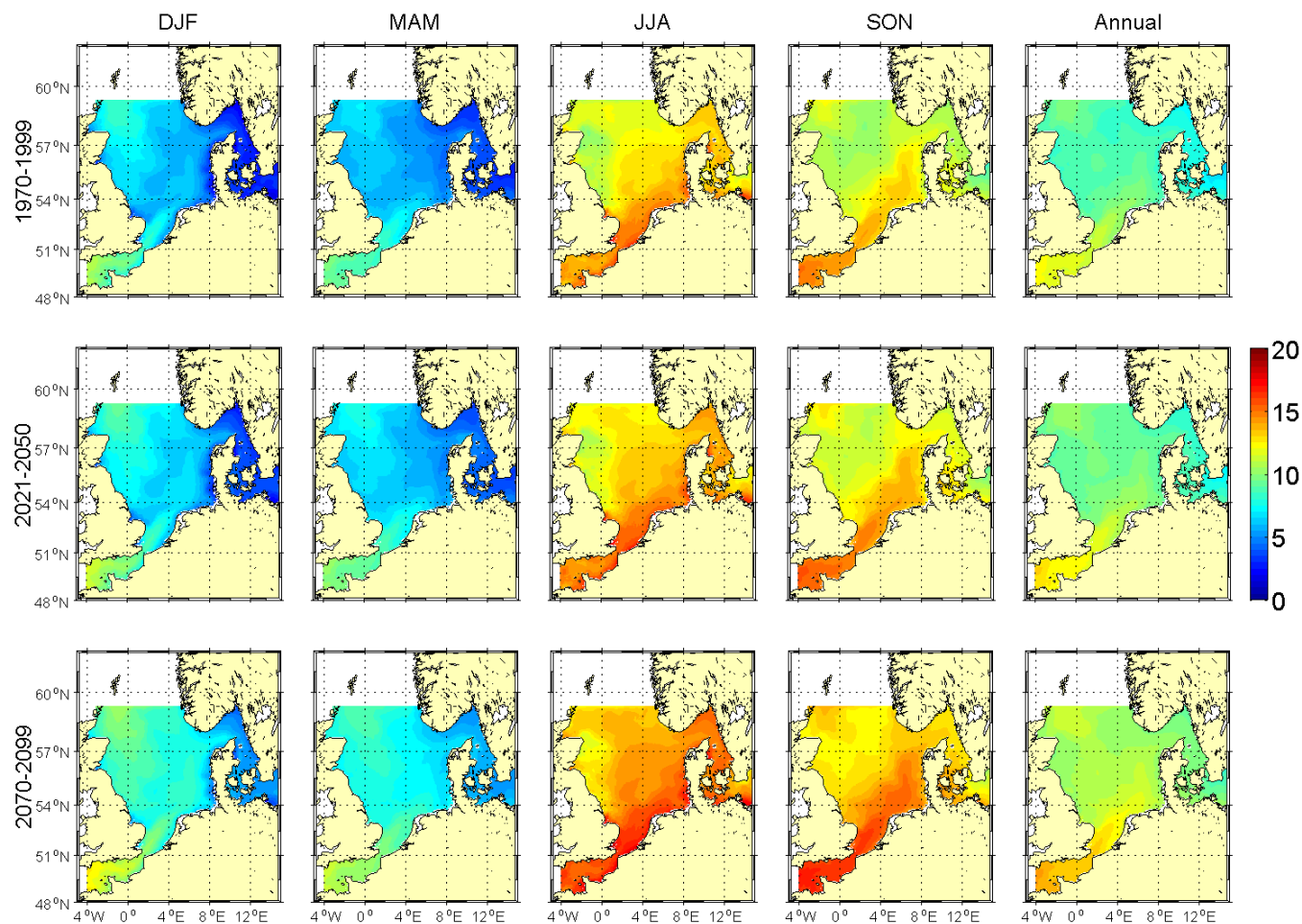


Figure 5.3.1A: Seasonal and annual means of sea surface temperature [°C] for NEMO-Nordic run 470 (A1B scenario run). The upper row shows averages for the period 1970-1999, the middle row for 2021-2050 and the lower row for 2070-2099.

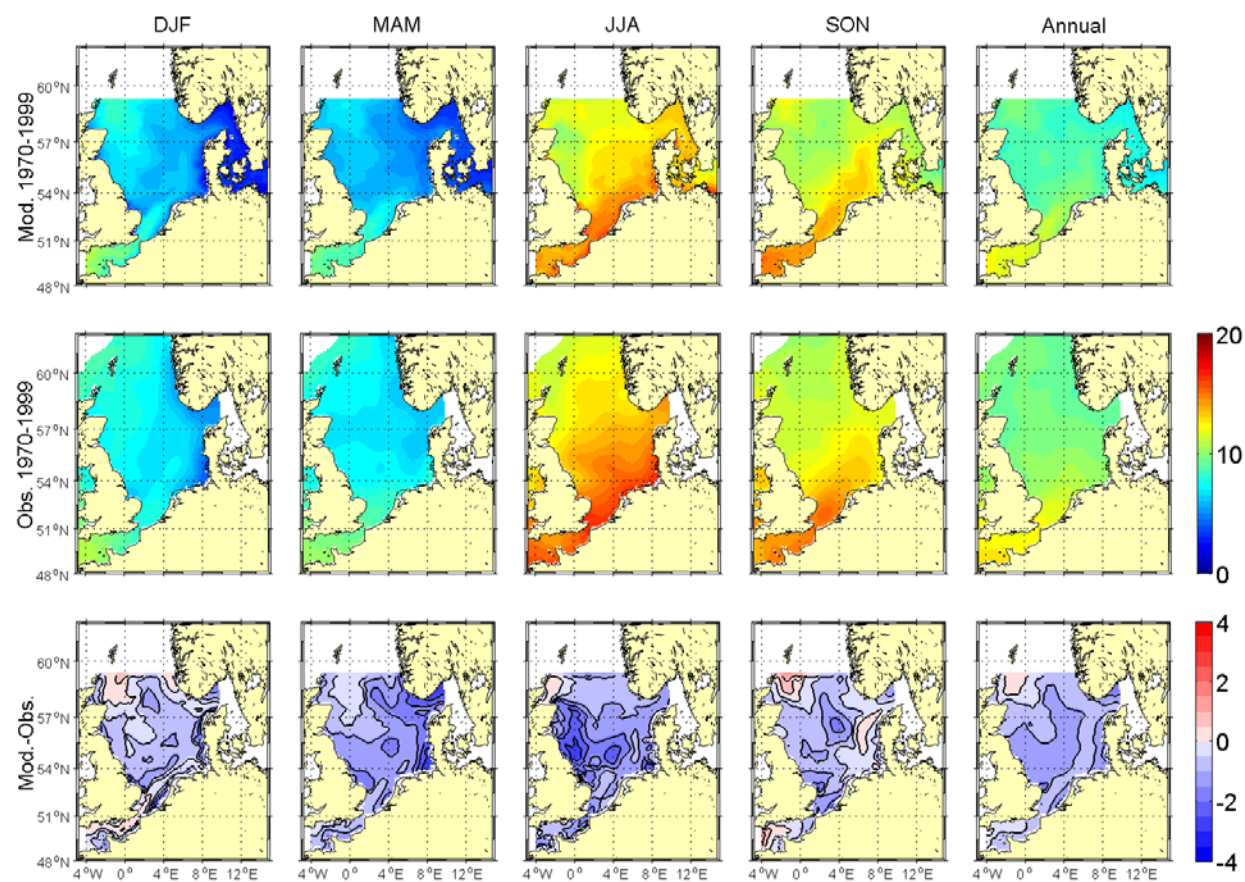


Figure 5.3.2A: Comparison of seasonal and annual means of sea surface temperature [°C] for NEMO-Nordic run 470 for the base period 1970-1999 with BHC means. The upper row shows average model distributions, the middle row observed climatological means and in the lower row the difference between the model results and the climatology.

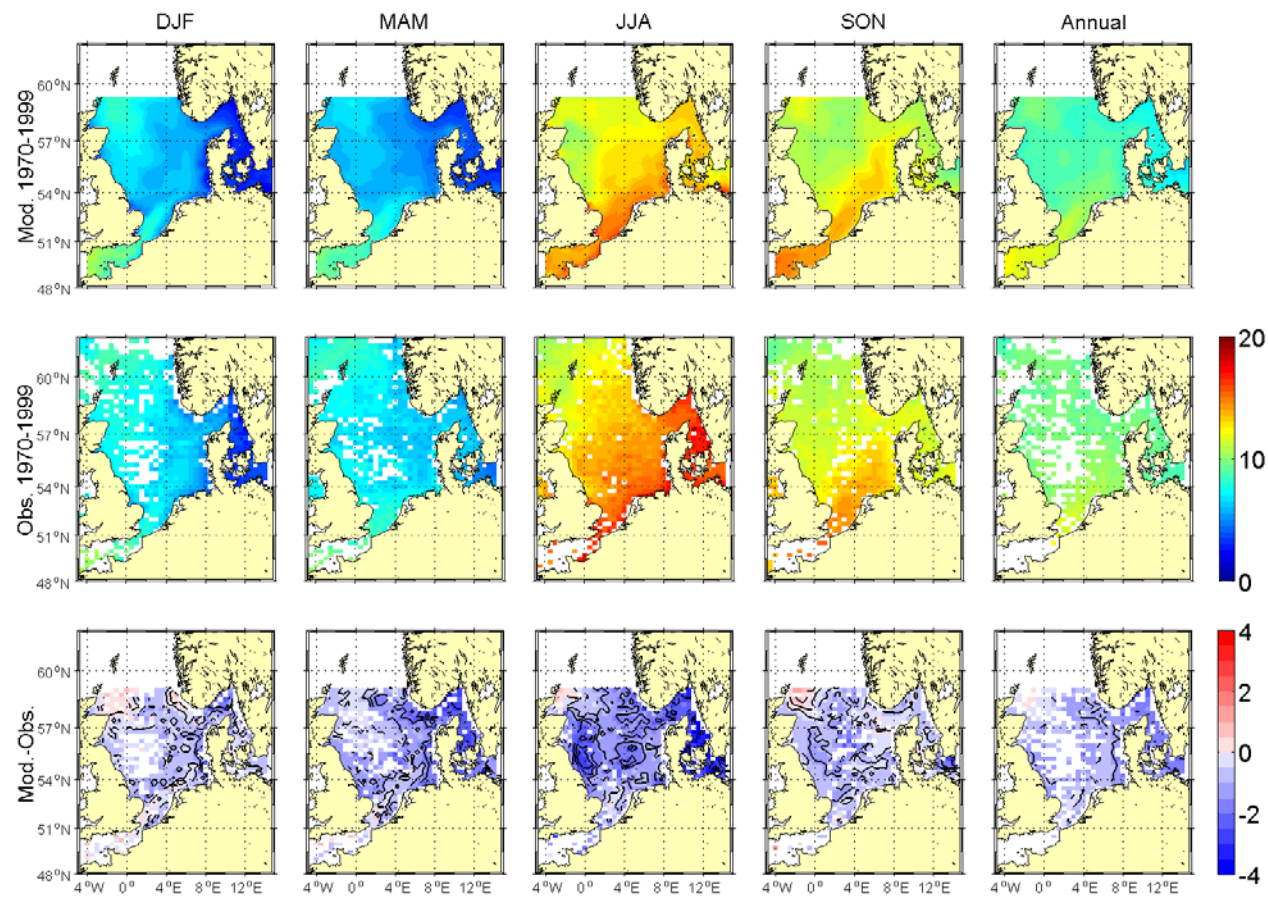


Figure 5.3.3A: Comparison of seasonal and annual means of sea surface temperature [°C] for NEMO-Nordic run 470 for the base period 1970-1999 with KNSC means. The upper row shows average model distributions, the middle row observed climatological means and the lower row the difference between the model results and the climatology.

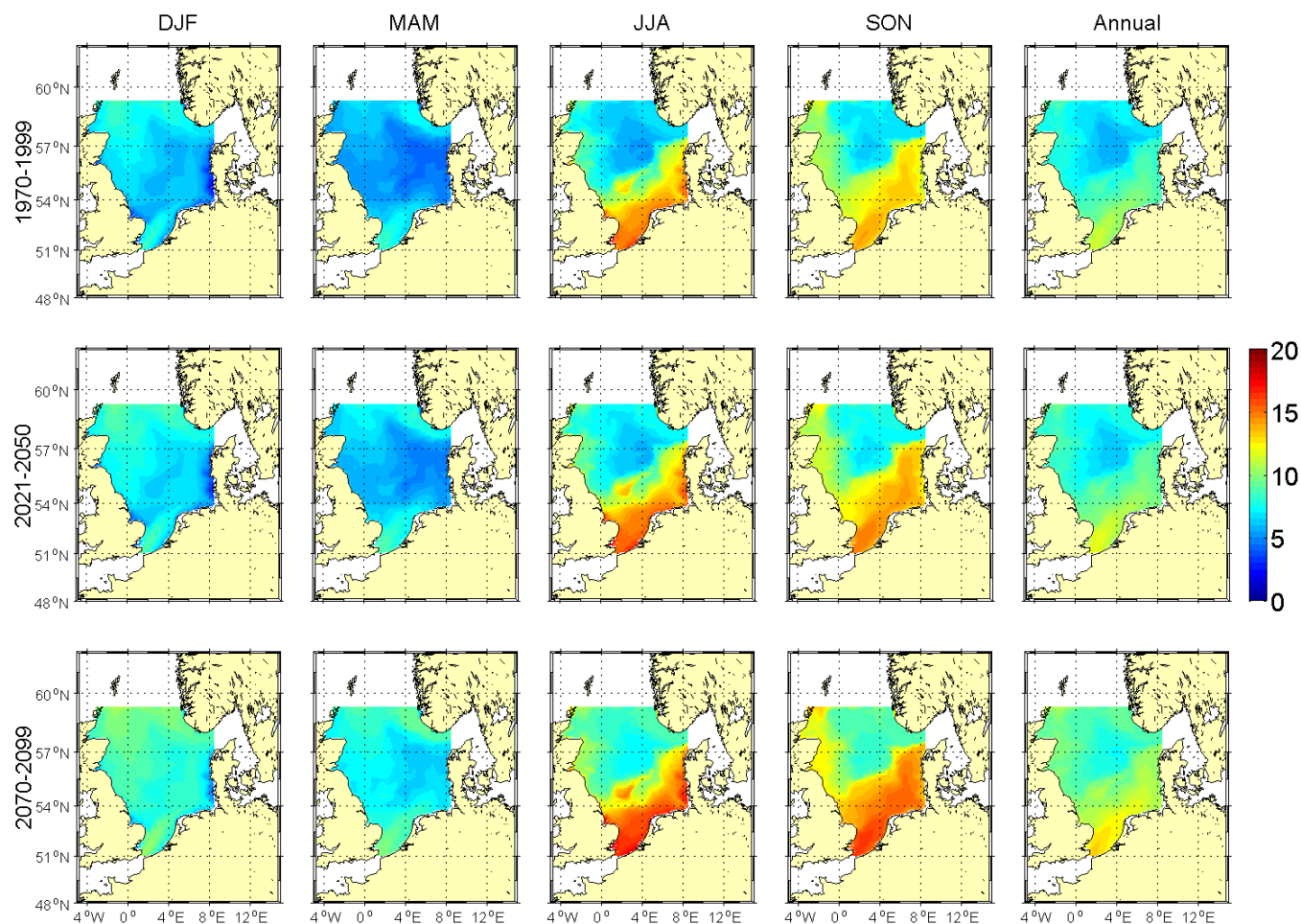


Figure 5.3.4A: Seasonal and annual means of bottom temperature [°C] for NEMO-Nordic run 470 (A1B scenario run). The upper row shows averages for the period 1970-1999, the middle row for 2021-2050 and the lower row for 2070-2099.

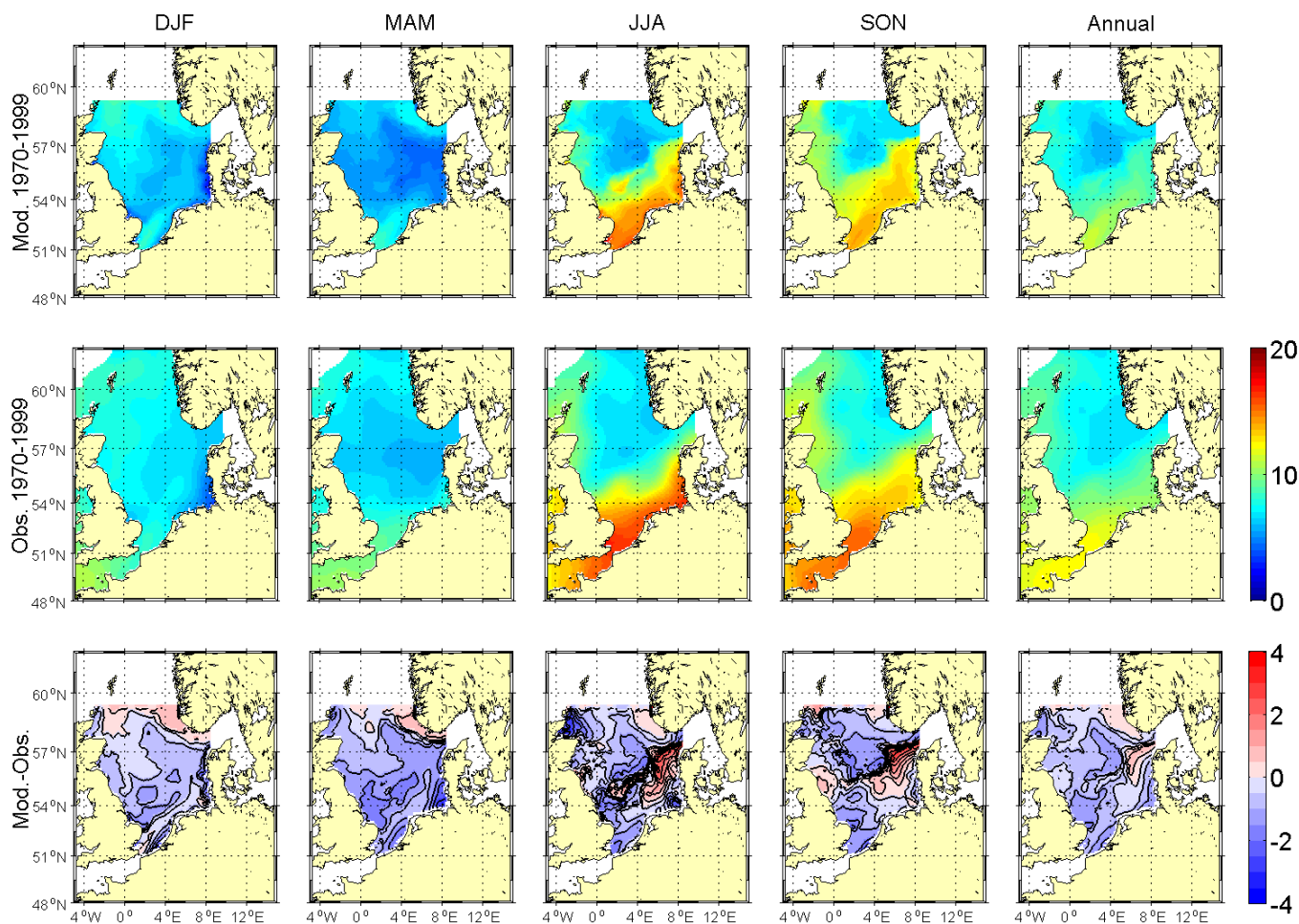
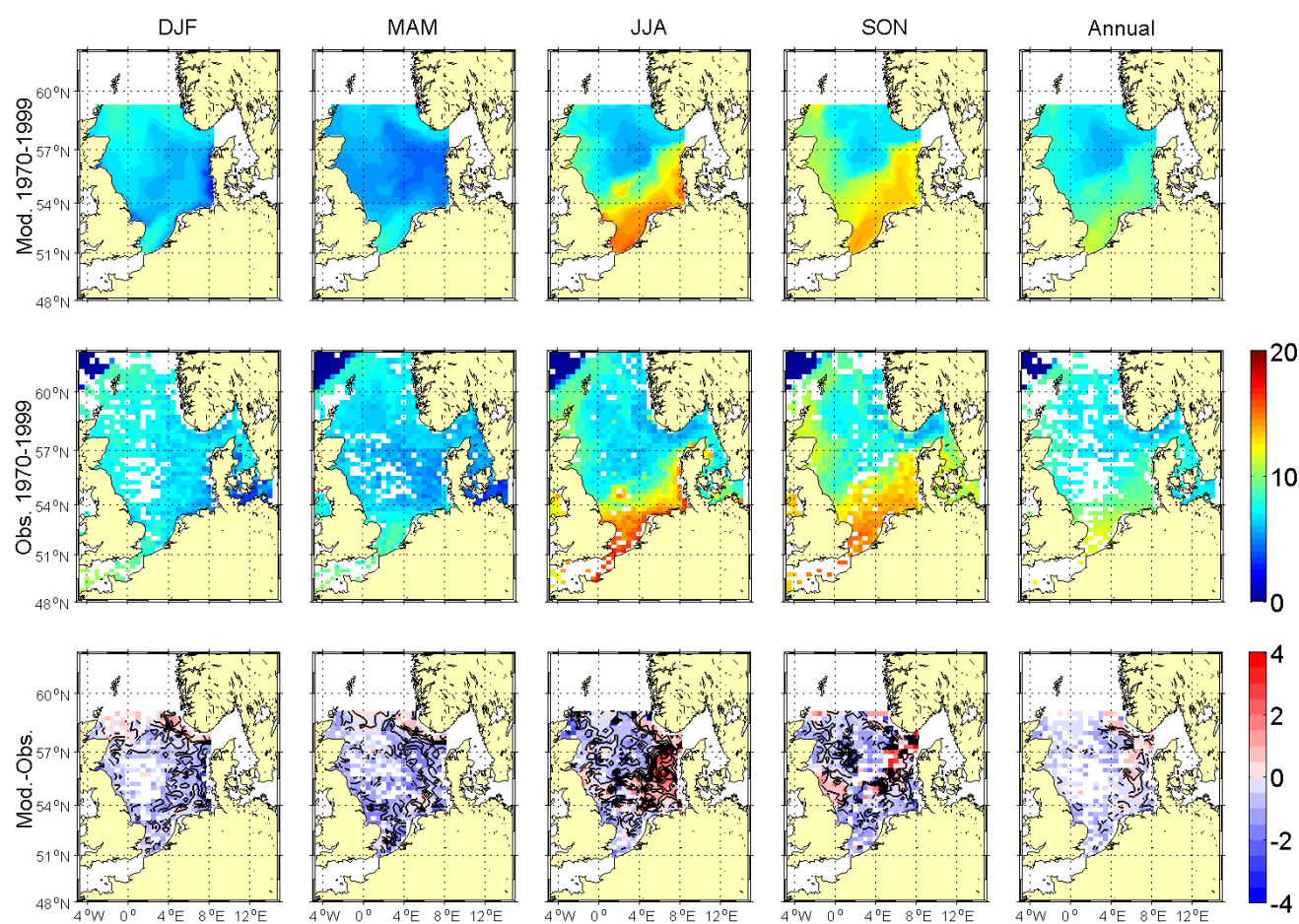


Figure 5.3.5A: Comparison of seasonal and annual means of bottom temperature [°C] for NEMO-Nordic run 470 for the base period 1970-1999 with BHC means. The upper row shows average model distributions, the middle row observed climatological means and the lower row the difference between the model results and the climatology.



Coupled Ocean
Atmosphere
Models

BSH
DWD
IfM Hamburg
MPI Hamburg
SMHI
AWI

Figure 5.3.6A: Comparison of seasonal and annual means of bottom temperature [°C] for NEMO-Nordic run 470 for the base period 1970-1999 with KNCS means. The upper row shows average model results, the middle row observed climatological means and the lower row the difference between the model results and the climatology.

Coupled Ocean
Atmosphere
Models

BSH
DWD
IfM Hamburg
MPI Hamburg
SMHI
AWI

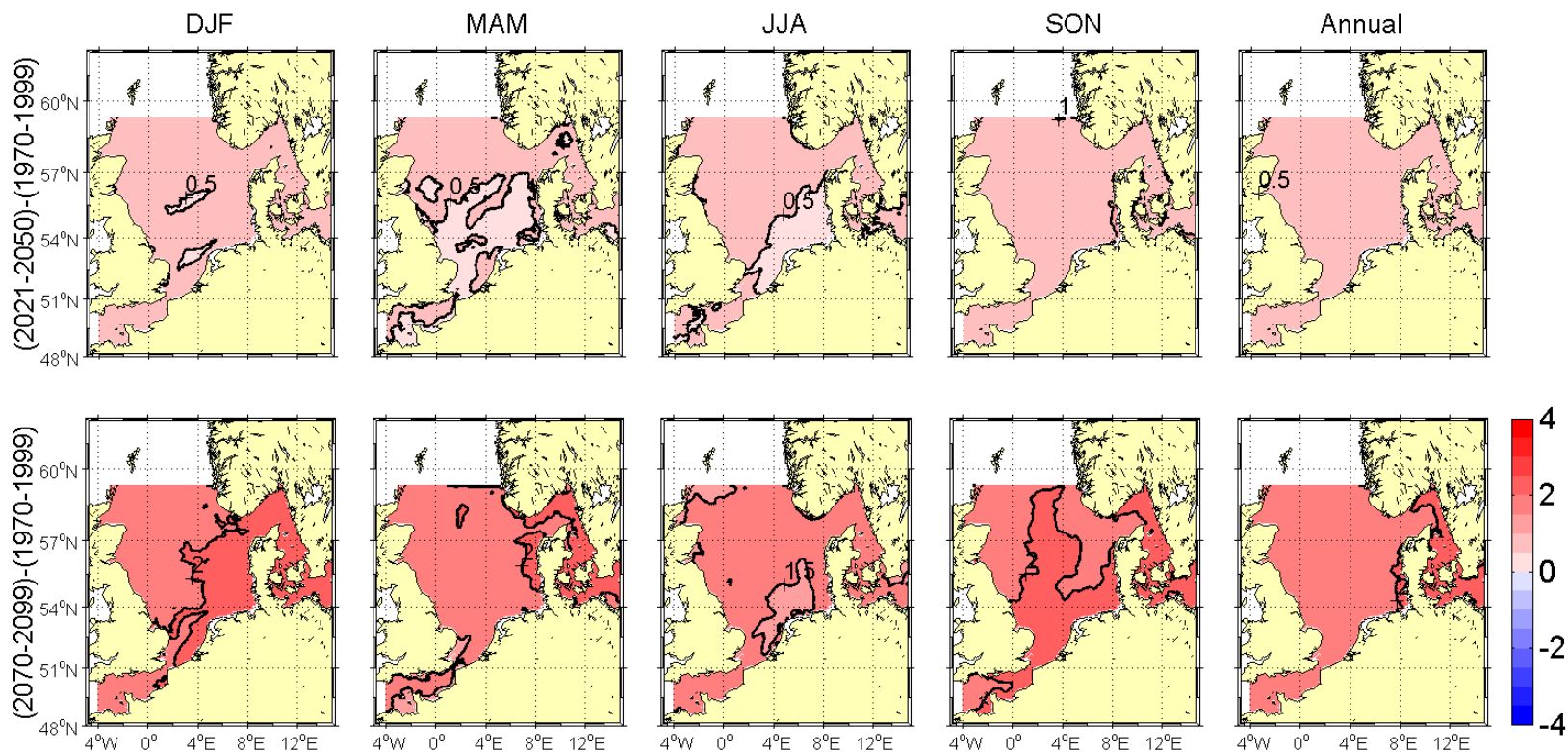


Figure 5.3.7A: Changes in seasonal and annual sea surface temperature [°C] for NEMO-Nordic run 470 (A1B scenario run). Upper panel from (1970-1999) to (2021-2050) and lower panel from (1970-1999) to (2070-2099). The contour interval is 0.5 °C. Selected isolines have been labelled for better orientation.

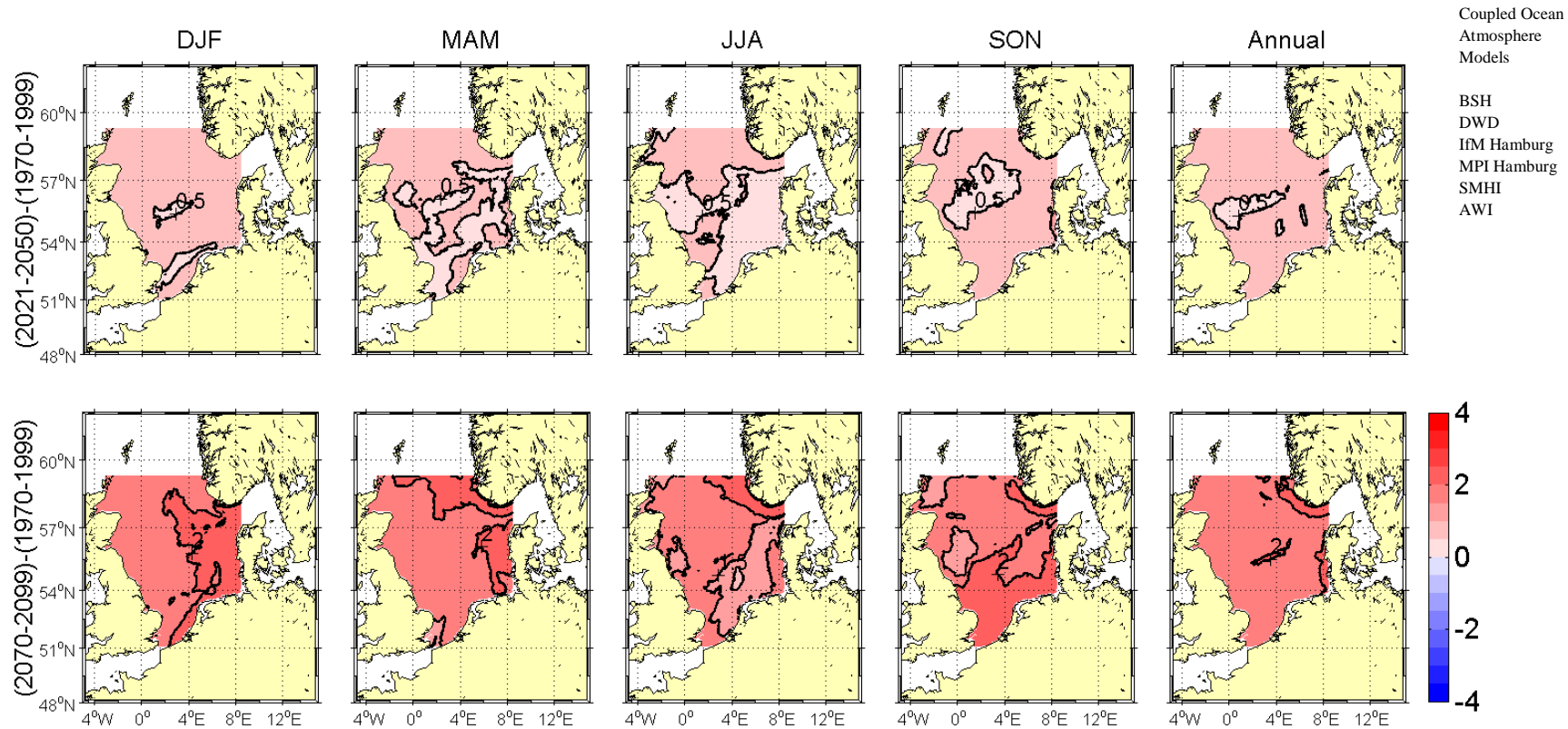


Figure 5.3.8A: Changes in seasonal and annual bottom temperature [°C] for NEMO-Nordic run 470 (A1B scenario run). Upper panel from (1970-1999) to (2021-2050) and lower panel from (1970-1999) to (2070-2099). The contour interval is 0.5 °C. Selected isolines have been labelled for better orientation.

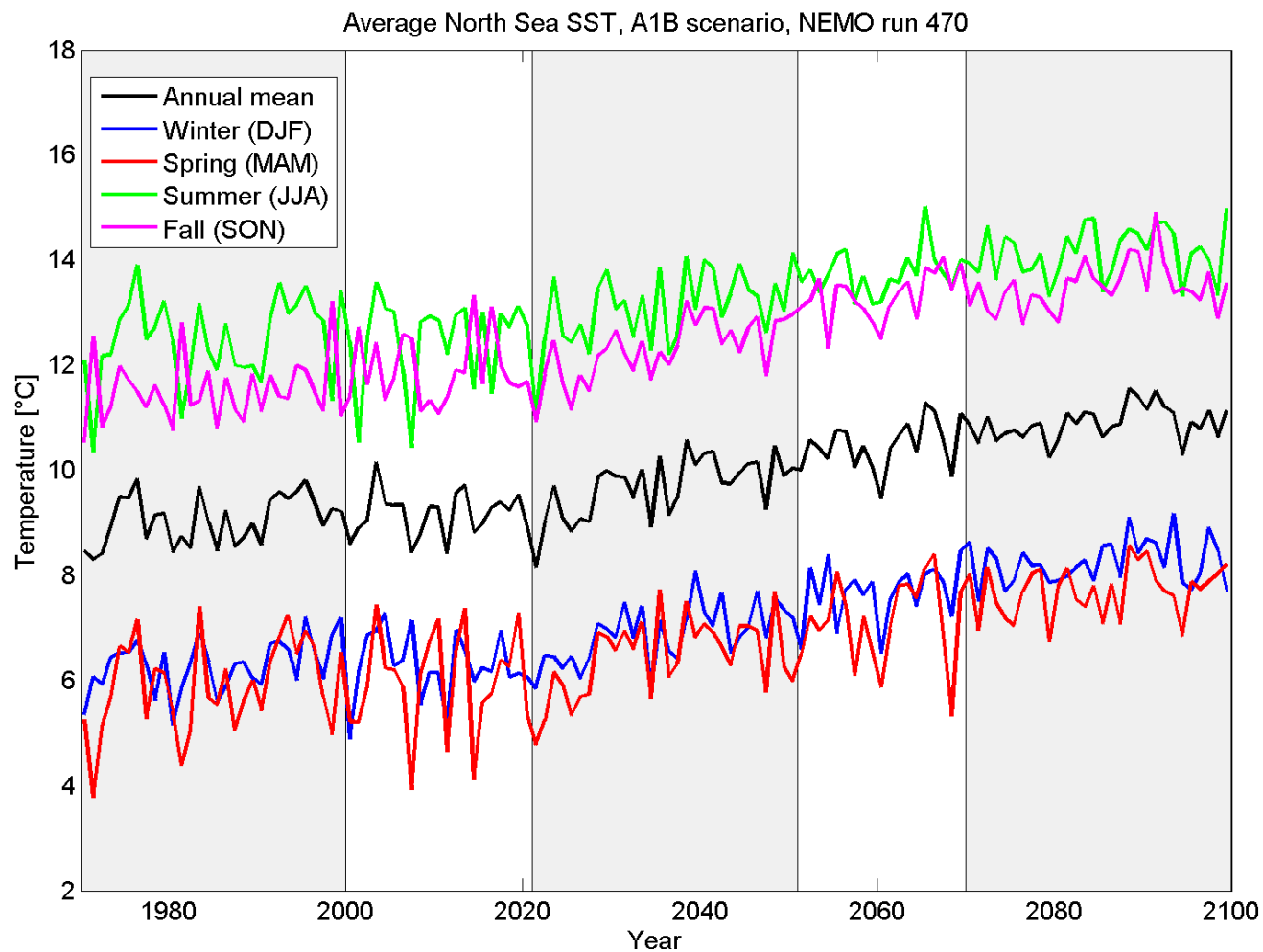


Figure 5.3.9A: Time series of seasonal and annual means of sea surface temperature [°C] for NEMO-Nordic run 470 (A1B scenario run) from 1970-2099. The temperatures represent averages over the North Sea area given in Figure 4.1.

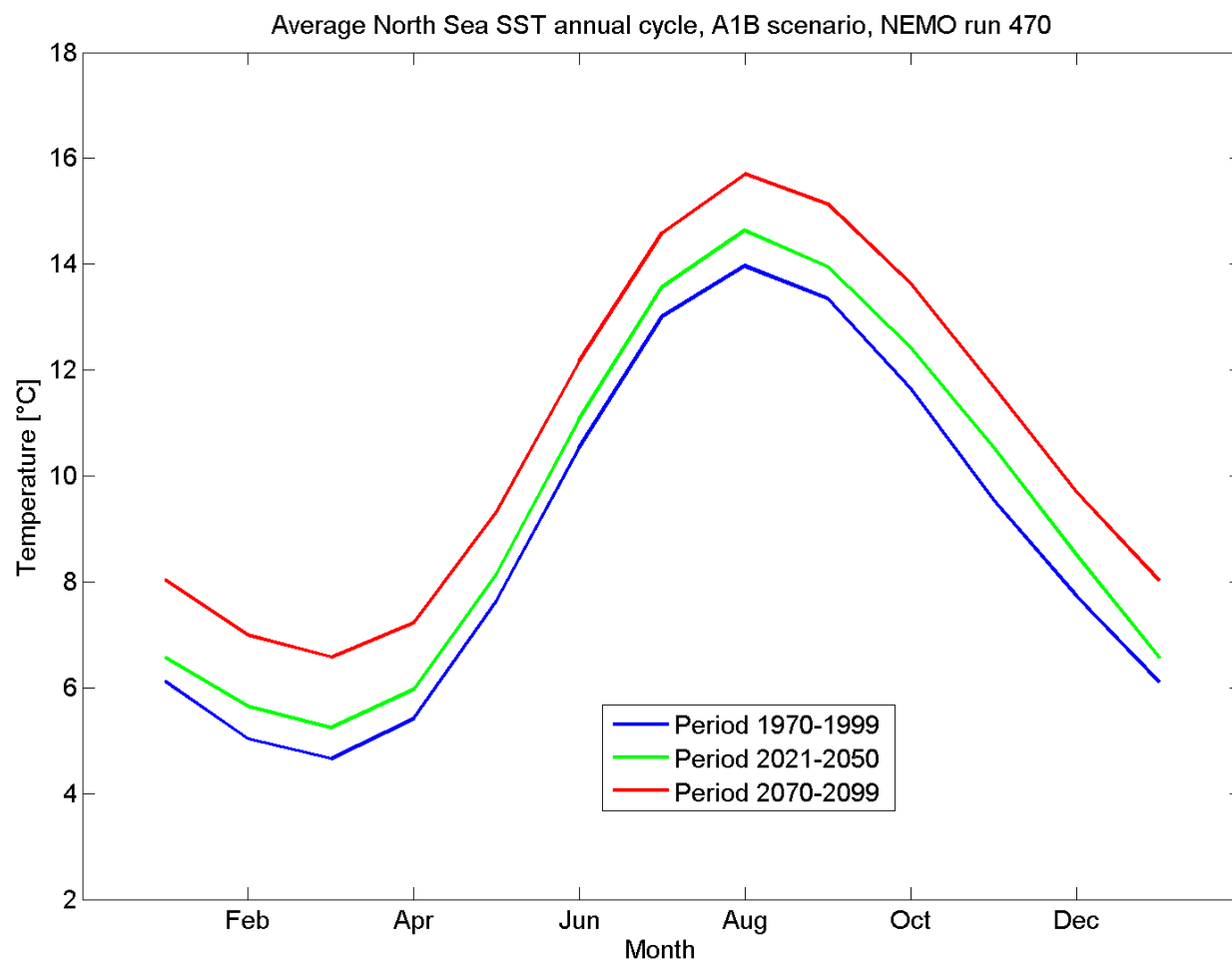


Figure 5.3.10A: The mean annual cycle of sea surface temperatures [°C] for NEMO-Nordic run 470 (A1B scenario run) for 1970-1999 (blue), 2021-2050 (green) and 2070-2099 (red). The means are representing averages over the North Sea area given in Figure 4.1.

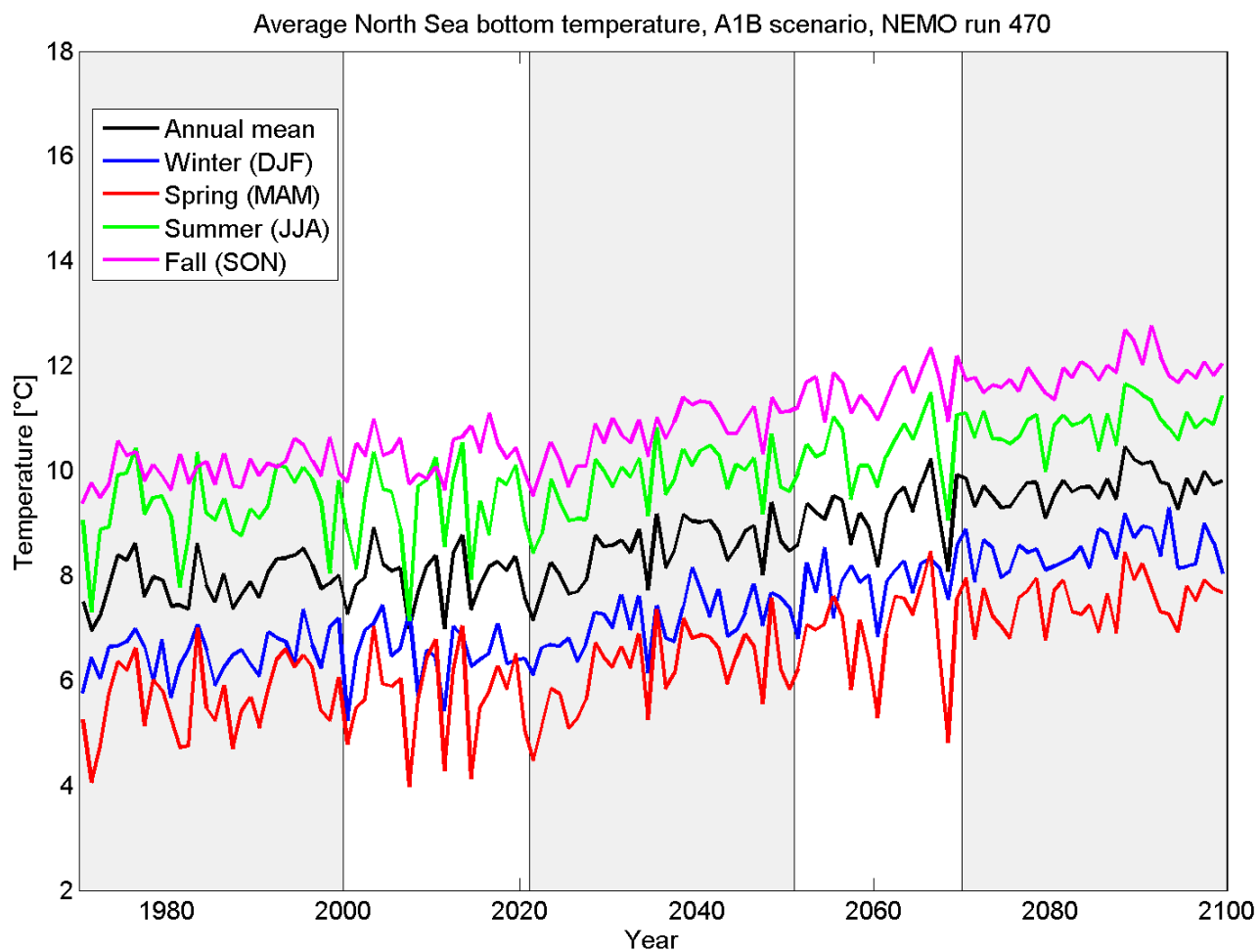


Figure 5.3.11A: Time series of seasonal and annual means of bottom temperature [°C] for NEMO-Nordic run 470 (A1B scenario run) from 1970-2099. The temperatures represent averages over the North Sea area given in Figure 4.1.

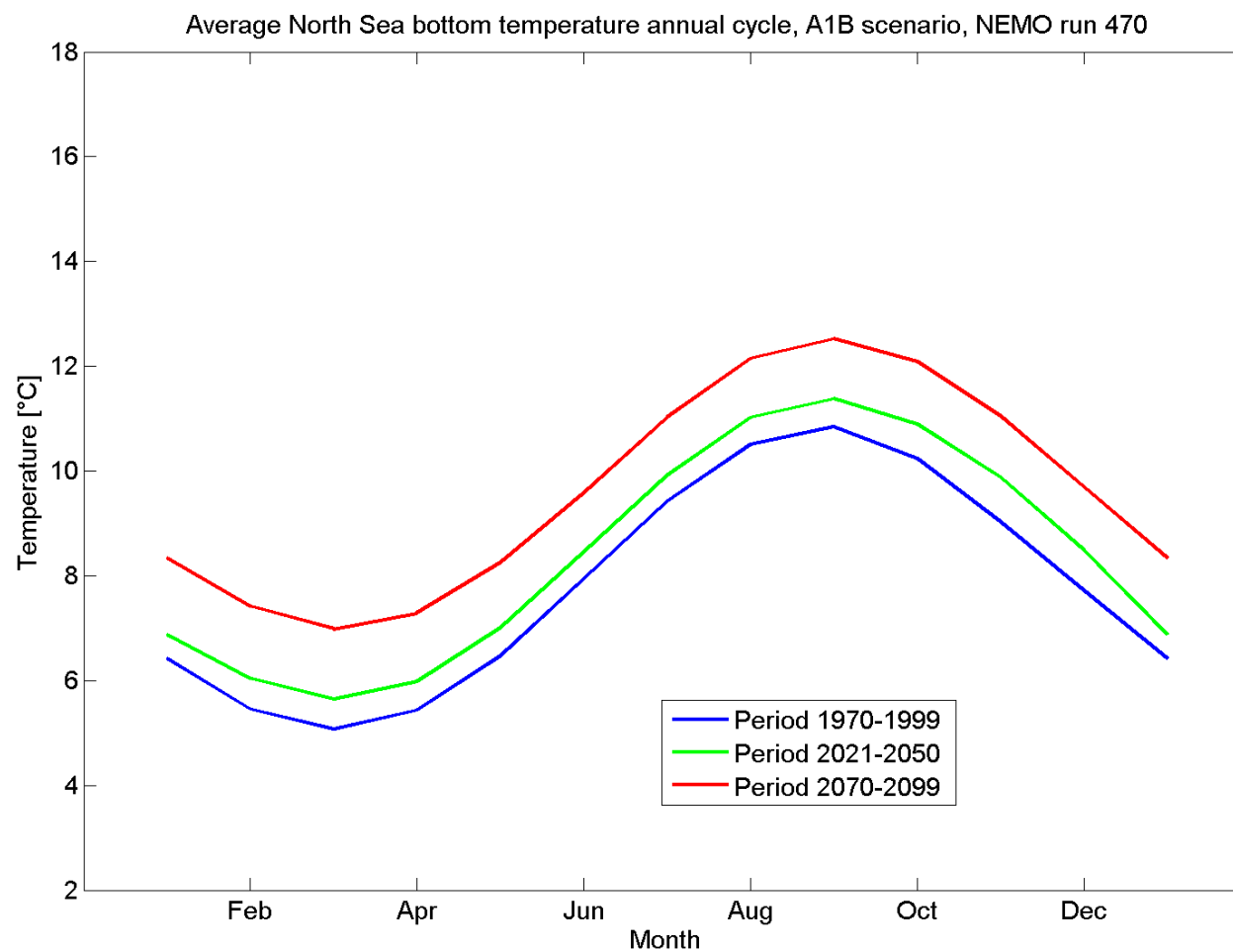


Figure 5.3.12A: The mean annual cycle of bottom temperatures [°C] for NEMO-Nordic run 470 (A1B scenario run) for 1970-1999 (blue), 2021-2050 (green) and 2070-2099 (red). The means are representing averages over the North Sea area given in Figure 4.1.

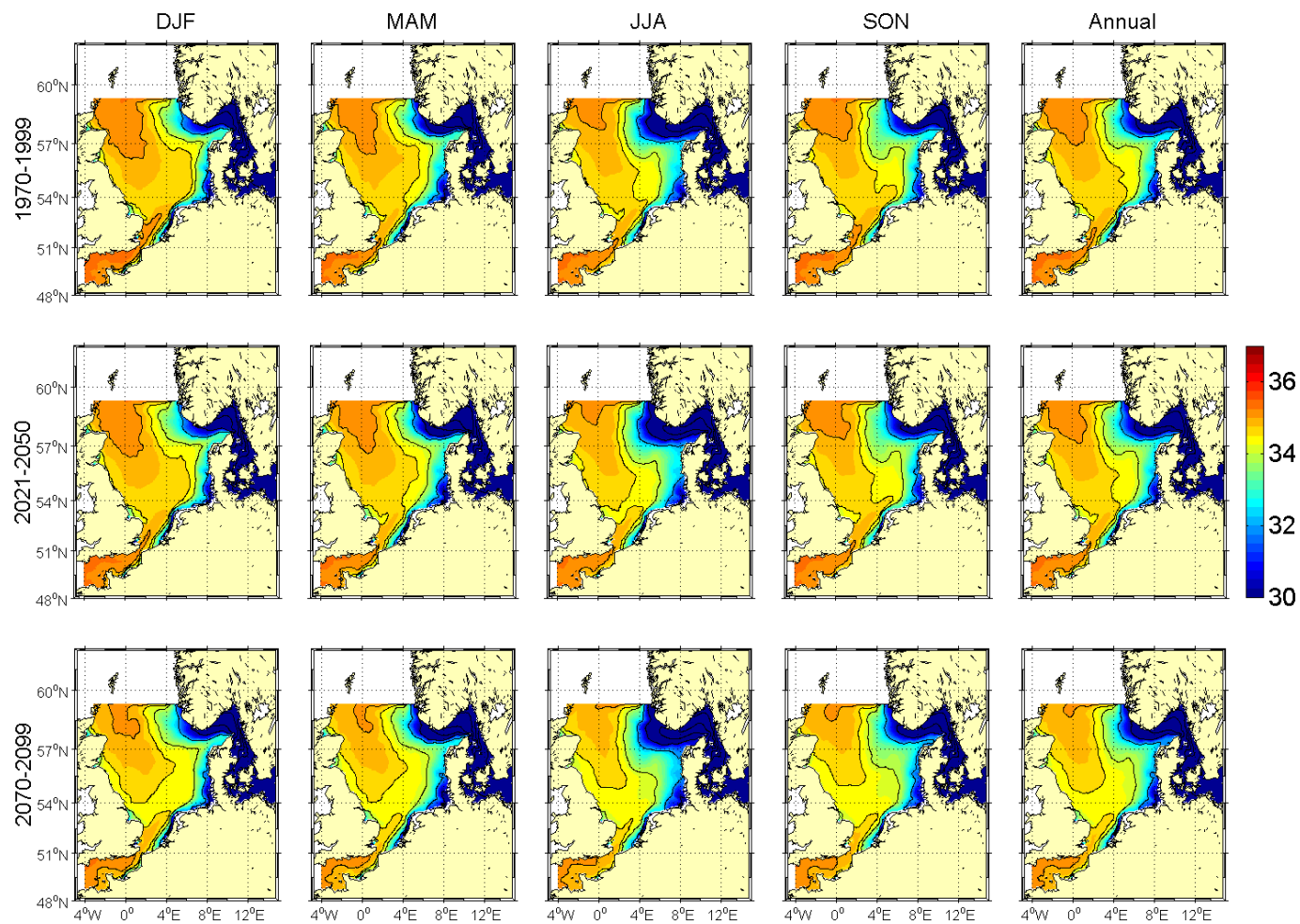


Figure 5.3.13A: Seasonal and annual means of sea surface salinity [psu] for NEMO-Nordic run 470 (A1B scenario run). The upper row shows averages for the period 1970-1999, the middle row for 2021-2050 and the lower row for 2070-2099.

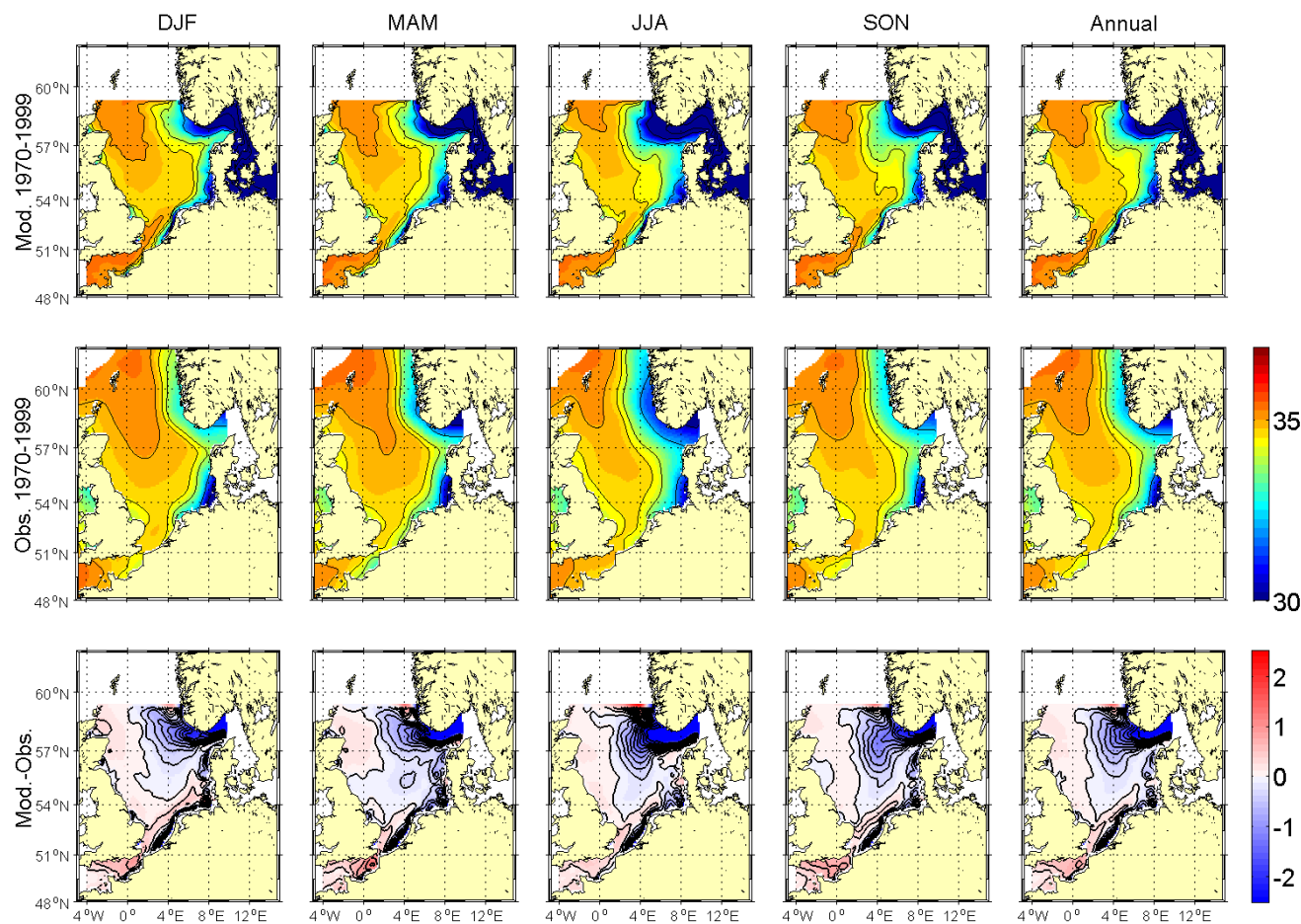


Figure 5.3.14A: Comparison of seasonal and annual means of sea surface salinity [psu] for NEMO-Nordic run 470 for the base period 1970-1999 with BHC means. The upper row shows average model distributions, the middle row observed climatological means and the lower row the difference between the model results and the climatology.

Coupled Ocean
Atmosphere
Models

BSH
DWD
IfM Hamburg
MPI Hamburg
SMHI
AWI

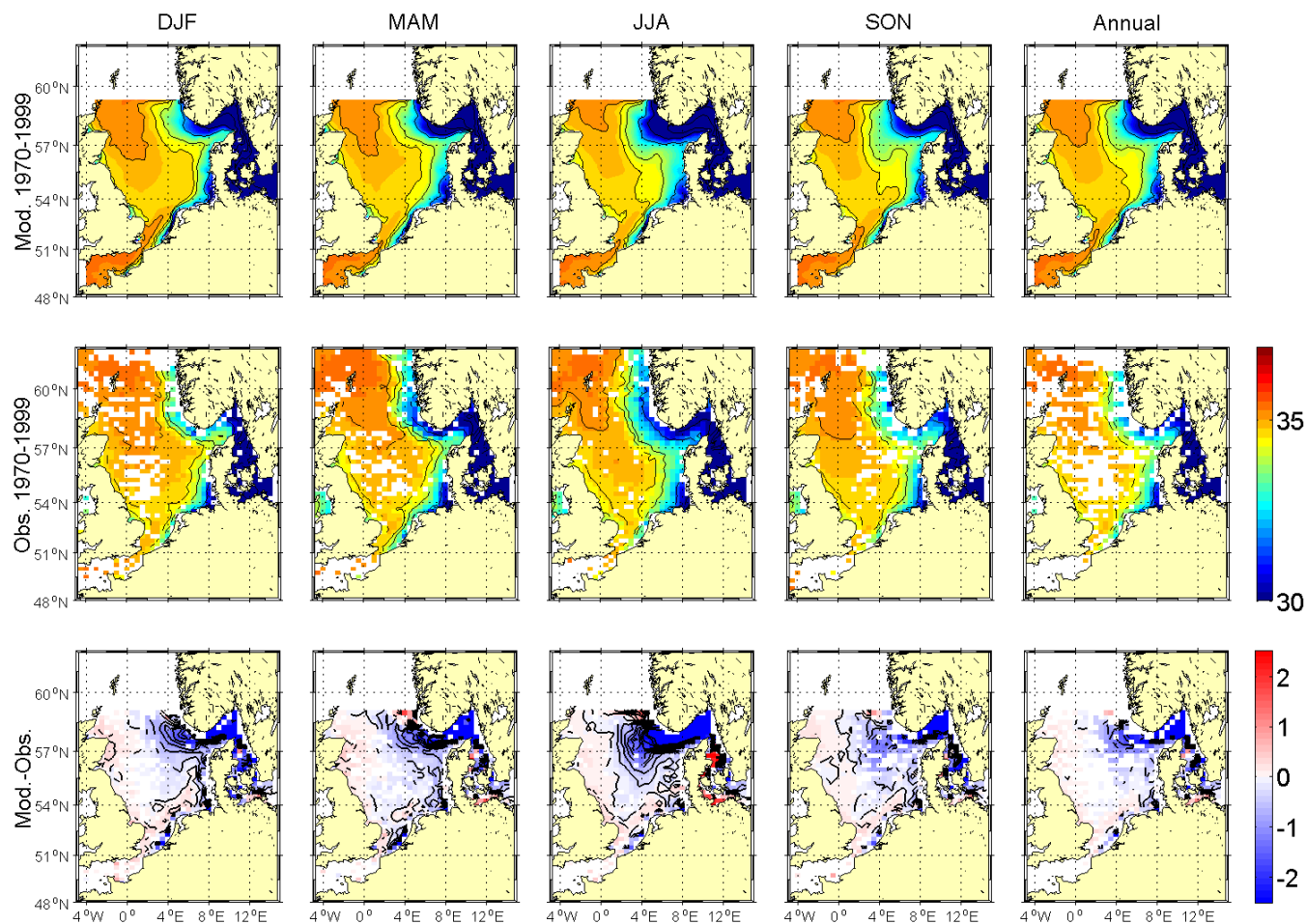


Figure 5.3.15A: Comparison of seasonal and annual means of sea surface salinity [psu] for NEMO-Nordic run 470 for the base period 1970-1999 with KNSC means. The upper row shows average model distributions, the middle row observed climatological means and the lower row the difference between the model results and the climatology.

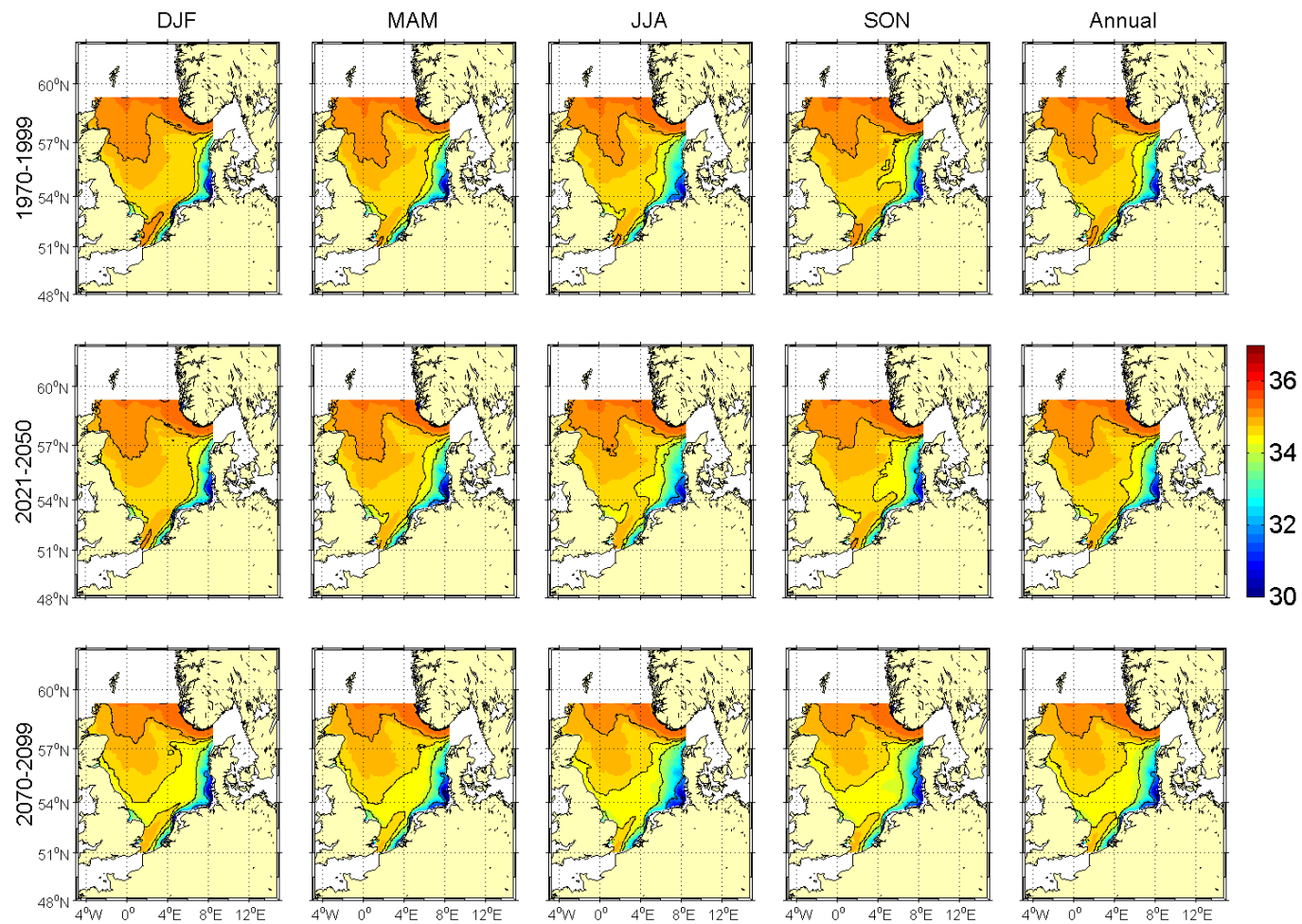


Figure 5.3.16A: Seasonal and annual means of bottom salinity [psu] for NEMO-Nordic run 470 (A1B scenario run). The upper row shows averages for the period 1970-1999, the middle row for 2021-2050 and the lower row for 2070-2099.

Coupled Ocean
Atmosphere
Models

BSH
DWD
IfM Hamburg
MPI Hamburg
SMHI
AWI

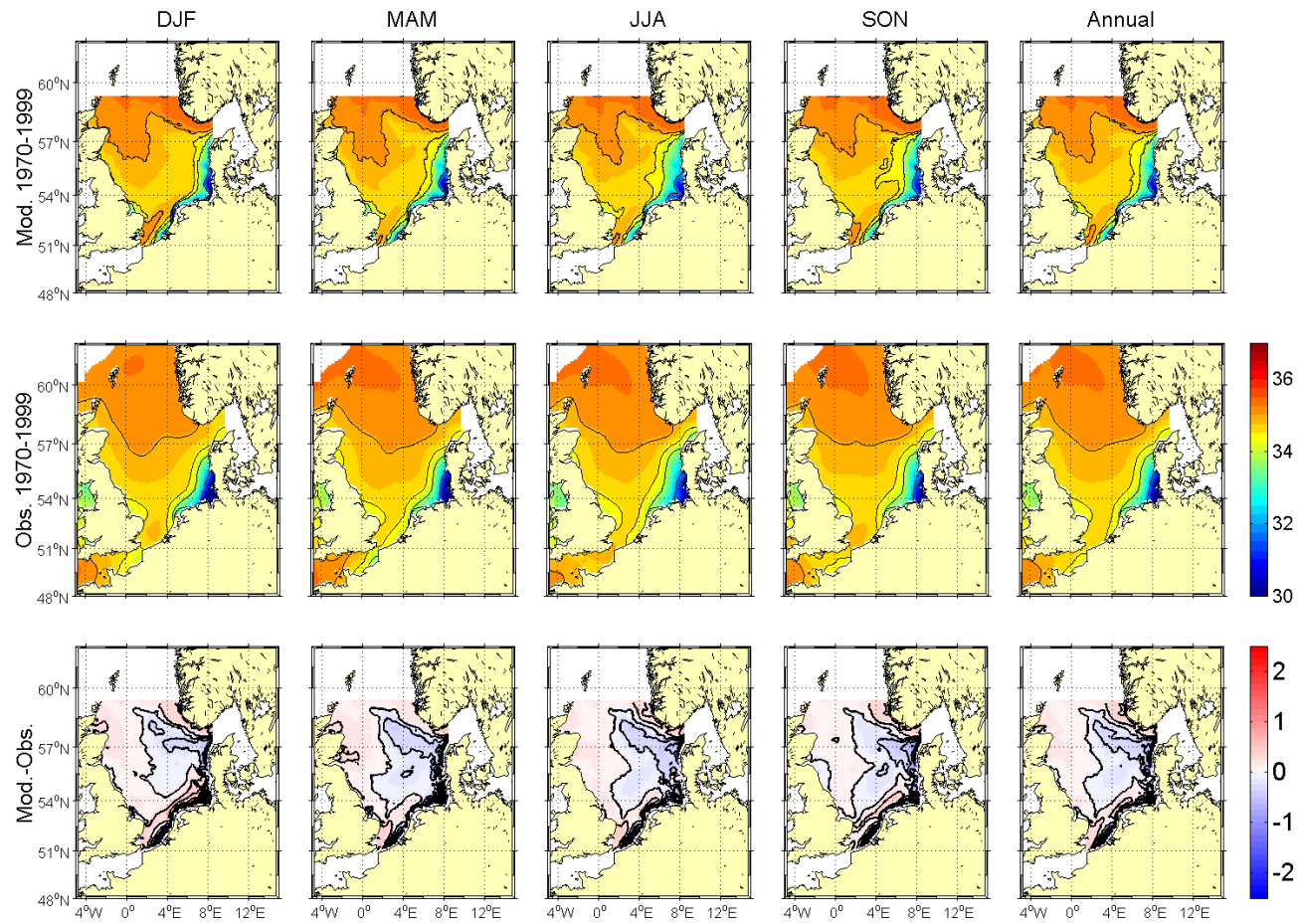


Figure 5.3.17A: Comparison of seasonal and annual means of bottom salinity [psu] for NEMO-Nordic run 470 for the base period 1970-1999 with BHC means. The upper row shows average model distributions, the middle row observed climatological means and the lower row the difference between the model results and the climatology.

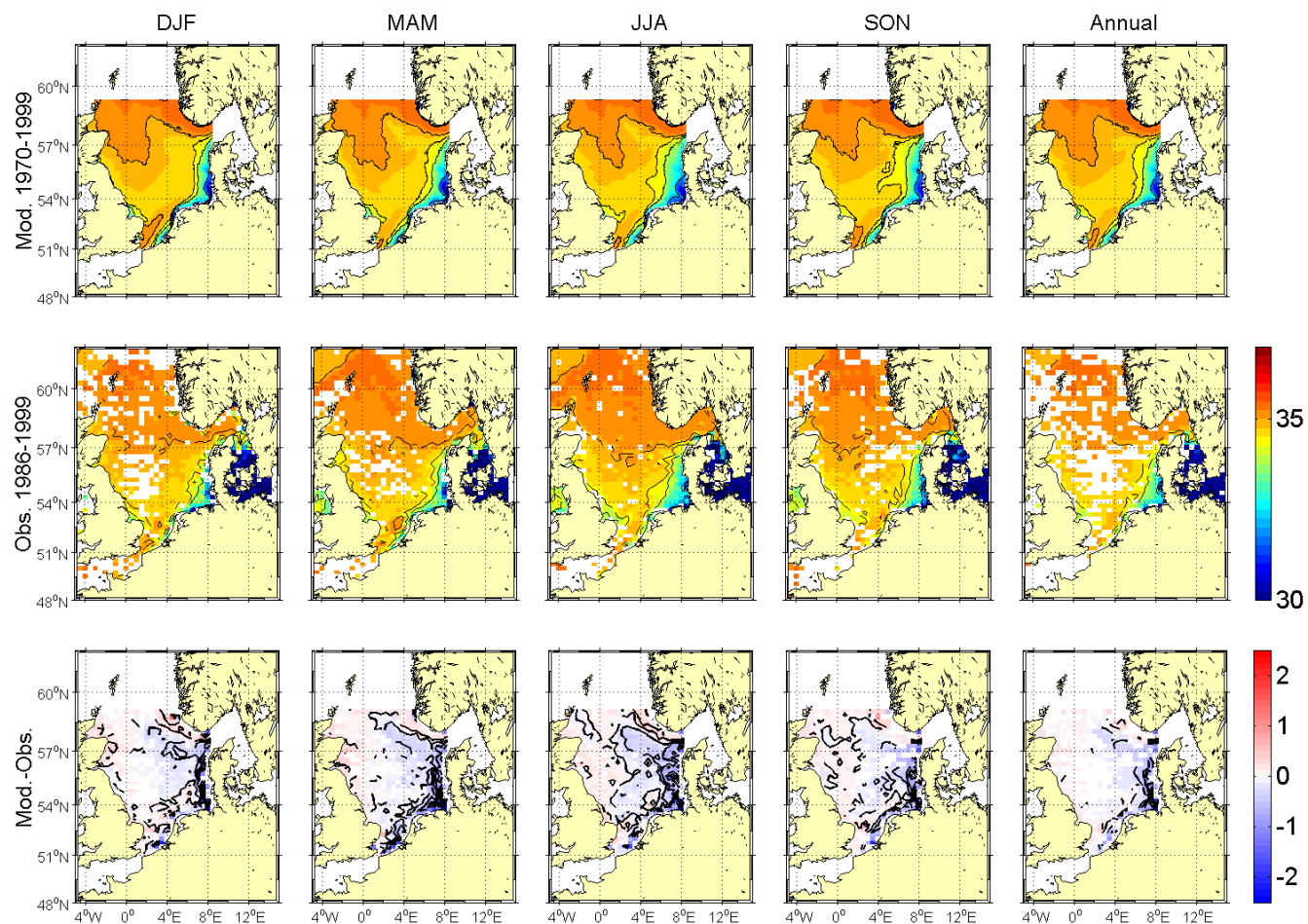


Figure 5.3.18A: Comparison of seasonal and annual means of bottom salinity [psu] for NEMO-Nordic run 470 for the base period 1970-1999 with KNSC means. The upper row shows average model results, the middle row observed climatological means and the lower row the difference between the model results and the climatology.

Coupled Ocean
Atmosphere
Models

BSH
DWD
IfM Hamburg
MPI Hamburg
SMHI
AWI

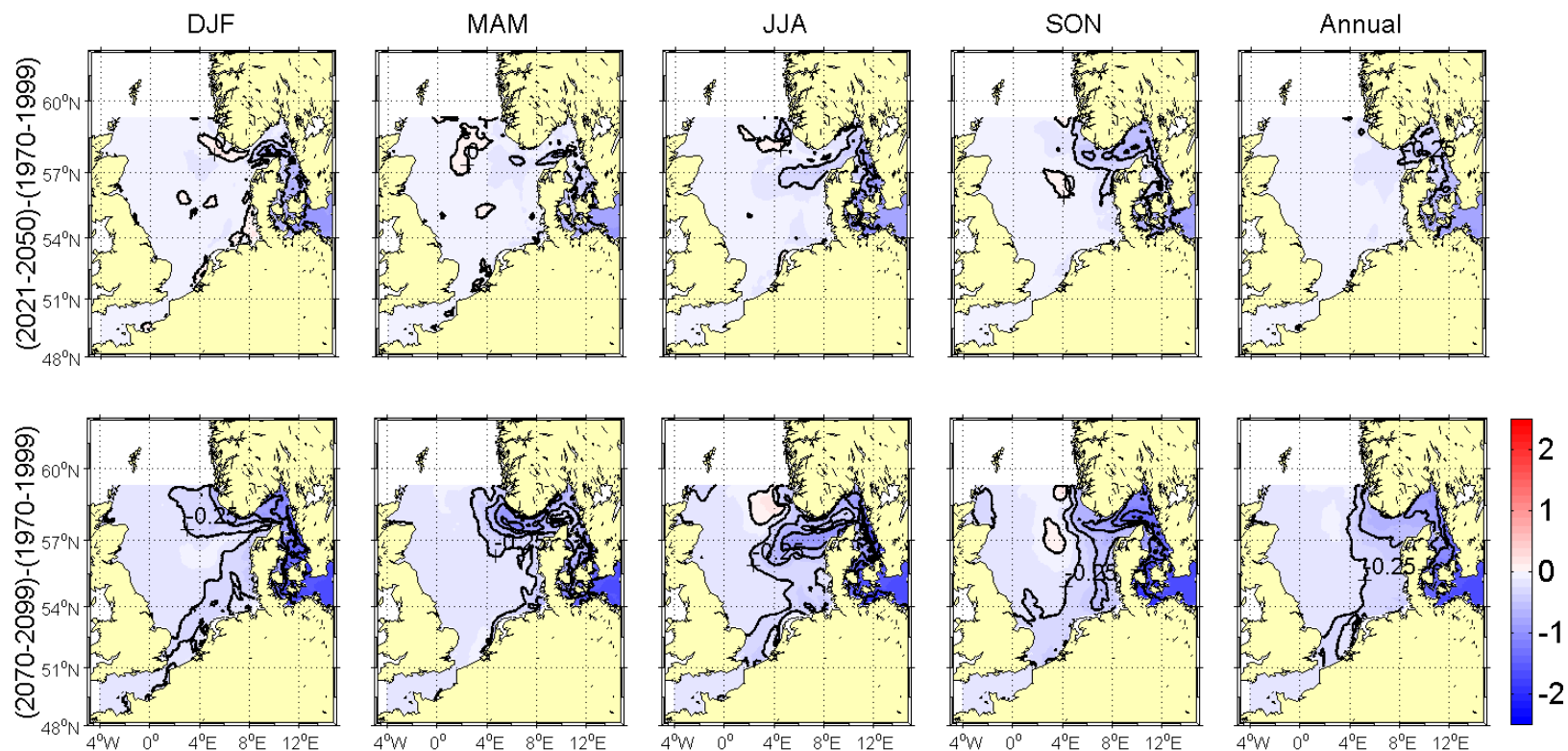


Figure 5.3.19A: Changes in seasonal and annual sea surface salinity [psu] for NEMO-Nordic run 470 (A1B scenario run). Upper panel from (1970-1999) to (2021-2050) and lower panel from (1970-1999) to (2070-2099). The contour interval is 0.25 psu. Selected isolines have been labelled for better orientation.

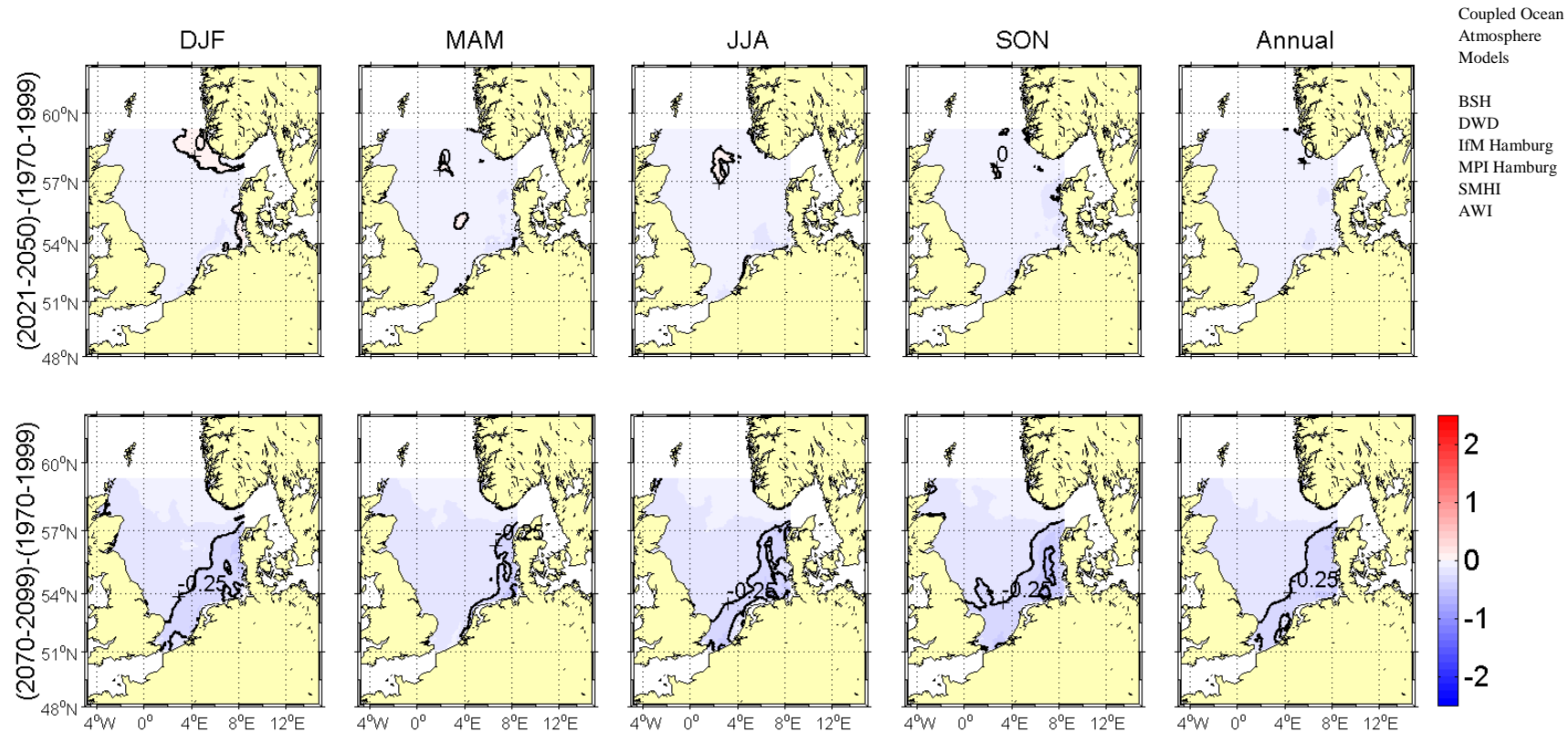


Figure 5.3.20A: Changes in seasonal and annual bottom salinity [psu] for NEMO-Nordic run 470 (A1B scenario run). Upper panel from (1970-1999) to (2021-2050) and lower panel from (1970-1999) to (2070-2099). The contour interval is 0.5 °C. Selected isolines have been labelled for better orientation.

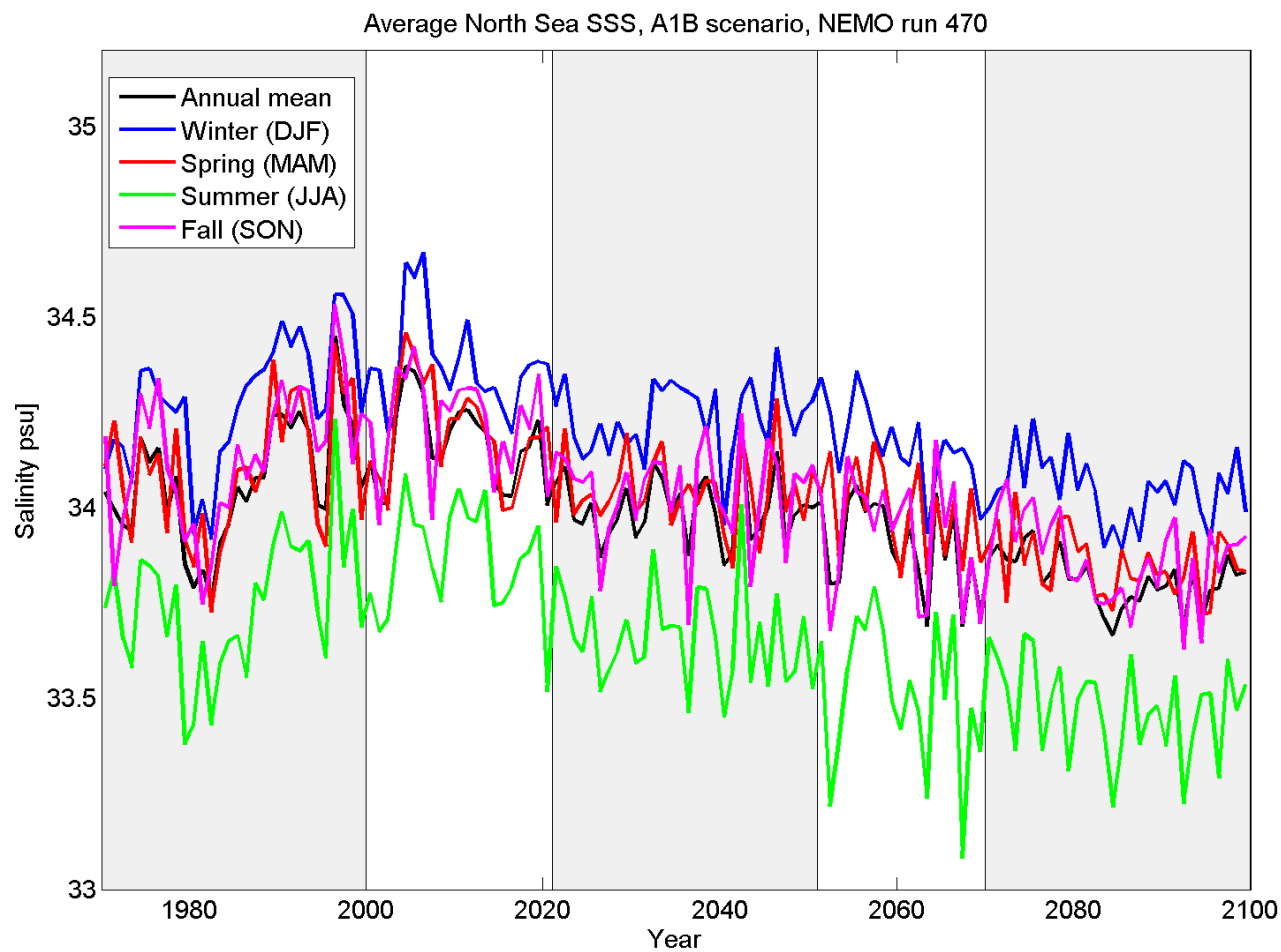


Figure 5.3.21A: Time series of seasonal and annual means of sea surface salinity [psu] for NEMO-Nordic run 470 (A1B scenario run) from 1970-2099. The salinities represent averages over the North Sea area given in Figure 4.1.

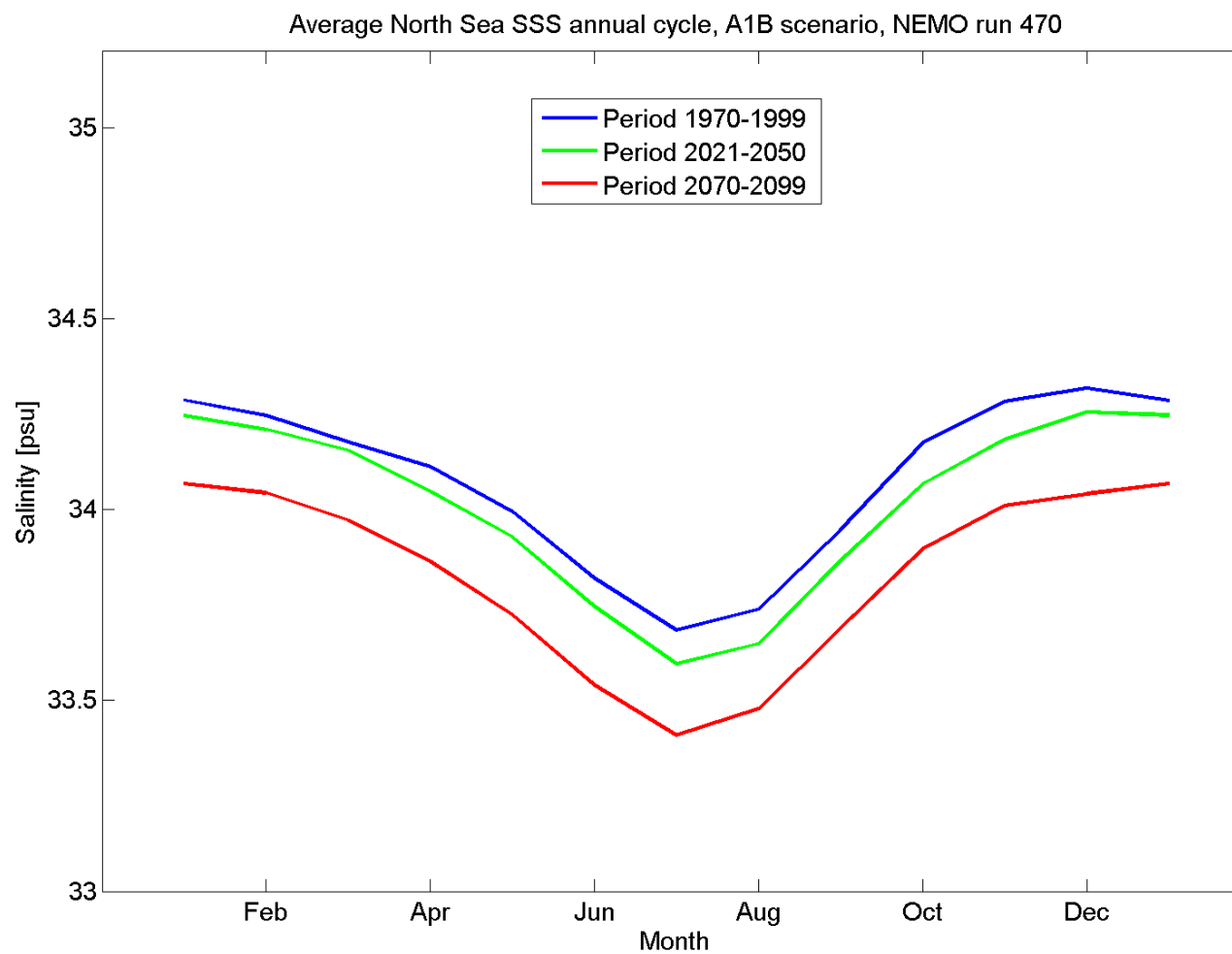


Figure 5.3.22A: The mean annual cycle of sea surface salinity [psu] for NEMO-Nordic run 470 (A1B scenario run) for 1970-1999 (blue), 2021-2050 (green) and 2070-2099 (red). The means are representing averages over the North Sea area given in Figure 4.1.

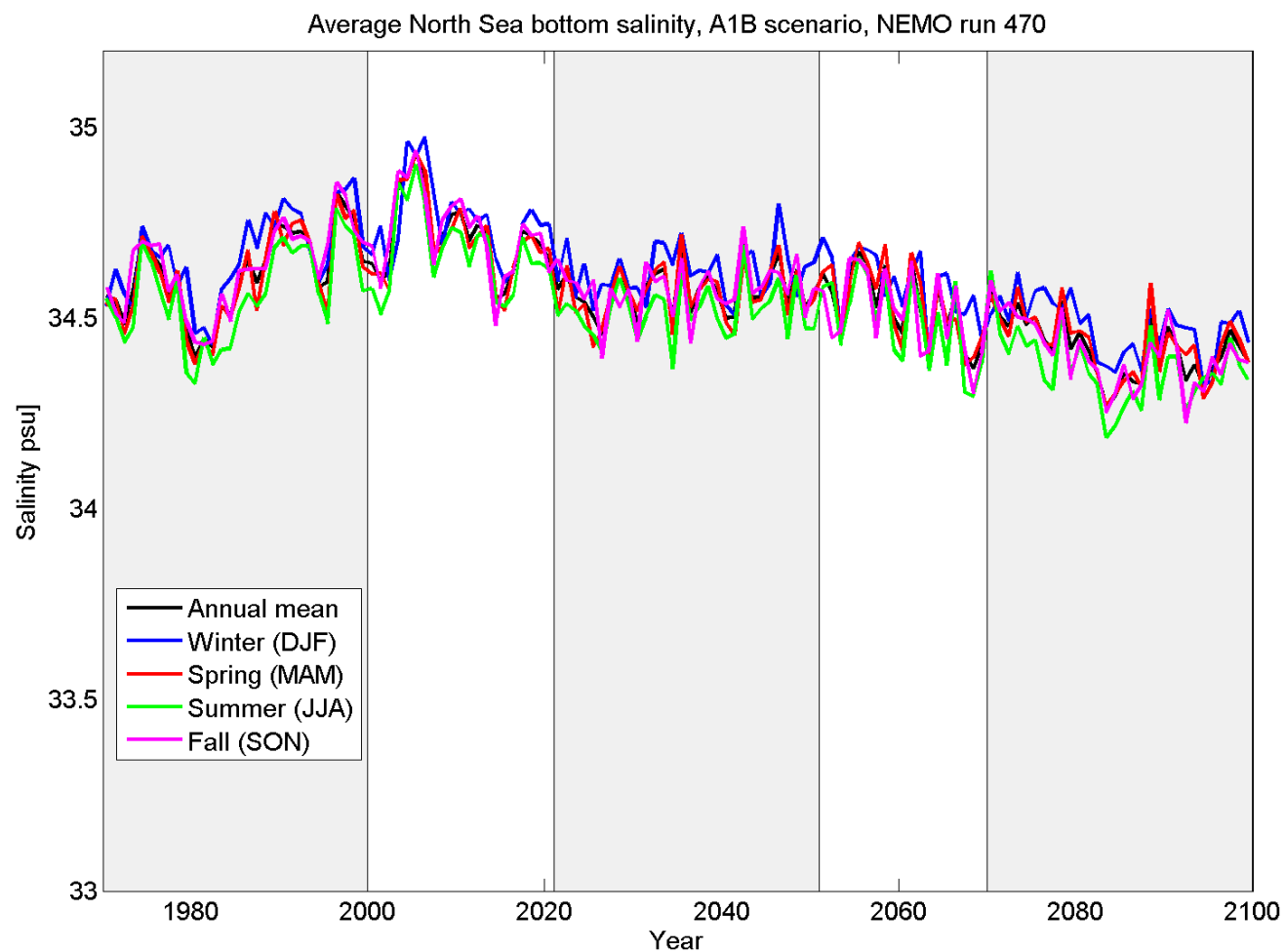


Figure 5.3.23A: Time series of seasonal and annual means of bottom salinity [psu] for NEMO-Nordic run 470 (A1B scenario run) from 1970-2099. The salinities represent averages over the North Sea area given in Figure 4.1.

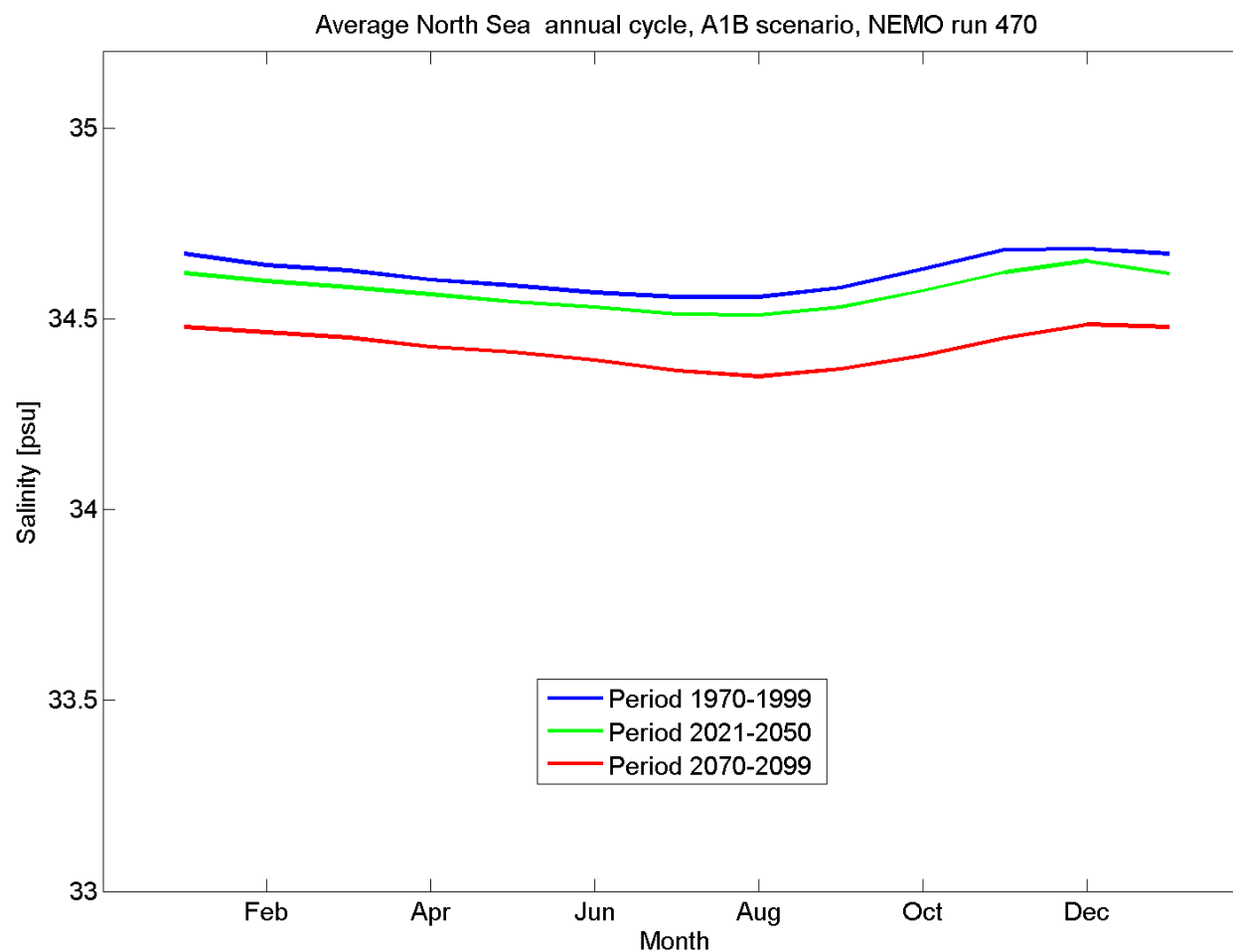


Figure 5.3.24A: The mean annual cycle of bottom salinity [psu] for NEMO-Nordic run 470 (A1B scenario run) for 1970-1999 (blue), 2021-2050 (green) and 2070-2099 (red). The means are representing averages over the North Sea area given in Figure 4.1.

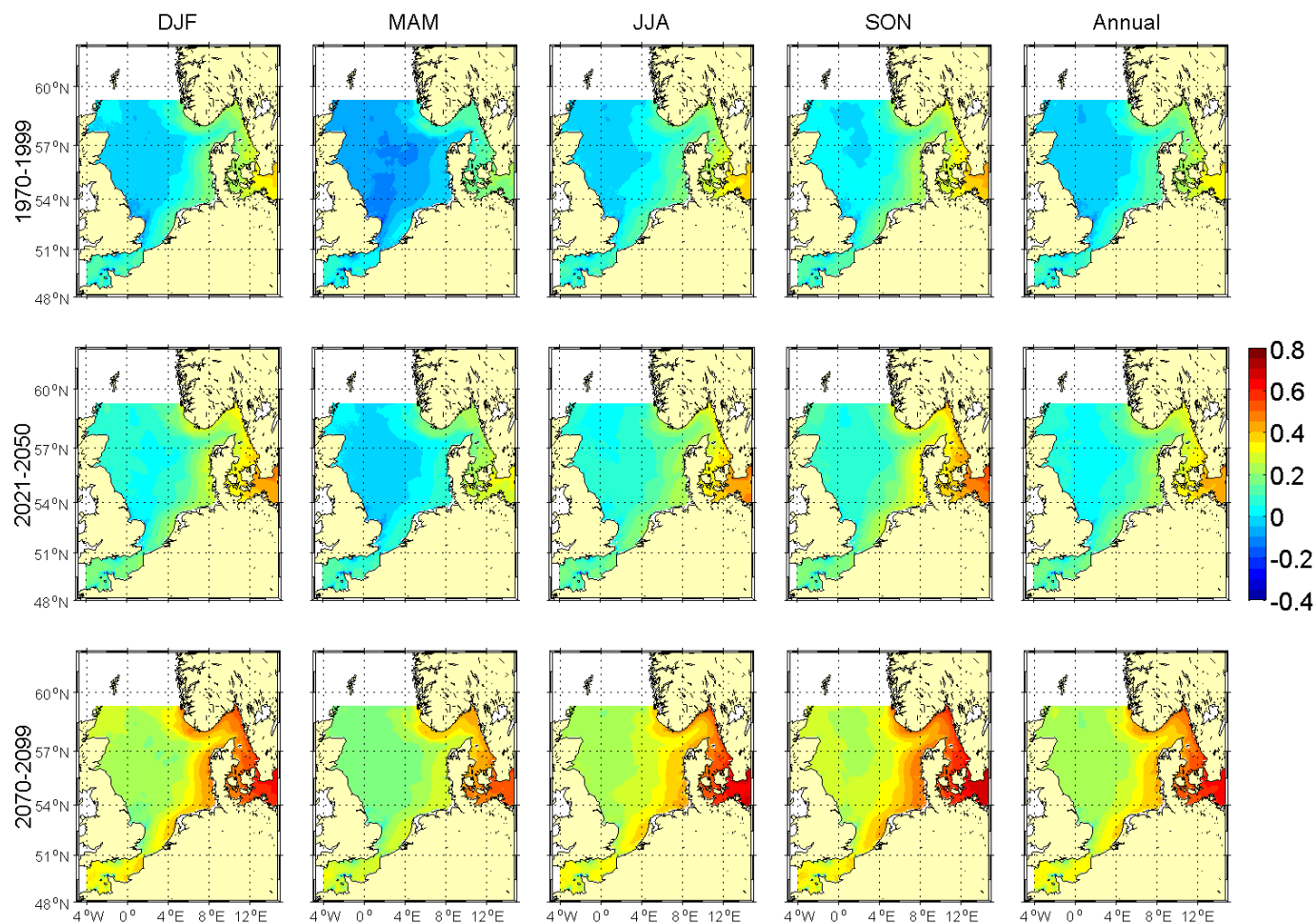


Figure 5.3.25A: Seasonal and annual means of sea surface height [m] for NEMO-Nordic run 470 (A1B scenario run). The upper row shows averages for the period 1970-1999, the middle row for 2021-2050 and the lower row for 2070-2099.

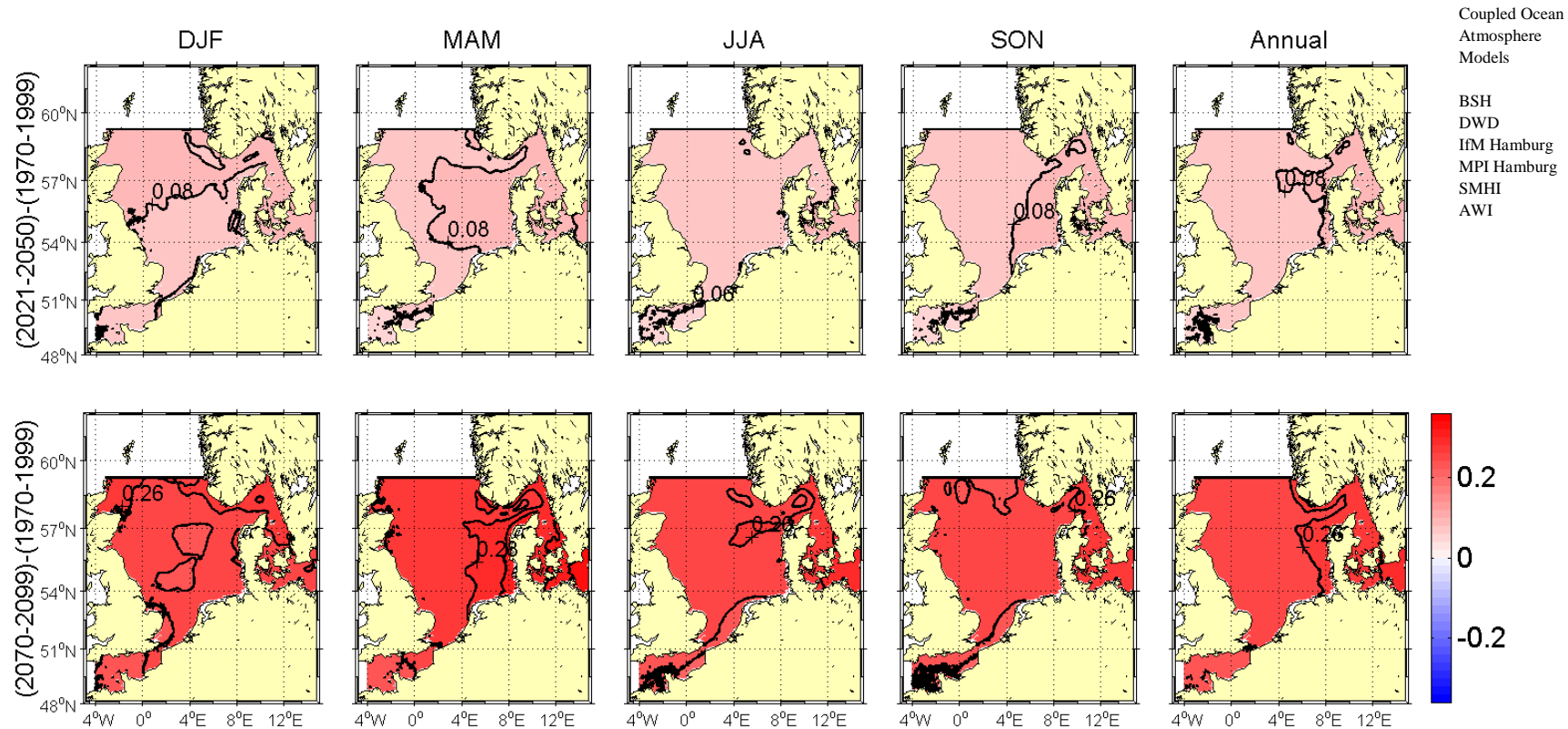


Figure 5.3.26A: Changes in seasonal and annual sea surface height [m] for NEMO-Nordic run 470 (A1B scenario run). Upper panel from (1970-1999) to (2021-2050) and lower panel from (1970-1999) to (2070-2099). The contour interval is 0.02 m. Selected isolines have been labelled for better orientation.

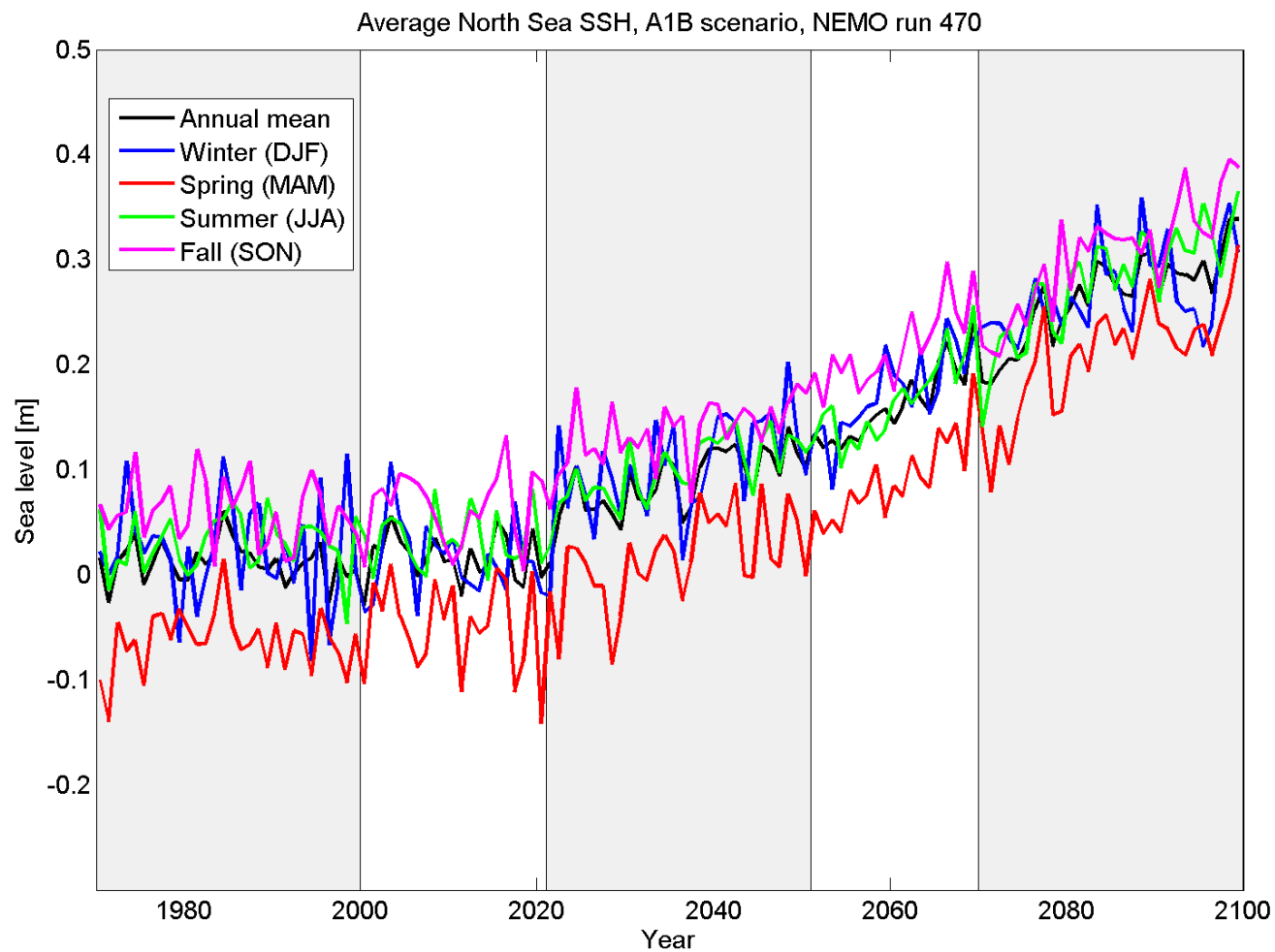


Figure 5.3.27A: Time series of seasonal and annual means of sea surface height [m] for NEMO-Nordic run 470 (A1B scenario run) from 1970-2099. The sea surface heights represent averages over the North Sea area given in Figure 4.1.

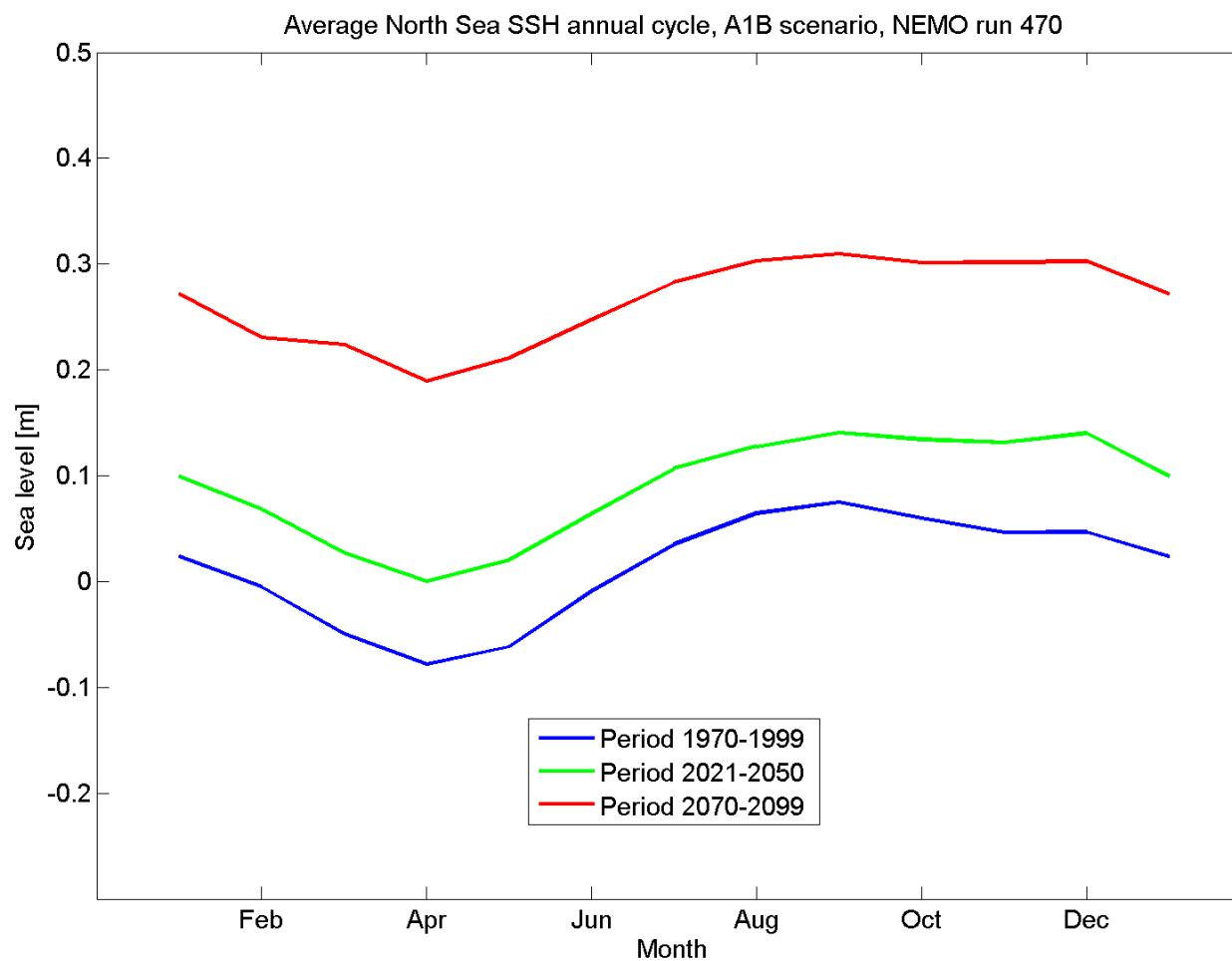


Figure 5.3.28A: The mean annual cycle of sea surface height [m] for NEMO-Nordic run 470 (A1B scenario run) for 1970-1999 (blue), 2021-2050 (green) and 2070-2099 (red). The means are representing averages over the North Sea area given in Figure 4.1.

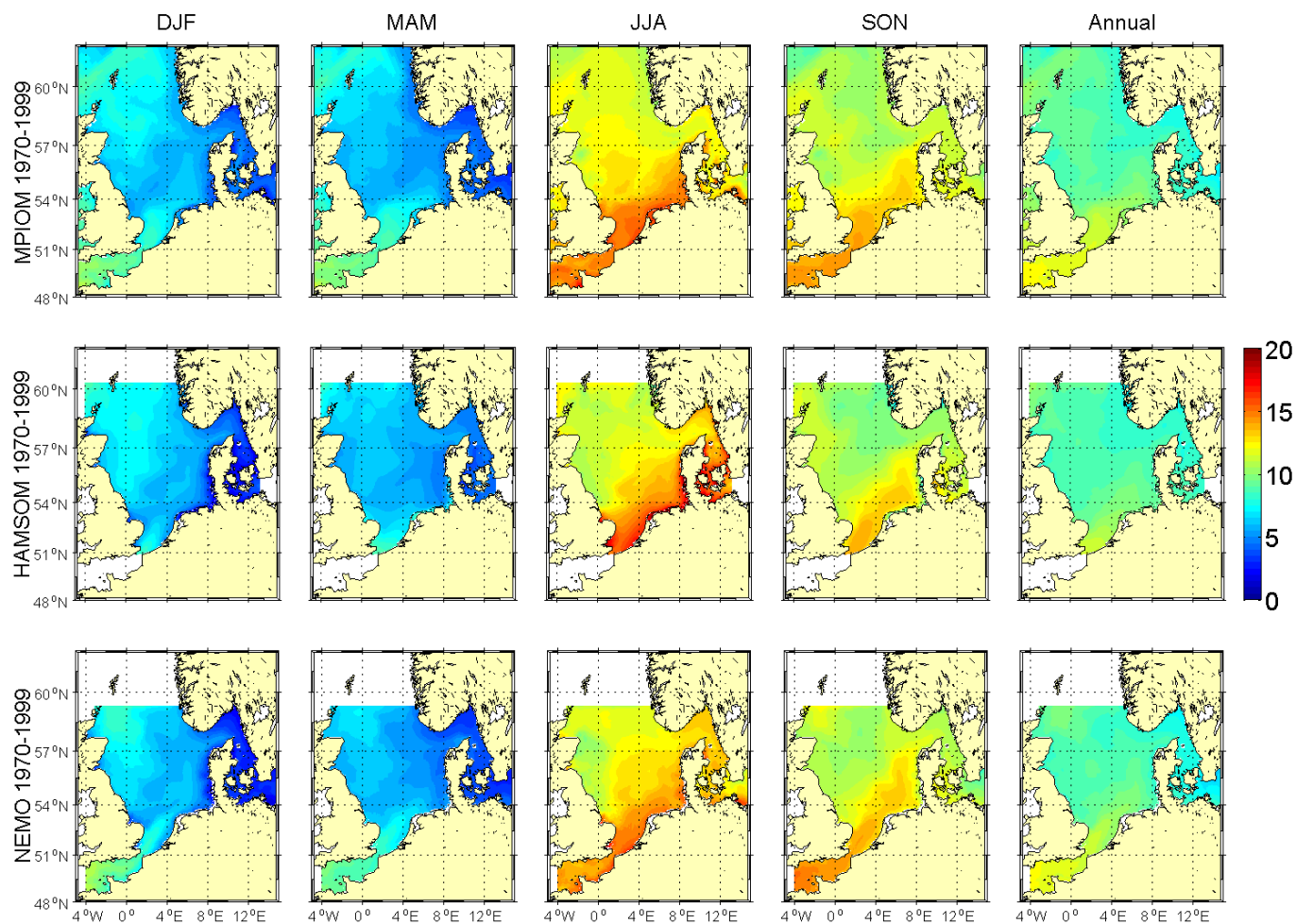


Figure 5.4.1A: Seasonal and annual means of sea surface temperature [°C] for the period 1970-1999. Upper row MPIOM run 215, middle row HAMSOM run 202 and lower row NEMO-Nordic run 470 (all A1B scenario).

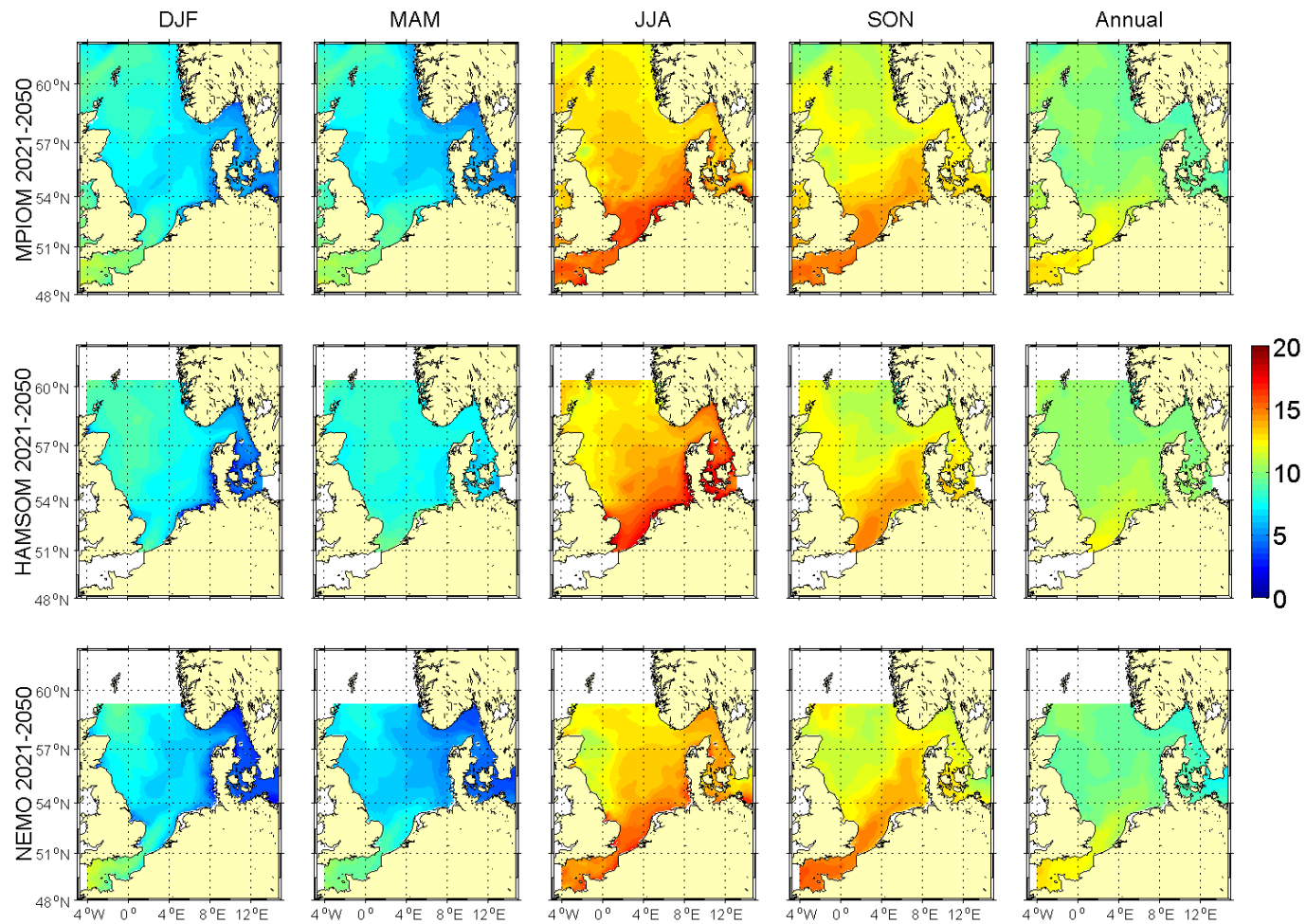


Figure 5.4.2A: Seasonal and annual means of sea surface temperature [°C] for the period 2021-2050. Upper row MPIOM run 215, middle row HAMSOM run 202 and lower row NEMO-Nordic run 470 (all A1B scenario).

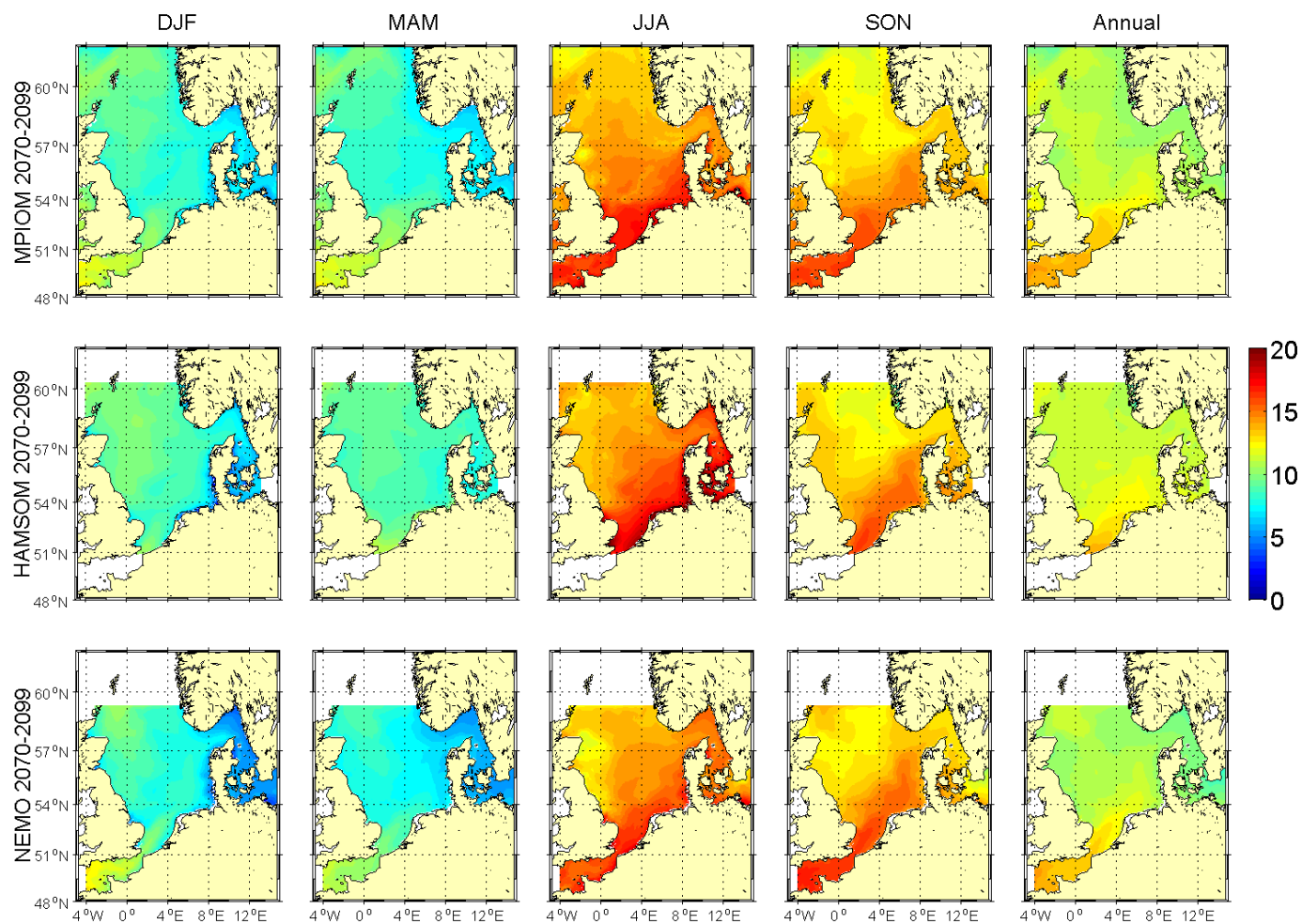
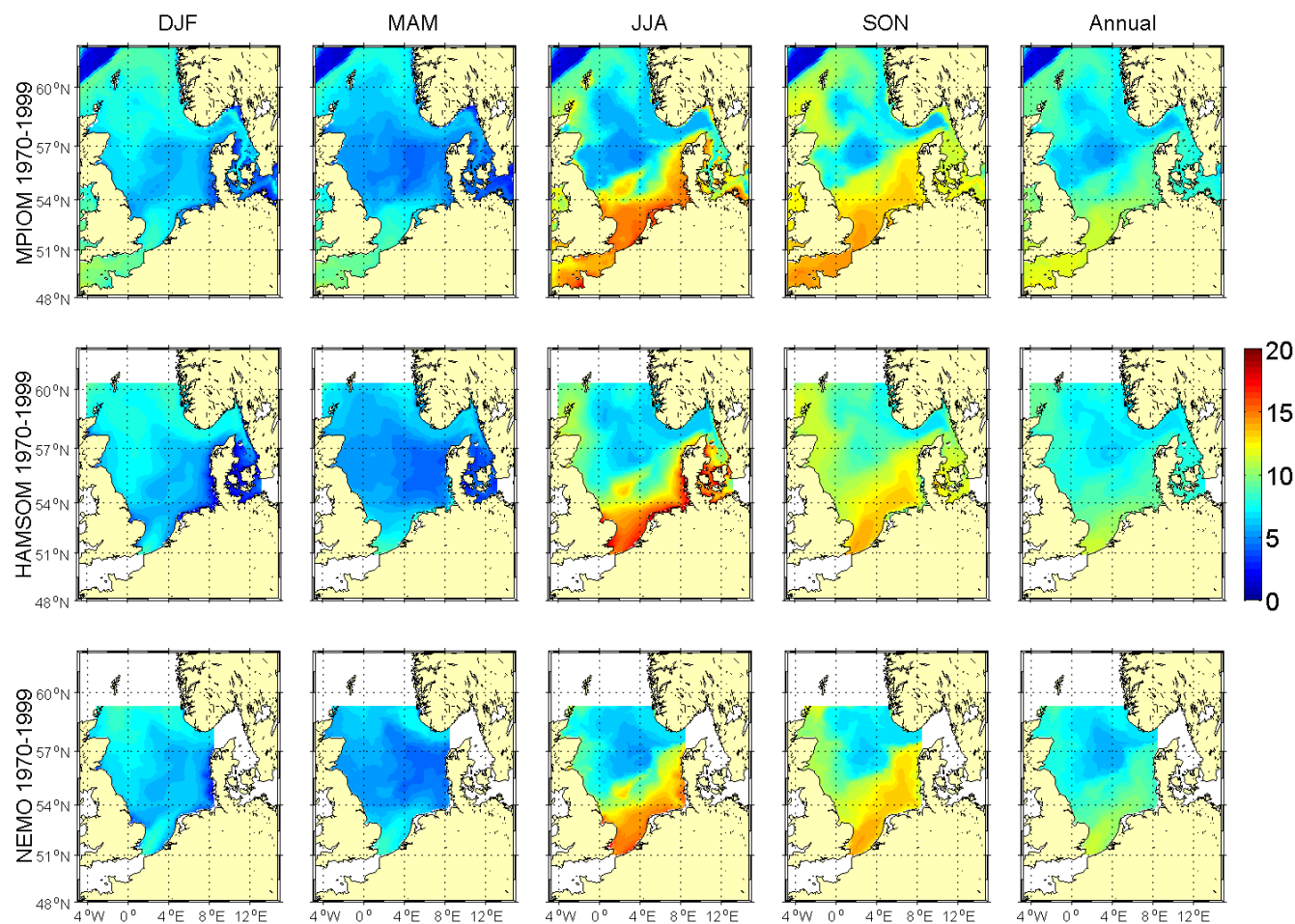


Figure 5.4.3A: Seasonal and annual means of sea surface temperature [°C] for the period 2070-2050. Upper row MPIOM run 215, middle row HAMSOM run 202 and lower row NEMO-Nordic run 470 (all A1B scenario).



Coupled Ocean
Atmosphere
Models

BSH
DWD
IfM Hamburg
MPI Hamburg
SMHI
AWI

Figure 5.4.4A: Seasonal and annual means of bottom temperature [°C] for the period 1970-1999. Upper row MPIOM run 215, middle row HAMSOM run 202 and lower row NEMO-Nordic run 470 (all A1B scenario).

Coupled Ocean
Atmosphere
Models

BSH
DWD
IfM Hamburg
MPI Hamburg
SMHI
AWI

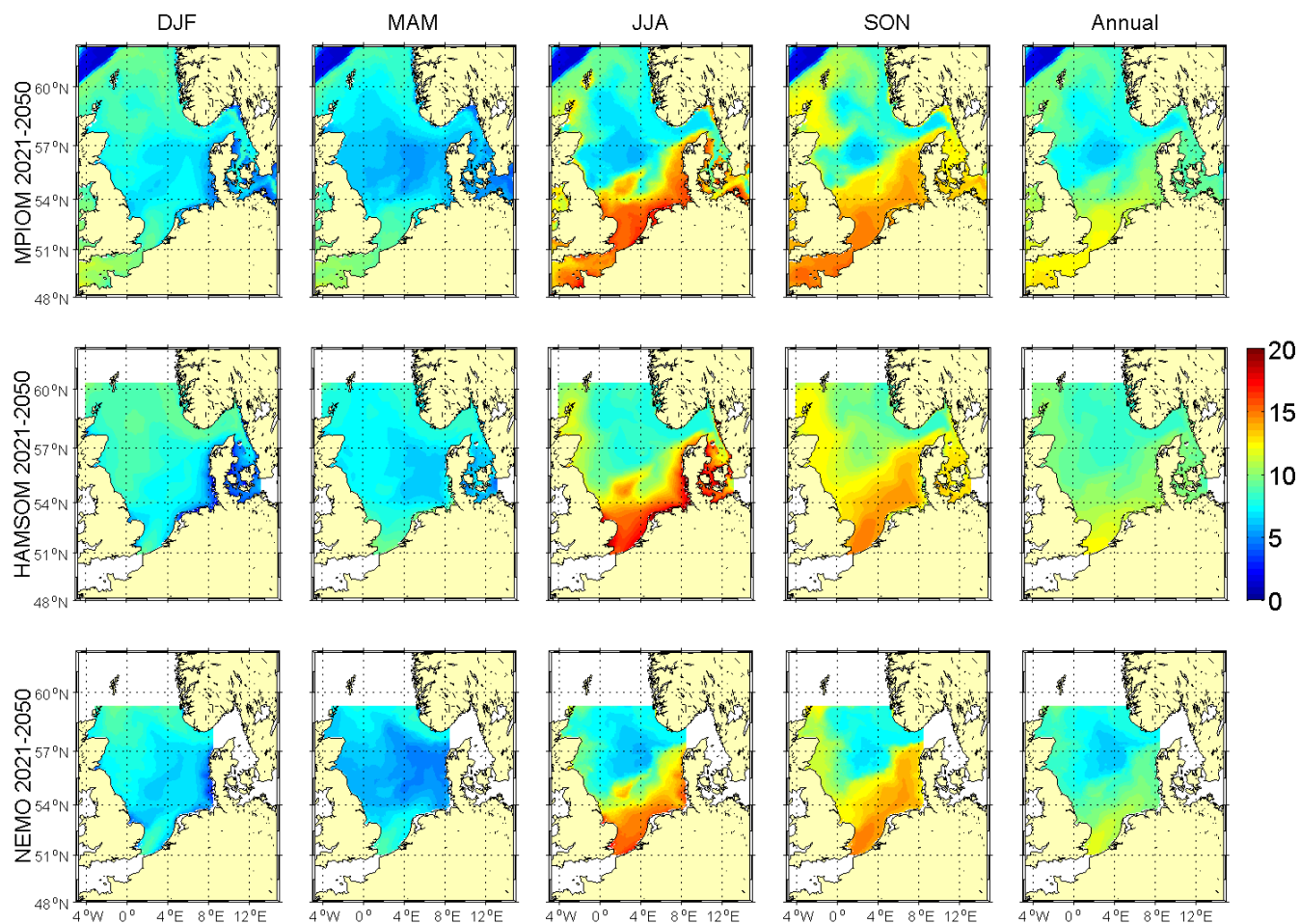


Figure 5.4.5A: Seasonal and annual means of bottom temperature [°C] for the period 2021-2050. Upper row MPIOM run 215, middle row HAMSOM run 202 and lower row NEMO-Nordic run 470 (all A1B scenario).

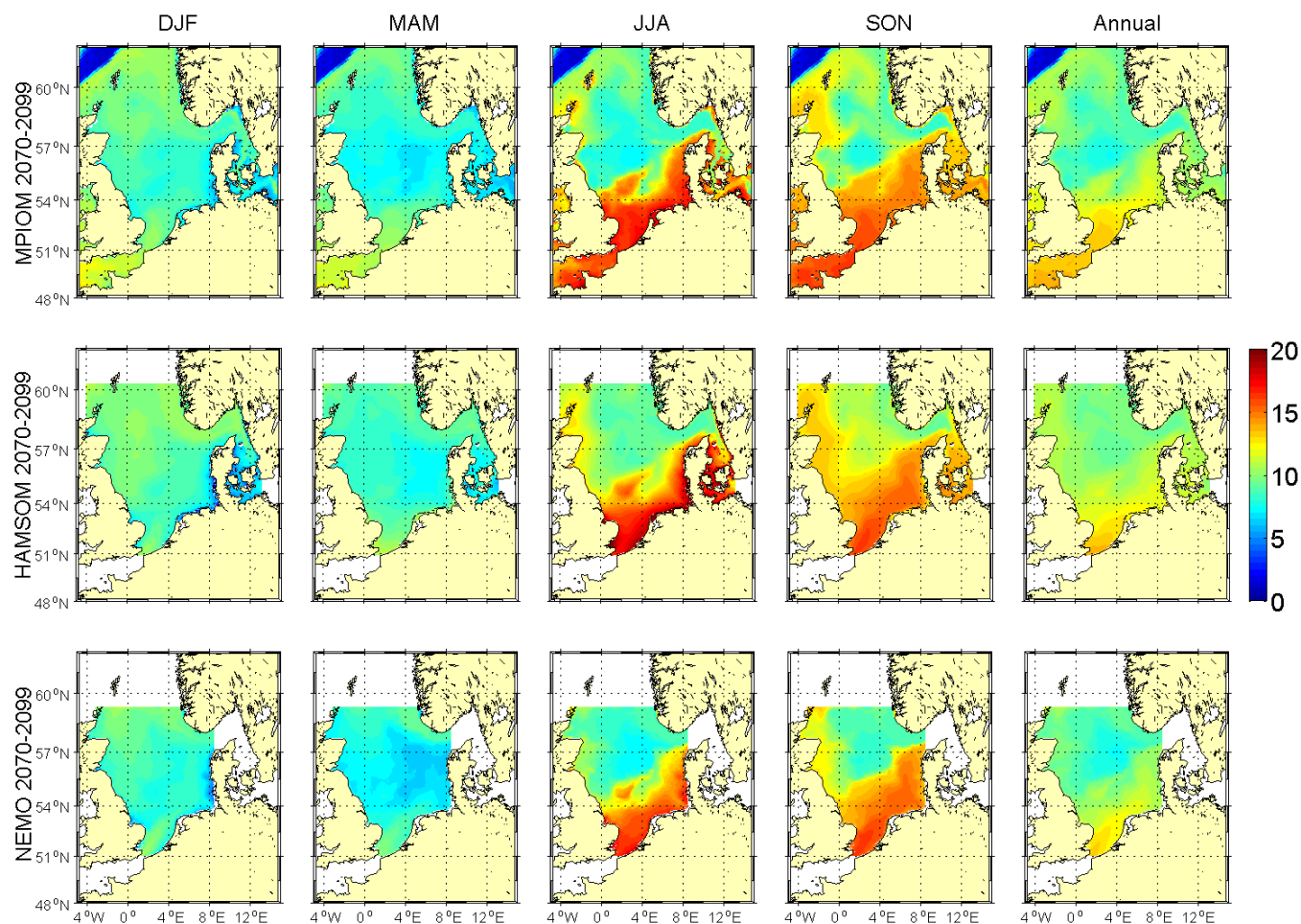


Figure 5.4.6A: Seasonal and annual means of bottom temperature [°C] for the period 2070-2050. Upper row MPIOM run 215, middle row HAMSOM run 202 and lower row NEMO-Nordic run 470 (all A1B scenario).

Coupled Ocean
Atmosphere
Models

BSH
DWD
IfM Hamburg
MPI Hamburg
SMHI
AWI

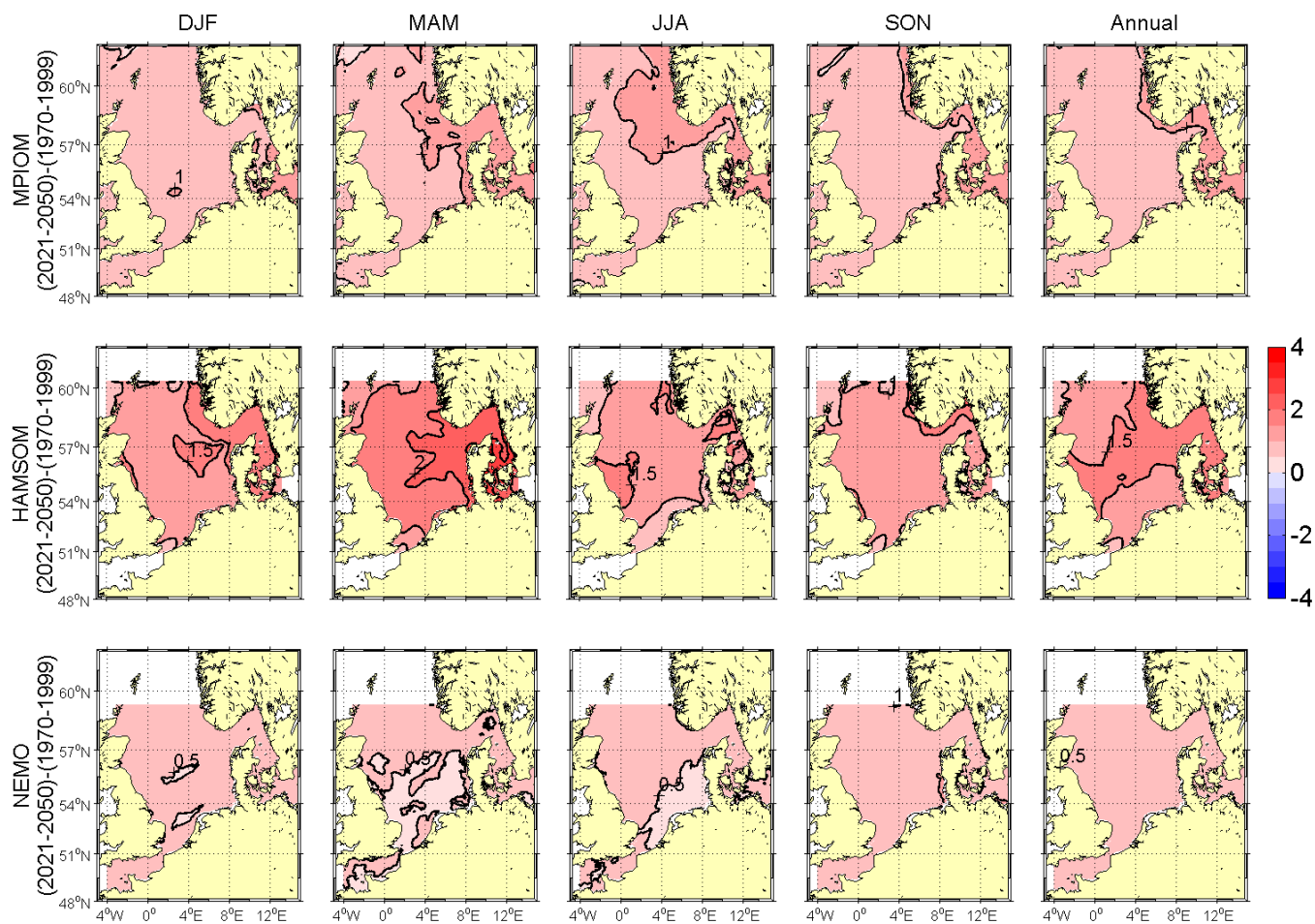
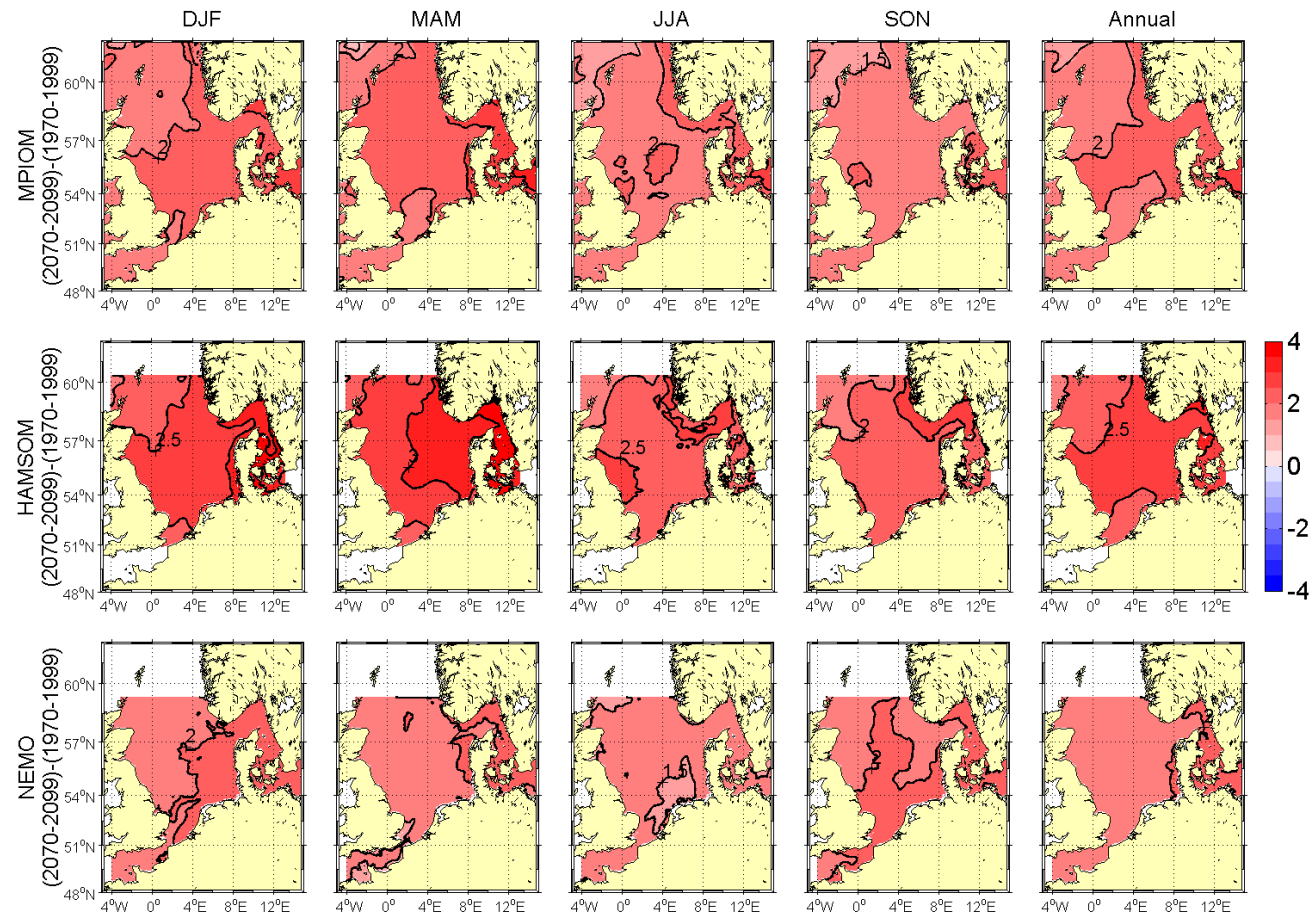


Figure 5.4.7A: Changes in seasonal and annual means of sea surface temperature [°C] from (1970-1999) to (2021-2050). Upper row MPIOM run 215, middle row HAMSOM run 202 and lower row NEMO-Nordic run 470 (all A1B scenario). Selected isolines have been labelled for better orientation, contour interval is 0.5 °C.



Coupled Ocean
Atmosphere
Models

BSH
DWD
IfM Hamburg
MPI Hamburg
SMHI
AWI

Figure 5.4.8A: Changes in seasonal and annual means of sea surface temperature [°C] from (1970-1999) to (2070-2099). Upper row MPIOM run 215, middle row HAMISOM run 202 and lower row NEMO-Nordic run 470 (all A1B scenario). Selected isolines have been labelled for better orientation, contour interval is 0.5 °C.

Coupled Ocean
Atmosphere
Models

BSH
DWD
IfM Hamburg
MPI Hamburg
SMHI
AWI

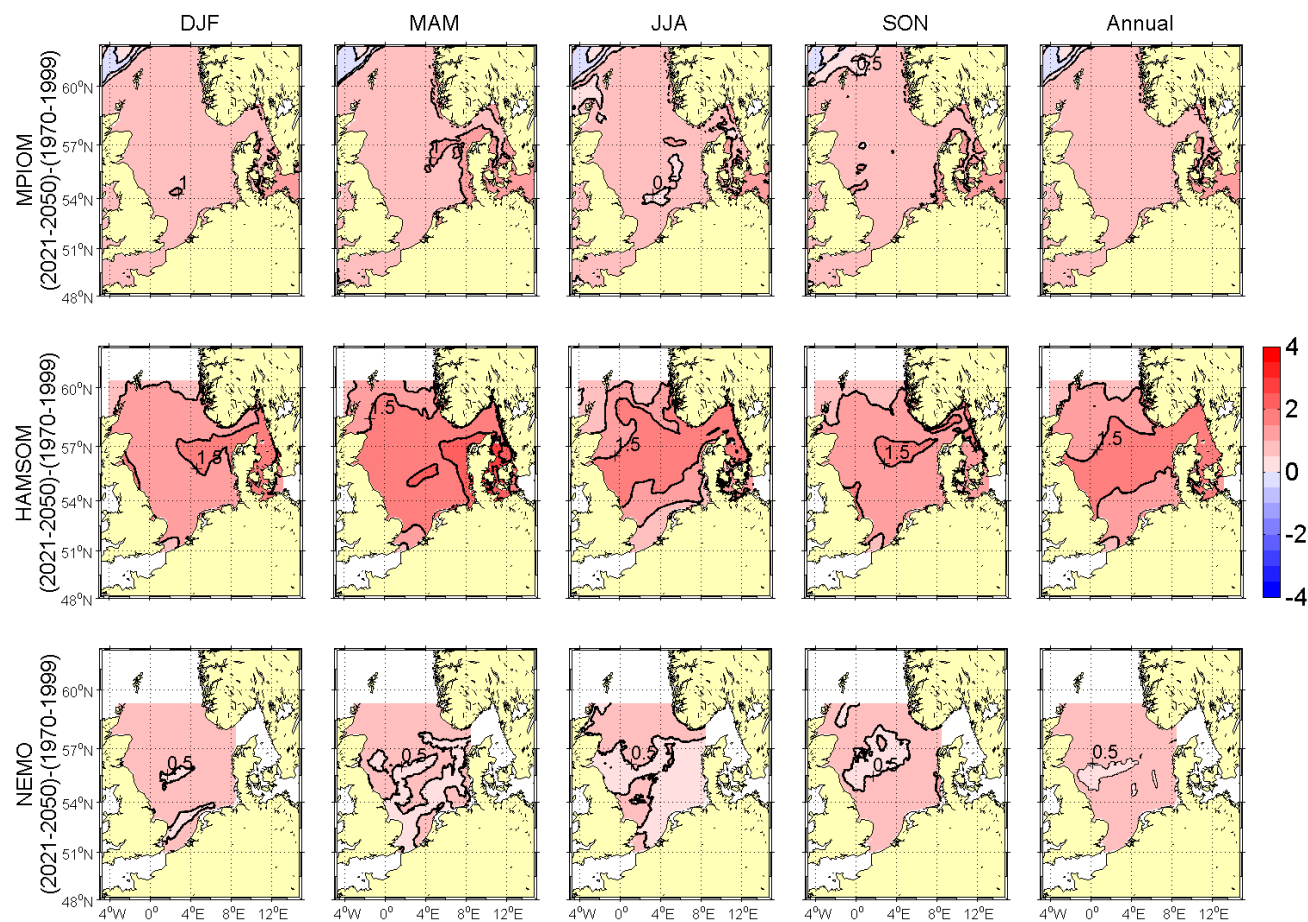


Figure 5.4.9A: Changes in seasonal and annual means of bottom temperature [°C] from (1970-1999) to (2021-2050). Upper row MPIOM run 215, middle row HAMSOM run 202 and lower row NEMO-Nordic run 470 (all A1B scenario). Selected isolines have been labelled for better orientation, contour interval is 0.5 °C.

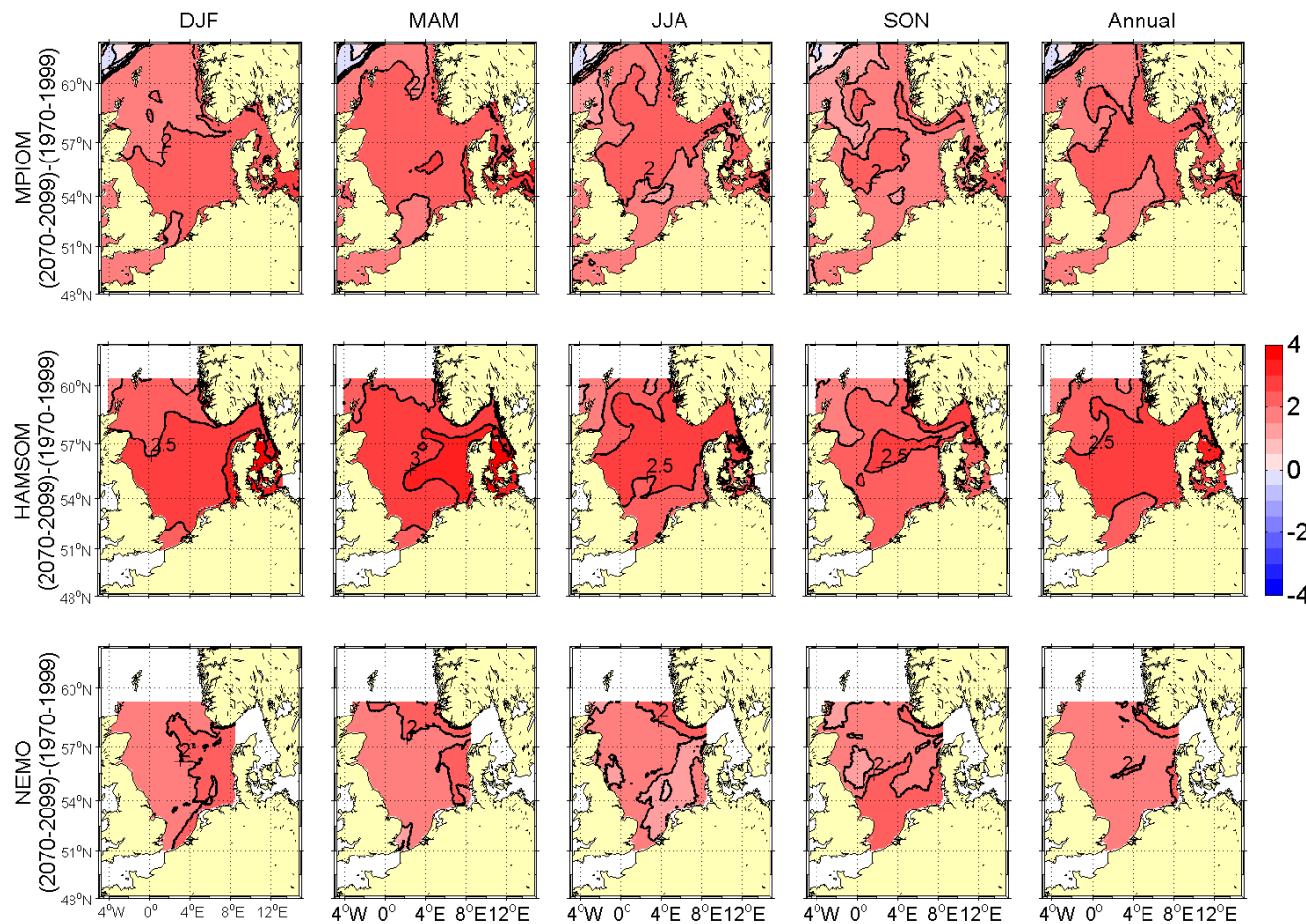


Figure 5.4.10A: Changes in seasonal and annual means of bottom temperature [°C] from (1970-1999) to (2070-2099). Upper row MPIOM run 215, middle row HAMSOM run 202 and lower row NEMO-Nordic run 470 (all A1B scenario). Selected isolines have been labelled for better orientation, contour interval is 0.5 °C.

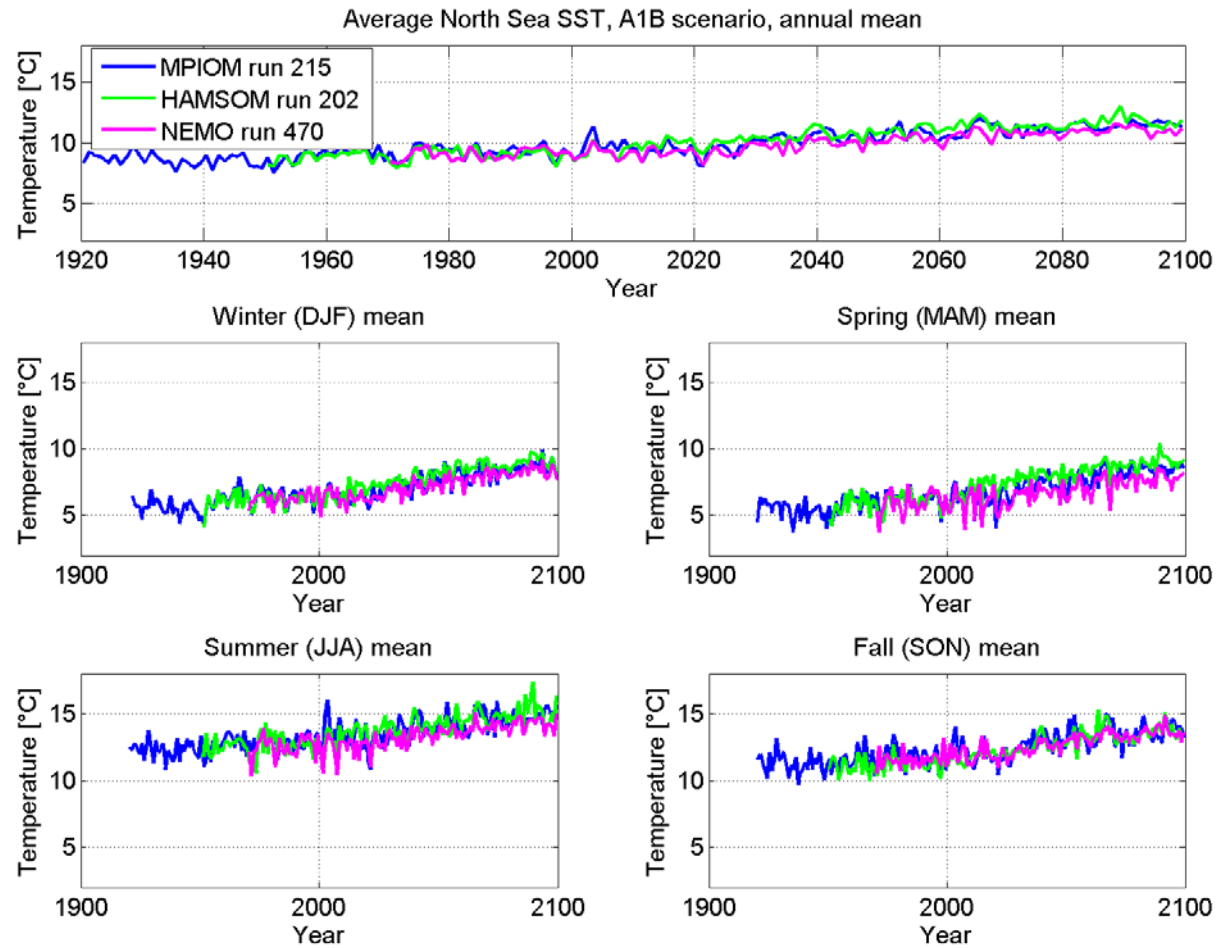


Figure 5.4.11A: Time series of seasonal and annual means of sea surface temperature [°C] for MPIOM run 215 (blue), HAMSOM run 202 (green) and NEMO-Nordic run 470 (magenta). The temperatures represent averages over the North Sea area given in Figure 4.1. Upper row annual means, lower rows seasonal means.

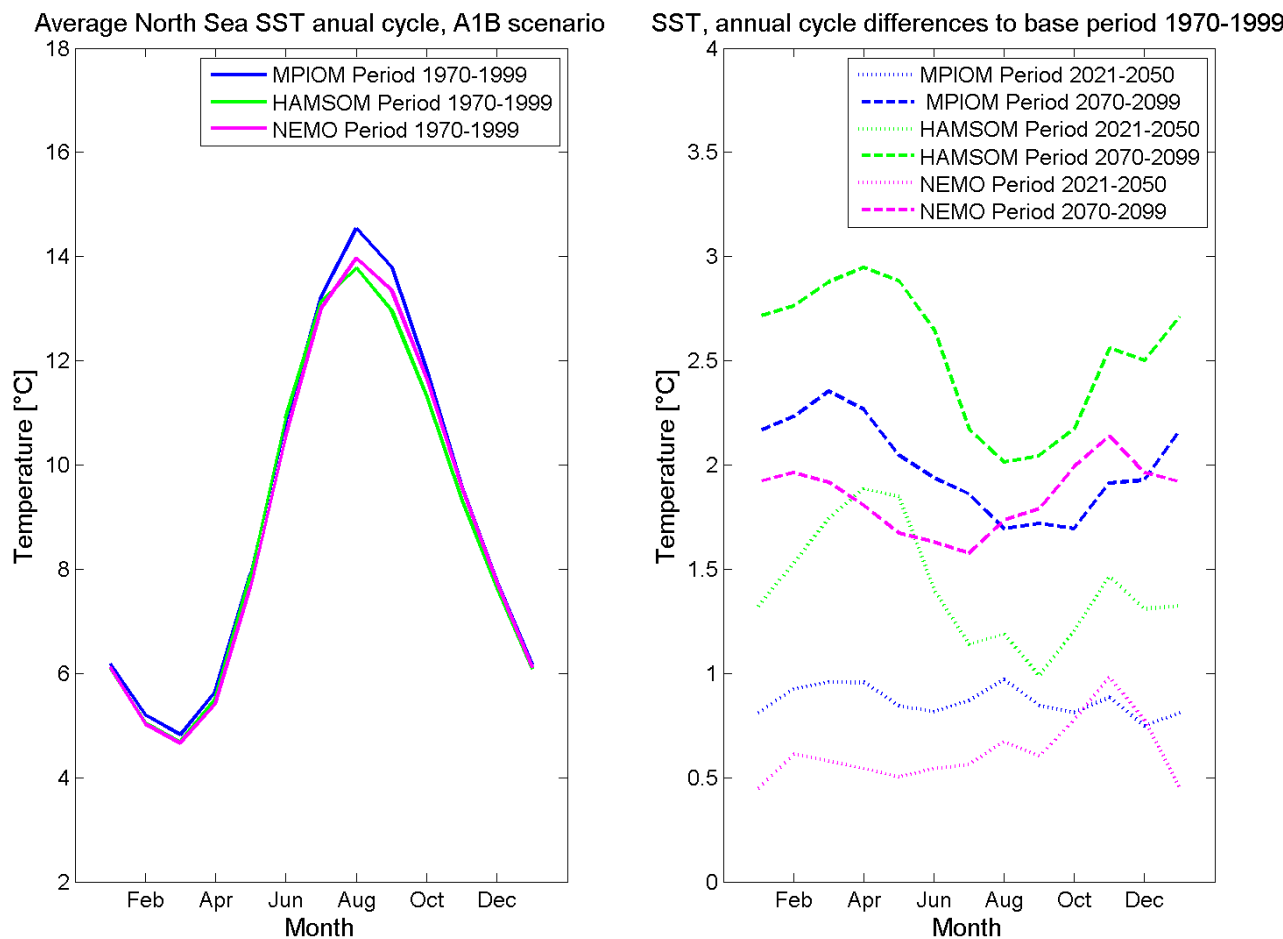


Figure 5.4.12A: left: mean annual cycle of sea surface temperatures [°C] for 1970-1990 for MPIOM run 215 (blue), HAMSOM run 202 (green) and NEMO-Nordic run 470 (blue). Right: differences in mean annual cycle to the averaging period 1970-1999, 2021-2050 as dotted line and 2070-2099 as dashed line. The means are representing averages over the North Sea area given in Figure 4.1.

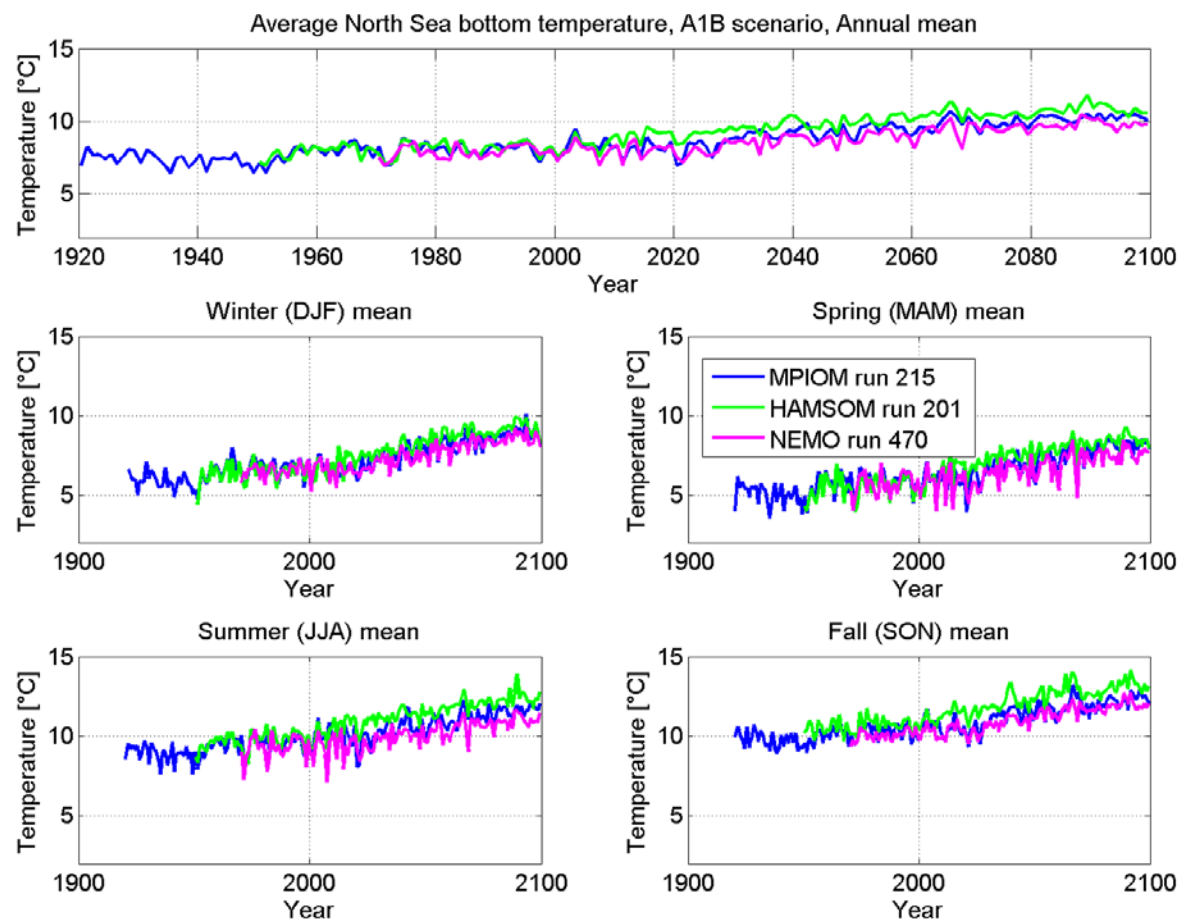


Figure 5.4.13A: Time series of seasonal and annual means of bottom temperature [°C] for MPIOM run 215 (blue), HAMSOM run 202 (green) and NEMO-Nordic run 470 (magenta). The temperatures represent averages over the North Sea area given in Figure 4.1. Upper row annual means, lower rows seasonal means.

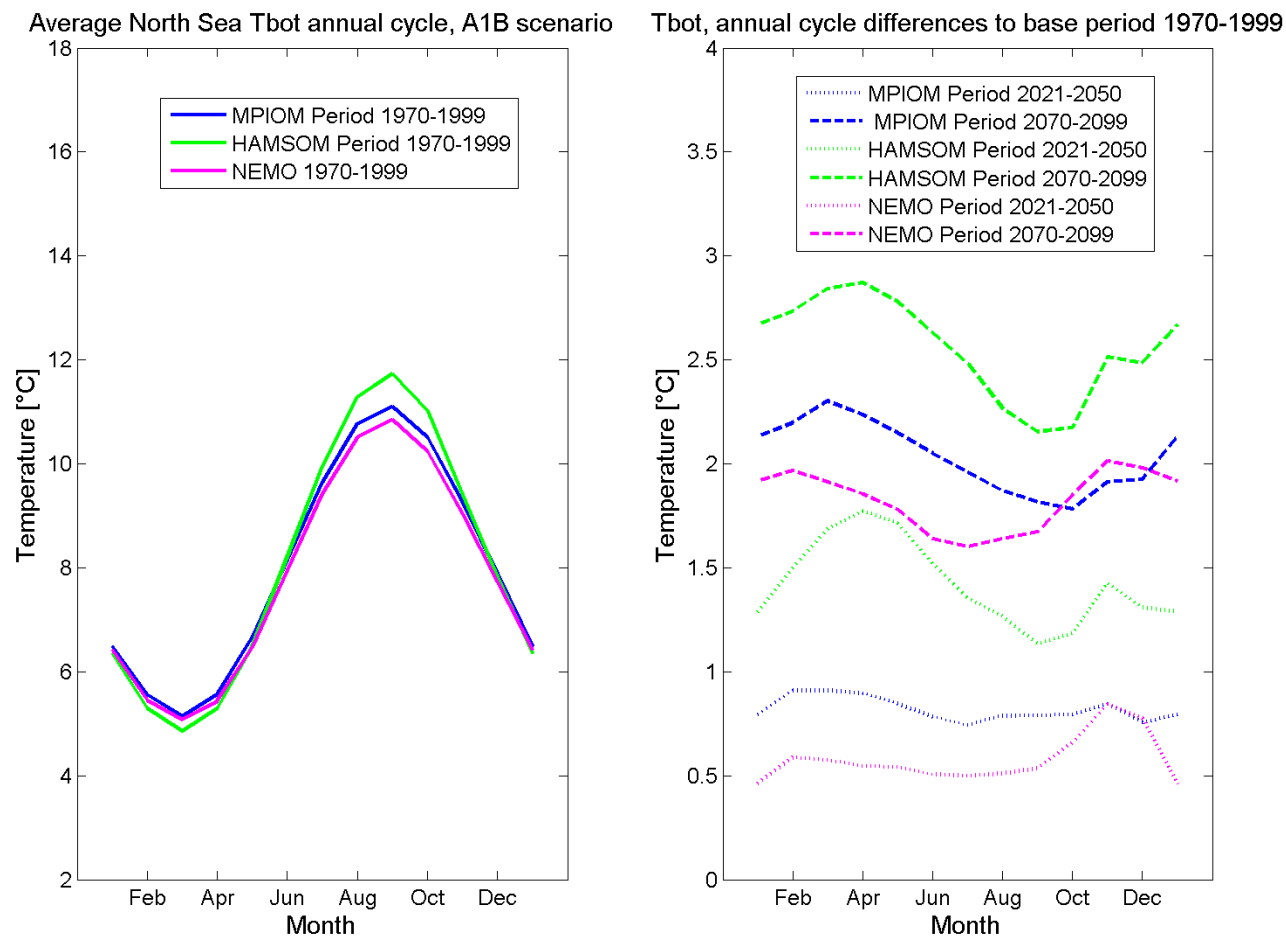


Figure 5.4.14A: left: mean annual cycle of bottom temperatures [°C] for 1970-1990 for MPIOM run 215 (blue), HAMSOM run 202 (green) and NEMO-Nordic run 470 (blue). Right: differences in mean annual cycle to the averaging period 1970-1999, 2021-2050 as dotted line and 2070-2099 as dashed line. The means are representing averages over the North Sea area given in Figure 4.1.

Coupled Ocean
Atmosphere
Models

BSH
DWD
IfM Hamburg
MPI Hamburg
SMHI
AWI

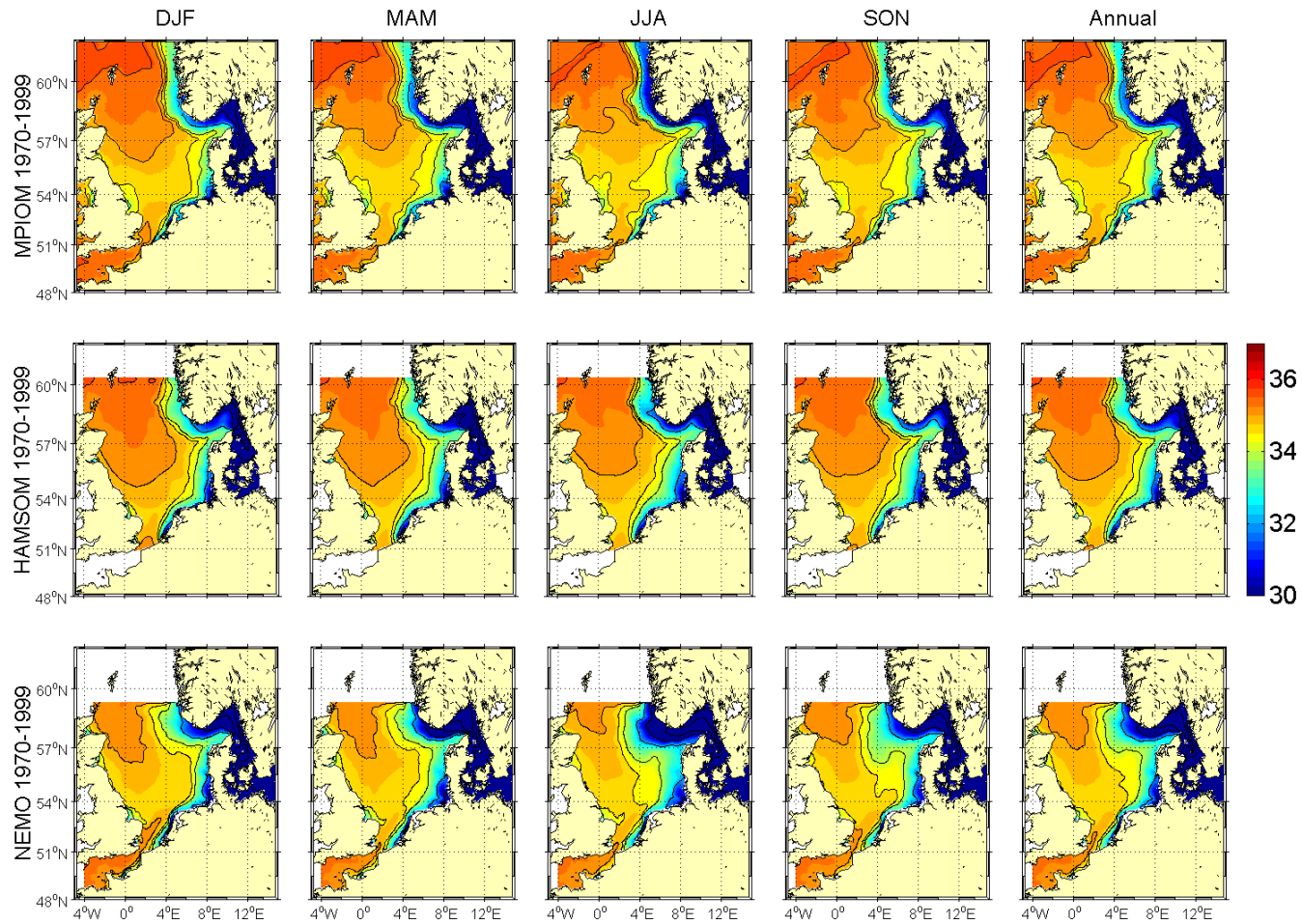


Figure 5.4.15A: Seasonal and annual means of sea surface salinity [psu] for the period 1970-1999. Upper row MPIOM run 215, middle row HAMSOM run 202 and lower row NEMO-Nordic run 470 (all A1B scenario).

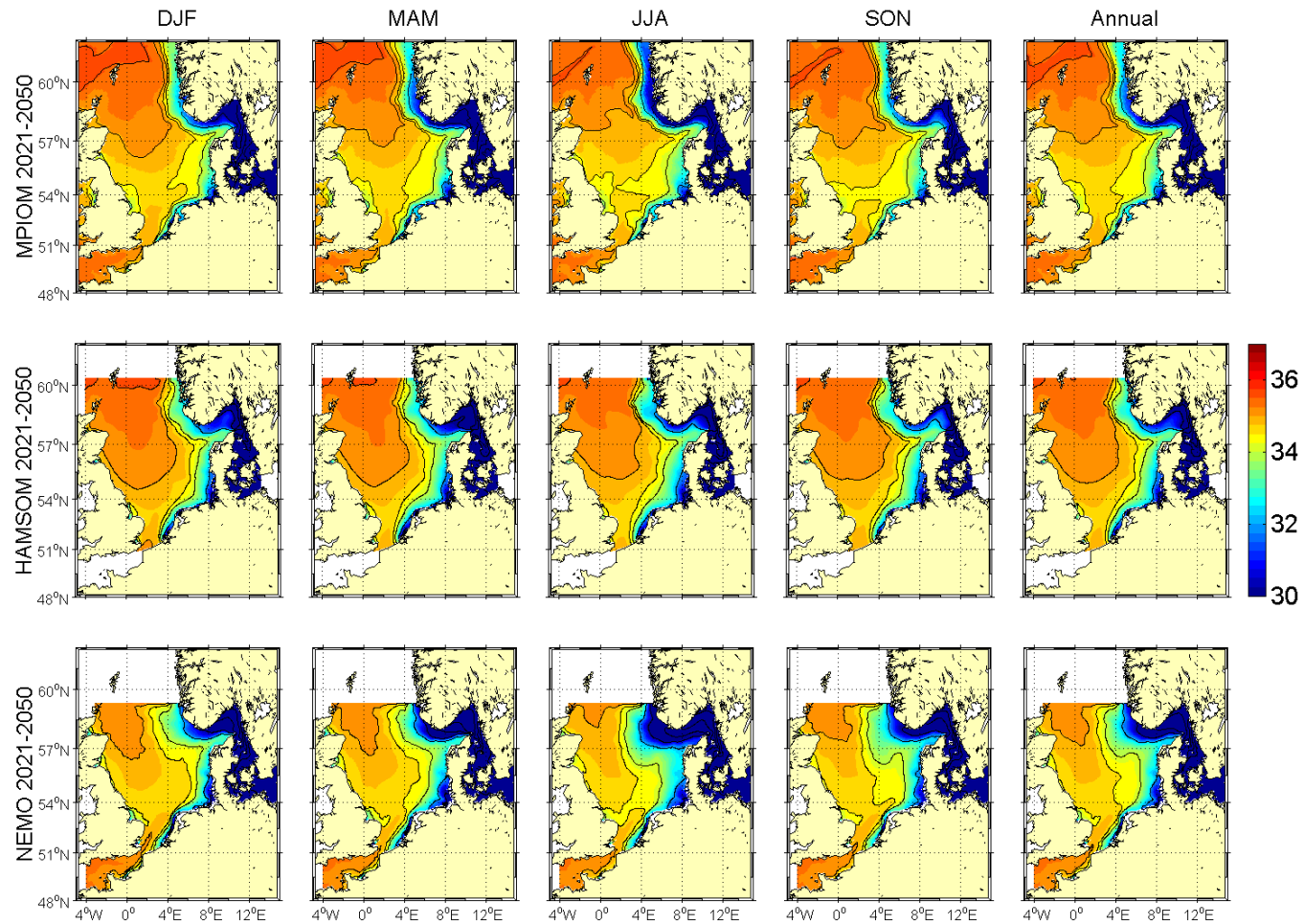


Figure 5.4.16A: Seasonal and annual means of sea surface salinity [psu] for the period 2021-2050. Upper row MPIOM run 215, middle row HAMSOM run 202 and lower row NEMO-Nordic run 470 (all A1B scenario).

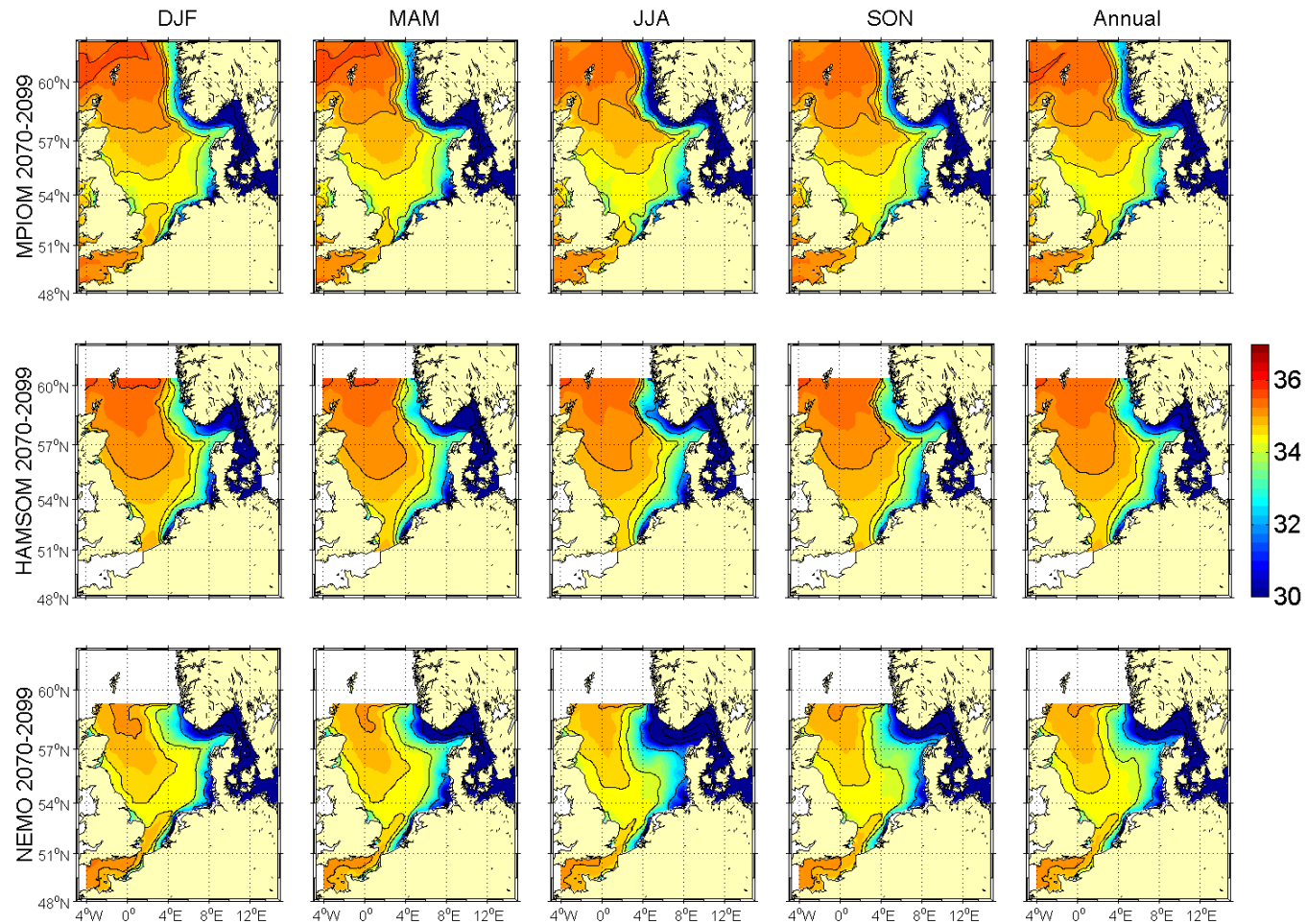


Figure 5.4.17A: Seasonal and annual means of sea surface salinity [psu] for the period 2070-2050. Upper row MPIOM run 215, middle row HAMSOM run 202 and lower row NEMO-Nordic run 470 (all A1B scenario).

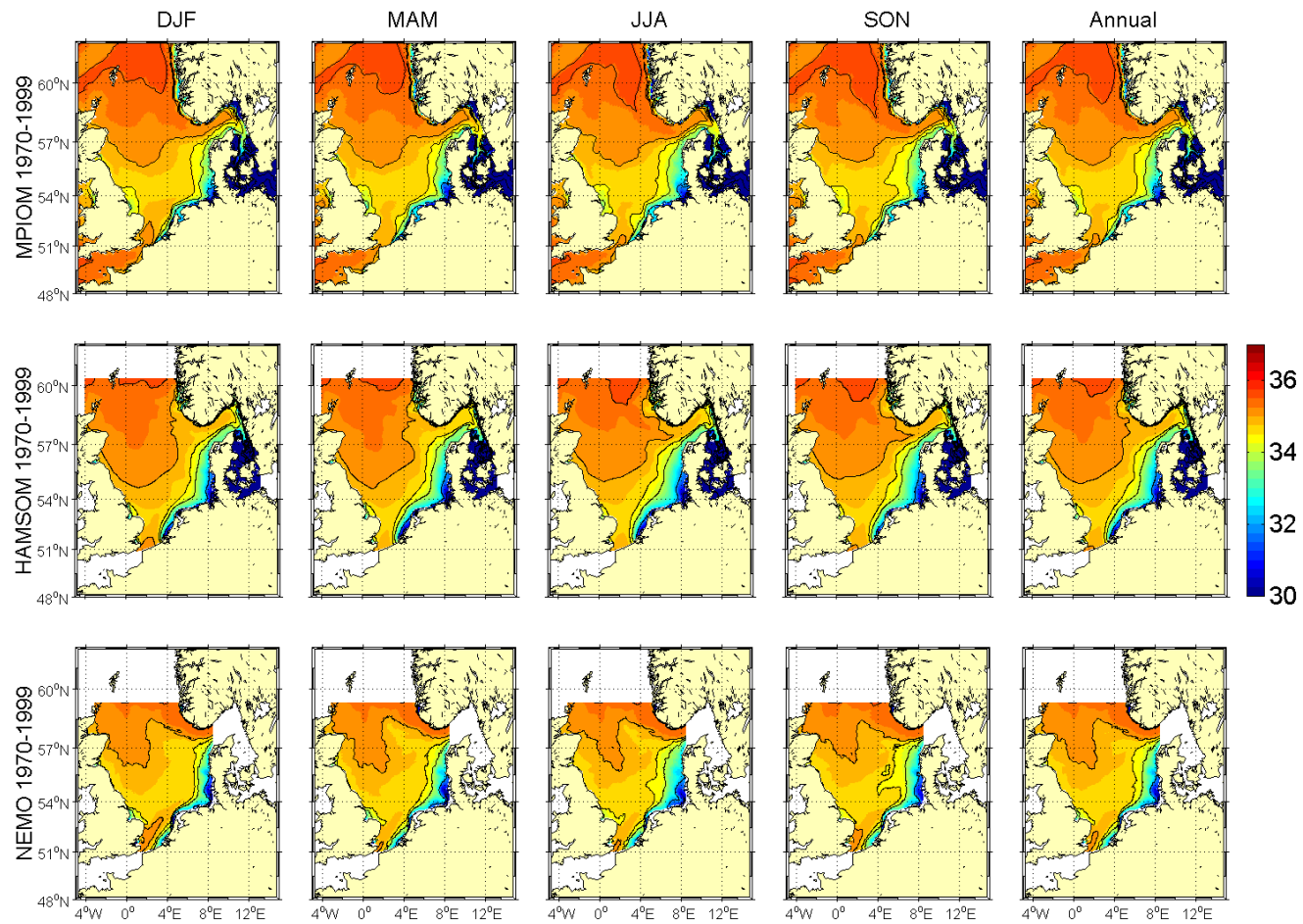


Figure 5.4.18A: Seasonal and annual means of bottom salinity [psu] for the period 1970-1999. Upper row MPIOM run 215, middle row HAMSOM run 202 and lower row NEMO-Nordic run 470 (all A1B scenario).

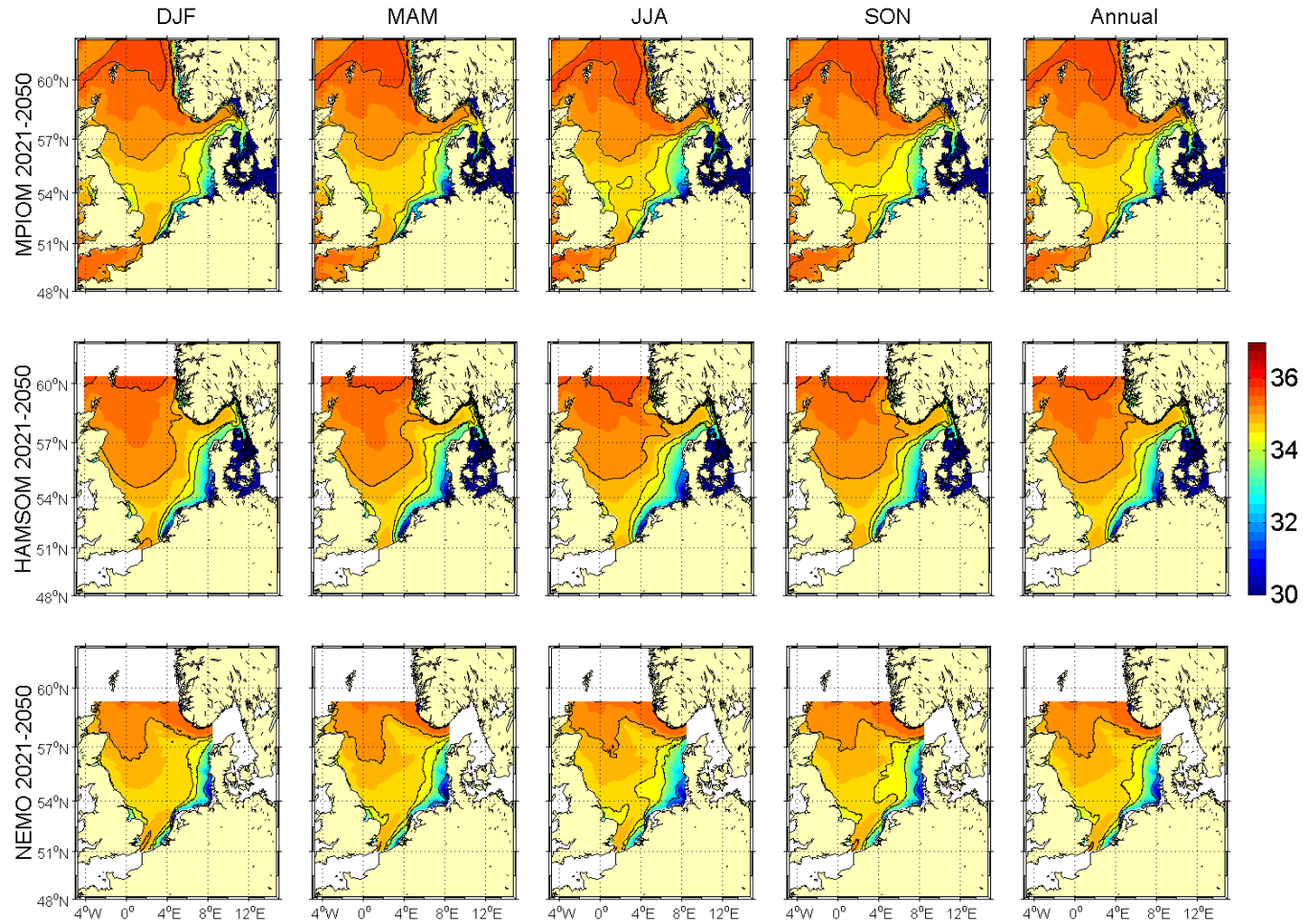


Figure 5.4.19A: Seasonal and annual means of bottom salinity [psu] for the period 2021-2050. Upper row MPIOM run 215, middle row HAMSOM run 202 and lower row NEMO-Nordic run 470 (all A1B scenario).

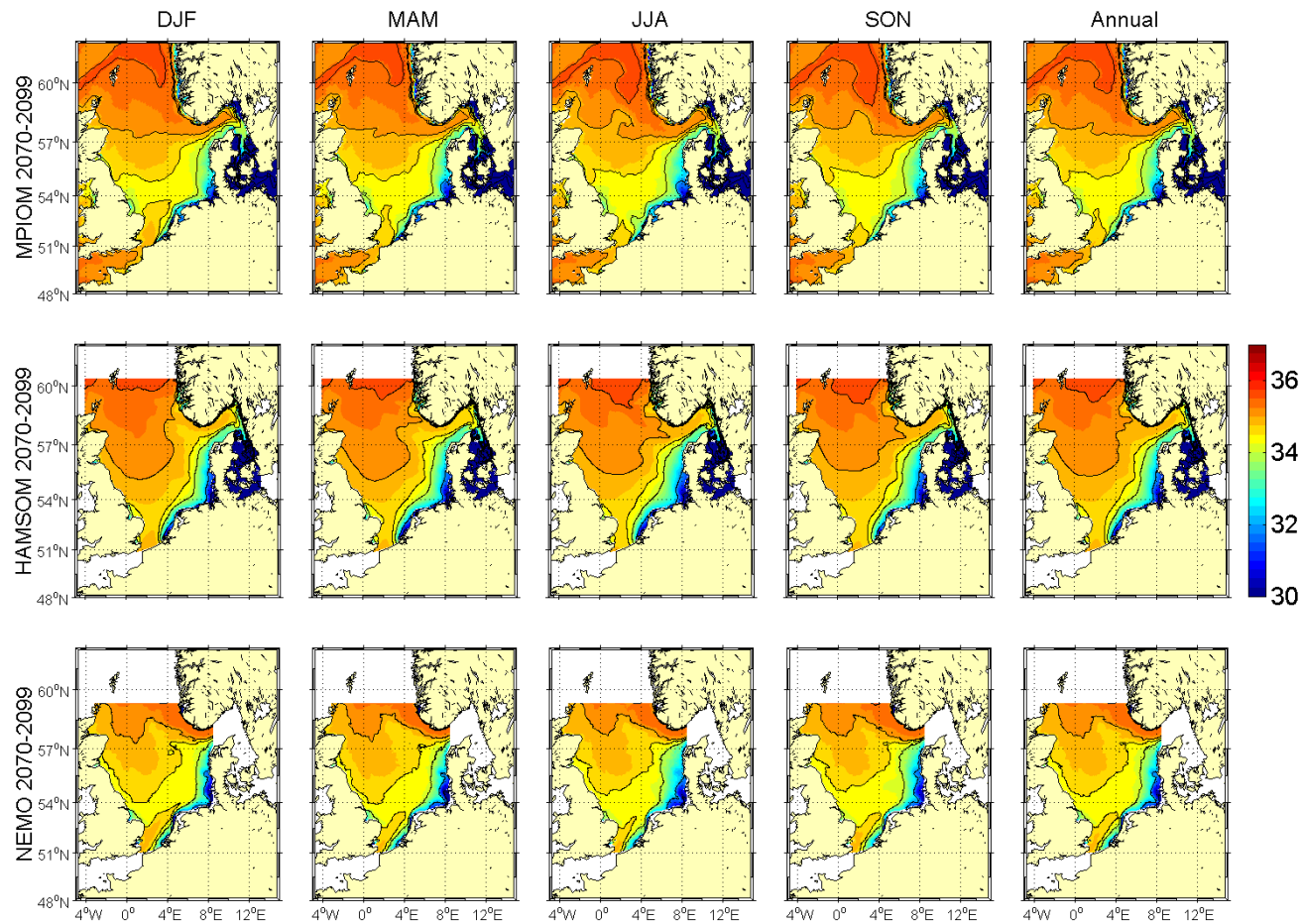


Figure 5.4.20A: Seasonal and annual means of bottom salinity [psu] for the period 2070-2099. Upper row MPIOM run 215, middle row HAMSOM run 202 and lower row NEMO-Nordic run 470 (all A1B scenario).

Coupled Ocean
Atmosphere
Models

BSH
DWD
IfM Hamburg
MPI Hamburg
SMHI
AWI

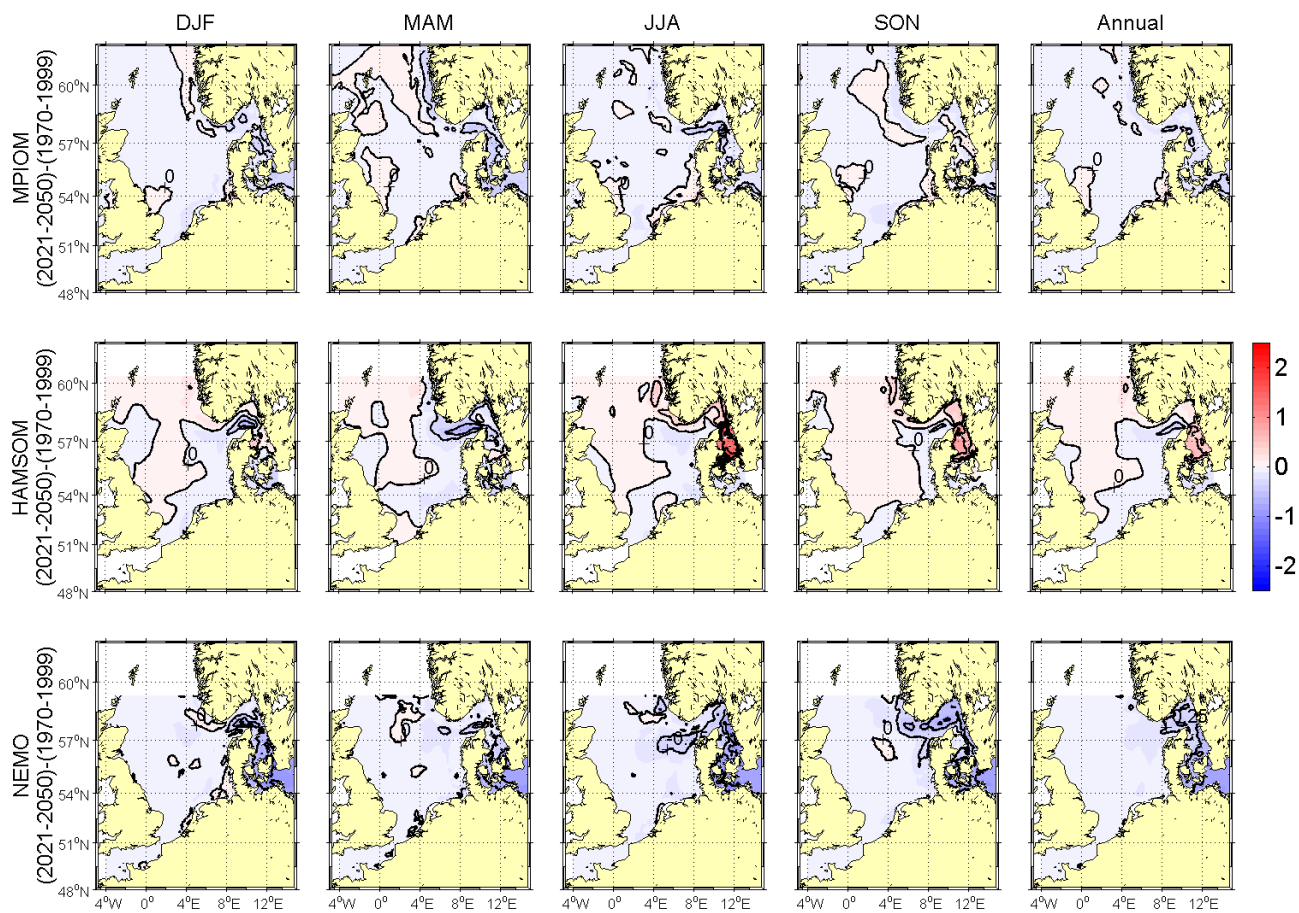


Figure 5.4.21A: Changes in seasonal and annual means of sea surface salinity [psu] from (1970-1999) to (2021-2050). Upper row MPIOM run 215, middle row HAMSOM run 202 and lower row NEMO-Nordic run 470 (all A1B scenario). Selected isolines have been labelled for better orientation, contour interval is 0.25 psu.

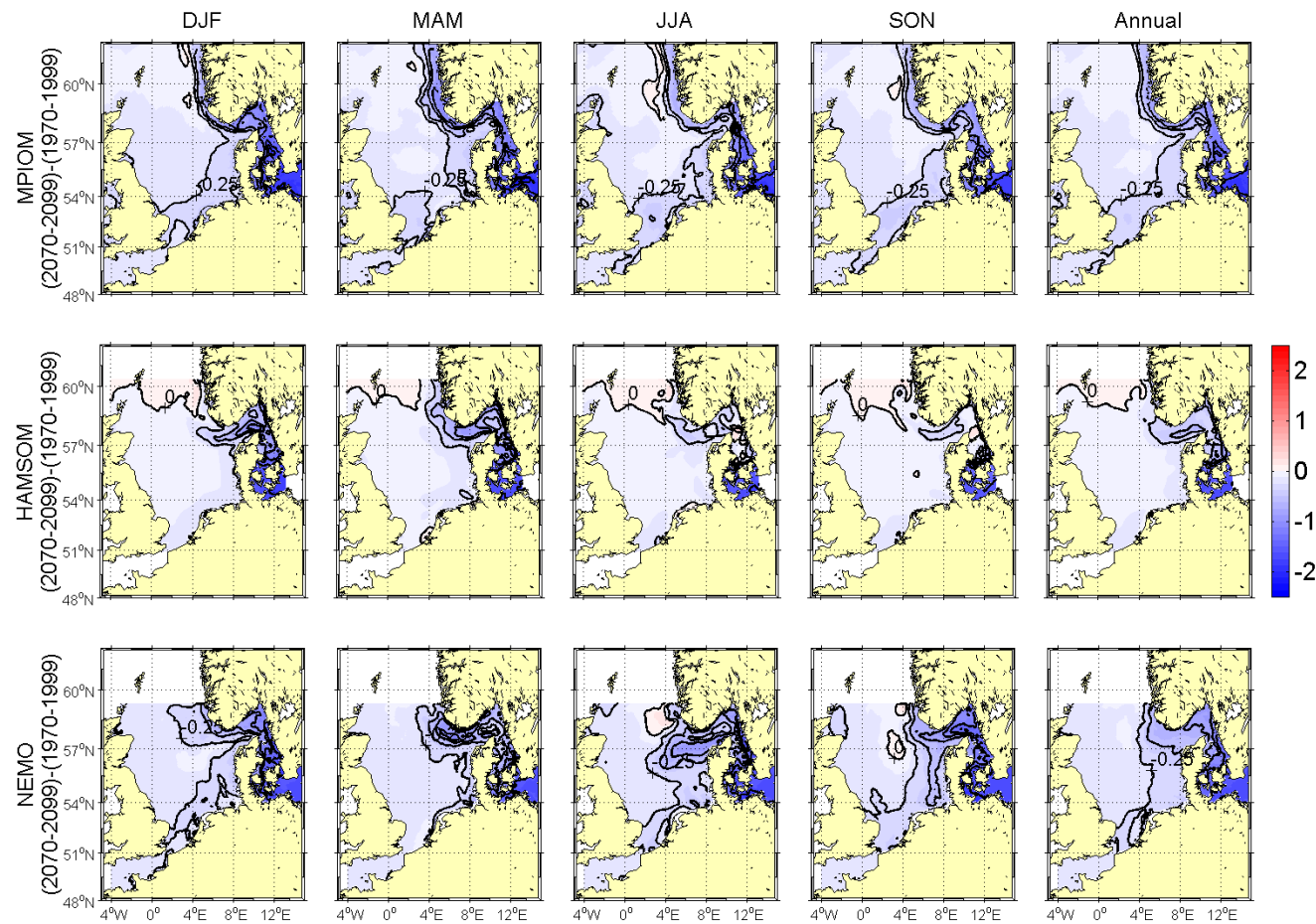


Figure 5.4.22A: Changes in seasonal and annual means of sea surface salinity [psu] from (1970-1999) to (2070-2099). Upper row MPIOM run 215, middle row HAMSOM run 202 and lower row NEMO-Nordic run 470 (all A1B scenario). Selected isolines have been labelled for better orientation, contour interval is 0.25 psu.

Coupled Ocean
Atmosphere
Models

BSH
DWD
IfM Hamburg
MPI Hamburg
SMHI
AWI

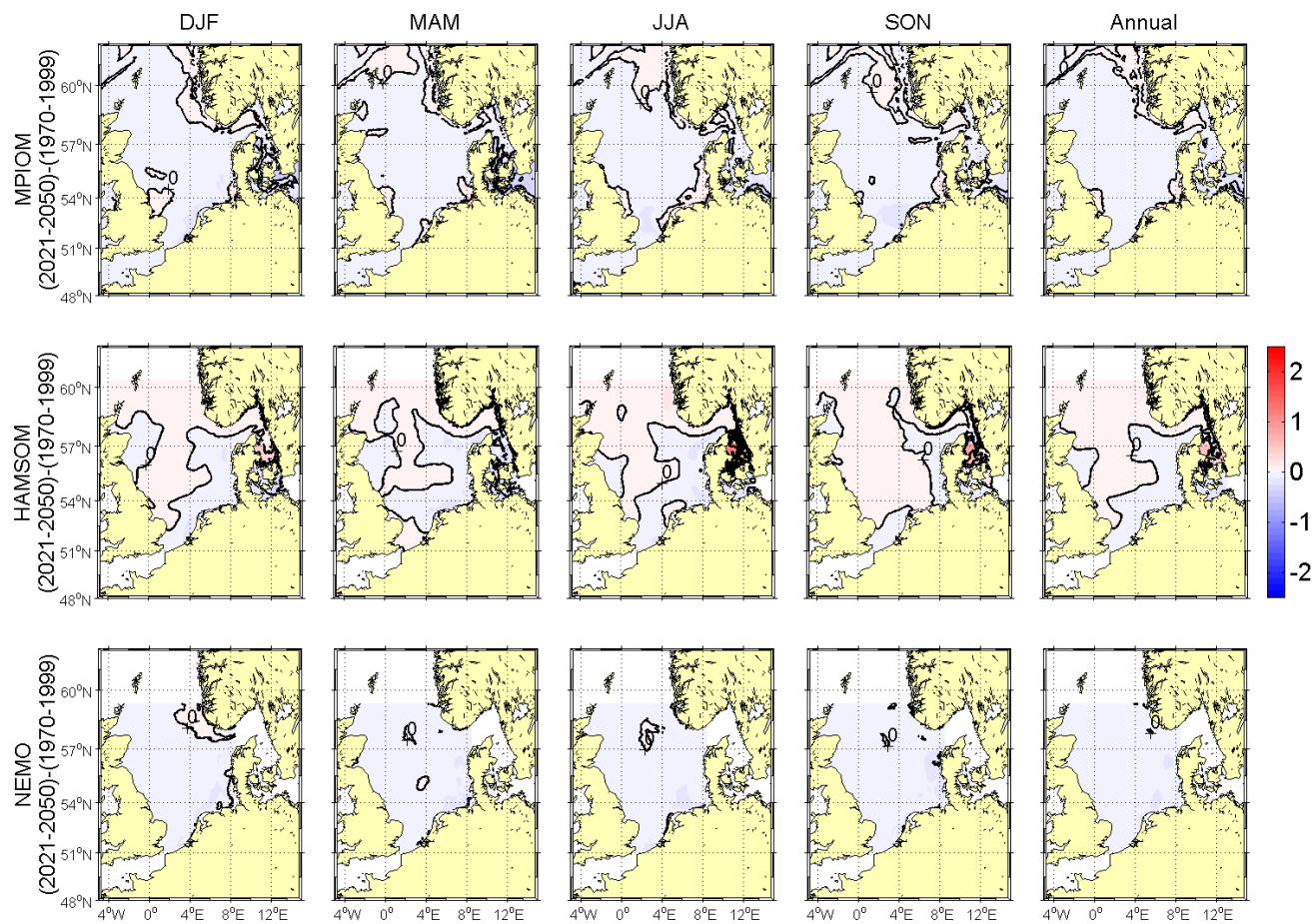


Figure 5.4.23A: Changes in seasonal and annual means of bottom salinity [psu] from (1970-1999) to (2021-2050). Upper row MPIOM run 215, middle row HAMSOM run 202 and lower row NEMO-Nordic run 470 (all A1B scenario). Selected isolines have been labelled for better orientation, contour interval is 0.25 psu.

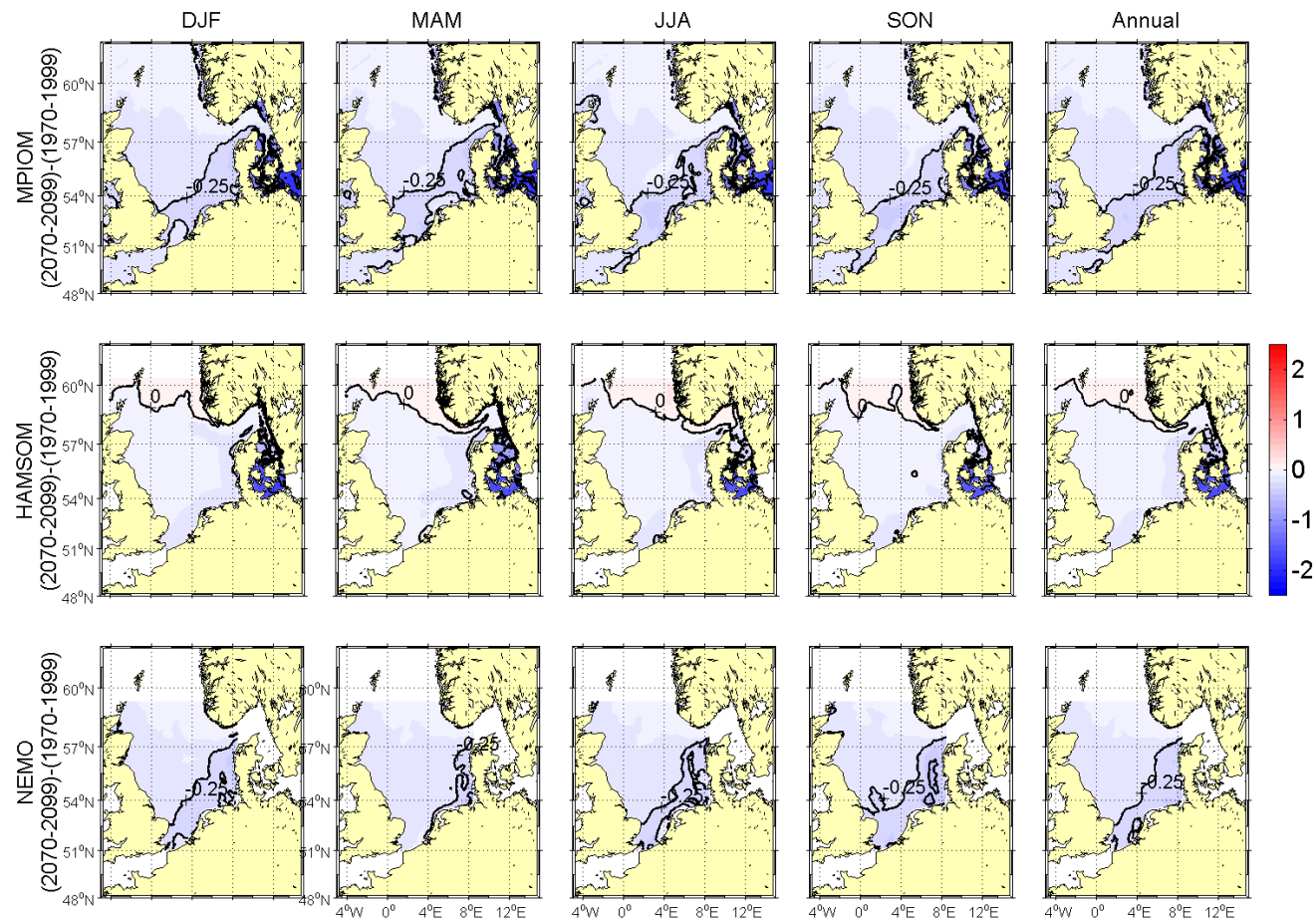


Figure 5.4.24A: Changes in seasonal and annual means of bottom salinity [psu] from (1970-1999) to (2070-2099). Upper row MPIOM run 215, middle row HAMSOM run 202 and lower row NEMO-Nordic run 470 (all A1B scenario). Selected isolines have been labelled for better orientation, contour interval is 0.25 psu.

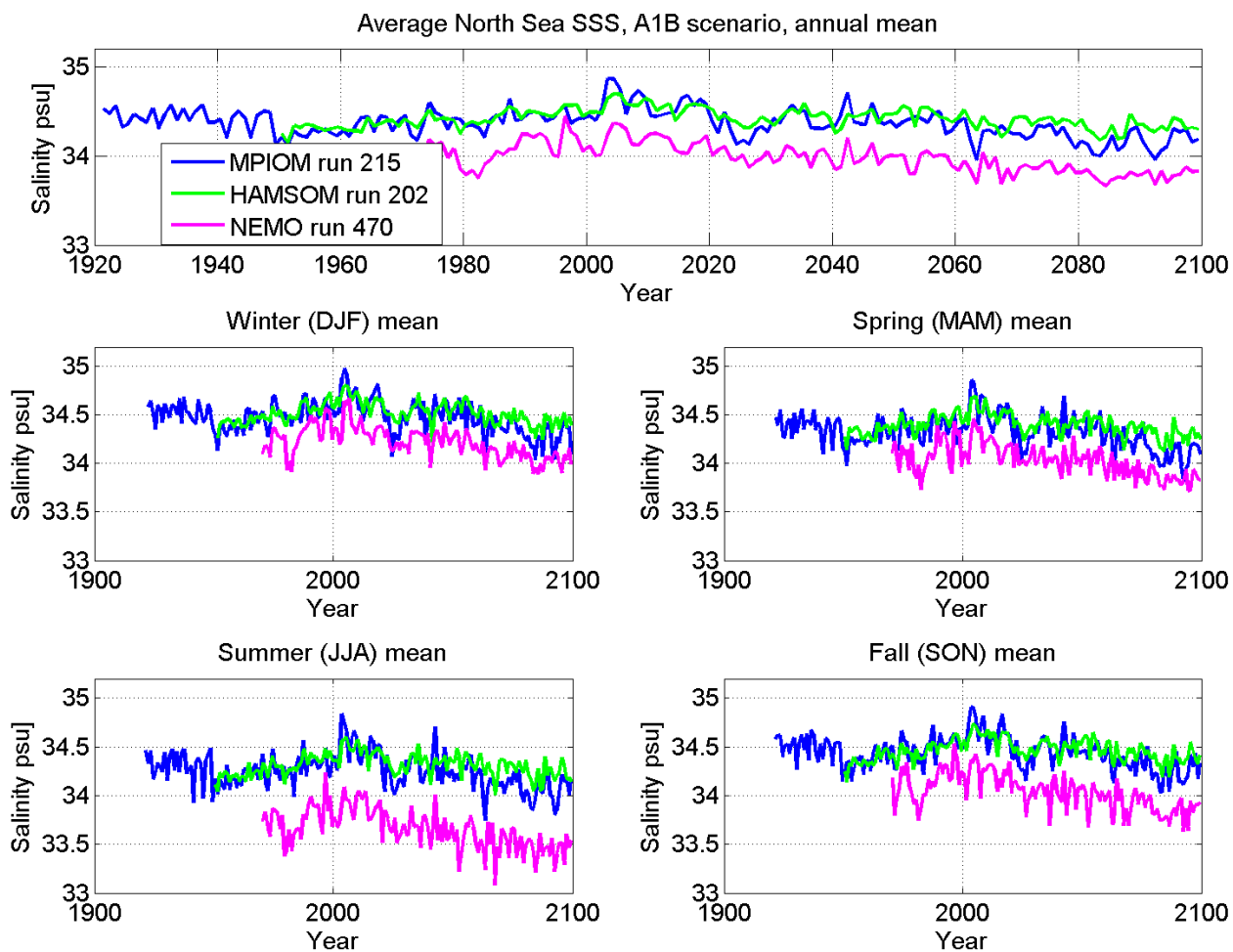


Figure 5.4.25A: Time series of seasonal and annual means of sea surface salinity [psu] for MPIOM run 215 (blue), HAMSOM run 202 (green) and NEMO-Nordic run 470 (magenta). The salinities represent averages over the North Sea area given in Figure 4.1. Upper row annual means, lower rows seasonal means.

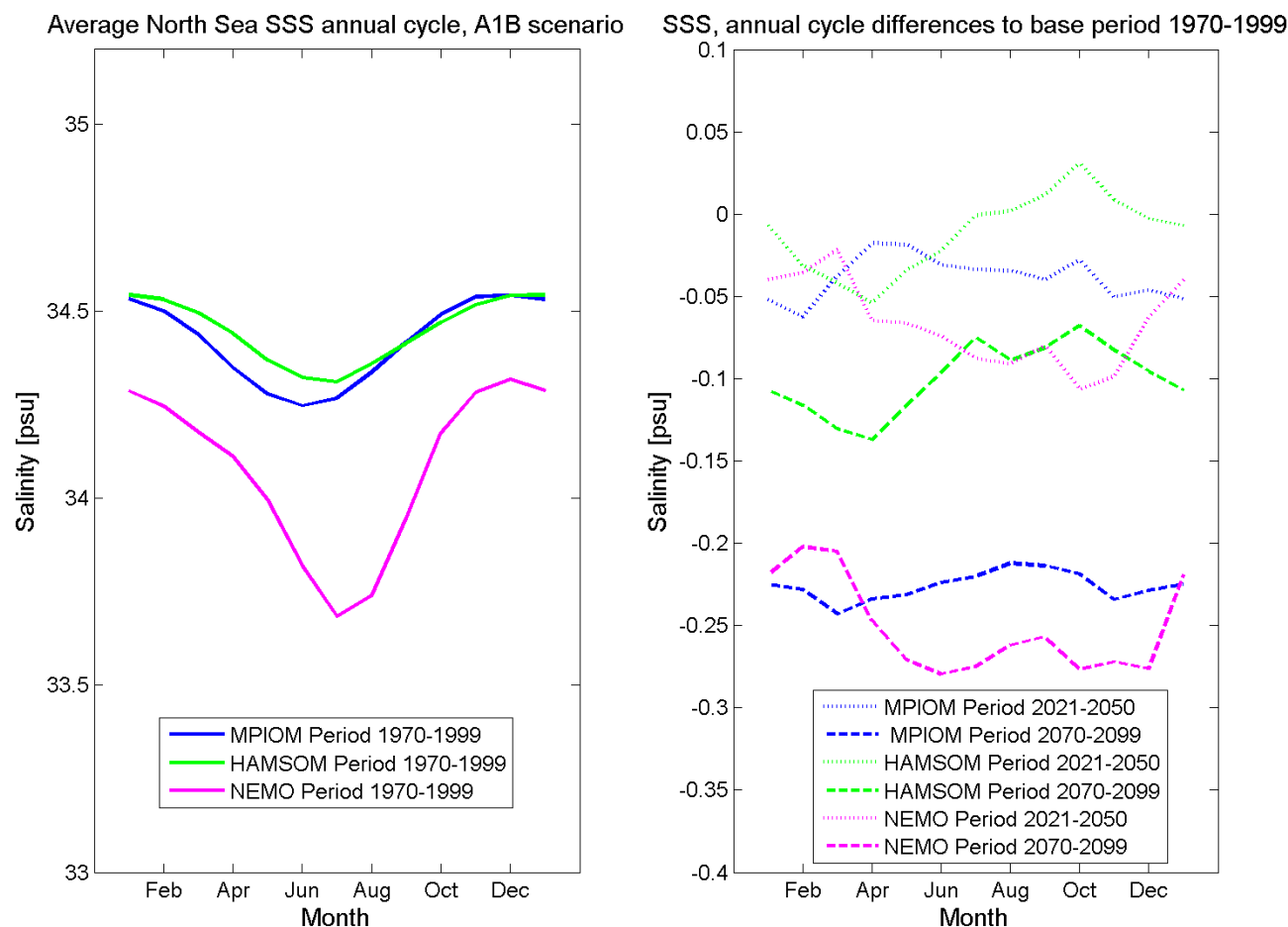


Figure 5.4.26A: left: mean annual cycle of sea surface salinity [psu] for 1970-1990 for MPIOM run 215 (blue), HAMSOM run 202 (green) and NEMO-Nordic run 470 (blue). Right: differences in mean annual cycle to the averaging period 1970-1999, 2021-2050 as dotted line and 2070-2099 as dashed line. The means are representing averages over the North Sea area given in Figure 4.1.

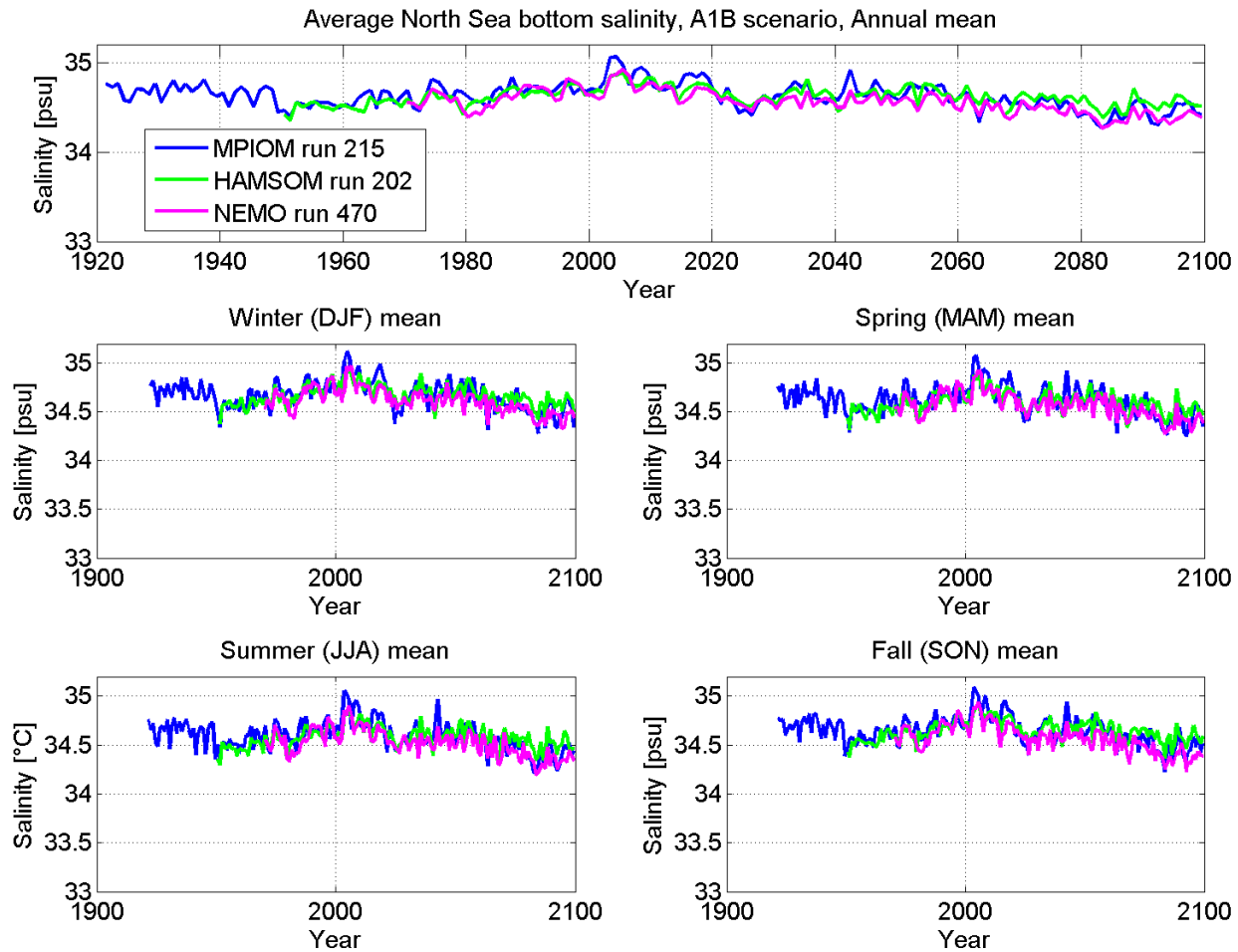


Figure 5.4.27A: Time series of seasonal and annual means of bottom salinity [psu] for MPIOM run 215 (blue), HAMSOM run 202 (green) and NEMO-Nordic run 470 (magenta). The salinities represent averages over the North Sea area given in Figure 4.1. Upper row annual means, lower rows seasonal means.

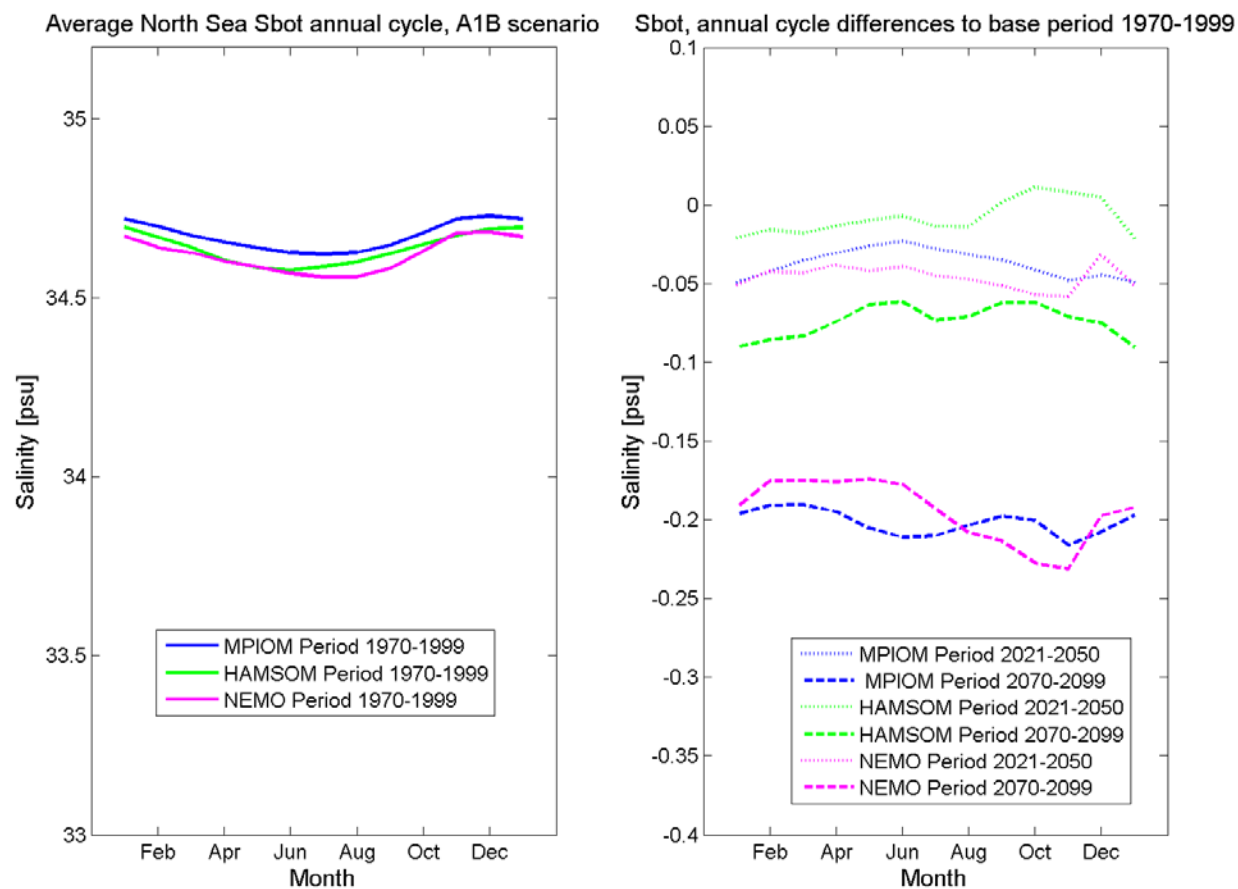


Figure 5.4.28A: left: mean annual cycle of bottom salinity [psu] for 1970-1990 for MPIOM run 215 (blue), HAMSOM run 202 (green) and NEMO-Nordic run 470 (blue). Right: differences in mean annual cycle to the averaging period 1970-1999, 2021-2050 as dotted line and 2070-2099 as dashed line. The means are representing averages over the North Sea area given in Figure 4.1.

Coupled Ocean
Atmosphere
Models

BSH
DWD
IfM Hamburg
MPI Hamburg
SMHI
AWI

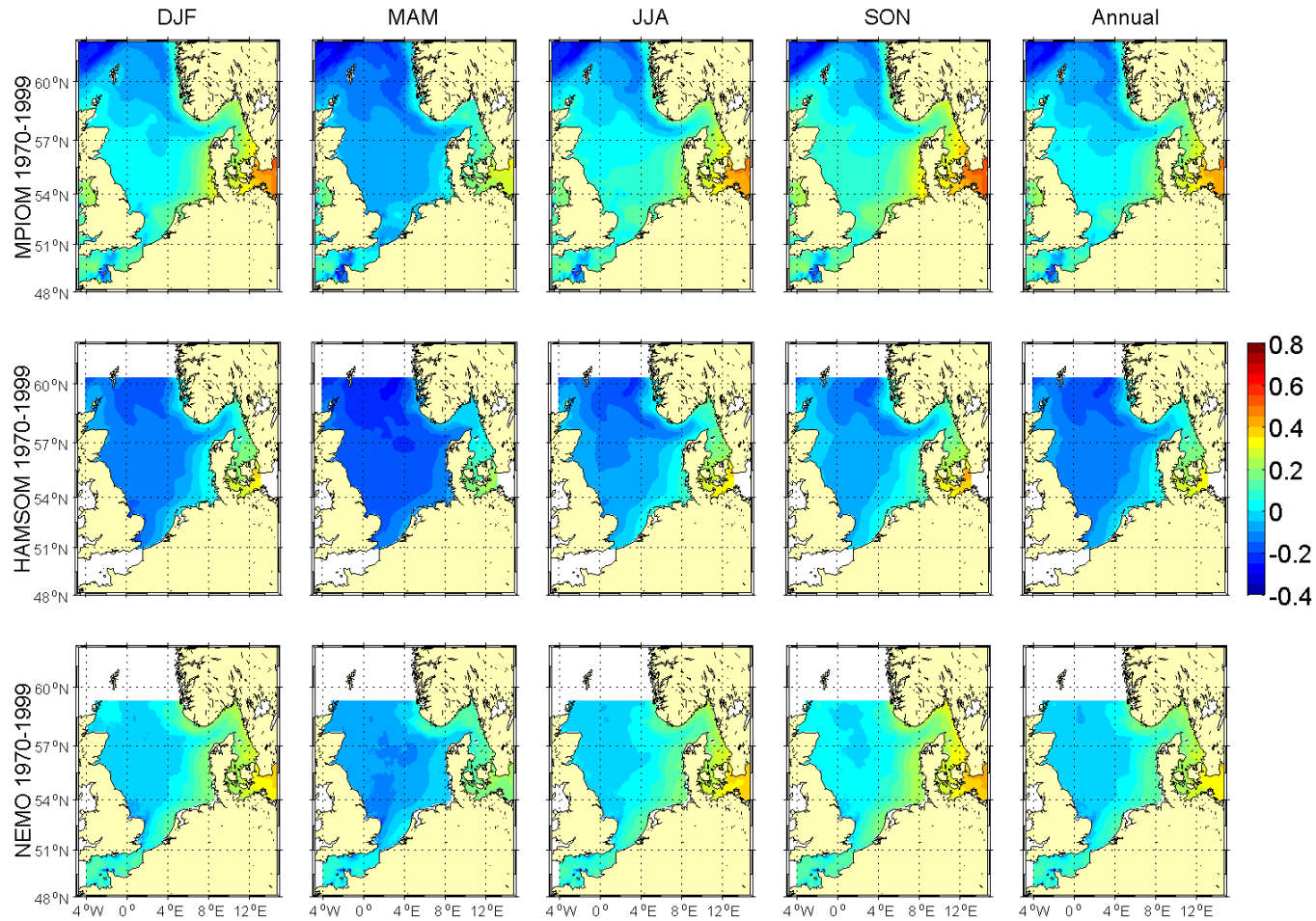


Figure 5.4.29A: Seasonal and annual means of sea surface height [m] for the period 1970-1999. Upper row MPIOM run 215, middle row HAMSOM run 202 and lower row NEMO-Nordic run 470 (all A1B scenario).

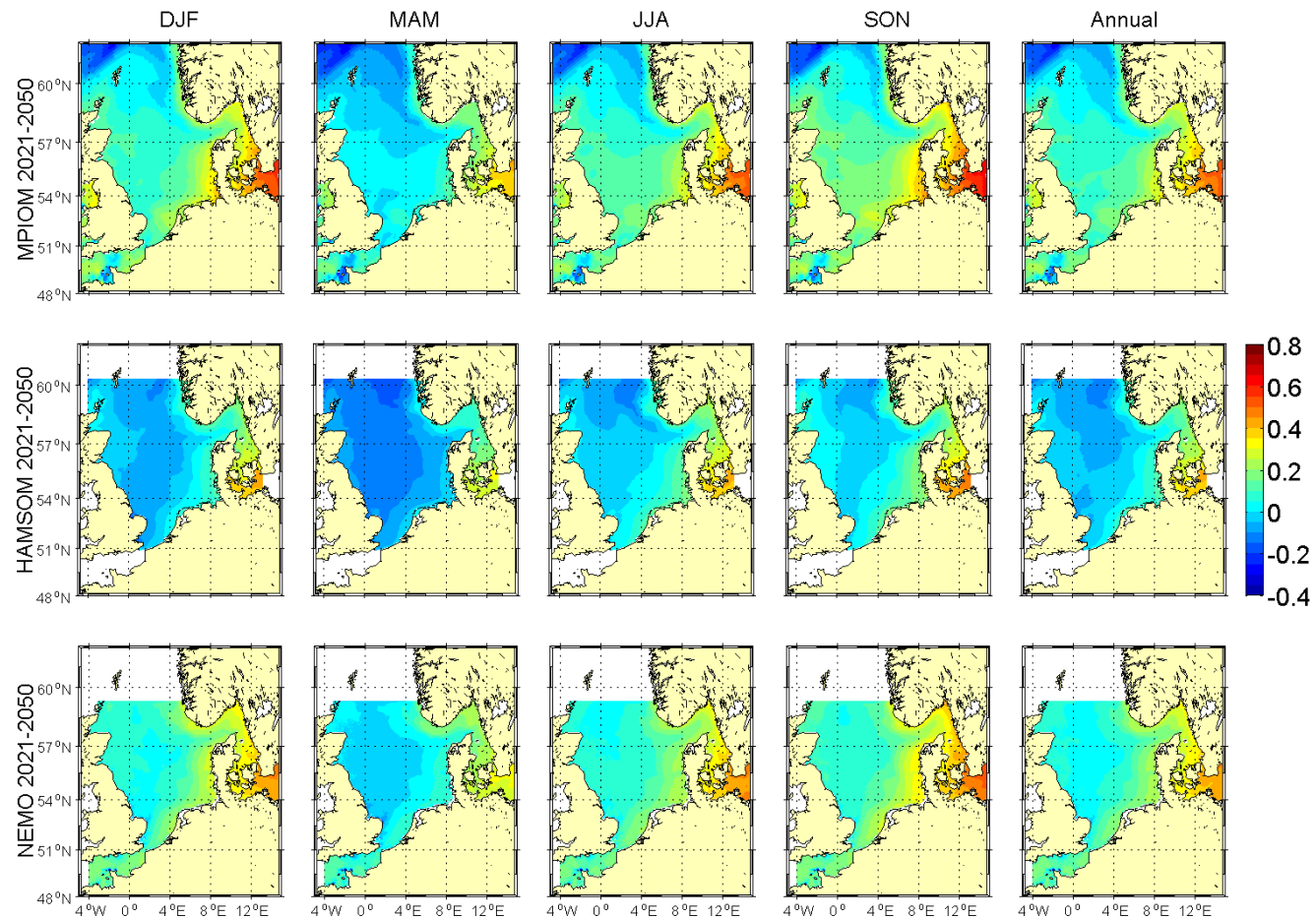


Figure 5.4.30A: Seasonal and annual means of sea surface height [m] for the period 2021-2050. Upper row MPIOM run 215, middle row HAMSOM run 202 and lower row NEMO-Nordic run 470 (all A1B scenario).

Coupled Ocean
Atmosphere
Models

BSH
DWD
IfM Hamburg
MPI Hamburg
SMHI
AWI

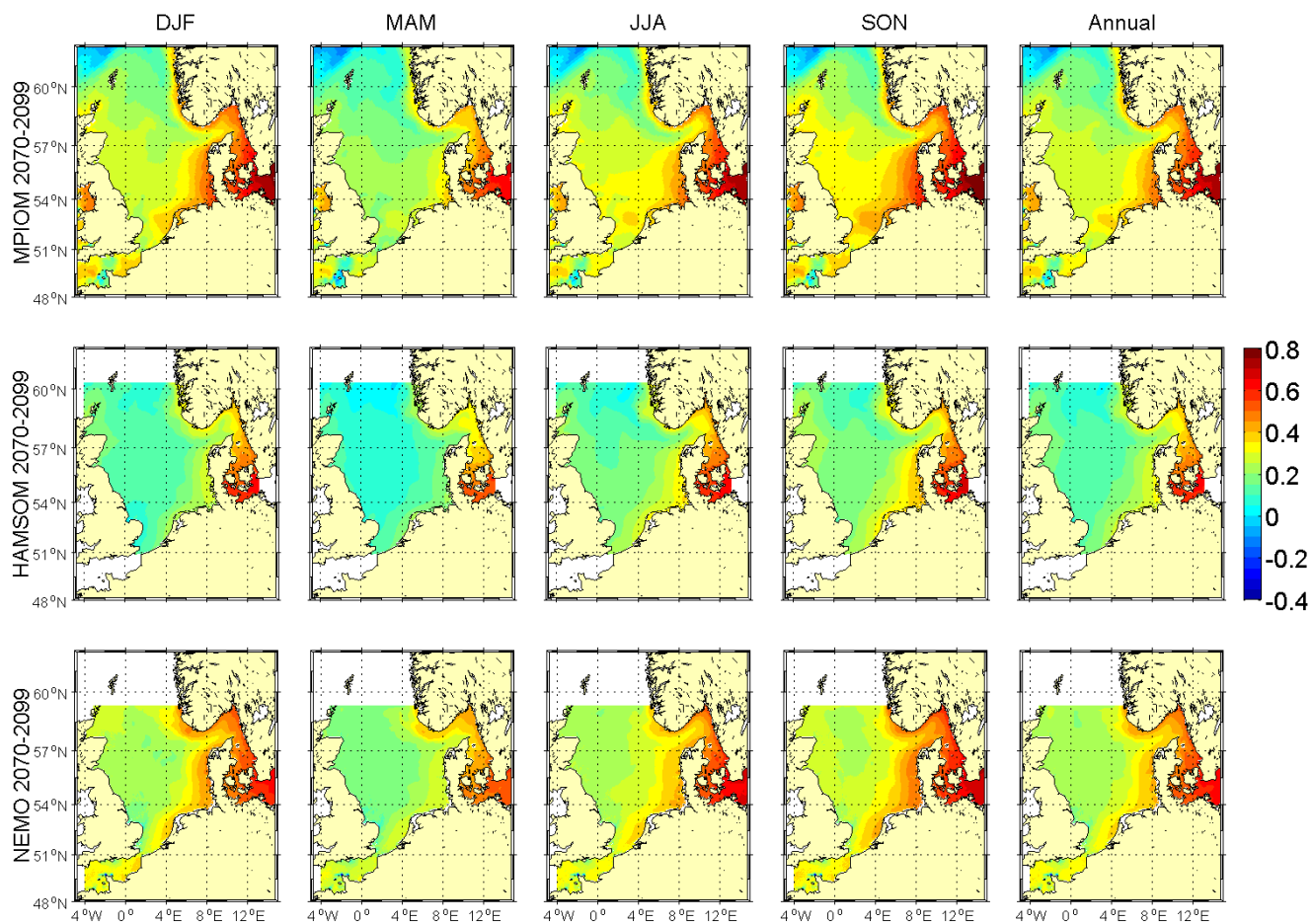


Figure 5.4.31A: Seasonal and annual means of sea surface height [m] for the period 2070-2099. Upper row MPIOM run 215, middle row HAMSOM run 202 and lower row NEMO-Nordic run 470 (all A1B scenario).



Coupled Ocean
Atmosphere
Models

BSH
DWD
IfM Hamburg
MPI Hamburg
SMHI
AWI

Figure 5.4.32A: Changes in seasonal and annual means of sea surface height [m] from (1970-1999) to (2021-2050). Upper row MPIOM run 215, middle row HAMSOM run 202 and lower row NEMO-Nordic run 470 (all A1B scenario). Selected isolines have been labelled for better orientation, contour interval is 0.02 m.

Coupled Ocean
Atmosphere
Models

BSH
DWD
IfM Hamburg
MPI Hamburg
SMHI
AWI

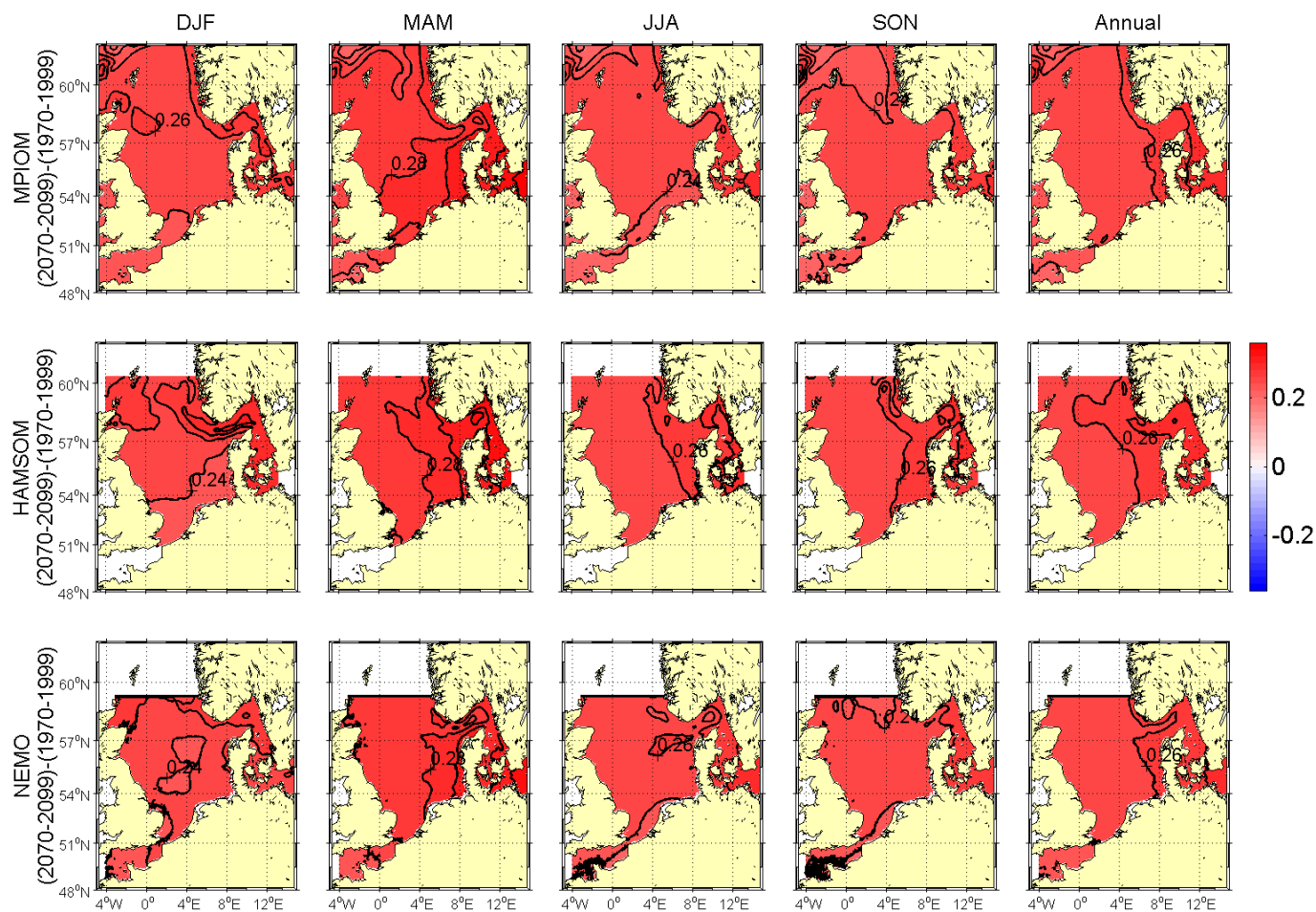


Figure 5.4.33A: Changes in seasonal and annual means of sea surface height [m] from (1970-1999) to (2070-2099). Upper row MPIOM run 215, middle row HAMSOM run 202 and lower row NEMO-Nordic run 470 (all A1B scenario). Selected isolines have been labelled for better orientation, contour interval is 0.02 m.

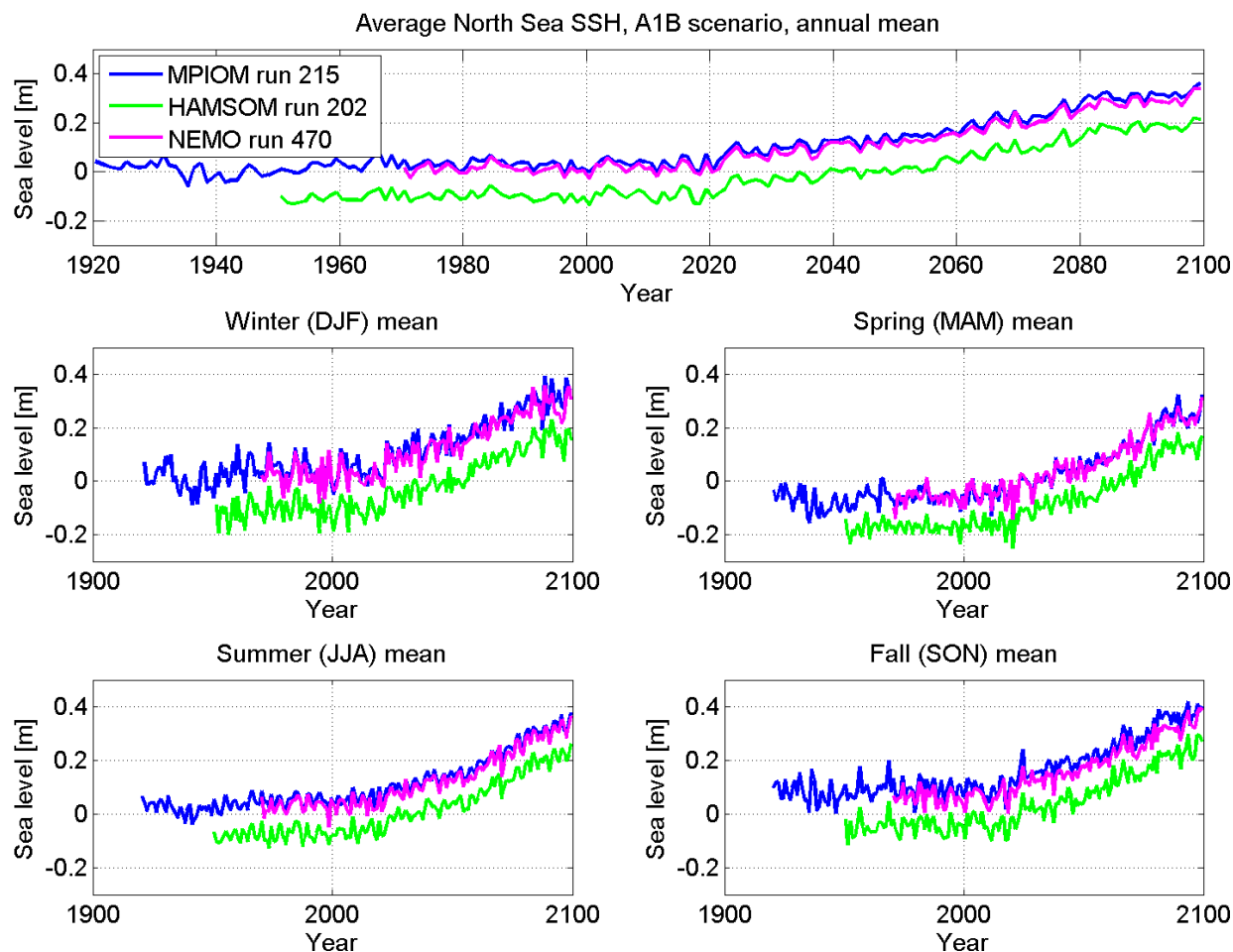


Figure 5.4.34A: Time series of seasonal and annual means of sea surface height [m] for MPIOM run 215 (blue), HAMSOM run 202 (green) and NEMO-Nordic run 470 (magenta). The sea surface heights represent averages over the North Sea area given in Figure 4.1. Upper row annual means, lower rows seasonal means.

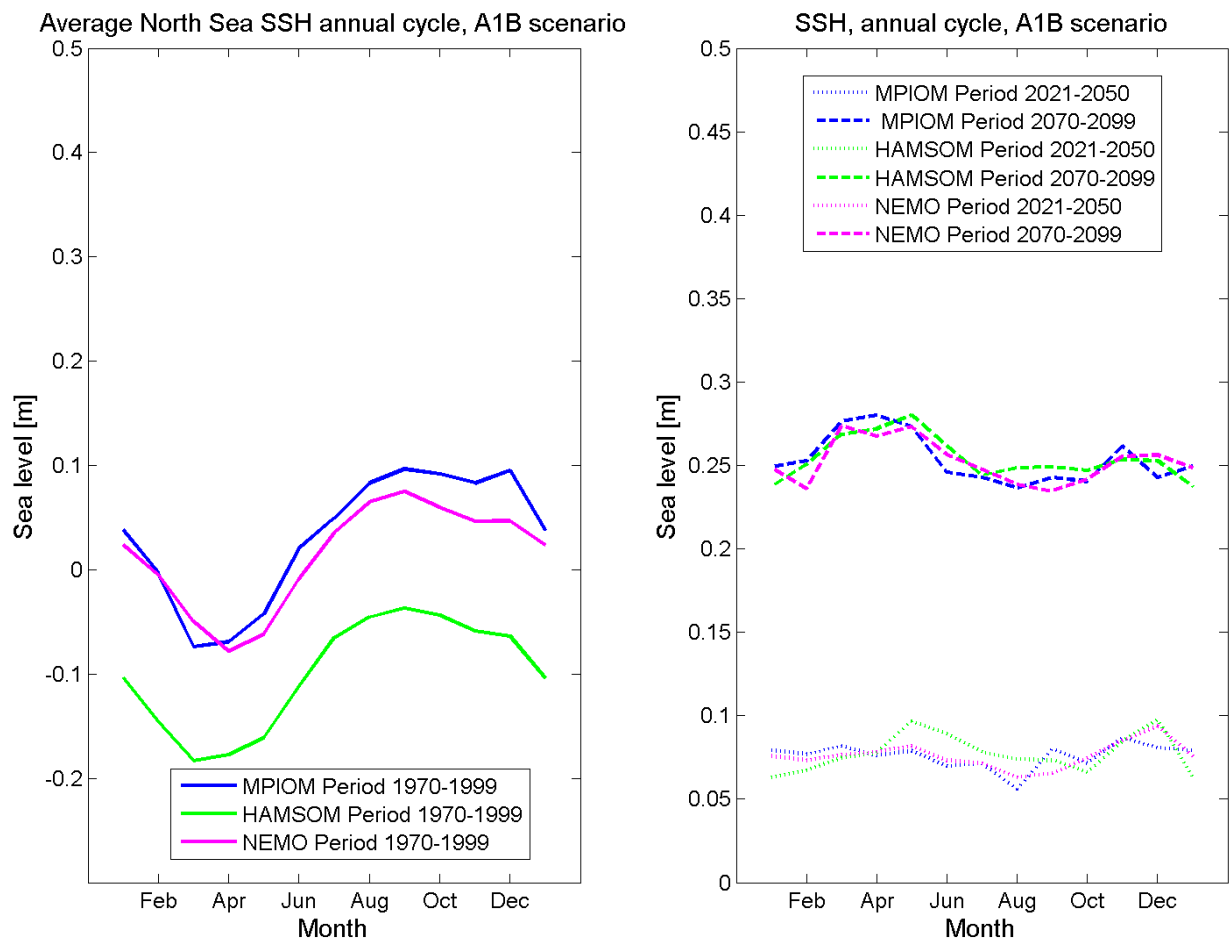


Figure 5.4.35A: left: mean annual cycle of sea surface height [m] for 1970-1990 for MPIOM run 215 (blue), HAMSOM run 202 (green) and NEMO-Nordic run 470 (blue). Right: differences in mean annual cycle to the averaging period 1970-1999, 2021-2050 as dotted line and 2070-2099 as dashed line. The means are representing averages over the North Sea area given in Figure 4.1.



Bundesanstalt für Wasserbau
Kompetenz für die Wasserstraßen

Bundesanstalt für Wasserbau (BAW)

Kußmaulstraße 17
76187 Karlsruhe

www.baw.de
info@baw.de

Bundesamt für Seeschifffahrt und Hydrographie (BSH)

Bernhard-Nocht-Straße 78
20359 Hamburg

www.bsh.de
posteingang@bsh.de



**BUNDESAMT FÜR
SEESCHIFFFAHRT
UND
HYDROGRAPHIE**



Deutscher Wetterdienst (DWD)

Frankfurter Straße 135
63067 Offenbach/Main

www.dwd.de
info@dwd.de

**Bundesanstalt für
Gewässerkunde (BfG)**

Am Mainzer Tor 1
56068 Koblenz

www.bafg.de
posteingang@bafg.de



IMPRESSUM

Herausgeber:

Bundesanstalt für Gewässerkunde
KLIWAS Koordination
Am Mainzer Tor 1
Postfach 20 02 53
56002 Koblenz
Tel.: 0261 / 1306-0
Fax: 0261 / 1306-5302
E-Mail: kliwas@bafg.de
Internet: <http://www.kliwas.de>

Redaktion: KLIWAS-Koordination
Bundesanstalt für Gewässerkunde

Autoren: Katharina Bülow¹, Christian Dieterich²,
Alberto Elizalde³, Matthias Gröger²,
Hartmut Heinrich¹, Sabine Hüttl-Kabus¹,
Birgit Klein¹, Bernhard Mayer⁴,
H.E. Markus Meier², Uwe Mikolajewicz³,
Nikesh Narayan¹, Thomas Pohlmann⁴,
Gudrun Rosenhagen⁵, Semjon Schimanke²,
Dmitry Sein⁶, Jian Su⁴

(1) BSH, (2) SMHI, (3) Max Planck Institute
for Meteorology, (4) Institute of Oceanography,
University Hamburg, (5) DWD, (6) AWI

Layout: Christin Hantsche und Tobias Knapp,
Bundesamt für Seeschifffahrt
und Hydrographie - Rostock

DOI: 10.5675/Kliwas_27/2014